

Regd. No. C-3911

VOL. 37

INDIAN JOURNAL OF PHYSICS

No. 1

(Published in collaboration with the Indian Physical Society)

AND

VOL. 46

PROCEEDINGS

No. 1

OF THE

INDIAN ASSOCIATION FOR THE
CULTIVATION OF SCIENCE

JANUARY 1963

PUBLISHED BY THE
INDIAN ASSOCIATION FOR THE CULTIVATION OF SCIENCE
JADAVPUR, CALCUTTA 32

BOARD OF EDITORS

K. BANERJEE	D. S. KOTHARI
D. M. BOSE	S. K. MITRA
S. N. BOSE	B. D. NAG CHAUDHURI
S. D. CHATTERJEE	K. R. RAO
P. S. GILL	D. B. SINHA
S. R. KHAISTGIR	S. C. SIKKAR (<i>Secretary</i>)
B. N. SRIVASTAVA	

EDITORIAL COLLABORATORS

PROF. R. K. ASUNDI, Ph.D., F.N.I.
PROF. D. BASU, Ph.D.
PROF. J. N. BHAR, D.Sc., F.N.I.
PROF. V. G. BHIDE, Ph.D. (Nag), Ph.D. (Lond).
PROF. A. BOSE, D.Sc., F.N.I.
PROF. S. K. CHAKRABARTY, D.Sc., F.N.I.
DR. J. S. CHATTERJEE
DR. K. DAS GUPTA, Ph.D.
PROF. N. N. DAS GUPTA, Ph.D., F.N.I.
J. DHAR, D.Phil. (So)
PROF. A. K. DUTTA, D.Sc., F.N.I.
PROF. C. S. GHOSH, M.Sc., S.M., F.N.I., M.I.E.E.
PROF. S. GHOSH, D.Sc., F.N.I.
PROF. S. N. GHOSH, D.Sc.
PROF. S. GUPTA, M.Sc., F.N.I.
PROF. D. N. KUNDU, Ph.D., F.N.I.
PROF. R. C. MAJUMDER, Ph.D., F.N.I.
PRINCIPAL Y. G. NAIK, Ph.D.
PROF. S. R. PALIT, D.Sc., F.R.I.C., F.N.I.
PROF. H. RAKSHIT, D.Sc., F.N.I.
PROF. A. SAHA, D.Sc., F.N.I.
DR. VIKRAM A. SARABHAI, M.A., Ph.D., F.N.I.
DR. A. K. S. GUPTA, D.Sc.
PROF. NAND LAL SINGH, D.Sc.
DR. M. S. SINHA, D.Sc., F.N.I.
PROF. N. R. TAWDE, Ph.D., F.N.I.
DR. P. VENKATESWARLU

Assistant Editor :

SRI T. N. MISRA, M.Sc.

Annual Subscription—

Inland Rs. 25.00

Foreign £ 2-10-0 or \$ 7.00

NOTICE

TO INTENDING AUTHORS

Manuscripts for publication should be sent to the Assistant Editor, *Indian Journal of Physics*, Jadavpur, Calcutta-32.

The manuscripts submitted must be type-written with double space on the foolscap paper with sufficient margin on the left and at the top. The original copy, and not the carbon copy, should be submitted. Each paper must contain an abstract at the beginning.

All references should be given in the text by quoting the surname of the author, followed by year of publication e.g., (Ghosh, 1954). The full reference should be given in a list at the end arranged alphabetically, as follows: Ghosh, D. K., 1954, *Ind. J. Phys.*, 2, 485.

Line diagrams should be drawn on white Bristol board or tracing paper with black India ink, and letters and numbers inside the diagrams should be written neatly in capital type with India ink. The size of the diagrams submitted and the lettering inside should be large enough so that it is legible after reduction to one-third the original size. A simple style of lettering such as gothic, with its uniform line width and no serifs should be used e.g.,

A·B·E·F·G·M·P·T·W·

Photographs submitted for publication should be printed on glossy paper with somewhat more contrast than that desired in the reproduction, and should, if possible, be mounted on thick white paper.

Captions to all figures should be typed on a separate sheet and attached at the end of the paper.

The mathematical expressions should be written carefully by hand. Care should be taken to distinguish between capital and small letters and superscripts and subscripts. Repetition of a complex expression should be avoided by representing it by a symbol. Green letters and unusual symbols should be identified in the margin. Fractional exponents should be used instead of roots.

Bengal Chemical and Pharmaceutical Works Ltd. **Pioneer Indian Manufacturers of Pharmaceuticals & Chemicals.**

Manufacturers of

Pharmaceutical Chemicals:

Caffeine and its salts, Strychnine Hydrochlor, Strychnine Sulphate, Brucine Sulphate, Potassium Citrate B.P., I.P., Sodium Citrate B.P., I.P., Potassium Acetate B.P., I.P., Potassium Iodide B.P., I.P., Sodium Iodide B.P., I.P., Ferri et Ammon Citrate B.P., I.P., Nicotinic Acid, B.P., Nicotinamide, B.P., and various other Pharmaceutical Chemicals.

Heavy & Reagent Quality Fine Chemicals:

Alum, Alum Sulphate (Iron Free), Ferro Alum, Zinc Chloride Tech. Naphthalene Pure, Sodium Citrate A.R., Potassium Citrate A.R., Magnesium Sulphate A.R., Sodium Sulphate Anhydrous A.R., Potassium Iodide A.R., Sodium Chloride A.R., Zinc Sulphate A.R., etc.

Please refer your enquiries for the above items and other chemicals in the line to :-

BENGAL CHEMICAL
6, GANESH CHUNDER AVENUE,
CALCUTTA-13, INDIA.

When you require

MEASURING INSTRUMENTS & PRECISION TEST-GEAR

for different purposes

make it a point to contact us

We supply :

Moving Coil Movements for Voltage or Current Measurements in any range, RF Signal Generators, RC Audio Generators, Maicom Test Instruments and Other Testing Equipment

We can also design to your requirements

Oscillographs, Signal Generators, Rectifier Units, Power Supply Units

State your detailed requirements and get our quotations

We have been designing and supplying to the market various Electrical and Electronic Equipment for over 15 years past.

Guaranteed Service.

Prompt Attention

RADIO ELECTRIC (PRIVATE) LTD.

2R LAMINGTON CHAMBERS, LAMINGTON ROAD, BOMBAY-4

IMPORTANT PUBLICATIONS

The following special publications of the Indian Association for the Cultivation of Science, Jadavpur, Calcutta, are available at the prices shown against each of them :—

TITLE	AUTHOR	PRICE
Magnetism—Report of the Symposium on Magnetism		Rs. 7 0 0
Iron Ores of India	Dr. M. S. Krishnan	5 0 0
Earthquakes in the Himalayan Region	Dr. S. K. Banerji	3 0 0
Methods in Scientific Research	Sir E. J. Russell	0 6 0
The Origin of the Planets	Sir James H. Jeans	0 6 0
Active Nitrogen A New Theory	Prof. S. K. Mitra	2 8 0
Theory of Valency and the Structure of Chemical Compounds.	Prof. P. Ray	
Petroleum Resources of India	D. N. Wadia	2 8 0
The Role of the Electrical Double-layer in the Electro Chemistry of Colloids.	J. N. Mukherjee	1 12 0
The Earth's Magnetism and its Changes	Prof. S. Chapman	1 0 0
Distribution of Anthocyanins	Robert Robinson	1 4 0
Lapmore, A New Antimalarial	Louis F. Fieser	1 0 0
Catalysts in Polymerization Reactions	H. Mark	1 8 0
Constitutional Problems Concerning Vat Dyes	Dr. K. Venkataratnam	1 0 0
Non-Aqueous Titration	Santi R. Palit, Mihir Nath Das and G. R. Somayajulu	3 0 0
Garnets and their Role in Nature	Sir Lewis I. Fieser	2 8 0

A discount of 25% is allowed to Booksellers and Agents

N O T I C E

No claims will be allowed for copies of journal lost in the mail or otherwise unless such claims are received within 4 months of the date of issue.

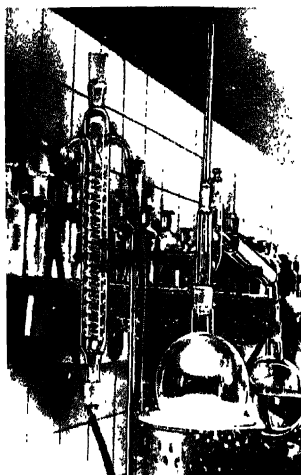
RATES OF ADVERTISEMENTS

1. Ordinary pages

Full page	Rs. 50/- per insertion
Half page	Rs. 28/- per insertion
 2. Pages facing 1st inside cover, 2nd inside cover and first and last page of book matter.

Full page	Rs. 55/- per insertion
Half page	Rs. 30/- per insertion
 3. Cover pages

by negotiation	Rs. 50/- per insertion
----------------	------------------------
- 25% commissions are allowed to *bona fide* publicity agents securing orders for advertisements.



For a specially high
working rate
in research and
works laboratories
RASOTHERM -Glass
FROM JENA

Laboratory Instruments, structural parts and apparatus of

R A S O T H E R M

are distinguished by a specially high chemical and thermic as well as mechanical resistance.



R A S O T H E R M

has an extremely low coefficient of expansion which permits special wall thicknesses

R A S O T H E R M

is free from potassium, arsenic, antimony and heavy metals

VEB JENA^{er} GLASWERK SCHOTT & GEN., JENA

GERMAN DEMOCRATIC REPUBLIC

General representation for India :

RAJ-DER-KAR & CO.

SADHANA RAYON HOUSE,
Dr D Naoji Road,
B O M B A Y

44/6. REGAL BUILDING
Cannaught Circus.
NEW DELHI - I



Laboratory Instruments for the DETERMINATION

OF

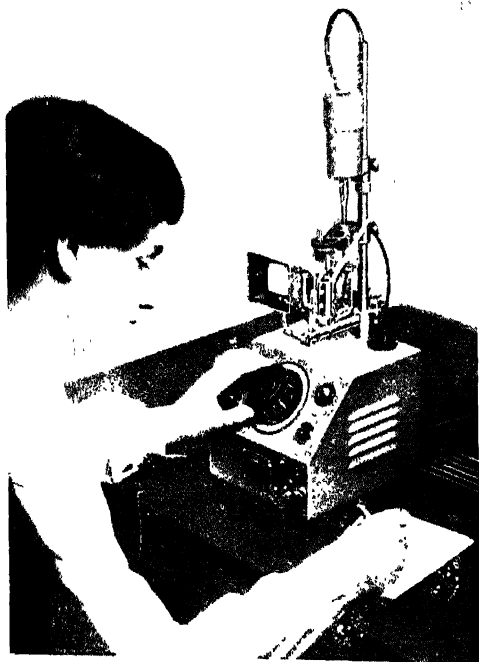
MELTING POINT

BOILING POINT

MOLECULAR

WEIGHT

FLOW POINT



In organic-chemical investigation and for Industrial purposes, the determination of melting point is the most important and generally applied method for the examination of known materials.

This new instrument of BUCHHI has proved by its daily use to meet entirely your requirements. This instrument also makes possible an exact recordable deter-

mination of melting point, and by changing some accessories, the determination of boiling point, molecular weight and flow point.

For further particulars, please write to :

Sole Distributors -

**THE SCIENTIFIC INSTRUMENT
CO., LD.**

ALLAHABAD BOMBAY CALCUTTA MADRAS
NEW DELHI

Head Office : 6, Tej Bahadur Sapru Road, Allahabad



INTERACTION OF 14.8 Mev NEUTRONS WITH ALUMINIUM

R. K. MOHINDRA AND H. S. HANS

DEPARTMENT OF PHYSICS, MUSLIM UNIVERSITY, ALIGARH

(Received February 5, 1962, Resubmitted September 21, 1962)

ABSTRACT The spectra of charged particles and neutrons from Al^{27} have been calculated on the basis of the compound nucleus theory using various level density formulae and taking into account the effect of volume direct interaction. The comparisons between the experimental and calculated spectra are presented in the form of actual particle spectra. The shapes of the calculated spectra for the various level density formulae are in rough agreement with the experimental results, but there are deviations in the absolute yield. Level density formulae due to Lang & LeCouteur and Newton gave better agreement with the experimental results than the simple formulae based on Fermi gas model and the constant temperature. Yield of (n, np) calculated on the basis of simple Fermi gas model formula, assuming the parameter a to be constant, is too high. All the calculated proton spectra are deficient in the high energy protons compared to the experimental values even after taking into account the contribution of the volume direct interaction.

INTRODUCTION

Recent comparison of Colli *et al.* (1959), Allan (1957), (1958); Kumabe *et al.* (1957); Graves and Rosen (1953); Paul and Clarke (1953) between experimental data on the various interaction cross-sections and the predictions of the compound nucleus theory have suggested that the theory is inadequate. In the experimental spectra there is excess of high and low energy particles. The excess of high energy particles has been explained partly by various authors [Brown and Muirhead (1957), Austern *et al.* (1953)] by taking into account direct interactions. On the other hand, several attempts have been made to explain to some extent the preponderance of low energy particles by taking into account (i) the evaporation of secondary particles from the residual nucleus, (ii) assuming the density distribution of the nucleus to be round edged Kikuchi (1957), (iii) the velocity dependent potential, (iv) the oscillations of the compound nucleus Nemeth (1958); (v) the particles are evaporated from an excited nucleus and the potential and transmission coefficients for an excited nucleus differ from those of a nucleus in ground state Nemeth (1960).

The present calculations were undertaken as an attempt to delineate the extent to which various level density formulae of the statistical theory and the theory of volume direct interaction can provide a valid description of the spectra of emitted particles due to the interaction of 14.8 Mev neutron with Al^{27} . We

have made calculations on the basis of compound nucleus for the spectra of emitted particles in (n, p) , (n, n') and (n, α) reactions making use of (i) the simple Fermi gas model level density formula due to Weisskopf (1952), (ii) the constant temperature formula, (iii) the level density formula due to Lang and LeCouteur (1954) and (iv) Newton's shell dependent formula (1956). It may be noted that the direct comparisons of calculated and the observed actual particle spectra provide a better test for the validity of the statistical theory rather than the comparisons in the form of level densities. Earlier, Mann and Nair (1960) reported similar calculations for the proton spectrum and using the simple Fermi gas model formula only.

THEORY

In the interaction of 14.8 Mev neutrons with Al^{27} ,

(i) the proton spectrum is mainly due to the following reactions:

$$[(n, p\gamma) + (n, pn)]_{\text{comp}, d\Omega} + [(n, np)]_{\text{comp}, d\Omega}$$

The contribution due to $(n, \alpha p)$ reaction has been found to be less than one millibarn and (n, pp') is not energetically possible because of the large separation energy of proton in ^{27}Mg .

(ii) the neutron spectra is mainly due to

$$[(n, n'\gamma) + (n, n'n'') + (n, n'p) + (n, n'\alpha)]_{\text{comp}, d\Omega} + [(n, \alpha n')]_{\text{comp}, d\Omega} + [(n, pn')]_{\text{comp}, d\Omega}$$

(iii) the alpha particle spectra are mainly due to

$$[(n, \alpha\gamma) + (n, \alpha n')]_{\text{comp}, d\Omega} + [(n, n'\alpha)]_{\text{comp}, d\Omega}$$

The primary particles are emitted both due to the evaporation process and direct interaction, while the secondary particles are mainly emitted due to evaporation.

COMPOUND NUCLEUS THEORY

The energy spectra of the (l, i) reaction due to incident particle l with energy E_l (14.8 Mev in the present case) is given by

$$\frac{\partial^2 \sigma_c(l, i)}{\partial E_i \partial \Omega} = \frac{\sigma_c(E_l)}{4\pi} \cdot \frac{2M_l}{h^2} \cdot \frac{E_l \sigma_i'(E_l) \omega_R(E_0 - E_i) dE_i}{\sum_K F_K(E_0)} \quad \dots (1)$$

where F_K is a quantity proportional to partial width for the disintegration with the emission of any particle K and is given by Blatt and Weisskopf (1952) as

$$F_K(E_0) = \frac{2M_K}{h^2} \int_{E_K}^{E_0} E_K \sigma_c^K(E_K) \omega_R(E_0 - E_K) dE_K \quad \dots (2)$$

where E_0 is the maximum available energy = the incident energy + Q value of the reaction, $\sigma_c^K(E_K)$ is the cross-section for the inverse reaction, ω_R is the level

Interaction of 14.8 Mev Neutrons with Aluminium

density of the residual nucleus, M_K is the mass of the emitted particle, and $\sum_K F_K(E_0)$ is extended over all kinds of partial widths

When the first particle i is emitted with small kinetic energy, the intermediate nucleus is often so highly excited that a second particle j can be evaporated if

$$E_i < E_0 - S_{ij}$$

where S_{ij} is the separation energy of the secondary particle j in the intermediate nucleus left after the evaporation of i .

The energy spectrum of secondary particles emitted after evaporation of the particle i is given by Hayakawa *et al.* (1955) as

$$\frac{\partial^2 \sigma_c(l, i, j)}{\partial E_j \partial \Omega} = \frac{\sigma_c(E_l)}{4\pi} \cdot \frac{1}{\sum_K F_K} \cdot \begin{cases} E_0 - S_{ij} - E_j \\ 0 \end{cases} \cdot \frac{2M_i}{\hbar^2} \cdot E_i \sigma_c'(E_i) \omega_R'(E_0 - E_i) \times \\ \frac{2M_j}{\hbar^2} \cdot \frac{E_j \sigma_c'(E_j) \omega_R'(E_0 - E_i - S_{ij} - E_j)}{\sum F_m(E_0 - E_i - S_{im})} dE_i \quad \dots \quad (3)$$

DIRECT INTERACTION

These formulae are the same as derived by Hayakawa *et al.* (1955) and Brown and Muirhead (1957) assuming the nucleus to be composed of two non-interacting Fermi gases and taking into account the Pauli exclusion principle. The direct collisions with the individual nucleons in the nucleus give rise to these reactions.

The energy spectrum of protons due to direct interaction is given by

$$\left[\frac{d\sigma_{np}}{d\epsilon_p} \right]_{dir} = \sigma_1 \left(\frac{d\sigma}{d\epsilon_0} \right)_{np}^p X_{np} \phi(\epsilon_p) \dots \quad (4)$$

$$[\rho_p \alpha_{np} X_{np}] [\rho_n \alpha_{nn} X_{nn}]$$

The neutrons can be emitted either due to the collision of the incident neutrons with the protons or the neutrons of the target nucleus.

The energy spectrum of neutrons due to (n, p) collisions is given by

$$\left[\frac{d\sigma_{np}}{d\epsilon_n} \right]_{dir} = \sigma_1 \frac{\rho_p \left(\frac{d\sigma}{d\epsilon_0} \right)_{np} X_{np} \phi(\epsilon_n)}{[\rho_p \alpha_{np} X_{np} + \rho_n \alpha_{nn} X_{nn}]} \dots \quad (5)$$

The part due to (n, n) collisions is given by

$$\left[\frac{d\sigma_{nn}}{d\epsilon_n} \right]_{dir} = \sigma_1 \frac{2\rho_n \left(\frac{d\sigma}{d\epsilon_0} \right)_{nn} X_{nn} \phi(\epsilon_n)}{[\rho_p \alpha_{np} X_{np} + \rho_n \alpha_{nn} X_{nn}]} \dots \quad (6)$$

where $\left(\frac{d\sigma}{d\epsilon_n}\right)_{np}$ is the cross-section for the production of a proton with energy ϵ_n in a single collision between the neutron and proton inside the nucleus and α is a factor which reduces the magnitude of X_{np} and X_{nn} due to Pauli exclusion principle. The values of $\left(\frac{d\sigma}{d\epsilon_0}\right)$ and α have been evaluated by the method of Mani and Nair (1960). ρ is the density of nucleons inside the nucleus, σ is the interaction cross-section. X_{np} and X_{nn} are free (n, p) and (n, n) collision cross-sections at 14 Mev. $\phi(\epsilon)$ is the total probability of escape for a particle with energy ϵ is given by

$$\phi(\epsilon) = \frac{P(\epsilon) \exp - \frac{0.75R}{\lambda(\epsilon_0)}}{1 + [1 - P(\epsilon)] \exp - \left[\frac{1.33R}{\lambda(\epsilon_0)} \right]}$$

$\lambda(\epsilon_0)$ is the mean free path of the nucleon inside the nucleus, P is the penetrability factor and for a square well potential is given by Mani and Nair (1960)

$$P(\epsilon) = \frac{\sigma_c(\epsilon)}{[\pi(R + \bar{\lambda})^2]}$$

where $R = 1.5A^{1/3}$, 10^{-13} cms, $\bar{\lambda} = \lambda/2\pi$ is the wavelength of the particle with energy ϵ and $\sigma_c(\epsilon)$ is the cross-section for the formation of the compound nucleus. For the case of a diffuse nuclear model an expression for P has been given by Kikuchi (1957) but we used only a square well potential.

Spectrum of secondary particles The spectrum of the secondary particles j boiling off the intermediate nucleus left after protons have been knocked out due to direct collisions is given by (Hayakawa *et al.* 1955)

$$\frac{\partial^2 \sigma(n, p, i)}{\partial E_j \partial \Omega} = \frac{1}{4\pi} \int_0^{E_0 - S_{ij} - E_j} \left(\frac{d\sigma_{np}}{d\epsilon_p} \right)_{dr} [1 - \phi(\epsilon_n)] \frac{2M_j}{\hbar^2} \cdot \frac{E_j \sigma_c^j(E_j) \omega_R^j(E_0 - S_{ij} - E_j - E_j) dE_i}{\sum_m F_m(E_0 - E_i - S_{im})} \dots (7)$$

Similarly, the spectra of particles boiling off the residual nucleus left after the first neutron has been knocked out

$$\frac{\partial^2 \sigma(n; n', j)}{\partial E_j \partial \Omega} = \frac{1}{4\pi} \int_0^{E_0 - S_{ij} - E_j} \left\{ \left(\frac{d\sigma_{np}}{d\epsilon_n} \right)_{dr} [1 - \phi(\epsilon_p)] + \left(\frac{d\sigma_{nn}}{d\epsilon_n} \right)_{dr} [1 - (\phi)\epsilon'_n] \right\} \cdot \frac{2M_j}{\hbar^2} \cdot \frac{E_j \sigma_c^j(E_j) \omega_R^j(E_0 - E_i - S_{ij} - E_j) dE_i}{\sum_m F_m(E_0 - E_i - S_{im})} \dots (8)$$

Differential cross-section of protons emitted due to direct interaction.

A calculation of the differential cross-section has been given by Hayakawa *et al.* (1955) and Brown and Muirhead (1957) for the production of a proton with energy ϵ and in a direction θ in the centre of mass system and their result is

$$\left[\frac{\partial^2 \sigma}{\partial \epsilon \partial \Omega} \right]_{av} = \left[\rho_p \alpha_{np} X_{np} + \rho_n \alpha_{nn} X_{nn} \right] \left[\rho_p \left(\frac{\partial^2 \sigma}{\partial \epsilon_0 \partial \Omega} \right)_{np} \right] \quad \dots \quad (9)$$

where

$$\left(\frac{\partial^2 \sigma}{\partial \epsilon_0 \partial \Omega} \right)_{np} = \frac{3 P P_1 X_{np}(P_1) M_p}{4 \pi q P_F^3} \log_e \frac{(\rho_2^4 + 2 b \rho_2^2 + c)^{1/2} + \rho_2^2 + b}{(\rho_1^4 + 2 b \rho_1^2 + c)^{1/2} + \rho_1^2 + b}$$

Where P_1 and P represent the momentum of the incident neutron and the emitted proton inside the nucleus, P_F is the Fermi momentum for the proton,

$$b = z_0^2 + q^2 - P^2, \quad c = (P^2 + q^2 - z_0^2)^2, \quad \rho_2^2 = P_F^2 - z_0^2, \\ \rho_1^2 = P_F^2 - 2Q + P^2 - Z_0^2 - P_1^2, \quad Z_0 = \frac{1}{2q}(P^2 + q^2 - P_1^2), \text{ and } q = |\vec{P} - \vec{P}_1|.$$

CALCULATIONS FOR THE EVAPORATION PROCESS

In order to carry out the calculations we have to consider the following quantities.

(i) cross-section for the formation of the compound nucleus. For protons and alphas calculated values of σ_c for square well potential have been listed by Blatt and Weisskopf (1952) for various $Z \leq 10$. For neutrons, values of σ_{cn} have been plotted in Fast Neutron Data Report (1951) for various A . We simply used the interpolated values.

(ii) Separation energies for various nuclei involved were calculated from the mass differences and beta disintegration energies given by King (1954) and Matlack and Everling (1957).

The values used are given below.

Nucleus	Sp in Mev	Sn in Mev
$^{27}_{17}\text{Al}$	8.3	13.0
$^{26}_{13}\text{Al}$	6.3	11.3
$^{27}_{12}\text{Mg}$	14.3	6.5
$^{26}_{12}\text{Mg}$	14.0	11.1
$^{21}_{11}\text{Na}$	10.6	7.0
$^{23}_{11}\text{Na}$	8.8	12.6

$T = 42 \text{ Mev}$

$X_{np} = 710 \text{ mbs}$ $X_{pn} \approx 200 \text{ mbs}$ (Hess, 1958)

$\sigma_T = \sigma_{TS} = 900 \text{ mbs}$ (Celli *et al.*, 1959)

$[\sigma(n, \gamma)]_{comp} = 92 \text{ mb}$ (Kumabe *et al.*, 1957)

$S_0 \text{ in } 11.11^{27} = 8 \text{ Mev}$ (Kumabe, 1958)

$[\sigma(n, p\gamma) + n, pn)]_{comp} = 85 \text{ mbs}$ (Glover *et al.* 1961)

(iii) Level densities :- The four formulae for level density have been employed. The evaluation of various parameters of the particular formula used along with its results is discussed below separately.

Simple Fermi gas model level density formula

This formula was first given by Blatt and Weisskopf and is frequently used for statistical theory calculations.

$$\omega(U) = C \exp(2\sigma' U^2) \quad \dots (10)$$

where U is the residual energy in the C.M. system. The parameters a and C of the above formula are not known. We eliminate the constant C and use ' a ' equal to 3 Mev^{-1} and 5 Mev^{-1} . From formula (1) we know,

$$\sigma(n, p\gamma + n, pn)]_{comp} = \frac{2M_p E_0}{h^2} \int_0^{E_0} E_p \sigma_n(E_p) \exp(2a^2 U^2) dE_p$$

$$\frac{\sum F_K(E_0)}{K}$$

using experimental value of $[\sigma(n, p\gamma) + \sigma(n, pn)]_{comp}$ we can write the energy spectrum of protons as

$$\left[\frac{\partial^2 \sigma_{np}}{\partial E_p \partial \Omega} \right] = \frac{[\sigma(n, p\gamma + n, pn)]_{comp}}{4\pi} \frac{E_p \sigma_n(E_p) \exp(2a^2 U^2) dE_p}{\int_0^{E_0} E_p \sigma_n(E_p) \exp(2a^2 U^2) dE_p} \quad \dots (11)$$

Similarly, (n, n') spectrum can be found if we use

$$[\sigma(n, n')]_{comp} = \sigma_{nnel} - [\sigma(n, p\gamma + n, pn)]_{comp+dir} - [\sigma(n, \alpha\gamma + n, \alpha n)]_{comp} - [\sigma(n, n')]_{dir}$$

where $[\sigma(n, n')]_{dir}$ and $[\sigma(n, p\gamma + n, pn)]_{dir}$ were found by formulae (4), (5) and (6). The value of estimated $\sigma(n, n')$ may introduce large errors and the result were checked by using another form

$$\frac{\partial^2 \sigma_{nn'}}{\partial E_n \partial \Omega} = \frac{[\sigma_n(E_n) + \sigma(n, \alpha)]}{4\pi} \frac{E_n \sigma_n(E_n) \omega(E_0 - E_n) dE_n}{F_p(E_0) + F_n(E_0)} \quad \dots (12)$$

This expression is quite insensitive to the value of $\sigma(n, \alpha)$ as this value is quite small as compared to $\sigma_n(E_n)$

The spectrum of (n, np) was evaluated with the help of formula (3) and (8) and ΣP_m was taken over (n, np) and $(n, 2n)$ only because we do not know C' for ${}_{11}\text{Na}^{23}$ nucleus in $(n, n'\alpha)$ reaction. The neglect of $(n, n'\alpha)$ introduces small error which may be estimated from the case where spectra have been calculated on the basis of Lang and LeCouteur formula and has been found to be of the order of 3% for 1.5 Mev, 6% for 2.5 Mev, 8% for 3.5 Mev and 15% for 4.5 Mev secondary protons. The value of C' was used according to the odd-even character of the nucleus from the relation, Moore (1960)

$$\frac{1}{2} C'_{\text{odd-odd}} = C'_{\text{even-odd}} = C'_{\text{odd-even}} = 5C'_{\text{even-even}}$$

Lang and LeCouteur level density formula

For a nucleus of atomic weight A and excitation energy U , the level spacing is

$$D_0 = \frac{1}{\omega_0} = 0.11 U^2 (U + t)^2 \exp \left[-2 \left(\frac{A U}{11} \right)^{1/3} - \frac{5}{32} (11 U)^{2/3} \right] \quad \dots (13)$$

where nuclear temperature

$$t = \left[\frac{10.5 U}{A} \right]^{1/2} - \frac{7.9}{A}$$

The effect of the pairing energy was not taken into account as it appears as a fictitious negative Q value and the high energy end of the spectrum is cut off. This will make the comparison with experiment difficult as in the high energy region we want to see the effect of volume direct interaction. Instead of it we performed the calculations with and without taking into account the odd-even characteristic of residual nuclei by the method suggested by Brown and Muirhead (1957).

Newton's level density formula

This shell dependent level spacing formula depends upon the densities of single particle orbits near the Fermi level in the nucleon gas. For a nucleus of excitation energy U , with Z protons and N neutrons,

$$D_0 = \frac{1}{\omega_0} = A^{5/4} (\hat{j}_N + 1)^{1/2} (\hat{j}_Z + 1)^{1/2} (2U + 3t)^2 \times \exp \{ 8.75 - 0.4982 (\hat{j}_N + \hat{j}_Z + 1)^{1/3} U^{1/2} \} \quad \dots (14)$$

D is in ev, U and t in Mev

Here \hat{j}_N, \hat{j}_Z are effective values of j and are tabulated by Newton (1956).

Nuclear temperature $t = [6\pi^{-2} G^{-1} U]^{1/2}$ where $G = 2\pi (\hat{j}_N + \hat{j}_Z + 1) A^{2/3}$
 $\alpha = 0.03772$

The level spacing approaches infinity at zero excitation energy which is the unattractive feature of the Newton's formula in our calculations. This may intro-

duce some error in the calculations as we simply extrapolated the curves to zero excitation energy. Cameron (1958) has given an improved formula which does go smoothly to zero excitation energy but it is too complicated. Again, the effect of pairing energy was not taken into account.

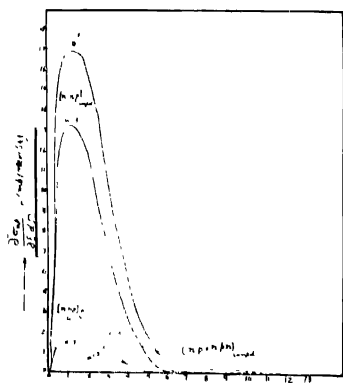
Constant temperature level density formula

$$\text{Here, } \rho(E_i) = C \exp - \left(\frac{E_i}{\theta} \right) \quad \dots (15)$$

where C is a constant and θ is the nuclear temperature. Calculations were made for the primary neutron and proton spectra using $\theta = 0.5$ Mev, 1 Mev, 1.3 Mev and 1.6 Mev. The shape of the spectrum depends more sensitively upon the value of θ as compared to the parameter 'a' in Weisskopf's formula. As θ is not known precisely in the case of (n, np) and $(n, 2n)$ processes, calculations were not carried out for secondary processes.

DISCUSSION AND RESULTS

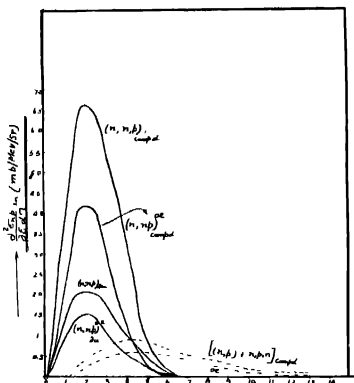
Proton spectra The calculated proton spectra are shown in fig. 1, 2 and 3. After adding the differential cross-section at 40° to the above curves the resultant curves are shown in fig. 4 along with the smoothed experimental curve of Glover and Weigold (1961) for the sake of comparison. The following points are worth mentioning



→ Proton energy in Mev.

Level density formula : $\omega(U) = C e^2 \sqrt{aU}$.

Figure (1) Energy spectra of protons for (n, p) and (n, np) reactions. Curves correspond to two different values of 'a' in the simple Fermi gas model formula.



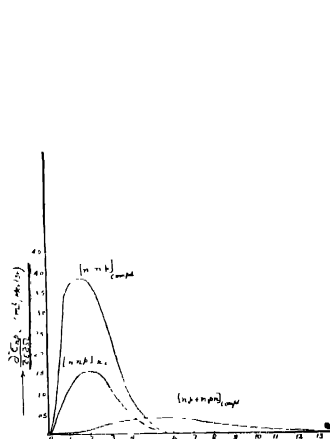
→ Proton energy in Mev.

Level density formula : Lang and LeCouteur.

Figure (2) Energy spectra of protons for (n, p) and (n, np) reactions calculated with Lang and LeCouteur formula. Oe denotes curves obtained without odd even effect and the remaining curves are without odd even effect.

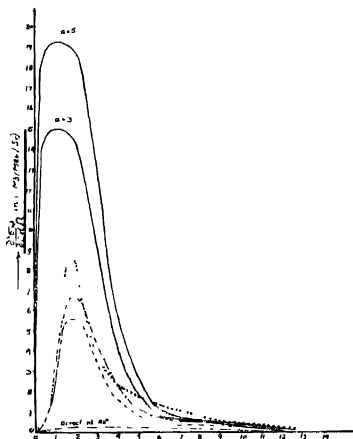
(i) In the case of simple Fermi gas model formula (10), we used the experimental value of $\sigma(n, p\gamma \rightarrow n, pn)$ rather than $\sigma(n, p\gamma)$ found by activation technique to eliminate the unknown constant C' and put the limits of the integral from zero to E_0 as in formula (11). The value of the calculated $\sigma(n, p\gamma \rightarrow n, pn)$ obtained by using $\sigma(n, p\gamma)$ is too high. This suggests that there may be competition between proton and γ -ray emission even if $E_p < E_n - S_n$, where S_n is the separation energy of neutron in the residual nucleus left after the evaporation of proton.

(ii) The calculated value of the spectra on the basis of the above formula is too high on the low energy region which is mainly due to (n, np) . This is probably because we used the same value of the parameter 'a' for the calculation of $\sigma(n, n')$, $\sigma(n, np)$ and $\sigma(n, 2n)$ as for $\sigma(n, p)$. By choosing suitable value of 'a' for each reaction, one may get better fit with the experiment. If we use the



→ Proton energy in Mev
Level density formula - Newton

Figure (3) Energy spectra of protons for (n, p) and (n, np) reactions calculated on the basis of Newton's formula.



→ Proton energy C M S. (Mev)
— — — Newton
- - - - - Lang Leuteur with odd even effect.
× × × Exptl points.
... Lang Leuteur without odd even effect

Figure (4) Resultant differential energy spectra of protons due to evaporation and direct interaction along with the experimental curve. The spectrum shown here are calculated for $\theta = 10^\circ$ to compare with experimental curve obtained at the same angle.

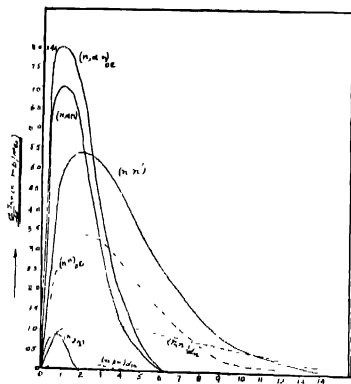
same value of $a = 3 \text{ Mev}^{-1}$ for (n, n') and (n, p) , the (n, n') spectrum is exaggerated in the low energy region and hence the (n, np) spectrum.

(iii) Curves of Fig. 2 show the various partial cross-sections calculated on the basis of Lang and LeCouteur formula with and without odd even effects. The oe -curve fits quite well with experimental values taking into account the uncertainties involved in the experimental points. It is evident that one should take into account the odd even effects.

(iv) Curves of fig. (3) give the various partial cross-sections calculated on the basis of Newton's shell-dependent level density formula. Fig. 4 shows that Newton's formula behaves nearly in the same way as that of Lang and LeCouteur with odd even effects.

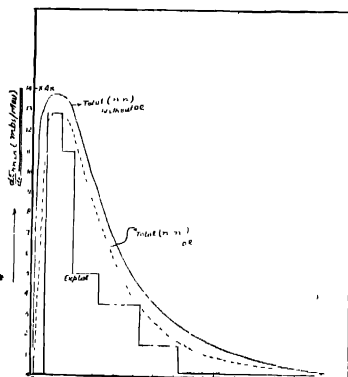
(v) All the calculated spectra are deficient in the high energy protons compared to the experimental spectra. This can be partly due to the deuteron contamination in the experiment and partly due to the fact that the theory of volume direct interaction may not take fully into account all the instantaneous emissions.

Neutron spectra. The calculated neutron energy spectra on the basis of Newton's and Lang and LeCouteur's formulae are shown in Fig 5 and 7.



→ Neutron energy in Mev.

Level density formula : Lang & LeCouteur.
Figure (5) Energy spectra of neutrons for (n, n') and $(n, \alpha n)$ calculated on the basis of Lang and LeCouteur formula. oe denotes curves obtained with odd even effects and the remaining curves are without odd even effects. The ordinate is to be multiplied by 4π to get absolute value



→ Neutron energy in Mev.

Level density formula : Lang & LeCouteur.
Figure (6) Energy spectra of neutrons due to the sum of various curves in fig (5). The dotted curve is with odd even effect and has been normalised with respect to the peak of the experimental histogram. The ordinate should be multiplied by 4π to get absolute value.

(i) Calculated $(n, \alpha n)$ contribution is quite significant in the low energy region and the contribution of $(n, 2n)$ is quite small.

(ii) Lang and LeCouteur's formula with odd-even effects and Newton's formula behave nearly in the same manner for the case of various partial cross-sections viz. $\sigma(n, \alpha n)$, $\sigma(n, n')$.

(iii) Calculated value of direct interaction cross-section for n, n' is about four times as compared to the n, p direct interaction cross-section. The higher value in the case of (n, n') is expected because of the collisions between identical particles.

(iv) The resultant neutron spectra are compared with the experimental curve of Stelson and Goodman (1951). The experimental curve has been normalized corresponding to the peak of the calculated spectra for the sake of comparison. The various spectra are shown in Figs. (6) and (7). The shapes are in rough agreement, but nothing can be concluded regarding the absolute yields.

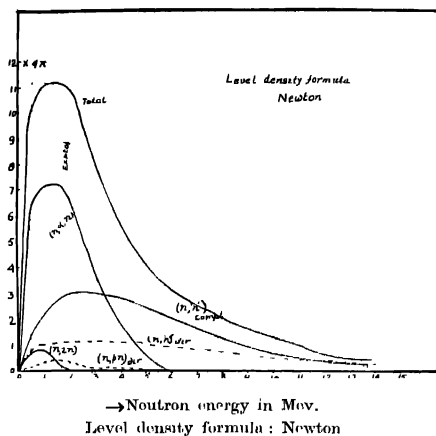


Figure (7) . Energy spectra of neutrons for $(n, n' x)$ and $(n, \alpha n)$ calculated on the basis of Newton's formula. The ordinate should be multiplied by 4π to get absolute value.

(v) The neutron spectrum was not calculated by using simple Fermi gas model formula (10) because we cannot eliminate C for calculating $\sigma(n, \alpha n)$ by the procedure used in the case of (n, np) . This is because C is assumed to be the same for isobaric nuclei. For the same reasons, we did not calculate the alpha particle spectrum by using the formula (10).

Alpha particle spectra. The alpha particle spectra calculated on the basis of Lang and LeCouteur formula with and without odd-even effects and Newton's formula are shown in Fig 8. The following points may be noted :

(i) As in the case of (n, p) and (n, n') the above two formulae due to Lang and LeCouteur with odd-even effects and Newton's behave nearly in the same manner and calculated total $\sigma(n, \alpha)$ is of the same order of magnitude in each case.

(ii) The calculated value of $\sigma(n, \alpha)$ is about five times higher than the experimental value. It is surprising that the above two formulae which give favourable results in case of (n, n') and (n, p) give too high a value in the case of (n, α) reac-

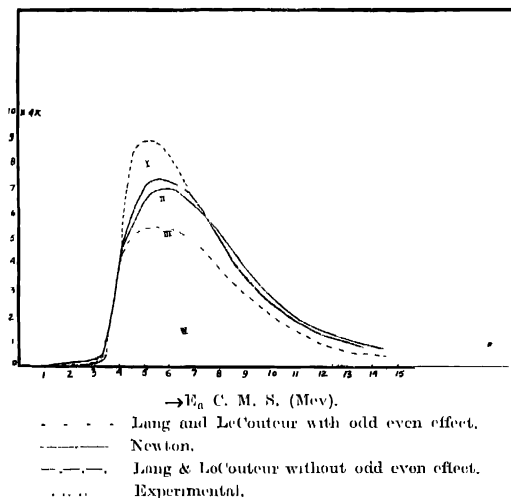


Figure (8) Calculated energy spectra of alphas along with the experimental curve. Dotted portion of curve (I) shows the calculated $(n, n' \alpha)$ contribution on the basis of Lang-LeCouteur formula. The ordinate should be multiplied by 4π to get absolute value.

tion which is supposed to be mainly due to the compound nucleus formation. The calculated curves have been compared with the experiment of Kumabe *et al.* (1957) in figure (8). The dotted part of curve I shows the contribution of $\sigma(n, n\alpha)$ calculated on the basis of Lang and LeCouteur formula.

ACKNOWLEDGMENTS

The authors are grateful to Prof. P. S. Gill for his kind encouragement. Thanks are due to Dr. C. S. Khurana and Mr. J. H. Naqvi for helpful discussions.

REFERENCES

- Allan, D., 1961, *Nuc. Phys.* **24**, 274.
 " 1957, *Proc. Phys. Soc.*, **A70**, 195.
 Austern, N., Butler, S. T. and MacManus, H., 1953, *Phys. Rev.*, **92**, 350.

- Brown, G. and Murhead, H., 1957, *Phil. Mag.*, **2**, 473.
- Blatt, J. M. and Weisskopf, V. F. Theoretical Nuclear Physics (Wiley, New York, 1952). Chapter VIII.
- Colli, L., Facchini, U., Iori, I., Mareazzan, M. G. and Sonn, A. M., 1959, *Nuovo Cimento*, **13**, 730.
- Cameron, A. G. W., 1957, *Can. J. Phys.*, **35**, 1021.
- Cameron, A. G. W., 1958, *Can. J. Phys.*, **36**, 1010.
- Final Report of Fast Neutron Data Project NYO -636, 1951.
- Glover, R. N. and Weigold, E., 1961, *Nuc. Phys.*, **24**, 630.
- Graves, E. R. and Rosen, L., 1953, *Phys. Rev.*, **89**, 343.
- Graves, E. R. and Rosen, L., 1957, *Phys. Rev.*, **107**, 824.
- Gugelot, P. C., 1951, *Phys. Rev.*, **81**, 51.
- Gugelot, P. C., 1954, *Phys. Rev.*, **93**, 425.
- Hayakawa, S., Kawai, M., and Kikuchi, K., 1955, *Prog. Theo. Phys.*, **13**, 413.
- Hess, W. N., 1958, *Rev. Mod. Phys.*, **30**, 368.
- Kikuchi, K., 1957, *Prog. Theo. Phys.*, **17**, 643.
- King, R. W., 1954, *Rev. Mod. Phys.*, **26**, 327.
- Kumabe, I., Takakoshi, E., Ogata, H., Tanabeke, Y. and Oki, S., 1957, *Phys. Rev.*, **106**, 155.
- Kumabe, I., 1958, *J. Phys. Soc. Japan*, **13**, 325.
- Lang, J. M. B. and LeCouteur, K. J., 1954, *Proc. Phys. Soc.*, **A67**, 586.
- Newton, T. D., 1956, *Can. J. Phys.*, **34**, 804.
- Nemeth, Judit, 1958, *Nuc. Phys.*, **6**, 686.
- Nemeth, Judit, 1960, *Nuc. Phys.*, **16**, 331.
- Mani, G. S. and Nair, K. G., 1960, *Ind. Acad. Sci.*, **51**, 243.
- Mattauch, J. and Everling, F., 1957, *Prog. Nucl. Phys.*, **6**, 233.
- Moore, Jr. R. G., 1960, *Rev. Mod. Phys.*, **32**, 101.
- Paul, E. B. and Clarke, R. L., 1953, *Can. J. Phys.*, **31**, 267.
- Stelson, P. H., and Goodman, C., 1951, *Phys. Rev.*, **83**, 69.

POTENTIAL ENERGY CURVES AND DISSOCIATION ENERGY OF THE PO MOLECULE

C. V. V. S. N. K. SANTHARAM AND P. TIRUVENGANNA RAO

SPECTROSCOPIC LABORATORIES, DEPARTMENT OF PHYSICS, ANDHRA UNIVERSITY
WALTAIR

(Received March 6, 1962)

ABSTRACT. From the observed head-head separations of the $C'-X^2\Pi$ system of PO reported by the authors (1962), approximate values of B_0' and τ_0' of the C' state have been estimated. Potential energy curves have been drawn for the X , B and C' levels of PO . Probable dissociation products of these states have been discussed. The dissociation energy of PO molecule is estimated as 6.8 e.v.

A study of the spectrum of the PO molecule by the authors (1962) excited in a high frequency discharge has led to the analysis and identification of two new doublet systems of bands in the ultraviolet region designated as $C'-X^2\Pi$ and $B'-X^2\Pi$. The bands of the $C'-X$ system were observed to be double double-headed and were accordingly ascribed to the transition $^2\Sigma$ (or $^2\Delta$)— $^2\Pi$. Neglecting what are likely to be small effects arising from Λ -type doubling, spin splitting and the influence of D terms, approximate B values for the vibrational levels of the upper C' state can be obtained from head-head separations. Treatment of the branch formulae gives

$$(R_{21})_{head} - (R_1)_{head} = \frac{2B'_1 B_1''}{B_1'' - B'_1}$$

$$(R_2)_{head} - (Q_2)_{head} = \frac{2B'_2 B_2''}{B_2'' - B'_2} \quad \dots \quad (1)$$

where B_1'' and B_2'' are the effective B -values for the $^2\Pi_{1/2}$ and $^2\Pi_{3/2}$ sub-levels, and

$$B_1'' = B_0''(1 - B_0''/A), \quad B_2'' = B_0''(1 + B_0''/A) \quad \dots \quad (2)$$

and B_0'' is the true value. Using the true B_0'' values of the ground state $X^2\Pi$ and A the coupling constant obtained by Suryanarayana Rao (1958) from the rotational analysis of the γ system, the effective B_1'' and B_2'' values are calculated according to relations (2). The head-head separations in the intense (0, 1), (0, 2), (0, 3), (0, 4) sub-bands and the derived values of B_0' according to relation (1) are shown in Table I.

TABLE I

The head-head separations in the (0, 1), (0, 2), (0, 3), (0, 4) sub-bands and the derived values of B'_0

v', v''	$R_2 - Q_2$	B'_0	$R_{21} - R_1$	B'_0
0, 1	10.4	0.638	11.9	0.644
0, 2	11.2	0.639	10.8	0.633
0, 3	12.7	0.643	13.4	0.643
0, 4	13.3	0.642	13.3	0.638

From these an approximate value of B'_0 was estimated as 0.64 cm^{-1} . The value of r'_0 was then obtained as 1.58 \AA from the relation $r_0 = \frac{4.1061}{\sqrt{\mu_A B_0}} \times 10^{-8}$ (Herzberg page 180).

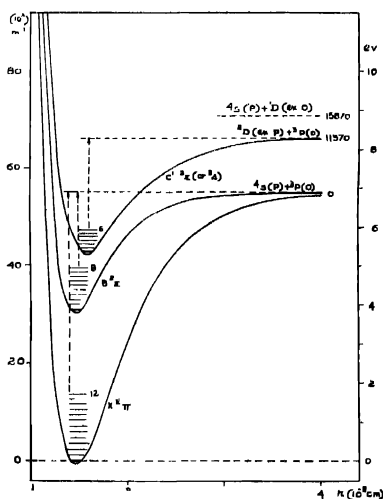


Fig. 1. Potential curves of the X , B and C' electronic states of the PO molecule.

Using the vibrational and rotational constants of the X , B and C' states, potential energy curves have been drawn adopting the Morse relation $U(r) = E_0 + D_0(1 - e^{-\beta(r-r_0)})^2$. These curves for the $X \ ^2\Pi$ ground state and the excited $B \ ^2\Sigma$ (the upper state of the β system) and $C' \ ^2\Sigma$ (or $^2\Delta$) states are shown in Fig. 1. For the C' state the value of r_0 ($\sim r_e$) is used in drawing the potential energy curve. The probable dissociation products are given on the right in Fig. 1.

A linear extrapolation of the vibrational levels of the ground state X gives a value 57000 cm^{-1} (7.1 e.v.) for the dissociation energy of the PO molecule. The vibrational analysis of the β system by K. Dressler (1955) shows that the vibrational levels of the B state converge very rapidly and therefore allow a reliable estimation of this dissociation energy. The linear extrapolation of the vibrational energy levels of the B state gives $D'_0 = 24000 \text{ cm}^{-1}$. Thus the convergence limit of the bands of the $B-X$ system is $30806 \pm 24000 = 54806 \text{ cm}^{-1}$ or approximately 55000 cm^{-1} , above the $v'' = 0$ of $X^2\Pi_1$ level.

A similar extrapolation of the vibrational levels of the C' excited state, whose spacings decrease uniformly, gives a value for D'_0 equal to $25,200 \text{ cm}^{-1}$. The convergence limit of the bands of the $C'-X$ system is $43650 \pm 25200 = 68850 \text{ cm}^{-1}$, above the $v'' = 0$ of $X^2\Pi_1$ level.

We may now discuss the probable dissociation products of the X , B , and C' states. The P atom has three low lying states 4S ground state and the two 2D , 2P metastable states. The oxygen atom has three low lying states. The 3P ground state and the metastable 1D and 1S states. The X ground state may be expected to dissociate into two normal atoms $^4S(P) + ^3P(O)$. This lowest combination ($^1S_u + ^3P_g$), according to Wigner and Witmer's rules, gives rise to one Σ^+ and one Π state with each of the multiplicities 2 and 4. The $^2\Pi$ state belonging to this combination can be correlated unambiguously with the observed $X^2\Pi$ ground state of PO . Assuming the validity of noncrossing rule, the $^2\Sigma$ state can be correlated with the observed first excited $B^2\Sigma$ state which has been established by Nandalal Singh (1959) from a detailed rotational analysis. Thus both the B and X states dissociate into two normal atoms. The second excited $A^2\Sigma^+$ state of PO may be assumed to dissociate into an excited P atom in a $4s$ orbit and unexcited $^3P(O)$ similar to the upper state of the γ system of NO .

From the observed convergence limit of 55000 cm^{-1} of the vibrational levels of the B state, we may therefore estimate the dissociation energy of the PO molecule as 55000 cm^{-1} (6.8 e.v.) which may be higher than the true value by an amount of about 0.1 e.v. The linear extrapolated value of the ground state vibrational energy levels is 57000 cm^{-1} . The fact that this is 5 per cent higher than the above value can reasonably be attributed to the uncertainty in the extrapolated value of the ground state.

The convergence limit of the C' state was obtained as 68850 cm^{-1} . The difference between the convergence limits of C' and B states is equal to 14000 cm^{-1} . This corresponds either to the excitation energy 11370 cm^{-1} of 2D state over the 4S state of the P atom or the excitation energy $15,870 \text{ cm}^{-1}$ of 1D above the 3P ground state of O atom. Thus the C' state may dissociate into either 2D (excited P) + 3P (unexcited O) or 4S (unexcited P) + 1D (excited O). As the linear extrapolated value D'_0 of the C' state will in general be higher than the true value, the true convergence limit of the C' state would be less than 68850 . So the difference

between the convergence limits of the C' and B states is expected to be less than 14000 cm^{-1} . Hence the C' state may not possibly dissociate into 4S (unexcited P) + 1D (excited 0). Further the C' state which should arise from a $^2\Sigma$ or $^2\Delta$ term cannot result from this combination. It may be reasonable to conclude that the C' state dissociates into a 2D (excited P) + 3P (unexcited 0). This combination gives rise to $\Sigma^+(2)$, Σ^- , $\Pi(3)$, $\Delta(2)$ and ϕ states with each of multiplicities 2 and 4. The C' state may therefore be identified as a $^2\Sigma$ (or $^2\Delta$) state of this combination. The difference between 14000 cm^{-1} and 11370 cm^{-1} can reasonably be attributed to the uncertainty in the linear extrapolated value of D'_0 of the C' state.

ACKNOWLEDGMENT

The authors wish to express their thanks to Prof. K. R. Rao for his kind interest in this work. One of the authors (C. V. V. S. N. K. Santharam) is grateful to the C.S.I.R. (Delhi) for the award of a Research Fellowship.

REFERENCES

- Dressler, K., 1955, *Helv. Phys. Acta*, **28**, 563-690.
 Nandalal Singh, 1959, *Can. Jour. Phys.*, **57**, 136.
 Santharam, C. V. V. S. N. K. and Rao, P. T., 1962, *Z. Physik* **168**, 553.
 Suryanarayana Rao, K., 1958, *Can. J. Phys.*, **36**, 1526.

ONE OPERATIONAL AMPLIFIER SIMULATES THIRD ORDER SYSTEMS WITH A LEADING-TIME CONSTANT

L. K. WADHWA AND JAGDISH CHANDRA

DEFENCE RESEARCH AND DEVELOPMENT LABORATORY, DELHI-6

(Received April 5, 1962)

ABSTRACT. The paper outlines a method for the simulation of third order linear systems with only one operational amplifier.

A particular class of the general third order systems, that is, systems with a leading time constant is considered in this paper.

Two basic circuits each consisting of one operational amplifier, four capacitors and five resistors are presented. The circuits are analysed and the conditions of physical realisability discussed and obtained.

The design formulae and procedure are also given.

INTRODUCTION

In previous communications (Wadhwa, 1961, 1962) on this subject three particular classes of the general third order linear systems were considered for simulation with only one operational amplifier. The purpose of this paper is to consider another particular class of systems, that is, third order systems with a leading time-constant, which are characterised by a transfer function of the form

$$F(S) = - \frac{b_0(b_1S+1)}{a_3S^3+a_2S^2+a_1S+1} \quad (1)$$

where a 's and b 's are positive and real constants, and S is the Laplace operator.

In principle, it should be possible to simulate the system of (1) with the aid of three capacitors and six resistors but the resulting network design formulae and the conditions of physical realisability become somewhat complicated. With the employment of four capacitors and five resistors, however, the design formulae and the conditions of physical realisability become simple and conveniently computable. It is primarily with a view to ensuring simplicity and convenience that in the networks presented in this paper four capacitors and five resistors have been used.

Of the various possible circuit each employing four capacitors and five resistors only two will be presented here; their design formulae obtained and conditions of physical realisability discussed.

Third order system simulation

A network for the simulation of third order systems is shown in Fig. 1 and its transfer function has been shown to be

$$\frac{E_0}{E_1} = - \frac{Y_1 Y_3 Y_6}{Y_6(Y_1 + Y_2 + Y_6)(Y_3 + Y_4 + Y_5 + Y_7) + Y_3 Y_6(Y_4 + Y_5 + Y_7) + Y_5 Y_7(Y_1 + Y_2 + Y_3 + Y_4) + Y_3 Y_6 Y_8} \quad \dots (2)$$

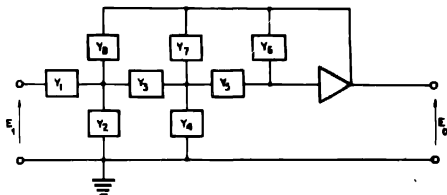


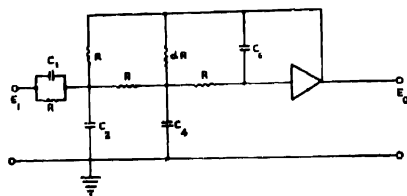
Fig. 1 Network for the simulation of third systems.

Simulation of the system of (1) with the network of Fig. 1 is possible if the admittances (Y 's) are properly chosen, and furthermore it should be obvious from (2) that at least three of the appropriate admittances will be required to be purely capacitive. As already mentioned the use of three capacitors gives inconveniently long design formulae and conditions of physical realizability while the use of four capacitors makes these simple and easily computable.

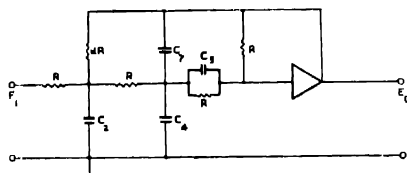
(a) Y_1, Y_2, Y_4 and Y_6 capacitive

A possible circuit for simulating the system of (1) is shown in Fig. (2a), in which

$$\left. \begin{aligned} Y_1 &= \left(SC_1 + \frac{1}{R} \right) \\ Y_2 &= SC_2 \\ Y_4 &= SC_4 \\ Y_6 &= SC_6 \\ Y_3 = Y_5 = Y_8 &= \frac{1}{R} \\ Y_7 &= \frac{1}{\alpha R} \end{aligned} \right\} \quad \dots (3)$$



(a)



(b)

Fig. 2. Network for the simulation of

$$\frac{E_0}{E_1} = - \frac{b_0(b_1 S + 1)}{a_2 S^2 + a_1 S + 1}$$

Substituting (3) into (2) and simplifying

$$\begin{aligned} \frac{E_0}{E_1} = & - \left(\frac{\alpha}{\alpha+3} \right) (RC_1 S + 1) \frac{\left(\frac{\alpha}{\alpha+3} \right) R^3 (C_1 + C_2) C_4 C_6 S^3 + R^2 C_6 \left[\frac{2\alpha+1}{\alpha+3} (C_1 + C_2) + \left(\frac{3\alpha}{\alpha+3} \right) C_4 \right] S^2}{\left(\frac{\alpha}{\alpha+3} \right) R (C_1 + C_2) + \left(\frac{5\alpha+3}{\alpha+3} \right) RC_6} S + 1 \end{aligned} \quad \dots (4)$$

Equations (1) and (4) will be identical if

$$b_0 = \left(\frac{\alpha}{\alpha+3} \right) \quad \dots (5)$$

$$b_1 = T_1 \quad \dots (6)$$

$$a_1 = \left(\frac{\alpha}{\alpha+3} \right) (T_1 + T_2) + \left(\frac{5\alpha+3}{\alpha+3} \right) T_1 \quad \dots (7)$$

$$a_2 = T_6 \left[\left(\frac{2\alpha + 1}{\alpha + 3} \right) (T_1 + T_2) + \left(\frac{3\alpha}{\alpha + 3} \right) \right] T_4 \quad \dots (8)$$

$$a_3 = \left(\frac{\alpha}{\alpha + 3} \right) (T_1 + T_2) T_4 T_6 \quad \dots (9)$$

where

$$T_n = RC_n \quad \dots (10)$$

Now, simulation of the system of (1) with the network of Fig. 2(a) is possible only if the values of α , T_1 , T_2 , T_4 , T_6 obtained as the solution of (5) through (9) are real and positive. It is required to determine, therefore, in terms of the given real and positive a 's and b 's, the values of α , T_1 , T_2 , T_4 , T_6 and find the conditions, if any, under which these can be real and positive.

Elimination of α , T_1 , T_2 , and T_6 from (5) through (9) gives a cubic

$$27b_0^3(a_1a_2 - 3a_3b_0)T_4^3 - 9b_0^2\{a_1a_3(5b_0 + 1) + a_2^2(4b_0 + 1)\}T_4^2 + 6a_2a_3b_0(4b_0 + 1)(5b_0 + 1)T_4 - a_3^2(4b_0 + 1)(5b_0 + 1)^2 = 0 \quad \dots (11)$$

which can have either one or three real roots depending on whether its discriminant is positive or negative.

Now, as shown in Appendix I, a set of real and positive α , T_1 , T_2 , T_4 , T_6 exists, provided that

$$b_0 < 1 \quad \dots (12)$$

and, either

$$\left. \begin{aligned} a_3 &> \frac{a_2b_1}{3} \\ a_1 &> \frac{3a_3b_0}{a_2} \end{aligned} \right\} \quad \dots (13)$$

$$\text{or} \quad \left. \begin{aligned} a_3 &< \frac{a_2b_1}{3} \\ a_1 &> \frac{3(4b_0 + 1)(a_2b_1 - 3a_3) + b_0b_1}{b_1^2(5b_0 + 1)} + b_0b_1 \end{aligned} \right\} \quad \dots (13a)$$

For the design of the network, circuit component values are required to be determined. The proper procedure for design would be to first check and see if the inequalities of (12) and either (13) or (13a) are satisfied. The satisfaction of these conditions signifies that the circuit of Fig. 2(a) for simulation of the system

of (1) is physically realisable. The circuit component values may then be obtained by solving the cubic of (11) for T_4 . Since α and T_1 are known directly from (5) and (6) respectively, then T_2 and T_6 may be obtained by solving (7) and (8). Having thus determined α , T_1 , T_2 , T_4 , T_6 , and choosing arbitrarily a convenient value for any one of the capacitors, the value of resistors and the remaining capacitors may be then determined with the aid of (10).

(b) Y_2 , Y_4 , Y_5 , and Y_7 capacitive

Another possible circuit for the simulation of the system of (1) is shown in Fig. 2(b), where

$$\left. \begin{aligned} Y_2 &= SC_2 \\ Y_4 &= SC_4 \\ Y_6 &= (SC_6 + 1/R) \\ Y_7 &= SC_7 \\ Y_1 &= Y_3 = Y_5 = 1/R \\ Y_8 &= 1/\alpha R \end{aligned} \right\} \dots (14)$$

Substituting (14) into (2) and simplifying

$$\begin{aligned} \frac{E_0}{E_1} = & \frac{\frac{\alpha}{3(\alpha+1)} \cdot (RC_6S+1)}{\frac{\alpha}{3(\alpha+1)} R^2(C_2C_5C_7S^3 + \left[\frac{\alpha}{3(\alpha+1)} R^2(C_4+C_6)C_2 + \frac{2\alpha}{3(\alpha+1)} R^2C_2C_7 \right.} \\ & + \frac{(2\alpha+1)}{3(\alpha+1)} R^2C_6C_7 \left. \right] S^2 + \left[\frac{2\alpha}{3(\alpha+1)} RC_2 + \frac{(2\alpha+1)}{3(\alpha+1)} RC_4 + \frac{2}{3} RC_6 \right.} \\ & \left. \left. + \frac{2(2\alpha+1)}{3(\alpha+1)} RC_7 \right] S + 1} \dots (15) \end{aligned}$$

Equations (1) and (15) will be identical if

$$b_0 = \frac{\alpha}{3(\alpha+1)} \dots (16)$$

$$b_1 = T_6 \dots (17)$$

$$a_1 = \frac{2\alpha}{3(\alpha+1)} T_2 + \frac{(2\alpha+1)}{3(\alpha+1)} T_4 + \frac{2}{3} T_6 + \frac{2(2\alpha+1)}{3(\alpha+1)} T_7 \dots (18)$$

$$a_2 = \frac{\alpha}{3(\alpha+1)} (T_4 + T_6) T_2 + \frac{2\alpha}{3(\alpha+1)} T_2 T_7 + \frac{(2\alpha+1)}{3(\alpha+1)} T_6 T_7 \quad \dots \quad (19)$$

$$a_3 = \frac{\alpha}{3(\alpha+1)} T_2 T_6 T_7 \quad \dots \quad (20)$$

where

$$T_n = RC_n \quad \dots \quad (21)$$

Elimination of α , T_4 , T_6 and T_7 from (16) through (20) gives a cubic

$$T_2^3 - \frac{1}{6b_0} [3a_1 + b_1(3b_0 - 1)] T_2^2 + \frac{a_2(3b_0 + 1)}{6b_0^2} T_2 - \frac{a_3(3b_0 + 1)^2}{18b_0^3} = 0 \quad \dots \quad (22)$$

which, as is obvious, can have no negative real roots and will have either one or three real positive roots depending on whether its discriminant Δ is positive or negative.

Now, as shown in Appendix II, if

$$b_0 < \text{Min} \left[\frac{1}{3}, \left\{ \frac{b_1}{144a_3} (3a_1 - 2b_1)^2 - \frac{1}{3} \right\}, \left\{ \frac{(a_2b_1 - 2a_3)^2}{4a_3b_1^3} - \frac{1}{3} \right\} \right] \quad \dots \quad (23)$$

$$(3a_1 - 2b_1) > 0$$

$$(a_2b_1 - 2a_3) > 0$$

then one set of positive real α , T_2 , T_4 , T_6 and T_7 exists, provided that either

$$\left. \begin{aligned} \Delta &= 4p^3 + 27q^2 > 0 \\ \text{and} \quad OQ &> OB > OP > OA \end{aligned} \right\} \quad \dots \quad (24)$$

$$\text{or} \quad \left. \begin{aligned} \Delta &< 0 \\ \text{and} \quad OB &> OQ > OA > OP \end{aligned} \right\} \quad \dots \quad (24a)$$

But, if (23) is satisfied and

$$\Delta < 0$$

$$\text{and either} \quad OB > OQ > OP > OA \quad \left\{ \quad \dots \quad (25) \right.$$

$$\text{or} \quad OQ > OB > OA > OP$$

then two sets of positive real values exist. And three sets of positive real values can exist if

$$\left. \begin{aligned} \Delta &< 0 \\ \text{and} \quad OQ &> OB > OP > OA \end{aligned} \right\} \quad \dots \quad (26)$$

where

$$\begin{aligned}
 OA &= \frac{b_1(3a_1 - 2b_1) - \sqrt{b_1^2(3a_1 - 2b_1)^2 - 48a_3b_1(3b_0 + 1)}}{12b_0b_1} \\
 OB &= \frac{b_1(3a_1 - 2b_1) + \sqrt{b_1^2(3a_1 - 2b_1)^2 - 48a_3b_1(3b_0 + 1)}}{12b_0b_1} \\
 OP &= \frac{(a_2b_1 - 2a_3) - \sqrt{(a_2b_1 - 2a_3)^2 - 4a_3b_1^3(b_0 + 1)}}{2b_0b_1^2} \\
 OQ &= \frac{(a_2b_1 - 2a_3) + \sqrt{(a_2b_1 - 2a_3)^2 - 4a_3b_1^3(b_0 + 1)}}{2b_0b_1^2} \\
 p &= \frac{a_2(3b_0 + 1)}{18b_0^2} - \frac{1}{3} \left[\frac{3a_1 + b_1(3b_0 - 1)}{6b_0} \right]^2 \\
 q &= \frac{a_1(3b_0 + 1)^2}{18b_0^3} + \frac{a_2(3b_0 + 1)[3a_1 + b_1(3b_0 - 1)]}{108b_0^3} \\
 &\quad - \frac{2}{27} \left[\frac{3a_1 + b_1(3b_0 - 1)}{6b_0} \right]^3
 \end{aligned} \tag{27}$$

To summarise, therefore, if (23) and either

$$OQ > OB > OP > OA \tag{28}$$

or

$$\Delta = 4p^3 + 27q^2 < 0 \tag{29}$$

are satisfied then it is possible to simulate the system of (1) with the circuit of Fig. 2(b). The circuit component values may be obtained with the aid of (16), (17), (22), (20), (18) and (21).

ACKNOWLEDGMENT

The authors wish to thank the Director, Defence Research and Development Laboratory, for his permission to publish this paper.

REFERENCES

- Wadhwa, L. K., 1961, *Seventh Congress, Indian Society of Theoretical and Applied Mechanics*, December.
- Wadhwa, L. K., 1962 *Proc. I.R.E.* **50** No. 2, pp. 201-202; 465; 1538.
- Wadhwa, L. K., 1962, *Jour. I.T.E.* **8** No. 1, pp. 61.

APPENDIX I

CONDITIONS UNDER WHICH THE CIRCUIT OF FIGURE 2(a) IS PHYSICALLY REALISABLE

Simulation of the system represented by (1) with the network of Fig. 2(a) is possible only if the values of α , T_1 , T_2 , T_4 and T_6 obtained as the solution of equations

$$b_0 = \frac{\alpha}{\alpha+3} \quad \dots \quad (1.1)$$

$$b_1 = T_1 \quad \dots \quad (1.2)$$

$$a_1 = \left(\frac{\alpha}{\alpha+3} \right) (T_1+T_2) + \left(\frac{5\alpha+3}{\alpha+3} \right) T_6 \quad \dots \quad (1.3)$$

$$a_2 = T_6 \left[\left(\frac{2\alpha+1}{\alpha+3} \right) (T_1+T_2) + \left(\frac{3\alpha}{\alpha+3} \right) T_4 \right] \quad \dots \quad (1.4)$$

$$a_3 = \left(\frac{\alpha}{\alpha+3} \right) (T_1+T_2)T_4T_6 \quad \dots \quad (1.5)$$

are real and positive; where a 's and b 's are real and positive constants.

It is, therefore, required to determine the conditions under which α , T_1 , T_2 , T_4 , T_6 can be real and positive; and graphical methods may be perhaps a convenient means of obtaining these.

Elimination of α , T_1 and T_4 from (1.1), (1.2), (1.3), (1.5) and (1.1), (1.2), (1.4), (1.5) give the following two equations

$$b_0T_2 + (4b_0+1)T_6 = (a_1 - b_0b_1) \quad \dots \quad (1.6)$$

$$\text{and} \quad T_6 = \frac{3a_2}{(5b_0+1)(T_2+b_1)} - \frac{9a_3}{(5b_0+1)(T_2+b_1)^2} \quad \dots \quad (1.7)$$

The intersection of the straight line of (1.6) and the curve of (1.7) in the first quadrant of the T_2-T_6 plane will give both T_2 and T_6 as real and positive. It is obvious from (1.1), (1.2) and (1.6) that the corresponding α , T_1 and T_4 are also real and positive, provided that

$$b_0 < 1 \quad \dots \quad (1.8)$$

It should be clear, therefore, that only the portion of the curves lying on the right of the T_6 -axis are of interest.

The intercepts that the straight line of (1.6) makes with the T_2 and T_0 -axes respectively, are given by

$$OA = T_2'' = \left(\frac{a_1 - b_0 b_1}{b_0} \right) \quad \dots \quad (1.9)$$

$$OB = T_0'' = \left(\frac{a_1 - b_0 b_1}{4b_0 + 1} \right) \quad \dots \quad (1.10)$$

which are real and, also positive if

$$a_1 > b_0 b_1 \quad \dots \quad (1.11)$$

Similarly, the curve of (1.7) will cut the axes at points P and Q whose T_2 and T_0 coordinates are respectively given by

$$OP = T_2'' = \left(\frac{3a_3 - a_2 b_1}{a_2} \right) \quad \dots \quad (1.12)$$

$$OQ = T_0'' = \frac{3(a_2 b_1 - 3a_3)}{b_1^2(5b_0 + 1)} \quad \dots \quad (1.13)$$

Now, if

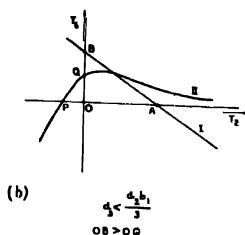
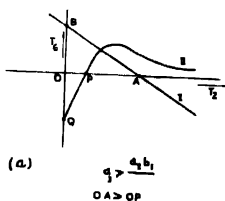
$$\left. \begin{aligned} (3a_3 - a_2 b_1) &> 0 \\ a_3 &> \frac{a_2 b_1}{3} \end{aligned} \right\} \quad \text{i.e.} \quad (1.14)$$

then the intercept OP is positive and OQ negative, but if

$$\left. \begin{aligned} (3a_3 - a_2 b_1) &< 0 \\ a_3 &< \frac{a_2 b_1}{3} \end{aligned} \right\} \quad \text{i.e.} \quad \dots \quad (1.15)$$

then the intercept OQ is positive and OP negative.

Therefore, if the conditions as expressed in (1.11) and either in (1.14) or (1.15) are satisfied then it is possible for a portion of the straight line and the curve to exist in the first quadrant and it may be possible, under certain conditions, for these to intersect each other at one or more points in that region. The sketches of the straight line of (1.6) and a portion of the curve of (1.7) lying on the right of the T_0 -axis are shown in Fig. 1.1.



$$\begin{aligned} \text{I} \quad & b_1 T_0 + (a_2 b_1 + 1) T_0 = (a_1 - b_1 b_0) \\ \text{II} \quad & T_0 = \frac{3a_1}{(5b_0 + 1)(T_0 + b_1)} - \frac{9a_2}{(5b_0 + 1)(T_0 + b_1)^2} \end{aligned}$$

Fig. 1. Condition under which the straight line and the curve can intersect each other in the first quadrant.

It is evident from the sketch of Fig. 1.1(a) that if (1.11) and (1.14) are satisfied and

$$OA > OP$$

$$\text{i.e.,} \quad a_1 > \frac{3a_2 b_0}{a_2} \quad \dots (1.16)$$

or, as seen from figure 1.1(b), if (1.11) and (1.15) are satisfied, and

$$OB > OQ$$

$$\text{i.e.,} \quad a_1 > \frac{3(4b_0 + 1)(a_2 b_1 - 3a_2)}{b_1^2(5b_0 + 1)} + b_0 b_1 \quad \dots (1.17)$$

then it is possible for the straight line and the curve to intersect each other in the first quadrant giving T_2 and T_0 as real and positive.

To summarise, therefore, if

$$b_0 < 1 \quad \dots \quad (1.8)$$

and, either

$$\left. \begin{aligned} a_3 &> \frac{a_2 b_1}{3} \\ a_1 &> \frac{3a_2 b_0}{a_2} \end{aligned} \right\} \quad \dots \quad (1.16a)$$

or

$$\left. \begin{aligned} a_3 &< \frac{a_2 b_1}{3} \\ a_1 &> \frac{3(4b_0+1)(a_2 b_1 - 3a_3)}{b_1^2(5b_0+1)} + b_0 b_1 \end{aligned} \right\} \quad \dots \quad (1.17a)$$

then the circuit of Fig. 2(a) for simulating the system of (1) is physically realisable.

APPENDIX II

CONDITIONS UNDER WHICH THE CIRCUIT OF FIG. 2(b) IS PHYSICALLY REALISABLE

If the values of α , T_2 , T_4 , T_5 and T_7 obtained as the solution of equations

$$b_0 = \frac{\alpha}{3(\alpha+1)} \quad \dots \quad (2.1)$$

$$b_1 = T_5 \quad \dots \quad (2.2)$$

$$a_1 = \frac{2\alpha}{3(\alpha+1)} T_2 + \frac{(2\alpha+1)}{3(\alpha+1)} + \frac{2}{3} T_5 + \frac{2(2\alpha+1)}{3(\alpha+1)} T_7 \quad \dots \quad (2.3)$$

$$a_2 = \frac{\alpha}{3(\alpha+1)} T_2(T_4+T_5) + \frac{2\alpha}{3(\alpha+1)} T_2 T_7 + \frac{(2\alpha+1)}{3(\alpha+1)} \cdot T_5 T_7 \quad \dots \quad (2.4)$$

$$a_3 = \frac{\alpha}{3(\alpha+1)} T_2 T_5 T_7 \quad \dots \quad (2.5)$$

are real and positive, then it is possible to simulate the system of (1) with the circuit of Fig. 2(b).

Elimination of α , T_5 and T_7 from (2.1), (2.2), (2.3), (2.5) and (2.1), (2.2), (2.4), (2.5) give the following two equations:

$$T_4 = \frac{(3a_1 - 2b_1)}{(3b_0 + 1)} - \frac{2a_3}{b_0 b_1 T_2} - \frac{6b_0}{(3b_0 + 1)} T_2 \quad \dots (2.6)$$

$$T_4 = \frac{(a_2 b_1 - 2a_3)}{b_0 b_1 T_2} - \frac{a_3(3b_0 + 1)}{3b_0^2 T_2^2} - b_1 \quad \dots (2.7)$$

The intersection of the curves of (2.6) and (2.7) in the first quadrant of the T_2 - T_4 plane will give both T_2 and T_4 as real and positive. It is evident from (2.1), (2.2) and (2.5) that the corresponding α , T_5 and T_7 will be also real and positive, provided that

$$b_0 < 1/3 \quad \dots (2.8)$$

The curve of (2.6) will cut the T_2 -axis (i.e. $T_4 = 0$) at two points A and B whose T_2 coordinates may be obtained by equating to zero the right hand side of (2.6) and solving the resulting quadratic

$$6b_0^2 b_1 T_2^2 - b_0 b_1 (3a_1 - 2b_1) T_2 + 2a_3(3b_0 + 1) = 0 \quad \dots (2.9)$$

whose roots are given by

$$T_{2(A, B)} = \frac{b_1(3a_1 - 2b_1) \pm \sqrt{b_1^2(3a_1 - 2b_1)^2 - 48a_3 b_1(3b_0 + 1)}}{12b_0 b_1} \quad \dots (2.10)$$

Now, A and B will be real, if

$$b_1(3a_1 - 2b_1)^2 > 48a_3(3b_0 + 1)$$

$$\text{i.e.} \quad b_0 < \frac{b_1}{144a_3} - \frac{(3a_1 - 2b_1)^2}{3} \quad \dots (2.11)$$

and their coordinates will be positive, if

$$(3a_1 - 2b_1) > 0 \quad \dots (2.12)$$

Similarly, (2.7) will cut the T_2 -axis at two points P and Q whose T_2 -coordinates are

$$T_{2(P, Q)} = \frac{(a_2 b_1 - 2a_3) \pm \sqrt{(a_2 b_1 - 2a_3)^2 - 4a_3 b_1^3(b_0 + 1/3)}}{2b_0 b_1^2} \quad \dots (2.13)$$

and which will be real and positive, if

$$\left. \begin{aligned} & (a_2 b_1 - 2a_3)^2 > 4a_3 b_1^3(b_0 + 1/3) \\ \text{i.e.} \quad & b_0 < \frac{(a_2 b_1 - 2a_3)^2}{4a_3 b_1^3} - \frac{1}{3} \end{aligned} \right\} \quad \dots (2.14)$$

and $(a_2 b_1 - 2a_3) > 0$

Therefore, if the conditions as expressed in (2.11), (2.12) and (2.14) are satisfied then it is possible for a portion of the curves of (2.6) and (2.7) to exist in the

first quadrant, and it may be possible, under certain conditions, for these to intersect each other at one or more points in that region.

Elimination of T_4 from (2.6) and (2.7) gives a cubic

$$T_2^3 - \frac{1}{6b_0} \{3a_1 + b_1(3b_0 + 1)\} T_2^2 + \frac{a_2(3b_0 + 1)}{6b_0^2} T_2 - \frac{a_3(3b_0 + 1)^2}{18b_0^3} = 0 \quad \dots (2.15)$$

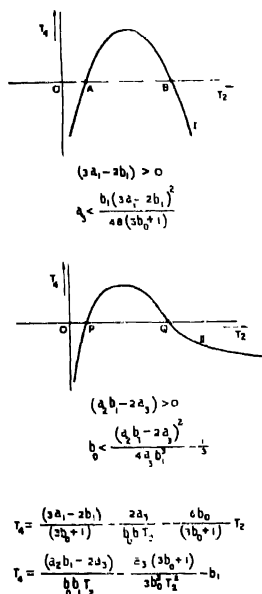


Fig. 2.1. Sketches of the curves for positive values of T_2 .

The real roots of (2.15) give the real points of intersection of the curves of (2.6) and (2.7). It is obvious, in view of (2.12), that (2.15) can have no negative real roots, therefore, the curves do not intersect at real points on the left of the T_4 -axis. If its discriminant Δ is positive then (2.15) will have one real root signifying that the curves intersect each other at one point on the right of T_4 -axis; and if Δ is negative then the curves can intersect each other at three points on the right of T_4 -axis. The sketches of portions of the curves lying on the right of the T_4 -axis are shown in Fig. 2.1.

Now, as evident from figure 2.1, if the points A and B interlace with the points P and Q , such that

$$OQ > OB > OP > OA \quad \dots (2.16)$$

then the curves will intersect each other at one point in the first quadrant if

$$\Delta = 4p^3 + 27q^2 > 0$$

and at three points if

$$\Delta < 0$$

Hence, at least one set of positive real α , T_2 , T_1 , T_5 , T_7 exist if (2.16) is satisfied, irrespective of whether Δ is positive or negative.

But if

$$\left. \begin{array}{l} \Delta < 0 \\ OB > OQ > OA > OP \end{array} \right\} \quad \dots \quad (2.17)$$

then one set of real positive values exists, and two real positive sets of values exist if

$$\left. \begin{array}{l} \Delta < 0 \\ OB > OQ > OP > OA \\ or \\ OQ > OB > OA > OP \end{array} \right\} \quad \dots \quad (2.18)$$

where

$$\left. \begin{array}{l} OA = \frac{b_1(3a_1 - 2b_1) - \sqrt{b_1^2(3a_1 - 2b_1)^2 - 48a_3b_1(3b_0 + 1)}}{12b_0b_1} \\ OB = \frac{b_1(3a_1 - 2b_1) + \sqrt{b_1^2(3a_1 - 2b_1)^2 - 48a_3b_1(3b_0 + 1)}}{12b_0b_1} \\ OP = \frac{(a_2b_1 - 2a_3) - \sqrt{(a_2b_1 - 2a_3)^2 - 4a_3b_1^3(b_0 + 1/3)}}{2b_0b_1^2} \\ OQ = \frac{(a_2b_1 - 2a_3) + \sqrt{(a_2b_1 - 2a_3)^2 - 4a_3b_1^3(b_0 + 1/3)}}{2b_0b_1^2} \\ p = \frac{a_2(3b_0 + 1)}{6b_0^2} - \frac{1}{3} \left[\frac{3a_1 + b_1(3b_0 - 1)}{6b_0} \right]^2 \\ q = \frac{-a_3(3b_0 + 1)^2}{18b_0^3} + \frac{a_3(3b_0 + 1)[3a_1 + b_1(3b_0 - 1)]}{108b_0^3} \\ \quad - \frac{2}{27} \left[\frac{3a_1 + b_1(3b_0 - 1)}{6b_0} \right]^3 \end{array} \right\} \quad \dots \quad (2.19)$$

To summarise, therefore, if

$$b_0 < \text{Min} \left[\frac{1}{3}, \left\{ \frac{b_1}{144a_1} (3a_1 - 2b_1)^2 - \frac{1}{3} \right\}, \left\{ \frac{(a_2b_1 - 2a_3)^2}{4a_3b_1^3} - \frac{1}{3} \right\} \right] \quad \dots (2.20)$$

$$(3a_1 - 2b_1) > 0$$

$$(a_2b_1 - 2a_3) > 0$$

$$\text{and either} \quad OQ > OB > OP > OA \quad \dots (2.16)'$$

$$\text{or} \quad \Delta = 4p^3 + 27q^2 < 0 \quad \dots (2.21)$$

then it is possible to simulate the system of (1) with the circuit of Fig. 2(b).

MEASUREMENT OF DIELECTRIC PROPERTIES OF METAL SULPHIDES

M. N. SHARMA AND S. S. GUPTA

DEPARTMENT OF PHYSICS, LUCKNOW UNIVERSITY, LUCKNOW

(Received June 1, 1962).

ABSTRACT Dielectric constants of some bivalent metal sulphides have been determined at radio frequency (7.25 Mc/s) using the method of mixtures. For ZnS, the force constant, K , has been evaluated and it compares well with other determinations. Compressibility, reststrahlen frequency, cohesive energy, ionic polarisation and Szeglet's short range correction factor 's', are subsequently calculated. The results are in good agreement with experimental values.

INTRODUCTION

Wiener (1910) has developed a formula taking into account the geometrical shape of the particles and their influence on the distribution of electric field, as the dielectric constant of crystalline powders depends also on the size and shape of the particles. Fricke (1924) has modified Wiener's formula and this modified formula has been used by us.

Compressibility and reststrahlen frequency of an ionic crystal are related to the dielectric constant and therefore they can be evaluated theoretically. Further, the force constant can also be evaluated with its help and if the law of interaction is known, interaction energy can also be computed. Dielectric constant data obtained experimentally for ZnS only has been treated for these properties, as the compressibilities and reststrahlen frequencies of other sulphides i.e. CaS, SrS and BaS are not known.

THEORY

Wiener's (1910) formula improved by Fricke (1924) for the case of spheroids immersed in a liquid medium, latter being continuous and homogeneous, is given as;

$$\frac{\epsilon_m - \epsilon_2}{\epsilon_m + u\epsilon_2} = v_1 \frac{\epsilon_1 - \epsilon_2}{\epsilon_1 + u\epsilon_2} \quad \dots (1)$$

where ϵ_m , ϵ_1 and ϵ_2 are the dielectric constants of the mixture and of the individual components, u is a factor depending on ϵ_1 , ϵ_2 and the geometry of the particles, v_1 is the volume ratio of the components to that of the whole mixture.

Since at radio frequencies ϵ_1 and ϵ_2 are complex quantities, u is also complex, u being unknown, it is difficult to solve equation (1), for ϵ_1 . Burton and Turnbull's

method for solving equation (1) for ϵ_1 has been used earlier by Pradhan and Gupta (1959), and Sharma, *et al.* (1962). We have also used Burton and Turnbolls' method. This affords a simple and adequate approach for determining the dielectric constants of crystalline solids using the method of mixtures.

EXPERIMENTAL PROCEDURE

The mixtures of different sulphides were formed into experimental pastes in the following way :

The crystalline sulphides were powdered in a mortar and filtered through a fine mesh (1000 B.S.) This supplies almost similar sized particles which is our main requirement. The binding medium was taken to be liquid paraffin, which has $\epsilon = 2.202$ and negligible dielectric loss. After efficient stirring homogeneous pastes having different known percentages of constituent sulphides were formed.

The dielectric constants of these pastes were determined by Hartshorn's method for the measurement of permittivity and power factor of dielectrics at radio frequencies, the method has been discussed in detail by Sharma (1960). Dielectric constants of mixtures thus measured are given in Table I.

The dielectric constants of metal sulphides were evaluated by the method described in preceding section, and are given in Table III, the constants used for obtaining these dielectric constants are given in Table II.

TABLE I
Dielectric constants of mixtures

BaS		SrS		ZnS		CaS	
Conc. of salt %	ϵ_m	Conc. of salt %	ϵ_m	Conc. of salt %	ϵ_m	Conc. of salt %	ϵ_m
10.010	2.843	10.100	2.652	10.090	2.539	9.963	2.492
20.520	3.571	19.930	3.057	14.730	2.752	19.130	2.757
29.060	4.103	29.060	3.580	20.070	2.938	27.740	3.021
39.900	4.963	39.090	4.190	24.650	3.067	40.060	3.211
50.350	5.665	—	—	—	—	50.630	3.807

TABLE II
Values of 'u' and 'x' for metal sulphides

Crystal	BaS	SrS	ZnS	CaS
u	2.475	1.875	1.050	1.600
x	0.690	0.590	0.530	0.440

CORRELATION OF DIELECTRIC CONSTANT
WITH OTHER PROPERTIES

The dielectric properties of ionic crystals are connected with the compressibilities, reststrahlen frequencies and interaction energies.

The potential energy $E(r)$ of the crystal per pair of ions can be written as :

$$E(r) = - \frac{\alpha e^2 Z^2}{r} + \phi(r) \quad \dots (2)$$

where, α , is the Madelung constant r is the inter-ionic distance and Z is the ionic valency of the crystal. $\phi(r)$ contains all the rest of the energy which is not contained in the electrostatic term. Various forms of $\phi(r)$ have been suggested but we have taken the simplest form of $\phi(r)$ i.e.

$$\phi(r) = \frac{B}{r^n} \quad \dots (3)$$

where B is a repulsive force parameter and n is a Born constant. Eq.(3) does not take into account the van der Waals forces as the required data of these force parameters are not known. Hence equation (2) takes the form

$$E(r) = - \frac{\alpha e^2 Z^2}{r} + \frac{B}{r^n} \quad \dots (4)$$

The force constants a_1 , used by Krishnan and Roy (1951) and K used by Born and Huang (1954) are given by

$$K = 2a_1 \quad \dots (5)$$

where

$$K = \frac{1}{3} \left[\frac{2\phi'(r)}{r} + \phi''(r) \right] \quad \dots (6)$$

in which $\phi'(r)$ and $\phi''(r)$ are the first and second derivative of the overlap potential between a positive and negative ion.

If we consider a uniformly polarized sphere in the absence of an external electric field, the only forces acting are due to $\phi(r)$ term as shown by Szigeti (1951), the Lorentz effective field F being equal to zero, and we can write a relation connecting K and β , (the compressibility) as,

$$K = \frac{3u}{\beta r^2} \quad \dots (7)$$

where u is the volume occupied by an ion pair. The force constant K , when $F = 0$, is connected with the reststrahlen frequency ω_0 as

$$K = \frac{\epsilon_0 + 2}{\epsilon_\infty + 2} m \omega_0^2 \quad \dots (8)$$

where ϵ_0 and ϵ_∞ are the static and high frequency dielectric constants and m is the reduced mass. Krishnan and Roy (1951) treat this problem in a slightly different way. As a result of lattice displacement, there is a development of a homogeneous electric polarization in the crystal and the value of the force coefficient K , instead of being only due to the $\phi(r)$ term will be less by an amount proportional to the force due to the polarization field.

From the polarization, the contribution to the force coefficient will be

$$2a_2 = -\frac{4}{3} \pi N e^2 \quad \dots (9)$$

and the total force coefficient then becomes

$$2a = 2a_1 + 2a_2 = m\omega_0^2 \quad \dots (10)$$

Therefore,

$$K = m\omega_0^2 - 2a_2 = 2a_1 \quad \dots (11)$$

Utilizing the experimentally determined values of the dielectric constant ϵ_0 , we can evaluate the value of the force coefficient K , provided we know the reststrahlen frequency ω_0 . This in turn will enable a determination of the interaction energy of the undeformed crystal as well as its compressibility. The values of β and K (from 11 and 8) are given in Tables V and VI respectively, where they have been compared with other determinations. Recently, compressibility data is available only for ZnS and hence one could also take the experimental value of β and use it to calculate K . This can then give the reststrahlen frequency using either equation (8) or (11). The value of ω_0 thus computed is given in Table VI. Using experimental ω_0 and experimental β , theoretical value of dielectric constant can also be computed for ZnS crystal this value of dielectric constant is given in Table VI, where it has been compared with experimental value.

The expression for interaction energy is given by the relation

$$U(r) = \frac{3r^2}{n(n-1)} \left[K - \frac{n(n-1)}{3r^2} \frac{\alpha e^2}{r} \right] \quad \dots (12)$$

where $n = 9$ for ZnS. The value of interaction energy using equation (12) is given in Table V.

RESULTS AND DISCUSSION

The dielectric constants of metal sulphides given in Table III show that the dielectric constant is maximum for BaS and minimum for CaS, i.e., it increases as the molecular weight of the ionic crystal decreases and vice versa. This behavior

Measurements of Dielectric Properties of Metal Sulphides 37

can be explained if we consider the ionic polarization of these crystals. The dielectric constant of a material can be attributed to polarizability and may be due to electronic, ionic or orientation factors. The electronic contribution arises from the displacement of electrons in an atom relative to the nucleus, i.e., from the deformation of the electronic shell about the nucleus. The ionic or atomic contribution is due to the displacement of a charged ion with respect to the other ions. If the substance is built up of molecules possessing permanent electric dipole moments the orientation or dipolar polarization occurs. In the case of ordinary ionic crystals there is no dipolar contribution, and ionic contribution is seldom larger than the electronic contribution.

The ionic and electronic contributions can be separated from the following relation;

$$\Delta\epsilon = (\epsilon_0 - n^2) \quad \dots \quad (13)$$

where ϵ_0 , the dielectric constant of the crystal, arises almost entirely from the electronic polarizability, n is the refractive index of crystal in the optical range (in the electrical frequency range, the dielectric constant arises from both ionic and electronic polarizabilities), and $\Delta\epsilon$ is the contribution due to ionic polarizability. The value of $\Delta\epsilon$ for ZnS is given in Table IV along with the value of n .

The magnitude of the electronic polarization is given by Szigeti (1949) as,

$$(c - n^2) = \left(\frac{n^2 + 2}{3} \right)^2 4\pi n \frac{(SZe)^2}{m\omega_i^2} \quad \dots \quad (14)$$

where c is the static dielectric constant, n the optical refractive index, ω_i the infra-red absorption frequency and m , the reduced mass of an ion pair defined by,

$$\frac{1}{m} = \frac{1}{m_1} + \frac{1}{m_2} \quad \dots \quad (15)$$

m_1 and m_2 being the masses of the two atoms. Z is the valency of the ions and e the electronic charge, S is defined by,

$$\mu_s(x) = SZex \quad \dots \quad (16)$$

where μ_s is the dipole moment per ion pair in a spontaneously polarized sphere, if x is the displacement of the two kinds of ions relative to each other. As the effective field vanishes in the Lorentz approximation, there should be no elec-

TABLE III

Dielectric constants of metal sulphides

Crystal	Structure	Present	Born and Huang (1954)
BaS	NaCl	19.230	—
SrS	NaCl	11.310	—
ZnS	Zinc-blende	8.780	8.300
CuS	NaCl	6.699	—

TABLE IV

Comparison of 'S' values for ZnS

ϵ	n^2	$\Delta\epsilon$	S Values	
			Present	Szigeti (1951)
8.78	5.07	3.71	0.516	0.480

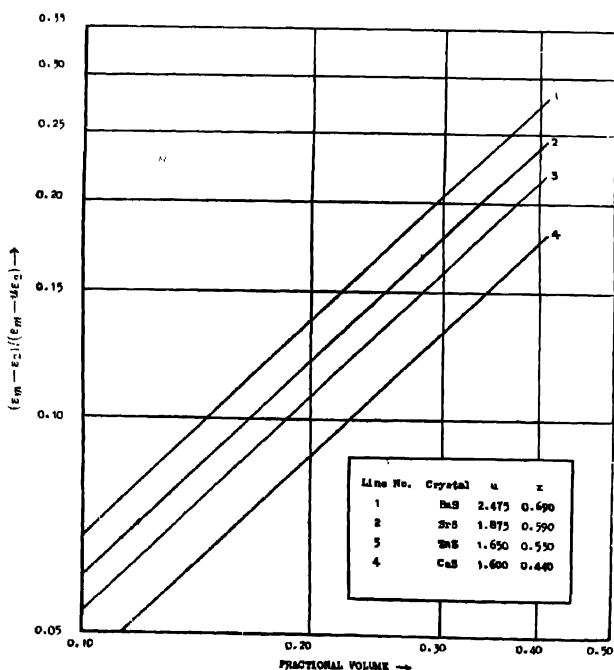


Fig. 1. Interpolation for obtaining 'X' values for different sulphides.

TABLE V
 Values of compressibility and cohesive energy for ZnS

Experimental	Compressibility ($\beta \times 10^{-12}$ cm./dyne)		Cohesive energy in K. cal. /mole			
	From equ. (11) and $\omega_{(expt.)}$	From equ. (11) and (14)	Observed	Using K from equ (8)		
				From equ (7)	K from $\beta_{(expt.)}$	K from equ. (14)
1 280	1.331	1.185	1 237	851.0	876.4	880.8
					878.8	875.6

 TABLE VI
 Values of reststrahlen frequency, force constant and dielectric constant

Reststrahlen frequency $\times 10^{-13}$		Force constant $\times 10^{-4}$				Dielectric constant	
Observed	From equ. (14) and $\epsilon_{(expt.)}$	Using $\beta_{(expt.)}$ and equ. (8)	Using $\beta_{(expt.)}$ and equ. (11)	From equ. (11)	From equ. (8)	From equ (7) and $\beta_{(expt.)}$	From equ. (14)
5.710	6.187	5.617	5.866	16.49	17.74	17.15	18.53
						Observed	Calculated
						8.78	8.42

tronic polarization in this case, and μ_e ought to be equal to zero. In other words, in Lorentz approximation S would be unity

Eq (8) holds better than equation (14), particularly for alkali halides as shown by Hardy (1960), who has given a detailed discussion of the importance of relations (8) and (14). The effect of equation (14) can be seen if one uses this relation and the experimental c_0 to calculate the compressibility which can be compared with the values given in Table V based on equation (8). The calculated value of S for ZnS employing equation (14) is given in Table IV along with Szigeti's value. A fair agreement is observed. The author's value is slightly higher than Szigeti's value showing that there is less overlap or short range interaction in the radio frequency region.

Comparison of various values in Tables V and VI shows that there is a reasonable agreement between themselves and also with the experimentally determined values.

A comparison of reststrahlen frequency indicates that the value of ω_0 calculated by using experimental β is in better agreement with the observed frequency, thus placing confidence in the experimental value of β .

Table V shows that the calculated value of β is smaller than experimental β . This is due to the fact that as a result of increasing electron sharing the distortions caused by the neighbouring ions are no longer sufficiently localised to be independent of each other.

In view of the fact that ZnS is less ionic than alkali halides studied earlier by Sharma, *et al.* (1962), much importance is to be attached to the remarkable agreement in the case of ZnS for various properties. It has been mentioned by Szigeti (1951) that the experimental data for some of the crystals, which are not alkali halides, may contain fairly large errors, and this may be the case for ZnS.

ACKNOWLEDGMENT

Authors are indebted to Prof. P. N. Sharma for guidance and encouragement. It is pleasure to acknowledge thanks to Dr. B. P. Pradhan for his valuable suggestions and discussions.

REFERENCES

- Born, M and Huang, K., 1954, "Dynamical Theory of Crystal Lattices" (Oxford at the Clarendon Press).
- Fricke, H., 1924, *Phys. Rev.*, **24**, 575.
- Gupta, R. C. and Pradhan, B. P., 1959, *Proc. Nat. Inst. Sc. India*, **25A**, 184
- Hardy, J. R., 1961, *Phil. Mag.*, **6**, 27.
- Krishnan, K. S. and Roy, S. K., 1951, *Proc. Roy. Soc. London*, **207A**.
- Pradhan, B. P. and Sharma, M. N., 1960, *Proc. Nat. Inst. Sc. India*, **26A**, 560.
- Sharma, M. N., Madan, M. P., and Pradhan, B. P. (unpublished).
- Szigeti, B., 1949, *Trans. Faraday Soc.*, **45**, 155.
- Szigeti, B., 1951, *Proc. Roy. Soc. London*, **204**, 51
- Wioner, R., 1910, *Ber. Sachs. Ges. (Akad.) Wiss.*, **62**, 256.

THE SPACE GROUPS OF CRYSTALS OF β -CHLORONAPHTHALENE AT DIFFERENT TEMPERATURES

NABA KUMAR BANERJEE AND S. C. SIRKAR

OPTICS DEPARTMENT,

INDIAN ASSOCIATION FOR THE CULTIVATION OF SCIENCE
CALCUTTA-32

(Received November 6, 1962)

Plates 1A & 1B

ABSTRACT. The Debye-Scherrer patterns of crystals of β -chloronaphthalene at 30°C and -180°C have been studied and analysed. As it was not possible to interpret the patterns satisfactorily single crystal rotation photographs about a -axis and another zone axis have been taken. The unit cell has been found to be different from that reported by Neuhaus. The dimensions of the unit cell observed are $a = 7.48$ Å, $b = 17.92$ Å, $c = 6.35$ Å and $\beta = 97^\circ 15'$, and there are 4 molecules in the unit cell. The density calculated is 1.270 which agrees with the observed value 1.266. The space group is $P2_1/m$ or $C2_2h$.

At -180°C the space group remains the same as at 30°C, but the a - and c -edges of the unit cell contract while the length along b -axis remains almost unchanged. The dimensions of the unit cell at -180°C are $a = 7.28$ Å, $b = 17.88$ Å, $c = 6.17$ Å and $\beta = 98^\circ 53'$.

INTRODUCTION

The Debye-Scherrer pattern of the crystals of β -chloronaphthalene was studied earlier by Neuhaus (1939) and he found the crystal to be monoclinic, the dimensions of the unit cell being $a = 7.65$ Å, $b = 5.93$ Å, $c = 18.4$ Å and $\beta = 103^\circ$. The density calculated on the basis of four molecules per unit cell was found to be 1.36, but the actual measurement gives the value 1.266 for the density at 16°C. Hence there seemed to be some discrepancy between these two values of the density. Also, the cell dimensions reported by Neuhaus does not account for satisfactorily all the spacings observed by him. It was, therefore, thought worthwhile to re-investigate the structure of the crystal. In this attempt, besides photographing the Debye-Scherrer patterns of the crystal at 30°C and -180°C, single crystal rotation photographs have also been taken by rotating the crystal about different axes. The results obtained in this case indicated that the cell dimensions are different from those reported by Neuhaus. These results are reported in the present paper.

EXPERIMENTAL

The compound β -chloronaphthalene was procured from an old stock supplied by Dr. Freunkel and Dr. Land of Germany. It was recrystallised from

solutions in benzene. The Debye-Scherrer patterns due to the crystals at about 30°C and also at the temperature of liquid oxygen were photographed using a camera used previously by Krishnamurti (1956). The diameter of the camera was determined by studying with it the Debye-Scherrer pattern due to aluminium powder and was found to be 8.72 cm. Although the substance is solid at the room temperature it was sealed in a Lindemann glass capillary tube to prevent rapid sublimation. A Seifert X-ray tube running at 32 K.V., 20 mA was used to photograph the patterns.

The crystals were in the form of flakes and in order to study single crystal rotation photographs such a crystal was sealed in a Lindemann glass capillary tube and the plane faces of the flake were made vertical by mounting the tube on a goniometer head. After several trials with different axes of rotation a photograph showing layer lines was obtained. The trial was continued with different axes in the plane of the large face of the flake. Altogether four photographs showing layer lines were obtained in this way.

RESULTS AND DISCUSSION

The Debye-Scherrer patterns and two of the rotation photographs are reproduced in Figs. 1, 2, and 3 and 4, Plates IA and IB. The spacings calculated from Debye-Scherrer rings are given in Tables I and II. It can be seen that a reflection corresponding to a spacing 8.96 Å occurs in the zero layer line in both the rotation photographs. As the axes of rotation lie in the plane face of the flake this spacing corresponds to that of the planes parallel to the large face of the crystal. Further, there are some reflections in Fig. 3 along two straight lines passing through the central spot and making an angle 7°15' with the zero layer line. Hence it is assumed that the *a*-axis is vertical in this case and the angle β is 97°15' and that the spacing mentioned above is due to planes normal to the *b*-axis. This spacing was taken as that due to 020 reflection. The primitive translation along *a*-axis derived from Fig. 2 is 7.48 Å. The *c*-axis could not be located and no rotation photographs about the *c*-axis could be taken. Table I, however, shows a strong reflection corresponding to a spacing 3.175 Å. Tentatively, this was assumed to be 002 reflection and the following cell dimensions were assumed for the crystal at 30°C.

$$\begin{aligned}a &= 7.48 \text{ Å} \\b &= 17.92 \text{ Å} \quad \beta = 97^\circ 15' \\c &= 6.35 \text{ Å}\end{aligned}$$

This gives four molecules per unit cell with the density 1.270, which agrees with the observed value 1.266 (Cook & Jones, 1953).

The spacings of the planes giving reflections in the rotation photographs were then determined from the position of the spots using the relation $\cos 2\theta = \cos \phi \cos \mu$, where θ is the Bragg angle, μ is the angle of elevation of the reflected

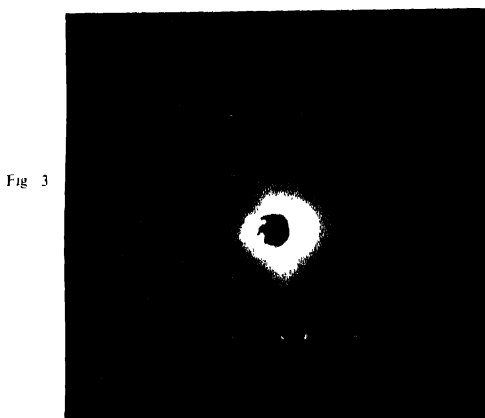


Fig 1 Debye-Scherrer pattern of β -chloronaphthalene at 30 C

Fig. 2 Debye-Scherrer pattern of β -chloronaphthalene at -180 C.

Fig 3. Single crystal rotation photograph of β -chloronaphthalene about a -axis.

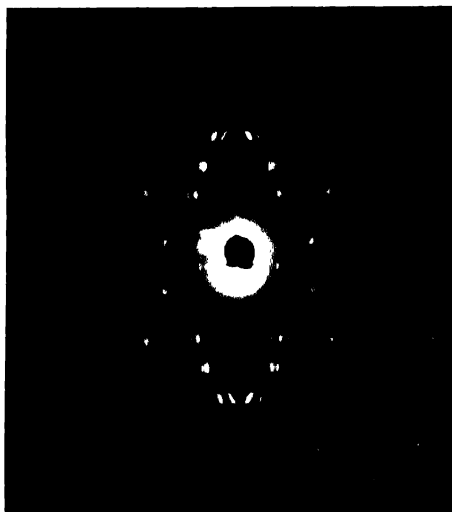


Fig. 4 Single crystal rotation photograph about a zone axis
of β -chloronaphthalene

The Space Groups of Crystals of β -Chloronaphthalene, etc. 43

ray above the equatorial plane and ϕ is the angle made by the direct ray with the projection of the reflected ray in the equatorial plane. The probable spacings of the different planes of the crystal having the cell dimensions given above were also calculated. These are given in Table III.

TABLE I
Spacings of β -chloronaphthalene at 30°C from Debye-Scherrer
photograph

Sr. No.	Visual Intensity	$\sin \theta$	Spacings observed by Neuhaus in A.U.	Observed spacings in A.U.	Calculated spacings in A.U.	Indices
1	vs	0860	8.95	8.96	8.96	020
2	vs	1664	4.63	4.63	4.65	130
3	m	1758	4.44	4.38	4.39	111
4	vs	2075	3.76	3.716	3.71	200
5	vs	2425	3.17	3.175	3.175	002
6	w	2619	2.96	2.95	2.95	151, 231
7	w	2802	2.76	2.748	2.74	112
8	w	3307	2.33	2.328	2.32	152
9	vw	3616		2.129	2.13	162
10	m	3991	1.93	1.929	1.93	103
11	m	4221	1.82	1.83	1.837	302

TABLE II
Spacings of β -chloronaphthalene at -180°C

$\sin \theta$ and Intensity	Spacings observed d in A.U.	Spacing calculated d in A.U.	Indices
.0861 vs	8.943	8.94	020
.1678 vs	4.59	4.59	130
.1824 m	4.22	4.217	111
.2139 vs	3.60	3.60	200
.2525 vs	3.049	3.049	002
.2646 w	2.91	2.919	151
.2905 w	2.65	2.64	112
.3374 w	2.288	2.289	152
.3609 vw	2.10	2.104	162
.4158 w	1.91	1.90	103

TABLE III
Spacings of β -chloronaphthalene

Sr. No.	Indices	Spacings in A.U. calculated	Spacings in A.U. observed	Figure Number in which observed
1	020	8.96	8.96	1, 3 and 4
2	130	4.65	4.63	1 and 4
3	101	4.53	4.535	3
4	040	4.48	4.47	3 and 4
5	121	4.45	4.46	4
6	111	4.30	4.38	3
7	200	3.71	3.71	1 and 3
8	220	3.428	3.42	1
9	211	3.33	3.33	3 and 4
10	002	3.175	3.175	1
11	221	3.14	3.13	3 and 4
12	201	3.07	3.08	4
13	102	3.04	3.03	4
14	231	2.95	2.95	1 and 4
	151	2.94	2.93	1
15	112	2.74	2.75	1 and 4
16	241	2.70	2.70	4
17	122	2.65	2.66	3
18	152	2.32	2.328	1 and 4
19	321	2.317	2.317	3
20	102	2.13	2.13	1
21	103	1.94	1.93	1 and 4
22	322	1.908	1.903	3
23	172	1.880	1.885	4
24	302	1.837	1.83	1
25	202	1.804	1.803	4

It can be seen from Table III that there is no restriction for the general planes of indices hkl and hol , but no reflection from planes of indices oko with odd values of k has been observed. Hence the space group is $P2_{1/m}$ or C_{2h}^2 .

The Crystal at -180°C .

It can be seen from a comparison of Tables I and II that almost all the reflections observed in the Debye-Scherrer pattern of the crystal at 30°C persist when the crystal is cooled to -180°C , but the spacings diminish a little. The primitive translation along b -axis, however, remains almost unchanged when the crystal is cooled to -180°C , although the a -axis and the c -axis contract to a large extent at the low temperature. The dimensions of the unit cell at -180°C are: $a = 7.28\text{\AA}$, $b = 17.88\text{\AA}$, $c = 6.17\text{\AA}$ and $\beta = 98^\circ 53'$.

ACKNOWLEDGMENT

The work was carried out under a scheme sanctioned by the Council of Scientific and Industrial Research and the authors' thanks are due to the Council for the financial help.

REFERENCES

- Cook, A. H. and Jones, E. R. H., 1953, *Dictionary of Organic Compounds*, p., 26, 526.
 Krishna Murti, G. S. R., 1956, *Ind. J. Phys.*, **30**, 537.
 Neuhaus, A., 1939, *Zeit. f. Krist.*, **101**, 177.

THE RAMAN AND INFRARED SPECTRA OF 2,4 AND 3,4-DICHLOROBENZYL CHLORIDE AND 1,2,4-TRIMETHYL BENZENE*

KRISHNA KUMAR DEB

OPTICS DEPARTMENT,

INDIAN ASSOCIATION FOR THE CULTIVATION OF SCIENCE,
CALCUTTA-32.

(Received November 14, 1962)

Plate II

ABSTRACT. The Raman and infrared spectra of 2,4-dichloro- and 3,4-dichlorobenzyl chloride and 1,2,4-trimethyl benzene have been studied and assignments of the observed frequencies to different vibrational modes of the molecules have been proposed. The Raman spectra of the compounds in the solid state at -180°C have also been investigated. In the case of the two isomeric dichlorobenzyl chlorides, some changes in some of the frequencies of the molecules are found to take place with solidification of the liquids. It has been concluded that the Cl atom of (CH_2Cl) group in the 2,4-dichlorobenzyl chloride molecule forms weak bonds with H atoms of the neighbouring molecule, while such hydrogen bonding does not take place in the case of the 3,4-isomer. The reason has been discussed.

Small changes in the spectra are also observed in the case of 1,2,4-trimethyl benzene and it has been concluded that no new intermolecular bonding takes place in this case at the low temperature.

INTRODUCTION

The Raman spectra of a large number of mono- and disubstituted benzenes in the solid state at low temperatures were studied by many previous workers (Biswas, 1954, 1955; Deb, 1960, 1961, 1962; Mukherjee, 1960) and those of some trisubstituted benzenes in the solid state at -180°C have been studied by the present author (Deb, 1960). It has been observed that some of the intramolecular vibrational modes of the molecules are affected by change of state and a few low frequency Raman lines are exhibited by the compounds at low temperature, the number of such lines depending on the nature and relative positions of the substituents. In continuation of these investigations, the Raman and infrared spectra of 2,4-dichlorobenzyl chloride, 3,4-dichlorobenzyl chloride and 1,2,4-trimethyl benzene have been studied under different conditions. The states of polarization of the Raman lines have also been determined. The results have

*Communicated by Prof. S. C. Sirkar.

been discussed in the present paper and an attempt has been made to assign the observed frequencies to appropriate vibrational modes of the molecules.

EXPERIMENTAL

The liquids 2,4-dichlorobenzyl chloride and 3, 4-dichlorobenzyl chloride supplied by Light and Co., England and 1, 2, 4-trimethyl benzene obtained from Eastman Kodak Co., U.S.A., were of chemically pure quality and they were further purified by distillation under reduced pressure. The arrangements for recording the Raman spectra in the liquid state and in the solid state at -180°C and for studying the state of polarisation of the Raman lines in the liquid state were the same as those used earlier (Deb, 1960). The spectra were recorded on Ilford Zenith plates with the help of a Fuess glass spectrograph having a dispersion of about $11\text{ \AA}/\text{mm}$ in the region 4047 \AA .

The infrared spectra of the liquids were recorded in the region from 607 cm^{-1} to 3600 cm^{-1} with the help of a Perkin-Elmer Model 21 spectrophotometer with NaCl optics. Films of the liquids of thickness of a few microns enclosed between two NaCl discs were used in recording the spectra due to the liquids.

RESULTS

The Raman spectra are shown in Figs. 1, 2 and 3, Plate II. The observed Raman shifts of the molecules in the liquid state and in the solid state at -180°C are tabulated in Tables I, II and III. The Raman frequencies of 1, 2, 4-trimethyl benzene in the liquid state reported by previous workers are also included in Table III. The state of polarisation of the Raman lines of the liquids are indicated by the letters 'P' and 'D' which mean partially polarised and totally depolarised respectively.

The infrared absorption curves of the liquids are shown in Figs. 4, 5 and 6 and the frequencies of the observed bands are tabulated in Table IV.

DISCUSSION OF RESULTS

(a) Assignments of the Raman lines

The molecules of 2, 4-dichlorobenzyl chloride, 3, 4-dichlorobenzyl chloride and 1, 2, 4-trimethyl benzene belong to the point group C_s . In such molecules the polarised Raman frequencies would belong to the symmetry class a' giving vibrations in the plane of the molecules while the depolarised Raman lines belong to the symmetry class a'' giving vibrations perpendicular to the plane of the molecule. Tentative assignments of the lines are given in the third column of Tables I and II and in the fourth column in Table III. The numbering of the modes of vibration has been made following that for the benzene ring made by Pitzer and Scott (1943).

It is seen from Table I, II and III that there are four totally depolarised Raman lines in the spectra due to 2, 4-dichlorobenzyl chloride and 3, 4-dichloro-

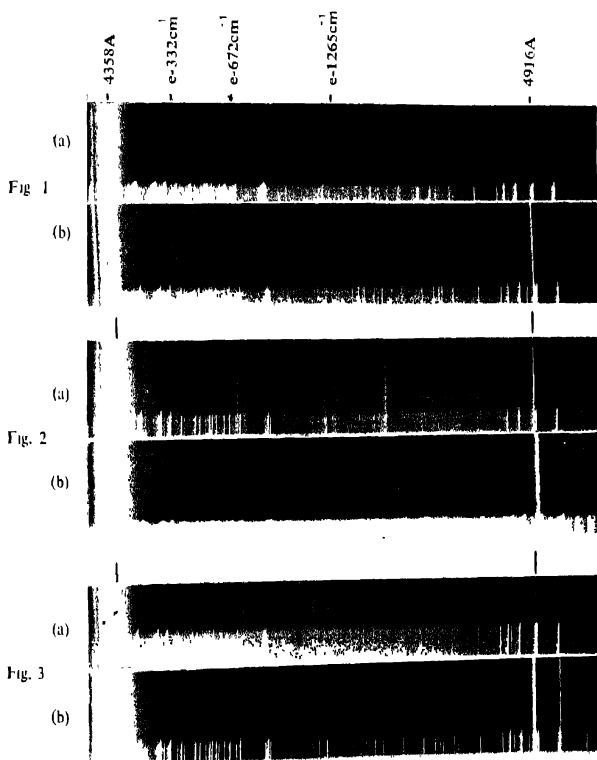


Fig. 1. (a) Raman spectrum of 2,4-dichlorobenzyl chloride, liquid at 32°C
 (b) " " " Solid at -180°C
 Fig. 2. (a) Raman spectrum of 3,4-dichlorobenzyl chloride, liquid at 32°C.
 (b) " " " " Solid at -180°C
 Fig. 3. (a) Raman spectrum of 1,2,4-trimethyl benzene, liquid at 32°C
 (b) " " " " Solid at -180°C.

benzyl chloride in the region below 400 cm^{-1} . As the molecules have no centre of symmetry, the out-of-plane degenerate mode No. 16 would be allowed and split up in those cases. The lines 171 and 98 cm^{-1} of 2, 4-dichlorobenzyl chloride and the lines 155 and 95 cm^{-1} of 3, 4-dichlorobenzyl chloride may correspond to the modes 16A and 16B of benzene. The Raman lines 210 and 182 cm^{-1} of the first compound and 250 cm^{-1} and 197 cm^{-1} of the second compound probably represent the out-of-plane bending oscillations of both C-Cl and C-H bonds corresponding to the modes 10A and 10B respectively. The modes 16A and 16B in the case of 1, 2, 4-trimethyl benzene seem to give the lines 210 and 145 cm^{-1} and the modes 10B and 10A probably give the lines 287 and 313 cm^{-1} respectively.

TABLE I
Raman spectra of 2, 4-dichlorobenzyl chloride

Raman shifts, in cm^{-1}		Symmetry class	Assignment Mode No (Pitzer and Scott, 1943)
Liquid at 30°C (Present author)	Solid at -180°C (Present author)		
98 (2b) D	98 (2)	a'' fundamental	16 B
171 (3) D	176 (1)	a'' „	16 A
182 (3) D	183 (1)	a'' „	10 B
210 (5) D	207 (1b)	a'' „	10 A
259 (1b) P		a' „	11 (C-Cl bonding in CH_2Cl gr.)
332 (6) P	335 (0)	a' „	6 A
396 (4) P	396 (0)	a' „	9 A
461 (3) P	460 (0)	a' „	6 B
557 (3) P	557 (0)	a' „	9 B
650 (2) D	651 (0)	a'' „	17 B
672 (12) P	664 (10)	a' „	1
720 (6) D	718 (2)	a'' „	17 A
737 (6) P	737 (2)	a' „	C-Cl stretching in CH_2Cl group
850 (3) P		a' „	19 A
1044 (2) D		a' „	8 A
1095 (4) P	1095 (0)	a' „	19 B
1145 (3) P	1149 (0)	a' „	7A
1214 (5) P	1218 (4)	a' „	7 B
1265 (8) P	1265 (2)	a' „	2
1296 (0)	1296 (0)		
1386 (0)			
1444 (1)			CH_2 bending oscillation in CH_2Cl group
1584 (12) D	1584 (6)	a' „	8 B
2068 (2b) P	2068 (1b)		CH_2 stretching oscillation in CH_2Cl gr.
3065 (4b) P	3064 (0)	a' „	CH valence oscillation, 7 B and 2 superposed

TABLE II
Raman spectra of 3,4-dichlorobenzyl chloride

Raman shifts in cm^{-1}		Symmetry class	Assignment Mode No. (Pitzer and Scott, 1943)
Liquid at 30°C (Present author)	Solid at -180°C (Present author)		
95 (2b) D	95 (2)	a'' fundamental	16 B
155 (6b) D	155 (2b)	a'' „	16 A
197 (5) D	197 (0b)	a'' „	10 B
250 (1b) D	245 (0)	a'' „	10 A, C-Cl bending in CH_2Cl group
333 (6) P	336 (1)	a' „	6 A
425 (3) P	425 (0)	a' „	9 A
465 (8) P	465 (1)	a' „	6 B
556 (4) P	556 (1)	a' „	9 B
661 (1) D	666 (0)	a'' „	17 B
680 (10) P	683 (8)	a' „	1
695 (1) D	695 (0)	a'' „	17 A
722 (8b) P	722 (3)	a' „	C-Cl stretching in CH_2Cl group
831 (0b) P			
879 (3b) P	879 (0b)	a' „	19 A
1034 (8) P	1034 (2)	a' „	19 B
1140 (8) P	1140 (1)	a' „	7 A
1215 (10) P	1217 (6)	a' „	7 B
1276 (8b) P	1276 (3b)	a' „	2 and 8A superposed
1446 (1)			CH_2 bending oscillation in CH_2Cl group
1593 (15) D	1595 (6)	a' „	8 B
2964 (4b) P	2964 (0b)		CH_2 stretching oscillation in CH_2Cl group
3060 (6b) P	3064 (0b)	a' „	CH valence oscillation, 7 B and 2 superposed

TABLE III

Raman spectra of 1, 2, 4-trimethyl benzene

Raman shifts in cm^{-1}			Assignment	
Pure liquid		Solid at -180°C Present author	Symmetry class	Assignment Mode No. (Pitzer and Scott, 1943)
Landolt- Börnstein Tables (1951)	Present author			
148 (2)	145 (0b)D	150 (1)	a'' fundamental	16 B
207 (4,7) D	210 (4b)D	212 (1)	a'' "	16 A
232 (1)	237 (1) D	238 (1)	a'' "	11
281 (2,0)P	287 (1) D		a'' "	10 B
318 (23,6)D	313 (6)D	313 (2)	a'' "	10 A
434 (6,4)P	437 (1)P		a' "	9 A
470 (19,8)P	475 (5)P	475 (2)	a' "	6 A
515 (1)				
537 (1)	538 (0)			
554 (29,6)P	558 (6) P	558 (3)	a' "	6 B
576 (2)				
603 (1,3) P				
686 (6,0)P				
716 (20,8) P	719 (3) P	718 (0)	a' "	9 B
743 (47,7) P	747 (10) P	747 (4)	a' "	1
806 (1,7) P	806 (0b) P			
871 (1,6) P	874 (0) P			
924 (14,6) P	928 (4) P	926 (0)	a' "	19 A
1023 (3,1) P	1020 (0vb)			
1095 (2)				
1124 (4,3)	1123 (2) P	1125 (2)	a' "	19 B
1148 (3,5)				
1157 (2)	1160 (1) P	1167 (2)	a' "	7 A
1188 (2,3)				
1209 (4,0)	1213 (1) P			
1243 (33,6) P	1246 (12) P	1243 (8)	a' "	2
1379 (25,4) P	1383 (8) P	1383 (2)	a' "	7 B
1444 (12,0)	1448 (4b) P	1448 (2)		CH bending in CH_3 group
	1545 (0)			
1576 (6,5) P	1582 (1) D		a' "	8 A
1618 (20,0) P	1620 (8) D	1616 (6)	a' "	8 B
2731 (1)	2736 (1) P			
2857 (3)	2859 (4) P	2860 (1)		CH oscillation in CH_3 group
2912 (6b)	2918 (8b) P	2911 (4b)		CH oscillation in CH_3 group
3038 (3)	3040 (6) P	3035 (2)	a' "	CH valence oscillation, 7 B and 2 superposed

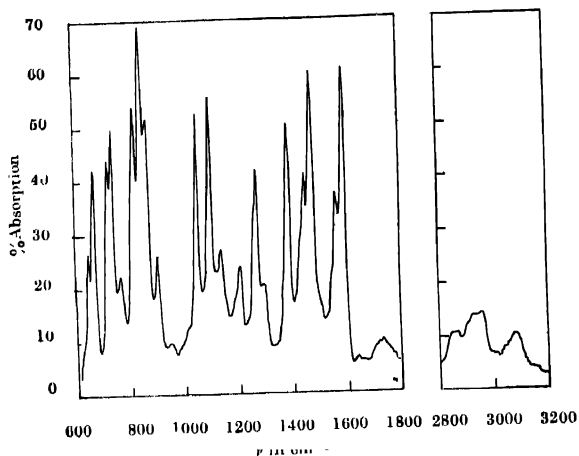


Fig. 4. Infra-red spectrum of 2,4-dichlorobenzyl chloride (liquid at 26°C).

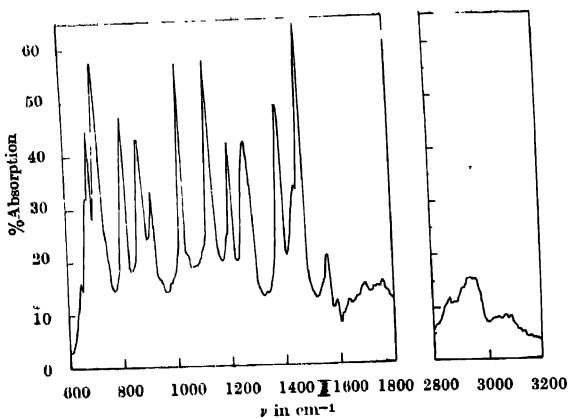


Fig. 5. Infra-red spectrum of 3,4-dichlorobenzyl chloride (liquid at 26°C).

TABLE IV

Infrared spectra of 2,4-dichloro- and 3,4-dichlorobenzyl chloride and 1,2,4-trimethyl benzene. Infra-red bands Wave number in cm^{-1} and Intensity

2,4-dichlorobenzyl chloride	3,4-dichlorobenzyl chloride	1,2,4-trimethyl benzene
650 (w)	650 (vw)	
672 (ms)	670 (w)	
	688 (ms)	700 (w)
725 (ms)	718 (s)	
742 (s)		742 (ms)
770 (vw)		760 (vw)
822 (s)	815 (ms)	800 (vs)
848 (vs)		
870 (s)	875 (ms)	870 (ms)
906 (w)	920 (w)	998 (ms)
1012 (vw)	1028 (s)	1020 (ms)
1055 (s)		1030 (ms)
1101 (s)	1130 (s)	1120 (w)
1140 (w)	1190 (vw)	1170 (vw)
1210 (w)	1206 (ms)	1210 (w)
1260 (ms)	1255 (ms)	1210 (w)
1272 (ms)	1265 (ms)	1250 (w)
1300 (w)	1285 (w)	1330 (w)
1365 (w)		
1390 (s)	1390 (ms)	1380 (ms)
1435 (ms)		1420 (ms)
1450 (ms)	1442 (w)	1450 (vs)
1465 (ms)		1465 (s)
	1470 (vs)	
1480 (s)		1500 (s)
1545 (w)	1540 (vw)	1530 (w)
1565 (ms)	1560 (vw)	1550 (w)
1593 (s)	1590 (vw)	1570 (w)
		1610 (ms)
		2730 (vw)
2862 (w)	2855 (w)	2865 (vs)
	2900 (w)	
2930 (w)	2940 (w)	2930 (vs)
2960 (w)		3010 (vs)
3060 (w)	3058 (vw)	

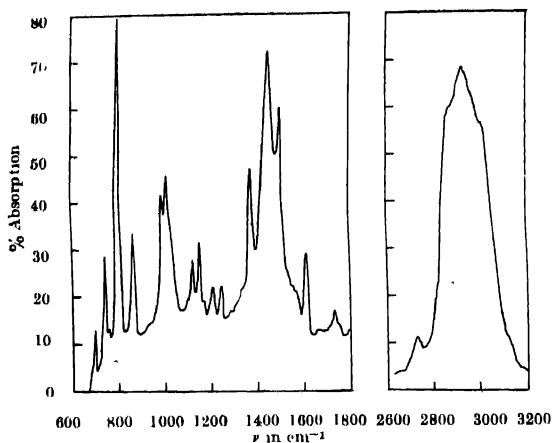


Fig. 6. Infra-red spectrum of 1, 2, 4 trimethyl benzene (liquid at 26°C.)

The degenerate mode No. 6 of benzene representing the in-plane bending oscillation of the carbon ring may correspond to the frequencies 332 and 461 cm^{-1} in the case of 2, 4-dichlorobenzyl chloride and to 333 and 465 cm^{-1} of 3, 4-dichlorobenzyl chloride. In the case of 1, 2, 4-trimethyl benzene the modes 6A and 6B probably give the lines 475 and 558 cm^{-1} respectively. The frequencies corresponding to the modes 8A and 8B may account for the lines 1044 and 1584 cm^{-1} respectively in the case of 2, 4-dichlorobenzyl chloride. The lines 1593 cm^{-1} in the case of 3, 4-dichlorobenzyl chloride corresponds to the mode 8B and the frequency corresponding to the mode 8A is probably superposed on the mode No. 2 of benzene giving a strong and broad line at 1276 cm^{-1} . The lines 1582 and 1620 cm^{-1} in the case of 1,2,4 trimethyl Benzene probably account for the modes 8A and 8B respectively. In the last case, in the mode 8A, the two diametrically opposite CH groups may be displaced simultaneously towards the centre of the molecule and in that case the frequency will not be much different from that of the corresponding mode 18B of the benzene molecule.

The superposition of the modes 7A and 2 give rise to a pure CH valence oscillation in two diametrically opposite C-H groups in the three molecules and gives the lines 3065, 3060 and 3040 cm^{-1} respectively in the three cases. The CH_2 valence oscillation in the CH_2Cl and CH_3 groups give the lines 2960, 2964 and 2918 cm^{-1} respectively. The other lines are assigned to different modes as shown in the Tables.

(b) *Changes in the Raman spectra with the solidification of the liquids*

It can be seen from Tables I and II that when 2, 4-dichloro and 3, 4-dichlorobenzyl chloride are solidified and cooled to -180°C , the Raman lines 332, 1265

and 3065 cm^{-1} due to the former liquid and the lines 197 , 333 and 1034 cm^{-1} due to the latter liquid become much weaker. Probably, these lines being highly polarised, they are partly absorbed while traversing the polycrystalline mass. Further, in the case of 2, 4 dichlorobenzyl chloride the line 672 cm^{-1} shifts to 664 cm^{-1} with solidification of the substance. This may be due to the formation of a weak bond between Cl atom of the CH_2Cl group and hydrogen atom of the neighbouring molecule. In the case of 3, 4-dichlorobenzyl chloride, however, no such shift of the line 680 cm^{-1} takes place. This may be explained on the assumption that the Cl atom in the CH_2Cl group is attached to the adjacent H atom in the same molecule so that it is no longer able to form intermolecular bond.

Small changes also occur in the case of 1, 2, 4-trimethyl benzene as can be seen from Table III. The line 1160 cm^{-1} corresponding to the mode 7A shifts to 1167 cm^{-1} and increases in intensity when the compound is solidified and cooled to -180°C . Also, the line 210 cm^{-1} due to a C—H out-of-plane bending oscillation becomes weaker under similar condition. These changes are obviously due to influence of crystal field on the molecule. The electronic spectra do not undergo any drastic change with the solidification of the liquid (Misra, 1962) and therefore, no new intermolecular bond-formation takes place in this case.

ACKNOWLEDGMENT

The author wishes to acknowledge his ever grateful indebtedness to Prof. S. C. Sirkar, D.Sc., F.N.I., for his kind help and inspiring guidance throughout the progress of the work.

REFERENCES

- Biswas, D. C., 1954a, *Ind. J. Phys.*, **28**, 54.
" " 1954b, *Ind. J. Phys.*, **28**, 423.
" " 1955a, *Ind. J. Phys.*, **29**, 74.
" " 1955 b, *Ind. J. Phys.*, **29**, 257.
Deb, K. K., 1960, *Ind. J. Phys.*, **34**, 247.
Deb, K. K. and Banerjee, S. B., 1960, *Ind. J. Phys.*, **34**, 554.
Deb, K. K., 1961, *Ind. J. Phys.*, **35**, 16.
Deb, K. K., 1962, *Ind. J. Phys.*, **36**, 159.
Landolt-Börnstein Tables, 1951, Zahlenwerte und Funktionen, 1 Band, Atom-und Molekular Physik, p. 499.
Misra, T. N., 1962, D. Phil. (Science) Thesis.
Mukherjee, D. K., 1960, *Ind. J. Phys.*, **34**, 402.
Pitzer, K. S. and Soot, D. W., 1943, *J. Am. Chem. Soc.*, **65**, 803.

INTERPENETRATION OF TWO IONIZED GAS CLOUDS-II

V. B. BHATIA

DEPARTMENT OF PHYSICS, S. D. COLLEGE, NEW DELHI-5

AND

J. N. TANDON

DEPARTMENT OF PHYSICS, UNIVERSITY OF DELHI, DELHI-6

(Received January 4, 1962)

ABSTRACT. Counterstreaming of two ionized gas clouds has been considered by taking account of the gas pressures of the two clouds. It is shown that the counterstreaming will, in general, be unstable

INTRODUCTION

Counterstreaming of two ionized gas clouds has been the subject of investigation in recent years (Kahn 1957, Parker 1958, Tandon 1961). It was shown that the counterstreaming, in general, is unstable except when the density of one of the streams is extremely low as compared with that of the other. Kahn suggested that the counterstreaming will be stopped because of this instability and a shock will be generated. Alternatively, Tandon (hereafter referred to as paper I) is of the opinion that the counterstreaming will not stop but the double stream will break into small clouds of space charge with a maximum length given by

$$\lambda_{max} = \sqrt{\frac{\pi m M U^2}{2 N_0 e^2 (m + M)}} \quad \dots (1)$$

when the two clouds are of equal particle density N_0 and are moving in the opposite directions with the velocity \vec{U} .

There is no experimental evidence to support one view or the other. However, the recent satellite observations (Arnoldy *et al.* 1960) showing that the outer radiation belt disrupts during a magnetic storm and that the intensity of radiation in the outer belt is much higher (about five times the pre-storm value) near the end of the storm which stays at this value for about 8 to 10 days before it begins to decrease, seems to support indirectly the views developed in paper I (Tandon, unpublished).

Earlier authors did not consider the effect of gas pressure which in many situations (solar ion streams, laboratory experimentation) is of considerable significance. In this note we discuss the effect of the pressure of the two streams on the stability criteria. It can be easily seen from paper I that the protons do

not appreciably change the stable length. We, therefore, assume that the protons provide a uniform back-ground of positive charge because of their heavier mass, although it may be mentioned that this assumption may not always hold good.

COUNTERSTREAMING OF CLOUDS

Following paper I we suppose that a completely ionized neutral gas cloud of initial uniform density N_{01} electrons per cm^3 is moving with initial uniform velocity \vec{V}_{01} . Let a similar stream with density N_{02} electrons per cm^3 be moving with a velocity $-\vec{V}_{02}$. We shall further assume that the temperatures of the two gas clouds are the same and that the particle collisions are negligible.

After the interaction there will be perturbations in the densities, velocities and pressures. Assuming isothermal changes, let the perturbations be given by

$$N_1 = N_{01} + n_1 \qquad N_2 = N_{02} + n_2 \qquad \dots (2)$$

$$\vec{V}_1 = \vec{V}_{01} + \vec{v}_1 \qquad \vec{V}_2 = -\vec{V}_{02} + \vec{v}_2 \qquad \dots (3)$$

where the small quantities denote the perturbation values which are of the first order.

The basic equations are the equations of motion

$$\left[\frac{\partial}{\partial t} + (\vec{V}_1 \cdot \text{grad}) \right] \vec{V}_1 = \frac{e}{m} \vec{E} - \frac{1}{N_1 m} \text{grad } p_1 \qquad \dots (4)$$

$$\left[\frac{\partial}{\partial t} + (\vec{V}_2 \cdot \text{grad}) \right] \vec{V}_2 = \frac{e}{m} \vec{E} - \frac{1}{N_2 m} \text{grad } p_2 \qquad \dots (5)$$

and the equations of continuity

$$\left[\frac{\partial}{\partial t} + (\vec{V}_1 \cdot \text{grad}) \right] \vec{V}_1 + N_1 \text{div } \vec{V}_1 = 0 \qquad \dots (6)$$

$$\left[\frac{\partial}{\partial t} + (\vec{V}_2 \cdot \text{grad}) \right] \vec{V}_2 + N_2 \text{div } \vec{V}_2 = 0 \qquad \dots (7)$$

where p_1 and p_2 are the electron gas pressures of the two clouds respectively, which are given by

$$p_1 = N_1 kT \quad \text{and} \quad p_2 = N_2 kT \qquad \dots (8)$$

and the electric field \vec{E} is given by

$$\text{div } \vec{E} = 4\pi e(n_1 + n_2) \qquad \dots (9)$$

(Combining equations (4) and (5) with the equations (2), (3), (6), (7) (8) and (9) we get

$$\left[\frac{\partial}{\partial t} + (\vec{V}_{01} \cdot \text{grad}) \right]^2 n_1 = -\omega_1^2 (n_1 + n_2) - \frac{u_1^2}{N_{01}} \nabla^2 n_1 \quad \dots \quad (10)$$

$$\left[\frac{\partial}{\partial t} + (\vec{V}_{02} \cdot \text{grad}) \right]^2 n_2 = -\omega_2^2 (n_1 + n_2) - \frac{u_2^2}{N_{02}} \nabla^2 n_2 \quad \dots \quad (11)$$

where $\omega_1 = \left(\frac{4\pi e^2 N_{01}}{m} \right)^{\frac{1}{2}}$ and $\omega_2 = \left(\frac{4\pi e^2 N_{02}}{m} \right)^{\frac{1}{2}}$ are the two plasma frequencies

and $u_1 = \left(\frac{N_{01} k T}{m} \right)^{\frac{1}{2}}$ and $u_2 = \left(\frac{N_{02} k T}{m} \right)^{\frac{1}{2}}$ are the Newtonian sound velocities.

Assuming the solutions of (10) and (11) of the form $e^{i\omega t + i\vec{k} \cdot \vec{r}}$, we have

$$\left\{ [\omega + (\vec{V}_{01} \cdot \vec{k})]^2 + \frac{u_1^2 k^2}{N_{01}} - \omega_1^2 \right\} n_{01} = \omega_1^2 n_{02} \quad \dots \quad (12)$$

$$\text{and} \quad \left\{ [\omega - (\vec{V}_{02} \cdot \vec{k})]^2 + \frac{u_2^2 k^2}{N_{02}} - \omega_2^2 \right\} n_{02} = \omega_2^2 n_{01} \quad \dots \quad (13)$$

Eliminating n_{01} and n_{02} from (12) and (13) we get the dispersion relation

$$\begin{aligned} & \left[\omega + (\vec{V}_{01} \cdot \vec{k}) \right]^2 \left[\omega - (\vec{V}_{02} \cdot \vec{k}) \right]^2 - \frac{u_1^2 k^2}{N_{01}} \left[\omega - (\vec{V}_{02} \cdot \vec{k}) \right]^2 + \frac{u_2^2 k^2}{N_{02}} \left[\omega + (\vec{V}_{01} \cdot \vec{k}) \right]^2 \\ & - \omega_2^2 \left[\omega + (\vec{V}_{01} \cdot \vec{k}) \right]^2 - \omega_1^2 \left[\omega - (\vec{V}_{02} \cdot \vec{k}) \right]^2 - k^2 \left[\frac{u_1^2 \omega_2^2}{N_{01}} + \frac{u_2^2 \omega_1^2}{N_{02}} \right] + \frac{u_1^2 u_2^2 k^4}{N_{01} N_{02}} \\ & = 0 \quad \dots \quad (14) \end{aligned}$$

we now put

$$\begin{aligned} \vec{V}_{01} + \vec{V}_{02} &= 2\vec{U} \\ \vec{V}_{01} - \vec{V}_{02} &= 2\vec{V} \\ p &= \omega + \vec{V} \cdot \vec{k} \\ \Omega &= \vec{U} \cdot \vec{k} \end{aligned} \quad \dots \quad (15)$$

and get the simplified dispersion relation

$$\begin{aligned} (p^2 - \Omega^2)^2 - (\omega_1^2 + \omega_2^2 - \chi_1^2 - \chi_2^2)(p^2 + \Omega^2) + 2p\Omega(\omega_1^2 - \omega_2^2 + \chi_2^2 - \chi_1^2) \\ - (\chi_1^2 \omega_2^2 + \chi_2^2 \omega_1^2) + \chi_1^2 \chi_2^2 = 0 \quad \dots \quad (16) \end{aligned}$$

where $\chi_1^2 = \frac{u_1^2 k^2}{N_{e1}}$ and $\chi_2^2 = \frac{u_2^2 k^2}{N_{e2}}$... (17)

Equation (16) is the general expression for the dispersion relation.

In order to get the physical insight, we assume that the two clouds have the same electron density. Thus $\omega_1^2 = \omega_2^2 = \omega_0^2$ (say) and $\chi_1^2 = \chi_2^2 = \chi^2$ (say) and equation (16) reduces to

$$p^4 - 2p^2(\Omega^2 + \omega_0^2 - \chi^2) + \Omega^4 - 2\Omega^2(\omega_0^2 - \chi^2) - 2\chi^2\omega_0^2 + \chi^4 = 0 \quad \dots (18)$$

which is quadratic in p^2 .

For very low values of gas pressure, it can easily be seen that χ^2 is negligibly small. Thus we have

$$p^4 - 2p^2(\Omega^2 + \omega_0^2) + \Omega^2(\Omega^2 - 2\omega_0^2) = 0 \quad \dots (19)$$

This is a similar expression as derived earlier in Paper I. From equation (18) it is evident that for all real values of k , p is complex when

either $\Omega^2 < 2\omega_0^2 - \chi^2$... (20)

$$\Omega^2 > \frac{4(\chi^2 - \omega_0^2)}{3} \quad \dots (21)$$

showing thereby that the counterstreaming will be unstable by overstability. It appears, therefore, that the counterstreaming is always unstable. The fluctuations of protons will not change these conditions considerably. This, therefore, does not change basically any of the results deduced in Paper I.

ACKNOWLEDGMENT

One of us (JNT) is grateful to the University Grants Commission, India, for the award of Senior fellowship.

REFERENCES

- Arnoldy, R. L., Hoffman, R. A. and Winckler, J. R., 1960, *J. Geophys. Res.*, **65**, 1361.
 Khan, F. D., 1957, *J. Fluid Mech.*, **2**, 601.
 Parker, E. N., 1958, *Phys. Rev.*, **112**, 1429
 Tandon, J. N., 1961, *Ind. J. Phys.*, **35**, 193.

CONTENTS

Indian Journal of Physics

Vol. 57, No. 1

January, 1965

Page

1. Interaction of 14.8 Mev Neutrons with Aluminium—R. K. Mohindra and H. S. Hans	1
2. Potential Energy Curves and Dissociation Energy of the PO Molecule—C. V. V. S. N. K. Santharam and P. Tiruvenganna Rao	14
3. One Operational Amplifier Simulates Third Order Systems with a Leading-Time Constant—L. K. Wadhwa and Jagdish Chandra	18
4. Measurement of Dielectric Properties of Metal Sulphides—M. N. Sharma and S. S. Gupta	33
5. The Space Groups of Crystals of β -Chloronaphthalene at Different Temperatures—Naba Kumar Banerjee and S. C. Sirkar	41
6. The Raman and Infrared Spectra of 2, 4-and 3, 4-Dichlorobenzyl Chloride and 1, 2, 4-Trimethyl Benzene—Krishna Kumar Deb	45
7. Interpenetration of two Ionized Gas Clouds-II—V. B. Bhatia and J. N. Tandon	54

Regd. No. C-3911

VOL. 37 INDIAN JOURNAL OF PHYSICS

No. 2

(Published in collaboration with the Indian Physical Society)

AND

VOL. 48

PROCEEDINGS

No. 2

OF THE

**INDIAN ASSOCIATION FOR THE
CULTIVATION OF SCIENCE**

FEBRUARY 1963

**PUBLISHED BY THE
INDIAN ASSOCIATION FOR THE CULTIVATION OF SCIENCE
3 ADAMPUR, CALCUTTA 11**

BOARD OF EDITORS

K. BANERJEE	D. S. KOTHARI
D. M. BOSE	S. K. MITRA
S. N. BOSE	B. D. NAG CHAUDHURI
S. D. CHATTERJEE	K. R. RAO
P. S. GILL	D. B. SINHA
S. R. KHASTGIR	S. C. SIKKAR (<i>Secretary</i>)
B. N. SRIVASTAVA	

EDITORIAL COLLABORATORS

PROF. R. K. ASUNDI, Ph.D., F.N.I.
PROF. D. BASU, Ph.D.
PROF. J. N. BHAR, D.Sc., F.N.I.
PROF. V. G. BHIDE, Ph.D.(Nag), Ph.D.(Lond).
PROF. A. BOSE, D.Sc., F.N.I.
PROF. S. K. CHAKRABARTY, D.Sc., F.N.I.
DR. J. S. CHATTERJEE
DR. K. DAS GUPTA, Ph.D.
PROF. N. N. DAS GUPTA, Ph.D., F.N.I.
DR. J. DHAR, D.Phil. (So)
PROF. A. K. DUTTA, D.Sc., F.N.I.
PROF. C. S. GHOSH, M.Sc., S.M., F.N.I., M.I.E.E.
PROF. S. GHOSH, D.Sc., F.N.I.
PROF. S. N. GHOSH, D.Sc.
PROF. S. GUPTA, M.Sc., F.N.I.
PROF. D. N. KUNDU, Ph.D., F.N.I.
PROF. R. C. MAJUMDER, Ph.D., F.N.I.
PRINCIPAL Y. G. NAIK, Ph.D.
PROF. S. R. PALIT, D.Sc., F.R.I.C., F.N.I.
PROF. H. RAKSHIT, D.Sc., F.N.I.
PROF. A. SAHA, D.Sc., F.N.I.
DR. VIJAYAM A. SARABHAI, M.A., Ph.D., F.N.I.
DR. A. K. SENGUPTA, D.Sc.
PROF. NAND LAL SINGH, D.Sc.
DR. M. S. SINHA, D.Sc., F.N.I.
PROF. N. R. TAWDE, Ph.D., F.N.I.
DR. P. VENKATESWARLU

Assistant Editor :

SRI T. N. MISRA, M.Sc.

Annual Subscription—

Inland Rs. 25.00

Foreign \$ 2-10-0 or \$ 7.00

NOTICE

TO INTENDING AUTHORS

Manuscripts for publication should be sent to the Assistant Editor, Indian Journal of Physics, Jadavpur, Calcutta-32.

The manuscripts submitted must be type-written with double space on thick foolscap paper with sufficient margin on the left and at the top. The original copy, and not the carbon copy, should be submitted. Each paper must contain an abstract at the beginning.

All references should be the text by quoting the surname of the author, followed by year of publication, e.g., (Ghosh, 1954). The full reference should be given in a list at the end, arranged alphabetically, as follows; Ghosh, D. K., 1954, *Ind. J. Phys.*, 28, 485.

Line diagrams should be drawn on white Bristol board or tracing paper with black India ink, and letters and numbers inside the diagrams should be written neatly in capital type with India ink. The size of the diagrams submitted and the lettering inside should be large enough so that it is legible after reduction to one-third the original size. A simple style of lettering such as gothic, with its uniform line width and no serifs should be used, e.g.,

A·B·E·F·G·M·P·T·W·

Photographs submitted for publication should be printed on glossy paper with somewhat more contrast than that desired in the reproduction, and should, if possible, be mounted on thick white paper.

Captions to all figures should be typed in a separate sheet and attached at the end of the paper.

The mathematical expressions should be written carefully by hand. Care should be taken to distinguish between capital and small letters and superscripts and subscripts. Repetition of a complex expression should be avoided by representing it by a symbol. Green letters and unusual symbols should be identified in the margin. Fractional exponents should be used instead of root signs.

Bengal Chemical and Pharmaceutical Works Ltd. **Pioneer Indian Manufacturers of Pharmaceuticals & Chemicals.**

Manufacturers of:

Pharmaceutical Chemicals:

Caffeine and its salts, Strychnine Hydrochlor, Strychnine Sulphate, Brucine Sulphate, Potassium Citrate B.P., I.P., Sodium Citrate B.P., I.P., Potassium Acetate B.P., I.P., Potassium Iodide B.P., I.P., Sodium Iodide B.P., I.P., Ferri et Ammon Citrate B.P., I.P., Nicotinic Acid, B.P., Nicotinamide, B.P., and various other Pharmaceutical Chemicals.

Heavy & Reagent Quality Fine Chemicals:

Alum, Alum Sulphate (Iron Free), Ferro Alum, Zinc Chloride Tech. Naphthalene Pure, Sodium Citrate A.R., Potassium Citrate A.R., Magnesium Sulphate A.R., Sodium Sulphate Anhydrous A.R., Potassium Iodide A.R., Sodium Chloride A.R., Zinc Sulphate A.R., etc.

Please refer your enquiries for the above items and other chemicals in the line to :—

BENGAL CHEMICAL

6, GANESH CHUNDER AVENUE,
CALCUTTA-13, INDIA.

B O R O S I L

LABORATORY GLASSWARE

such as

FLASKS, BEAKERS, CONDENSERS, MEASURING FLASKS, MEASURING CYLINDERS,
PIPETTES & ANY SPECIAL APPARATUS MADE TO DESIGN

and

PENICILIN VIALS, VACCINE BULBS—WHITE & AMBER

●
ALL OTHER APPARATUS & EQUIPMENT MANUFACTURED TO CLIENT'S DESIGN

INDUSTRIAL & ENGINEERING APPARATUS CO. PRIVATE LIMITED

CHOTANI ESTATES, PROCTOR ROAD, GRANT ROAD, BOMBAY 7

— JUST PUBLISHED —**FIELDS AND CIRCUITS IN ELECTRICAL MACHINES**

By

N. KESAVAMURTHI, *Professor of Electrical Engineering, Indian Institute of Technology, Kharagpur.*

AND

R. E. BRIDFORD, *Asst. Professor of Electrical Engineering, Indian Institute of Technology, Bombay.*

These eminent Professors associated with premier Technical Institutions, present, in an easy-to-understand manner, an integrated account of MAGNETIC FIELD THEORY with special reference to ELECTRICAL MACHINE PROBLEMS. The book develops from the fundamentals the Mathematical expressions for various field quantities and the laws governing them. *Major portion of this book has been included in curriculum for Post Graduate Course in Electrical Engineering and Electrical Machine Design with selected topics for the Final Year Students in Electrical Engineering in the leading Institutions*

FIRST AUTHORITATIVE INDIAN PUBLICATION ON THE SUBJECT—PROFUSELY
ILLUSTRATED WITH HUNDREDS OF DIAGRAMS.

Royal 8vo — Rexine & Gold Embossed — Pp. 384 —

Rs. 20.50

THACKER, SPINK & CO. (1933) PRIVATE, LTD.

(PUBLISHERS & BOOKSELLERS SINCE 1819)

3, Esplanade East, Calcutta-1**NON-AQUEOUS TITRATION**

A monograph on acid-base titrations in organic solvents

By

PROF. SANTI R. PALIT, D.Sc., F.R.I.C., F.N.I.

DR. MIHIR NATH DAS, D.Phil.

AND

MR. G. R. SOMAYAJULU, M.Sc.

This book is a comprehensive survey of the recently developed methods of acid-base titrations in non-aqueous solvents. Acid-base concept, as developed by Lowry-Brönsted and Lewis is succinctly presented in this slender volume. The subject is divided into two classes, viz. titration of weak bases and titration of weak acids. The method of 'glycolic titration' is described at a great length as also the method of 'acetic titration' including its recent modifications for the estimation of weak bases. Various methods for the titration of weak acids are duly described. A reference list of all pertinent publications is included in this book.

122 pages with 23 diagrams (1954)

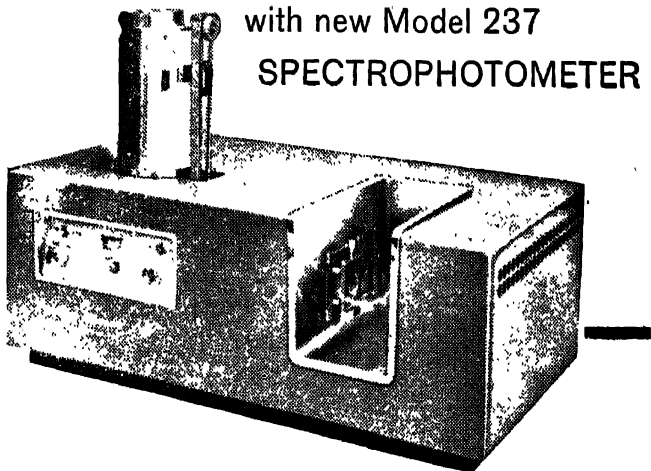
Inland Rs. 3 only. Foreign (including postage) \$ 1.00 or 5s.

Published by

INDIAN ASSOCIATION FOR THE CULTIVATION OF SCIENCE

JADAVPUR, CALCUTTA-32, INDIA

Now...grating resolution
over fundamental IR range
with new Model 237
SPECTROPHOTOMETER



You can now have the advantages of high-resolution analysis over the entire infrared spectral range of fundamental analytical importance—4000 to 625 wavenumbers (2.5 to 16 microns)...even if your budget is limited. The New Perkin-Elmer Model 237 Double-Grating Spectrophotometer, latest in P-E's low-cost Infracord line, makes this possible.

Basic to this high performance at low cost is the Model 237's grating-filter design. the dispersing power of gratings, used only in their first orders, is complemented by filters to eliminate higher orders of radiation. The result is outstanding spectral purity achieved with simplicity and dependability of mechanical operation previously not available.

Flexible Presentation. You can specify a Model 237 recording in either linear wavelength or linear wavenumbers, as you prefer. Full wavelength coverage is divided into two ranges. 4000-1300 and 2000-625 wavenumbers, or 2.5-7.7 and 5.0-16 microns. The analyst selects the range he desires by the flick of a panel switch, thus assuring maximum legibility of fine structural detail.

Two scanning rates for each range are available: fast (8 minutes) rate for survey scans or spectra of materials with relatively few narrow spectral bands; slow (24 minutes) rate provides details of very complex spectra. Here, too, a panel switch puts both speeds at the analyst's fingertips.

Optional auxiliary recorders are available to give you continuous spectra at fixed wavelengths or to let you expand or compress ordinate or abscissa. The chart ordinate—a full 15 centimeters—provides maximum accuracy in recording band intensities.

INSTRUMENT DIVISION
Perkin-Elmer Corporation
NORWALK CONNECTICUT

Sold and serviced in India exclusively by

BLUE ★ STAR

**BLUE STAR ENGINEERING
CO. (Calcutta) PRIVATE LTD.**
7 HARE STREET, CALCUTTA 1
Also at BOMBAY • DELHI
MADRAS • JAMSHEDPUR

IMPORTANT PUBLICATIONS

The following special publications of the Indian Association for the Cultivation of Science, Jadavpur, Calcutta, are available at the prices shown against each of them :—

TITLE	AUTHOR	PRICE
Magnetism .. Report of the Symposium on Magnetism		Rs. 7 0 0
Iron Ores of India ..	Dr. M. S. Krishnan	5 0 0
Earthquakes in the Himalayan Region ..	Dr. S. K. Banerji	3 0 0
Methods in Scientific Research ..	Sir E. J. Russell	0 6 0
The Origin of the Planets ..	Sir James H. Jeans	0 6 0
Active Nitrogen— A New Theory.	Prof. S. K. Mitra	2 8 0
Theory of Valency and the Structure of Chemical Compounds. ..	Prof. P. Ray	3 0 0
Petroleum Resources of India ..	D. N. Wadia	2 8 0
The Role of the Electrical Double-layer in the Electro-Chemistry of Colloids. ..	J. N. Mukherjee	1 12 0
The Earth's Magnetism and its Changes ..	Prof. S. Chapman	1 0 0
Distribution of Anthocyanins ..	Robert Robinson	1 4 0
Lapinone, A New Antimalarial ..	Louis F. Fieser	1 0 0
Catalysts in Polymerization Reactions ..	H. Mark	1 8 0
Constitutional Problems Concerning Vat Dyes.	Dr. K. Venkataraman	1 0 0
Non-Aqueous Titration ..	Santi R. Palit, Mihir Nath Das and G. R. Somayajulu	3 0 0
Garnets and their Role in Nature ..	Sir Lewis L. Fermor	2 8 0

A discount of 25% is allowed to Booksellers and Agents.

NOTICE

No claims will be allowed for copies of journal lost in the mail or otherwise unless such claims are received within 4 months of the date of issue.

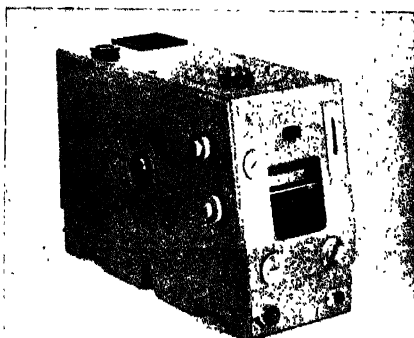
RATES OF ADVERTISEMENTS

- Ordinary pages :

Full page ..	Rs. 50/- per insertion
Half page ..	Rs. 28/- per insertion
 - Pages facing 1st inside cover, 2nd inside cover and first and last page of book matter :

Full page ..	Rs. 55/- per insertion
Half page ..	Rs. 30/- per insertion
 - Cover pages .. by negotiation
- 25% commissions are allowed to *bona fide* publicity agents securing orders for advertisements.

ZEISS Mirror Monochromator "SPM 2"



- * Represents a high quality new development in the field of optophysical measuring instruments.
- * It combines versatility of application with simplicity of operation.
- * It can be used for the production of monochromatic radiation in the wavelength region from 0.193 to 40 microns by using interchangeable prisms and diffraction grating.
- * The respective wavelength scale can be read in projection.



VEB Carl Zeiss JENA
(German Democratic Republic)

Sole Agents in India :

GORDHANDAS DESAI PRIVATE LIMITED

PHEROZSHAH MEHTA ROAD, BOMBAY 1

Branches at :

**P/7, Mission Row Extension,
CALCUTTA 1.**

**4/2B, Asaf Ali Road,
NEW DELHI 1.**

**22, Linghi Chetty Street,
MADRAS 1.**

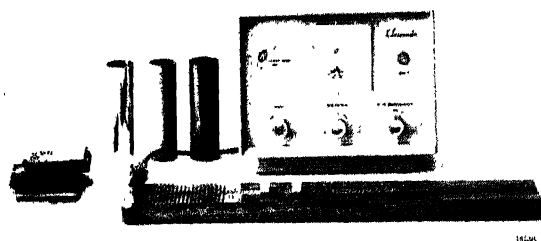
Nuclear



Chicago

WORLD FAMOUS
NUCLEONIC INSTRUMENT
MANUFACTURERS

Presenting
TRAINING INSTRUMENT: CLASSMASTER



Model 1613A

The Model 1613-A Class Master is a complete system for radiation demonstration. It consists of sturdy ratemeter, G-M detector, calibrated experiment board, two radiation sources etc. The manual covers absorption, scattering, coincidence loss, detector efficiency and other phenomena of interest to the students of Physics, Chemistry and Biology Classes.

For further particulars, please write to :

Sole Distributors .

**THE SCIENTIFIC INSTRUMENT
COMPANY, LIMITED.**

ALLAHABAD BOMBAY CALCUTTA MADRAS
NEW DELHI

Head Office : 6, Tej Bahadur Sapru Road, Allahabad



A COMPARATIVE STUDY OF THE FLUORESCENCE AND THE EMISSION SPECTRA OF ANISOLE

SATYA PRAKASH AND NAND LAL SINGH

DEPARTMENT OF SPECTROSCOPY,
BANARAS HINDU UNIVERSITY,
VARANASI-5.

(Received June 4, 1962)

Plate III

ABSTRACT. The fluorescence and emission spectra of anisole vapour have been photographed in the near ultraviolet region. The two spectra are compared and their vibrational structure has been discussed on the basis of 13 ground state frequencies observed in the fluorescence spectrum and 15 ground state and 7 excited state frequencies observed in the emission spectrum.

INTRODUCTION

The present paper deals with the investigation of the fluorescence and emission spectra of anisole vapour. A preliminary report on the fluorescence spectrum has already been published (Prakash, 1962). The fluorescence was excited by condensed manganese spark lines and it lies in the near ultraviolet region. The emission spectrum of the molecule first photographed by Singh (1958) in this laboratory was excited by transformer discharge. This spectrum also lies in the near ultraviolet region, but is more extended. Both the processes involve transitions from an excited electronic state to the various vibrational levels of the ground electronic state. A comparative study of the two spectra has provided better information about the vibrational structure of the states involved.

EXPERIMENTAL

Fluorescence spectrum

The fluorescence spectrum of anisole vapour has been recorded following the technique of Bass and Sponer (1950). The exciting source was a condensed manganese spark working at 15000 volts drawn from a Hilger 1/4 KW transformer with a condenser of capacity .05 μ F kept in the circuit parallel to the spark gap. A horn shaped fluorescence cell of pyrex glass fitted with three quartz windows was used. The liquid was obtained from E. Merck, Darmstadt and was of their extra pure quality. It was used as such without further purification. The liquid at room temperature was contained in a small bulb attached to a side tube of the fluorescence cell. The vapour pressure of the chemical was about 7 to

8 mm of mercury. The exciting radiation was focussed on the entrance window by a short focus quartz lens. A concave mirror with a wide aperture was used at the back of the spark source to increase the intensity of the exciting radiation.

The fluorescent radiation was received in a direction at right angles to the incident beam and was photographed on the Hilger medium quartz spectrograph having an aperture $f/12$ and dispersion of $13 \text{ \AA}/\text{mm}$ in the region around 2700 \AA . The cell was placed very close to the slit of the spectrograph. The intensity of the fluorescent radiation was further increased by placing a plane mirror behind the cell and facing the slit of the spectrograph. Kodak II-0 plates were used and an exposure of 110 hours was found sufficient to record the spectrum with a slit width of 35 microns.

Emission spectrum

The emission spectrum of anisole has been obtained by uncondensed transformer discharge through flowing vapour. The usual π type discharge tube, 75 cm. long, fitted with internal aluminum electrodes was used. The tube was sealed off at one end and the other end was closed with a quartz window. A bulb, containing liquid anisole was attached to the discharge tube through a nail trap. This served to control the flow of vapour in the discharge tube. The tube was evacuated by means of a vacuum pump through a U-shaped glass tube kept immersed in ice and salt mixture to condense the vapour coming from the discharge tube. At a regulated flow of the vapour a light blue discharge was found to emit the bands. This type of discharge was maintained throughout the experiment by controlling the output of the transformer at about 3000 volts by means of a variac, put in the primary of the transformer.

The spectrum was photographed on Zeiss medium quartz spectrograph with slit width of 35 microns. Kodak II-0 plates were used to photograph the spectrum with different times of exposures varying from 1 to 4 hours.

R E S U L T S

Both the fluorescence and emission spectra reproduced in Fig. 1 seem to be alike and lie in the region 2700 \AA to 3100 \AA . The bands in the emission spectrum are sharper and more extended than those in the fluorescence spectrum. The bands in both the cases are red degraded and are masked by a strong continuum covering the entire region of the spectra. The intensities of the bands on the shorter wavelength side of the spectrum have been reduced due to self-absorption by the unexcited vapour lying near the window.

The bands were measured using Hilger L76 comparator with a least count of .001 mm. The wavenumbers are accurate up to $\pm 8 \text{ cm}^{-1}$ for fluorescence bands and up to $\pm 5 \text{ cm}^{-1}$ for emission bands.

The fluorescence and emission bands are collected in Table I, together with their wavenumbers, the intensities, the separations from 0, 0 band and their

assignments. The figures in parentheses give the difference in wave-numbers between the observed and assigned values. The notations used to indicate the intensities of the bands are as follows .-

vw-very weak, w-weak, mw-medium to weak, m-medium, ms-medium to strong, s-strong, vs-very strong. d-diffuse, b-broad.

In Table II, a comparison between the fundamental ground state frequencies observed in fluorescence, emission, absorption and Raman spectra is given.

DISCUSSION

If we take OCH_3 to behave like an atom X , the approximate symmetry of anisole is C_{2v} . Though this is not rigorously true, it serves our purpose to explain the gross structure of the spectrum. From the work of Sponer and Teller (1941) it can be concluded that the spectra of mono-substituted benzenes observed in the ultraviolet region corresponds to the electronic transition ${}^1B_1 \rightarrow {}^1A_1$, between the totally symmetric ground state (A_1) and a non-totally symmetric excited state (B_1). In an allowed transition, we expect strong 0, 0 band, which, however, in our case has appeared as a self-absorption band. We further expect strong totally symmetric vibrations (a_1) and weak non-totally symmetric vibrations (a_2 and b_1) to appear in our spectra. The non-totally symmetric vibrations (b_2) should occur with even quanta only and in combination with non-totally symmetric vibrations (a_2 and b_1).

The strong absorption band due to self-absorption at 36386 cm^{-1} in the fluorescence spectrum or at 36387 cm^{-1} in the emission spectrum is purely due to an electronic transition and is taken as the 0,0 band in the present analysis. This is in agreement with the value 36389 cm^{-1} measured in ultraviolet absorption (Sreeramanurthy 1950) spectrum.

The analysis of the fluorescence bands shows the following ground state frequencies : 265, 450, 522, 555, 611, 788, 818, 1000, 1029, 1178, 1250, 1310 and 1597 cm^{-1} . A similar analysis of the emission bands shows all the above frequencies observed in the fluorescence spectrum with an addition of two frequencies, namely, 209 and 1065 cm^{-1} . Other frequencies are 265, 448, 520, 551, 615, 785, 820, 996, 1023, 1180, 1251, 1302 and 1599 cm^{-1} . These correspond well with values mentioned in the case of fluorescence.

The frequencies 788, 1000, 1029 and 1250 cm^{-1} in the fluorescence are correlated with 785, 996, 1023 and 1251 cm^{-1} in the emission spectrum. They are excited strongly and are observed in combination and overtones. This has led us to believe that they are totally symmetric vibrations. The corresponding Raman frequencies (Kohlrusch and Pongratz, 1934) are at 781, 991, 1020 and 1244 cm^{-1} respectively. The vibrations—785 and $\sim 1251\text{ cm}^{-1}$ in our spectra are X sensitive corresponding to the frequencies 785 and 1210 cm^{-1} observed in toluene (Pitzer and Scott, 1943). The frequency ~ 996 is the strongest and

corresponds to breathing vibration. The vibration $\sim 1023\text{ cm}^{-1}$ is due to C-H in-plane bending vibration. This is inferred by comparing with frequencies 1024 , 1029 and 1030 cm^{-1} occurring in phenol (Evans 1960), aniline (Evans 1960) and toluene (Pitzer and Scott, 1943).

The vibrations 1178 , 1310 and 1557 cm^{-1} observed in the fluorescence spectrum also occur in emission with the values 1180 , 1302 and 1599 cm^{-1} respectively. The true intensities of the bands involving these vibrations cannot be visualized as the bands have been completely masked by the strong continuum predominating in that region. These can be correlated with frequencies 1177 , 1209 and 1603 cm^{-1} in the Raman spectrum. The frequency 1180 can be assigned to C-H inplane bending vibration of type a_1 by analogy with the frequencies 1170 , 1176 and 1178 occurring in phenol, aniline and toluene respectively. The remaining two vibrations lie in the region of C-C stretching vibrations, but the spectra do not give any definite information about their species.

A very weak frequency 1065 cm^{-1} has been recorded in emission spectrum. It finds the proper correlation with the frequency 1072 cm^{-1} in the Raman spectrum.

A medium to weak frequency 818 cm^{-1} in the fluorescence or 820 cm^{-1} in the emission spectrum is correlated with the frequency 816 cm^{-1} in the Raman spectrum. This frequency is expected to be a_2 , C-H out-of-plane bending vibration, split out of 849 cm^{-1} vibration of benzene.

The weak frequency 611 cm^{-1} in the fluorescence or 614 cm^{-1} in the emission spectrum is the non-totally symmetric part of 606 cm^{-1} vibration of benzene. The corresponding part in the Raman spectrum is at 612 cm^{-1} .

A strong vibration 551 cm^{-1} occurs in the emission spectrum and is also found in combination with totally symmetric vibrations. This may be taken as a fundamental vibration, but no corresponding frequency in the Raman spectrum is reported. It occurs in fluorescence with weaker intensity.

The frequencies 520 , 448 , 265 and 209 cm^{-1} are observed with weaker intensities in the emission spectrum. They lie in the region of self-absorption and no definite information about their species could be gathered from the spectrum. They are correlated with frequencies 529 , 441 , 264 and 210 cm^{-1} in the Raman spectrum. In the fluorescence spectrum they are more uncertain. However, the two low vibrations 209 and 265 cm^{-1} may be assigned to bending modes.

The emission spectrum also extends towards shorter wavelength side of the $0,0$ band. The bands appear due to self-absorption and involve the excited state frequencies 184 , 252 , 495 , 522 , 759 , 934 and 954 cm^{-1} .

The frequencies 30 , 56 and 230 cm^{-1} observed in the fluorescence are in close agreement with the values 28 , 58 and 230 cm^{-1} in the emission spectrum. They are assigned to difference frequencies arising out of $1-1$ transitions of some

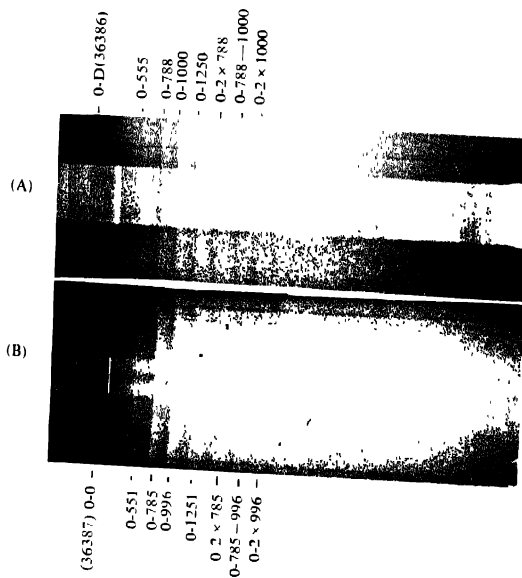


Fig. 1. (A) Fluorescence and (B) emission spectra of anisole vapour.

TABLE I

Fluorescence and emission bands of anisole

Fluorescence spectrum				Emission spectrum			
Wave-number	Intensity	Separation from 0,0	Assignment	Wave-number	Intensity	Separation from 0,0	Assignment
				37341	m	954	0 + 954 (0)
				37321	m	934	0 + 934 (0)
				37146	m	759	0 + 759 (0)
				37119	mw	732	0 + 759 - 28 (1)
				37087	w	700	0 + 759 - 58 (-1)
				36909	m	522	0 + 522 (0)
				36882	m	495	0 + 495 (0)
				36847	mw	460	0 + 522 - 58 (4)
				36812	vw	425	
				36752	mw	365	0 + 2 × 184 (3)
				36678	w	291	0 + 522 - 230 (-1)
				36639	w	252	0 + 252 (0)
36386	vs	0	0 - 0 (0)	36387	vs	0	0 - 0 (0)
36356	s	-30	0 - 30 (0)	36359	m	-28	0 - 28 (0)
				36351	w	-36	
36330	s	-56	0 - 56 (0)	36329	msb	-58	0 - 58 (0)
36299	w	-87	0 - 56 - 30 (-1)	36299	msb	-88	0 - 58 - 28 (-2)
				36291	vw	96	0 - 614 + 522 (-4)
36266	w	-120	0 - 2 × 56 (-8)	36272	mw	-115	0 - 2 × 58 (1)
				36242	vw	145	
				36178	vw	-200	0 - 209 (0)
36153	mw	-233	0 - 230 (-3)	36158	m	-229	0 - 230 (1)
36121	vw	-265	0 - 265 (0)	36122	vw	-265	0 - 265 (0)
				35973	vw	-414	0 - 2 × 209 (4)
35936	vw	-450	0 - 450 (0)	35939	vw	-448	0 - 448 (0)
				35927	vw	-460	0 - 2 × 230 (0)
35864	vw	-522	0 - 522 (0)	35869	vw	-518	0 - 520 (2)
			0 - 2 × 230 - 56 (-6)				0 - 2 × 230 - 58 (0)
35831	mw	-555	0 - 555 (0)	35836	m	-551	0 - 551 (0)
				35812	vw	-575	0 - 551 - 28 (4)
35775	w	-611	0 - 611 (0)	35770	w	-617	0 - 614 (-3)
35752	vw	-634	0 - 611 - 30 (-3)				
35718	vw	-668	0 - 611 - 56 (-1)	35720	vw	-667	0 - 614 - 58 (5)
				35685	vw	-702	
				35648	vw	-730	
35598	ms	-788	0 - 788 (0)	35602	ms	-785	0 - 785 (0)
35569	mw	-818	0 - 818 (0)	35567	mw	-820	0 - 820 (0)
35542	w	-844	0 - 788 - 56 (0)	35546	w	-841	0 - 785 - 58 (2)

TABLE I (cont'd).

Fluorescence spectrum				Emission spectrum			
Wave-number	Intensity	Separation from 0,0	Assignment	Wave-number	Intensity	Separation from 0,0	Assignment
35506	w	-880	0-818-56 (-6)	35508	vw	-879	0-820-58 (-1)
35486	w	-900	0-788-2 \times 56 (0)	35491	vw	-896	0-785-2 \times 58 (5)
35418	vw	-908	0-522-450 (4)	35417	w	-970	0-448-520 (-2)
35400	vw	-986					
35386	ms	-1000	0-1000 (0)	35391	ms	-996	0-996 (0)
35357	m	-1029	0-1029 (0)	35364	m	-1023	0-1023 (0)
35330	mw	-1056	0-1000-56 (0)	35338	w	-1049	0-996-58 (5)
				35322	vw	-1065	0-1005 (0)
35306	mw	-1080	0-1029-56 (5)	35305	vw	-1082	0-1023-58 (-1)
35279	w	-1107	0-1000-2 \times 56 (5)	35276	vw	-1111	0-996-2 \times 58 (1)
35250	w	-1136	0-611-522 (-3)	35247	vw	-1140	0-1023-2 \times 58 (-1)
35208	w	-1178	0-1178 (0)	35207	w	-1180	0-1180 (0)
35167	w	-1219	0-2 \times 611 (3)	35162	w	-1225	0-2 \times 614 (3)
35136	w	-1250	0-1250 (0)	35136	m	-1251	0-1251 (0)
35108	w	-1278	0-1250-30 (2)	35109	vw	-1278	0-1251-28 (1)
35076	vw	-1310	0-1310 (0)	35085	w	-1302	0-1302 (0)
				35050	vw	-1337	0-785-551 (-1)
35020	vw	-1366	0-1310-56 (0)	34844	vw	-1543	0-996-551 (4)
34816	w	-1570	0-2 \times 788 (6)	34813	w	-1574	0-2 \times 785 (-4)
34789	w	-1597	0-1597 (0)	34788	w	-1599	0-1599 (0)
34753	vw	-1633	0-2 \times 788-56 (-1)	34757	vw	-1630	0-2 \times 785-58 (-2)
				34742	vw	-1645	0-2 \times 820 (-5)
34723	vw	-1663					
34697	wl	-1789	0-1000-788 (-1)	34606	mw	-1781	0-996-785 (0)
34668	vwd	-1818	0-1029-788 (-1)	34581	w	-1806	0-1023-785 (2)
				34558	vw	-1829	0-996-785-58 (10)
				34529	vw	-1858	0-1023-785-58 (8)
34385	vwd	-2001	0-2 \times 1000 (-1)	34387	vwd	-2000	0-2 \times 996 (8)
34360	vwd	-2020	0-1000-1029 (9)	34357	vwd	-2030	0-996-1023 (-11)

TABLE I (contd.).

Fluorescence spectrum				Emission spectrum			
Wave-number	Intensity	Separation from 0,0	Assignment	Wave-number	Intensity	Separation from 0,0	Assignment
34332	vwd	-2054	0-2×1029 (4)	34335	vwd	-2052	0-2×1023 (6)
34300	vwd	-2086	0-1000-1020 -56(1)	34307	vwd	-2080	0-996-1023- 58 (-3)
	vwd	-2121		34264	vwd	-2123	
				34205	vwd	-2182	0-1180- 996 (-4)
				34146	vwd	-2241	0-996-1251 (6)
				34120	vwd	-2267	0-1023-1251 (7)
				34088	vwd	-2299	0-996-1251- 58 (6)
				34052	vwd	-2335	0-1023-1251- 58 (-3)
				34025	vwd	-2362	
				34001	vwd	-2386	
				33942	vwd	-2445	0-1251- 1180 (-14)
				33828	vwd	-2559	0-996-2× 785 (7)

TABLE II

Comparison between the fundamental ground state vibrations of anisole

Raman Kohlrausch and Pongratz	Fluorescence	Emission	Absorption Sreeramamurty	Assignment
	Present Research			
210	—	209	210	b_2 nontotally symmetric
264	265	265	264	nontotally symmetric
441	450	448	440	—
520	522	520	523	—
—	555	551	—	a_1
612	611	614	610	b_1 ring def. ip
781	788	785	786	a_1 X sensitive stretch.
816	818	820	818	a_1 C-H bend. op
991	1000	996	987	a_1 ring breathing
1020	1029	1023	1029	a_1 C-H bend. ip
1072	—	1065	1055	b_1 C-H bend. ip
1177	1178	1180	—	a_1 C-H bend. ip
1244	1250	1251	—	a_1 X sensitive stretch.
1299	1310	1302	—	—
1603	1597	1599	—	ring stretch.

ip—inplane

op—out of plane

suitable non-totally symmetric vibrations. The difference frequency 28 cm^{-1} may be explained as $0-210 \pm 184\text{ cm}^{-1}$. No definite assignments could be given for the other two difference frequencies.

A C K N O W L E D G M E N T

The authors are thankful to Dr. K. N. Upadhyya for many valuable suggestions. One of the authors (S. P.) is grateful to C.S.I.R. for financial assistance.

R E F E R E N C E S

- Bas, A. M. and Sponer, H., 1950, *Optical Soc. Am.*, **40**, 389.
Evans, J. C., 1960, *Spectrochimica Acta*, **16**, 428.
Evans, J. C., 1960, *Spectrochimica Acta*, **16**, 1382.
Kohlrausch, K. W. F. and Pongratz, A., 1934, *Monat für Chem.* **65**, 6.
Pitzer, K. S. and Scott, D. W., 1943, *J. Am. Chem. Soc.*, **65**, 824.
Prakash, S., 1962, *Nature*, **193**, 268.
Sponer, H. and Teller, E., 1941, *Phys. Rev.*, **13**, 75.
Sreenannamurti, K., 1950, *Ind. J. Phys.*, **24**, 421.

A STUDY ON RECORDING AND REPRODUCTION OF DIGITAL DATA ON AND FROM MAGNETIC DRUM SURFACE

DWIJESH DUTTA MAJUMDAR

INDIAN STATISTICAL INSTITUTE, CALCUTTA-35

(Received June 6, 1962)

ABSTRACT. The basic requirements and role of storage section in all Information Processing System is explained with reference to digital data recording and reproduction on and from magnetic drum surface. A comprehensive theoretical and experimental investigation accompanied by physical interpretations of the process of digital data recording and reproduction on and from ferromagnetic layer surface of Magnetic Drum Memory is presented. The associated boundary value problem has been solved to find the distribution of the fringing field in the ferromagnetic layer and analytic expressions for the output of a write-read system is presented in terms of the basic system parameters. As a result of the investigations basic requirements for achieving high resolution pulse recording on a magnetic surface are shown to be high coercivity, low permeability, rectangular B-H loop characteristics, thin coating, optimum recording current and an optimum pole face configuration for having maximum flux gradient on the surface for a particular head-to-medium separation and coating thickness.

INTRODUCTION

The basic requirements of a storage device or memory system of any of the Information Processing System (IPS) are as follows :-

- a) Physical stability of the stored data, so that the information can be retained for an extended period, if desired.
- b) Combination of both physical properties of nonvolatility and alterability.
- c) Total capacity of the device to hold binary information should be high enough.
- d) "Access time" or maximum waiting time for reading from or writing on to a desired address location should be as small as possible.

Using well-known physical principles involved in audio-recording on magnetic surfaces, Digital Information Storage Systems are built (Bigelow, 1948; Booth, 1949; Dutta Majumdar, 1958; Dutta Majumdar, 1961) which satisfies all the above requirements.

In the system under investigation binary information are recorded on a magnetizable surface coated on a rotating nonmagnetic metallic cylinder known as "Magnetic Drum Memory".

Pulse recording on magnetic drum surface has attained a unique position, in the field of digital data storage, because both the basic requirements of a binary memory, ability to record two states of a binary digit, and to consult the stored data at anytime are satisfied in this type with simplicity and economy. Theoretical and experimental investigations on optimum design of magnetic drum stores, for serial, serial parallel, or parallel type of digital computers were undertaken by the present author, several aspects of which were published in different technical journals (Dutta Majumdar, 1958, 1959, 1961, 1962). In this paper the mathematics and physics involved in the process of pulse recording and reproduction on and from a moving magnetic surface with the help of a magnetic head is studied. Field configuration in and around the gap of the magnetic head is deduced, computed numerically and plotted, which gives a qualitative insight into the problem of head design. Calculation of the magnetic field in the ferromagnetic layer of the drum in certain cases is presented following a method similar to that of (Karqvist, 1954), from which variation of the field components with permeability, layer thickness, airgap and other factors involved in the process are studied briefly. Linear boundary value problem for the two-dimensional static field and the one-dimensional transient field has been studied. Pulse frequency has been assumed low enough to neglect eddy current losses in the head and layer that are made of spinel material. The results of some experimental investigations, carried out with a practical magnetic drum storage system, designed and built here, providing reasonable balance between conflicting requirements of access time, storage capacity, reliability, size and cost, are presented and analysed.

Physics involved in the process of magnetic recording in general is rather complicated by the facts that, the particles subjected to the recording field are not of uniform sizes, and the variation of the amplitude of the applied field are different at different depths thereby causing variations in the associated magnetic properties, and once the signal is recorded an interaction occurs between places of different magnetization giving rise to a demagnetization field, and an intricate interdependence of all these and many other parameters. But in saturation type pulse recording the errors involved in the simplifying assumptions made in theoretical deductions are less important, and experimental studies on variation of different parameters involved can be made with sufficient accuracy. The present study involving comprehensive theoretical and experimental investigations has provided us a guide to the design of record/reproduce head, and optimization of the whole system for high density storage of digital data. The details of the experimental investigation could not be given here to reduce the size of the paper, only the salient features have been presented.

Principles of magnetic data recording and reproduction.

In digital computers, binary system of notation, where every digit is either a "0" or a "1", is invariably used. And this in magnetic data recording storage

means that the magnetic material on the surface is either saturated in a positive or in a negative sense, or completely unmagnetized. Depending upon this basic fact several methods of recording digits are possible, Return to Zero ($R-Z$), Non-Return to Zero ($N-R-Z$), phase modulation methods etc. $N-R-Z$ method enables a much higher pulse packing density than the other methods maintaining the same degree of reliability. $N-R-Z$ method is being used in the system under investigation

When the individual writing current pulses are spread out in time or distance, so that they occupy a full bit cell the recording method is called a $N-R-Z$ method. Pulses lose their individuality, and the writing current waveform does not return to zero between successive 1's or successive 0's. Instead, the moving magnetic surface, is continuously magnetized to saturation in one direction or the other with the direction of magnetization being reversed, when a "1" follows a "0", or when a "0" follows a "1". The playback signal using a

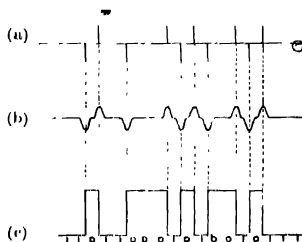


Fig 1. (a) Binary current waveform for $N-R-Z$ Method of recording (b) Actual p.b. signal, (c) Ideal p.b. signal

conventional type of head is approximately proportional to the rate of change of flux on the surface. The actual playback signal is shown in fig. (1b). But in ideal case when reading a flux pattern as shown in fig. (1a), the output should be a series of narrow pulses as shown in fig. (1c) corresponding to the flux changes. The original information is extracted from the presence or absence of these pulses. The widening of the output pulses as explained above seriously limits the pulse packing density because the flux changes must be separated sufficiently so that the pulses do not interact.

Magnetic model for write read process using saturation type recording.

The process consists in (1) switching of the state of magnetization of the ferromagnetic surface (Write Process),

(2) self demagnetization of the recorded signal,

(3) playback of the recorded signal (Read process).

The necessary aspects of the problem are to determine the magnetization of the ferromagnetic surface before and after the process of self demagnetization.

Attenuation factors for sinusoidal treatments has been developed and reported in the literature (Wallace, 1951, Begun, 1949, Westmijze, 1953). Now the magnetic model that explains $a-c$ magnetization can be applied with suitable simplifying assumptions, and the recorded pulse magnetization developed in the form of a harmonic series.

The model that explains $a-c$ magnetization is rather simple. In a particle a number of magnetic states are possible, each of which corresponds to a minimum of potential energy and is separated from other minima by potential barriers. Another simplifying assumption that can be made is that these barriers are of equal height. With the application of the magnetic field, the potential energy of these states will be diminished where the direction of the field is more in accord with the direction of the magnetization. Hence the potential barriers will decrease on the one side and will increase on the other side of the potential minimum. For a certain value of the applied field strength the first barriers will have disappeared and the magnetization will jump to a state with lower energy. Since all the barriers were supposed to be of equal height they will be crossed at the same field strength and therefore saturation will be obtained. Reversal of the field effects the saturation in the opposite direction. For an $a-c$ field of sufficient strength the magnetization will alternate between two directions. Now in the process of saturation type digital recording applied magnetic field, of sufficient amplitude to saturate the ferromagnetic surface reverses (switches) its direction of magnetization as steeply as possible when a "1" follows a "0" or vice-versa. So such a magnetization if developed in the form of a harmonic series, and the attenuation factors developed for sinusoidal treatments referred earlier, can be applied term by term to the total available flux to give the flux passing through the read coil, and by differentiation, the resultant head output voltage is obtained.

Field configuration in and around the gap of the magnetic head.

Before proceeding with the difficult problem of determining the ultimate magnetization of the element on the magnetizable surface in front of the record/read head, we intend to determine the nature of the field configuration in and around the gap. From this investigation we shall be in a position to approximate a potential distribution between the corners of the recording head. The problem has been tackled by Booth and Westmijze. It has been solved in a somewhat different method and is presented here.

At the outset it is assumed that the permeability μ of the head is infinity and that of the layer material is unity.

We approximate a practical head (Fig. 2) such that its left pole piece is bounded by the plane $y=0$ from $x=-a$ to $x=-l/2$, and by the plane $x=-l/2$. The right pole piece is symmetrical with respect to the plane $x=0$. This is the case of semi-infinite gap and bears close resemblance to practical heads, but the calculations are rather difficult to carry

out. The other two models, that of infinite gap and thin gap, also treated by Westmijze, are not of much practical use, and so will not be dealt with here.

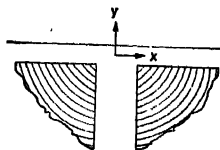


Fig. 2. An approximate practical magnetic head (semi infinite gap).

Looking normal to the gap surface, the gap is infinitely extended in the $-ve$ direction (fig. 2). The assumption that μ of the head material is infinite can be easily approximated as the permeability of the head materials ranges from 10,000 to 100,000 (radometal, mumetal, permalloy, etc.) and they are not used near the saturation region. The pole surface may then be said to represent a set of magnetic equipotentials.

Supposing there is an one turn coil in the head, and a current I is passed through it, then there will be a magnetic potential difference I between the pole pieces. So the potential function $V(x, y)$ has to satisfy the boundary condition $V = I/2$ and $-I/2$, respectively for the two pole pieces. It is clear from the symmetry that $V(x, y) = 0$ at $x = 0$. We shall apply Schwarz-Christoffel transformation in solving this problems, and then shall numerically compute the equipotential profiles and the lines of forces. (The computation was done in the electronic computer HEC2M).

Equipotential profiles and lines of forces.

We now picture the head on the positive side of the axis in the Z -plane with magnetic pole potentials, $\phi = \pm I/2 = \pm V$.

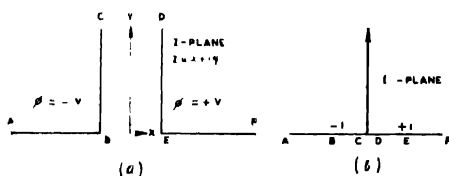
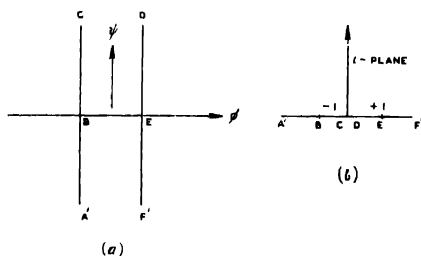
Application of the Schwarz-Christoffel Transformation gives us the equation from which the transformation of the contour ABCDEF in Z -plane into the W -plane is found. Let length of the head gap to be $2a$.

$$\text{then} \quad \frac{\partial \phi}{\partial x} = \frac{V}{a} = \frac{\partial \psi}{\partial y} \quad \therefore \quad \psi = \frac{V}{a} y + k.$$

Let $\psi = 0$ at B and E .

From Fig. 3(a) and 3(b)

$$\begin{aligned} \frac{dz}{dt} &= A(t+1)^{\frac{1}{2}}(t-0)(t-1)^{\frac{1}{2}} \\ &= A \left(\sqrt{\frac{t^2-1}{t}} \right). \end{aligned} \quad (1)$$

Fig. 3. (a) Z -plane, (b) t -planeFig. 4. (a) W -plane, (b) t -plane

From Fig. 4(a) and (b)

$$\frac{dW}{dt} = B(t+1)^0 \cdot t^{-1} \cdot (t-1)^0 = \frac{B}{t} \quad (2)$$

$$\therefore W = B \log t + C.$$

$$\text{At } E, t = 1, W = V, \therefore C = V.$$

$$\text{At } B, t = -1, W = -V$$

$$\therefore B = \pm \frac{2V}{i\pi}$$

$$\text{We take } W = \frac{2V}{i\pi} \log t + V.$$

$$= -\frac{2iV}{\pi} \log t + V \quad (3)$$

Since this satisfies the conditions

$$t \rightarrow 0, \text{ (along real axis), } \psi \rightarrow \infty.$$

$$t \rightarrow \pm \infty \text{ (" ") } \psi \rightarrow \infty$$

From equation (1)

$$Z = A \int \frac{\sqrt{t^2 - 1}}{t} dt + D$$

which on integration yields

$$Z = A \left(\sqrt{t^2 - 1} - \cos^{-1} \frac{1}{t} \right) + D$$

We have $Z = +a$ at $t = +1$, $\therefore D = a$

and $Z = -a$ at $t = -1$, $\therefore -a = A\{\cos^{-1}(-1)\} + a$

$$\therefore A = \pm \frac{2a}{\pi}$$

Now we have

$$Z = \frac{2a}{\pi} \left(\sqrt{t^2 - 1} - \cos^{-1} \frac{1}{t} \right) + a \quad (4)$$

(valid for $x \rightarrow 0$)

From equation (3) we have $t = e^{-\frac{\pi}{2V} \left(\frac{W}{V} - 1 \right)}$

This when expanded gives

$$t = -1 + e^{-\frac{\pi\psi}{2V}} \left[\cos \frac{\pi\phi}{2V} + i \sin \frac{\pi\phi}{2V} \right]$$

Substituting the value of t in equation (4),

$$Z = \frac{2a}{\pi} \left[\sqrt{-1 - e^{\frac{\pi\psi}{V}}} \left\{ \cos \frac{\pi\phi}{V} + i \sin \frac{\pi\phi}{V} \right\} - \cos^{-1} \left\{ e^{\frac{\pi\psi}{2V}} \left\{ i \cos \frac{\pi\phi}{2V} + \sin \frac{\pi\phi}{2V} \right\} \right\} \right] + a. \quad (5)$$

We take

$$\cos^{-1} \left\{ e^{\frac{\pi\psi}{2V}} \sin \frac{\pi\phi}{2V} + i e^{\frac{\pi\psi}{2V}} \cos \frac{\pi\phi}{2V} \right\} = C - iD.$$

This on solution leads to

$$C = \cos^{-1} \left[\frac{1}{\sqrt{2}} \sqrt{\left(e^{\frac{\pi\psi}{V}} + 1 \right) - e^{\frac{\pi\psi}{2V}} \left\{ e^{\frac{\pi\psi}{V}} + e^{-\frac{\pi\psi}{V}} + 2 \cos \frac{\pi\phi}{V} \right\}} \right] \quad (6)$$

$$D = \cos^{-1} \left[\frac{1}{\sqrt{2}} \sqrt{\left(e^{\frac{\pi\psi}{V}} + 1 \right) + e^{\frac{\pi\psi}{2V}} \left\{ e^{\frac{\pi\psi}{V}} + e^{-\frac{\pi\psi}{V}} + 2 \cos \frac{\pi\phi}{V} \right\}} \right] \quad (7)$$

Now we take

$$-1 + e^{-\frac{\pi\psi}{V}} A \left\{ \cos \frac{\pi\phi}{V} + i \sin \frac{\pi\phi}{V} \right\} = A' - iB' = Re^{i\theta}.$$

$$A' = R \cos \theta \quad \text{and} \quad B' = R \sin \theta.$$

$$R = e^{-\frac{\pi\psi}{2V}} \left\{ e^{\frac{\psi\pi}{V}} + e^{-\frac{\pi\psi}{V}} + 2 \cos \frac{\pi\phi}{V} \right\} \quad (8)$$

and

$$\tan \theta = - \frac{e^{-\frac{\pi\psi}{V}} \sin \frac{\pi\phi}{V}}{1 + e^{-\frac{\pi\psi}{V}} \cos \frac{\pi\phi}{V}}. \quad (9)$$

The equation (5) can now be written as

$$Z = x + iy$$

$$\frac{2a}{\pi} \left[\sqrt{R} e^{-i\theta} - (C' + iD) \right] + a$$

$$= \frac{2a}{\pi} (A - C') + a + i(D - B) \frac{2a}{\pi}.$$

where

$$\sqrt{R} \cos \theta/2 = A \quad \text{and} \quad \sqrt{R} \sin \theta/2 = B.$$

Therefore,

$$x = \frac{2a}{\pi} (A - C') + a \quad (10)$$

$$y = \frac{2a}{\pi} (D - B)$$

and,

$$\begin{aligned} A &= \sqrt{R} \cos \frac{\theta}{2} = \sqrt{\frac{R}{2}} (1 + \cos \theta) \\ B &= \sqrt{R} \sin \frac{\theta}{2} = \sqrt{\frac{R}{2}} (1 + \cos \theta) \end{aligned} \quad (11)$$

Substituting the value of $\tan \theta$ from equation (9), we have

$$\cos \theta = \frac{1}{\sqrt{1 + \tan^2 \theta}}$$

$$= \pm \sqrt{\frac{e^{\pi\psi/V} + e^{-\pi\psi/V} \cos^2 \frac{\pi\phi}{2} + 2 \cos \frac{\pi\phi}{2}}{e^{\pi\psi/V} + e^{-\pi\psi/V} + 2 \cos \frac{\pi\phi}{2}}} \quad (12)$$

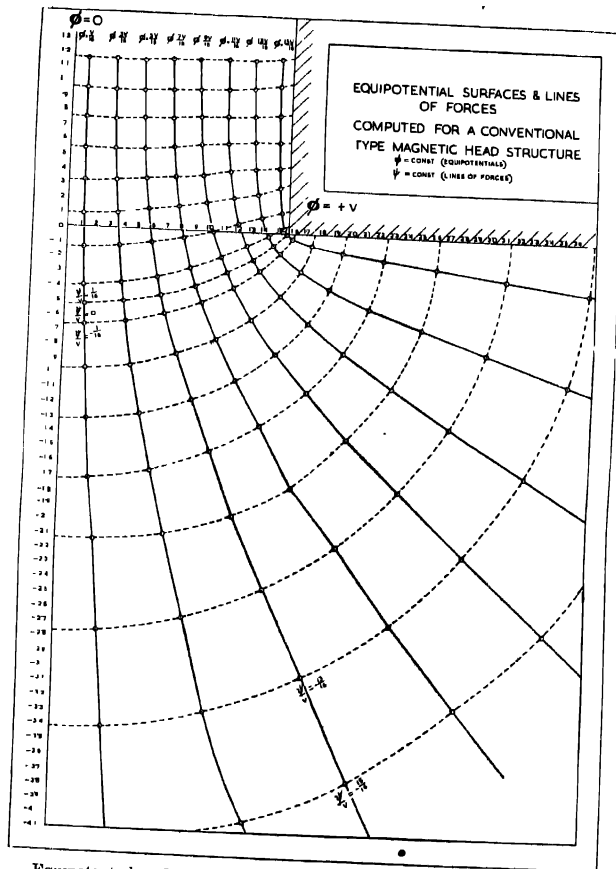


Fig. 5. Equipotential surfaces and lines of forces computed for a conventional type magnetic head structure.

$\phi = \text{const. (equipotentials)}$

$\psi = \text{const. (lines of forces)}$

Using equations (6), (7) (10), (11) and (12), the sets of magnetic equipotential profiles and lines of forces are computed and plotted as shown in the Figure 5.

SOLUTION OF BOUNDARY VALUE PROBLEM TO
FIND DISTRIBUTION OF FRINGING FIELD
OF A SEMI-INFINITE POLE GAP IN
FERRO-MAGNETIC LAYER OF A
MAGNETIC DRUM

Though the problem is non-linear, the linear case gives a first approximation, which in some cases seems to be satisfactory (Wallace, 1951; Karlqvist, 1954; Booth, 1952). Linear boundary value problem for the two dimensional static field and the one dimensional transient field has been solved and will be dealt with here.

The notations for the physical parameters are :

μ - layer permeability, d - layer thickness, N - half the pole distance b - head-to-layer distance, B_0 - induction in the pole gap measured in volt-sec per sq. meter, $B_0 = \mu_0 V/N$, V = magnetic potential of the head. $\mu_0 = 4\pi \times 10^{-7}$ in MKS system.

The investigations on the potential between the corners of the head treated with conformal mapping, shows that the magnetic potential distribution along $y = 0$ can be safely assumed to be linear.

Thus

$$\left. \begin{aligned} v &= -V & x < -N \\ v &= V \cdot x/N & -N < x < N \\ v &= +V & x > N \end{aligned} \right\} \quad \dots (13)$$

So the boundary value problem reduces in finding the magnetic potential $v(x, y)$ in the region $y > 0$, $-\infty < x < \infty$, when the potential along $y = 0$ is prescribed. The magnetizing vector is then,

$$H = -\text{Grad } v(x, y) \quad \dots (14)$$

The potential satisfies the equation,

$$\frac{\partial}{\partial x} \mu \frac{\partial V}{\partial x} + \frac{\partial}{\partial y} \mu \frac{\partial V}{\partial y} = 0 \quad \dots (15)$$

We assume μ , the layer permeability as constant, and we get the Laplace's equation:

$$\Delta v = 0, \quad \text{where} \quad \Delta = \frac{\partial^2}{\partial x^2} + \frac{\partial^2}{\partial y^2} \quad \dots (16)$$

usually the equation (15) is a non-linear equation

Boundary conditions :

We take v_1 = the potential above the layer ($b \rightarrow 0$).

$$v_2 = \text{''} \quad \text{''} \quad \text{in} \quad \text{''} \quad \text{''} \quad (b \rightarrow 0),$$

$$v_3 = \text{''} \quad \text{''} \quad \text{''} \quad \text{''} \quad \text{''} \quad (c \rightarrow 0),$$

$$v_4 = \text{''} \quad \text{''} \quad \text{below} \quad \text{''} \quad \text{''} \quad (c \rightarrow 0),$$

then boundary conditions along $y = b$ and $y = b + d$ (on the two sides of the layer) are,

$$\frac{\partial V_1}{\partial y} = \mu \frac{\partial V_2}{\partial y} \quad \dots \quad (17)$$

$$\mu \frac{\partial V_3}{\partial y} = \frac{\partial V_4}{\partial y} \quad \dots \quad (18)$$

Equations (15) and (16) are elliptic equations.

The non-stationary one-dimensional field can be computed from the equation:

$$\frac{\partial^2 H}{\partial x^2} = \sigma \mu \mu_0 \frac{\partial H}{\partial t} \quad \dots \quad (19)$$

σ = conductivity of the layer, μ = permeability of the layer and is assumed constant.

Idealisation of the problem.

The 1st approximation is to regard the drum surface as plane. The Drum diameter is about 200 mm. and the gap is about .02 mm. The variation of the head to layer distance due to the curvature of the drum surface is less than 10% for the interval $0 < x < 10N$. The factor b/N is usually between 0.5 and 2. The length of the Read/Record head is about 100 to 200 times that of the gap width, and so for all practical purposes, we can assume the head length as infinite. The width of the head is also about 100 times the gap width, and so our two dimensional treatment of the problem will be satisfactory. The permeability of the head is very high, and so the lines of force will leave the head surface nearly perpendicularly. The magnetic potential of the head is therefore assumed constant and is $+Ve$ on the right half and $-Ve$ on the left half of the head. How the pole length influences the field in the layer was investigated by Booth (Booth, 1952); here we shall study the potential between the corners of the head.

The boundary value problem.

We have to find out the potential $v(x, y)$ from the solution of Laplace's equation, subject to the conditions,

$$V = 0 \quad \text{when} \quad y = \infty \quad \dots \quad (20)$$

$$V = f(x) \quad \text{when} \quad y = 0 \quad \dots \quad (21)$$

Fourier's Integral solution for this is

$$V = \frac{1}{\pi} \int_0^{\infty} d\alpha \int_{-\infty}^{\infty} e^{-\alpha y} f(\lambda) \cos \alpha(\lambda - x) \cdot d\lambda \quad \dots \quad (22)$$

Following the same course as in Byerly (pp 78-79).

We obtain

$$v(x, y) = \frac{1}{2b} \sin \frac{\pi y}{b} \int_{-\infty}^{\infty} f(\lambda) \frac{d\lambda}{\cosh \frac{\pi}{b} (\lambda - x) - \cos \frac{\pi y}{b}} \quad \dots \quad (23)$$

And when $b = \infty$ we deduce the formula,

$$v(x, y) = \frac{y}{\pi} \int_{-\infty}^{\infty} f(\lambda) \frac{d\lambda}{y^2 + (\lambda - x)^2} \quad \dots \quad (24)$$

The field for $\mu = \alpha$ is obtained from the equation (23) defined by the equation (13), as :

$$H_y(x, b) = \frac{H_0}{\pi} \log \frac{\cosh \frac{\pi(x+N)}{2b}}{\cosh \frac{\pi(x-N)}{2b}} \quad \dots \quad (25)$$

This is not of much practical use. We get the field for the case $\mu = 1$ from the equation (24), which will be of great practical use. The field is always computed from equation (14). The field is given by the equations -

$$H_x(x, y) = -\frac{H_0}{\pi} \left[\tan^{-1} \frac{N+x}{y} + \tan^{-1} \frac{N-x}{y} \right] \quad \dots \quad (26)$$

$$H_y(x, y) = \frac{H_0}{2\pi} \log \frac{y^2 + (N+x)^2}{y^2 + (N-x)^2} \quad \dots \quad (27)$$

In the above equations we have the field given explicitly as simple functions of $x+y$, and it is easy to compute actual field. The approximation is satisfactory upto y greater than $0.5N$. The pole gap field intensity H_0 is estimated from a magneto motive force reluctance relationship, where the reluctance of the head core is piecewise calculated. We have

$$H_0 = \frac{4\pi n_1 i}{g_1 \left[1 + \frac{R_p}{R_g} \right]} \quad \dots \quad (28)$$

where R_p = reluctance of the head core, R_{g1} = Reluctance of the head pole gap, n_1 is the number of turns on the write coil and

$$\frac{R_p}{R_{g1}} = \frac{A_{g1}}{g_1} \left[\frac{g_2}{A_{g2}} + \sum_{i=1}^n \frac{l_i}{\mu_1 l_{p1}} \right] \quad (29)$$

g_1 = length of pole gap in the write read head (cm),

g_2 = average length of the rear gap (cm),

A_{g1} = area of the pole gap (cm²), A_{g2} = area of the rear gap (cm²)

μ_1 = initial permeability of the head core material at the frequency of operation.

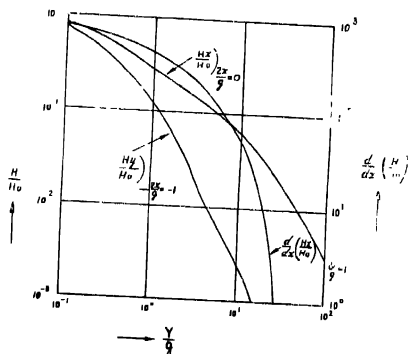


Fig. 6 Fringing field components H_x , H_y , and the gradient $\frac{\partial H_x}{\partial x}$,

The validity of the above equations was checked by Kostyshin and Roshon ((Kostyshin and Roshon 1959) with the help of a Hall-probe, the vertical component of the fringing field of a magnetic recording head with a .001 inch pole gap was mapped. The observed and calculated fields agreed to within 4%.

Equations (26) and (27) in terms of the above parameters can be written as

$$H_x(x, y) = -\frac{H_0}{\pi} \left\{ \tan^{-1} \left[\frac{1 + \frac{2x}{g_1}}{\frac{2y}{g_1}} \right] + \tan^{-1} \left[\frac{1 - \frac{2x}{g_1}}{\frac{2y}{g_1}} \right] \right\} \quad \dots (30)$$

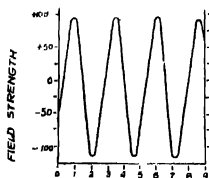
$$H_y(x, y) = \frac{H_0}{\pi} \left\{ \frac{\left(\frac{2y}{g_1}\right)^2 + \left(1 + \frac{2x}{g_1}\right)^2}{\left(\frac{2y}{g_1}\right)^2 + \left(1 - \frac{2x}{g_1}\right)^2} \right\} \quad \dots (31)$$

Maximum values of the fringing field components H_x , H_y , and the gradient $\frac{\partial H_x}{\partial x}$ at the point of inflection of the curve are shown in the Fig. 6.

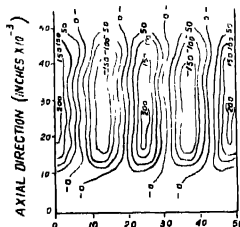
The point of inflexion of H_x and the \max^m value of H_y are assumed to occur at $x_1 = \frac{1}{2} g_1/2$, for all values of y

The analytical expressions for other two cases, μ greater than 1 but infinite layer thickness and μ greater than 1 and finite layer thickness can be deduced using Fourier's transform method, but for all practical purposes expressions (26) and (27) or (30) and (31) offer very good approximation (We are using spinel material of very low μ as our ferromagnetic layer)

It is seen that at a distance greater than one tenth of the pole gap, the intensity of the longitudinal (X) component is always greater than the vertical (Y) component. For a typical recording head at a distance equal to the pole gap the intensities of the longitudinal (X) and the vertical (Y) field components may be of the order of 1200 and 700 oersteds respectively. The 1200 oersteds field is sufficient to saturate any of the commonly used storage media in the longitudinal direction. Moreover, because of the shearing of the loop (Began, S. J.) in the vertical direction due to adverse demagnetization conditions, the 700 oersted



Direction of recording (inches $\times 10^{-3}$)
Fig. 7. Magnetic field strength normal to oxide recording media.



Direction of recording (inches $\times 10^{-3}$)
Fig. 8. Distribution of Magnetic field strength normal to the recording media, signal array continuous series of "ones" Isobars are in oersteds.

field is insufficient to saturate the medium in the vertical direction. So we take it for granted that the magnetization is predominantly of longitudinal nature. This statement was made by the author in a note presented to the Roorki Session of the Indian Science Congress (Dutta Majumdar, 1958) and has been demonstrated by Kostyshin and others (Kostyshin, Roshon etc., 1959) by mapping the fringing fields of signals stored on oxide and on nickel cobalt plated surfaces with a Hall probe and is reproduced here (Fig. 7 and 8). Before going into the more rigorous harmonic analysis and other things, we would like to show how most of the engineering design conditions are derived from the equations (26) and (27).

From (26) and (27) we can compute longitudinal and vertical components of magnetic flux vectors in the media as follows (Fig. 9) :

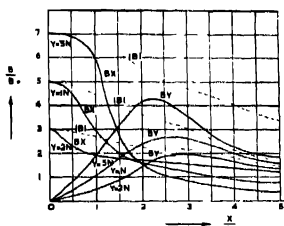


Fig. 9. Graphical plots of equations 32, 33, and 34.

We ha

$$B_x = \frac{B_0}{\pi} \left[\tan^{-1} \frac{N_+ X}{Y} + \tan^{-1} \frac{N_- X}{Y} \right] \quad \dots \quad (32)$$

$$B_{\theta} = -\frac{B_0}{2\pi} \left[\log \frac{Y^2 + (N-X)^2}{Y^2 + (N+X)^2} \right] \quad \dots (33)$$

$$|B| = \sqrt{B_x^2 + B_y^2} \quad \dots \quad (34)$$

COMPUTATION OF PLAYBACK VOLTAGE PULSE
FROM EQUATION (32)

Considering the idealised play back head to be a semi infinite block of high permeability material with the flat face at a distance b above the recording surface, the P , B , signal will be proportional to the rate of change of the X -component of the flux.

Using the method of images, the value of the flux density in the head can be shown to be the same as though the head filled all of space and the intensity of magnetization in the recording medium were $\frac{2\mu}{\mu+1}$ times the value actually present.

So,

$$B_x = -\frac{2\mu B_0}{\pi(\mu - 1)} \left[\tan^{-1} \frac{N}{Y} + \tan^{-1} \frac{N-X}{Y} \right] \quad \dots \quad (35)$$

If δ is the thickness of the medium the total flux per unit width will be

$$\phi_x = \int_{b+\delta/2}^{\bar{y}} B_x dy \quad \dots \quad (36)$$

The output voltage will be proportional to the rate of change of ϕ_x ; therefore,

$$e(x) = C' \frac{d\phi_x}{dt} = C' \frac{dx}{dt} \cdot \frac{d\phi_x}{dx} = v \cdot C' \frac{d}{dx} \int_{b+\delta/2}^{\infty} B_x dy$$

$$= v \cdot C' \int_{b+\delta/2}^{\infty} \frac{d}{dx} B_x dy \quad \dots (37)$$

$$e(x) = \frac{2\mu r B_0}{\pi(\mu + 1)} \int_{b+\delta/2}^{\infty} \left[\frac{y}{y^2 + (N+x)^2} - \frac{y}{y^2 + (N-x)^2} \right] dy.$$

$$= \frac{\mu r B_0}{\pi(\mu + 1)} \left[\log \frac{y^2 + (N+x)^2}{y^2 + (N-x)^2} \right]_{b+\delta/2}^{\infty}$$

$$\frac{\mu r B_0}{\pi(\mu + 1)} \cdot \log \left[\frac{\left(b + \frac{\delta}{2} \right)^2 + (N-x)^2}{\left(b + \frac{\delta}{2} \right)^2 + (N+x)^2} \right] \quad \dots (38)$$

where C' = constant of proportionality and V = velocity of the surface. The equation (38) if slightly modified as

$$e(x) = \frac{\mu r B_0}{\pi(\mu + 1)} \log \left[\frac{(b + \delta/2 - a)^2 + (N-x)^2}{(b + \delta/2 - a)^2 + (N+x)^2} \right] \quad \dots (39)$$

where 'a' is greater than '0' and is a recording constant which incorporates the magnetic properties of the medium. The above expression relates the playback voltage "e" from an ideal head with different physical parameters. These and their graphical plots can be used for design purposes. If the value of 'a' is determined indirectly, the maximum pulse amplitude and the pulse width at a certain clipping level can be determined.

Demagnetisation curve of layer material.

The portion of the hysteresis loop that lies in the second quadrant between residual induction, B_r , and coercive force H_c , is called demagnetization curve. The quantities most used in evaluating the quality of materials are H_c , B_r , and the products $H_c B_r$, $(BH)_m$, the latter being the maximum product of B and H for points on the demagnetization curve (-ve sign omitted). A given value of magnetic material will produce highest field in a given air space when the induction

B in the material is that for which the energy product BH is a maximum (Evershed, 1958).

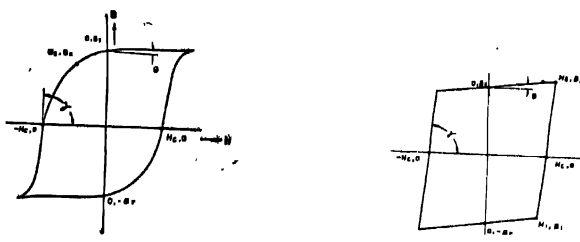


Fig 10. (a) A hysteresis loop, demagnetization curve approximated to a rectangular hyperbola, (b) hysteresis loop linearized to a parallelogram.

As an empirical mathematical relation the demagnetization curve can be simulated by a rectangular hyperbola (Bozorth, 1951) defined by three points $B_r(H = 0)$, (B_a, H_a) , $-H_c(B = 0)$ as shown in Fig. (10a)

The shape of the demagnetization curve between B_r and H_c is fixed by what is often called the fullness factor, defined by

$$\gamma = \frac{(BH)_m}{B_r H_c} \quad \dots (40)$$

and the squareness factor, S , defined retentively by the ratio of the B_r to the asymptotic magnetization predicted by the hyperbola and is given by the equation

$$S = \frac{m+h-1}{mh} \quad \dots (41)$$

where

$$m = \frac{B_a}{B_r}, \text{ and } h = -\frac{H_a}{H_c},$$

S is related to γ by

$$S = 1 - (\gamma - 1)^2 \quad \dots (42)$$

Using the general expression for a rectangular hyperbola

$$(x - x_0)(y - y_0) = C_0^2 \quad \dots (43)$$

and making substitutions and simplifications, the second quadrant of the hysteresis loop is given by the equation :

$$B = \frac{B_r(1 - H/H_c)}{1 - S(H/H_c)} \quad \dots (44)$$

The reversible permeability μ_2 , of the storage medium, considered constant (Westmijze, 1953), is defined by the slope of the hyperbola at the point $(0, B_r)$, where

$$\mu_2 = 1 + \tan \theta \quad \dots (45)$$

and
$$\tan \theta = \frac{B_r}{H_e} (1 - S) \quad \dots (46)$$

So it is seen that the reversible permeability μ_2 , is dependent on the squariness factor S . The slope of the hyperbola at the point $(H_e, 0)$ is given by the equation :

$$\tan \alpha = \frac{B_r}{H_e} \left(\frac{1}{1 - S} \right) \quad \dots (47)$$

Write process. For the write process only, we linearize the entire hysteresis loop to a parallelogram (fig. 10b), then the field intensities at the beginning and at the end are given by the equations :

$$H_1 = \frac{H_e}{2 - S}, \quad H_2 = \frac{H_e}{S} \quad \dots (48)$$

From the mathematical and physical analysis earlier we assumed the magnetization of the medium as predominantly longitudinal. In the mechanics of NRZ recording, the longitudinal component of magnetization may be represented by a trapezoid. The transition length of magnetization (Fig. 11) is equal to the average dynamic transition length b_d with a lower limit imposed by the static transition length b_s .

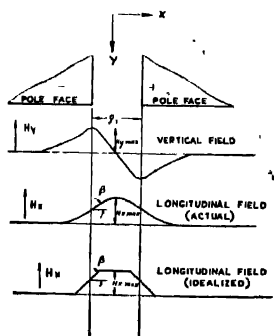


Fig. 11. Longitudinal component approximated to a trapezoid

The static transition length b_s is determined by the shape of the hysteresis loop of the layer material and the pattern of the fringing field at the pole gap.

And the dynamic transition length is determined by the time constants of the write circuitry, the relative velocity of the head and storage medium, and the reluctance of the head core.

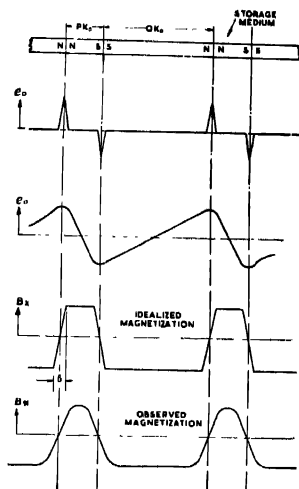


Fig. 12. A typical signal array where a succession of ones are separated by p and q 'bit' lengths.

For the typical signal array (Fig. 12) where a succession of ones are separated by p and q bit length, the resultant magnetization is described by the Fourier Series (Kostyshin, 1961) :

$$B = \sum_{n=1}^{\infty} B_0 \left\{ \frac{p-q}{p+q} + \frac{4}{n\pi} \cdot \sin \frac{n\pi}{1 + \frac{q}{p}} \cdot \frac{\sin \frac{n\pi b}{(p+q)K_0}}{\frac{n\pi b}{(p+q)K_0}} \cdot \cos \frac{2n\pi x}{(p+q)K_0} \right\} \dots (49)$$

The corresponding harmonic wave length and the equivalent harmonic frequency are defined by the equations :

$$\lambda_n = \frac{(p+q)K_0}{n} \dots (50)$$

$$f_n = \frac{nV}{(p+q)K_0} \dots (51)$$

Self Demagnetisation of the recorded signal.

As soon as the recording head is removed from the vicinity of the recorded cell, the boundary conditions change resulting in a demagnetizing field H_d and a quiescent magnetization B_d . During reading operation, the boundary conditions similar to those of Write process are re-established, and ideally at least the demagnetizing field is reduced to zero, and the resulting magnetization B_n (the initial magnetization considered for the Read process) is slightly lower than the retentivity of the storage medium. This is due to the nonlinear character of the hysteresis loop and the constancy of the reversible permeability of the medium.

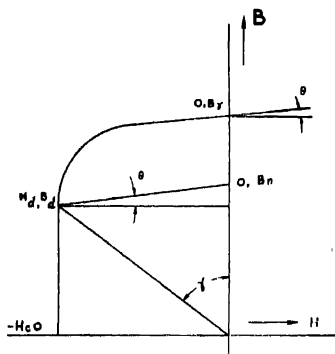


Fig. 13. Demagnetization curve.

It is a standard practice to define a demagnetization factor (Westmijze, 1953) as

$$D_n = \tan \gamma = - \frac{H_d}{B_d} \quad \dots \quad (52)$$

B_n is then determined by the values of H_d and B_d and by the angle defined by the reversible permeability of the storage medium as shown in Fig. 13 (Bozorth, 1951)

Assuming the magnetization to be constant throughout the depth the average demagnetization factor is defined by the equation .

$$D_n = \frac{\int_{b_1}^{b_1+d} D_n dy}{\int_{b_1}^{b_1+d} dy} \quad \dots \quad (53)$$

b_1 = head to storage medium distance during write process and d = layer thickness. D_n is determined from an expression for H_d and B_d similar to that given by Westmijze (Westmijze, 1953) which need not be treated here

The resultant initial harmonic magnetization after self-demagnetization is given by the equation (Kostyshyn, 1961) ·

$$B_n = H_e \left\{ \left[\frac{1 + \bar{D}_n(\mu_2 - 1)}{2SD_n} \right] \left[1 + D_n \frac{B_r}{H_e} - \left(1 + D_n \frac{B_r}{H_e} \right) \times \left(2 - 4S + D_n \frac{B_r}{H_e} \right)^{1/2} \right] \right\} \quad (54)$$

Process of play back :

The next problem obviously is to determine the total quantity of fringing flux of the stored bit in the cell that passes through the read coil when there is a reading operation. Westmijze (Westmijze, 1953) has described the loss term, assuming of course the head permeability as infinity and a non-zero head to layer spacing due to physical dimensions of the head to medium gap, the thickness of the medium and the reversible permeability of the medium. Total flux through the head coil can thus be determined which on differentiation gives the output voltage of the read coil. By considering an equivalent read circuit, the loading effect of the amplifier, the line and the stray capacitance of the read coil can be taken account of. Following the above logic, the expression for the head output voltage, for the signal array described by equation (49), is given by the equation ·

$$E_0 = \sum_{n=1}^{\infty} X_n Y_n C_n E_n L_n B_n \{ 4N_2 W V \} \sin \frac{n\pi}{1+g/p} \sin \frac{\pi}{\lambda_n} \left\{ X + \frac{g_1}{2} \right\} \cdot 10^{-8} \text{ volt.} \quad \dots (55)$$

where,

$$X_n = \frac{1}{1 + \frac{R_p}{R_{g_1}}} \quad R_p = \text{reluctance of the head core} \quad \dots (56)$$

R_{g_1} = reluctance of the head pole gap

$$Y_n = \frac{\sin \frac{\pi g_1}{\lambda_n}}{\frac{\pi g_1}{\lambda_n}} \quad \dots (57)$$

$$C_n = \frac{1}{n\pi} \left\{ \frac{\tanh \frac{\pi d}{\lambda_n}}{\cosh \frac{\pi b}{\lambda_n}} \cdot \frac{1 + \frac{1}{\mu_2} \tanh \frac{\pi d}{2\lambda_n}}{1 + \tanh \frac{\pi b_2}{\lambda_n} + \tanh \frac{\pi d}{\lambda_n} \left[\frac{1}{\mu_2} + \mu_2 \tanh \frac{\pi b}{\lambda_n} \right]} \right\} \dots (58)$$

$$E_n = \frac{\sin \frac{\pi b}{\lambda_n}}{\frac{\pi b}{\lambda_n}}, \dots (59)$$

$$L_n = \frac{1}{1 + \frac{Z_1}{Z_n}} \dots (60)$$

N_2 = No. of turns on read coil.

W = width of the head at pole tips (cm.).

V = relative velocity of head and storage medium (cm. per Sec.).

Z_1 = Load impedance of the read network (ohm).

Z_n = equivalent impedance of the read head (ohm).

The reluctance ratio R_p/R_{p1} is given in equation (29), from which X_n is known and the expression for B_n is given by equation (54). The above equations can be programmed for any Electronic Computer and can be applied to various head-recording media systems, and it is possible to study on an analytic basis the effect of varying single parameters of a system.

The case of one dimensional transient field.

In the ferromagnetic layer of a DRUM MEMORY switching the state of magnetization of the specified region on the memory drum surface is accomplished by reversing the direction of an electric current in the write coil of the magnetic recording head. In order to study the transient field associated with this phenomena, it can be assumed that a polarised electro-magnetic wave with the components H_x and E_z comes perpendicular to the ferromagnetic layer.

The electro-magnetic field must satisfy the Maxwell's fundamental equations, and so the corresponding differential equation can be derived from them.

We assume μ = permeability of the layer

K = constant

σ = conductivity of the layer (1/ohm-meter).

$\mu_0 = 4\pi 10^{-7}$ in MKS system = 1.257×10^{-6} (henry/meter)

E = electric intensity (volts/meter)

B = magnetic Induction (weber/meter)

D = electric displacement (coulombs/meter²)

H = magnetic intensity (amperes/meter)

J = current, density (amperes/meter²)

ρ = charge density (coloumbs/meter²)

Maxwells' Equations are :

$$\left. \begin{array}{l} \Delta \times E = - \frac{\partial B}{\partial t} \\ \Delta \times H = J + \frac{\partial D}{\partial t} \end{array} \right\} \begin{array}{l} \Delta \cdot B = 0 \\ \Delta \cdot D = \rho \end{array} \quad \dots \quad (61)$$

In a homogeneous isotropic medium we have the additional relations

$$D = KE, \quad B = \mu H, \quad \text{and} \quad J = \sigma E.$$

From the above relations we have,

$$\left. \begin{array}{l} \Delta \times E = \mu \frac{\partial H}{\partial t} \\ \Delta \times H = \sigma E \end{array} \right\} \quad \dots \quad (62)$$

We have $H_y = H_z = 0$, and $E_x = E_y = 0$,

$$\Delta \times H = \left| \begin{array}{ccc} i & j & K \\ \frac{\partial}{\partial x} & \frac{\partial}{\partial y} & \frac{\partial}{\partial z} \\ H_x & 0 & 0 \end{array} \right|$$

$$\therefore \frac{\partial H_x}{\partial z} = 0, \quad K \frac{\partial H_x}{\partial y} = K \sigma E_z.$$

And

$$\begin{aligned} \Delta \times E &= \left| \begin{array}{ccc} i & j & K \\ \frac{\partial}{\partial x} & \frac{\partial}{\partial y} & \frac{\partial}{\partial z} \\ 0 & 0 & E \end{array} \right| \\ &= i \frac{\partial E_z}{\partial y} - j \frac{\partial E_z}{\partial x} \end{aligned}$$

$$\text{but } \frac{\partial E_z}{\partial x} = 0,$$

$$\therefore \frac{\partial H_x}{\partial y} = \sigma E_z$$

and

$$\frac{\partial E_z}{\partial y} = \mu \frac{\partial H_x}{\partial t}$$

Therefore,

$$\frac{\partial^2 H_x}{\partial y^2} = \sigma \frac{\partial E_z}{\partial y} = \mu \sigma \frac{\partial H_x}{\partial t}$$

In rationalised M.K.S. system

$$\frac{\partial^2 H_x}{\partial y^2} = \sigma \mu \mu_0 \frac{\partial H_x}{\partial t} \quad \dots (63)$$

The non-stationary one dimensional field can be computed from equation (63) which is a parabolic differential equation and will be solved using Laplace's transforms.

The equation (63) is to be solved for infinite layer and for finite layer.

Infinite layer : The wave is applied suddenly at $t = 0$, and the air gap b is assumed to be zero. The initial value problem is .

$$H_{(0,t)} = H_0, \quad H_{(\infty,t)} = 0, \quad H_{(y,0)} = 0.$$

(X - coordinate has been replaced by y)

[Laplace transform $f(p)$ of the function $F(t)$ is defined by

$$f(p) = \int_0^\infty e^{-pt} F(t) dt]$$

Then the Laplace transform of the equation (63) can be written as

$$h = \frac{H_0}{p} e^{-ky\sqrt{p}}, \quad K^2 = \sigma \mu \mu_0.$$

The corresponding time function is

$$H_{y,t} = H_0 \operatorname{erfc} \cdot y \sqrt{\frac{\sigma \mu \mu_0}{4t}} \quad \dots (64)$$

is defined by the equation

$$\operatorname{erfc} x = 1 - \operatorname{erf} x = \frac{2}{\sqrt{\pi}} \int_0^x e^{-t^2} dt.$$

Finite layer thickness : While considering this case we have to assume that the Z -component of electric intensity, E_z , is continuous on the other side of the

layer, that is, at the point $y = d$, then if σ_1 and σ_2 represent conductivities of the layer material and drum material respectively

$$\lim_{y \rightarrow d-0} \sigma_2 \frac{\partial H}{\partial y} = \lim_{y \rightarrow d+0} \sigma_1 \frac{\partial H}{\partial y}.$$

$$y \rightarrow d-0 \qquad y \rightarrow d+0$$

The conductivity of the ferromagnetic layer material σ_1 can be considered as zero in comparison with that of the drum material (usually brass).

We have the Laplace transform

$$h = H_0 \frac{e^{-(y-d)K/\sqrt{p}}}{\cosh Kd\sqrt{p}}$$

and the corresponding time function is,

$$H_{(d,t)} = 2H_0 \sum_{n=0}^{\infty} (-1)^n \operatorname{erfc} \left[(2n+1)d\sqrt{\frac{\sigma\mu}{4t}} \right] \quad \dots (65)$$

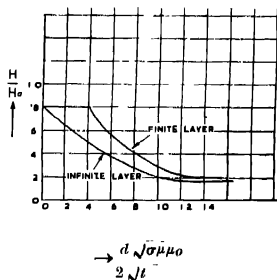


Fig. 14. Magnetic field in transient case.

From these two cases one can compute the transient time of the layer material, and their dependence on σ , μ , and d .

EXPERIMENTAL INVESTIGATION

In order to carry out a thorough investigation on the problems and limitations associated with arriving at a wholly rational design of a magnetic drum store, an experimental magnetic drum unit was designed, constructed, coated, and finished by ourselves in our Laboratory. The engineering description, the drum coating technique, and its digital data recording and reproduction techniques were described earlier (Dutta Majumdar, 1961).

For experimental purposes, factors that affect pulse resolution should be broadly classified as (a) frequency dependent factors and (b) wavelength dependent factors. Frequency dependent factors in pulse recording are (1) recording current and flux rise time, (2) frequency response of the amplifiers, (3) frequency response of the magnetic heads. It is obvious that the frequency dependent factors can be made very negligible. Wave length dependent factors are considered to be more basic with respect to the recording and reading out of the pulses and here the results of the theoretical investigations presented earlier are of great help. In our magnetic model of Write-Read process using saturation type recording we have explained that the process consists in (1) switching of the state of magnetization, (2) self-demagnetization of the recorded signal and (3) playback of the recorded signal. It has been explained in an earlier publication (Dutta Majumdar, 1959) how the variables involved in the process are interrelated in a complex manner. For the clarity of the concept the variable factors can be combined and grouped as (1) Recording process limitations and (2) Playback process limitations. The limitations due to magnetic characteristics of the layer surface are of course, involved in both.

RECORDING PROCESS LIMITATION

Several important limitations of recording process are associated with what is known as Record-Head Trailing Effect, which is commonly defined as the demagnetization of the surface still within the field of the head as it changes polarity.

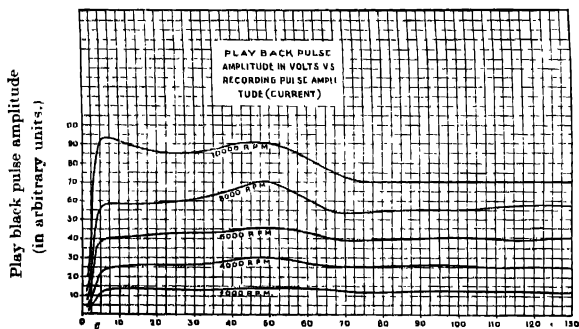


Fig. 15. Variation of P.B. Pulse amplitude (volts) with recording pulse amplitude (current).

In Fig. 15 the variation of P.B. pulse amplitude with recording pulse amplitude is plotted. If the field gradient across the record head had no influence on the flux pattern, one would expect the pulse width and amplitude to remain constant after saturation. But it is seen that they are dependent on recording current. The increase in pulse width and decrease in amplitude may be attributed to the

“record-head trailing effect.” At the moment of flux reversal in the head, all particles under the trailing pole face are magnetized to a varying degree dependent on the gradient across the head. The actual field pattern in the coating will

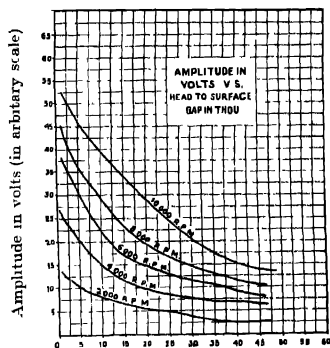


Fig. 16. Variation of P.B. pulse amplitude with head-to-surface gap (in thou.).

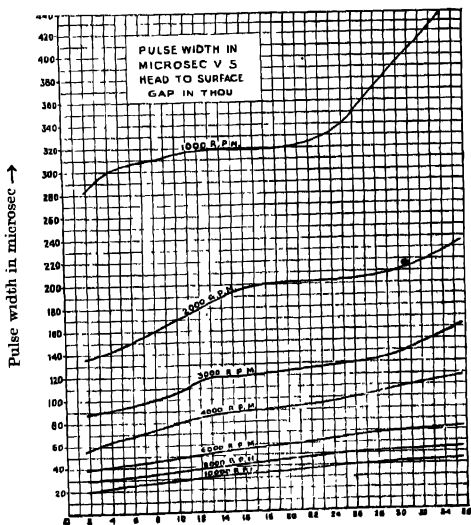


Fig. 17. Variation of P.B. pulse width in microsecond with head-to-surface gap (in thou.);

depend on the permeability of the material saturated to a constant value at distances from the gap. This record head trailing effect is dependent on the $B-H$ characteristics of the medium, recording current, coating thickness, head to medium separation and gap width of the record head

In Figs. 16 and 17 variation of P.B. pulse amplitude and width with Head to Surface gap are plotted for different speeds. In amplitude versus head to surface gap curves it is seen that at higher speeds it tends to become linear. In Fig. 17 it is seen that the pulse width increases with gap distance, at lower speeds the rate of increase is sharper than at higher speeds. It is seen that at 8000 r.p.m. and above, the P.B. pulse amplitude is much less affected by gap variation.

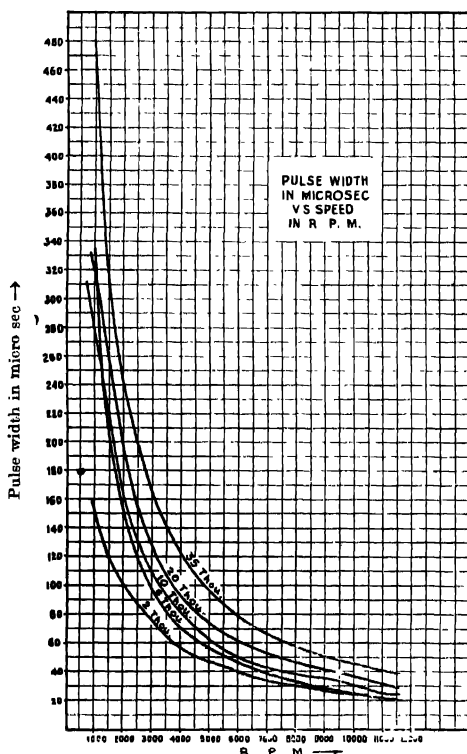


Fig. 18. Variation of P.B. pulse width in microsec. with rotational speed in r.p.m.,

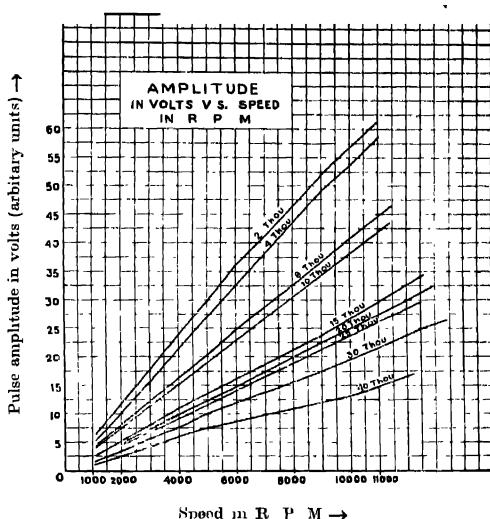


Fig. 19. Variation of P.B. pulse amplitude with rotational speed in

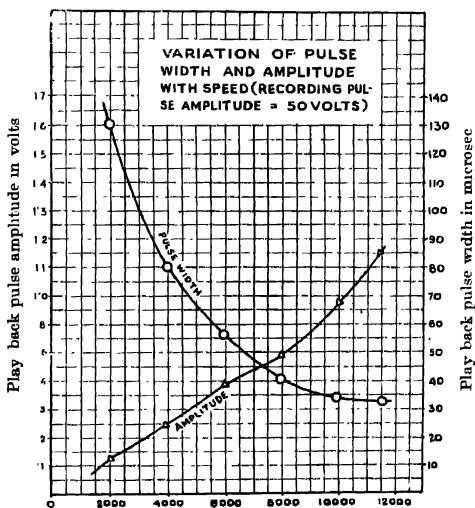


Fig. 20. Variation of P.B. pulse amplitude and width, with speed in r.p.m. (for a constant recording pulse amplitude).

Pulse width in microsecond versus rotational speed in r.p.m. is plotted in Fig. 18. The curves seem to approximate rectangular hyperbola. Here also it is seen that the effect of speed variation on playback pulse width is much less affected at speed above 8000 r.p.m. In Fig. 19 and 20 where variation of pulse width and amplitude with rotational speed is plotted, the amplitude is seen to rise linearly with speed.

Effect of recording mmf.

The position of maximum flux gradient is the effective recording point, which will depend on the magnetic medium and the recording field strength. We can see it from our theoretical results that the relative distribution of the horizontal and vertical components of the magnetization will depend on the recording field strength and the coating thickness. It has been observed experimentally that a current greater than that required to saturate the surface results in reduction in amplitude and increase in pulse width and consequent loss of resolution. It has been shown earlier in connection with equations (30) and (31) that the longitudinal component is responsible for recording. But if the recording current is increased beyond the saturation current the vertical component becomes predominant, which results in a shift of the effective recording point further away from the centre of the gap, and increases the total distance over which the flux is changing, which obviously results in the increase of pulse width and loss of resolution.

Effect of recording head gap width.

This effect is same as that of the effect of the trailing field gradient as explained earlier. If the gap width is very small, the field gradient will be greater at the pole face surface which will enable us to use a very thin magnetic coating which is desirable from many other considerations. Naturally for thick coatings a wider gap will be desirable to set up a sufficiently strong field to saturate those particles some distance from the pole face. In a nutshell the optimum record head gap will depend on the coating thickness, the $B-H$ characteristics of the layer surface and the separation between the record head and layer surface.

Effect of separation between record head and layer surface :

With increase in separation the layer surface is subject to a diminished recording field gradient, which will widen the flux distribution resulting in the loss of resolution. This loss can be minimised by using a coating with a rectangular $B-H$ characteristics, and by designing a record head that gives maximum field gradient for the particular separation being used.

Effect of magnetic characteristics of the coating material .

Earlier we have tried to explain, on theoretical grounds, the demagnetization curve of the layer material, (equations 40 through 47) and, self-Demagnetization of the recorded signal (equations 52, 53, 54). Now we apply the term "self-

demagnetization effect" to pulse widening caused by the field within the coating. The field in the coating due to the volume element dv will be $dH = \frac{\text{Div } I \, dv}{r^2}$ where I is the intensity of magnetization, $\text{Div } I$ is the "volume density of magnetic charge" and r is the distance from the volume element dv to the point (x, y, z) in the coating. The total field at (x, y, z) will be

$$H = \int \frac{\text{Div } I \, dv}{r^2} \quad \dots (66)$$

This field within the coating will act on the particles and tend to reorient the particles and thereby reduce the resolution. This effect can be reduced by using a coating material with high coercivity to remanence ratio which will minimize reorientation of particles, and having a rectangular $B-H$ loop characteristics. The demagnetizing field is less with thin coating than with thick coating. Thus from all considerations a considerable improvement w.r.t. resolution is achieved with nearly rectangular hysteresis loop material and a thin coating

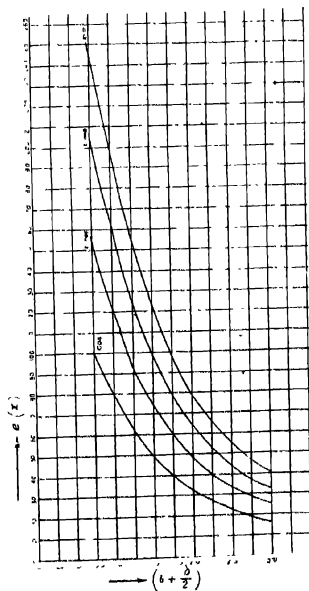


Fig. 21. Computation of P.B. voltage from equation (38) for different physical parameters.

PLAYBACK PROCESS LIMITATIONS

An expression was derived earlier (equation 38), showing how the P.B. signal characteristics depend on coating thickness, head to medium separation and a recording constant (a computed plot of equation 38 is given in Fig. 21). And another expression for the head output voltage, for the signal array using NRZ recording, and described by equation (49) was given by the equation (54) using harmonic analysis. A detailed analysis of the playback process limitations from these deductions will not be attempted here to keep the size of the paper within a reasonable limit, only the salient features will be stated. Theoretical and experimental findings on pulse width and amplitude as a function of separation between P.B. head and layer surface agree well, and the difference may be attributed to the self-demagnetization and record head trailing effects which are dependent on coating thickness.

Effect of p.b. head gap width.

It can be stated from physical reasonings that the sensitivity contour of the P.B. head should be wide and sharply defined enough to be able to intercept as much flux as is possible during reading operation from the recorded spots. The total flux intercepted by the head will be

$$\phi_d = \int_{x-\omega/2}^{x+\omega/2} \phi_e dx$$

Therefore,

$$e_x = K \frac{d}{dx} \int_{x-\omega/2}^{x+\omega/2} \phi_x dx \quad \dots (67)$$

where K is proportionality constant involving number of turns in the head, surface speed and all other variables including ω , (ω = width of the P.B. head sensitivity contour). Using the formula of Leibnitz, (67) becomes

$$e_x = K[\phi_{x+\omega/2} - \phi_{x-\omega/2}] \quad \dots (68)$$

The maximum signal amplitude is

$$e_{max} = e_0 = K[\phi_{\omega/2} - \phi_{-\omega/2}]$$

But

$$\phi_{\omega/2} = \phi_{-\omega/2} \therefore e_{max} = 2K\phi_{\omega/2}$$

For pulse width at N per cent of the peak amplitude the following equation must hold

$$0.02N\phi_{\omega/2} = \phi_{x_N+\omega/2} - \phi_{x_N-\omega/2} \quad \dots (69)$$

x_N is the head position where the amplitude has dropped to N per cent of the peak value. The solution for $2x_N$ will give pulse width as a function of gap width.

But the above equation can not be solved directly as ϕ is a transcendental function. The equation can be solved graphically for particular systems. One point should be marked here is that the effective gap width is not necessarily the physical gap width. And the effective gap width is to be determined, by measuring the wavelength where the 1st minima in signal occurred (Bagun, 1955). So if the pulse width is not to exceed certain limit of an absolute minimum, the effective gap width for the system can be determined. In general, it would be desirable to use the largest gap width consistent with satisfactory performance.

CONCLUSIONS

A comprehensive theoretical and experimental investigation on digital data recording and reproduction on and from ferromagnetic layer surface of magnetic drum memory has been presented. The boundary value problem has been solved to find the distribution of the fringing field in the ferromagnetic layer surface. Analytic expressions for the output of a Write-Read system employing saturation recording on a magnetic medium in terms of the basic system parameters have been presented.

The variables involved in the process of pulse recording on a moving magnetic surface and their influences were experimentally studied with a practical magnetic drum storage system, which has special features for studying the influence of different parameters.

Both theoretical and experimental investigations, and physical analysis of the factors involved in the process lead to the conclusion that the following are the basic requirements for achieving high resolution pulse recording on magnetic surface :

- 1) Recording pole face configuration for having maximum flux gradient on the surface for a particular head to medium separation.
- 2) Rectangular B - H loop characteristics of the coating material to reduce the record head trailing effect and the self-demagnetization effect.
- 3) High ratio of H_c to B_r to reduce the self-demagnetization effect.
- 4) Optimum recording current.
- 5) Minimum coating thickness consistent with satisfactory operation to reduce the record head trailing effect, self-demagnetization effect, and loss of resolution in the P.B. process.
- 6) Minimum head to coating separation to reduce record head trailing effect and loss of resolution in the P.B. process.
- 7) Largest effective gap width which will give required resolution for the particular coating, record head and head to coating separation so that tolerances involved in the construction of the head can be relaxed and the performance characteristics made more uniform.

ACKNOWLEDGMENT

The author wishes to thank Sri S. K. Mitra, Head of the Computer Development and Research Division, I.S.I., for his kind interest in the work, Sri K. M. Patnaik, for his arduous assistance in the work, Sri S. Basu and Sri. R. Biswas, for their help in carrying out the experiment and Sarbasree Ambarish Ghosh, Dipak Dutta and Mohit Roy, for their help in doing numerical calculations in the electronic computer HEC2M. The author is indebted to Professor J. N. Bhar, Head of the Institute of Radio Physics and Electronics, for his help and encouragement in doing the work. The author also wishes to express his gratitude to Professor P. C. Mahalanobis, Director of the Institute, for providing funds for the research projects.

REFERENCES

- Begun S. J., 1949, "Magnetic Recording, Murray Hill Books Inc.
 Bigelow, J. H. and others, 1948, 'First Progress Report . . . I.A.S. Princeton.
 Booth, A. D., 1949, July, *Electronic Engineering*.
 Booth, A. D., 1952, *Brit. Jour. Appl. Phys.*, **3**.
 Bozorth, R. M., 1951, "Ferromagnetism pp. 351-53.
 Byerly, W. E., "Fourier's Series and Spher. and Ellips Harmonics, Grinn and Company.
 Dutta Majumdar D., 1958, *Electronic Engineering*, 702-5.
 " " " 1959, *J. Inst. Telecomm. Engrs.*, **5**, **4**, 211-22.
 Dutta Majumdar D., 1961, *Proc. Ind. Sc. Congress, Roorkee, Session*.
 " " " 1961, *J. Inst. Telecomm. Engrs.*, **7**, **1**, 27-36 ;
 " " " and Biswas, R. 1962 (Communicated) I.G.P.
 Evershed, E., 1958, *J.I.E.E.*,
 Karlqvist, O., 1954, *T. R. I. T.*, Sweden.
 Kostyshyn, B., 1961, *IRE Conv. Proceedings*
 Kostyshyn, B., Roshon, D., 1959, *Proc. IRE.*, **47**, 451.
 Wallace, R. L., Jr., 1951, *B. S. T. J.*, **30**, 1146-73.
 Westmijze, W. K., 1953, Philips Research Report, Vol. 8.

INFLUENCE OF PERMANENT ELECTRIC MOMENT ON THE ABSORPTION SPECTRA OF POLAR ORGANIC MOLECULES IN THE CRYSTALLINE STATE

S. C. SARKAR

OPTICS DEPARTMENT, INDIAN ASSOCIATION FOR THE CULTIVATION OF SCIENCE, CALCUTTA-32

(Received, December 18, 1962)

ABSTRACT Expressions for the energies of interaction of the three components of the transition moment of a polar molecule along three rectangular axes in the crystal with the permanent dipoles of the nearest neighbours have been derived. It has been shown that as these energies of the three components are different from each other the absorption band is expected to be split up into three components, as observed experimentally in many cases.

INTRODUCTION

It has been pointed out earlier (Sirkar, 1961) that the ultraviolet absorption spectra of many aromatic polar molecules in the crystalline state show splitting of individual bands into three components. It was suggested that this splitting might be due to interaction between the transition moment of the molecule and the permanent dipoles of the surrounding molecules. An attempt has been made in this note to explain in more detail how such splitting originates.

In Davydov's theory (Davydov, 1948) of factor group splitting in the case of crystals like those of anthracene or naphthalene belonging to the space group C_{2h}^{2h} with two centrosymmetrical molecules per unit cell, two wave functions of the unit cell are given by

$$\gamma^a = \frac{1}{\sqrt{2}}(\psi_1 + \psi_2)$$

$$\gamma^b = \frac{1}{\sqrt{2}}(\psi_1 - \psi_2),$$

where ψ_1 and ψ_2 are respectively the wave functions of the crystal when the first and the second molecule in a particular unit cell are excited.

The wave function of the whole crystal is built up with the help of γ^a and γ^b for individual unit cells using the expression given by Seitz (1936) as the suitable representation of the translational group. Denoting the wave function of the k -th representation by $\phi^{a,\beta}(k_a, k_b, k_c)$ corresponding to $\gamma^{a,\beta}$, we have

$$\phi^{a,\beta}(k_a, k_b, k_c) = \frac{1}{\sqrt{N/2}} \sum_{\mu, \nu, \omega} e^{i(k_a a \mu + k_b b \nu + k_c c \omega)} \gamma^{a,\beta}_{(\mu, \nu, \omega)} \dots \quad (2)$$

where k_a, k_b, k_c are the resolved parts of the wave vector along the crystal axes and μ, ν, ω are the number of translations along a, b, c axes required to reach the unit cell under consideration. Here the summation is to be taken over the unit cells in the crystal. Putting this expression for $\phi^{\alpha\beta}(k_a, k_b, k_c)$ in the Schrödinger equation and obtaining suitable Hermitian scalar products, the expression for the excitation energy of the crystal corresponding to the wave function ϕ^α of the crystal is given by

$$\begin{aligned} \Delta E^\alpha = & w'_p - w_p + D + C + \sum_{l \neq p} \langle \phi'_p \phi_l | V_{pl} | \phi_p \phi'_l \rangle \\ = & \Delta w_p + D + C + I_{pl} \end{aligned} \quad (3)$$

where
$$D = \sum_l \langle \phi'_p \phi_l | V_{pl} | \phi'_p \phi_l - \phi_p \phi_l | V_{pl} | \phi_p \phi_l \rangle, \quad (4)$$

I_{pl} is the resonance interaction integral, w'_p and w_p are the excited state and ground state energies of the p -th molecule in the vapour state, all the other molecules being in the ground state, ϕ'_p and ϕ_p are the corresponding wave functions of the molecule, V_{pl} is the potential energy operator for the interaction between the p -th and l -th molecules, the summation being taken over all the molecules except the p -th one, and C is the energy of interaction between the two molecules of the unit cell.

Similarly,

$$\Delta E^\beta = w'_p - w_p - C + D + I_{pl}' \quad (5)$$

So,
$$\Delta E^\alpha - \Delta E^\beta = 2C + I_{pl} - I_{pl}' \quad (6)$$

In Davydov's theory applied to the crystal of anthracene it has been assumed (Craig and Hobbins, 1955) that the transition moment in the plane of the molecule in the unit cell can be resolved along the b -axis and in the ac plane of the crystal, respectively and that the former component corresponds to the wave function ϕ^β and the latter to ϕ^α . The splitting between these two components is given by Eqn.(6). It has been pointed out earlier (Sirkar, 1961) that when the value of the oscillator strength f is very small the fourth term in Eqn. (3) produces the splitting only with a shifted component having negligible intensity.

An attempt is now made to calculate the interaction of neighbouring permanent dipoles on the transition moment of polar molecules in the crystalline state by applying Davydov's theory in a modified form.

Davydov's theory extended to polar molecules

According to Davydov's theory the second term D in the expression for the excitation energy (Eqn. 3) gives the difference between the integral of interaction of a molecule in the excited state with all the other unexcited molecules in the crystal and the interaction between the molecule in the ground state and all other

unexcited molecules. The value of D remains the same for both the wave functions ϕ^a and ϕ^b . Hence, the corresponding components of the band being shifted by the same amount by this term, no splitting is produced by these interactions. If it is assumed that the molecules in the crystal have permanent dipoles, the interaction between the transition moment of any molecule and all other molecules in the lattice is to be taken into consideration. As pointed out earlier (Sirkar, 1961) the expression for the interaction between two transition moments can be modified to obtain the interaction between a neighbouring permanent moment and the transition moment. This interaction I is given by

$$I = -e \frac{|M_k| \mu_l}{r_{kl}^3} \{ 2 \cos \theta_{lx} \cos \theta_{lr} - \cos \theta_{ly} \cos \theta_{ky} - \cos \theta_{lz} \cos \theta_{kz} \} \quad (7)$$

where μ_l and $|M_k|$ are respectively the permanent moment of the l -th molecule and the transition moment of the k -th molecule, r_{kl} is the distance between the molecules θ_{lx} , θ_{ly} , θ_{lz} are the angles made by the dipole with r_{kl} and two other rectangular axes perpendicular to r_{kl} and θ_{ky} , θ_{kz} are the angles made by transition moment with r_{kl} and two other axes parallel to the y and z axes mentioned above.

Taking the case of a monoclinic crystal with the dimensions a , b , c and β of the unit cell and assuming that the transition moment can be resolved into three components $|M_x|$, $|M_y|$ and $|M_z|$ along the directions of $a \cos \beta$, b - and c -axes, the interaction I_x between $|M_x|$ and the permanent dipoles of the nearest translationally equivalent molecules calculated from Eqn. (7) is given by

$$I_x = -e |M| \mu \cos \theta_1 \cos \theta_1' \left\{ \frac{2 \cos^2(\beta - 90^\circ)}{a^3} - \frac{1}{b^3} - \frac{1}{c^3} \right\} \quad \dots \quad (8)$$

Here θ_1 , θ_2 and θ_3 are the angles made by the transition moment and θ_1' , θ_2' and θ_3' are those made by the permanent dipole with the directions of $a \cos \beta$, b -axis and c -axis respectively. Similarly, the interaction between the component of $|M_y|$ along the b -axis and the nearest neighbouring dipoles is given by

$$I_y = -e |M| \mu \cos \theta_2 \cos \theta_2' \left\{ \frac{2}{b^3} - \frac{1}{a^3} - \frac{1}{c^3} \right\} \quad \dots \quad (9)$$

and

$$I_z = -e |M| \mu \cos \theta_3 \cos \theta_3' \left\{ \frac{2}{c^3} - \frac{1}{a^3} - \frac{1}{b^3} \right\} \quad \dots \quad (10)$$

It is evident from Eqns.(8), (9) and (10) that the interactions of the different components of the transition moment with the permanent dipoles of the nearest neighbours are different from each other. Hence, these components in the ab-

sorption spectra are expected to be separated from each other, the magnitude of separation depending on the differences of the axial lengths of the unit cell and the orientations of $[M]$ and μ with respect to the axes.

If there be two molecules in the unit cell, the interactions $I'_x I'_y$ and I'_z between the components $|M_x|$, $|M_y|$ and $|M_z|$ of the first molecule with the permanent dipole of the second molecule are to be added to I_x , I_y and I_z respectively and it is evident that interactions $(I_x + I'_x)$, $(I_y + I'_y)$ and $(I_z + I'_z)$ will be quite different from each other.

ACKNOWLEDGMENT

The author's thanks are due to Professor D. Basu for many helpful discussions.

REFERENCES

- Craig, D. P. and Hobbs, P. C., 1955, *J. Chem. Soc.*, p. 539.
Davydov, A. S., 1948, *J. Exp. Theor. Phys.*, **18**, 210.
Satz, F., 1936, *Ann. Math.*, **37**, 17.
Sirkar, S. C., 1961, *Proc. Nat. Inst. Science, India*, **27A**, 568.

LATTICE ENERGY OF ALKALI HALIDES

S. CHATTERJEE

DEPARTMENT OF GENERAL PHYSICS AND X-RAYS,
INDIAN ASSOCIATION FOR THE CULTIVATION OF SCIENCE, CALCUTTA-32.

(Received December 18, 1962)

ABSTRACT. Lattice energy of the alkali halides has been calculated by assuming the potential function in the form

$$\phi(r) = -\frac{\alpha e^2}{r} + \frac{B}{r^n} - \frac{C}{r^6} - \frac{D}{r^8} + \epsilon_0$$

where the index n and the constant B have been determined from the equilibrium conditions and the experimental data on the compressibility and the inter-ionic distance. The values of ϕ for the alkali halides are found to be very close to the experimental values as well as to the values calculated from the exponential form of the potential function. The values of compressibility and thermal expansion are also calculated and the agreement with the experimental values is excellent.

INTRODUCTION

The theory of ionic crystals was first developed by Born and later extended by Born and Mayer (1932) and several others. The interaction energy consists of an attractive and a repulsive term in addition to the Coulomb term. The most widely used forms for the repulsive potential are an exponential variation with the distance or simply an inverse power variation. Results of quantum-mechanical calculation favour the exponential form whereas the inverse power form has the advantage of greater simplicity. The former was utilised by Born and Mayer (1932), Huggins (1937), Cubicciotti (1959) and others, but is extremely cumbersome to use. It is, therefore, worthwhile to find out whether the simpler inverse power law is equally satisfactory.

In an ionic crystal the inverse power law appears to be a good choice because there the distance between two ions does not vary widely. In fact the inter-ionic distance will be near about that corresponding to the potential minimum. The energy per cell in an ionic crystal may be therefore represented as

$$\phi(r) = -\frac{\alpha e^2}{r} + \frac{B}{r^n} - \frac{C}{r^6} - \frac{D}{r^8} + \epsilon_0 \quad \dots (1)$$

where α is the Madelung's constant, e the electronic charge, r the interionic distance and B the repulsive parameter. C represents the van der Waal attraction, D the dipole-quadrupole interaction and ϵ_0 is the zero-point vibrational energy.

B and n are to be found out from the equilibrium relations (Born and Huang, 1954).

$$r \left(\frac{d\phi}{dr} \right)_{r=r_0} = \frac{3eT}{\beta} \left(\frac{1}{V} \frac{\partial V}{\partial T} \right)_P \quad \dots (2)$$

$$r \left(\frac{d^2\phi}{dr^2} \right)_{r=r_0} = \frac{9v}{\beta} F_{T,P} \quad \dots (3)$$

where

$$F_{T,P} = 1 + \frac{T}{\beta} \left(\frac{\partial \beta}{\partial T} \right)_P + \frac{T}{\beta^2 V} \left(\frac{\partial V}{\partial T} \right)_P \left(\frac{\partial \beta}{\partial P} \right)_T + \frac{2T}{3V} \left(\frac{\partial V}{\partial T} \right)_P$$

and β is the compressibility. If V is the molar volume, then $v = V/N = Kr^3$ in which K is a constant that is characteristic of the type of the lattice.

Recently, Sharma and Mudan (1961) have assumed the value

$$\phi(r) = -\frac{\alpha e^2}{r} + \frac{B}{r^{12}} - \frac{C}{r^6}.$$

They argued that in ionic crystals the ions are of the same electronic structure as the inert gas molecules and therefore it is possible to describe a number of properties of ionic crystals with the help of Lennard-Jones (12, 6) potential in conjunction with the Coulomb energy. They have calculated only for a few alkali halides and the results are none too satisfactory when compared with the experimental values. The assumption of the value 12 for the index is, however, open to question as Born found the value 9 to be more satisfactory with n actually varying from 6 to 12. Born, however, did not take the attraction terms involving the inverse powers 6 and 8. Therefore, we thought it desirable to include the attraction terms also in the Born expression to find out a better value of n from the experimental data and see if it is permissible to take $n = 12$ in conformity with the well-known Lennard-Jones potential

CALCULATION OF THE POTENTIAL PARAMETERS B AND n .

From (1) we can write

$$r \frac{d\phi}{dr} = -\frac{\alpha e^2}{r} - \frac{n\beta}{r^n} + \frac{6C}{r^6} + \frac{8D}{r^8} \quad \dots (4)$$

$$r^2 \frac{d^2\phi}{dr^2} = -\frac{2\alpha e^2}{r} + \frac{n(n+1)B}{r^n} - \frac{42C}{r^6} - \frac{72D}{r^8} \quad \dots (5)$$

Thus combining (2) and (3) with (4) and (5) we get

$$n = \frac{9Kr^3}{\beta} F_{T,P} \left[\frac{2\alpha e^2}{r} + \frac{42C}{r^6} + \frac{72D}{r^8} - \frac{\alpha e^2}{r} + \frac{6C}{r^4} + \frac{8D}{r^6} - \frac{3kr^3}{\beta} \left(\frac{T}{V} \frac{\partial V}{\partial T} \right)_P \right]^{-1} \quad \dots (6)$$

$$B = \frac{r^n}{n} \left[\frac{\alpha e^2}{r} + \frac{6C}{r^6} + \frac{8D}{r^8} - \frac{3Kr^3}{\beta} \frac{T}{V} \left(\frac{\partial V}{\partial T} \right)_P \right]. \quad \dots (7)$$

The experimental values for the inter-ionic distances were obtained from N. B. S. Circ. (1953-1957) excepting LiI and RbF whose values were taken from M. L. Huggins (1937). The experimental values of compressibility were taken from K. Spangenberg (1956), K. Spangenberg and S. Haussühl (1957) and Bridgeman (1940). Values of C , D were taken from Mayer (1933). Using these values n is found out from Eq. (6).

The values so obtained are recorded in column 3 of Table I, along with the values obtained by Born. It will be seen that the values of n now lie in a much closer range (from 6.43 to 10.66). The values for CsCl structure are seen to be higher than those for NaCl structure. Further in the NaCl structure, it increases slightly as we pass from Li to Rb, i.e., as the radius of the alkali ion increases. It also increases slightly with the increase of the radius of the halogen ion, but the increase with the positive ion radius is more marked.

CALCULATION OF THE CRYSTAL PROPERTIES

(a) Lattice energy

Once the parameters B and n are calculated it remains only to know the zero point energy ϵ_0 . The Van der Waal's constants C and D were estimated by Mayer (1933) by careful analysis of optical data. These were tabulated by Huggins (1937). This has been calculated by Cubicciotti (1959, 1961).

TABLE I

Substance	Value of n (Born)	n from Eq. (6)	Substance	Value of n (Born)	n from Eq. (6)
Li F	6	6.43	Rb F	8.5	8.37
Cl	7	6.92	Cl	9.5	9.59
Br	7.5	7.33	Br	10.0	9.75
I	8.5	7.87	I	11.0	10.49
Na F	7	6.59	Cs F	9.5	8.90
Cl	8	8.68	Cs Cl	10.5	10.66
Br	8.5	8.60	Br	11.6	10.47
I	9.5	9.07	I	12.0	10.28
K F	8	7.79			
Cl	9	8.93			
Br	9.5	9.36			
I	10.5	9.6			

The individual terms in Eq. (1) have been calculated for $r = r_0$, the equilibrium ionic distance. These terms are summed up and recorded in Table II, along with the experimental values and also the theoretical values calculated by other workers.

It will be seen that the values obtained are almost as good as those obtained by Cubicciotti by using the exponential form which involves complicated calculations.

(b) *Crystal compressibilities:*

From the knowledge of B, n, C, D we can calculate the crystal compressibilities which can be compared with the observed values. From equation (3) we have

TABLE II

Substance	Value of n	Lattice energy in K cal/mole			
		Present work	Experimental	Calculated by Mard H	Calculated by Cubicciotti
Li F	6.43	240.0		240.1	246.8
	6.02	198.7	198.1	199.2	202.0
	7.33	188.12	180.3	188.3	190.7
	7.87	175.3	181.1	174.1	176.8
Na F	6.59	217.4		213.4	218.7
	8.68	187.2	182.8	183.1	185.9
	8.60	176.7	173.3	174.6	176.7
	9.07	164.9	166.4	163.9	164.9
K F	7.79	194.5		189.7	194.4
	8.93	168.0	164.4	165.4	169.4
	9.36	162.4	156.2	159.3	162.4
	9.60	152.7	151.5	150.8	153.0
Rb F	8.37	187.2		181.4	185.9
	9.59	163.4	160.5	160.7	164.0
	9.75	156.7	153.3	153.5	157.5
	10.49	148.9	149.0	145.3	148.7
Cs F	8.96	178.0		173.7	178.7
Cs	10.66	156.2	155.1	152.2	155.9
	10.47	150.2	148.6	146.3	151.1
	10.28	141.1	145.3	139.1	143.7

$$\beta = 9Kr^3 F_{T,P} / \left[-\frac{2\alpha e^2}{r} + \frac{n(n+1)B}{r^n} - \frac{42C}{r^6} - \frac{72D}{r^8} \right] \quad \dots (8)$$

The quantity $F_{T,P}$ was calculated at $T = 298^\circ\text{K}$. The values of β thus obtained are given in Table III along with the experimentally observed values. The agreement is excellent.

TABLE III

Substance		$F_{T,P}$ at $T=298^\circ\text{K}$	$\beta \times 10^{-12}$ Exp.	$\beta \times 10^{-12}$ Calc.	$\alpha' \times 10^{-5}$ Expt.	$\alpha' \times 10^{-5}$ Calc.
Li	F	9899	1.43	1.43	9.2	9.18
	Cl	8843	3.17	3.14	12.2	12.24
	Br	8803	3.90	3.90	14.0	14.00
	I	9192	5.3	5.30	16.7	16.7
Na	F	.824	2.06	2.05	9.8	9.956
	Cl	1.0332	3.97	3.97	11.0	11.01
	Br	.9591	4.75	4.75	11.9	11.88
	I	.9949	6.21	6.35	13.5	13.56
K	F	.8897	3.14	3.14	10.0	10.0
	Cl	.9601	5.50	5.30	10.1	9.93
	Br	1.0074	6.45	6.45	11.0	11.07
	I	.9784	8.07	8.06	12.5	12.00
Rb	F	.9470	3.66	3.66	9.5	9.5
	Cl	1.028	6.16	6.16	9.85	9.57
	Br	1.0457	7.38	7.31	10.4	9.81
	I	1.0786	9.00	9.00	11.9	11.14
Cs	F	.9443	4.25	4.25	9.5	9.49
	Cl	1.0078	5.55	5.55	13.65	13.65
	Br	.9568	6.28	6.30	13.9	13.97
	I	1.0062	7.83	7.83	14.6	16.27

(c) *Thermal expansion*

The thermal expansion can also be calculated and compared with the experimental values. Dividing (2) by (3) and using (4) and (5) we obtain for the coefficient of thermal expansion α' the relation

$$\alpha' = \frac{3E\tau_0}{T} \left[\frac{\alpha e^2}{r} - \frac{nB}{r^n} + \frac{6c}{r^6} + \frac{8D}{r^8} - \frac{2\alpha e^2}{r} + \frac{n(n+1)B}{r^n} - \frac{42C}{r^6} + \frac{72D}{r^8} \right] \quad \dots (9)$$

The values of α' calculated from (9) are given in Table III along with the experimental values. The agreement with the experimental values is again quite satisfactory, except in the case of CsI where probably some of the experimental data utilised are in error.

ACKNOWLEDGMENT

The author is grateful to Prof. B. N. Srivastava, D.Sc., F.N.I., for suggesting the problem and continued guidance throughout the progress of the work.

REFERENCES

- Born, M., and Huang, K., 1954, *Dynamical Theory of Crystal Lattices*.
 Born, M. and Mayer, J., 1932, Zur Gitter Theorie der Ionenkristalle, *Zett.f. Physik*, **75**, 1.
 Bridgeman, P., 1940, *Proc. Am. Acad. Arts. Sci.*, **74**, 21.
 Cubicciotti, D., 1959, *J. Chem. Phys.*, **31**, 1646.
 Cubicciotti, D., 1961, *J. Chem. Phys.*, **34**, 2189.
 Huggins, M. L., 1937, *J. Chem. Phys.*, **5**, 143.
 Huggins, M. L., and Mayer, J., 1933, *J. Chem. Phys.*, **1**, 643.
 Mayer, J., 1933, *J. Chem. Phys.*, **1**, 270.
 N. B. S. Circular (1953-1957) No. 530, Vols. 1-7.
 Sharma, M. N., and Madan, M. P., 1961, *Ind. J. Phys.*, **35**, 596.
 Spangenberg, K., 1950, *Naturwissenschaften*, **43**, 394.
 Spangenberg, K., and Haussühl, S., 1957, *Z. Krist.*, **109**, 422.

THERMAL DIFFUSION OF BINARY GASEOUS MIXTURES

S. C. SAXENA AND S. M. DAVE

PHYSICS DEPARTMENT, RAJASTHAN UNIVERSITY, JAIPUR, INDIA

(Received June 12, 1962)

ABSTRACT. Rigorous theoretical formulae according to Chapman and Cowling, and Kihara approximation schemes have been derived for the thermal diffusion factor of such binary mixtures where the lighter component is in trace, from the known expressions for the general case. These formulae are further simplified by expanding in powers of the ratio of molecular masses. The latter expressions are simpler and preferable for numerical computation. Simple numerical calculations reveal that the convergence of the theoretical formulae for this case is poorer as compared to the other end of the composition range, the magnitude depends upon the system and the temperature range.

INTRODUCTION

Recent attempts, Weissman, Saxena and Mason (1961), Saxena and Mason (1959), Heymann and Kistemaker (1959), Mundy (1958), Grew, Johnson and Neal (1954), and Grew and Ibbs (1952), to measure accurately the thermal diffusion factor, α_T , have necessitated an accurate knowledge of the theoretical expression for α_T , so that a precise interpretation of the experimental data may be possible. A considerable achievement is due to Mason (1957), who extended the formulae to higher approximations and performed calculations for some ideal mixtures. Real systems differ from these ideal mixtures and the conclusions derived from the latter may not hold for the former, at least quantitatively. For this reason, Saxena and Dave (1961) investigated the binary mixtures where the heavier component was in trace. In this paper those binary mixtures are considered which have the lighter component in trace, and therefore provide the other end of the composition range. These two investigations together besides enabling to estimate the entire composition dependence of α_T also facilitate analysis of experimental data of binary systems where one component is a radioactive gas and is in trace. A knowledge of the appropriateness of these approximation schemes at the two limiting ends may also provide some clue for the use of these schemes in assessing α_T expression for the middle range of the composition. Theoretical expressions of α_T derived according to the approximation procedures of Chapman and Cowling (1952) and Kihara (1949, 1953) have been considered. The rigorous expressions are further simplified by expanding in powers of M , where $M = (M_2/M_1)$ and M_2 and M_1 are the molecular weights of the lighter and heavier components respectively. Convergence errors as well as the adequacies

of the simpler expressions are investigated by performing calculations for the specific systems. Some preliminary results have been reported by us (1962) earlier.

F O R M U L A E F O R α_T

Chapman and Cowling Method

The general m -th approximation to α_T is given by Chapman and Cowling (1952). To the first approximation for binary systems when the lighter component is in trace we get

$$[\alpha_T]_1 = \frac{5}{2} \left[\left(\frac{M_1 + M_2}{2M_1} \right)^{\frac{1}{2}} \left(\frac{a_{10}^{(1)} - a_{-1-1}^{(1)} - a_{10}^{(1)} - a_{-1-1}^{(1)}}{a_{11}^{(1)} a_{-1-1}^{(1)}} \right) + \frac{a_{-10}^{(1)}}{a_{-1-1}^{(1)}} \left(\frac{M_1 + M_2}{2M_2} \right)^{\frac{1}{2}} \right] \quad \dots (1)$$

The various a_{ij} are functions of molecular weights of the two gases, and collision integrals, and are given by Mason (1954, 1957). Equation (1) can be put in the more familiar form as follows :

$$[\alpha_T]_1 = (6C_{12}^* - 5)(S_1/Q_1), \quad \dots (2)$$

where

$$S_1 = \frac{M_1}{M_2} \left(\frac{2M_2}{M_1 + M_2} \right)^{\frac{1}{2}} Z' - \frac{4M_1 M_2 A_{12}^*}{(M_1 + M_2)^2} - \frac{15M_2(M_2 - M_1)}{2(M_1 + M_2)^2}, \quad \dots (3)$$

$$Q_1 = \frac{2Z'}{M_2(M_1 + M_2)} \left(\frac{2M_2}{M_1 + M_2} \right)^{\frac{1}{2}} \left[\left(\frac{5}{2} - \frac{6}{5} B_{12}^* \right) M_1^2 + 3M_2^2 + \frac{8}{5} M_1 M_2 A_{12}^* \right], \quad \dots (4)$$

$$A_{12}^* = \frac{\Omega_{12}^{(2,2)*}}{\Omega_{12}^{(1,1)*}}, \quad B_{12}^* = \frac{5\Omega_{12}^{(1,2)*} - 4\Omega_{12}^{(1,3)*}}{\Omega_{12}^{(1,1)*}},$$

$$C_{12}^* = \frac{\Omega_{12}^{(1,2)*}}{\Omega_{12}^{(1,1)*}} \quad \text{and} \quad Z' = \frac{\Omega_{11}^{(2,2)*} \sigma_{11}^2}{\Omega_{11}^{(1,1)*} \sigma_{12}^2} \quad \dots (5)$$

Here $\Omega_{ij}^{(l,n)*}$ are dimensionless reduced collision integrals and are defined so as to be equal to unity for rigid spherical molecules of mutual diameter σ_{ij} , Hirschfelder,

Curtiss and Bird (1954). For such mixtures, the second approximation to α_T is given by

$$[\alpha_T]_2 = \frac{5}{2} \left[\left(\frac{M_1 + M_2}{2M_1} \right)^{\frac{1}{2}} \{ (a'_{-1-1} a'_{-2-2} - a'^2_{-1-2}) (a''_{11} a''_{22} - a''^2_{12}) \}^{-1} \right. \\
+ \{ (a_{10} a''_{22} - a''_{12} a_{02}) (a'_{-1-1} a'_{-2-2} - a'^2_{-1-2}) \\
+ (a_{1-1} a''_{22} - a''_{12} a_{2-1}) (a_{-20} a'_{-1-2} - a_{-10} a'_{-2-2}) \\
+ (a_{1-2} a''_{22} - a''_{12} a_{2-2}) (a_{-10} a'_{-1-2} - a_{-20} a'_{-1-1}) \} \\
\left. + \left(\frac{M_1 + M_2}{2M_2} \right)^{\frac{1}{2}} \left(\frac{a_{-10}}{a'_{-1-1}} \right) \left(1 - \frac{a_{-20} a'_{-1-2}}{a_{-10} a'_{-2-2}} \right) \left(1 - \frac{a'^2_{-1-2}}{a'_{-1-1} a'_{-2-2}} \right)^{-1} \right] \dots \quad (6)$$

Considerable simplification occurs in the expressions of α_T if they are expanded in terms of the ratio (M_2/M_1) . Thus, for the first approximation we get

$$[\alpha_T]_1 = \frac{(6C_{12}^* - 5)}{2Y} \left[1 - \left(\frac{8A_{12}^*}{5Y} - 1 \right) M + \frac{15}{2\sqrt{2}Z} \left(1 - \frac{8}{15} A_{12}^* \right) M^{3/2} \right. \\
\left. - \frac{3}{Y} \left\{ 1 - \frac{8}{15} A_{12}^* \left(\frac{8A_{12}^*}{5Y} - 1 \right) \right\} M^2 + \dots \right], \quad (7)$$

where

$$Y = (1/10)(25 - 12B_{12}^*), \quad (8)$$

Similarly, for the second approximation we get

$$[\alpha_T]_2 = [\alpha_T]_1^2 (1 + B_1 M + B_2 M^2) [(1 - B_{14})^{-1} \\
\{ 1 - B_{14}(B_3 + B_6)(1 - B_{14})^{-1} M + B_{14}(1 - B_{14})^{-1} \\
(B_{14}(B_3 + B_6)^2(1 - B_{14})^{-1} + B_4 + B_6 + B_3 B_6) M^2 \}] \\
[1 - (1 + B_6 M + B_6 M^2)(B_9 B_{13}/B_{10})] - \frac{5\sqrt{2}}{16Z} \\
(6C_{12}^* - 5)(1 - B)^{-1} (5B_{10} Y - 4B_9^2)^{-1} [10Y B_{10} - B B_9^2 \\
- B_{11}(B_{10} - B_9 B_{13}) - B_{12}(10Y B_{13} - 8B_9)] M^{3/2} \\
+ \dots \quad (9)$$

where

$$[\alpha_T]_1^2 = (6C_{12}^* - 5)/2Y, \\
B = (8E_{11}^* - 7)^2(77 - 112E_{11}^* + 80F_{11}^*)^{-1}, \\
B_1 = 1 - (8A_{12}^*/5Y),$$

$$B_2 = (8A_{12}^*/5Y)^2 - (15 + 8A_{12}^*)(5Y)^{-1},$$

$$B_3 = (7A_{12}^* - 8H_{12}^*)(B_0)^{-1} - (8A_{12}^*/5Y),$$

$$B_4 = \frac{21(5 - 6C_{12}^*)}{8B_0} - \frac{3}{Y} - \frac{8A_{12}^*(7A_{12}^* - 8H_{12}^*)}{5YB_0},$$

$$B_5 = (7A_{12}^* - 8H_{12}^*)B_0^{-1} - B_7B_{10}^{-1} - \frac{64A_{12}^{*2}}{25Y^2},$$

$$B_6 = \frac{21(5 - 6C_{12}^*)}{8B_0} + \frac{B_7(7A_{12}^* - 8H_{12}^*)}{B_0B_{10}} + \frac{B_7^2}{B_{10}^2} - \frac{B_8}{B_{10}},$$

$$B_7 = (49/2)A_{12}^* - 56H_{12}^* + 40F_{12}^*A_{12}^*,$$

$$B_8 = (735/16) + 12K_{12}^* - 9C_{12}^* - (81/4)B_{12}^*,$$

$$B_9 = (175/32) + (225/16)C_{12}^* - 15G_{12}^* - (57/8)B_{12}^*,$$

$$B_{10} = (1225/128) + (315/4)C_{12}^* - (399/16)B_{12}^* + 45J_{12}^* - 105G_{12}^*,$$

$$B_{11} = 55 - 12B_{12}^* - 16J_{12}^*,$$

$$B_{12} = (595/32) + (3/16)C_{12}^* - (57/8)B_{12}^* - 15G_{12}^* - 7A_{12}^* + 8H_{12}^*,$$

$$B_{13} = \left[1 - \frac{3(5 - 4B_{12}^*)}{4(6C_{12}^* - 5)} \right]$$

$$B_{14} = 4B_0^2 + 5B_{10}Y,$$

and

$$E_{ij}^* = \frac{\Omega_i^{(2,3)*}}{\Omega_0^{(2,2)*}}, \quad F_{ij}^* = \frac{\Omega_i^{(2,4)*}}{\Omega_j^{(2,2)*}}$$

$$G_{ij} = \frac{\Omega_j^{(1,4)*}}{\Omega_j^{(1,1)*}}, \quad H_{ij}^* = \frac{\Omega_j^{(2,3)*}}{\Omega_j^{(1,1)*}},$$

$$J_{ij}^* = \frac{\Omega_{ij}^{(1,5)*}}{\Omega_{ij}^{(1,1)*}}, \quad K_{ij}^* = \frac{\Omega_{ij}^{(3,3)*}}{\Omega_{ij}^{(1,1)*}}. \quad \dots \quad (10)$$

If we put $M = 0$ in Eqs (7) and (9), α_T expressions corresponding to Lorentzian gas mixtures result. These are

$$[\alpha_T]_1 = [\alpha_T]_1^a,$$

$$[\alpha_T]_2 = [\alpha_T]_1 [1 - (B_9 B_{13}/B_{10})] [1 - (4B_9^2/5Y B_{10})]^{-1}.$$

These expressions were earlier derived by Mason (1957).

Kihara and Extended Kihara Methods

To the first approximation when the lighter component is in trace the thermal

diffusion factor, $[\alpha'_T]_1$, is again given by an expression similar to Eq. (2), except Q_1 which is now defined as follows.

$$Q'_1 = \frac{2Z'}{M_2(M_1 + M_2)} \left(\frac{2M_2}{M_1 + M_2} \right)^{\frac{1}{2}} \left[M_1^2 + 3M_2^2 + \frac{8}{5} M_1 M_2 A_{12}^* \right] \dots \quad (11)$$

The second approximation to α_T for such mixtures is

$$[\alpha'_T]_2 = [\alpha_T]_1 (1 + K'_1) + K'_2,$$

where

$$K'_1 = \frac{C''_{-1-1} C''_{-2-2}}{C''_{-1-1} C''_{-2-2}} + \frac{C''_{12}}{C''_{11} C''_{22}}, \quad (12)$$

and

$$\begin{aligned} K'_2 = & \frac{5}{2} \left(\frac{M_1 + M_2}{2M_1} \right)^{\frac{1}{2}} \left[\frac{\alpha_{-10}}{C''_{11}} \frac{C'_{1-2} C''_{-1-2}}{C''_{-1-1} C''_{-2-2}} + \frac{\alpha_{10}}{C''_{11}} \frac{C''_{1-2}}{C''_{-1-1} C''_{-2-2}} \right. \\ & + \frac{C'_{-12}}{C''_{22} C''_{-1-1} C''_{11}} \frac{C'_{1-2}}{C''_{-2-2} C''_{-1-1} C''_{11}} - \frac{\alpha_{0-2}}{C''_{11}} \frac{C'_{1-2}}{C''_{-2-2}} \\ & + \left. \frac{\alpha_{0-2}}{C''_{11}} \frac{C'_{1-1}}{C''_{-1-1} C''_{-2-2}} - \frac{\alpha_{20}}{C''_{11}} \frac{C'_{12}}{C''_{22}} + \frac{\alpha_{-20}}{C''_{11} C''_{22}} \frac{C'_{12}}{C''_{-2-2}} \right] \\ & - \frac{5}{2} \left(\frac{M_1 + M_2}{2M_2} \right)^{\frac{1}{2}} \left[\frac{\alpha_{0-2}}{C''_{-1-1} C''_{-2-2}} + \frac{\alpha_{0-1}}{C''_{11} C''_{22}} \frac{C'_{12}}{C''_{-1-1}} \right] \dots \quad (13) \end{aligned}$$

The various α_{ij} and C_{ij} are defined by Mason (1954, 1957). Equations (11) and (12) are much simplified by expanding in powers of M . Thus, we have

$$\begin{aligned} [\alpha'_T]_1 = & \frac{1}{2} (6C_{12}^* - 5) \left[1 + \left(\frac{8}{5} A_{12}^* - 1 \right) M + \frac{15}{2\sqrt{2}Z'} \left(1 - \frac{8A_{12}^*}{15} \right) M^{3/2} \right. \\ & \left. - 3 \left\{ 1 - \frac{8}{15} A_{12}^* \left(\frac{8}{5} A_{12}^* - 1 \right) \right\} M^2 + \dots \right], \quad \dots \quad (14) \end{aligned}$$

and

$$[\alpha'_T]_2 = [\alpha_T]_1 \left\{ 1 + \frac{7}{25} (6C_{12}^* - 5)^2 + \frac{2}{5} (6C_{12}^* - 5) B_{13} \right\}$$

$$\begin{aligned}
& - \left\{ [\alpha_T]_1 (8B_{15} + \frac{24}{5} A_{12}^*) + \frac{1}{84} (8E_{11}^* - 7)^2 (6C'_{12}^* - 5) \right. \\
& \quad \left(\frac{8}{5} A_{12}^* - 1 \right) - \frac{(6C'_{12}^* - 5)^2}{5} B_{13} \left(4B_{15} + \frac{24}{5} A_{12}^* - 1 \right) \Big\} M \\
& + \frac{(6C'_{12}^* - 5)^2}{5\sqrt{2}} \left\{ \frac{7}{4} (6C'_{12}^* - 5) - 7(6C'_{12}^* - 5)(1 + B_{15}) \right. \\
& \quad \left. - 10B_{13}(1 + B_{15}) + 2(5 - 2A_{12}^*)B_{13} \right\} M^{3/2} \\
& - \left[[\alpha_T]_1 \left\{ 3 - \frac{448A_{12}^{*2}}{25} + \frac{192}{35} K_{12}^* - \frac{192}{5} A_{12}^* B_{15} \right. \right. \\
& \quad \left. \left. - 16B_{15}^2 \right\} - \left\{ \frac{1}{84} (8E_{11}^* - 7)^2 (6C'_{12}^* - 5) \right. \right. \\
& \quad \left. \left. \left(3 - \frac{64A_{12}^{*2}}{25} + \frac{8A_{12}^*}{5} \right) - \frac{B_{13}}{5} (6C'_{12}^* - 5)^2 \right. \right. \\
& \quad \left. \left. \left(\frac{448}{25} A_{12}^{*2} - 6 - \frac{192}{35} K_{12}^* - \frac{24}{5} A_{12}^* + \frac{96}{5} A_{12}^* B_{15} - 4B_{15} \right) \right\} \right] M^2 + \dots \quad (15)
\end{aligned}$$

where

$$B_{15} = \frac{2(7A_{12}^* - 8H_{12}^*)}{7(6C'_{12}^* - 5)}.$$

In writing Eq. (15) it has been tacitly assumed that $[\alpha_T]_1 = [\alpha'_T]_1$ in K'_2 for a Lorentzian gas mixture. This procedure is valid and consistent with the Kihara approximation scheme was brought to our notice by Prof. E. A. Mason, and we are extremely grateful to him for this suggestion. If $M_1 \gg M_2$ so that M can be neglected, we get the following simple expressions for $[\alpha'_T]_1$, and $[\alpha'_T]_2$ respectively :

$$[\alpha'_T]_1^a = (1/2)(6C'_{12}^* - 5), \quad \dots \quad (16)$$

and

$$[\alpha'_T]_2^a = [\alpha_T]_1^a \left[1 + \frac{7}{25} (6C'_{12}^* - 5)^2 + \frac{2}{5} (6C'_{12}^* - 5) - \frac{3}{10} (5 - 4B_{12}^*) \right]. \quad \dots \quad (17)$$

These expressions have been already derived by Mason (1957) for a Lorentzian gas mixture.

DISCUSSION

The formulae derived in the previous section will be extremely useful for calculating the thermal diffusion factor of binary mixtures when the lighter component is in trace or is a radioactive tracer. The experiments of the latter type are not yet performed though data on such systems will be interesting to determine. Before putting any confidence in the various formulae it will be essential to estimate their adequacy. In this section we will report the results of numerical calculations for a few mixtures to throw light on this point. Numerical computations of this nature for ideal Lorentzian gas mixtures were performed by Mason (1957). The values of thermal diffusion factor obtained by considering terms having powers of M as zero, one, one and a half, and two will be referred to as $[\alpha'_T]^a$, $[\alpha'_T]^b$, $[\alpha'_T]^{b'}$ and $[\alpha'_T]^c$ respectively.

TABLE I

Various calculated values of α'_T as a function of temperature for Ar-Xe and He-Xe mixtures with the lighter component present only in trace

System	T °K	$[\alpha'_T]_1$	$[\alpha'_T]_2$	$[\alpha'_T]^a_2$	$[\alpha'_T]^b_2$	$[\alpha'_T]^{b'}_2$	$[\alpha'_T]^c_2$
Ar-Xe	100	-0.0248	-0.0250	-0.0245	-0.0251	-0.0251	-0.0247
	200	0.0326	0.0305	0.0282	0.0312	0.0318	0.0296
	300	0.0909	0.0880	0.0855	0.0870	0.0867	0.0866
	400	0.143	0.133	0.133	0.132	0.129	0.131
	500	0.171	0.163	0.170	0.160	0.155	0.160
	700	0.209	0.199	0.214	0.193	0.183	0.199
	900	0.229	0.223	0.242	0.212	0.200	0.222
He-Xe	200	0.270	0.255	0.257	0.254	0.254	0.255
	300	0.307	0.301	0.307	0.303	0.303	0.303
	500	0.329	0.340	0.346	0.341	0.341	0.341
	700	0.332	0.340	0.353	0.348	0.347	0.350
	900	0.335	0.350	0.355	0.349	0.348	0.349

The calculated values of the thermal diffusion factor as a function of temperature for the Ar-Xe system, Ar, present only in trace, and He-Xe system with He in trace, are recorded in Tables I and II. These calculations are according to the familiar Lennard-Jones (12-6) intermolecular potential in conjunction with the

potential parameters of Lunbeck (1951). It is seen from Table I that for the Ar-Xe system where the value of M is appreciable, consideration of terms upto M^2 is sufficient. For systems where M is small $[\alpha'_T]_2^b$ may be even sufficient. Thus, for the He-Xe system we find that the contribution of terms having powers of M greater than one is negligible, so that $[\alpha'_T]_2 = [\alpha'_T]_2^b$. It is important to notice in Table I that the convergence of α'_T is poor though the degree depends on the specific system and temperature range, and will have to be investigated in each case individually. Simpler formulae worked out in this paper are specially suited for this work. In any case it seems very likely that the convergence error in most of the cases will be greater than the precision of the experimental measurements. Some caution is, therefore, needed for interpreting experimental data on this end of the composition range.

TABLE II

Calculated values of α_T as a function of temperature for Ar-Xe and He-Xe systems when the lighter component is present in trace

System	T °K	$[\alpha_T]_1$	$[\alpha_T]_2$	$[\alpha_T]_2^{\text{approx}}$
Ar-Xe	100	-0.0250	-0.0234	-0.0181
	300	0.0896	0.0887	0.0977
	500	0.159	0.167	0.200
	700	0.189	0.202	0.238
	900	0.206	0.212	0.248
He-Xe	300	0.260	0.280	0.279
	500	0.284	0.309	0.304
	700	0.288	0.295	0.306
	900	0.285	0.318	0.313

*Values obtained according to Eqs. (9) and (10).

Similarly, computed values of α_T for these two systems and as a function of temperature are reported in Table II. Some conclusions are straightforward. The convergence of α_T is quite poor in this case too and is worse than on Kihara approximation scheme for these two systems. Unlike Kihara approximation results, the simpler and approximate formula derived on Chapman-Cowling scheme has poor validity for the Ar-Xe mixtures; however, it is somewhat adequate for the He-Xe system,

CONCLUSION

The convergence of the theoretical expressions for α_T is poor for approximately Lorentzian gas mixtures i.e. $X_1 \rightarrow X_2$ but $M_1 \rightarrow M_2$ is not necessarily true. The degree differs from mixture to mixture and the temperature range and will have to be investigated individually. Simpler formulae derived in this paper will facilitate such an investigation and will considerably reduce the computational labour. It would be very interesting to develop a third approximation scheme which may have better convergence error than either of the two discussed in this paper.

REFERENCES

- Chapman, S. and Cowling, T. G., 1952, *The Mathematical Theory of Non-Uniform Gases* (Cambridge University Press).
- Grew, K. E., and Ibb, T. L., 1952, *Thermal Diffusion in Gases* (Cambridge University Press).
- Grew, K. E., Johnson, F. A., and Neul, W. E. J., 1954, *Proc. Roy. Soc.*, **224**, 513.
- Heymann, D. and Kistemaker, J., 1959, *Physica*, **25**, 556.
- Hirschfelder, J. O., Curtiss, C. F., and Bird, R. B., 1954, *Molecular Theory of Gases and Liquids* (John Wiley and Sons, Inc., New York).
- Kihara, T., 1949, *Imperfect Gases*, Originally published in Japanese (Asakura Bookstore, Tokyo, and translated into English by the U.S. office of Air Research Wright-Patterson Air Force Base).
- Kihara, T., 1953, *Revs. Modern Phys.*, **25**, 831.
- Lunbeck, R. J., 1951, Thesis, Amsterdam.
- Mason, E. A., 1954, *J. Chem. Phys.*, **22**, 169.
- Mason, E. A., 1957, *J. Chem. Phys.*, **27**, 75, 782.
- Mundy, J. N., 1956, Thesis, University of Exeter.
- Saxena, S. C., and Mason, E. A., 1959, *Mol. Phys.*, **2**, 379.
- Saxena, S. C., and Dave, S. M., 1961, *Revs. Modern Phys.*, **33**, 148.
- , 1962, *Molecular Phys.*, to be published.
- Weissman, S., Saxena, S. C., and Mason, E. A., 1961, *Phys. Fluids*, **4**, 643.

INDIAN JOURNAL OF PHYSICS. VOL. 36, 1962

Statement about ownership and other particulars about FORM IV

1. Place of Publication ... 2 and 3, Lady Willingdon Road, Calcutta-32
2. Periodicity of its publication ... Monthly
3. Printer's Name ... Kalipada Mukherjee
- Nationality ... Indian,
- Address ... Eka Press, 204/1, B. T. Road, Alambazar, Calcutta-35.
4. Publisher's Name ... Samarendra Nath Sen
- Nationality ... Indian,
- Address ... Registrar, Indian Association for the Cultivation of Science, 2 and 3, Lady Willingdon Road, Jadavpur, Calcutta-32.
5. Editors' Names
 1. Prof. K. Banerjee, Indian, Director, I. A. C. S., Jadavpur, Calcutta-32.
 2. Prof. D. M. Bose, Indian, Director, Bose Institute, 93/1, Acharya Prafulla Ch. Road, Calcutta-9.
 3. Prof. S. N. Bose, Indian, National Professor 22, Iswarmill Lane, Calcutta-6.
 4. Prof. S. D. Chatterjee, Indian, Head of the Dept. of Physics, Jadavpur University, Jadavpur, Calcutta-32.
 5. Prof. P. S. Gill, Indian, Prof. of Physics, Muslim University, Aligarh.
 6. Prof. S. R. Khastgir, Indian, Khira Prof. of Physics, University College of Science, 92, Acharya Prafulla Ch. Road, Calcutta-9.
 7. Prof. D. S. Kothari, Indian Prof. of Physics Delhi University, Delhi.
 8. Prof. S. K. Mitra, Indian, National Professor, Institute of Radio Physics & Electronics, 92, Acharya Prafulla Ch. Road, Calcutta-9.
 9. Prof. B. D. Nag Chaudhuri, Indian, Director, Saha Institute of Nuclear Physics, 92, Acharya Prafulla Ch. Rd. Calcutta-9.
 10. Prof. K. R. Rao, Indian, Principal & Head of the Dept. of Physics, Andhra University, Waltair.
 11. Dr. D. B. Sinha, Indian, Dept. of Applied Physics, University College of Science, 92, Acharya Prafulla Ch. Road, Calcutta-9.
 12. Prof. S. C. Sarkar (Secy. Board of Editors) Indian, Indian Association for the Cultivation of Sci. Jadavpur, Calcutta-32.
 13. Prof. B. N. Srivastava, Indian, I.A.C.S., Jadavpur, Calcutta-32.
6. Name and address of the proprietor... Indian Association for the Cultivation of Science, Jadavpur, Calcutta-32.

I, Samarendra Nath Sen, hereby declare that the particulars given above are true to the best of my knowledge and belief.

(Sd) Samarendra Nath Sen,

Signature of Publisher

Date 16-3-62

CONTENTS

Indian Journal of Physics

Vol. 37, No. 2

February, 1985

	PAGE
8. A Comparative Study of the Fluorescence and the Emission Spectra of Anisole—Satya Prakash and Nand Lal Singh	59
9. A Study on Recording and Reproduction of Digital Data on and from Magnetic Drum Surface—Dwijesh Dutta Majumdar	67
10. Influence of Permanent Electric Moment on the Absorption Spectra of Polar Organic Molecules in the Crystalline State—S. C. Sirkar	101
11. Lattice Energy of Alkali Halides—S. Chatterjee	105
12. Thermal Diffusion of Binary Gaseous Mixtures—S. C. Saxena and S. M. Dave	111

Regd. No. C-3911

VOL. 37

INDIAN JOURNAL OF PHYSICS

No. 3

(Published in collaboration with the Indian Physical Society)

AND

VOL. 46

PROCEEDINGS

No. 3

OF THE

**INDIAN ASSOCIATION FOR THE
CULTIVATION OF SCIENCE**

MARCH 1963

PUBLISHED BY THE
INDIAN ASSOCIATION FOR THE CULTIVATION OF SCIENCE
JADAVPUR, CALCUTTA 22

BOARD OF EDITORS

K. BANERJEE	D. S. KOTTHARI
D. M. BOSE	S. K. MITRA
S. N. BOSE	B. D. NAG CHAUDHURI
S. D. CHATTERJEE	K. R. RAO
P. S. GILL	D. B. SINHA
S. R. KHASTOIR	S. C. SIKKAR (<i>Secretary</i>)
B. N. SRIVASTAVA	

EDITORIAL COLLABORATORS

PROF. R. K. ASUNDI, Ph.D., F.N.I.	
PROF. D. BASU, Ph.D.	
PROF. J. N. BHAR, D.Sc., F.N.I.	
PROF. V. G. BHIDR, Ph.D. (Nag), Ph.D. (Lond).	
PROF. A. BOSE, D.Sc., F.N.I.	
PROF. S. K. CHAKRABARTY, D.Sc., F.N.I.	
DR. J. S. CHATTERJEE	
DR. K. DAS GUPTA, Ph.D.	
PROF. N. N. DAS GUPTA, Ph.D., F.N.I.	
DR. J. DEAR, D.Phil. (Sc)	
PROF. A. K. DUTTA, D.Sc., F.N.I.	
PROF. C. S. GHOSH, M.Sc., S.M., F.N.I.,	M.I.E.E.
PROF. S. GHOSH, D.Sc., F.N.I.	
PROF. S. N. GHOSH, D.Sc.	
PROF. S. GUPTA, M.Sc., F.N.I.	
PROF. D. N. KUNDU, Ph.D., F.N.I.	
PROF. R. C. MAJUMDER, Ph.D., F.N.I.	
PRINCIPAL Y. G. NAIK, Ph.D.	
PROF. S. R. PALIT, D.Sc., F.R.I.C., F.N.I.	
PROF. H. RAKSHIT, D.Sc., F.N.I.	
PROF. A. SAHA, D.Sc., F.N.I.	
DR. VIKRAM A. SARABHAI, M.A., Ph.D., F.N.I.	
DR. A. K. SENGUPTA, D.Sc.	
PROF. NAND LAL SINGH, D.Sc.	
DR. M. S. SINHA, D.Sc., F.N.I.	
PROF. N. R. TAWDE, Ph.D., F.N.I.	
DR. P. VENKATESWARLU	

Assistant Editor :

SRI T. N. MURA, M.Sc.

Annual Subscription—

Inland Rs. 25.00

Foreign £ 2-10-0 or \$ 7.00

NOTICE

TO INTENDING AUTHORS

Manuscripts for publication should be sent to the Assistant Editor, Indian Journal of Physics, Jadavpur, Calcutta-22.

The manuscripts submitted must be type-written with double space on thick foolscap paper with sufficient margin on the left and at the top. The original copy, and not the carbon copy, should be submitted. Each paper must contain an abstract at the beginning.

All references should be given in the text by quoting the surname of the author, followed by year of publication, e.g., (Ghosh, 1954). The full reference should be given in a list at the end, arranged alphabetically, as follows; Ghosh, D. K., 1954, *Ind. J. Phys.*, 28, 486.

Line diagrams should be drawn on white Bristol board or tracing paper with black India ink, and letters and numbers inside the diagrams should be written neatly in capital type with India ink. The size of the diagrams submitted and the lettering inside should be large enough so that it is legible after reduction to one-third the original size. A simple style of lettering such as gothic, with its uniform line width and no serifs should be used, e.g.,

A · B · E · F · G · M · P · T · W ·

Photographs submitted for publication should be printed on glossy paper with somewhat more contrast than that desired in the reproduction, and should, if possible, be mounted on thick white paper.

Captions to all figures should be typed in a separate sheet and attached at the end of the paper.

The mathematical expressions should be written carefully by hand. Care should be taken to distinguish between capital and small letters and superscripts and subscripts. Repetition of a complex expression should be avoided by representing it by a symbol. Green letters and unusual symbols should be identified in the margin. Fractional exponents should be used instead of root signs.

Bengal Chemical and Pharmaceutical Works Ltd. Pioneer Indian Manufacturers of Pharmaceuticals & Chemicals.

Manufacturers of:

Pharmaceutical Chemicals:

Caffeine and its salts, Strychnine Hydrochlor, Strychnine Sulphate, Brucine Sulphate, Potassium Citrate B.P., I.P., Sodium Citrate B.P., I.P., Potassium Acetate B.P., I.P., Potassium Iodide B.P., I.P., Sodium Iodide B.P., I.P., Ferri et Ammon Citrate B.P., I.P., Nicotinic Acid, B.P., Nicotinamide, B.P., and various other Pharmaceutical Chemicals.

Heavy & Reagent Quality Fine Chemicals:

Alum, Alum Sulphate (Iron Free), Ferro Alum, Zinc Chloride Tech. Naphthalene Pure, Sodium Citrate A.R., Potassium Citrate A.R., Magnesium Sulphate A.R., Sodium Sulphate Anhydrous A.R., Potassium Iodide A.R., Sodium Chloride A.R., Zinc Sulphate A.R., etc.

Please refer your enquiries for the above items and other chemicals in the line to :—

BENGAL CHEMICAL

6, GANESH CHUNDER AVENUE,
CALCUTTA-13, INDIA.

NON-AQUEOUS TITRATION

A monograph on acid-base titrations in organic solvents

By

PROF. SANTI R. PALIT, D.Sc., F.R.I.C., F.N.I.

DR. MIHIR NATH DAS, D.Phil.

AND

MR. G. R. SOMAYAJULU, M.Sc.

This book is a comprehensive survey of the recently developed methods on acid-base titrations in non-aqueous solvents. Acid-base concept, as developed by Lowry-Brönsted and Lewis is succinctly presented in this slender volume. titration of weak bases and titration 'titration' is described at a great length acetous titration' including its recent modifications for the estimation of weak bases. Various methods for the titration of weak acids are duly described. A reference list of all pertinent publications is included in this book.

122 pages with 23 diagrams (1954)

Inland Rs. 3 only. Foreign (including postage) \$ 1.00 or 5s.

Published by

INDIAN ASSOCIATION FOR THE CULTIVATION OF SCIENCE
JADAVPUR, CALCUTTA-32, INDIA

**Measure
and plot changes
in variables
as they occur...
with**

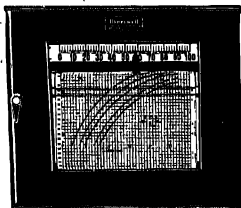
Electronik

instruments for research

Here's an exceptional group of instruments to measure and record your research findings swiftly, surely, conveniently. These Electronik instruments for research can speed completion of your projects by eliminating many of the tedious time-consuming details of test work

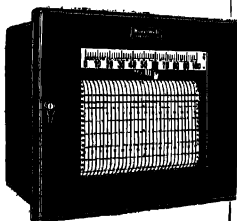
Electronik

FUNCTION PLOTTER automatically and continuously plots a curve which shows the relationship of one variable to another. Typical uses: speed versus torque, stress versus strain, temperature versus pressure, plate voltage versus plate current (and other electron tube characteristics), and many other variable relationships



Electronik

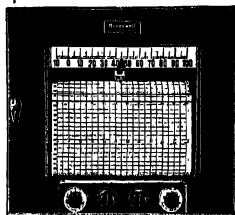
accurately measure d.c. potentials as low as 0.1 microvolt and spans as narrow as 100 microvolts. Available as a precision indicator, circular chart recorder and strip chart recorder. Useful (with appropriate primary measuring elements) for measuring differential temperatures and slight variations in the temperatures of small objects through the use of radiation pyrometry.



PSB-4122/63

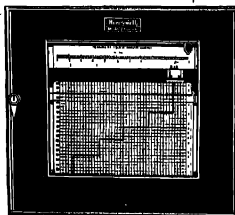
Electronik

ADJUSTABLE SPAN RECORDER measures spans and magnitudes of a variety of emf. Instrument calibration can be in terms of any variable reducible to d.c. voltage. Can be used with thermocouples, strain gauges, tachometers and other transducers



Electronik

EXTENDED RANGE RECORDER facilitates measurement of any linear variable whose values change over a wide range, and where precise evaluation and good resolution are important. This instrument is particularly suited to the measurement of forces in conjunction with a strain gauge bridge



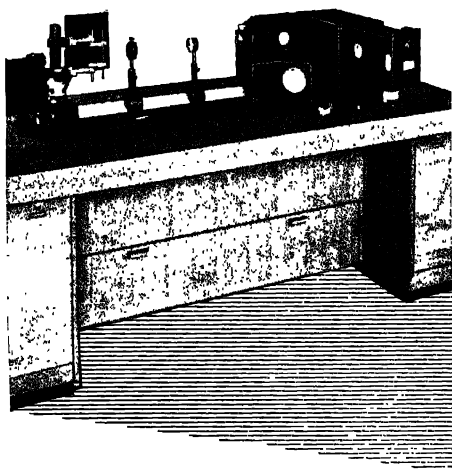
Honeywell

[H] First in Control

Sold and serviced in India exclusively by

BLUE STAR

**BLUE STAR ENGINEERING
CO. (Calcutta) PRIVATE LTD.**
7 HARE STREET, CALCUTTA 1
Also at BOMBAY • DELHI
MADRAS • JAMSHEDPUR



ZEISS THREE-PRISM SPECTROGRAPH

A glass-type spectrograph with Foresterling set of prisms of high-power and resolving capacity, large dispersion and excellent definition of lines, self-contained construction.

Equipment with 3 cameras : Camera $f = 12$ cm $F/2.4$ and camera $f = 27$ cm $F/5.4$ for feeble-light phenomena (Raman effect, fluorescence of flame-spectra, etc.)

Autocollimation camera $f = 130$ cm $F/26$ for taking complex emission spectra in the visible region (special type steel, rare earth etc.)

Solves all spectra-chemical problems of organic and inorganic nature.

VEB Carl Zeiss JENA

SOLE AGENTS IN INDIA

GORDHANDAS DESAI PRIVATE, LTD.

PHEROZSHAH MEHTA, ROAD, BOMBAY 1.

Branches :

22, Lingh Chetty Street
MADRAS-1.

P-7, Mission Row Extension
CALCUTTA-1.

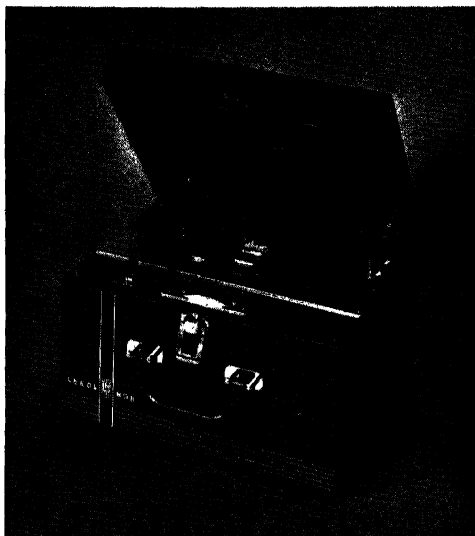
4/2B Asaf Ali Road
NEW DELHI.

Leeds



Northrup

**FOR PRECISE
MEASUREMENTS OF
TEMPERATURES &
MILLIVOLTS**



The use of this three-dial 8686 Portable Potentiometer is rapidly spreading in research laboratories. It features a central reading windowwhere measured values appear as a row of digits plus a scale value.....for rapid reading of test results. Wide operating range from -10.1 to $+100.1$ mv; accuracy with and without reference junction compensation: $\pm(0.05\%$ of reading $+6\mu v$) and $\pm(0.05\%$ of reading $+3\mu v$) respectively.

For further particulars, please write to :

The Sole Distributors for Laboratory Equipments

**THE SCIENTIFIC INSTRUMENT
COMPANY, LIMITED.**

ALLAHABAD BOMBAY CALCUTTA MADRAS
NEW DELHI

Head Office : 6, Tej Bahadur Sapru Road, Allahabad



VIBRATIONAL SPECTRA, APPROXIMATE POTENTIAL CONSTANTS AND CALCULATED THERMODYNAMIC PROPERTIES OF BENZOPHENONE

P. G. PURANIK AND E. V. RAO

DEPARTMENT OF PHYSICS, UNIVERSITY COLLEGE OF SCIENCE,
OSMANIA UNIVERSITY, HYDERABAD-7.

(Received August 8, 1962)

ABSTRACT. Benzophenone has been subjected to normal coordinate treatment assuming the phenyl groups to be point masses. The Wilson $F-G$ matrix method has been employed to obtain the secular equation in order to calculate the fundamental frequencies. In calculating the thermodynamic properties, contributions from the ring frequencies are also included.

INTRODUCTION

The infrared spectrum of benzophenone is not found in literature in all its aspects, although several workers mention the carbonyl frequency. However, the Raman spectrum of benzophenone has been recorded among others by Kohlrausch and Pongratz (1934), Lestrade (1952) and Puranik (1953). No attempt appears to have been made to subject the molecule to normal coordinate treatment.

EXPERIMENTAL

The infrared spectrum was recorded with a Perkin-Elmer Infrared Spectrophotometer Model 21 with NaCl optics. The spectrum was recorded in nujol mull and in solutions of CCl_4 . The spectrum in solutions of CCl_4 was more extensive but it did not exhibit any shift in the frequencies recorded in the mull.

The Raman spectrum of molten benzophenone was recorded by using a Hilger Raman Source Unit and Fuess Glass Spectrograph having a dispersion of $19\text{\AA}/\text{mm}$ in $\lambda 4358$ region. In order to get the spectrum of molten benzophenone, the melt is poured in the Raman tube in the Unit and the flow of the cooling water circulation is slowed down and regulated so as to keep the temperature of the cell slightly above 49°C which is the melting point of benzophenone. In this way the substance can be retained in molten state for a considerable time.

Benzophenone of Merck make was recrystallised by dissolving it in anhydrous absolute ethyl alcohol.

RESULTS

The Raman spectrum of benzophenone melt and its infrared spectrum in solutions in CCl_4 are given in Table I. The Raman spectrum of the substance as

recorded by Lestrade is given for comparison. The present results, however, agree more closely with those reported by Kohlrausch and Pongratz. The assignments proposed are also indicated in Table I.

TABLE I
Raman and infrared frequencies in cm^{-1}

Raman		Infrared	Assignments
Authors	Lestrade	Authors	
148 (2)	—	—	
221 (2)	223 (5)	—	
277 (2)	—	—	R-C-R deformation.
—	387 (1)	—	
406 (2)	410 (1)	—	C (ν_{2a}) ring
567 (2)	559 (1)	—	C-C=O deformation.
—	579 (2)	—	
616 (3)	612 (5)	—	C (ν_{2g}) ring.
—	—	609 (s)	C-H out-of-plane bending.
721 (2)	—	717 (m)	
764 (2)	—	—	
810 (1)	—	—	
845 (2)	—	845 (w)	
—	—	917 (s)	C-H out-of-plane bending.
—	943 (1)	939 (m)	
—	—	971 (w)	1674-699 = 975.
1003 (5)	996 (10)	—	C-C (ν_{2g}) ring.
1027 (3)	1023 (3)	1028 (m)	
			C-H in-plane bending.
		1136 (m)	
1151 (4b)	1155 (5)	1148 (m)	C-R symmetric stretch.
		1176 (w)	559 + 612 = 1171,
		1220 (w)	
		1249 (w)	845 + 406 = 1251.
1281 (1)	1282 (3)	1274 (vs)	C-R antisymmetric stretch.
—		1307 (s)	
1322 (1)		1316 (s)	1600-277 = 1328.
—		1389 (w)	1603-221 = 1382.
1448 (0)	1451 (1)	1449 (s)	1600-148 = 1452.
—	—	1475 (sh)	
1492 (0)	1491 (1)	1493 (m)	721 + 764 = 1485.
	1542 (1)		
	1578 (1)	1581 (m)	ring.
1600 (7)	1600 (10)	1603 (s)	C=C stretch.
1658 (5)	1661 (5)	1674 (vs)	C=O stretch.
—	—	1689 (w)	2 × 845 = 1690.
3052 (2b)	—	3053 (w)	C-H stretch.

NORMAL COORDINATE TREATMENT

If the phenyl groups in benzophenone are assumed to be point masses the molecule can be treated as a four body problem having the symmetry of the point group C_{2v} with a distribution ($3A_1, 2B_1, B_2$). All the normal vibrations are both Raman and infrared active. The Normal coordinate treatment has been carried out by the authors according to the Wilson F-G matrix method. The following symbols are used for the equilibrium values of bond distances and interbond angles which are shown in the Fig. 1.

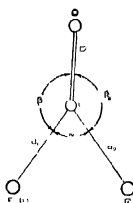


Fig. 1

In accordance with the above notation an example of the possible types of the potential constants arising out of different interactions are

$f_d = \text{C-R stretching constant.}$

$f_\alpha = \text{<RCR bending constant.}$

$f_{\alpha\beta} = \text{<RCR and C = O angle bond interaction constant.}$

$f'_{\alpha\beta} = \text{C-R and <OCR bond-angle interaction constant, the prime indicating that the bond and the angle do not have a common bond.}$

The most general quadratic expression for the potential energy has the coefficients given in Table II.

TABLE II

	ΔD	Δd_1	Δd_2	$\Delta \alpha$	$\Delta \beta_1$	$\Delta \beta_2$
ΔD	f_D	f_{Dd}	f_{Dd}	$f_{D\alpha}$	$f_{D\beta}$	$f_{D\beta}$
Δd_1		f_d	f_{dd}	$f_{d\alpha}$	$f'_{d\beta}$	$f_{d\beta}$
Δd_2			f_d	$f_{d\alpha}$	$f_{d\beta}$	$f'_{d\beta}$
$\Delta \alpha$				f_α	$f_{\alpha\beta}$	$f_{\alpha\beta}$
$\Delta \beta_1$					f_β	$f_{\beta\beta}$
$\Delta \beta_2$						f_β

The symmetry coordinates for the
Type A_1

$$R_1 = \Delta D.$$

$$R_2 = 1/\sqrt{2}(\Delta d_1 + \Delta d_2).$$

$$R_3 = 1/\sqrt{6}(2\Delta\alpha - \Delta\beta_1 - \Delta\beta_2).$$

Type B_1

$$R_4 = 1/\sqrt{2}(\Delta d_1 - \Delta d_2).$$

$$R_5 = 1/\sqrt{2}(\Delta\beta_1 - \Delta\beta_2)$$

The symmetry coordinates are normalised and orthogonal. From the potential energy matrix and the matrix formed from the coefficients contained in the symmetry coordinates the F matrix elements are formed. The F matrices are as follows. For type A_1

$$\begin{pmatrix} F_{11} & F_{12} & F_{13} \\ & F_{22} & F_{23} \\ & & F_{33} \end{pmatrix} = \begin{pmatrix} f_D & \sqrt{2}f_{Dd} & \sqrt{(2/3)}(f_{D\alpha} - f_{D\beta}) \\ f_d + f_{dd} & 1/\sqrt{3}(2f_{d\alpha} - f_{d\beta} - f'_{d\beta}) & \\ & 1/3d^2(2f_{\alpha} + f_{\beta} + f_{\beta\beta} - 4f_{\beta\alpha}) & \end{pmatrix}$$

For type B_1

$$\begin{pmatrix} F_{44} & F_{45} \\ & F_{55} \end{pmatrix} = \begin{pmatrix} f_d & f_{dd} & f_{d\beta} - f'_{d\beta} \\ & & f_{\beta} - f_{\beta\beta} \end{pmatrix}$$

The structural parameters of benzophenone were not available to the authors, either from X-ray or electron diffraction data. However, the values of bond distances given by Karl Hauptman *et al.* (1957) for *p,p'*-dimethoxy benzophenone and the value of inter bond angles given by Glasston (1935) are found suitable for the molecule under investigation in calculating the G matrix elements. These values are :

$C-R = 1.46 \text{ \AA}$, $C-O = 1.3 \text{ \AA}$, $\angle RCR = 131^\circ$ and $\angle O = C-R = 114^\circ 30'$. The elements of G matrices were evaluated with the help of Decius (1948) Tables. The actual values of the elements of G matrices for classes A_1 and B_1 are given below. The out of plane vibrations falling under the class B_2 have not been discussed in this paper.

$$\begin{pmatrix} G_{11} & G_{12} & G_{13} \\ & G_{22} & G_{23} \\ & & G_{33} \end{pmatrix} = \begin{pmatrix} 8.7820 \times 10^{22} & -2.9418 \times 10^{22} & 7.6582 \times 10^{30} \\ & 2.5067 \times 10^{22} & -4.4914 \times 10^{30} \\ & & 1.2791 \times 10^{39} \end{pmatrix}$$

$$\begin{pmatrix} G_{44} & G_{45} \\ & G_{55} \end{pmatrix} = \begin{pmatrix} 9.0887 \times 10^{22} & -9.5886 \times 10^{30} \\ & 1.5856 \times 10^{39} \end{pmatrix}$$

The potential constants for the molecules having similar structures as benzophenone were transferred to this molecule. Probably in view of the fact that the phenyl groups are assumed to be point masses the bond-angle and the angle-angle interaction terms were very critical. After a few modifications the observed frequencies were reproduced by calculations, the difference in their values being well within one per cent. The potential constants* thus finally arrived at are $f_D = 13.0$, $f_d = 7.25$, $f_a = 1.5$, $f_\beta = 1.73$, $f_{dd} = 2.75$, $f_{da} = -1.5$, $f_{d\beta} = 1.17$, $f'_{d\beta} = 0.626$, $f_{D\alpha} = 1.2$, $f_{D\beta} = -2.0$, $f_{\alpha\beta} = 0.4$ and $f_{\beta\beta} = -0.33$.

The observed and the calculated values of the frequencies of the normal vibrations considering the phenyl group to be a point mass are given in Table III.

TABLE III

Type	observed		Calculated
	Raman	Infrared	
	1658	1674	1664
A_1	1151	1148	1150
	277	—	273
B_1	1281	1274	1278
	567	—	561

THERMODYNAMIC PROPERTIES

The heat content, free energy, entropy and heat capacity at constant pressure for benzophenone with rigid rotator and harmonic oscillator approximation have been calculated. The contributions from the normal vibrations discussed in this paper and the contributions from the ring frequencies are included in calculating the thermodynamic properties, for the ideal gaseous state at one atmospheric pressure for twelve temperatures in 100-1000°K range. Since no data were available for the vibrational frequencies in the gaseous state of the molecule, the observed values as recorded by the authors are used. The thermodynamic properties are given in Table IV.

*Bond constants and bond-bond interaction constants are given in md/Å, bond-angle interaction terms in md/rad, angle constants and angle-angle interaction constants are given in mdÅ/rad².

TABLE IV

Heat content, free energy, entropy and heat capacity for benzophenone

T°K	$(H_0 - H_0^c)/T_0$	$(H - H_0^c)/T$	S°	C_p°
100	9.01	50.78	59.79	11.30
200	11.76	57.82	69.58	18.07
273	14.12	61.81	75.95	23.57
303	15.33	63.35	78.68	26.65
400	19.11	67.73	87.51	33.51
500	22.90	71.75	95.98	40.30
600	26.62	75.39	104.01	46.87
700	29.51	80.23	111.24	50.43
800	32.33	84.89	118.23	53.83
900	35.12	89.44	125.09	57.12
1000	37.86	93.85	131.71	62.33

N, B The moments of inertia of the molecule in a w.u.A² are $I_x = 54.945$, $I_y = 272.194$ and $I_z = 327.130$. The temperatures are given in K and the other quantities are in cal. deg⁻¹ mole⁻¹.

REFERENCES

- Deerus, J. C., 1948, *J. Chem. Phys.*, **16**, 1025.
 Glasston, 1935, Annual reports, pp 134.
 Kaile Hauptmann et al., 1957, *Acta Cryst.*, **10**, 481.
 Kohlrusch, K. W. F., Pongratz, A., 1934, *S. B. Akad. Wiss. Wien*, **143**, 288.
 Lestrade, M., 1952 Theses pour le grade Docteurs Sciences Physiques de l'Université de Poitiers.
 Puranik, P. G., 1953, Thesis for Ph. D degree of the Osmania University.

DISCRETE FREQUENCIES IN A LATTICE PERTURBED BY ISOTOPE DEFECTS

J. MAHANTY AND RAM KISHORE SHARMA

PHYSICS DEPARTMENT, PUNJAB UNIVERSITY, CHANDIGARH-3

(Received April 21, 1962)

ABSTRACT. An investigation is made of the process of generation of discrete vibration frequencies outside the allowed frequency band of a lattice when it is perturbed by the change of the mass of an atom. A criterion for monatomic lattices is described which enables one to predict whether in the perturbed state of the lattice, the discrete frequency generated from any branch is independent of the other branches. Finally, the discrete frequencies in the case of several linear lattice models are evaluated.

INTRODUCTION

The problem of generation of discrete vibrational frequencies due to isotope defects in a lattice has been studied by Lifshitz (1943a, 1943b, 1944, 1956), and by Montroll and Potts (1955, 1956). The general techniques developed by them have been applied mostly to a lattice model in which there is no coupling between the various components of the displacements of the atoms. Recently, Nardolli (1960) has studied the problem in the case of cubic lattices. The object of this paper is to discuss a few lattice models in which there is coupling between the displacements; but still it is possible to evaluate the discrete frequencies due to an isotope defect exactly.

THE SECULAR EQUATION FOR THE DISCRETE FREQUENCY

We will adopt here the notation of Lifshitz (1943a) with slight changes. The lattice under consideration has N unit cells in each of which there are p atoms, the mass of the s -th atom being m_s . The coordinate of the unit cell is given by the vector q , whose dimension equals the dimension of the lattice. Periodic boundary conditions will be used throughout.

The eigenfrequencies of the unperturbed lattice are the roots of the equation

$$|\hat{A} - I\omega^2| = 0 \quad \dots (1)$$

where the dynamical matrix \hat{A} is determined from the equations of motion of the atoms in the lattice. Each element of \hat{A} has six indices, three for the row and

three for the column. The following equation gives the correspondence between this notation and that of Born and Huang (1954);

$$A_{q-q'}(s, j | s', j') = \frac{1}{\sqrt{m_s m_{s'}}} \phi_{jj'} \left(\begin{array}{c} q-q' \\ s \quad s' \end{array} \right) \quad \dots (2)$$

The index j refers to the component of the displacement of the atoms.

In the presence of an isotope defect of mass $m_{s'}$ at the s -th position in the q -th unit cell, the eigenfrequencies are the roots of the equation

$$|\hat{I} - \hat{G}(\omega) \hat{\Lambda}| = 0 \quad \dots (3)$$

where $\hat{G}(\omega) = (\hat{A} - \hat{I}\omega^2)^{-1}$ and $\hat{\Lambda}$ is the perturbation matrix. In this case $\hat{\Lambda}$ is a diagonal matrix whose elements are given by

$$\Lambda_{q'-q''}(s', j' | s'', j'') = e_s \omega^2 \delta_{j'j''} \delta_{s's} \delta_{q'q} \delta_{q''q} \delta_{s''s} \quad \dots (4)$$

where

$$e_s = 1 - \frac{m'_s}{m_s}.$$

In a three dimensional lattice, for example, there will be only three nonvanishing elements in $\hat{\Lambda}$, and they will be the diagonal elements characterised by the indices q, s , and the three values of j .

The determinant in equation (3) can be reduced to the form

$$\begin{vmatrix} 1 + e_s \omega^2 G_0(s, 1 | s, 1) & e_s \omega^2 G_0(s, 1 | s, 2) & e_s \omega^2 G_0(s, 1 | s, 3) \\ e_s \omega^2 G_0(s, 2 | s, 1) & 1 + e_s \omega^2 G_0(s, 2 | s, 2) & e_s \omega^2 G_0(s, 2 | s, 3) \\ e_s \omega^2 G_0(s, 3 | s, 1) & e_s \omega^2 G_0(s, 3 | s, 2) & 1 + e_s \omega^2 G_0(s, 3 | s, 3) \end{vmatrix} = 0 \quad \dots (5)$$

The evaluation of the elements of \hat{G} matrix which occur in equation (5) can be done by the bilinear formula for the matrix elements of a function of an operator.

The eigenvectors of \hat{A} span a space of $3pN$ dimensions, and constitute an orthogonal set. (The degenerate eigenvectors can be orthogonalised in the usual way). For convenience we will use the symbol $|k, r\rangle$ for a typical normalised eigenvector of \hat{A} , where k can take up N values inside the unit cell of the reciprocal lattice, of volume $(2\pi)^3/N$, and r can take up $3p$ values.

Each eigenvector of \hat{A} has $3pN$ components. We will denote a typical component by the symbol $|k, r; q, s, j\rangle$. These components are known to be of the form (Lifshitz, 1943a)

$$|k, r; q, s, j\rangle = \frac{1}{\sqrt{N}} Q_r^{sj}(k) \exp \left(\frac{2\pi i}{N} k \cdot q \right) \quad \dots (6)$$

where $Q_r^{s,j}(k)$ is the (s, j) -th component of the r -th eigenvector of a $3p \times 3p$ Hermitian matrix \hat{a}_k which is related to \hat{A} by the equation

$$a_k(s, j | s', j') = \sum_q A_q(s, j | s', j') \exp \left(\frac{2\pi i}{N} k \cdot q \right) \quad \dots (7)$$

The eigenvalues of \hat{a}_k are the $3p$ branch (squared) frequencies $\omega_r(k)$ for a given value of k . The branch index r can take up $3p$ values. In each branch there are N frequencies corresponding to the N values of k .

By the bilinear formula, the matrix element of \hat{G} is

$$\begin{aligned} G_{q-q'}(s, j | s', j') &= \sum_{k, r} \frac{\langle k, r, q', s', j' | k, r; q, s, j \rangle}{\omega_r^2(k) - \omega^2} \\ &= \frac{1}{(2\pi)^3} \sum_r \int_{V^*} \frac{d^3k Q_r^{s,j}(k) Q_r^{*s',j'}(k) \exp [2\pi i k \cdot (q - q')]}{\omega_r^2(k) - \omega^2} \quad \dots (8) \end{aligned}$$

In this, the summation over k has been replaced by an integration. V^* is the volume of the unit cell of the reciprocal lattice*.

In particular, the elements of \hat{G} that occur in equation (5) are given by

$$G_0(s, j | s', j') = \frac{1}{(2\pi)^3} \sum_r \int_{V^*} \frac{d^3k Q_r^{s,j}(k) Q_r^{*s',j'}(k)}{\omega_r^2(k) - \omega^2} \quad \dots (9)$$

Actual computation of the discrete frequencies has been done in those lattice models in which there is no coupling between the various components of the displacements of the atoms, since the evaluation of the matrix elements of \hat{G} is easy for such models. We will now prove a theorem that if a certain criterion is satisfied in a lattice model, an isotope defect perturbs each frequency branch separately, and evaluation of the matrix elements of \hat{G} is somewhat simpler even in the presence of coupling between the displacement components.

Only monatomic lattices can satisfy this criterion. We will evaluate the discrete frequencies in certain linear lattice models satisfying this criterion, and it will be shown that when this criterion is satisfied, the range of interaction between

In this equation the vector k is normalised in such a way that the volume V^ equals $(2\pi)^3$.

the atoms is of no consequence, as far as the solvability of the problem is concerned.

THE CRITERION FOR THE UNMIXING OF THE PERTURBATION IN DIFFERENT BRANCHES

Let us consider a monatomic lattice model ($p = 1$), in which each atom has three degrees of freedom, and in which the elements of \hat{A} satisfy the equation

$$A_{q' - q''}(j' | j'') = U_{q' - q''} \alpha(j' | j'') \quad \dots \quad (10)$$

where $\alpha(j' | j'')$ is a number independent of q .

The dynamical matrices corresponding to the various branches are obtained by a similarity transformation

$$\hat{P} \hat{A} \hat{P}^{-1} = \hat{B} \quad \dots \quad (11)$$

where \hat{B} is a matrix of the form

$$B = \begin{bmatrix} \hat{X} & \hat{O} & \hat{O} \\ \hat{O} & \hat{Y} & \hat{O} \\ \hat{O} & \hat{O} & \hat{Z} \end{bmatrix} \quad (12)$$

Here \hat{X} , \hat{Y} , and \hat{Z} are $N \times N$ submatrices.

In this model it is easily shown that the elements of \hat{P} are

$$P_{q' - q''}(j' | j'') = \delta_{q' q''} \beta(j' | j'') \quad \dots \quad (13)$$

and

$$\begin{aligned} \hat{X} &= x \hat{C} \\ \hat{Y} &= y \hat{C} \\ \hat{Z} &= z \hat{C} \end{aligned} \quad \dots \quad (14)$$

where x , y , and z are pure numbers and \hat{C} is a $N \times N$ cyclic matrix. x , y and z are, in fact, the eigenvalues of the 3×3 matrix $\hat{\alpha}$ whose elements are $\alpha(j' | j'')$. Using equation (11) it can be shown that the 3×3 matrix $\hat{\beta}$ whose elements are $\beta(j' | j'')$ diagonalises $\hat{\alpha}$ by the similarity transformation

$$\hat{\beta} \hat{\alpha} \hat{\beta}^{-1} = \begin{bmatrix} x & o & o \\ o & y & o \\ o & o & z \end{bmatrix} \quad \dots \quad (15)$$

The wellknown symmetry properties of \hat{A} require that $\hat{\alpha}$ must be a symmetric matrix, so that $\hat{\beta}$ must be an orthogonal matrix satisfying the condition,

$$\sum_j \beta(j|j') \beta(j|j'') = \delta_{j',j''} \quad \dots \quad (16)$$

The matrix $\hat{\Lambda}$ for isotope defects can be written in the form

$$\hat{\Lambda} = \begin{bmatrix} \hat{S} & \hat{O} & \hat{O} \\ \hat{O} & \hat{S} & \hat{O} \\ \hat{O} & \hat{O} & \hat{S} \end{bmatrix} \quad \dots \quad (17)$$

where \hat{S} is a $N \times N$ diagonal submatrix. Using equation (16) and the fact that \hat{S} commutes with each of the submatrices of \hat{P} (which are diagonal), it is easily shown that for this model

$$\hat{P} \hat{\Lambda} \hat{P}^{-1} = \hat{\Lambda} \quad \dots \quad (18)$$

Therefore, if we perform a similarity transformation with respect to \hat{P} on equation (3), we obtain

$$|\hat{T} + \hat{G}(x)\hat{S}| |\hat{T} + \hat{G}(y)\hat{S}| |\hat{T} + \hat{G}(z)\hat{S}| = 0 \quad \dots \quad (19)$$

where all matrices are now $N \times N$, and

$$\begin{aligned} \hat{G}(x) &= [x\hat{C} - \hat{I}\omega^2]^{-1} \\ \hat{G}(y) &= [y\hat{C} - \hat{I}\omega^2]^{-1} \\ \hat{G}(z) &= [z\hat{C} - \hat{I}\omega^2]^{-1} \end{aligned} \quad \dots \quad (20)$$

From equation (19) it is apparent that in a monatomic lattice satisfying the criterion of equation (10), the effect of isotope defects on each frequency branch is independent of the other branches.

With a single isotope defect, equation (19) reduces to the three equations

$$1 + \frac{\epsilon\omega^2}{(2\pi)^3} \int_{V^*} \frac{d^3k}{\omega_x^2(k) - \omega^2} = 0 \quad \dots \quad (21a)$$

$$1 + \frac{c\omega^2}{(2\pi)^3} \int_{V^*} \frac{d^3k}{\omega_y^2(k) - \omega^2} = 0 \quad \dots \quad (21b)$$

$$1 + \frac{\epsilon\omega^2}{(2\pi)^3} \int_{V^*} \frac{d^3k}{\omega_z^2(k) - \omega^2} = 0 \quad \dots \quad (21c)$$

An example

As a simple example of a physical lattice model satisfying the criterion of equation (10), we consider the case of a linear chain with nearest neighbour interactions and three degrees of freedom per atom. If $u_n \exp(i\omega t)$, $v_n \exp(i\omega t)$, and $w_n \exp(i\omega t)$ denote the two transverse and one longitudinal components respectively of the n -th atom from equilibrium, the equations of motion can be written in the form

$$\begin{aligned} m\omega^2 u_n &= \gamma_1(2u_n - u_{n-1} - u_{n+1}) + \gamma_2(2v_n - v_{n-1} - v_{n+1}) + \gamma_3(2w_n - w_{n-1} - w_{n+1}); \\ m\omega^2 v_n &= \gamma_2(2u_n - u_{n-1} - u_{n+1}) + \gamma_1(2v_n - v_{n-1} - v_{n+1}) + \gamma_3(2w_n - w_{n-1} - w_{n+1}), \\ m\omega^2 w_n &= \gamma_3(2u_n - u_{n-1} - u_{n+1}) + \gamma_3(2v_n - v_{n-1} - v_{n+1}) + \gamma_4(2w_n - w_{n-1} - w_{n+1}); \end{aligned} \quad \dots \quad (22)$$

Here γ_2 is the coupling between u and v components, and γ_1 is the coupling between u and w or between v and w components respectively.

The matrix $\hat{\alpha}$ in this case is of the form

$$\hat{\alpha} = \begin{bmatrix} \gamma_1 & \gamma_2 & \gamma_3 \\ m & m & m \\ \gamma_2 & \gamma_1 & \gamma_3 \\ m & m & m \\ \gamma_3 & \gamma_3 & \gamma_4 \\ m & m & m \end{bmatrix} \quad \dots \quad (23)$$

and the $N \times N$ matrix \hat{C} is of the form

$$\hat{C} = \begin{bmatrix} 2 & -1 & 0 & 0 & \dots & \dots & 0 & -1 \\ -1 & 2 & -1 & 0 & \dots & \dots & 0 & 0 \\ 0 & -1 & 2 & -1 & \dots & \dots & 0 & 0 \\ \vdots & \vdots & \vdots & \vdots & & & \vdots & \vdots \\ -1 & 0 & 0 & 0 & & & -1 & 2 \end{bmatrix} \quad \dots \quad (25)$$

The three eigenvalues of $\hat{\alpha}$, which we denote as before by x , y , and z , are easily obtained and are given by the equations

$$x = \frac{1}{m} (\gamma_1 - \gamma_2)$$

$$y = \frac{1}{2m} [\gamma_1 + \gamma_2 + \gamma_4] + \sqrt{(\gamma_1 + \gamma_2 - \gamma_4)^2 + 8\gamma_3^2}$$

$$z = \frac{1}{2m} [(\gamma_1 + \gamma_2 + \gamma_4) - \sqrt{(\gamma_1 + \gamma_2 - \gamma_4)^2 + 8\gamma_3^2}] \quad \dots \quad (25)$$

The eigenfrequencies in the various branches as functions of k (which is a one dimensional vector in this case) is obtained by taking the Fourier transform of \hat{B} in accordance with the formula of equation (7);

$$\omega_x^2(k) = 2x(1 - \cos k)$$

$$\omega_y^2(k) = 2y(1 - \cos k)$$

$$\omega_z^2(k) = 2z(1 - \cos k) \quad \dots \quad (26)$$

We will discuss the equation for the discrete frequency generated from one of the branches only. Equation (21a) can be written in the following form by substituting for the denominator of the integrand from equation (26);

$$1 + \frac{\epsilon\omega^2}{2\pi} \int_{-\pi}^{\pi} \frac{dk}{2x(1 - \cos k) - \omega^2} = 0 \quad \dots \quad (27)$$

For discrete frequencies we are interested in the region $\omega^2 > \omega_{xL}^2$, where $\omega_{xL}^2 = 4x$, the maximum frequency of that branch. In this region equation (27) reduces to the form

$$1 - \frac{\epsilon\omega}{\sqrt{\omega^2 - \omega_{xL}^2}} = 0 \quad \dots \quad (28)$$

A solution of this equation for $\omega > \omega_{xL}$ can exist only for positive ϵ , i.e., for a lighter isotope defect, and this solution is

$$\omega_{x0} = \frac{\omega_{xL}}{\sqrt{1 - \epsilon^2}} \quad \dots \quad (29)$$

The treatment of the other two secular equations proceeds along identical lines.

Thus, in this example, a single lighter isotope defect generates three discrete frequencies, one from each of the acoustic branches. However, for small ϵ the physical observable discrete frequency is the one, which is above the maximum frequency of the stiffest branch, since the other two discrete frequencies will lie submerged among the quasicontinuum of frequencies of the stiffest branch.

A LINEAR LATTICE WITH LONG RANGE INTERACTIONS

In a linear lattice with long range interactions, the equations of motion can be written in the form (with infinite number of atoms)

$$m\omega^2 u_n = \sum_p [\Gamma_p^{(u,u)}(2u_n - u_{n-p} - u_{n+p}) + \Gamma_p^{(u,v)}(2v_n - v_{n-p} - v_{n+p})$$

$$+ \Gamma_p^{(u,w)}(2w_n - w_{n-p} - w_{n+p})]; \quad \dots \quad (30)$$

with two similar equations for the other two components. Here $\Gamma_p^{(u,v)}$ is the coupling constant between the u -displacement of an atom and the v -displacement of its p -th neighbour.

A physically reasonable assumption to make on the properties of the coupling constants is that they all depend on the distance of separation of the interacting atoms in accordance with the same law. In that case, one can write

$$\Gamma_p^{(u,v)} = \gamma^{(u,v)} f(p) \quad \dots (31)$$

where the function $f(p)$ suitably describes the dependence of the coupling constants on the distance of separation of the atoms.

This model satisfies the criterion of equation (10). The matrix $\hat{\alpha}$ will have the same form as in equation (23), if we use the following equivalences,

$$\begin{aligned} \gamma^{(u,u)} &= \gamma^{(v,v)} = \gamma_1, & \gamma^{(u,v)} &= \gamma^{(v,u)} = \gamma_2; \\ \gamma^{(u,w)} &= \gamma^{(w,u)} = \gamma^{(v,w)} = \gamma^{(w,v)} = \gamma_3; & \gamma^{(w,w)} &= \gamma_4. \end{aligned}$$

The matrix \hat{C} is now of the form

$$\hat{C} = \begin{vmatrix} 2 \sum_p f(p) & -f(1) & -f(2) & \dots & \dots \\ -f(1) & 2 \sum_p f(p) & -f(1) & \dots & \dots \\ -f(2) & -f(1) & 2 \sum_p f(p) & \dots & \dots \\ -f(3) & -f(2) & -f(1) & \dots & \dots \\ \vdots & \vdots & \vdots & \ddots & \ddots \end{vmatrix} \quad \dots (32)$$

The eigenfrequencies of the various branches are

$$\omega_x^2(k) = 2x \left[\sum_{p=1}^{\infty} f(p) - \sum_{p=1}^{\infty} f(p) \cos pk \right] \quad \dots (33)$$

with two similar equations for the other two branches. The maximum frequency of the branch is evidently $4x \left[\sum_{p=0}^{\infty} f(2p+1) \right]$. As before, we will evaluate the discrete frequency generated from one of the branches only. The secular equation is

$$1 + \frac{\epsilon \omega^2}{2\pi} \int_0^{\infty} \frac{dk}{2x \left[\sum_p \{f(p) - f(p) \cos pk\} - \omega^2 \right]} = 0 \quad \dots (34)$$

The integral in equation (34) can be done exactly for several assumed forms of $f(p)$. We give below the results for the discrete frequency arising outside the band in a few cases.

$$(i) \quad f(p) = \exp(-p\sigma).$$

The integral in equation (34) can be done exactly for $\omega^2 > \omega_{xL}^2$, and in terms of a variable $\theta = \cosh^{-1}\omega/\omega_{xL}$, the discrete frequency is the root of the equation

$$\coth \left(\theta + \frac{\sigma}{2} \right) = \frac{1}{\epsilon} \tanh \theta \quad \dots (35)$$

It is easy to show graphically and otherwise that for values of ϵ in the range $0 < \epsilon < 1$ a solution of this transcendental equation must exist, and hence a discrete frequency must arise. For very small values of ϵ , the discrete frequency is

$$\omega_{x0} \simeq \omega_{xL} \left(1 + \frac{\epsilon^2}{2} \coth^2 \frac{\sigma}{2} \right) \quad \dots (36)$$

$$(ii) \quad f(p) = (p)^{-2r}; \quad r = \text{Integer}.$$

The series occurring in the denominator of the integrand in equation (34) can be summed exactly in accordance with the formulae (Jeffreys and Jeffreys, 1956),

$$\sum_{p=1}^{\infty} (p)^{-2r} \cos pk = \frac{(-1)^{r-1}}{2} \cdot (4\pi^2)^r \left[P_{2r} \left(\frac{k}{2\pi} \right) + b_{2r} \right]$$

$$\text{and} \quad \sum_{p=1}^{\infty} (p)^{-2r} = \zeta(2r)$$

where P_{2r} and b_{2r} are respectively the Bernoulli polynomial and the Bernoulli number of order $2r$ respectively, and $\zeta(2r)$ is the Riemann Zeta function. $\zeta(2r)$ is related to b_{2r} through the equation

$$\zeta(2r) = \frac{(-1)^{r-1}}{2} (4\pi^2)^r b_{2r}$$

The first few Bernoulli polynomials are

$$P_2(x) = \frac{1}{6} (x^3 - x); \quad P_4(x) = \frac{1}{24} (x^5 - 2x^3 + x^2);$$

$$P_6(x) = \frac{1}{720} \left(x^7 - 3x^5 + \frac{5}{2} x^4 - \frac{1}{2} x^2 \right);$$

$$P_8(x) = \frac{1}{40320} \left(x^9 - 4x^7 + \frac{14}{3} x^6 - \frac{7}{3} x^4 + \frac{2}{3} x^2 \right).$$

The first few Bernoulli numbers are

$$b_2 = \frac{1}{12}; \quad b_4 = -\frac{1}{720}; \quad b_6 = \frac{1}{30240}; \quad b_8 = -\frac{1}{1209600}.$$

The equation for the discrete frequency for $r = 1$ is (with $\eta = \frac{\omega}{\omega_{xL}}$

$$\frac{\eta^2}{\sqrt{\eta^2 - 1}} \sin^{-1} \frac{1}{\eta} = \frac{1}{c} \quad \dots \quad (37)$$

A solution of this equation will always exist for $0 < c < 1$, and for $c < 1$, the discrete frequency is

$$\omega_{x0} \cong \omega_{xL} \left(1 + \frac{c^2 \pi^2}{8} \right) \quad \dots \quad (38)$$

For $r = 2$, the equation for the discrete frequency is

$$\frac{\eta}{4\sqrt{1+\eta}} \log \frac{\sqrt{1+\eta}+1}{\sqrt{1+\eta}-1} + \frac{\eta}{2\sqrt{\eta-1}} \sin^{-1} \frac{1}{\eta} = \frac{1}{c} \quad \dots \quad (39)$$

In this case also, a solution will always exist for $0 < c < 1$, and for $c < 1$ the discrete frequency is given by

$$\omega_{x0} \cong \omega_{xL} \left(1 + \frac{c^2 \pi^2}{16} \right) \quad \dots \quad (40)$$

CONCLUSION

If the condition described in equation (10) does not hold for any given lattice model, the perturbation due to the isotope defect mixes up the various frequency branches, so that it may not be possible to find a one to one correspondence between the discrete frequencies and the unperturbed frequency branches. The models discussed here are one dimensional, but there is no essential complication in the case of two and three dimensional crystals as long as they satisfy the criterion of equation (10). For three dimensional crystals the evaluation of the integrals in equation (21) can be done numerically if one knows the frequency distribution function of the unperturbed lattice. Whether any actual crystals can be adequately represented by a model satisfying the criterion of equation (10) must remain an open question.

Discrete Frequencies in a Lattice Perturbed by Isotope, etc. 137

We have seen that the difference between the discrete frequency and the maximum frequency of any branch depends on ϵ^2 . This property is related to the existence of the square root singularity in the frequency distribution function of a linear lattice. A simple proof of the fact that for small ϵ one can expect the discrete frequency to depend on ϵ^2 irrespective of the details of the law of interaction between the atoms in a linear lattice is given in the Appendix.

APPENDIX

When ϵ is very small, a solution of equation (34) would exist only if ω is slightly greater than ω_{xL} . Let

$$\sum_{p=1}^{\infty} [f(p) - f(p) \cos pk] = F(k).$$

$F(k)$ has a maximum at $k = \pi$, and evidently

$$\omega_{xL}^2 = 2xF(\pi).$$

In the neighbourhood of this maximum we can expand $F(k)$ in a power series in $k' = k - \pi$. Remembering that most of the contribution to the integral comes from the neighbourhood of $k' \cong 0$, we can write the integral in equation (34) in the form

$$-\int_{-\infty}^{\infty} \frac{dk'}{(\omega^2 - \omega_{xL}^2) - xF''(\pi)k'^2} = \frac{\pi}{xF''(\pi)} \frac{1}{\sqrt{\omega^2 - \omega_{xL}^2}}.$$

We thus get the following approximate secular equation for the discrete frequency for small ϵ ;

$$1 - \frac{\epsilon\omega^2}{2\sqrt{xF''(\pi)}} \frac{1}{\sqrt{\omega^2 - \omega_{xL}^2}} \cong 0.$$

The solution of this equation is

$$\omega_{x0} = \omega_{xL} \left[1 + \frac{F(\pi)}{4F''(\pi)} \epsilon^2 \right].$$

ACKNOWLEDGMENT

One of the authors (R.K.S.) is indebted to the authorities of the Punjab University for the award of a research scholarship.

REFERENCES

- Jeffreys, H. and Jeffreys, B. S., 1956, *Methods of Mathematical Physics*, (Cambridge University Press), p. 388.
- Lifshitz, I. M., 1943a, *J. Phys. USSR*, **7**, 215.
- Lifshitz, I. M., 1943b, *J. Phys. USSR*, **7**, 240.
- Lifshitz, I. M., 1944, *J. Phys. USSR*, **8**, 89. **4**, 716.
- Montroll, E. W., and Potts, R. B., 1955, *Phys. Rev.*, **100**, 525.
- Montroll, E. W. and Potts, R. B., 1956, *Phys Rev.*, **102**, 72.
- Nardelli, G. F., 1960, Dynamics of Cubic Crystal Lattices Perturbed by a Local Change of Mass, (Tech. Rep., Institute of Physics, University of Milan).

HYDROGEN BONDING IN ANILINE AND SOME SUBSTITUTED ANILINES IN DIFFERENT ENVIRONMENTS

K. C. MEDHI AND G. S. KASTHA

OPTICS DEPARTMENT, INDIAN ASSOCIATION FOR THE CULTIVATION OF SCIENCE, CALCUTTA-32

(Received January 16, 1963)

ABSTRACT. A comparative study on the shifts in the frequencies of infrared absorption bands due to the symmetric and asymmetric N-H stretching vibrations of aniline and some methoxy- and ethoxy anilines in the liquid state and in solutions in some polar solvents relative to those of the respective compounds in dilute CCl_4 solution has been made. The shifts observed with all the compounds in different environments have been attributed to the formation of intermolecular hydrogen bonds and it has been pointed out that the strength of the hydrogen bond depends on the electronic nature of the substituents and is affected by steric interactions between the molecules of the same type in the pure liquids and in the case of solutions of the ortho-compounds between the solvent and the solute molecules.

INTRODUCTION

Though inference about the formation of intermolecular hydrogen bonds, in solutions of aniline in polar solvents, between the solute molecules of aniline and molecules of the polar solvents, e.g., chloroform, tetrahydrofuran and dioxane was made by some workers (Krueger and Thompson, 1957; Whetsel, 1962), it was Bellamy, Hallam and Williams (1958) who pointed out that solvent-solute dipolar interactions are mainly responsible for the formation of such hydrogen bridges. Later, Cutmore and Hallam (1962) extended these investigations to some substituted aniline compounds and showed that the relative shifts may be related to the pK_a values of the amines provided that due considerations of other solvation interactions, such as structural effects are taken into account. But it seems that very little work on the influence of structure of the molecules of both the solute and solvent on the strength of intermolecular hydrogen bridges has been carried out. Recently, Medhi, *et al.* (1962) showed that hydrogen bonding in toluidines in the pure compounds and in solutions in polar solvents depends on the relative positions of the substituents and the Hammett σ -factor of the CH_3 group in the ring of the aniline molecule. In order to understand how the formation of hydrogen bonds in substituted anilines in different environments depends on the electronic nature and positions of the substituent groups and also on the characteristics of the polar solvents, the infrared spectra of some methoxy and ethoxy anilines in the pure state and in solutions in some polar solvents have been

investigated and the results have been compared with those obtained with aniline under similar conditions.

EXPERIMENTAL

Pure samples of aniline, *o*-, *m*- and *p*-anisidine and *o*- and *m*-phenetidine supplied by reputed firms of U.S.A. and England were fractionated and the appropriate fractions were further distilled under reduced pressure. The solvents were also carefully purified and dried. A Perkin-Elmer Model 21 spectrophotometer provided with rock salt optics was used to record all the spectra due to the pure compounds and their solutions with arrangements described in a previous paper (Banerjee and Kastha, 1962). The absorption bands due to N-H stretching vibrations of aniline in very dilute CCl_4 solution were recorded from time to time to check the reliability of the recorded spectra.

RESULTS AND DISCUSSION

The symmetric (ν_s) and asymmetric (ν_a) N-H stretching vibrational frequencies in cm^{-1} for the compounds are given in Table I. Table II contains the values of the shifts in cm^{-1} of the frequencies of symmetric and asymmetric vibrations (denoted respectively by $\Delta\nu_s$ and $\Delta\nu_a$) and their mean values for all the compounds in different environments relative to the frequencies of the respective compounds in 1% carbon tetrachloride solution. The values of Hammett σ -factors for some of these compounds given by Krueger and Thompson (1957) are included in both the Tables.

(a) Aniline

The two bands at 3402 and 3476 cm^{-1} of aniline in 1% CCl_4 solution shift respectively to 3398 and 3460 cm^{-1} in 1% solution of the compound in chloroform and with the increase in concentration of the chloroform solution the centres of these two bands further shift to lower frequencies. Doublet structure of the two bands in chloroform solution as reported by some workers (Krueger and Thompson, 1957; Moritz, 1962; Whetsel, 1962) has not been detected, but the band at 3460 cm^{-1} in 1% solution of aniline in chloroform is rather broad and the strength of absorption in the region between the two bands is found to increase markedly with increase in the concentration of aniline in the chloroform solution. In contrast to the proton-donor solvent chloroform, the proton-acceptor solvents acetone, ether, tetrahydrofuran and pyridine shift the N-H stretching vibrational frequencies to lower frequencies by larger amounts. The shift is largest in the case of pyridine solution and of the three other polar solvents, each containing an oxygen atom with lone electron pairs, tetrahydrofuran produces larger shifts than either acetone or ether both of which shift the N-H stretching frequencies by almost the same amount. The shifts in these frequencies of aniline in the liquid state are intermediate between those in tetrahydrofuran and in pyridine solutions,

Not only the frequencies of N-H stretching vibrations of aniline are changed but also the width and the strength of these absorption bands are affected by the polar solvents. The band 3476 cm^{-1} of aniline dissolved in pyridine becomes broad and is weakened in such a way that its presence in 1% solution is almost undiscernible and in solutions of higher concentrations it appears only as a hump. In the case of solutions in acetone, ether and tetrahydrofuran the ratio of the strength of the band due to symmetric vibration to its asymmetric counterpart is greater than that in CCl_4 solution. In the pure liquid and in solution in chloroform this ratio remains almost the same as in the solution in carbon tetrachloride.

The changes observed in solutions of aniline in polar solvents evidently arise from the formation of intermolecular hydrogen bridges between the hydrogen atoms of the NH_2 group of aniline molecule and the N-atom of pyridine or the oxygen atom of acetone, ether and tetrahydrofuran. The hydrogen bond in the pure liquid involves the hydrogen atom of the N-H bond of an aniline molecule and the N-atom of NH_2 group in a neighbouring molecule. The large shifts observed in the case of the pure liquid and in solution of pyridine indicate the formation of fairly strong $\text{N-H}\cdots\text{N}$ bonds.

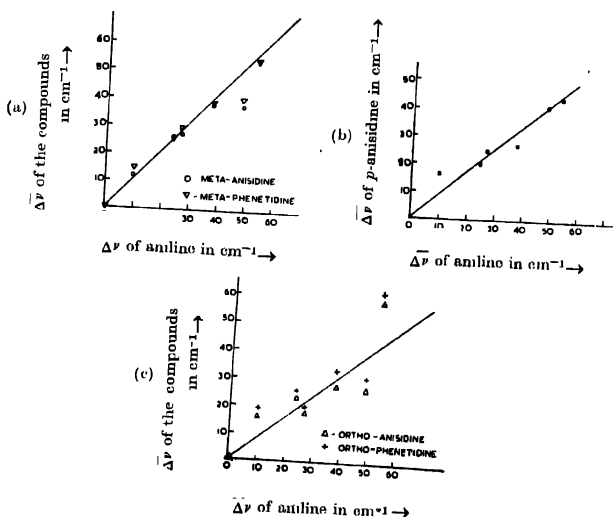


Fig. 1. Plot of mean solvent shifts ($\bar{\Delta\nu}$) in cm^{-1} of (a) *m*-anisidine and *m*-phenetidine, (b) *p*-anisidine, (c) *o*-anisidine and *o*-phenetidine, against those of aniline

(b) *Substituted anilines*

The N-H stretching vibrational frequencies of the ortho- and meta-isomers of anisidine and phenetidine in 1% CCl_4 solution are higher than those of aniline

in the same solution while in the case of para-anisidine these frequencies are lower than those of aniline. The observed variations in the frequency of N-H vibrations of these compounds in solutions of CCl_4 and other solvents with the Hammett σ -factor of the substituent methoxy and ethoxy groups are similar to those reported by Krueger and Thompson (1957). The nature of the solvent shifts ($\Delta\nu_s$ and $\Delta\nu_d$) for all the substituted anilines in different solvents in general is the same as that observed with aniline under similar condition and this is clearly seen from the graphs in Fig. 1., where the mean values of the shifts $\Delta\nu_s$ and $\Delta\nu_d$ for each of the compounds have been plotted against the corresponding quantities for aniline. It is seen from the graphs that for all the compounds the mean solvent shifts are linearly related to those of aniline. The slope of the straight line is slightly greater than unity for the meta-compounds and for the ortho-compounds and para-anisidine the slopes are much less than unity. The unit slope of the straight line for meta-anisidine and meta-phenetidine indicates that the causes producing the solvent shifts in aniline and in the meta-compounds are almost similar, but the value less than unity of the slope for ortho-anisidine, ortho-phenetidine and para-anisidine points to the fact that the causes producing the solvent shifts are not operative in these compounds as effectively as in aniline. The proximity of the OMe and the OEt groups to the NH_2 group in the ortho-compounds and the negative value of Hammett σ -factor for *p*-anisidine may

TABLE I
N-H stretching frequencies in cm^{-1}

Compound and Hammett σ	Pure		Solution in						Type of vibra- tion
	Liquid	Solid	CCl_4	HCCl_3	$(\text{C}_2\text{H}_5)_2\text{CO}$	$(\text{C}_2\text{H}_5)_2\text{O}$	$(\text{CH}_3)_2\text{O}$	$\text{C}_6\text{H}_5\text{N}$	
Aniline $\sigma = 0.0$	3360 3420		3402 3476	3398 3460	3380 3450	3376 3448	3304 3438	3340 3430	ν_s ν_d
Meta- anisidine $\sigma = +0.115$	3372 3437		3404 3480	3400 3460	3381 3452	3380 3450	3308 3440	3340 3436	ν_s ν_d
Meta- Phenetidine $\sigma = +0.150$	3367 3434		3403 3478	3391 3461	3380 3451	3373 3450	3362 3442	3341 3432	ν_s ν_d
Para- Anisidine $\sigma = -0.268$	3353 3420	3307 3386	3395 3460	3380 3443	3375 3440	3366 3440	3362 3439	3342 3425	ν_s ν_d
Ortho- Anisidine	3380 3452		3405 3480	3393 3460	3384 3455	3380 3470	3370 3460	3328 3440	ν_s ν_d
Ortho- Phenetidine	3370 3454		3403 3483	3390 3458	3376 3459	3377 3469	3363 3457	3323 3440	ν_s ν_d

TABLE II
Solvent shifts in cm^{-1}
Mean values are given in brackets
Compound and Hammett σ

Solution in	Aniline $\sigma = 0.0$		<i>m</i> -Anisidine $\sigma = +0.115$		<i>m</i> -Phenetidine $\sigma = +0.150$		<i>p</i> -Anisidine $\sigma = -0.268$		<i>o</i> -Anisidine		<i>o</i> -Phenetidine	
	$\Delta\nu_s$	$\Delta\nu_a$	$\Delta\nu_s$	$\Delta\nu_a$	$\Delta\nu_s$	$\Delta\nu_a$	$\Delta\nu_s$	$\Delta\nu_a$	$\Delta\nu_s$	$\Delta\nu_a$	$\Delta\nu_s$	$\Delta\nu_a$
CHCl_3	4	16	4	20	12	17	15	17	12	20	13	25
	(10)		(12)		(14.5)		(16)		(16)		(19)	
$(\text{CH}_3)_2\text{CO}$	22	26	23	28	23	27	20	20	21	25	27	24
	(24)		(25.5)		(25)		(20)		(23)		(25.5)	
$(\text{C}_2\text{H}_5)_2\text{O}$	26	28	24	30	30	28	29	20	25	10	26	14
	(27)		(27)		(29)		(24.5)		(17.5)		(20)	
$(\text{CH}_2)_4\text{O}$	38	38	36	40	41	36	33	21	35	20	40	26
	(38)		(38)		(38.5)		(27)		(27.5)		(33)	
	62	46	64	44	62	46	53	35	77	40	80	43
	(54)		(54)		(54)		(44)		(58.5)		(61.5)	
Liquid	42	56	32	43	36	44	42	40			33	29
	(49)		(37.5)		(40)		(41)		(26.5)		(31)	

be responsible for such shielding effect. Like the solvent shift, the changes in the width and intensity of the bands of the compounds in different environments also follow the same pattern as in the case of aniline.

A careful examination of Table II reveals that the solvent shifts for meta-anisidine and meta-phenetidine are slightly greater than the corresponding shifts for para-anisidine. The slightly positive value of the Hammett σ factor of meta-anisidine and meta-phenetidine makes the H-atoms in the NH_2 group slightly more positive and consequently the intermolecular N-H...N and N-H...O bridges are stronger in these cases than in the case of para-anisidine where the Hammett σ -factor is negative. The proximity of the methoxy and the ethoxy group to the NH_2 group in the ortho-compounds and consequent steric interaction complicate the simple interpretation. However, the largest solvent shift observed with these compounds in pyridine solution definitely indicates stronger N-H...N bonds and hence larger positive charge on the H-atoms of the NH_2 group of the compounds as compared to aniline, meta-anisidine and meta-phenetidine. Not only the influence of the steric effect of the solute molecules but also that of solvent molecules on the strength of the intermolecular N-H...O hydrogen bonds is to be considered. A comparison of the mean solvent shifts for the ortho-compounds in solutions of acetone, ether and tetrahydrofuran shows that the shifts in acetone and tetrahydrofuran are larger than the mean shift in ether solution.

This seems to indicate that the interaction of the steric hindrances of the OMe group or the OEt group in the ortho-compounds with the C_2H_5 group of ether molecule makes the N-H...O bonds weaker in comparison to that in the solution in acetone or tetrahydrofuran.

ACKNOWLEDGMENT

The authors' grateful thanks are due to Professor S. C. Sirkar, D.Sc., F.N.I., for his kind interest in the work.

REFERENCES

- Banerjee, S. B. and Kastha, G. S., 1962, *Ind. J. Phys.*, **36**, 163.
Bellamy, L. J., Hallam, H. E., and Williams, R. L., 1958, *Trans. Farad. Soc.*, **54**, 1120.
Cutmore, E. A. and Hallam, H. E., 1962, *Trans. Farad. Soc.*, **58**, 40.
Krueger, P. J. and Thompson, H. W., 1957, *Proc. Roy. Soc.*, **243A**, 143.
Medhi, K. C., Banerjee, S. B. and Kastha, G. S., 1962, *Ind. J. Phys.*, **36**, 457.
Moritz, A. G., 1962, *Spectrochim. Acta.*, **17**, 365.
Whetzel, K. B., 1962, *Spectrochim. Acta.*, **17**, 614.

OBSERVATION OF 'HAMMER' STARS CAUSED BY Li⁹—DECAY

G. C. DEKA AND K. M. PATHAK

DEPARTMENT OF PHYSICS, COTTON COLLEGE, GAUHATI

(Received September 1, 1962)

Plate IV

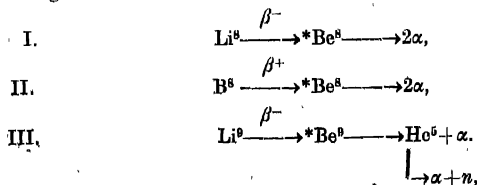
ABSTRACT. In a systematic area scanning of emulsion pellicles irradiated with the separated beam of 4.0 GeV/c negative pions, 290 double stars—so-called 'hammer' stars—have been observed and carefully measured. It is seen that 35 of these events have got some features which distinguish them from the ordinary 'hammer' tracks usually caused by Li⁸-decay. From their kinematical analyses, these 35 events can be interpreted as due to the radio-active decays of the Li⁹-nuclei. Also the energy levels of Be⁸ can be calculated from their analyses.

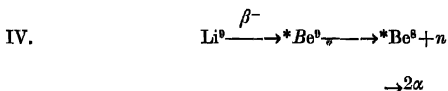
INTRODUCTION

'Hammer' tracks caused by the radio-active decay of Li⁸ have been of interest since its first discovery by Powell and Occhialini in 1947. Even at present quite a number of workers in different laboratories have been doing experiments to study in details the emission of 'hammer' tracks in the high energy interactions initiated by protons and pions. Very recently the Warsaw group has made an attempt to investigate thoroughly the emission frequency of 'hammer' tracks caused not only by decays of Li⁸, but also by the similar decays of Li⁹ and B⁸ nuclei at different incident energy in the GeV region. They have discussed in their paper all about the possibility of emission and the kinematics and their work is still continued. Our group has also been engaged in such problems for the last two years. We have recently reported a conspicuous event which seems to be a possible example of Li⁹ 'hammer' track. In this paper we are reporting a few more 'hammer' tracks which are kinematically possible to be due to Li⁹ decays.

Possible reactions :

The characteristic 'hammer' tracks are assumed to be the results of the following reactions :





Li^9 and B^8 -decays are kinematically indistinguishable. But as the Li^9 -decay in the final stage is a three-body-decay, in principle, alpha tracks should be non-collinear; and if the range and the angle measurements for alpha tracks are possible, then the Be^9 or He^6 energy levels for the assumed scheme can be calculated from the following formulae:

Energy levels in Mev

$$\text{I. } \text{Be}^9: E_9 = 5(E_1 + E_2) - 8\sqrt{E_1 E_2} \cos \psi + 1.57.$$

$$\text{II. } \text{Be}^8: E_8 = 0.5(E_1 + E_2) + \sqrt{E_1 E_2} \cos \psi - .094.$$

$$\text{III. } \text{He}^6: E_6 = 3.2 E_1 + 5E_2 - 8\sqrt{E_1 E_2} \cos \psi - .96.$$

where E_1 and E_2 are energies of alphas (in Mev) in the L-system and ψ is the angle between the direction of one alpha-track and the extension of the other.

EXPERIMENTAL PROCEDURE

A stack of Ilford G_5 emulsions was exposed at the Berkeley Bevatron to a negative pion beam of 4.6 Gev/c. The beam flux was $\approx 10^6/\text{cm}^2$. The plates were area scanned under low magnification (225X). About 30,000 stars with $N_\alpha \geq 6$ have been seen and 290 'hammer' tracks are recorded. Of these 'hammer' tracks, 35 are found to have the alpha tracks that are non-collinear in direction and unequal in ranges. Measurements are made under higher magnification and by two observers independently so as to minimise the bias.

Identification of Li^9 'hammer' tracks:

The Li^9 'hammer' track was first detected by Gardner (1951) and later was confirmed by Holt (1952) who obtained a life time of 0.17 sec for its beta-decay. It should be very hard to distinguish 'hammer' tracks produced by Li^9 , B^8 , and Li^9 in emulsions. However, whereas the angle between the alpha-particles from the Li^9 and B^8 decays would not exceed 6° , the presence of the neutron in the Li^9 -decay (reaction III and IV) would allow much greater disparity between the momenta taken by the two alpha particles and thus give greater angles between their directions of motion and also greater differences in their ranges. Such differences were calculated by Christy *et al.* (1947). And on the basis of such calculations Fry (1953) and Munir (1956) reported two 'hammer' tracks which were interpreted as being due to decays of Li^9 . Fry found in his event the angle of non-collinearity of 40° between the alpha-particles; and the calculated total energy release to conserve momentum indicated that the Be^9 was probably created in the

6.8 Mev excited state although the measurements errors were large in computing this excitation energy.

Our sample of 35 events which are assumed to be all due to Li^0 decay may be an admixture of several things, e.g. a scattering, a small collision star, a capture star, or a decay of hyperfragment etc., which may produce a non-collinear star of two short tracks with the appearance of a 'hammer' track. To minimise these biases we examined carefully every star for the presence of the electron track, any light π -track associated with the star and the pair of alpha- tracks; also we examined closely the parent track for its possible charge, any coulomb scattering at the end and any tapering which usually indicate the stopping of the particle. And thus it is easy to eliminate the first three biases when the parent track is long enough. The possibility of a hyperfragment decay is very low because it is unlikely that a π^- -track from hyperfragment decay will be missed from observations. Finally, on the basis of the kinematical analysis of the alpha pair we accept these 35 events as due to Li^0 -decays.

RESULTS

The following histograms represent the experimental results.

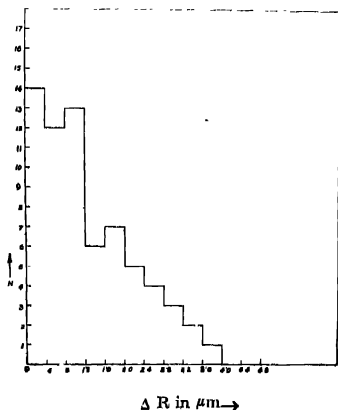


Fig. 1. Histogram showing the ΔR -distribution of the alpha-pairs, excluding those with $\Delta R = 0$, $\psi = 0$.

Fig. 1. shows the ΔR distribution of alpha-pairs. It includes alpha-pairs having any dip angle with respect to the emulsion plane. It has been found that there are as many as 9 non-collinear pairs having the range difference greater than 2.5μ .

Fig. 2. shows the distribution of the angles (ψ) of non-collinear alpha-pairs. We have found 15 events having $\psi \geq 15^\circ$ which indicates frequent occurrence

of larger angle $\psi \geq 15^\circ$, hence a relatively high yield of Li^9 -‘hammer’ tracks. But it cannot be overlooked that the large uncertainty in depth measurements

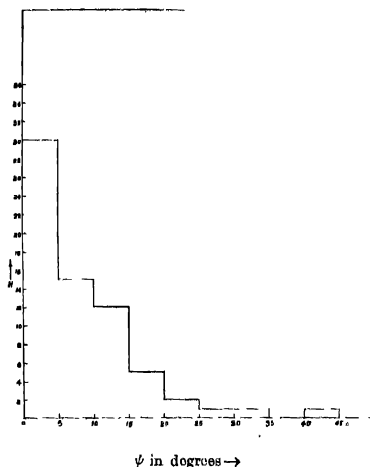


Fig. 2. Histogram showing the ψ -distribution of the alpha-pairs, excluding pairs with $\Delta R = 0$, and $\psi = 0$.

may easily be responsible for such large values of ψ . It has, however, been estimated that the uncertainty for the angle due to undetected multiple Coulomb scattering and for the angle measurement between two short tracks ($\leq 5\mu$) is nearly 8° ; this is to be added to the real spread of 6° of usual Li^9 ‘hammer’ tracks.

Fig. 3. shows the ΔR vs ψ distribution. As the ΔR and ψ distributions (Fig. 1 and 2) are likely to be biased because of the large experimental errors, we have tried to detect any grouping of the events by plotting the values of ΔR and ψ for the alpha-pairs of all the collinear and non-collinear events. This distribution indicates that alpha pairs with larger ψ have rather larger ΔR , and hence a sort of grouping too.

Fig. 4. shows the distribution of E_α for Be^9 nucleus. The histogram has a peak at ≈ 6.7 Mev. with no other distinguishing peaks. The known energy levels of Be^9 nucleus have also been shown in the graph for comparison. It appears as if most of these possible Be^9 nuclei are decaying from the known level at ≈ 6.7 Mev.

Fig. 5. shows microphotographs of a few conspicuous non-collinear events which could be interpreted as Li^9 -‘hammer’ tracks.

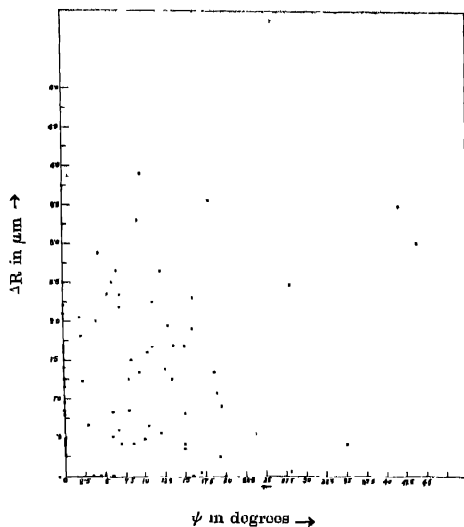


Fig. 3. ΔR vs ψ distribution for alpha-pairs.

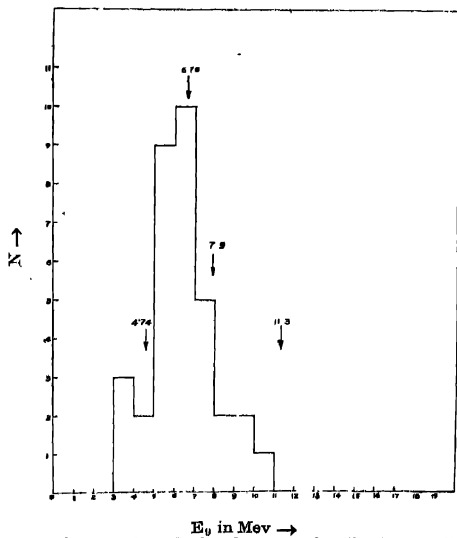


Fig. 4. Histogram showing the calculated energy distribution of Be^0 ; the values of the known energy levels in Be^0 are also shown in the figures for comparison.

ACKNOWLEDGMENT

We express our gratitude to the Govt. of Assam for providing us the facilities for such a piece of research work in the department of Physics, Cotton College, Gauhati. We must thank Sri H. C. Goswami, the Principal of the college, and many of our colleagues for their constant encouragement and helpful advice. We are also grateful to the Department of Atomic Energy, Govt. of India, for their annual financial aid. We like to thank Sri T. Baruah for his help in the scanning work.

REFERENCES

- Christy, R. F., Cohen, E. R., Fowler, W. A., Lauritsen, C. C., and Lauritsen, T., 1947, *Phys. Rev.*, **72**, 698.
- Deka, G. C., and Pathak, K. M., 1962 *Ind. Jour. Phys.*, **36**, 105.
- Fry, W. F., 1953, *Phys. Rev.*, **89**, 325.
- Gajewski, W., Pniewski, J., Pniewski, T., Sieminska, J., Soltan, M., Soltynski, K., and Suchozowska, J., 1961, *Polish Academy of Sciences*, Report No. 286/VI, Dec.
- Gardner, W. L., Knoble, N., and Mayer, B. J., 1951, *Phys. Rev.*, **83**, 1054.
- Holt, R. B., Thorne, R. N., and Watwisk, R. W., 1952, *Phys. Rev.*, **87**, 378.
- Munir, B. A., 1950, *Phil. Mag.*, **1**, 355.
- Powell, C. F., and Oechelham, G. P. S., 1947, *Nature*, **159**, 53.

DEKA & PATHAK

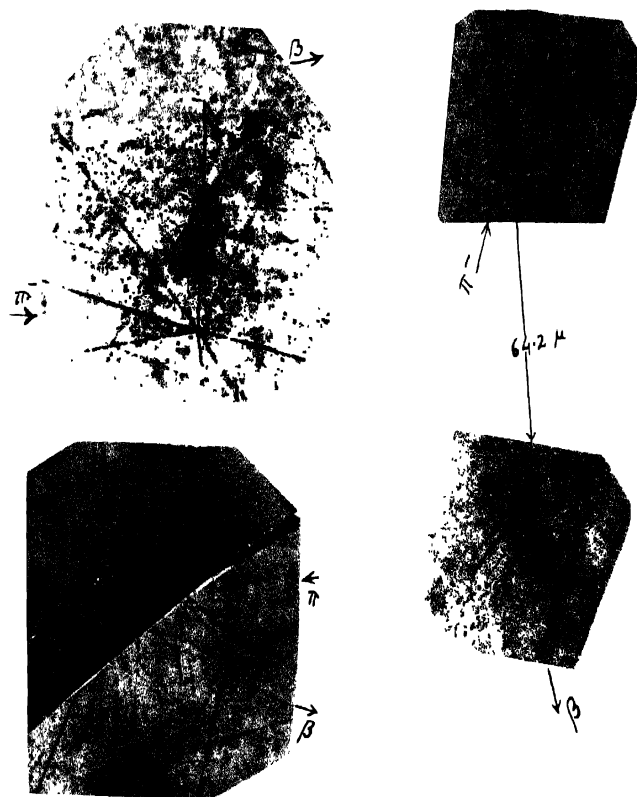


Fig. 5. Three non-collinear 'hammar' tracks

ON THE TEMPERATURE-EFFECT OF THE DAILY VARIATION OF COSMIC RAY MESON INTENSITY

R. P. KANE

PHYSICAL RESEARCH LABORATORY, AHMEDABAD, INDIA

(Received June 11, 1962)

ABSTRACT. The effect of the daily variation of atmospheric temperature on the daily variation of cosmic ray meson intensity recorded at ground level is discussed. Estimates of possible magnitudes of temperature effect are critically examined and shown to be rather unsatisfactory. Using for the temperature coefficient an *ad hoc* value of $0.02\%/^{\circ}\text{C}$ of ground temperature, past results regarding long-term changes of the amplitudes and hours of maxima of the first and second harmonic of daily variation of cosmic ray meson intensity are re-examined. It is shown that the temperature correction causes appreciable changes. However, in view of the divergent estimates of the temperature effects obtained so far, it is emphasised that a rigorous attempt at accurate experimental determination of daily variation of upper atmospheric temperatures is urgently needed.

INTRODUCTION

The atmospheric effects of cosmic ray intensity may be classified as :-

- (a) Barometric pressure effect.
- (b) Effect of liquid water content of over-hanging clouds.
- (c) Effect of passage of cold and warm air fronts.
- (d) Effect of snow deposition above the instrument.
- (e) Effects due to temperature distribution in the atmosphere.

Amongst these, the pure absorption effects (a) and (d) are well understood. For neutron intensity, the barometric pressure coefficient is about $0.96\%/\text{mm.Hg}$. (It is not quite known whether it is the same for high and low altitudes). For mesons, it is $0.22\%/\text{mm.Hg}$ for high latitude sea-level stations. As shown by Wada (1960), it reduces to $0.19\%/\text{mm.Hg}$ for equatorial, sea-level mesons. Also, both these coefficients increase rapidly with altitude, e.g., the value for mesons at Huancayo (alt. 3.4km) at equator is about $0.33\%/\text{mm.Hg}$. If the barometric pressure records at ground level are available, the barometric pressure effect can be adequately corrected for. Absorption due to deposition of snow above the instrument can also be corrected for if the snow thickness can be measured. Usually, workers prefer to eliminate this effect by continuously melting the snow by artificially heating the roof.

The effect of liquid water content of over-hanging clouds is a very uncertain factor (Arakawa, 1959). Since it does not affect the barometric pressure recorded

at ground, it is not taken care of by barometric correction. The effect is negligible for mesons but can be quite large $\sim(1.2\%)$ for neutrons. There is no simple way of correcting for it.

Effect of the passage of warm and cold air fronts seems to be more prominent for mesons than for neutrons. In principle, it can be corrected for if the temperature distribution of the atmosphere is known. However, in the dynamic, rapidly changing conditions of the atmosphere during storms, it is difficult to determine the temperature distribution. Hence, a correction becomes difficult.

The temperature distribution in the atmosphere directly affects the heights of the meson formation layers. Due to the limited life-times of mesons, their decay probabilities and hence their intensities at ground level are affected. For neutron intensity, the temperature distribution plays negligible role. For mesons, the variations at ground are adequately represented by the equation (Dorman, 1957)

$$\frac{\delta N_\mu}{N_\mu} = \beta \cdot \delta h_0 + \int_{h_0}^{h_1} W(h) \cdot \delta T(h) \cdot dh \quad (1)$$

where $\delta N_\mu/N_\mu$ is the fractional change of μ meson intensity at the atmospheric depth h_0 , β is the barometric coefficient, δh_0 is the actual change in barometric pressure at depth h_0 , $W(h)$ is the temperature-coefficient density and $\delta T(h)$, the actual temperature change at an atmospheric depth, h . As already mentioned, β is precisely known. The values of $W(h)$ for various atmospheric depths are also precisely known from theoretical calculations by Dorman. Therefore, to evaluate (1), one needs records of ground level pressure changes (δh_0) as also of the atmospheric temperature distribution $\delta T(h)$. In practice, the integral may be broken up into summation over a series of isobaric levels (say, 100 mb apart) for each of which the average temperature change δT may be available from Radiosonde data.

Now, Radio-sonde data are usually available for any station from only one or two flights a day. For correcting the *daily mean intensity* of μ mesons, one can use the averages of these flights for every isobaric level. However, if the correction $\delta N_\mu/N_\mu$ is needed for daily variation of cosmic rays, one either needs values of $\delta T(h)$ also at small time intervals, or, one has to know precise relations (theoretical or empirical) between variations of ground level temperature and simultaneous variations of temperatures at various atmosphere depths. Unfortunately, the altitude dependence of the daily variation of atmospheric temperature is not precisely known. Various workers have given various estimates. Some of these are experimental determinations, most of which are often considered of doubtful accuracy because of what are known as "Radiation errors" (Bracefield, 1948). There are several theoretical estimates too. Table I gives a summary of presently available information.

TABLE I

Investigator	Place	Season	Amplitude of daily variation at														
			Km. 0	0.3	0.5	1.0	1.5	2.0	3.0	4.0	10.0	15.0	20.0	30.0			
			Mb. 1000	975	955	900	845	800	700	610	260	120	55	10			
Van Bemmelen (1916)	Batavia,		5	0.7	0.4	0.7	0.4										
		(Arbitrary)															
Barkov (1917)	Lindenberg		5	1.9	1.2	0.9	0.4										
Dines (1919)	Drexel, U.S.A.		5		1.1	0.8	0.6										
Schmidt (1925)	Eiffel Tower, Paris		5	2.2													
Geiger <i>et al.</i> (1932)	Gross Arbor, Bavaria																
Wolf <i>et al.</i> (1940)	U.S.A.	Summer															
		Winter															
Piegsa (1947)	Liverpool, U.K.																
Scherlag (1948)	Germany																
Kay (1951)	British Isles																
Brunt (1952)	Lunderberg	Summer	5														
		Winter	5														
Venkatesvaran and Desai (1953)	Almedabad, India																
Belmont (1954)	Greenland																
Scruse (1956)	U.K.																
Kanuner (1956)	U.S.S.R.		5		2.0												
Harris (1959)	U.S.A.		5		1.8												
Chiu (1959)	U.S.A.	Summer															
		Winter															
Pant (1960)	India																
Jordan (1960)	Tropical Pacific																
Rangarajan and Sikka (1962)	India																
Haurwitz (1936)	Theoretical																
Elaesser (1940)	"																
Beers (1944)	"																
Penner (1948)	"																
Wexler (1950)	"																
London (1951)	"																
Johnson (1953)	"																
Pressman (1955)	"																

As can be seen from Table I, evidence regarding ranges of daily temperature at different altitudes is very uncertain indeed. While some workers claim no significant ranges, some others claim ranges as high as 5°C even at 15 km. altitudes. Now in equation (1), if the integral is replaced by a summation, the temperature effect could be represented by

$$\frac{\delta N_{\mu}}{N_{\mu}} = \sum K_i \delta T_i \quad \dots (2)$$

where K_i is the partial temperature-coefficient and T_i is the average temperature variation of the i -th layer. For K , Dorman's calculated values are as shown in Table II.

TABLE II

$H(\text{mb})$	1000	900	800	700	600	500	400	300	200	100
$K_i (\% / ^{\circ}\text{C})$ (negative)	.020	.021	.022	.024	.025	.026	.028	.033	.038	.031

If, as an extreme assumption, the diurnal variation of ground temperature is depicted to the same extent by all layers high up in air, the integrated effect would be about 0.27% per degree change at ground, which for a sea-level station like Ahmedabad, India, where ground temperature amplitudes can be as high as $\pm 10^{\circ}\text{C}$, would imply a diurnal contribution of about 2.7% oppositely correlated to ground temperature. On the other hand, if the diurnal variation of temperature reduces rapidly with altitude and is negligible after 2 km. altitude, the total contribution would reduce to about 0.3% or less. Considering the fact that the average amplitudes for meson telescopes for groups of days are only of the order of 0.5% or less, the uncertainty due to temperature correction is a very disconcerting feature indeed.

In view of the lack of proper information about diurnal variation of upper atmosphere temperatures, workers have attempted to estimate *indirectly* the contribution of temperature effect to the diurnal variation of cosmic ray mesons. In the next section, such attempts by other workers as also some analysis by the present author will be discussed.

EXPERIMENTAL STUDIES

From comparison of the average diurnal variation curves for different seasons, Dorman (1957) has concluded that the total contribution of temperature effect to diurnal variation of cosmic ray mesons is of the order of 0.10 to 0.30% depending upon the season. From the approximately linear motions of the tips of the vectors representing the first harmonic on a harmonic dial for 1953-54-55, Glokova (1960) has concluded that the daily variation of meson intensity is the resultant of a variable vector of external origin and a constant vector of most probably atmos-

pheric origin. From the data of several Ionisation chambers and meson telescopes, the constant vector seems to be of amplitude between about 0.05 and 0.12% and an hour of maximum in the early morning. This could be interpreted as the expected temperature effect. Unfortunately, the amplitudes differ largely from place to place. Also, the method gives only approximate estimates of the constant vector. The estimates could be wrong if the external vector had changed in both amplitude and phase from month to month.

Quenby and Thambyahpillai (1960) have estimated the temperature effect from a comparison of neutron monitor and Ionisation chamber data for Huancayo. Their basic idea is this. The neutron intensity is affected by atmospheric pressure but not by atmospheric temperature distribution. Also, for an equatorial station like Huancayo, the coupling constants for neutron and meson intensity are somewhat similar. (Webber and Quenby, 1959) In addition, a neutron pile and an ionisation chamber have roughly similar zenith angle responses. Hence, effects shown by the neutron pile and the ionisation chamber at equator (after proper barometric correction is applied to both) will be similar except for a possible temperature effect in the meson intensity (ionisation chamber) If periods are chosen when the daily variation for the neutron pile is negligibly small, the ionisation chamber will have no daily variation of extra-terrestrial origin. Hence an observed daily variation, if any, can be attributed to atmospheric temperature variations only.

Using this elegant idea, Quenby and Thambyahpillai (1960) selected months when the monthly average diurnal variations for Huancayo neutron pile were negligibly small ($<0.1\%$). They found that the average diurnal variation for the ionisation chamber for the same periods showed amplitudes of about 0.11% with the hour of maximum at 05.30 hrs (L.T) which is in very good negative correlation with the diurnal ground temperature wave at Huancayo. The period studied was 1953-55.

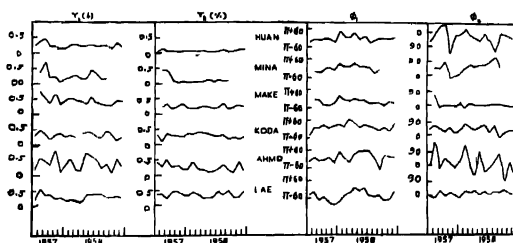


Fig. 1.—Monthly average amplitudes (r_1 , r_2) and hours of maxima (ϕ_1 , ϕ_2) of first and second harmonics of daily variation of neutron intensity at the equatorial station of Huancayo, Mina Aguilar, Makerere, Kodaikanal, Ahmedabad and Lae.

During the I.G.Y., several neutron monitors, meson telescopes and ionisation chambers were operating simultaneously all over the world. An attempt was made to use these to estimate the contribution of temperature effect. The equatorial stations where neutron and meson data were recorded simultaneously were Kodaikanal, Ahmedabad, Lac, Makerere and Huancayo. Now, following Quenby and Thambyahpillai's method, one should first separate out the months for which the average monthly amplitudes for neutrons are negligibly small. It was found, however, that the average daily variation amplitudes were rather high (0.2% or more) throughout the I.G.Y. period. The values of the monthly average amplitudes (r_1 and r_2) and hours of maxima (ϕ_1 and ϕ_2) of the first and second harmonics for several equatorial neutron monitors are plotted in Fig. 1. It may be noted that :

- (a) For most of the months, r_1 is $> 0.2\%$, in some cases as high as 0.6% . The value of r_2 is comparatively small.
- (b) Values of r_1 are not similar at all stations. Some stations (e.g. Ahmedabad) show much larger fluctuations of r_1 as compared to other stations. The pressure coefficient used for all these data is the same, about $0.72\%/mb.Hg$. Statistical errors are negligibly small. Dissimilarity between the number of days in the same month for different stations could be a possible cause. Also improper working of the instruments is not ruled out. The erratic fluctuations of the hour of maximum indicate possibly the same cause.

For these reasons, it became difficult to select months of negligibly low amplitudes. Nevertheless, the following grouping was adopted :

Group A—(Low amplitudes) Jul., Dec. 1957; Jan. Mar. Apr. Aug. Oct. Dec., 1958.

Group B—(Medium „) Oct. 1957, Feb., Jul., Sep., Nov., 1958.

Group C—(High „) Aug., Sep., Nov. 1957; May, June, 1958.

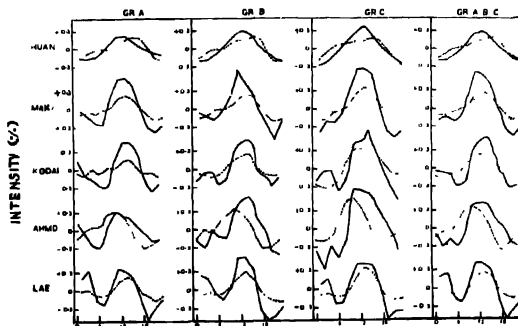


Fig. 2—Average diurnal variation curves for neutrons (full lines) and mesons (dotted lines) for Huancayo, Makerere, Kodaikanal, Ahmedabad and Lac for months of Low (Gr. A), Medium (Gr. B) and High (Gr. C) amplitudes r_1 .

Fig. 2 shows the average diurnal variation curves for neutrons and mesons (Ionisation chamber for Huancayo and cubical mesons for the others) for the three groups for various stations. In general, the mesons do show lesser amplitudes than neutrons and the difference indicates a negative correlation with an average ground temperature curve for the meson intensity. However, the differences are different from place to place. If all these are considered as fault-free and if it is assumed that the neutron and meson curves would have looked alike if the mesons were corrected for temperature effect, the temperature effect would amount to anything from 0.0 to 0.5%. This is rather a large contribution.

Amongst the various data referred to above, those for Huancayo neutrons and meson appeared to be the most reliable. Hence, a separate analysis was made for Huancayo, dividing the 1 G.Y. period into 4 groups as follows :

Group 1—(Very low amplitudes) Jul , Dec., 1957; Jan. Oct., 1958.

Group 2—(Low amplitudes) Oct. Nov , 1957, Apr., May, Jul., Sep . Dec., 1958

Group 3—(Medium amplitudes) Feb., Mar., Jun, Aug., 1958.

Group 4—(High amplitudes) Aug., Sep., 1957; Nov., 1958.

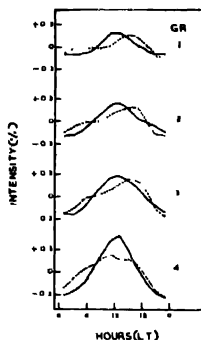


Fig. 3—Average diurnal variation at Huancayo for neutrons (full lines) and mesons (dotted lines) for months of Very Low (Gr 1), Low (Gr. 2), Medium (Gr 3) and High (Gr. 4) amplitudes r_1 .

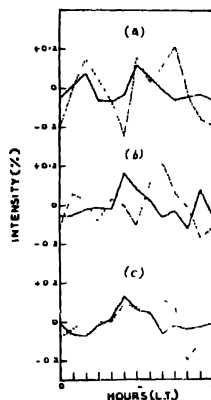


Fig. 4—Average diurnal variation at Huancayo for neutrons (full lines) and mesons (dotted lines) for days on which r_1 values were in the ranges (a) 0.00--0.10%, (b) 0.11--0.15%, (c) 0.16--0.00%.

Fig. 3 shows the average daily variation curves for those 4 groups for Huancayo neutron (full lines) and Ionisation Chamber (dotted lines). Here again, if it is assumed that neutrons and mesons should show similar variations but for the temperature effect on mesons, the temperature effect amounts to as large as 0.3% for Group 4. On the other hand, in Groups 1, 2, 3, the amplitudes of neu-

trons and mesons are almost alike but the hours of maxima are earlier for neutrons. It seems, therefore, that the assumption regarding similarity of daily variations for mesons and neutrons is not fully justified and the temperature effect estimated by the above method would be only approximate.

As it was not possible to pick out months showing average diurnal variation amplitudes less than $\sim 0.15\%$ for neutrons, an attempt was made to examine *individual days* and choose those of negligible amplitudes. For this, the neutron intensity at Huancaayo was used and the bi-hourly deviations from mean for every day for which data were available during I.G.Y. were harmonically analysed, after applying linear correction for long term changes by calculating running averages over 12 successive bi-hourly values as usual. Days were then sorted out according to values of the amplitude r_1 of the first harmonic lying in the following ranges :

Range (a)	$0.00 \leq r_1 \leq 0.10\%$
„ (b)	$0.11 \leq r_1 \leq 0.15\%$
„ (c)	$0.16 \leq r_1 \leq 0.20\%$

For days in each range, the average daily variation for neutrons and mesons was computed. The results are shown in Fig. 4. A very interesting point to note is that whereas days are chosen so as to have negligible amplitudes r_1 , the final curves do not show negligible deviations. This is because the amplitude r_2 of the second harmonic is not simultaneously negligible. Most of the curves in Fig. 4 are with two maxima during 24 hours, indicating an appreciable contribution of second harmonic. If an additional condition is imposed viz. that r_2 also should be in the same range as r_1 , the number of days in each group becomes very small, and the method cannot be pursued further. Table III gives the amplitudes and hours of maxima of the first and second harmonic for curves in Fig. 4.

It will be seen from Table III that the Neutron minus Meson curve which is expected to show an hour of maximum coinciding with that of ground temperature curve, does not show the effect either for the first or for the second harmonic. In fact, the phases of the two are in opposition which would imply a "Positive Temperature effect"!

It would be seen from the above discussion that the method suggested by Quenby and Thambyahpillai fails when applied to the I.G.Y. data. A possible reason could be that whereas in the period 1953-55 studied by them, the solar activity was low and the spectrum of the anisotropy causing daily variation was flat enough to give similar results for neutrons and mesons at equator, the increased solar activity during the I.G.Y. might have created complications.

Because of the failure of this method, a different approach was attempted. It is well-known that the daily variation of cosmic rays changes from month to month. The changes could be due to seasonal variations of ground temperature

TABLE III

Component	Group (a)			Group (b)			Group (c)		
	r_1 (%)	ϕ_1	r_2 (%)	ϕ_1	r_2 (%)	ϕ_2	r_1 (%)	ϕ_1	r_2 (%)
Neutrons	0.026	$\pi - 9^\circ$	0.054	-52°	0.056	$\pi - 25^\circ$	0.057	$\pi - 12^\circ$	0.045
						-31°			-41°
Mesons	0.062	$\pi + 40^\circ$	0.150	$\pi - 52^\circ$	0.062	$\pi - 33^\circ$	0.097	$\pi - 57^\circ$	
							0.091	$\pi - 7^\circ$	0.047
									$\pi - 81^\circ$
Neutrons minus mesons	0.049	$+63^\circ$	0.146	-31°	0.058	-89°	0.151	-47°	
							0.034	-2°	0.086
									-62°
ground temperature	5.9°C	$\pi - 28^\circ$	1.3°C	-9°	5.9°C	$\pi + 28^\circ$	1.3°C	$\pi - 28^\circ$	1.3°C
							5.9°C		-9°

or due to sidereal effects or due to long-term changes of the solar component which may be misinterpreted as seasonal effects. In practice, it is almost impossible to separate the three, specially from a limited amount of data. However, during the last 25 years, Forbush and his coworkers (1948, 1957; 1961) have done an admirable job of obtaining more or less continuous and reliable data from Ionisation chambers at Huancayo, Cheltenham (recently shifted to Fredericksburg) and Christchurch. One can, therefore, adopt the following argument :

From data for a few years, the seasonal variation cannot be properly studied because the solar vector also changes from month to month. However, if continuous data for, say, 2 solar cycles (22 successive years) are available, the long-term linear trends in daily variation would be greatly minimised. The following procedure could now be adopted :

- (i) Evaluate the monthly average daily variation curves (bi-hourly % deviations) for any station for $22 \times 12 = 264$ consecutive months.
- (ii) Average data for similar months, thus yielding 12 daily variation curves for January to December.
- (iii) Find the yearly average curve by combining the 12 monthly curves and subtract this from the curve for each month yielding thus a set of 12 bi-hourly percentage deviations from mean for each month.
- (iv) From data of ground temperature for any 3-4 successive years, evaluate a set similar to (iii) above.

Since monthly average ground temperature daily variation does not change much from year to year, an average for any 3-4 consecutive years would be a good representative for any period. Because we have subtracted the yearly average

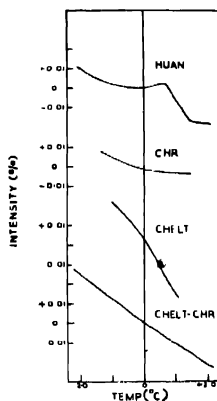


Fig. 5—Cosmic ray meson intensity *vs* ground temperature (from daily variation curves).

from the monthly curves for temperature also, the sets of 12 bi-hourly values of cosmic rays and ground temperature for every month can be directly compared. If a sidereal variation does not exist, one would expect a perfect negative correlation between the two.

The above procedure was adopted for the Ionisation Chamber data at Huancayo for the period 1937-59. It was noticed that the correlation coefficients did not exceed 0.5 for any month. Also, the coefficients were sometimes positive. It was obvious, therefore, that temperature variations were not the only cause of the month-to-month changes of daily variation. A possible sidereal variation could be the disturbing factor. Also, long-term changes in the solar factor may not have been completely eliminated. There was no straight-forward method of estimating these or applying corrections for the same. A statistical approach could be to give weightage to temperature deviations only. Thus, the 12 sets of 12 bi-hourly values of cosmic rays were grouped in such a way that the corresponding temperature deviations lay in fixed ranges. Fig. 5 shows the plot of average cosmic ray values vs temperature ranges. In general, lower temperatures are associated with higher cosmic ray intensities and vice versa. But an actual correlation analysis yields a regression coefficient of only $-0.007\%/^{\circ}\text{C}$. At Huancayo, the yearly average amplitude of ground temperature is about $\pm 7^{\circ}\text{C}$. Hence the contribution to cosmic ray meson intensity would be only 0.05% in contrast to 0.11% reported by Quenby and Thambyahpillai.

Using data for about 20 years for Ionisation chambers at Cheltenham and Christchurch, a similar analysis was carried out. These results are also shown in Fig. 5. The coefficient for Christchurch is very low, about $-0.004\%/^{\circ}\text{C}$, but for Cheltenham, it is quite high, about $-0.029\%/^{\circ}\text{C}$ (temperature data for Washington D. C. were used). Now, if there is a sidereal effect affecting all these data, it is expected to be the same for Cheltenham and Christchurch and hence should cancel out in their difference. On the other hand, since these two stations are in different hemispheres, temperature differences will persist. Hence, a similar analysis was carried out for Cheltenham minus Christchurch, adopting a similar procedure for ground temperatures also. The plot is shown in Fig. 5. The regression coefficient is $-0.011\%/^{\circ}\text{C}$.

For the period 1936-40, Hogg (1949) has published Ionisation chamber data for Canberra. When a similar analysis was carried out for these data, it yielded a positive correlation between cosmic ray intensity and ground temperature. Data for Ionisation Chamber at Itabashi (Japan) for the period 1953-60 were also analysed. A negligible correlation between cosmic rays mesons and ground temperature was obtained.

Table IV summarises the various estimates of temperature effect referred to so far.

IMPLICATIONS OF TEMPERATURE CORRECTION

From the evidence presented so far it seems that the situation regarding the estimation of temperature effect on the daily variation of cosmic ray mesons is very unsatisfactory indeed. Not only is the magnitude of the effect not precisely known but even the upper limit of the effect expected is difficult to determine. From some results, it would seem as if the effect is probably less than about 0.15% for yearly average curves. On the other hand, some data on upper air temperatures would put an upper limit as high as 0.5%. In studies with narrow

TABLE IV

Source of information	Total temperature effect on cosmic rays (%)	Temperature coefficient (%°C of ground temperature)
From experimentally determined daily variation of upper air temperature	0 to 2.0	0 to 0.3
Beer's relation (Table I)	0.20	0.03
Quonby and Thambyahpillai,		
High altitude	0.11	—
Sea-level	0.16	—
Dorman's estimate	0.10 to 0.30	—
Present analysis :—		
Comparison of <i>N</i> and <i>M</i> curves,	0 to 0.5	
Seasonal variation analysis,		
Huancayo	0.05	0.007
Christchurch	0.03	0.004
Cheltenham	0.20	0.029
(Chert-Christ)	0.08	0.011
Canberra	Positive effect	
Itabashi	Negligible	
Glokova, from long-term changes of daily variation during solar minimum	0.05 to 0.12	

angle telescopes, one usually finds daily amplitudes as high as 1.0%. It is, therefore, argued that the pollution due to temperature effect on such days would be small. It must be remembered, however, that on individual days, the daily range of ground temperature, specially at sea-level inland stations, can be quite large. Table V gives the maximum, minimum and average monthly range for 1959 for Ahmedabad, India (sea-level, geographic lat. 23°. ON, long. 72° 5E).

TABLE V

Month	Ground temperature range ($^{\circ}\text{C}$)		
	Maximum	Minimum	Monthly average
January	20.0	9.1	15.3
February	20.1	10.6	10.2
March	20.5	10.5	10.6
April	20.2	9.3	14.5
May	17.0	10.6	13.9
June	15.6	5.6	10.3
July	8.5	0.9	4.8
August	6.2	0.9	4.3
September	10.1	2.0	5.4
October	16.1	3.7	9.5
November	16.7	4.7	13.8
December	18.7	6.5	15.3

Thus, in the winter months, one encounters days of temperature range as high as 20°C , which will give an amplitude of about $\pm 10^{\circ}\text{C}$, while in monsoon months, the range may drop down to 0.9°C yielding an amplitude of $\pm 0.5^{\circ}\text{C}$ only. As shown in Table IV, the temperature coefficients may be anything from 0 to $0.2\%/^{\circ}\text{C}$ and thus daily temperature effects may amount to as much as 1.0% or more. The precise contribution depends upon the precise value of the coefficient which itself may be different for different locations and for different seasons. Thus, there is no reason to be complacent about temperature corrections at any period.

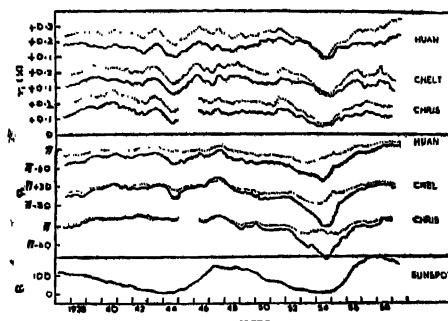


Fig. 6—Long-term changes of the amplitude r_1 and hour of maximum ϕ_1 of the first harmonic before (full lines) and after (dotted lines) temperature correction,

It would be interesting to examine at this stage the implications of a temperature correction to daily variation of meson intensity in the light of the various results that have been published in the past. Sarabhai and Kane (1953), Thambyahpillai and Elliot (1953) and Sarabhai *et al.* (1954) have shown that the yearly average amplitude and phase of daily variation of cosmic ray meson intensity show fluctuations in relation to the 11 year and 22 year solar cycle. Fig. 6 is a plot of the amplitudes r_1 and hours of maximum ϕ_1 of the first harmonic, each point being obtained as running average of 12 consecutive monthly values. Full lines represent data corrected for barometric pressure only and are similar to those illustrated in the publications referred to above, except for the period 1946-58 for Huancayo. For this station the pressure records were read wrongly in this period (Forbush and Beach, 1961) and hence the data published earlier were wrongly pressure-corrected. The necessary changes in the vectors a_1 and b_1 and hence in r_1 and ϕ_1 are given by Forbush and Beach and have been used in the present analysis for obtaining the curves for Huancayo in Fig. 6. The dotted lines in Fig. 6 represent the amplitudes and hours of maximum after correcting for temperature effect by using a coefficient of 0.02% per °C of ground temperature. For Huancayo, it amounts to adding a vector of amplitude of about 0.12% parallel to ground temperature vector and is roughly the same as Quenby and Thambyahpillai's estimate of temperature effect.

As can be seen from Fig. 6 the correction for temperature effect does the following

- a) The amplitude r_1 is now in general larger than before and remains essentially constant except near the solar minimum years of 1944 and 1954 when the amplitudes go down. The depression in 1954 is conspicuously larger and is spread over longer period (1952-55) in contrast to that in 1944 (1944-45 only). It possibly indicates a minor 11 year cycle included in a major 22 year cycle. The forthcoming solar minimum will soon give a part confirmation of this pattern.
- b) The hour of maximum ϕ_1 without temperature correction shows a shift towards earlier hours during solar minimum, which is more marked for 1954 (about 8 hours) than in 1944 (about 3 hours) indicating an 11 year cycle within a 22 year cycle. It is interesting to note that, after temperature correction, the variations in hour of maximum are reduced considerably. In 1944 the shift is not even discernable. In 1954, it amounts to only about 3 hours. The 22 year cycle becomes more obvious and the minor 11 year cycle disappears. Here again, confirmation over one more 22 year cycle is necessary.

The actual amount of shift in the hour of maximum is directly related to changes in the energy spectrum of the anisotropy of daily variation and its direction in space. Assuming that the energy spectrum remains constant and the

average geomagnetic deflection for cosmic rays arriving at Huancayo is about 90° , the normal hour of maximum at about 12 noon for Huancayo indicates an anisotropy in the 18 hr. direction. In 1944 it shifts by 3 hours and in 1954 by 8-9 hours thus crossing the earth-sun line by 1954. If, however, a temperature correction is applied, the direction changes utmost by 3 hours and hence is always on the same side of the earth-sun line. This would have an important bearing on the theories of daily variation.

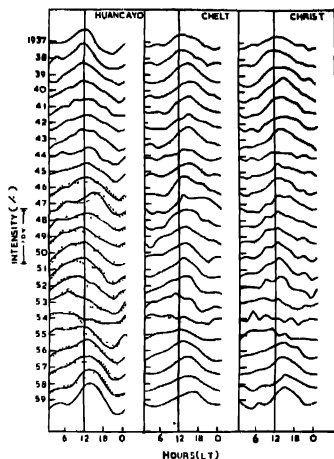


Fig. 7—Daily variation curves for Huancayo, Cheltenham and Christchurch for 23 years. For Huancayo, the dotted curves for 1946-58 are the wrongly pressure-corrected ones.

The shifting of the hour of maxima by as much as 8 hours had indicated another possibility. Sarabhai *et al.* (1955) have shown that from 1937 to 1954, the daily variation curves had undergone a drastic change from curves of day-time maximum to night-time maximum. Unfortunately, the conclusion was based mainly on the Carnegie Institution data for Huancayo for which the data for 1946-58 are wrongly pressure-corrected as stated earlier. Fig. 7 shows the average daily variation curves for 23 years (1937-59) for ionisation chambers at Huancayo, Cheltenham and Christchurch. For Huancayo, the dotted lines represent the earlier data which were wrongly pressure-corrected. The full lines are for properly pressure-corrected data. As can be seen for Huancayo, the hour of maximum is at about local noon from 1937 to 1945. From 1946 onwards, it looks as if a second peak is developing at or before 06 hours. The effect is more prominent in the dotted curves (wrongly pressure-corrected) but is seen in the full curves also. By 1954, the original day-time peak has disappeared leaving only one peak during night-time, again more prominent in dotted curves. For Cheltenham and Christ-

church, the effect is not so clear but in 1954 there does appear a possibility of night-time maximum.

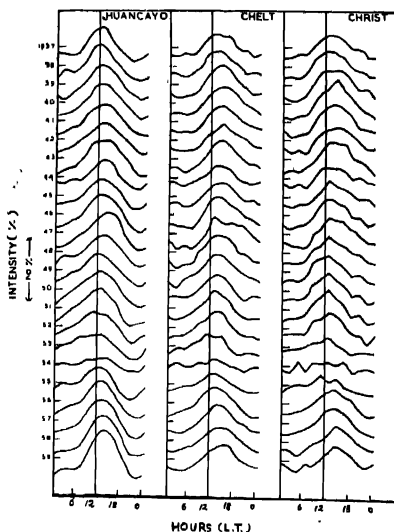


Fig. 8—Daily variation curves for Huancaayo, Cheltenham and Christchurch after temperature correction.

Fig. 8 shows the yearly average daily variation curves after correction for temperature effect ($0.02\%/^{\circ}\text{C}$). A marked change from Fig. 7 is obvious. The hour of maximum is throughout in the noon or afternoon and all that happens in 1954 is a drastic reduction of amplitude. In particular, there is no indication of a night-time component of daily variation in any year.

The shifting of the hour of maximum to early morning or night hours during 1953-54 has been reported by several other workers. Thus, Possener and Heerden (1956) report that during July, Aug., Sep. of 1953 and June 1954, the hour of maximum of meson intensity measured by inclined (North, South) as well as vertical telescopes at Manchester and London was between midnight and early morning. Steinmaurer and Gheri (1955) report the same behaviour for Ionisation chamber at Hafelekar for 1953-54. Yagi and Ueno (1956) report a similar shift for data from counter telescopes and Ionisation chamber operated at Nagoya and Tokyo, Japan, during 1953-54. Thus all these data show night-time or early morning maxima in 1953-54. However, all refer to meson intensity. The question arises whether all these are subject to errors due to temperature correction and if so, to what extent. Since neutron monitor data are not affected by

temperature, it would be interesting to compare these results with neutron monitor data. For the monitor operative at Manchester and later at London, Possener and Hoerden (1956) report that the corresponding amplitudes during 1953-54 were not significantly different from zero. From data for Huancayo and Climax neutron monitors, Conforto and Simpson (1957) report that the monthly average vector drifted counter-clockwise during 1954 yielding an *yearly average* amplitude for Huancayo almost zero. For Climax, the average amplitude reduced considerably during 1954 and the hour of maximum shifted to *later* hours in the afternoon. Thus, in general, the neutron monitors showed negligible average amplitudes in 1953-54 and no night-time maxima. This would indicate that the night-time maxima seen in 1953-54 for meson intensities was mainly a temperature effect.

It must be remarked here that such comparisons with neutron monitors are not wholly desirable, because, the purpose of operating meson telescopes is to have an intensity record of mean energy response different from that of a neutron monitor. Thus, one would like to study the *differential* behaviour of neutron and meson intensities rather than equate the two. Therefore, an independent measure of the expected temperature effect would be desirable. If one assumes equality of neutron and meson effects, some very awkward conclusions follow. Thus Yagi and Ueno (1956) have reported that during 1954, the average amplitude for narrow angle telescopes was 0.3% and the hour of maximum was about 06 hours L.T. If the neutron monitor intensity were any valid comparison, the actual external anisotropy for the same period was zero and hence the temperature effect for narrow angle telescope intensity would work out to 0.3%, in contrast to 0.12% that we have used for correcting the Carnegie Institution data. It is difficult to judge whether such comparisons are invalid or whether temperature effects are really so large. The latter would prove a very disconcerting feature indeed.

It would be interesting to study the behaviour of the amplitude r_2 and hour of maximum ϕ_2 of the second harmonic also. In the past, Sarabhai and Sastry (1960) have reported that the hour of maximum ϕ_2 shifts by as much as 10 hours in 19 years (1939-56) for Huancayo. Here again, the conclusion was based on data which were wrongly pressure-corrected for Huancayo as mentioned earlier. Since pressure curve is predominantly semidiurnal, the error will be largest for the second harmonic of cosmic rays. In the diagram shown by Sarabhai and Sastry in their publication, the value of ϕ_2 changes abruptly from 1946 onwards. This is exactly the period when the wrong pressure correction crept in!

Fig. 9 shows the plots of r_2 and ϕ_2 for Huancayo, Cheltenham and Christchurch, using the properly pressure-corrected data for Huancayo. Following may be noted :

- a) The amplitude r_2 is small throughout, of the order of 0.10% for Huancayo and lesser for Cheltenham and Christchurch. For Huancayo, r_2

increases soon after the solar minima of 1944 and 1954 from values as low as 0.02% to as high as 0.10%. However, r_2 is high at other periods too. Thus, no one-to-one relation with solar cycle is indicated. At Cheltenham and Christchurch, r_2 fluctuates between 0.02% and 0.07% but no correlation between these two stations or with Huancayo or with sunspot cycle is discernable.

- b) The hour of maximum ϕ_2 fluctuates between 0 and 90° (i.e. a fluctuation of about 3 hours) for all stations. However, no intercorrelation between the 3 stations or of any of them with solar cycle is indicated. The large fluctuation of 10 hours (300°) reported by Sarabhai and Sastry is not visible. Also the dotted curves show much reduced fluctuations indicating an appreciable temperature effect.

It seems, therefore, that the second harmonic does not have any definite relation with solar cycle, except perhaps for Huancayo where the amplitude fluctuation shows some relation. This could be an effect confined to equatorial region. It must be noted, however, that the amplitudes are very small (<0.1%) and even small errors in barometric correction could cause large differences. It is also not yet known whether the second harmonic is a meaningful independent quantity. It may as well be an accessory of the first harmonic controlling its sharpness of occurrence.

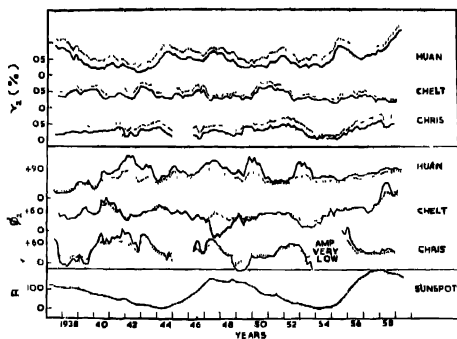


Fig 9 - Long-term changes of the amplitude r_2 and hour of maximum ϕ_2 of the second harmonic before (full lines) and after (dotted lines) temperature correction.

From the average data for 23 years, one can study the sidereal variation; because, the month-to-month change of the solar vector is likely to be very small for averages over such large periods. Fig. 10 shows the monthly average vectors of the first harmonic for Huancayo, Cheltenham and Christchurch after deducting the yearly average vectors from each month. Full curves represent only pressure-corrected data while dotted curves are with additional temperature correction.

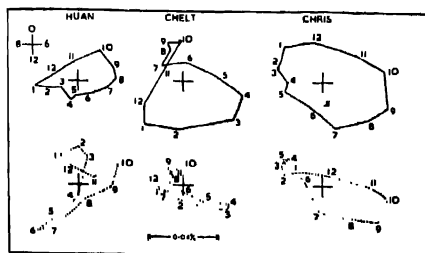


Fig. 10—Harmonic dials for the monthly minus yearly average vectors before (full curves) and after (dotted curves) temperature correction.

Each point is a running average of 3 consecutive months. An anti-clockwise shift of the monthly vector is clear for all stations for pressure-corrected vectors but not for pressure and temperature-corrected vectors. In the absence of a precise knowledge of the magnitude of the temperature effect, valid conclusions regarding sidereal anisotropy are difficult.

CONCLUSION

It is clear from the above discussion that the temperature effect may play a very vital role in the study of the daily variation of ground level meson intensity, specially if the expected amplitudes of external effect are comparable to the expected temperature effect. Unfortunately, there is no way of estimating the latter except by actual measurement of daily variation of upper air temperature. As shown in Table I, the information on this point is very unsatisfactory. Recently some workers of the India Meteorological Department carried out an extensive investigation at four Indian stations (Calcutta, New Delhi, Bombay, Madras, all sea-level stations) for four representative months January, April, July, October. The instruments used were by no means fault-free and, after applying rigorous statistical tests, the following conclusions were arrived at :

- a) Diurnal variation of temperature is generally significant in the lower levels up to 700 mb. only. Under stable conditions such as in January in New Delhi, the daily variation is hardly noticed even at 900 mb. But in July when convection and eddy conduction is very effective, the variation extends even up to 500 mb.
- b) Amplitude of daily variation is about 3°C at 900 mb. reducing to about 1.5°C at 700 mb. Significant values for levels above 700 mb. are also observed but radiation errors are not ruled out.

Such, perhaps, is the situation for all such measurements ! It is interesting to note that whereas a tremendous effort has been put so far and is still continuing to be put, for the continuous recording of cosmic ray meson intensity at ground

levels, not even a fraction of this is devoted by these workers to the measurements of upper air temperature which are so vitally needed for temperature correction. In a recent paper, Teweles and Finger (1960) have done a detailed analysis of comparative the various Radio sonde instruments used in U.S.A.

TABLE VI

Instrument	Solar radiation temperature correction.
(1) Conventional duct-type (double or single) Radiosonde with internally-mounted thermometer.	Radiation error increases rapidly with altitude in middle and upper stratosphere.
(2) Externally mounted (outrigger) white-coated thermometer.	Reflects away 95% of solar radiation. Still radiation error is $\sim 2.0^{\circ}\text{C}$ at 25 mib level with smaller errors below and larger errors above this altitude.
(3) Externally mounted, silvered thermistors employing very small bead and fine tungsten wire (Ney <i>et al.</i> , 1958).	Relatively costly. Presents problems of electrical circuitry. But radiation errors small.

Table VI briefly summarises the types of instruments presently used and their merits and demerits, which are most probably similar for Radio-sonde instruments used all over the world. Workers in several countries have determined radiational temperature corrections for their own instruments. Those differ largely from each other, which may be partly due to differences in the instruments at different places and partly because the determined corrections could be erroneous as shown by Teweles and Finger. With uncertainties as large as 2.0°C , the problem of determining the true daily variation of upper air atmospheric temperatures is very formidable indeed. It is unimaginable, however, that it is so difficult as to be beyond the reach of modern technological advance. The instrument of Ney *et al* (1958) is already an indicator of the improvement that can be achieved. The reason for apathy is obviously the lack of realisation of the vital role temperature correction may play in the study of the daily variation of cosmic ray mesons at ground level. It is hoped the present article will serve some useful purpose in bringing out the importance of such a correction and the effort needed to collect the necessary temperature data.

ACKNOWLEDGMENTS

The author is grateful to the various workers who kindly supplied cosmic ray data as well as ground temperature data used in the present analysis. Thanks are due to Prof. V. A. Sarabhai for discussions, to Mr. Bhavsar and others for computational assistance and to Atomic Energy Commission of India for financial support.

On the Temperature-Effect of the Daily Variation, etc. 171

REFERENCES

- Arakawa, H., 1959, *Jour. Geophys. Res.*, **64**, 625.
- Barkow, E., 1917, *Beit. Z. Phys. dev. frei Atmos.*, **7**, 30.
- Beers, N. R., 1944, *J. Met.*, **4**, 78.
- Belmont, A. D., 1954, *Sci. Rep. No. 1, Arctic, Met. Res. Project*, Univ. of California.
- Bracefield, C. J., 1948, *J. Met.*, **5**, 147.
- Brunt, D., (1952), "*Physical and Dynamical Meteorology*", *The Synthesis of the Cambridge Univ. Press*, p. 24.
- Chiu, W. C., 1959, *J. Met.*, **16**, 354.
- Conforto, A. M. and Simpson, J. A., 1957, *Nuovo Cimento*, **6**, 1052.
- Dinos, W. H., 1919, *Q. Jour. Roy. Met. Soc.*, **45**, 41.
- Dorman, L. I., 1957, "*Cosmic Ray Variations*", *State Publishing House, Technical and Theoretical Literature, Moscow*.
- Elsasser, W. M., 1940, *Month. Weath. Rev.*, **68**, 185.
- Forbush, S. I. and Lange, L., 1948, 1957, *Cosmic Ray Results*, *Carn. Inst. Washington Publ. No. 175*.
- Forbush, S. I. and Beach, L., 1961, *Cosmic Ray Results*, *Carn. Inst. Washington Publ. No. 175*.
- Geiger, R., Woolfe, M. and Scip, L. Ph., 1950, "*The Climate Near the Ground*", *Harvard Univ. Press*, p. 248.
- Glokova, E. S., 1960, *Proc. Moscow Cosmic Ray Conf. IV*, 243.
- Hartus, M. F., 1959, *Jour. Geophys. Res.*, **64**, 983.
- Haurwitz, B., 1936, *Trans. Roy. Soc. Canada, Sec. III*, 3rd series, **30**, 1.
- Hogg, A. R., 1949, *Memoirs of the Commonwealth Observatory, Canberra*, No. 10.
- Johnson, F. S., 1953, *Bull. Amer. Meteor. Soc.*, **34**, 106.
- Jordan, C. L., 1960, *J. Met.*, **17**, 569.
- Kammer, N. S., 1956, *Trudy TSAO*, Issue, **16**, 48.
- Kay, R. H., 1951, *Q. Jour. Roy. Met. Soc.*, **77**, 427.
- London, J., 1951, *Prog. Rep. 131.05 Project No. 131, Contract No. 1.F. 19* (122)-165, *N.Y. Univ.*
- Ney, E. P., Mass, R. and Huch, W., 1958, *Conf. on the High Atmos.*, *El. Press, Texas, U.S.A.*
- Pant, P. S., 1960, *Ind. Jour. Meteor. Geophys.*, **11**, 371.
- Pennier, C. M., 1948, *J. Met.*, **5**, 2, 69.
- Piegss, J., (1947), *Air Ministry, Met. Res. Ctee. M.R.P.*, No. 349 (U.K.).
- Possener, M. and Heerden, I. J. Van, 1956, *Phil. Mag.*, **1**, 253.
- Prossman, J., 1955, *Bull. Amer. Meteor. Soc.*, **36**, 220.
- Quenby, J. J. and Thambyahpillai, T., 1960, *Phil. Mag.*, **5**, 585.
- Rangarajan, S. and Sikka, D. R., 1962, "*The Diurnal Variations of Upper Air Temperatures over India*" (under publication).
- Sarabhai, V. A. and Kano, R. P., 1953, *Phys. Rev.*, **90**, 204.
- Sarabhai, V. A., Desai, U. D. and Venkatesan, D., 1954, *Phys. Rev.*, **96**, 469.
- Sarabhai, V. A., Desai, U. D. and Venkatesan, D., 1955, *Phys. Rev.*, **99**, 1490.
- Sarabhai, V. A. and Sastry, T. S. G., 1960, *Proc. Moscow Cosmic Ray Conf. IV*, 235.
- Scherlag, R., 1948, *Wetteranalyse und Wetterprognose*, *Springer Verlag, Berlin*, p. 31.
- Schmidt, W., 1945, "*Handbook of Meteorology*", *McGraw Hill Book Co.*, p. 468.
- Scrase, F. J., 1956, *Meteor. Mag.*, **85**, 65.
- Steinmaurer, R. and Gheri, H., 1955, *Naturwissen*, **42**, 294.
- Towolos, S. and Finger, F. G., 1960, *J. Met.*, **17**, 177.

- Thambyahpillai, T. and Elliot, H., 1953, *Nature*, **171**, 918.
- Van Bemmelen, W., 1916, *K. Mag. en. Meteor. Obs. te. Batavia*, **4**, 38.
- Venkateswaran, S. V. and Desai, U. D., 1953, *Proc. Ind. Acad. Sc.*, **38A**, 427.
- Wada, M., 1960, *Sci. Papers I. P.C.R. (Japan)*, **54**, 335.
- Webber, W. R. and Quenby, J. J., 1959, *Phil. Mag.*, **4**, 654.
- Wexler, H., 1950, *Tellus*, **2**, 262.
- Wolf, O. R., Hodge, M. W. and Obloy, S. J., 1946, *Misc. Rep. No. 21, Dep. Met. Univ. Chicago*
- Yagi, T. and Ueno, H., 1956, *J. Geomag. Geoelect.*, **3**, 93.

THE ELECTRONIC SPECTRA OF SOME TRISUBSTITUTED BENZENES IN DIFFERENT STATES-I*

T. N. MISRA

OPTICS DEPARTMENT, INDIAN ASSOCIATION FOR THE CULTIVATION OF SCIENCE,
CALCUTTA-32

(Received January 7, 1963)

ABSTRACT. The near ultraviolet absorption spectra of 1, 2, 3-trichloro- and 1, 2, 3-trihydroxybenzene have been studied in the liquid state, solid state at room temperature and at -180°C and also in rigid glass media in alcohol at the same temperature. In the liquid state and in the solid state at room temperature both the substances yield weak, broad, diffuse bands showing the characteristics of forbidden transition as in free molecules due to cancellation of three migration moment vectors. At -180°C , the transition becomes allowed and the band systems consists of sharp bands with the 0, 0 band at 35347 cm^{-1} for 1, 2, 3-trichlorobenzene and at 36109 cm^{-1} for 1, 2, 3-trihydroxybenzene. The other bands are satisfactorily assigned to excited state vibrational frequencies. The structure of the bands in the rigid glass at -180°C is similar to that of pure crystals at same temperature except that it is at higher energy region and in 1, 2, 3-trihydroxybenzene the bands are sharper.

These results indicate that a perturbation on the energy states of these molecules occur at -180°C . It has been pointed out that the interaction of permanent dipoles of the neighbouring molecules on the transition moment of the molecules in the lattice might play a dominant role in determining the energy states of molecular crystals.

INTRODUCTION

The intensity of absorption and structure of bands in the electronic spectra of trisubstituted benzenes are known to depend on the symmetry of the molecules. In symmetrical trisubstituted benzenes the 0,0 band in the near ultraviolet absorption spectra is forbidden in the vapour state as in benzene, whereas in the spectra of 1, 2, 4-trisubstituted benzenes the 0,0 band is allowed (Sponer, 1947). Sklar (1942) calculated the contributions from the substituents to the migrational transition moment and found that they annul one another in the first order in 1, 2, 3-trisubstituted benzenes, when the substituents at the positions are the same. Thus theoretically, the spectra should appear in these cases only through vibrational moments i.e. by distorting the symmetry of the molecule through excitation of vibrations. In 1, 2, 4-trisubstituted benzene, however, the three migration moment vectors are added up to give a large resultant migration moment and the spectra are expected to be allowed with a strong 0,0 band. The influence of intermolecular field on the electronic spectra of a few trisubstituted benzene has recently been studied by a number of workers. It has been observed

*Communicated by Prof. S. C. Sirkar.

that the symmetrically forbidden transitions in 1,3,5-trichlorobenzene (Banerjee, 1957) and 1,3,5-trimethylbenzene (Sen, 1959) become allowed in pure crystals when cooled to -180°C . Schnepf (1959) studied the polarised electronic spectra of orientated single crystal of 1,3,5-trichlorobenzene at -180°C and concluded that the appearance of the 0,0 band was due to change in symmetry of the molecule. Roy (1958) observed that in the spectrum of the substance dispersed in rigid glass media at -180°C also, the 0,0 band was present. In the present work, investigations on the electronic spectra of trisubstituted benzenes in different states have been extended to the molecules of 1,2,3-trichlorobenzene and 1,2,3-trihydroxybenzene.

EXPERIMENTAL

The experimental set up was the same as described in an earlier paper (Misra, 1960). Chemically pure 1,2,3-trichloro- and trihydroxybenzene supplied by Dr. Theodor Schuchardt of Munich and E. Merck & Co respectively were repeatedly crystallised from solutions in alcohol and the crystals were further purified by vacuum sublimation before use.

Thin films of the substances of thicknesses of the order of a few microns were required to produce bands in the solid state. To study the absorption spectra in the liquid state, the thin film of substances enclosed between two quartz plates was placed in a heating chamber which was kept at temperatures about 5°C above the respective melting points of the substances.

The solvent used to study the absorption spectra of the substances in solution and in rigid glass media at -180°C was ethyl alcohol. The solvent was found to produce no absorption band in the region under consideration. A brass cell of thickness 1 cm provided with quartz windows was used to study the absorption spectra of the substance in solution and in rigid glass and the strength of the solution was .01% by weight in each case.

Spectrograms were taken on Agfa Isopan films backed by a metal sheet with a Hilger E 1 spectrograph giving a dispersion of the order of 3 Å per mm. in the region of 2600 Å. Iron arc spectrum was photographed on each spectrogram as a comparison. Microphotometric records were taken with a Kipp and Zonen self-recording microphotometer. The absorption spectra were calibrated with the help of microphotometric records of iron arc lines using the method described in an earlier paper (Sirkar and Misra, 1959).

RESULTS AND DISCUSSION

The microphotometric records of the absorption spectra of the 1,2,3-trichlorobenzene and 1,2,3-trihydroxybenzene are given in Figs. 1—4 and the positions of the bands in wave numbers, their visual strengths of absorption and probable assignments are given in Tables 1-111.

The results have been discussed in the following sections.

1,2,3-Trichlorobenzene

The near ultraviolet absorption spectra of 1,2,3-trichlorobenzene along with those for 1,3,5- and 1,2,4-trichlorobenzene were studied by Conrad-Billroth (1932) in hexane solution and several distinct maxima were observed. Though the absorption is strong in the case of 1, 2, 4-trichlorobenzene, the other two compounds exhibit very feeble absorption. This shows the characteristics of forbidden transition. The absorption spectrum of 1, 2, 3-trichlorobenzene in the vapour phase was studied by Sponer (1947) who observed that the structure of the spectrum was different from that of the other two isomers. It consists of three broad, diffuse and weak bands which are separated from each other by about 995 cm^{-1} . No band due to $1 \rightarrow 0$ transition in the vapour phase was observed and therefore it was suggested that the $0,0$ band might be present in the first weak group. The centre of the first group is at about 35910 cm^{-1} , but as the transition is ordinarily forbidden, the $0,0$ band cannot be strong and therefore it cannot be at the centre of the first band. It has been observed in the present investigation that in the liquid state at 70°C also 1, 2, 3-trichlorobenzene shows three broad bands (Fig. 1, Table I), the centre of the bands being at 35535 cm^{-1} , 36607 cm^{-1} and 37681 cm^{-1} , respectively the difference between successive bands

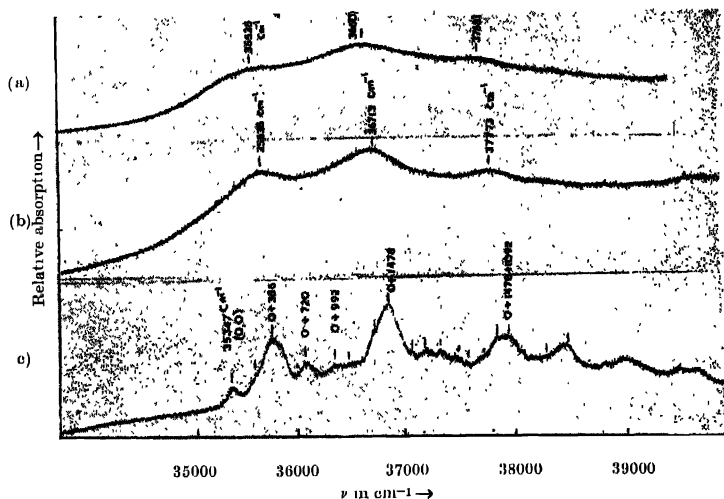


Fig. 1. Microphotometric records of the ultraviolet absorption spectra of 1,2,3-trichlorobenzene in different states.

(a) liquid state at 70°C . (b) solid state at 32°C . (c) solid state at -180°C .

TABLE I

Ultraviolet absorption bands of 1, 2, 3-trichlorobenzene in different states

Liquid at 70°C		Solid at 32°C		Crystal at -180°C	
Wave No. in cm ⁻¹	Difference	Wave No. in cm ⁻¹	Difference	Wave No. in cm ⁻¹	Assignment
35535 (vs)	1072	35638 (s)	1075	35347 (ms)	0,0
36007 (s)	1072	36713 (s)	1075	35616 (w)	0+269
37081 (s)		37773 (s)		35733 (vs)	0+386
				35837 (w)	0+490
				36002 (vw)	0+269+386
				36067 (ms)	0+269+490
					0+720
				36223 (w)	0+386+490
				36339 (m)	0+992
				36439 (m)	0+1092
				36557 (vw)	0+1210
				36725 (mw)	0+992+386
					0+1092+269
				36825 (vs)	0+1478
					0+1092+386
				36929 (w)	0+1092+490
				37059 (mw)	0+720+992
				37159 (m)	0+720+1092
				37316 (m)	0+1092+490+386
					0+1478+490
					0+2×992
				37431 (m)	0+992+1092
				37531 (mw)	0+2×1092
				37649 (w)	0+1092+1210
				37717 (w)	0+2×992+386
				37817 (m)	0+2×1092+269
					0+1092+992+386
				38033 (w)	0+2×1092+490
					0+1478+1210
				38151 (w)	0+1092+992+720
				38251 (vw)	0+2×1092+720
				38413 (s)	0+2×1092+386
					+490
					0+1478+1092+490
				38523 (w)	0+2×1092+992
				38800 (m)	0+2×992+1478
					0+2×992+1092+
					386
				39009 (ms)	0+2×1092+1478
				39409 (m)	0+2×992+2+1092

being about 1072 cm^{-1} . Thus it appears that on liquefaction of the vapour, the band system is shifted by about 375 cm^{-1} towards red.

When the liquid is solidified at the room temperature the bands become a little sharper but no further resolution of the structure of the bands takes place and the spectrum consists of three broad bands as in the liquid state, the centres of the bands being now at 35638 cm^{-1} , 36713 cm^{-1} and 37773 cm^{-1} respectively. Thus the band system is shifted by about 272 cm^{-1} towards red from its position in the vapour phase.

When the temperature of the crystals is lowered to -180°C each of the three bands is split up into a number of bands and the spectrum consists of strong sharp bands as in the case of allowed transition. The very strong band at 35733 cm^{-1} was approximately at the centre of a number of bands. The first band on the long wavelength side at 35347 cm^{-1} was taken as the 0, 0 band of the system. All the other bands in the spectrum could then be explained satisfactorily in terms of excited state frequencies 269, 386, 490, 992, 1092, 1210 and 1478 cm^{-1} and their combinations. These frequencies correspond respectively to the ground state Raman frequencies 333, 486, 505, 1076, 1151, 1248 and 1554 cm^{-1} as given in Landolt-Bornstein's Tables (1951). No Raman-shift of 720 cm^{-1} was given

TABLE 11
Ultraviolet absorption bands of 1, 2, 3-trichlorobenzene
in alcohol

In solution at 32°C		In rigid glass media at -180°C	
Wave No. in cm^{-1}	Difference	Wave No. in cm^{-1}	Assignment
		35463 (s)	0, 0
		35719 (w)	0+256
35652 (s)	1050	35844 (vs)	0+381
36702 (vs)		35947 (w)	0+484
	1050		
		36197 (ms)	0+256+484
			0+734
37753 (s)		36538 (ms)	0+1075
		36903 (vs)	0+1440
		37177 (m)	0+256+381+1075
		37281 (m)	0+734+1075
		37386 (m)	0+484+1440
		37870 (m)	0+2×1075+256
		37997 (ms)	0+2×1075+381
			0+1440+1075
		38479 (ms)	0+2×1075+381+484
			0+1440+1075+484
		39043 (ms)	0+2+1075+1440

in Landolt-Bornstein's Tables but such a frequency is usually observed in other 1, 2, 3-trisubstituted benzenes such as trimethylbenzene, trihydroxybenzene (Landolt-Bornstein's Table, 1951). Thus the very strong band at 35733 cm^{-1} which is at a distance of 386 cm^{-1} from the 0,0 band represents the centre of the broad band observed in the spectrum due to the crystal at room temperature. Hence the 0, 0 band is on the long wavelength side of the centre of the first broad band observed in the case of the liquid and it has been concluded that the 0,0 band appears only when the crystals are cooled to -180°C .

When the substance is dissolved in alcohol, three broad bands, as those due to the liquid state and solid state at 32°C , are observed, the centres of the bands being at 35652 cm^{-1} , 36702 cm^{-1} and 37753 cm^{-1} respectively (Fig. 2 Table II). In hexane solution (Conrad-Billroth, 1932) the first broad band was approximately at 35700 cm^{-1} . Thus in alcohol solution at room temperature, the band system is shifted towards red from its position in hexane solution and it is approximately in the same position as in pure the spectrum of crystals at the room temperature.

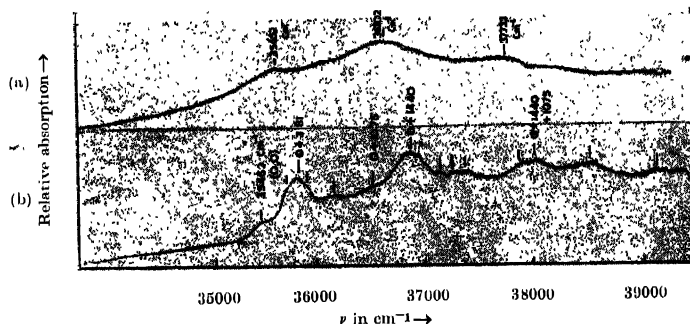


Fig. 2. Microphotometric records of the ultraviolet absorption spectra of 1,2,3-trichlorobenzene.

(a) alcohol solution at 32°C .

(b) Rigid Glass Medium at -180°C .

The assignments of the bands due to crystals at -180°C are supported by the spectra of the substance dispersed in rigid glass medium in alcohol at -180°C . The structure of the bands in rigid glass is similar to that due to pure crystals at -180°C . The first band of medium strength is now at 35463 cm^{-1} and taking this as the 0, 0 band, the other bands can be assigned to upper state fundamentals 256, 381, 484, 734, 1075 and 1440 cm^{-1} and their combinations. Thus the 0, 0 band of 1, 2, 3-trichlorobenzene in frozen alcohol at -180°C is at a distance of 116 cm^{-1} on the high energy side of the 0, 0 band due to the pure crystals at -180°C and the upper state fundamentals in the two cases agree fairly well with each other.

Thus it is seen that in the spectra of the substance in rigid glass media at -180°C and also of the pure crystals at -180°C the strength of absorption is much larger than that in free molecules and the broad bands of crystals at room temperature are resolved into a number of sharp bands in the former case. In rigid glass, the bands are less sharp than in pure crystals at -180°C but the structure of the spectrum is the same in both the cases. These results indicate that transition which is forbidden in free molecules due to cancellation of three migrational moment vectors, becomes allowed probably due to some distortion in the symmetry of the molecules at -180°C . The weak 0, 0 band in the spectrum due to the crystals at -180°C indicate that though the transition is allowed at this temperature, the magnitude of the transition moment is very small and its interaction with the permanent dipole of the neighbouring molecule is expected to be very weak. It has been proposed by Sirkar (1962, 1963) that such interaction might be partly responsible for producing large splitting of electronic bands in crystals of polar molecules. In the present case, the interaction may be too weak to produce any detectable splitting of the bands and actually no splitting has been observed.

1,2,3-Trihydroxybenzene

Little work has been done on the electronic spectra of pyrogallol in the near ultraviolet region. Leonard Jurd (1957) observed the absorption maximum of the substance at 2670 Å in solution in alcohol at room temperature. Shergina *et. al.* (1959) also reported similar observations. In the present investigation, the ultraviolet absorption spectra of the substance were investigated in the liquid and solid states at room temperature and also at -180°C . The spectrum of the substance in solution in alcohol at -180°C was also photographed in order to verify the assignments of the bands due to the polycrystalline mass at -180°C .

In the liquid state, a broad region of absorption extending from 35627 cm^{-1} to 38156 cm^{-1} was observed without any discrete structure. When the liquid was solidified at the room temperature, three broad bands were observed, the centres of the bands being at 35999 cm^{-1} , 36678 cm^{-1} and 37246 cm^{-1} respectively.

When the solid is cooled down to -180°C , the spectrum consists of strong but broad bands and eight strong bands are clearly resolved. No other bands were observed on the long wavelength side of the strong band at 36109 cm^{-1} and this was taken as the 0, 0 band of the system then the other bands represented excited state frequencies 429, 537, 675, 972, 1237 and 1463 cm^{-1} which correspond to the Raman frequencies 466, 573, 767, 1015, 1237 and 1473 cm^{-1} (Landolt-Bornstein's Tables 1951). A strong Raman line 1386 cm^{-1} has been reported in these Tables and the band due to the corresponding upper state frequency is

probably not resolved from the two bands representing the frequencies 1237 and 1463 cm^{-1} .

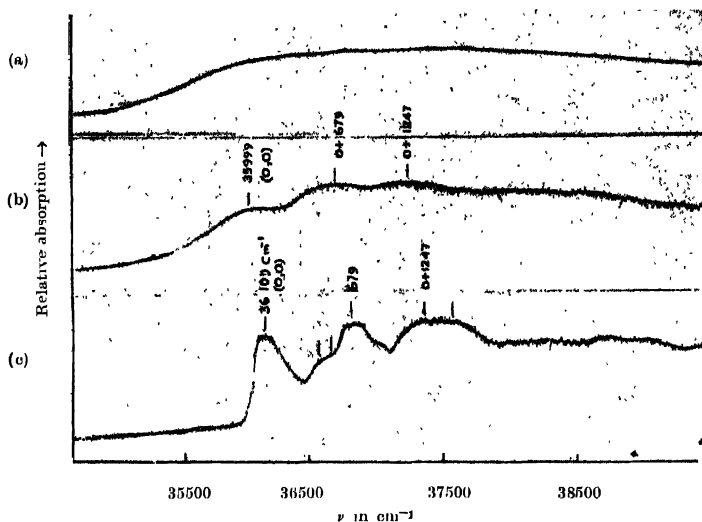


Fig. 3. Microphotometric records of the ultraviolet absorption spectra of 1,2,3-trihydroxybenzene in different states.
(a) liquid at 140°C (b) Solid at 32°C (c) solid at -180°C .

TABLE III

Ultraviolet absorption bands of pyrogallol

Liquid at 140°C	Solid at room temperature		Solid at -180°C		Rigid glass at -180°C in alcohol	
	Wave No. in cm^{-1}	Assignment	Wave No. in cm^{-1}	Assignment	Wave No. in cm^{-1}	Assignment
Broad absorption region extending from 36027 cm^{-1} to 38156 cm^{-1}	35999 (m)	0,0	36109 (vs)	0,0	35857 (s)	0,0
			36538 (m)	0 + 429	36273 (me)	0 + 416
	36678 (s)	0 + 679				
			36646 (m)	0 + 537	36392 (m)	0 + 535
	37246 (s)	0 + 1247				
			36784 (vs)	0 + 675	36526 (ms)	0 + 669
			37081 (w)	0 + 972	37081 (s)	0 + 1224
			37346 (s)	0 + 1237	37274 (s)	0 + 1427
			37572 (s)	0 + 1463		

In the case of the solution in alcohol at -180°C , the structure of the spectrum resembles that due to pure crystals at -180°C except that in the latter case the bands are strong but quite broad while in the former case the bands are sharp. The first band on the long wavelength side assigned as the 0, 0 band is pure crystals of 1, 2, 3-trihydroxybenzene at -180°C is quite strong compared to that in 1, 2, 3-trichlorobenzene and the transition moment has a larger value in the former than in the latter molecule. The broadness of the bands probably indicates that the bands are split up in the spectrum due to pure crystals at -180°C and the split components are not resolved. The 0, 0 band in this case is at 35857 cm^{-1} and the other bands represent upper state fundamentals

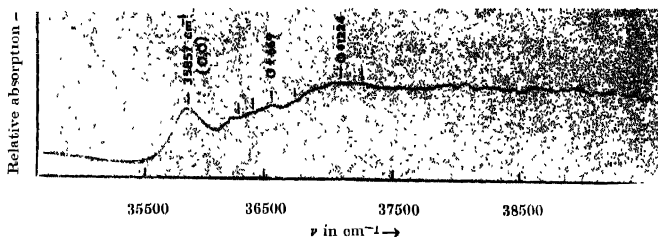


Fig. 4. Microphotometric records of ultraviolet absorption spectrum of 1,2,3-trihydroxybenzene in rigid glass medium at -180°C .

416, 535, 669, 1224 and 1427 cm^{-1} which agree fairly well with the values in the case of the pure crystals at -180°C . Thus the 0, 0 band in pure crystals at -180°C is shifted towards the higher energy region by about 252 cm^{-1} with respect to that due to rigid glass medium at the same temperature.

These results indicate that the symmetry of the molecule is disturbed at low temperature and the transition which is forbidden in the free molecule is made allowed as in the case of 1, 2, 3-trichlorobenzene. Further interaction of permanent dipoles of the neighbouring molecules on the transition moment of the molecules in the lattice plays a dominant role in determining the energy states of molecular crystals.

ACKNOWLEDGMENT

The author is grateful to Professor S. C. Sirkar, D.Sc., F.N.I. for his kind interest and guidance in the work.

REFERENCES

- Banerjee, S. R., 1957, *Ind. J. Phys.*, **31**, 483.
- Conrad-Billroth, H., 1932, *Z. f. Phys. Chem.*, **B19**, 76.
- Jurd, L., 1957, *J. Am. Chem. Soc.*, **79**, 3445.
- Landolt and Bornstein, 1951, *Zahlenwerte und Funktionen I Band, Teil 2*, p. 523 and p.498

- Misra, T. N., 1960, *Ind. J. Phys.*, **34**, 381.
Roy, S. B., 1957, *Ind. J. Phys.*, **31**, 588.
Schoepp, O. P., 1959, *J. Chem. Phys.*, **30**, 863.
Sen, S. K., 1959, *Ind. J. Phys.*, **33**, 41.
Shergina, N. I., et al., 1959, *Hua Hsiieh Hsueh Pao*, **25**, 236.
Sirkar, S. C., and Misra, T. N., 1959, *Ind. J. Phys.*, **33**, 45.
Sirkar, S. C., 1962, *Proc. Nat. Inst. Sci. of India*, **27A**, 568.
Sirkar, S. C., 1963, *Ind. J. Phys.*, **37**, 101,
Sklar, A. L., 1942, *Rev. Mod. Phys.*, **41**, 281.
Sponer, H., 1947, *Chem. Rev.*, **41**, 281.

Letters to the Editor

The Board of Editors will not hold itself responsible for opinions expressed in the letters published in this section. The notes containing reports of new work communicated for this section should not contain many figures and should not exceed 500 words in length. The contributions must reach the Assistant Editor not later than the 15th of the second month preceding that of the issue in which the letter is to appear. No proof will be sent to the authors.

1

ON NUCLEAR BINDING ENERGY

A. K. DUTTA

DEPARTMENT OF PURE PHYSICS

UNIVERSITY COLLEGE OF SCIENCE, CALCUTTA

(Received February 12, 1963)

A smooth curve, drawn over the plots of nuclear binding energy against mass number, is likely to be fitted in by a number of relationships with four or more variable parameters and corresponding adjustable constants. A theoretical significance given to the parameters, in any of these possible relationships, would not necessarily imply that the interpretation should be valid. This is all the more true when the experimental points lie scattered about the mean graph.

It is, therefore, more reasonable to be guided by the binding energy data, in an attempt to find a suitable relation for nuclear energy. It may be observed that in the usual Bethe-Weizsacker relation, the term denoting the binding energy per nucleon becomes inflated to a value of the order of -17 mev. per nucleon, in place of the maximum experimental value of -8.794 mev per nucleon, in the region near mass number 60, at mass number 62. This will be seen from the nuclear mass table of Everling *et al.* (1960). This inflation was necessary to counteract the effect of the other terms considered in the relation. It has been further noted that the binding energies for other mass numbers decrease on both sides of the region of maximum, in terms of the square of the mass number deviation, with only one adjustable constant associated with it. To make a closer fit with the large amount of binding energy data slight adjustments of the maximum binding energy and the corresponding mass number are helpful and we obtain.

$$E = \sim 8.728A + a(A-63.5)^2 \text{ mev.}, \text{ where } a = 9.181 \times 10^{-3}$$

This is transformed to

$$E = (-9.893A - 37.0) - 9.181 \times 10^{-3}A, \text{ in mev. units.}$$

The first part in the transformed relation signifies the usual binding energy per nucleon. The second term is the disruption energy, increasing proportionally with the square of the mass number. The constant term in the first part signifies that the nuclear binding energy of this character would come into operation only with nuclei having larger mass number than 3.75 for which E is zero, i.e. from mass number 4.

The relationship obtains the binding energies of all the 1600 nuclei, from carbon ($Z = 6$) to Fermium ($Z = 100$), tabulated by Everling, *et al.* with an average fluctuation of less than ± 3 mev., for any mass number. A few nuclei which have larger deviation in binding energy from the mean value for a mass number, obtain deviations of the order of ± 10 mev. Magnitudes of deviations calculated by Bethe-Weiszacker relation (Dutta *et al.* 1962) are generally much larger.

It appears that the fluctuations also can be expressed in terms of suitable additional or modified terms which are necessarily functions of N and Z . This will be attempted in a more detail paper with co-workers.

REFERENCES

- Everling, F., Konig, L. A. Mathunch, J. H. E., 1960, *Nuclear Physics*, **18**, 529.
 Dutta, A. K., Pal, B., Das Gupta, A., Choudhury, N., 1962, *Indian Jour. Physics*, **36**, 497.

IMPORTANT PUBLICATIONS

The following special publications of the Indian Association for the Cultivation of Science, Jadavpur, Calcutta, are available at the prices shown against each of them :—

TITLE	AUTHOR	PRICE
Magnetism .. Report of the Symposium on Magnetism		Rs. 7 0 0
Iron Ores of India	.. Dr. M. S. Krishnan	5 0 0
Earthquakes in the Himalayan Region	.. Dr. S. K. Banerji	3 0 0
Methods in Scientific Research	.. Sir E. J. Russell	0 6 0
The Origin of the Planets	.. Sir James H. Jeans	0 6 0
Active Nitrogen— A New Theory.	.. Prof. S. K. Mitra	2 8 0
Theory of Valency and the Structure of Chemical Compounds.	.. Prof. P. Ray	3 0 0
Petroleum Resources of India	.. D. N. Wadia	2 8 0
The Role of the Electrical Double-layer in the Electro-Chemistry of Colloids.	.. J. N. Mukherjee	1 12 0
The Earth's Magnetism and its Changes	.. Prof. S. Chapman	1 0 0
Distribution of Anthocyanins	.. Robert Robinson	1 4 0
Lapinone, A New Antimalarial	.. Louis F. Fieser	1 0 0
Catalysts in Polymerization Reactions	.. H. Mark	1 8 0
Constitutional Problems Concerning Vat Dyes.	.. Dr. K. Venkataraman	1 0 0
Non-Aqueous Titration	.. Santi R. Palit, Mihir Nath Das and G. R. Somayajulu	3 0 0
Garnets and their Role in Nature	.. Sir Lewis I. Fermor	2 8 0

A discount of 25% is allowed to Booksellers and Agents.

NOTICE

No claims will be allowed for copies of journal lost in the mail or otherwise unless such claims are received within 4 months of the date of issue.

RATES OF ADVERTISEMENTS

1. Ordinary pages :

Full page	Rs. 50/- per insertion
Half page	Rs. 25/- per insertion
 2. Pages facing 1st inside cover, 2nd inside cover and first and last page of book matter :

Full page	Rs. 55/- per insertion
Half page	Rs. 30/- per insertion
 3. Cover pages by negotiation
- 25% commissions are allowed to bona fide publicity agents securing orders for advertisements.

CONTENTS

Indian Journal of Physics

Vol. 37, No. 3

March, 1963

PAGE

13. Vibrational Spectra, Approximate Potential Constants and Calculated Thermodynamic Properties of Benzophenone—P. G. Puranik and E. V. Rao 121
14. Discrete Frequencies in a Lattice Perturbed by Isotope Defects—J. Mahanti and Ram Kishore Sharma 127
15. Hydrogen Bonding in Aniline and some Substituted Anilines in Different Environments—K. C. Medhi and G. S. Kastha 139
16. Observation of Hammer stars Caused by Li^3 -Decay—G. C. Deka and K. M. Pathak 145
17. On the Temperature-Effect of the Daily Variation of Cosmic Ray Meson Intensity—R. P. Kane 151
18. The Electronic Spectra of some Trisubstituted Benzenes in Different States—I—T. N. Misra 173

LETTER TO THE EDITOR

1. On Nuclear Binding Energy—A. K. Dutta 183

Regd. No. C-3911

VOL. 37

INDIAN JOURNAL OF PHYSICS

No. 4

(Published in collaboration with the Indian Physical Society)

AND

VOL. 46

PROCEEDINGS

No. 4

OF THE

INDIAN ASSOCIATION FOR THE
CULTIVATION OF SCIENCE

APRIL 1963

PUBLISHED BY THE
INDIAN ASSOCIATION FOR THE CULTIVATION OF SCIENCE
JADAVPUR, CALCUTTA 32

BOARD OF EDITORS

K. BANERJEE	D. S. KOTHARI
D. M. BOSE	S. K. MITRA
S. N. BOSE	B. D. NAG CHAUDHURI
S. D. CHATTERJEE	K. R. RAO
P. S. GILL	D. B. SINHA
S. R. KHASTGIR	S. C. SIKHAR (Secretary)
B. N. SRIVASTAVA	

EDITORIAL COLLABORATORS

PROF. R. K. ASUNDI, Ph.D., F.N.I.	
PROF. D. BASU, Ph.D.	
PROF. J. N. BHAR, D.Sc., F.N.I.	
PROF. V. G. BHIDE, Ph.D.(Nag), Ph.D.(Lond).	
PROF. A. BOSE, D.Sc., F.N.I.	
PROF. S. K. CHAKRABARTY, D.Sc., F.N.I.	
DR. J. S. CHATTERJEE	
DR. K. DAS GUPTA, Ph.D.	
PROF. N. N. DAS GUPTA, Ph.D., F.N.I.	
DR. J. DEAR, D.Phil (So)	
PROF. A. K. DUTTA, D.Sc., F.N.I.	
PROF. C. S. GHOSH, M.Sc., S.M., F.N.I.,	M.I.E.E.
PROF. S. GHOSH, D.Sc., F.N.I.	
PROF. S. N. GHOSH, D.Sc.	
PROF. S. GUPTA, M.Sc., F.N.I.	
PROF. D. N. KUNDU, Ph.D., F.N.I.	
PROF. R. C. MAJUMDER, Ph.D., F.N.I.	
PRINCIPAL Y. G. NAIK, Ph.D.	
PROF. S. R. PALIT, D.Sc., F.R.I.C., F.N.I.	
PROF. H. RAKSHIT, D.Sc., F.N.I.	
PROF. A. SAHA, D.Sc., F.N.I.	
DR. VIKRAM A. SARABHAI, M.A., Ph.D., F.N.I.	
DR. A. K. SENGUPTA, D.Sc.	
PROF. NAND LAL SINGH, D.Sc.	
DR. M. S. SINHA, D.Sc., F.N.I.	
PROF. N. R. TAWDE, Ph.D., F.N.I.	
DR. P. VENKATESWARLU	

Assistant Editor :

SRI T. N. MISRA, M.Sc.

Annual Subscription—

Inland Rs. 25.00

Foreign £ 2-10-0 or \$ 7.00

NOTICE

TO INTENDING AUTHORS

Manuscripts for publication should be sent to the Assistant Editor, Indian Journal of Physics, Jadavpur, Calcutta-32.

The manuscripts submitted must be type-written with double space on thick foolscap paper with sufficient margin on the left and at the top. The original copy, and not the carbon copy, should be submitted. Each paper must contain an abstract at the beginning.

All references should be given in the text by quoting the surname of the author, followed by year of publication, e.g., (Ghosh, 1954). The full reference should be given in a list at the arranged alphabetically, as follow. Ghosh, D. K., 1954, *Ind. J. Phys.*, 28, 485.

Line diagrams should be drawn on white Bristol board or tracing paper with black India ink, and letters and numbers inside the diagrams should be written neatly in capital type with India ink. The size of the diagrams submitted and the lettering inside should be large enough so that it is legible after reduction to one-third the original size. A simple style of lettering such as gothic, with its uniform line width and no serifs should be used, e.g.,

A·B·E·F·G·M·P·T·W·

Photographs submitted for publication should be printed on glossy paper with somewhat more contrast than that desired in the reproduction, and should, if possible, be mounted on thick white paper.

Captions to all figures should be typed in a separate sheet and attached at the end of the paper.

The mathematical expressions should be written carefully by hand. Care should be taken to distinguish between capital and small letters and superscripts and subscripts. Repetition of a complex expression should be avoided by representing it by a symbol. Green letters and unusual symbols should be identified in the margin. Fractional exponents should be used instead of root signs.

Bengal Chemical and Pharmaceutical Works Ltd.

Pioneer Indian Manufacturers of Pharmaceuticals & Chemicals.

Manufacturers of:

Pharmaceutical Chemicals:

Caffeine and its salts, Strychnine Hydrochlor, Strychnine Sulphate, Brucine Sulphate, Potassium Citrate B.P., I.P., Sodium Citrate B.P., I.P., Potassium Acetate B.P., I.P., Potassium Iodide B.P., I.P., Sodium Iodide B.P., I.P., Ferri et Ammon Citrate B.P., I.P., Nicotinic Acid, B.P., Nicotinamide, B.P., and various other Pharmaceutical Chemicals.

Heavy & Reagent Quality Fine Chemicals:

Alum, Alum Sulphate (Iron Free), Ferro Alum, Zinc Chloride Tech. Naphthalene Pure, Sodium Citrate A.R., Potassium Citrate A.R., Magnesium Sulphate A.R., Sodium Sulphate Anhydrous A.R., Potassium Iodide A.R., Sodium Chloride A.R., Zinc Sulphate A.R., etc.

Please refer your enquiries for the above items and other chemicals in the line to :—

BENGAL CHEMICAL
6, GANESH CHUNDER AVENUE,
CALCUTTA-13, INDIA.

NON-AQUEOUS TITRATION

A monograph on acid-base titrations in organic solvents

By

PROF. SANTI R. PALIT, D.Sc., F.R.I.C., F.N.I.

DR. MIHIR NATH DAS, D.Phil.

AND

MR. G. R. SOMAYAJULU, M.Sc.

This book is a comprehensive survey of the recently developed methods on acid-base titrations in non-aqueous solvents. Acid-base concept, as developed by Lowry-Brønsted and Lewis is succinctly presented in this slender volume.

including the estimation of weak bases. Various methods for the titration of weak acids are duly described. A reference list of all pertinent publications is included in this book.

122 pages with 23 diagrams (1954)

Inland Rs. 3 only. Foreign (including postage) \$ 1.00 or 5s.

Published by

INDIAN ASSOCIATION FOR THE CULTIVATION OF SCIENCE
JADAVPUR, CALCUTTA-32, INDIA

IMPORTANT PUBLICATIONS

The following special publications of the Indian Association for the Cultivation of Science, Jadavpur, Calcutta, are available at the prices shown against each of them :—

TITLE	AUTHOR	PRICE
Magnetism .. Report of the Symposium on Magnetism		Rs. 7 0 0
Iron Ores of India ..	Dr. M. S. Krishnan	5 0 0
Earthquakes in the Himalayan Region ..	Dr. S. K. Banerji	3 0 0
Methods in Scientific Research ..	Sir E. J. Russell	0 6 0
The Origin of the Planets ..	Sir James H. Jeans	0 6 0
Active Nitrogen— ..	Prof. S. K. Mitra	2 8 0
A New Theory		
Theory of Valency and the Structure of ..	Prof. P. Ray	3 0 0
Chemical Compounds.		
Petroleum Resources of India ..	D. N. Wadia	2 8 0
The Role of the Electrical Double-layer ..	J. N. Mukherjee	1 12 0
in the Electro-Chemistry of Colloids.		
The Earth's Magnetism and its Changes ..	Prof. S. Chapman	1 0 0
Distribution of Anthocyanins ..	Robert Robinson	1 4 0
Lapinone, A New Antimalarial ..	Louis F. Fieser	1 0 0
Catalysts in Polymerization Reactions ..	H. Mark	1 8 0
Constitutional Problems Concerning ..	Dr. K. Venkataraman	1 0 0
Vat Dyes.		
Non-Aqueous Titration ..	Santi R. Palit, Mihir Nath Das and G. R. Somayajulu	3 0 0
Garnets and their Role in Nature ..	Sir Lewis L. Fermor	2 8 0

A discount of 25% is allowed to Booksellers and Agents.

NOTICE

No claims will be allowed for copies of journal lost in the mail or otherwise unless such claims are received within 4 months of the date of issue.

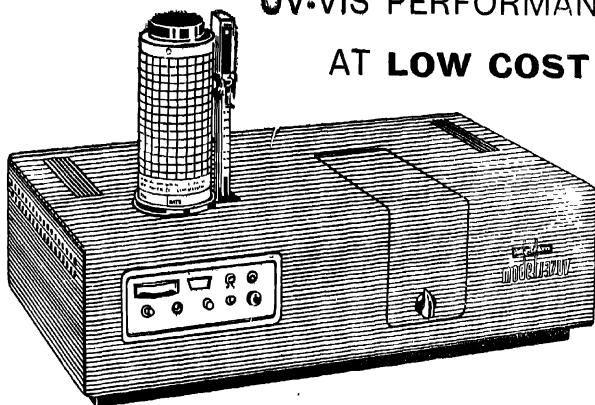
RATES OF ADVERTISEMENTS

- Ordinary pages :

Full page	Rs. 50/- per insertion
Half page	Rs. 28/- per insertion
 - Pages facing 1st inside cover, 2nd inside cover and first and last page of book matter :

Full page	Rs. 55/- per insertion
Half page	Rs. 30/- per insertion
 - Cover pages by negotiation
- 25% commissions are allowed to *bona fide* publicity agents securing orders for advertisements.

NEW SPECTROPHOTOMETER GIVES HIGHEST UV-VIS PERFORMANCE AT LOW COST



A new ultraviolet-visible spectrophotometer—the Perkin-Elmer Model 202—provides photometric and wavelength capabilities you expect from more expensive instruments. Its low price brings it within the range of any lab budget.

The Model 202 covers two regions: 190 to 390 $m\mu$ in the ultraviolet, and 350 to 750 $m\mu$ in the visible. Two scanning speeds—two and eight minutes per scan—are available for survey or precise work.

FEATURES

- **EASE OF OPERATION.** Minimum controls, plus Automatic Gain Control and slit programming, makes the Model 202 easy to run. Records linearly in absorbance units (0-1.5).
- **OPTICAL NULL RECORDING.** For high accuracy in quantitative analysis, plus high reproducibility.
- **AUTOMATIC GAIN CONTROL.** An exclusive feature, automatically increases energy of the system in high absorption areas. Makes the most difficult differential analyses routine.

Notebook-size Chart: Spectra of each range recorded on standard 8½ x 11 chart, with large ordinate for accuracy. Linear wavelength presentation. Specifications are:

	ULTRAVIOLET	VISIBLE
Resolution	0.2 $m\mu$ at 250 $m\mu$	1.5 $m\mu$ at 600 $m\mu$
Photometric accuracy in absorbance units	± 0.1	± 0.1
Photometric reproducibility in absorbance units	0.05	0.05
Wavelength accuracy	$\pm 0.5 m\mu$	$\pm 1.0 m\mu$
Wavelength reproducibility	0.3 $m\mu$	0.5 $m\mu$

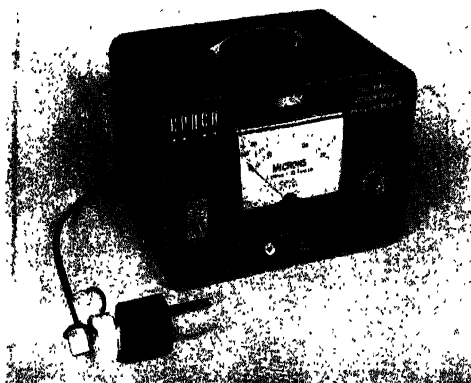
Perkin-Elmer

Sold and serviced in India exclusively by

BLUE STAR

**BLUE STAR ENGINEERING
CO. (Calcutta) Private LTD.**
7 HARE STREET, CALCUTTA 1
Also at BOMBAY • DELHI • MADRAS

CENCO DISCHARGE VACUUM GAUGE AND CONTROLLER



Measures vacuum from 0.001 micron to 20 microns of mercury. Gives direct readings using cold cathode discharge principles. Instantly self starting at any pressure from 760mm down to 0.001 micron. Measures total pressure of all condensable vapours and permanent gases present in a vacuum system. Automatic on.off switching action for operations performed within or outside of the vacuum system. A specific value can be pre-set. Designed also to operate an auxiliary power relay.

For further particulars, please write to :

The Sole Distributors

**THE SCIENTIFIC INSTRUMENT
COMPANY, LIMITED.**

ALLAHABAD BOMBAY CALCUTTA MADRAS
NEW DELHI

Head Office : 6, Tej Bahadur Sapru Road, Allahabad



EFFECT OF IONIC CURRENTS ON HEAT-TRANSFER

S. C. BHAND, M. S. GAUR AND D. V. GOGATE

PHYSICS DEPARTMENT, MADHAV COLLEGE, VIKRAM UNIVERSITY, UJJAIN

(Received August 22, 1962)

ABSTRACT. Electrolytic (ionic) currents are produced in a weak electrolyte giving rise to the generation of bubbles and their effect on heat transfer is studied. Thin platinum wires were used as heating surfaces and the enhancement of heat transfer under controlled bubble generation was determined for different values of the excess of temperature $\Delta\theta$ of the heating surface over the surrounding liquid. Changes in the value of the heat transfer coefficient ' h ' resulting from variation in the area of the heating surface and in the excess of temperature $\Delta\theta$ are exhibited graphically and the peak value of ' h ' obtained under the above conditions is then determined.

INTRODUCTION

Heat transfer between a heating solid surface and a boiling liquid has been the subject of many investigations during recent years (Nukiyama 1934; Drew and Mueller, 1937; Addoms, 1948; Bromley, 1950; Rao, Desai and Gogate, 1960). In the process of heat transfer in boiling liquids, the increase of temperature of the heating surface causes an increase in the rate of bubble evolution and also in the number of bubble nucleation-sites. These two effects can be simulated by electrolytic generation of bubbles and there is the added advantage that it can be controlled independently of the heating surface temperature. It thus offers possibilities of a better understanding of the mechanism by which heat is transferred. In our experiments bubbles are produced electrolytically on a heated platinum wire immersed in a dilute electrolyte.

Mixon and du Pont (1959) have investigated the influence of electrolytic bubble evolution on heat-transfer and have concluded that there is a slight but inconclusive evidence that an increase in the ionic current lowers the attainable heat flux in the high current region.

In a preliminary note Eddie, Rao and Gogate (1961) have briefly described the changes in the heat transfer coefficient ' h ' resulting from the production of ionic currents under a constant difference of temp. $\Delta\theta$ between a heated platinum wire and the surrounding liquid. It appears from their results that there is a sudden fall in the value of ' h ' immediately after the peak value (h_{max}) is reached. But they do not seem to have obtained any definite and reliable observations for the sudden fall in ' h ' with increase in the strength of the ionic currents.

The work reported in this paper was undertaken to examine heat transfer enhancement resulting from the controlled bubble generation by means of ionic

currents and to investigate the lowering of heat flux in the high ionic current region.

EXPERIMENTAL

A thin platinum wire (about 0.1 m.m. in diameter and 10 cms. in length) was stretched horizontally along the axis of a hollow metal cylinder open at both ends and the system (wire and the metal cylinder) was kept immersed in a trough containing a very dilute electrolyte, say water, containing a few drops of dilute sulphuric acid (Fig. 1). A potential difference ranging from 10 to 100 volts

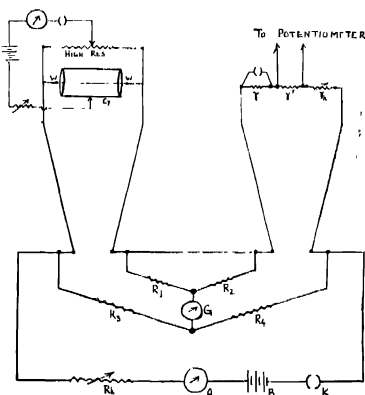


Fig. 1. (a) WW, platinum wire, (b) Cy, cylinder, (c) r, r' —standard low resistances

(using a dry battery) was established between the wire and metal cylinder giving rise to a radial-electric field. The ionic (electrolytic) currents generated in this way, were measured by means of milli-ammeter.

Measurements of the current flowing through the wire and its resistance are used for determining both the power input and the temperature of the wire. Under equilibrium conditions, the heat input to the wire becomes identical to the heat transfer from the wire to the liquid.

For the accurate determination of the current flowing through the platinum wire the latter was made to form one arm of a low resistance bridge (Kelvin's Double Bridge) as shown in Fig. 1. In the other arm (balancing arm), two standard low resistances r, r' (each fraction of an ohm) are connected in series with a small variable resistance. One of the two low resistances (r) is shunted by a key so that it can be introduced into the circuit when desired. The potential drop across the second low resistance (r') is measured by means of a potentiometer and from this the accurate value of the current passing through the platinum wire can be easily determined.

To start the experiment a very small current of the order of 10 m. a. (which does not heat the wire appreciably) is passed through the platinum wire, which is kept in one arm of the low resistance bridge referred to above and a balance is obtained by adjusting the resistances in the other arm of the bridge. The additional standard low resistance (r) is now introduced, and this disturbs the balance previously obtained. The current in the platinum wire is now gradually increased to restore the balance. The change in temperature $\Delta\theta$, can be calculated by means of the relation $\Delta\theta = (r/R_0\alpha)$, where r , the additional standard low resistance introduced in balancing arm, R_0 , the resistance of the platinum wire at 0°C and α , the temp. coefft. of resistance for the wire, are known.

If now some potential difference is established between the platinum wire and the metal cylinder, electrolysis starts in the liquid and ionic currents begin to flow between the wire and the cylinder. Bubbles are found to rise from different points on the wire due to evolution of gas in the process of electrolysis and the temp. of the wire is slightly lowered. The wire is now brought back to its initial temperature (temperature before the commencement of ionic currents) by passing a little more current through it from the battery and the heat exchange between it and the surrounding liquid is then measured. The heat flux q/A (A = surface area, $2\pi rl$ of the wire) for unit difference of temperature between the wire and the surrounding liquid is known as the heat transfer coefficient ' h '. We have investigated the variation of ' h ' with increasing values of $\Delta\theta$ for different strengths of ionic currents and with platinum wires of different diameters. The different values of $\Delta\theta$ could be obtained by choosing suitable values of the additional standard low resistance ' r ' in the balancing arm. A typical set of observations showing the variation of the heat transfer coefficient ' h ' with the strength of the ionic current ' i ' for a fixed value of $\Delta\theta$ is given in Table I.

TABLE I

Wire diameter = 0.10 m.m., $\Delta\theta = 6.3^\circ\text{C}$, $h_0 = 0.0873$ cal./sq. cm./sec/ $^\circ\text{C}$

Sl. No	i in milli-amp	Log i	h Cal/sq cm./ "C/sec.	(h/h_0)
1	20	1.30	0.1107	1.268
2	40	1.60	0.1274	1.458
3	60	1.78	0.1348	1.545
4	80	1.90	0.1368	1.567
5	100	2.00	0.1351	1.547
6	120	2.08	0.1310	1.501
7	140	2.14	0.1148	1.314
8	160	2.20	0.1029	1.179
9	180	2.25	0.0983	1.126
10	200	2.30	0.0909	1.041
11	220	2.34	0.0862	0.988
12	240	2.38	0.0726	0.831
13	260	2.41	0.0615	0.705

RESULTS AND DISCUSSION

In studying the variation of ' h ' with ionic current, the difference of temp. $\Delta\theta$ between the wire and the surrounding liquid was kept constant by keeping a definite value of ' r ', in the balancing arm. The values of $(h/h_0)^*$, where h_0 is the heat transfer coefficient in the absence of ionic currents, were then plotted against $\log i$, where ' i ' is the strength of ionic current in milliamperes. One such plot is shown in Fig. 2 (curve A), where the value of $\Delta\theta$ was maintained constant at 6.3°C.

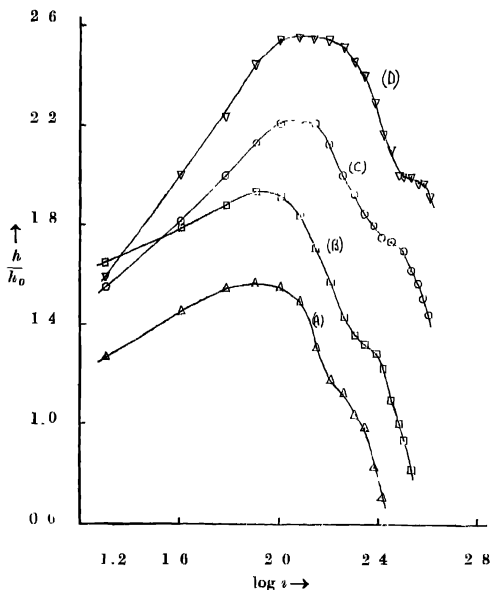


Fig. 2. The plot of (h/h_0) against $\log i$ (i , being ionic current in milliamperes) using platinum wire of diameter 0.10 mm., at different values of $\Delta\theta$ (A) 6.3°C, (B) 10.0°C, (C) 15.2°C, (D) 20.1°C.

This process was repeated for the values of $\Delta\theta = 10.0^\circ\text{C}$, 15.2°C, and 20.1°C and the resulting graphs B, C, D are shown in Fig. 2. It is obvious from these graphs that there is a definite increase in the peak value of ' h ' with increasing values of $\Delta\theta$. For instance, at the value of $\Delta\theta = 6.3^\circ\text{C}$, $(h/h_0)_{\text{max}}$ is equal to 1.567 whereas with $\Delta\theta = 20.1^\circ\text{C}$, $(h/h_0)_{\text{max}}$ comes out to be 2.559.

* It is found more convenient to use the ratio (h/h_0) than ' h ' alone, while considering the variation of heat transfer with increase in the ionic currents because, though the values of ' h ' may vary for different sets of observations under different conditions of temperature, pressure, humidity etc., the value of (h/h_0) remains sufficiently consistent and uniform.

The effect of varying the diameter of the platinum wire on the rate of heat transfer was then studied. For this purpose, wires of four different diameters were used. The variation of ' h ' with ionic currents for these wires of different diameters is depicted in Fig. 3. The different curves of Fig. 3, clearly indicate

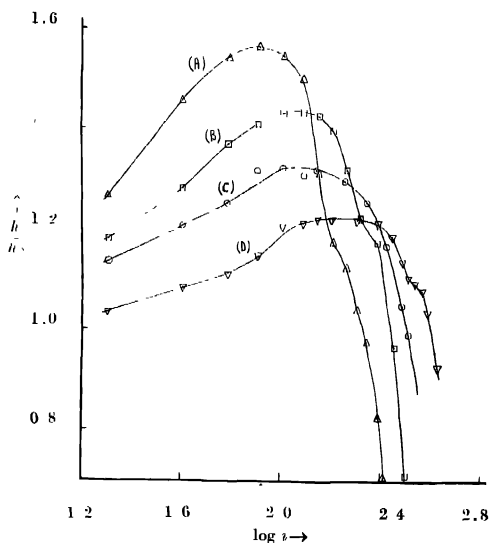


Fig. 3 The plot of (h/h_0) against $\log i$ maintaining $\Delta\theta = 6.3^\circ\text{C}$ and using platinum wires of different diameters, (A) 0.10 mm., (B) 0.19 mm., (C) 0.31 mm., (D) 0.37 mm.

that the maximum rate of heat transfer (h_{max}) goes on falling slowly as the diameter of the wire increases though in this case the change in the peak value of ' h ' is not very great even when the diameter of the wire is increased to four times its original value.

The variation of the peak value of ' h ' with (i) increase in the value of $\Delta\theta$ and (ii) increase in the diameter of the platinum wire is shown in Table II.

TABLE II

Sl No.	Wire diameter - 0.10 mm		$\Delta\theta = 6.3^\circ\text{C}$	
	$\Delta\theta$ in $^\circ\text{C}$	$(h/h_0)_{max}$	wire diameter in mm.	$(h/h_0)_{max}$
1	6.3	1.567	0.10	1.567
2	10.0	1.938	0.19	1.433
3	15.2	2.222	0.31	1.323
4	20.1	2.559	0.37	1.226

Our results indicate very clearly that for every value of $\Delta\theta$ there is a definite enhancement of heat transfer up to a certain value of ionic current and this is followed by a regular decrease in heat transfer in the higher ionic current region.

Moreover the graphs of Fig. 2 and 3 can be taken as a conclusive evidence to show that though ' h ' becomes maximum for an optimum value of i , it goes on falling gradually and not suddenly as reported by Edkie, Rao and Gogate (1961) with increasing strengths of ionic currents.

In calculating $\Delta\theta$ we cannot suppose that the temp. of the platinum wire alone is raised up to a certain point by the current passing through it and that the temperature of the surrounding liquid remains constant, though the rise in temperature of the liquid is made negligibly small by employing a large quantity of the liquid and very thin platinum wires. A correction for this very small change in $\Delta\theta$ was however applied by plotting change in $\Delta\theta$ against time and the values of $\Delta\theta$ corrected in this way were used for determining the value of ' h '.

In the above experiments the platinum wire was always kept at a positive potential with respect to the cylinder. We have checked up that the nature of the phenomena as shown by the graphs of Fig. 2 and 3 remains unaltered by reversing the polarity, though it causes a slight change in the value of ' h '.

CONCLUSIONS

- (a) There is an optimum value of ' i ' (the strength of the ionic current) for which the heat transfer coefficient ' h ' becomes maximum.
- (b) The value of ' h ' goes on falling gradually after attaining the peak value (h_{max}^m) with increase in the strength of ionic currents.
- (c) The enhancement of heat transfer becomes greater when the difference of temperature $\Delta\theta$ between the heating surface and the surrounding liquid is increased.
- (d) For a given value of $\Delta\theta$, the rate of heat transfer goes on falling when the area of the heating surface is enlarged.

ACKNOWLEDGMENTS

We wish to express our deep sense of gratitude to Principal Dr. S. M. Singh 'Suman' for giving us all necessary facilities to carry on this investigation in the Madhav College. We are also grateful to our Vice-Chancellor Dr. G. L. Datta for his constant encouragement in this work.

REFERENCES

- Addoms, J. N. 1948, cited in 'Heat-Transmission' by William H. Mc Adams (McGraw-Hill Book Co. Inc., New York), 1954, 382.
- Bronley, L. A. 1950, *Chem. Eng. Progr.*, **46**, 221.
- Drew, T. B. and Mueller, A. C., 1937, *Trans. Am. Inst. Chem. Engrs.*, **33**, 449.
- Edkie, R. G., Rao, R. D. and Gogate, D. V., 1961, *J. Sci. & Industr. Res.*, **20B**, 548.
- Mixon, F. O. and du Pont, E. I., 1959, *Chem. Eng. Progr.*, **55**, 49.
- Nukiyama, S., 1934, *J. Soc. Mech. Engrs. (Japan)*, **37**, 367, S53-54.
- Rao, R. D., Desai, H. S. and Gogate, D. V., 1960, *Ind. J. Phys.*, **34**, 456.

A STUDY ON THE DISCHARGE OF CONDENSER USING A TRANSISTORIZED BLOCKING OSCILLATOR

R. R. DUTTA GUPTA

INSTITUTE OF RADIO PHYSICS AND ELECTRONICS, UNIVERSITY OF CALCUTTA

(Received August 30, 1962)

ABSTRACT The problem of discharge of a condenser with the help of a transistorized blocking oscillator is investigated, both the grounded base and the grounded emitter mode of operation being considered. The optimum turns ratio of the feedback transformer for maximum discharge has been found out. Expressions for voltage swing are found out by theoretical analysis and confirmed by experimental measurements. A comparison of the relative merits of the grounded base and the grounded emitter modes reveals that a larger voltage swing should be obtainable with the latter mode; however, conditions requiring optimum performance of the grounded emitter mode cannot be realised in practice. A versatile generator of staircase waveform which may find use in special fields of application has also been incidentally developed.

INTRODUCTION

Transistorized blocking oscillators have been used as generators of rectangular pulses (Wrathall, 1956 and Tendick, 1956), pulse lengtheners and pulse frequency dividers (Butler, 1959). Linvill and Mattson (1955) have shown that a blocking oscillator using a junction transistor of a few megacycles alpha cut-off frequency could be used to obtain fast risetime by a proper choice of the feedback transformer.

In pulse techniques, ordinary blocking oscillators are frequently used for discharging a condenser (Chance *et al.*, 1949). The potentiality of a transistorized blocking oscillator as a means for such discharge has not, however, been investigated uptill now. In the present paper an account is given of such an investigation using both the grounded-base and grounded emitter configurations of the oscillator. The general principle of operation of a transistorized blocking oscillator is first described. This is followed by a theoretical analysis of the two modes of operation in Sec. 3. The results are extended in Sec. 4 to include the effect of delay caused by the transistor on the discharge of the condenser. Relative merits and demerits of the two modes of operation are critically examined in Sec. 5. The voltage swing due to discharge is shown to be larger with the grounded emitter mode. For both the modes, the transformer requirements for optimum discharge of a condenser are calculated. It is found that these requirements are different from those derived for minimum pulse rise-time by Linvill and Mattson. Thus, with a transformer designed to ensure the maximum discharge of a condenser, the speed of switching of the blocking oscillator would be somewhat sacrificed.

A free running blocking oscillator as a medium of condenser discharge is described in Sec. 6. It is shown that such a circuit arrangement may be designed in a manner so as to function as a generator of staircase waveform. Experimental evidences in support of results obtained in Sec. 3-6 are presented in Sec. 7.

TRANSISTORIZED BLOCKING OSCILLATOR AND ITS USE FOR CONDENSER DISCHARGE

The basic blocking oscillator circuit of the grounded base mode considered by Linvill and Mattson is shown in Fig. 1. It can either be triggered or free running depending upon the value of V_r . In either case, the oscillator possesses three distinct states, viz., the OFF, the regenerative and the ON states. Let us consider a triggered oscillator. In the OFF state the transistor and the diode D_1 and D_2 are non-conducting and the collector is at a potential $(V_1 + V_2)$. With a triggering pulse applied, the emitter begins to draw current. This produces a collector current which in turn sends a larger emitter current because of the regenerative feedback via the transformer T . This constitutes the regenerative state of the oscillator. During this period the collector potential falls steadily until it reaches a value V_1 . At this state D_1 begins to conduct and the collector potential is clamped to the value V_1 - hole storage effect being thus eliminated. This latter is the primary function of D_1 . Since the collector potential no longer changes after this state, further regeneration is stopped and the second state is, therefore, complete. After this the transistor is in the third state, viz., the ON state. The voltage source V_2 , however, tends to send through the magnetising

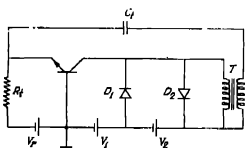


Fig. 1. Blocking oscillator circuit.

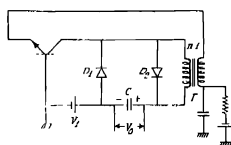


Fig. 2. Blocking oscillator circuit discharging a condenser

inductance of the transformer a current that increases almost linearly with time. This current is in a direction opposite to that in D_1 . Hence, the current through D_1 is gradually transferred, as it were, to the magnetising inductance until it becomes non-conducting again. After this the collector voltage begins to rise causing a regenerative cycle leading to a rapid transition of the oscillator towards the OFF state. After the collector has attained the value $(V_1 + V_2)$ the diode D_2 prevents any further rise, thus protecting the transistor against a high reverse bias. The cycle of operation is then complete. The oscillator continues in the OFF state till a fresh cycle is initiated by another pulse. If instead of a battery V_2 we have a condenser C charged to V_2 then the same cycle as above will be traced upon application of a triggering pulse.

For the free running case, the OFF state is reached because of the charges stored in the condenser C_1 . A fresh cycle starts when this has been discharged via R_1 to an extent so as to bias the emitter-base junction in the forward direction.

ANALYSIS OF THE TRANSISTOR BLOCKING OSCILLATOR OPERATION

In the present section simple analysis of the operation of a blocking oscillator will be given for both the grounded base and the grounded emitter mode of operation. The line of treatment will follow closely that of Linvill and Mattson. We shall first consider the grounded base configuration.

(a) *Grounded base configuration*

The essential details of a transistor blocking oscillator operating in the grounded base mode is shown in Fig. 2, where C is the condenser to be discharged by the oscillator. Diods D_1 and D_2 perform the same functions as described already in the preceding section. T is the feedback transformer with a turns ratio of $n : 1$. C is initially charged to the potential V_0 . During the process of charging, the blocking oscillator is in the OFF state, the discharge is initiated by switching it into the ON-state with the help of a triggering pulse. Alternatively, the blocking oscillator may be a free-running one allowing periodic charging and discharging of the condenser C . It will be convenient to consider separately the conditions during the regeneration and the ON-state of the oscillator.

(i) *Oscillator at the regenerative or the switch-on time.* At the regenerative or the switch-on time the circuit is unstable. Linvill and Mattson assumed that once the emitter is forward-biased, the circuit behaves in an essentially linear manner. Now the capacitance C , with the voltage V_0 across it, may be treated as a voltage source V_0 at this instant. Analysis of this period would, therefore, be the same as that given by Linvill and Mattson. The equivalent circuit given by them is reproduced in Fig. 3 in which the symbols have the following meanings

C_0 = collector to base capacitance, r_b = base resistance, L_e = leakage inductance $= (1 - k^2)L_m$, L_m = magnetising inductance of the transformer, k = coefficient of coupling and i_n = equivalent current generator. In this equivalent circuit the emitter resistance and the collector conductance have been assumed

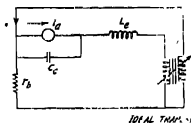
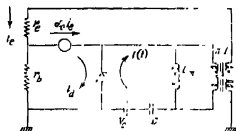


Fig. 3. Blocking oscillator equivalent circuit at switch-on time.



Ideal transformer.

Fig. 4. Equivalent circuit of the blocking oscillator during the ON period.

to be negligible and the low frequency short circuit current unity. Further, both the diodes D_1 and D_2 are considered to be open circuit.

Starting with the characteristic equation, giving the natural frequencies of the equivalent circuit of Fig. 3, these authors have shown that the magnetising inductance L_m is related to the turns ratio n and the coefficient of coupling k as

$$L_m = \frac{(n-1)^2}{g_b \omega_{ab}} \cdot x^2 - \left[\frac{(n-1)}{g_b \omega_{ab}} + \frac{1}{\omega_{ab}^2 C_c} \right] \cdot x + \frac{(n-1)}{C_c \omega_{ab}}, \quad \dots (1)$$

where $x = \frac{p}{\omega_{ab}}$ = the ratio between the positive real root of the characteristic equation of the circuit and the common base angular cut-off frequency of the transistor, and

$$g_b = \frac{1}{r_b}$$

The fastest speed of operation requires the highest possible value of x . The highest attainable value of x is, however, limited by the fact that L_m must always be positive. Basing arguments around this requirement Linvill and Mattson have given the following relation giving the value of turns ratio required for a given x or speed of response.

$$n = n_m = 1 + \frac{g_b}{2C_c \omega_{ab}(x^2 + x)}. \quad \dots (2)$$

For a transistor having $r_b = 100$ ohms, $C_c = 10$ pf, $\omega_{ab} = 2\pi \times 3.5 \times 10^6$, eqn.(2) gives for $x = 2$ (maximum permissible for L_m positive),

$$n_m \simeq 5. \quad \dots (3)$$

This means that with a transistor of 3.5 Mc/s cut-off frequency one can get as low a rise-time as 0.1μ sec. by using a transformer turns ratio 5.

(ii) *Oscillator during the ON period* : After the oscillator has been switched on, the equivalent circuit takes the form as shown in Fig. 4 provided the effects of C_c , L_c and diffusion delay are negligible. This is the same circuit as derived by Linvill and Mattson excepting for the inclusion of the condenser C in the arm containing V_0 . When the oscillator is switched on, diode D_1 presents a short circuit, D_2 an open circuit and the voltage V_0 appears directly across the combi-

nation L_m and C . Applying the operational method to the loop containing these elements we have,

$$I(p) = \frac{V_0/p}{pL_m + 1/pC} = CV_0 \cdot \frac{1}{\sqrt{L_m C}} \cdot \frac{1/\sqrt{L_m C}}{p^2 + 1/L_m C}$$

or,
$$i(t) = V_0 \sqrt{\frac{C}{L_m}} \sin \omega t, \quad \dots \quad (4)$$

where
$$\omega = \frac{1}{\sqrt{L_m C}}. \quad \dots \quad (5)$$

The voltage waveform across the condenser is then given by

$$V_c = V_0 + \frac{1}{C} \int_0^t i(t) dt$$

or,
$$V_c = V_0 \cos \omega t. \quad \dots \quad (6)$$

The diode current i_d is then obtained as

$$i_d = \frac{V_0 \cos \omega t}{n[r_e + r_b(1 - \alpha_0)]} \left(\alpha_0 - \frac{1}{n} \right). \quad \dots \quad (7)$$

The first factor on the right hand side of the equation is the emitter current at any instant. i_d is then the difference between the currents flowing through the collector and the emitter referred to the primary side of the transformer

When i_d has been transferred to L_m , the ON condition is terminated and the discharge stopped. This evidently happens when $i(t) = i_d$. This last condition determines the pulse duration τ . Putting $t = \tau$ in eqns. (4) and (7), we get,

$$V_0 \sqrt{\frac{C}{L_m}} \sin \omega \tau = \frac{V_0 \cos \omega \tau}{n[r_e + r_b(1 - \alpha_0)]} \left(\alpha_0 - \frac{1}{n} \right),$$

or,
$$\tan \omega \tau = \sqrt{\frac{L_m}{C}} \cdot \frac{(\alpha_0 n - 1)}{n^2[r_e + r_b(1 - \alpha_0)]}. \quad \dots \quad (8)$$

The voltage V_c across C at time τ is of course given by,

$$V_{c\tau} = V_0 \cos \omega \tau, \quad \dots \quad (9)$$

according to eqn. (7), and the voltage swing or the amplitude of discharge by,

$$A = V_0(1 - \cos \omega \tau). \quad \dots \quad (10)$$

From eqns. (8) and (10), we readily obtain,

$$A = V_0 \left[1 - \frac{1}{\left[1 + \frac{L_m}{C} \frac{(\alpha_0 n - 1)}{n^2 [r_e + r_b(1 - \alpha_0)]} \right]^2} \right] \quad \dots (11)$$

Referring back to eqns. (8) and (9), it is clear that the maximum discharge of C should be obtained if the transformer turns ratio be so chosen as to maximise the value of $\tan \omega \tau$. For the latter condition to be satisfied

$$\frac{\partial}{\partial n} (\tan \omega \tau) = 0$$

$$\text{or,} \quad \frac{\partial}{\partial n} \left[\sqrt{\frac{L_m}{C}} \cdot \frac{(\alpha_0 n - 1)}{n^2 [r_e + r_b(1 - \alpha_0)]} \right] = 0,$$

$$\text{giving,} \quad n = n_{max} = \frac{2}{\alpha_0} \quad \dots (12)$$

$$\begin{aligned} \text{Taking,} \quad \alpha_0 &\simeq 1, \\ n_{max} &= 2. \end{aligned} \quad \dots (13)$$

Referring to eqns.(2) and (3) we find that this value of n is very much different from that required for the speed of switching determined by the condition $x = 2$. Also, unlike the latter case, α_0 is the single transistor parameter that determines the optimum value of n for maximum discharge of condenser. Since α_0 may be taken to be unity for all practical junction transistors the optimum value of n should be sensibly independent of the type of transistor used and is roughly equal to 2.

Substituting (12) in (11), the amplitude of discharge for optimum turns ratio is found to be,

$$A = V_0 \left[1 - \frac{1}{\left[1 + \frac{L_m}{C} \frac{\alpha_0^2}{4[r_e + r_b(1 - \alpha_0)]} \right]^2} \right] \quad \dots (14)$$

It may be seen from (11) and (14), that the higher is the value of L_m/C and lower is the transistor input resistance, the more complete is the discharge of the condenser.

(b) *Grounded emitter configuration*

Analysis of the grounded emitter configuration of the blocking oscillator is

essentially the same as that for the grounded base mode. As before we shall again consider separately the regenerative and the ON state of the oscillator.

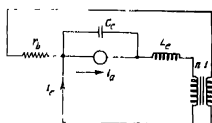


Fig. 5. Grounded emitter equivalent circuit at the switch-on time of the blocking oscillator

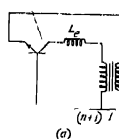
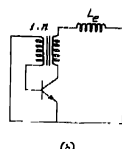


Fig. 6 Correspondence between grounded base and grounded emitter mode of operation.

(a) Grounded base mode



(b) Grounded emitter mode.

(i) *Oscillator at the Switch-on time* : The equivalent circuit for the grounded base case at the switch ON time was given in Fig. 3. Redrawing it for the grounded emitter case as in Fig. 5, we can find the relation between emitter and collector currents,

$$i_e = \alpha i_a + n i_a$$

$$\text{or,} \quad i_e \simeq i_a(n+1) \quad \dots (15)$$

Again referring to Fig. 3, if the transformer turns ratio for the grounded base mode is v then

$$i_e = i_a \cdot v. \quad \dots (16)$$

Since however, for the same regeneration speed, i.e., for identical switch on time, i_e 's should be equal for both the grounded emitter and the grounded base modes for a fixed i_a , it is clear by comparing eqns (15) and (16) that,

$$v = (n+1) \quad (17)$$

In fact this same result has also been given by Tendick (1956). It states that for the same speed of switching the correspondence, as shown in Fig. 6, must exist between the grounded base and the grounded emitter modes.

(ii) *Oscillator during the ON-period* : Analysis would be in the same line as in the grounded base mode. The equivalent circuit for this case during the ON-state is as shown in Fig. 7 in which β_0 is the grounded emitter current gain. Other notations are the same as in the grounded base mode. As before, we can write,

$$i_d = \frac{V_0 \cos \omega t}{n[r_b + \beta_0 r_e]} \left(\beta_0 - \frac{1}{n} \right) \quad \dots (18)$$

and,

$$i(t) = V_0 \sqrt{\frac{C}{L_m}} \sin \omega t. \quad \dots (4)$$

Again the pulse duration τ_e is obtained by putting $t = \tau_e$ in equation (4) and (18) and equating the two. This gives

$$\tan \omega \tau_e = \sqrt{\frac{L_m}{C}} \cdot \frac{\beta_0 n - 1}{n^2(r_b + \beta_0 r_e)}, \quad \dots (19)$$

the amplitude of discharge is now given by,

$$A_e = V_0 \left[1 - \frac{1}{\left[1 + \frac{L_m}{C} \left[\frac{\beta_0 n - 1}{n^2(r_b + \beta_0 r_e)} \right]^2 \right]^{\frac{1}{2}}} \right] \quad \dots (20)$$

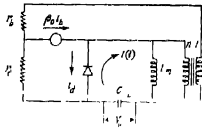


Fig. 7. Grounded emitter equivalent circuit during the ON-state of the blocking oscillator.

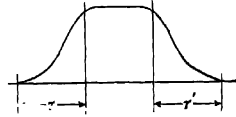


Fig. 8. Switching on and switching off times of a transistor.

Usually, $\beta_0 n \gg 1$ and hence eqn. (20) may be re-written as,

$$A_e = V_0 \left[1 - \frac{1}{\left[1 + \frac{L_m}{n^2 C} \left[\frac{\beta_0}{(r_b + \beta_0 r_e)} \right]^2 \right]^{\frac{1}{2}}} \right] \quad \dots (21)$$

Other things remaining constant the maximum discharge is obtained for a turns ratio determined by the condition,

$$\frac{\partial}{\partial n} (\tan \omega \tau_e) = 0$$

whence we get from eqn. (19),

$$n = \frac{2}{\beta_0} \quad \dots (22)$$

Generally, $\beta_0 \gg 1$ and hence $n \ll 1$, i.e., use must be made of a step up transformer. Noting that the base is a lower impedance point than the collector the feedback stability with such a step-up transformer from collector to base will be rather unsatisfactory and the switching of the oscillator may therefore be quite uncertain. To avoid this one might choose a unity transformer ratio as the

limiting case for the grounded emitter configuration thus sacrificing a little the optimum condition of operation. The result thus obtained may be compared with those of a grounded base configuration under optimum condition with $n = 2$ in order to assess the relative excellence of the two modes as media for a condenser discharge.

EFFECT OF DELAY ON DISCHARGE

In the foregoing analysis the effect of delay was completely ignored. In a practical transistor finite times are elapsed during both the switching on and switching off process. These times are of the same order of magnitude. During these periods τ and τ' the current does not remain constant but varies in the manner shown in Fig. 8 and voltage across the condenser is discharged by small amounts. A simple procedure for estimating the extent of discharge of the condenser voltage due to these currents would be to assume the existence of an additional current of magnitude equal to that of the main pulse and of duration τ —the switching on time.

Diode current equations, however, are still valid provided that we allow for an additional discharge of the condenser corresponding to this delay time.

Moll (1954) has given the following switch on times (τ) for the common base and the common emitter configurations.

Common base :

$$\tau = \frac{1}{\omega_{ab}} \ln \frac{I_c}{I_e - 0.9I_c} \quad \dots \quad (23)$$

Common emitter :

$$\tau = \frac{1}{(1 - \alpha_0)\omega_{ab}} \ln \frac{I_b}{I_b - 0.9 \frac{1 - \alpha_0}{\alpha_0} I_e} \quad \dots \quad (24)$$

where, I_e , I_b , I_c are at any instant the emitter, the base and the collector currents respectively.

It is obvious that in the mode of operation described above

$$\frac{I_c}{\alpha_0} = I_e$$

and

$$I_c \frac{1 - \alpha_0}{\alpha_0} = I_b.$$

Equations (23) and (24) then reduce to

$$\tau = \frac{2.30}{\omega_{ab}} \simeq \frac{0.4}{f_{ab}}, \quad \dots (25)$$

and

$$\tau = \frac{2.30}{(1-\alpha_0)\omega_{\tau b}} \simeq \frac{0.4}{f_{ab}|\beta_0|} \quad \dots (26)$$

respectively.

The condenser discharges by a small amount during this interval and the change in the condenser voltage due to this initial discharge is given by

$$A_i = V_0(1 - \cos \omega\tau). \quad \dots (27)$$

Since $\omega\tau$ is small, $\cos \omega\tau$ can be expanded retaining only the first two terms. We thus get,

$$A_i \simeq V_0 \cdot \frac{\omega^2 \tau^2}{2}. \quad \dots (28)$$

Inserting the values of τ as given by (25) and (26), we get, for the common base,

$$A_i = 0.08 V_0 (\omega/f_{ab})^2 \quad \dots (29)$$

and for the common emitter,

$$A_i = 0.08 V_0 (\beta \omega/f_{ab})^2. \quad \dots (30)$$

For the typical values,

$$f_{ab} = 3.5 \text{ Mc/s}, \quad \beta_0 = 40 \text{ and } L_m = 300 \mu H, \quad C = 0.47 \mu F,$$

we get from (5), (29) and (30) for the common base mode

$$A_i = 4.6 \times 10^{-3} V_0, \quad \dots (31)$$

and for the common emitter mode,

$$A_i \simeq 0.07 V_0. \quad \dots (32)$$

Eqs. (31) and (32) indicate that the effect of delay is negligible in the case of common base configuration but it is not so in the common emitter case. Hence, adding (21) and (32) the total amplitude of discharge for the common emitter configuration is found to be,

$$A = V_0 \left[1.07 - \left[1 + \frac{L_m}{n^2 C} \left(\frac{1}{\tau_b + \beta_0 \tau_e} \right)^2 \right]^{-1} \right]. \quad \dots (33)$$

COMPARISON BETWEEN COMMON-BASE AND COMMON-
EMITTER CONFIGURATIONS

At this stage it would be instructive to compare the performances of the common-base and common-emitter modes of operation of the blocking oscillator as the discharge element for a condenser. As was explained before, for stability of operation $n = 1$ for the common-emitter configuration. From eqn. (33) the amplitude of discharge A_1 under the condition is found to be

$$A_1 = V_0 \left[1.07 - \frac{1}{\left[1 + \frac{L_m}{C} \left(\frac{\beta_0}{r_b + \beta_0 r_e} \right)^2 \right]^{\frac{1}{2}}} \right] \quad \dots (34)$$

For the common-base mode the amplitude for maximum discharge is given by eqn. (14). Denoting this by A_2 we have from (14) and (4),

$$\frac{A_1}{A_2} = \frac{1.07 - \frac{1}{\left[1 + \frac{L_m}{C} \left\{ \frac{\beta_0}{r_b + \beta_0 r_e} \right\}^2 \right]^{\frac{1}{2}}}}{1 - \frac{1}{\left[1 + \frac{L_m}{C} \left\{ \frac{\alpha_0^2}{4[r_e + r_b(1 - \alpha_0)]} \right\}^2 \right]^{\frac{1}{2}}}} \quad \dots (35)$$

Taking $\alpha_0 \simeq 1$ and $\frac{1}{1 - \alpha_0} \simeq \beta_0$, eqn.(35) is reduced to

$$\frac{A_1}{A_2} = \frac{1.07 - \frac{1}{\left[1 + \frac{L_m}{C} \left\{ \frac{\beta_0}{r_b + \beta_0 r_e} \right\}^2 \right]^{\frac{1}{2}}}}{1 - \frac{1}{\left[1 + \frac{L_m}{C} \left\{ \frac{\beta_0}{4(r_b + \beta_0 r_e)} \right\}^2 \right]^{\frac{1}{2}}}} \quad \dots (36)$$

or,

$$\frac{A_1}{A_2} \simeq \frac{1 - \frac{1}{\left[1 + \frac{L_m}{C} \left\{ \frac{\beta_0}{r_b + \beta_0 r_e} \right\}^2 \right]^{\frac{1}{2}}}}{1 - \frac{1}{\left[1 + \frac{L_m}{C} \left\{ \frac{\beta_0}{4(r_b + \beta_0 r_e)} \right\}^2 \right]^{\frac{1}{2}}}} \quad \dots (37)$$

which is always greater than unity. Hence, we find from eqn. (37) that, compared with the grounded-base configuration, a grounded-emitter blocking oscillator should give a wider voltage swing during the discharge of a condenser even though

it cannot be operated under the optimum condition. From the point of view of voltage swing the use of this latter mode is then seen to be more advantageous. The exact margin of advantage thus obtainable is, however, dependent on the value of L_m/C .

USE OF A FREE-RUNNING BLOCKING OSCILLATOR AND GENERATION OF STAIRCASE WAVEFORM

In the foregoing analysis considerations had been restricted to a single shot blocking oscillator. For this the condenser is not fully discharged during a pulse but the voltage across the condenser at the end of discharge is

$$V_{cr} = V_0 \cos \omega\tau \quad \dots (9)$$

With the charging circuit off or with a charging circuit of sufficiently large time constant this voltage will be maintained across the condenser after the blocking oscillator switches to the *OFF* state. An interesting possibility arises if instead of a single shot oscillator, use is made of a free running one having a low duty cycle. After a time equal to the quiescent period of the blocking oscillator, the condenser will start discharging again. If the condenser does not receive any appreciable additional charge during this period the initial voltage across it for this second phase of discharge would be $V_0 \cos \omega\tau$ instead of V_0 . This process would repeat itself until the condenser has been completely discharged. In other words, the condenser will discharge in several steps giving rise to a staircase waveform. The condenser voltages $V_1, V_2 \dots, V_r$, at the end of the 1st, 2nd, ..., r -th phase of the discharge are given by

$$\begin{aligned} V_1 &= V_0 \cos \omega\tau \\ V_2 &= V_1 \cos \omega\tau = V_0 \cos^2 \omega\tau \\ \dots &\quad \dots \quad \dots \quad \dots \\ V_r &= V_{r-1} \cos \omega\tau = V_0 \cos^r \omega\tau, \quad \dots (38) \end{aligned}$$

so that

$$\frac{V_r}{V_0} = \cos^r \omega\tau. \quad \dots (39)$$

The number of steps required for the voltage to discharge to 10% of its initial value V_0 is obtained from the relation

$$\cos^r \omega\tau = 0.1$$

$$\text{or,} \quad r = -1/\log_{10} \cos \omega\tau. \quad \dots (40)$$

EXPERIMENTAL RESULTS AND DISCUSSIONS

In this section we would describe the results of experiments on condenser discharge using single shot blocking oscillators of both the grounded base and

the grounded-emitter mode. The results would be compared with the theoretical relations derived in the preceding sections.

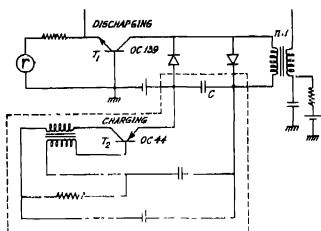


Fig. 9(a). Circuit details of the experimental blocking oscillator in the grounded base mode.

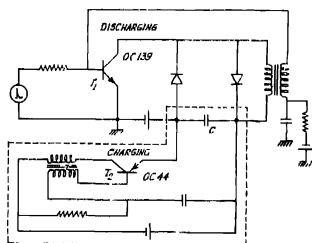


Fig. 9(b). Circuit details of the experimental blocking oscillator in the grounded emitter mode.

The circuit details of the experimental blocking oscillators of the grounded base and grounded-emitter modes are given in Figs. 9(a) and 9(b). In these transistors OC139 are in the blocking oscillator discharging circuit under investigation and OC44 in the charging circuit. T_1 being an $n-p-n$ transistor the triggering is achieved by applying a negative pulse at the emitter point in Fig. 9(a) and positive pulse at the base in Fig. 9(b). Transistor T_2 charges the condenser C (see Appendix).

(i) Common-base mode

(a) *Variation of amplitude with C* . Study of the variation of amplitude A with C using the circuit shown in Fig. 9(a) was made for $V_0 = 3$ volts with two different values of n , viz., 2 and 5. Experimental values of the amplitude for six different values of C are given in column 3, Tables I and II.

Referring to eqn. (11) and expanding we can write,

$$A = V_0 \frac{L_m}{2C} \left[\frac{(\alpha_0^n - 1)}{n^2[r_e + r_b(1 - \alpha_0)]} \right]^2, \quad \dots (41)$$

$$\text{or,} \quad C.A \simeq \frac{V_0 L_m}{2} \left[\frac{\beta_0(n-1)}{n^2(r_b + \beta_0 r_e)} \right]^2, \quad \dots (42)$$

which is a constant for a given value of n and V_0 . Column 4 in Tables I and II confirm the expectation. Now, a direct measurement gave $L_m = 300 \mu H$, $\beta_0 = 40$, $r_b = 100$ ohms and $r_e = 30$ ohms. The last columns of the tables give the product $C.A.$ as obtained from eqn. (42) and these values.

These are seen to agree closely with the experimental values in columns 4.

TABLE I

n	$C(\mu F)$	A (volts)	$C.A.$	$C.A.$ (calculated)
2	0.1	0.28	0.028	0.027
	0.23	0.12	0.028	
	0.33	0.09	0.030	
	0.47	0.06	0.028	
	0.57	0.05	0.029	
	0.94	0.03	0.028	

TABLE II

n	C (μF)	A (volts)	$C.A.$	$C.A.$ (calculated)
5	0.1	0.114	0.011	0.011
	0.23	0.045	0.011	
	0.33	0.030	0.010	
	0.47	0.024	0.011	
	0.57	0.018	0.010	
	0.94	0.012	0.011	

(b) *Variation of amplitude with n* It is also of interest to study the variation of A with the turns ratio n for a fixed value of C . Experimental results obtained with $C = 0.47\mu F$ are shown in column 3, Table III. Calculated values, based on eqn. (41) and on the simplifying assumptions $\alpha_0 \simeq 1$, $(1 - \alpha_0) \simeq 1/\beta_0$, and given in the last column are in fair agreement with these results.

TABLE III

C (μF)	n	A (volts)	A (volts) calculated
0.47	5	0.024	0.023
	3	0.042	0.045
	2	0.060	0.057
	1	0	—

(ii) Common-emitter mode

(a) *Variation of amplitude with C* : Experiments on the common emitter mode were carried out with the circuit shown in Fig. 9(b) with $n = 1$. Table IV, columns 3 and 4 give the observed and calculated values of A for different values of C . Calculations were made using eqn. (33), the numerical values of the various parameters being the same as those mentioned in Sec. 3(i) for the common-base mode. Again, the experimental results seem to agree closely with the calculated values. It may be noted that in eqn. (33) the second term under the square root sign is high compared to unity and hence for this case $C.A. \neq a$ constant for a given value of n .

TABLE IV

n	C (μF)	Amplitude (volts)	Amplitude (volts) calculated
1	0.23	1.20	1.17
	0.33	1.00	0.99
	0.47	0.87	0.84
	0.57	0.76	0.75
	0.94	0.57	0.57

(b) *Variation of amplitude with n* : Table V gives the experimental and calculated results for the variation of amplitude with n for $C = 0.47\mu F$ for the common-emitter configuration. Calculations are again based on eqn. (33), with the values mentioned before. Agreement between the experimental and the theoretical values is once again very satisfactory.

TABLE V

C (μF)	n	A (volts)	A (volts) calculated
0.47	1	0.87	0.84
	2	0.42	0.42
	3	0.36	0.33
	5	0.24	0.25

(iii) *Comparison between common-emitter and common-base configurations*

To check eqn. (37), Tables I and IV were used to obtain the experimental values of A_1/A_2 for different values of C . These values are recorded in column 2, Table VI. In this A_1 corresponds to amplitude for $n = 1$ for the common-emitter and

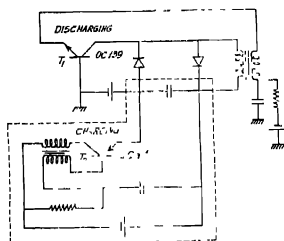


Fig. 10(a). Grounded base configuration of the staircase waveform generator

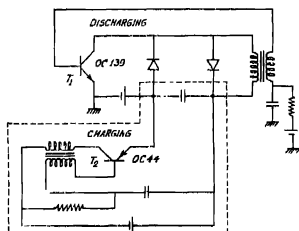


Fig. 10(b) Grounded emitter configuration of the staircase waveform generator.

A_2 to the configuration for the optimum condition $n = 2$ for the common base configuration. Calculated values of A_1/A_2 , as given by eqn. (37), are shown in column 3, Table VI. The extent of agreement between the two sets of values is obviously quite satisfactory.

TABLE VI

C (μF)	A_1/A_2 experimental	A_1/A_2 calculated
0.23	10.0	9.8
0.33	11.1	12.4
0.47	14.5	14.0
0.57	15.2	15.0
0.94	19.0	19.0



Fig. 11. Staircase waveform with equal steps.

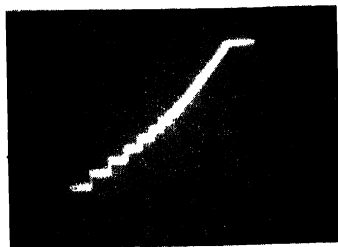


Fig. 12. Staircase waveform with unequal steps.

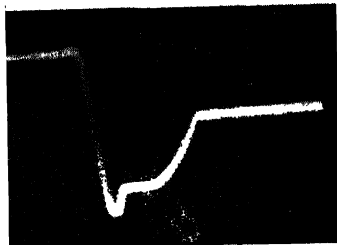


Fig. 13. Trailing edge of a step of the waveform in fig. 11.

(iv) Generation of staircase waveform

For generation of staircase waveform Figs. 9(a) and 9(b) were modified by biasing the discharging transistor T_1 in the forward direction and withdrawing the triggering arrangements, [Figs. 10(a) and (10(b))]. Under this condition they functioned as free-running oscillators. The general pattern of the condenser

discharge generating staircase waveform is shown in Figs. 11 and 12. It is clear that if the discharge in a given step is restricted to a rather smaller value as in the case of Fig. 11, the successive steps become fairly equal. This is to be expected from eqn. (39) which requires that for small values of $\omega\tau$

$$\frac{V_r}{V_0} \simeq \left(1 - \frac{r\omega^2\tau^2}{2} \right) \quad \dots \quad (43)$$

Also, the trailing end of each step should conform to eqn. (6) and this is illustrated in Fig. 13 which is merely a record of the waveform shown in Fig. 11 on an expanded time base.

CONCLUSION

A detailed study on the discharge of condenser by a transistorized blocking oscillator has been made. The experimental results have been found to agree well with the result of theoretical analysis. From the point of view of voltage swing during discharge, a grounded-emitter mode of operation appears to be satisfactory even though it cannot be operated under optimum conditions. Also, by referring to Figs. 6(a) and (b) it is seen that identical speed of switching is obtained for $n = 1$ for the grounded emitter and $n = 2$ for the grounded base grounded modes respectively which means that speed of operation is not sacrificed in using a emitter oscillator although it gives a greater voltage swing.

An incidental development of the study is the possibility of the generation of staircase waveform with the advantage of having adjustable number of steps in a given time. This may be useful in counter circuits and in the quantization of information.

ACKNOWLEDGMENTS

The author intends to thank Prof. J. N. Bhar for his kind interest and helpful advice. He is particularly indebted to Prof. S. Deb for his constant guidance throughout the course of the work. Thanks are also extended to the Council of Scientific and Industrial Research for appointing him as Pool Officer and to Messrs Philips India Ltd. for providing with ferrite cores in connection with the experiment.

REFERENCES

- Butler, F., 1959, *Electronic Engineering*, **31**, 72.
- Chance, B., et. al. 1949, *Waveforms, Radiation Laboratory Series*, **19**, 235.
- Linvill, J. G., and Mattson, R. H., 1955, *Proc. I.R.E.*, **43**, 1632.
- Moll, J. L., 1954, *Proc. I.R.E.*, **42**, 1773.
- Tondick, F. H. Jr., 1950, *B.S.T.J.*, **35**, 1085.
- Wrathall, L. R., 1950, *B.S.T.J.*, **35**, 1059.

A P P E N D I X

The charging circuit as mentioned in the text is shown inside the dotted line enclosure in Figs. 9(a), 9(b), 10(a) and 10(b). It may be seen by referring to these figures that it is another blocking oscillator, the regeneration of which is provided by the transformer at the collector of the transistor T_2 . The condenser C to be charged is placed in the emitter circuit of T_2 .

On completing a discharge stroke, transistor T_1 remains quiescent so that when T_2 charges the condenser C there is no loading due to T_1 . Similarly, in between the quiescent periods of T_2 when T_1 discharges the condenser C there is also no loading effect present. Thus, it follows that working of T_1 and T_2 is independent of each other.

It may be shown from a simple analysis of the charging circuit that under such conditions, the voltage to which the condenser C may be charged is given by

$$V_0 = \frac{nE}{n+1} \quad (44)$$

where V_0 = voltage to which C is charged,

E = H.T. voltage of T_2 ,

n = turns ratio of the transformer at the collector of T_2 .

In our case, we choose, $E = 6$ volts and $n = 1$, so that V_0 becomes equal to 3 volts.

GAMMA-GAMMA COINCIDENCES IN Pd^{105}

R. BHATTACHARYYA

Saha Institute of Nuclear Physics, CALCUTTA.

(Received October 3, 1962)

ABSTRACT. Gamma spectrum and gamma-gamma coincidence spectra measured with NaI (Tl) scintillation spectrometers reveal a 770 keV level and 420, 390 keV gamma rays in Pd^{105} . A decay scheme, based on these results and the results previously obtained has been proposed. These results are essentially in agreement with the recently reported work of Suter *et al.*

INTRODUCTION

The level scheme of Pd^{105} is complicated due to the presence of several closely-lying excited states. The high resolution β spectrometer measurements and e - γ coincidences of Suter *et al.* (1961) and the total absorption γ spectrometer measurements and angular correlation measurements by Bhattacharyya (1962) have revealed many features of the level scheme and have modified some of the previous findings (Nuclear data sheets). The γ spectrum and the coincidence spectra have been studied by Raether (1958) and other workers (Hayward, 1956), who reported strong coincidence pairs of 64-281, 319-331 and 654-438 keV γ rays and some weak coincidences between 281 keV γ ray and the γ rays in the 300-400 keV range.

The present work was undertaken to study from the γ - γ coincidences, the weaker coincidence pairs which were reported in the earlier works and to fit these findings into a level scheme.

SOURCE

The source was prepared by bombarding $\text{Rh}[\text{Rh}^{103}(\alpha, 2n)\text{Ag}^{105}]$ in the Birmingham Cyclotron and was sent to us after chemical separation of Ag from Rh. Half-life measurements did not reveal any measurable 8.3 day Ag^{106} activity. However, the experiment was started about 50 days after bombardment in order to allow Ag^{106} activity, if any, to decay down to a negligible value.

GAMMA-SPECTRA

The γ -spectra presented in Fig. 1 were recorded with a $1\frac{1}{2}$ " dia. $\times 1\frac{1}{2}$ " thick NaI(Tl) phosphor and with a $1\frac{1}{2}$ " dia. $\times \frac{1}{4}$ " thick NaI(Tl) phosphor (for low energies). In each case a RCA 6810A type photomultiplier with a single channel pulse height analyser was used. Analysis of the γ spectra of Fig. 1 yields, besides the prominent ones, a few weak peaks. The results are summarised in Table 1. The spectrum

obtained with the thin phosphor does not reveal any low energy γ rays other than the 21 keV X-rays and the 64 keV one.

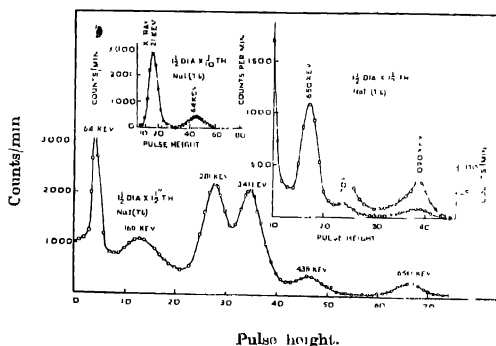


Fig. 1. Gamma spectra of Pd^{105} .

TABLE I

Energies and intensities of the γ rays of Pd^{105}

Gamma-energy (keV)	Corrected relative intensity $\pm 10\%$ (I)	Multipolarity assigned from α_L and K/L values measured in a Siegbahn-Statis beta-spectrometer
64	67	M_1
115	2	Intensity very small
160	10	$E1$
180	3	$E2$ or $M2$; $E2$ closer to theoretical value.
230	2.5	Intensity very small
280	75	$E2$
320		
	Small	$E2$ or $M2$
330		
341	100	$E2$
390	7	Intensity very small
420	Small	Intensity very small
438	23	$E2$
650	32	$E1$
770	4.5	Intensity very small
1090	7	$E1$

GAMMA-GAMMA COINCIDENCES

Coincidence spectra were recorded with two phosphor photomultiplier combinations fitted to a slow-fast coincidence assembly. RCA 6810A photomultipliers with $1\frac{1}{2}$ " dia. $\times 1\frac{1}{2}$ " thick NaI(Tl) phosphors were used in both the channels. A single channel analyser was used to record the coincidence spectrum. Coin-

cidences were measured between the integral γ spectrum and (i) the 64 keV γ ray (Fig. 2), (ii) the 280 keV γ ray (Fig. 3) and (iii) the 320 keV γ ray (Fig. 4). The coincidence resolving time was ~ 20 ns.

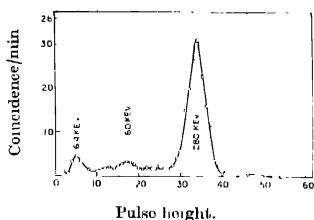


Fig. 2. Gamma spectrum in coincidence with the 64 keV gamma ray

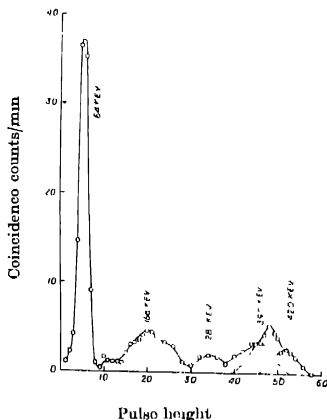


Fig. 3. Gamma spectrum in coincidence with the 280 keV gamma ray.

The spectrum of fig. 2 shows a prominent peak at 280 keV. The other small peaks are mainly due to the various coincidences with the Compton distributions near the 64 keV region. However, this spectrum shows a somewhat larger peak at 160 keV. Thus 64 keV γ ray is in cascade with 280 keV and probably with the weak 160 keV γ ray. The spectrum of fig. 3 supports the existence of the strong 64-280 keV cascade and shows weak but definite peaks at 390 and 420 keV. The peak at 160 keV in this spectrum as well as in fig. 2 indicates the existence of a 160-64-280 keV cascade.

In measuring the spectrum of Fig. 4, the channel selecting the 320 keV γ rays was wide enough to admit the strong 280 keV and 345 keV γ rays partially and the weak 330 keV fully. The peaks at 64, 160 (not separate from a 185 keV peak), 390 and 420 keV, are due to coincidence with 280 keV γ ray. The composite peak arising from 320-330 keV cascade is seen in the spectrum. The broad peak near 180 keV is due to both 160 and 185 keV γ rays. The 185 keV radiation may then be probably in coincidence with the 320 and 330 keV γ rays. However, the possibility of existence of the 185-306 keV cascade (Nuclear data sheets) instead of the above one, cannot be ignored on the basis of γ - γ coincidences only.

DISCUSSION ON THE DECAY SCHEME

With reference to the results discussed above and those reported earlier the decay scheme of fig. 5 has been drawn.

No coincidences were found with the 1090 keV γ ray. The total absorption spectrum (Bhattacharyya, 1962) suggests that the 1090 keV is the highest excited state of Pd^{105} decaying partially ($\sim 20\%$) to the ground state. The decay of this state proceeds predominantly through the 642-438 keV cascade ($\sim 60\%$) and a weaker 420-390-280 keV triple cascade ($\sim 20\%$).

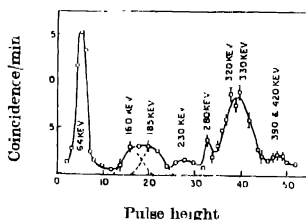


Fig 4. Gamma spectrum in coincidence with the 320 keV gamma ray.

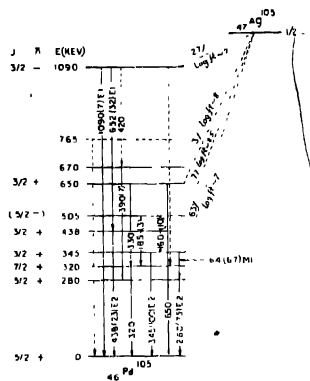


Fig 5 Proposed decay-scheme of Ag^{105}

From the angular correlation of 652-438 keV cascade and from the fact that 1090 keV is an E1 transition, the spin-parity of this state is found to be $3/2^-$ which, however, is not supported by the first forbidden nature of the capture transition to this state.

A 765 keV γ ray reported by McGowan (Nuclear data sheets) was also found in the present work. The 770-320 keV cascade in Pd^{105} may possibly be identified with the 743-344 keV cascade reported by Suter *et al.* (1961).

None of the 642 and the 438 keV γ rays was found to have any coincidence with any other γ ray, except between themselves. Table I shows that the 650 keV γ intensity is higher than that of the 438 keV. This seems to point out that there is a level near 650 keV which decays partly through a direct transition to the ground state. With the help of the decay scheme of Raether (1958) and our coincidence spectra, it can be seen that the 670 and 650 keV states decay through 390-280 keV and 330-320 keV cascades respectively. In absence of any broadening of the peak (Fig. 1) at 650 keV on the higher energy side, it can be concluded that there is no direct transition from the 670 keV level to the ground state. The 438 keV state is only fed from the 1090 keV state through the emission of the 650 keV γ ray as there is no evidence of a direct electron capture decay to this state. It is known that this 438 keV γ ray is emitted from a 438 keV state by an E2 transi-

sion from the coulomb-excitation experiments (Temmer *et al.*, 1956) Values of internal conversion co-efficients and results of angular correlation support a $3/2(\text{E}1) \rightarrow 3/2(\text{E}2) \rightarrow 5/2$ transition for the 652-438 keV cascade. E1 nature of the 1090 keV transition also supports this view.

The existence of a 319 keV level of Pd^{105} is known from a 5% branching (Nuclear data sheets) from Rh^{106} . If we also postulate the existence of a level at 320 keV, then the 330-320 keV cascade seems to originate from the 650 keV level. Angular correlation data indicate spin values of $3/2$ and $7/2$ to the 650 and 320 keV levels with both members of the cascade as quadrupole. The first forbidden nature of the capture transition from Ag^{106} to the 650 keV level of Pd^{105} supports an even parity assignment. The 650 keV level can therefore be assigned spin parity $3/2^+$.

The 505 keV state obtained by capture feeding, de-excites by emitting a 160 keV γ ray followed by a 345 keV γ ray. Probably, there is no direct transition to the ground state. The 345 keV state is also very strongly fed by capture. The enhanced intensity of the 280 keV ($I_{280} = 75$) with respect to the 64 keV ($I_{64} = 67$) can be explained by adding the intensity of the 390 keV ($I_{390} = 7$) to the intensity of the 64 keV γ ray. Since the 345 keV and the 280 keV transitions are E2 and the 64 is M1 the spin-parities of the 280 and 345 keV states are $5/2^+$ and $3/2^+$ respectively, and since the 160 keV transition is assigned as E1, the 505 keV state seems to have a spin-parity $5/2^-$. The first-forbidden capture decay, however, requires this state to be of even parity.

We have not come across any literature in which the decay properties of Ag^{106} has been discussed in terms of a model. The observed properties of the levels of Pd^{105} cannot be adequately explained by considering the neutrons in different states of seniority unless explicit calculations are done.

The reduced transition probability $B(\text{E}2)$ for the 266 keV state (identified as 280 keV in our case) has been measured (Temmer *et al.*, 1956) to be 70 times faster than the single particle estimate, while the 433 keV (438 in our measurement) is 25 times faster. The explanation of the level characteristics may require the introduction of particle and vibrational type of excitation for this nucleus.

ACKNOWLEDGMENTS

The author is grateful to Prof. A. K. Saha for his keen interest in the work and to Dr. S. Chatterjee, Mr. A. K. Sengupta and Dr. P. N. Mukherjee for helpful discussions.

REFERENCES

- Bhattacharyya, R., 1962, *Nucl. Cimento*, **24**, 1000.
- Hayward, R. W. and Hoppes D. D., 1956, *Bull. Am. Phys. Soc.*, **2**, No. 1, 42
- Nuclear Data sheets, National Academy of Sciences, National Research Council, Washington D. C.*
- Raother, M., 1958, *Zeit. f. Physik*, **150**, 38.
- Sutor, T., Reyes-Sutor, P., Schonor, W., Ausa and Backstrom, G., 1962, *Arkiv F. Fysik* **20**, 431.
- Temmer, G. M. and Heydenberg, N. P., 1956, *Phys. Rev.*, **104**, 967.

A CIRCUIT FOR A SELF-STROBED READING METHOD IN MAGNETIC DRUM DIGITAL STORES

D. DUTTA MAJUMDAR AND R. BISWAS

INDIAN STATISTICAL INSTITUTE
CALCUTTA

(Received June, 4, 1962)

ABSTRACT A method that provides accurately timed output pulses that do not require clock pulses for their identification is described. The detailed circuit diagram used in association with the particular Magnetic Drum Memory is presented. The method is simple and elegant and is relatively insensitive to noise pulses in comparison with other methods.

INTRODUCTION

Well-known physical principles involved in audio recording on magnetic surface have offered a very successful method of storing digital data and instructions in all Information Processing systems (Booth, 1949). A comprehensive investigation was undertaken by one of the authors (Dutta Majumdar, 1959) on different aspects of design, development and applications of magnetic drum digital storage systems in this Laboratory (Electronics Research Laboratory of I.S.I.). The present circuit was designed, constructed and experimented with the magnetic drum store designed and built here (Dutta Majumdar, '61)

In drum stores it is customary to divide the magnetic surface into the cells each having a finite area. For recording binary information, the pulse currents of appropriate polarity are fed into a coil wound on a magnetic core which is almost magnetically complete except for a small airgap in the vicinity of the recording medium which is moved relative to this head. Either state of a binary digit is defined by the magnetic configuration of the cell. When the medium is moved relative to a pick-up head in close proximity of the digit cell, the fluxes associated with the digit cell will take up the minimum reluctance path along the pick-up head, and a voltage will be developed across the windings in the head approximately proportional to the time and space derivatives of the stored flux-pattern. The nature of the voltage wave form will give a clear indication of the state of magnetization of the medium. Different methods of recording and reproduction of digits are treated in text books (Booth, A.D., Wilkes, M. V. etc) in detail.

A Reading-Writing circuit for Return to Zero (RZ) method was described earlier (Dutta Majumdar, 1958) in connection with a track switching circuit. There the output of the read amplifier enters the strobing circuit where it is interpreted. That is, the read output wave form is examined at the second peak of

the differential flux waveform by means of a set of very sharp pulses called strobing pulses derived from clock pulses. In this paper a reading method and the corresponding circuit is described in which accurately timed output pulses are obtained that do not require clock-pulses for their identification

SELF-STROBED READING METHOD

The method consists in inverting and delaying the output waveform and then combining it with the original waveform in a gate or AND circuit. In Fig. 1(a) the writing current waveform which is similar to that of RZ method is shown,

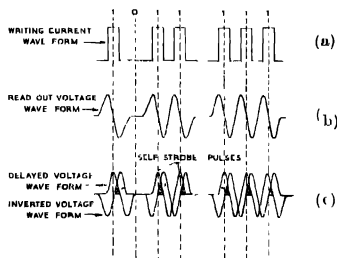


Fig. 1 Self-strobed reading method.

and the corresponding output voltage waveform is indicated in Fig. 1(b). At this point it should be noted that the point at which the output signal crosses the axis from the positive to the negative side is an accurate indication of the location of the stored '1'. In Fig. 1(c) the output waveform is duplicated twice, where it is shown after an inversion in one case and after a small amount of delay in the other case. If these waveforms are applied to an 'AND' gate that is responsive to voltage of positive polarity, sharp pulses as indicated by the darkened areas at the intersection of these two waveforms will be obtained. These pulses when properly amplified represent the stored binary information.

DESCRIPTION OF THE CIRCUIT

A functional block diagram of the circuit is shown in Fig. 2, and the actual circuit diagram is shown in Fig. 3. The output from the magnetic head is fed to

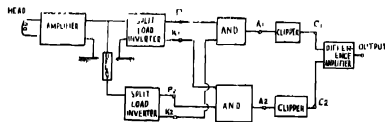


Fig. 2 Functional block diagram of the self-strobed reading method.

a conventional R-C coupled amplifier. The amplified output is fed to two split load inverters, one being fed direct, and the other through a delay line.

negative pulses for "0" are obtained (Fig. 5 two photographs are shown.) If instead of two channels before the 'AND' gates only one channel is used, there can be only sharp self-strobed positive pulses for '1's, whereas those for '0's will be

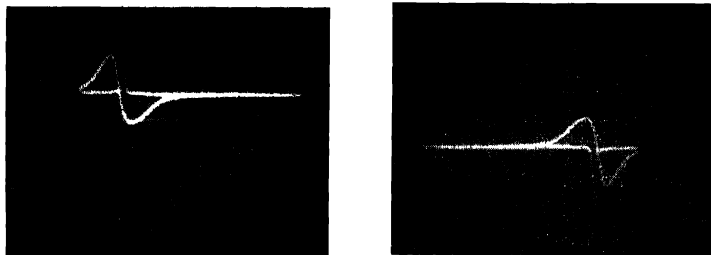


Fig. 5(a) self-strobed sharp positive pulse for a "one". (b) sharp negative pulse for a "Zero".

absent. The present circuit was designed for the particular head output pulse amplitude (about 0.75 volts), and for a particular Drum Speed (about 6000 r.p.m.). With the variation of these and other requirements the circuit constants will be different, but the general scheme can remain same. By selecting the delay and the associated circuit constants a compromise is to be made between the amplitude of the signal through the gate and the accuracy in locating the cross over point. Another advantage of this sensing method is its relative insensitivity to noise pulses.

ACKNOWLEDGMENT

The authors wish to thank Sri S. K. Mitra, Head of the Department of Electronic Computers, I.S.I., for his constant encouragement and Sri S. C. Majumdar, now in Institute of Nuclear Physics, who was associated with the work while he was taking his practical training in this Laboratory. The authors are grateful to Prof. J. N. Bhar, D. Sc., F.N.I. for his kind interest in the work. Authors are also grateful to Prof P. C. Mahalanobis, F.R.S., for providing funds for the research projects.

REFERENCES

- Booth, A. D., July, 1949, *Electronic Engineering*.
- Booth, A. D., and Booth, K, Automatic Digital Calculators.
- Dutta Majumdar, D., Dec. 1958, *Electronic Engineering*, 702-5.
- Dutta Majumdar, D., 1959, *J. Inst. Telecom. Engineers.*, 5, 4, 211-22.
- Dutta Majumdar, D., 1961, *J. Inst., Telecom. Engineers.*, 7, 1, 27-36.
- Wilkes, M. V., Automatic Digital Computers.

DETECTION OF INVARIANCE, TOTAL SYMMETRY AND PARTIAL SYMMETRY OF SWITCHING FUNCTIONS

SUNIL RANJAN DAS

INSTITUTE OF RADIO PHYSICS AND ELECTRONICS,
UNIVERSITY OF CALCUTTA

(Received September 6, 1962)

ABSTRACT. The paper suggests a method of identification of total or partial symmetry of a switching function based on the application of the principle of residue test. The invariance of a switching function under a single permutation of two variables can be readily detected from a knowledge of the equality of some of the residues of expansion about those two variables. This procedure of identifying invariance under a single interchange of two variables is then directly extended and applied for the identification of total or partial symmetry of a switching function, the variables of symmetry of which may be either all unprimed, all primed or of mixed nature. The method claims the additional advantage of giving all the relevant information regarding the various alternative representations of symmetries of a switching function with the corresponding n -numbers.

INTRODUCTION

A switching function of n variables which might be either all unprimed, all primed or mixed is said to possess total symmetry in these variables if any interchange of the variables leaves the function identically the same, i.e., invariant. A switching function which remains invariant under any interchange of variables which also might be all unprimed, all primed or mixed, belonging to a subset of the set of n variables is said to exhibit partial symmetry in these variables of the subset. Importance of detection and recognition of total or partial symmetry associated with a switching function lies in the method of special economical synthesis procedure for the realisation of such functions (Shannon, 1938 and 1949; Washburn, 1949; Keister, Ritchie and Washburn, 1951; G. Epstein, 1958).

Methods have been suggested by several authors for the detection of total symmetries of switching functions (Caldwell, 1954; Marcus, 1956; McCluskey, Jr., 1956; T. Singer, 1957; Choudhury and Basu, 1962; Mukhopadhyay, 1962). The method described by Caldwell consists in detecting and recognising total symmetry of switching functions by observing certain definite patterns in an extended Karnaugh map (Veitch, 1952; Karnaugh, 1953). The chief disadvantage of this method is that for functions of variables exceeding four, the recognition of symmetries becomes quite difficult. The methods of detection as suggested by Marcus and McCluskey can be applied to switching functions of any number

of variables. But these methods do not give any suggestion as to the various alternative forms of representation of symmetries with the corresponding α -numbers of a given switching function. Singer suggested the use of a set of decomposition charts (or "symmetry charts" as he called them) for the detection of total or partial symmetry of switching functions under all permutations of switching variables.

This detection of invariant patterns on the decomposition charts as suggested by Singer is analogous to the recognition of the properties of the residues of expansion of the given switching function about the row variables or column variables. The invariance of a switching function under a single interchange of two variables is readily detected from the equality of the definite groups of residues of expansion about these two variables. The purpose of the present paper is to suggest and develop a method based on the residue test of Boolean functions by numerical methods (Mullin and Kellner, 1955) for the detection of all types of symmetries of switching functions. To detect total symmetry we require only comparison of residues of expansion associated with n expansions. These expansions will also give us all the alternative forms of representation of symmetries of the function with the corresponding α -numbers. By utilising this principle of expansion and comparison of the residues of expansion for equality by numerical methods, the partial symmetry of a switching function with respect to the variables which might be all unprimed, all primed or mixed, can also be detected. Alternative representations of partial symmetries, if any, can be found out by this same method.

INVARIANCE OF A SWITCHING FUNCTION UNDER A SINGLE INTERCHANGE OF TWO VARIABLES

Any switching function $F(x_{n-1}, x_{n-2}, \dots, x_0)$ of n binary variables $x_{n-1}, x_{n-2}, \dots, x_0$, when expanded about any two variables, let us say, x_{n-1} and x_{n-2} , can be written as

$$F(x_{n-1}, x_{n-2}, \dots, x_0) = x_{n-1} x_{n-2} R_0 + x_{n-1} x'_{n-2} R_1 + x'_{n-1} x_{n-2} R_2 + x'_{n-1} x'_{n-2} R_3 \quad \dots \quad (1)$$

where R_0, R_1, R_2 and R_3 are the residual functions of expansions of $(n-2)$ variables, not including x_{n-1} and x_{n-2} .

From equation (1) it is seen that for the function $F(x_{n-1}, x_{n-2}, \dots, x_0)$ to remain invariant under different permutation and negation operations of the two variables x_{n-1} and x_{n-2} , the following conditions must be satisfied :

- (i) When both the variables x_{n-1} and x_{n-2} are unprimed, for invariance under single permutation, $R_1 = R_2$.
- (ii) When both the variables x_{n-1} and x_{n-2} are primed, for invariance under single permutation, $R_0 = R_3$.

(iii) When one of the variables is primed and the other unprimed, that is, when x_{n-1} is primed and x_{n-2} is unprimed or x_{n-1} is unprimed and x_{n-2} is primed, then for invariance under permutation, $R_0 = R_1 = R_2 = R_3$, i.e., all the four residues of expansion are identical. When this last condition is satisfied, it is implied that conditions (i) and (ii) are necessarily satisfied, and x_{n-1} and x_{n-2} can be eliminated from the expression of the function.

Therefore in order to detect the invariance of a switching function under a single interchange of two variables (the variables being either both primed, both unprimed or mixed) we need only expand the function about these two variables and compare the different residues of expansion for equality. This expansion and subsequent comparison of the residues of expansion to detect invariance can be done very effectively by utilising the method of residue test as applied to Boolean functions expressed in decimal mode.

When the residue test is applied to a transmission function expressed as a standard sum it is merely necessary to carry out a process of factoring in order to find the residues. Taking a function $F = (x'_3x_2x'_1x_0 + x'_3x_2x_1x_0 + x'_3x'_2x_1x_0 + x_3x_2x_1x_0)$, to apply the residue tests to the x_2 variable, we may perform the expansion by factoring out x_2 and x'_2 to obtain $F = x_2(x'_3x'_1x_0 + x'_3x_1x_0 + x_3x_1x_0) + x'_2(x_3x_1x_0)$.

In order to evaluate the residues of expansion about any variable of a given switching function by numerical methods, we are to know for the given binary digit position in the binary number representation of the function whether the digit is a zero or an one, corresponding to the primed and unprimed literal in the algebraic expression and then to group the terms to form "1" residue and "0" residue.

This can be done very easily if we note that as in a decimal number shifting of decimal point one digit position to the left is equivalent to dividing the number by 10, so also shifting of binary point one digit position to the left is equivalent to the division of the binary number by 2. Taking a binary number 111101 whose decimal equivalent is 61 and which might be thought to represent one of the terms in a standard sum expression of a given switching function, if we now want to know whether the third digit from the left in this particular binary number is a 0 or an 1, without actually writing the same but from a knowledge of its decimal counterpart, what we should do in fact is as follows (Mullin and Kellner, 1955).

Let us take the binary number 111101 and putting a binary point after the third digit from the left, write it as 111.101, decimal equivalent of which is

$$2^2 + 2^1 + 2^0 + 2^{-1} + 2^{-2} = 4 + 2 + 1 + 1/2 + 1/8 = 7\frac{5}{8} \quad \dots \quad (2)$$

Thus we see that by putting the binary point at the position mentioned, we have practically divided the original binary number by 2^3 or its equivalent decimal

value 61 by 8. Discarding all the binary digits to the right of the binary point we now obtain 111 which is equivalent to the decimal number 7, an integer which can be obtained independently from the number $7\frac{5}{8}$ by discarding the fractional part $5/8$. This integral part of the decimal quotient $7\frac{5}{8}$ or 7 is an odd number, a fact which goes to imply that the right hand digit of its binary equivalent (111) is unity. If the whole number part of the quotient had been even, the digit at the extreme right of the equivalent binary number would have been zero.

From this analysis, the general procedure for identifying a primed or an unprimed literal in a term of the standard sum expression (which is the same as to know whether the digit which represents it in the equivalent binary form is a 0 or an 1) of a switching function may be stated thus : We should divide the binary number equivalent of the term by that power of 2 which places the binary point to the right of the digit whose identity is to be disclosed, an operation which is the same as to divide the decimal counterpart of the same binary number by that same power of 2 and to note whether the integral part of the decimal quotient obtained thereby is an even or an odd integer, an even integer denoting a primed and an odd integer an unprimed literal.

Example :

To illustrate the principle, let us take an example

$$F(x_3, x_2, x_1, x_0) = \Sigma(4, 6, 8, 12) \quad (3)$$

To apply the residue test to the x_2 variable we see that in the binary number representation of the function, the binary point should be shifted two digit positions to the left which requires that its decimal counterpart be divided by 4. Thus dividing by 4, the results obtained for different terms of the transmission are :

$$\frac{4}{4} = 1+, \text{ odd}; \frac{6}{4} = 1+, \text{ odd}; \frac{8}{4} = 2+, \text{ even}; \text{ and } \frac{12}{4} = 3+, \text{ odd}.$$

Hence the residues can be written by grouping the decimal numbers, as

$$F(x_3, x_2, x_1, x_0) = x_2(4, 6, 12) + x'_2(8) \quad \dots (4)$$

Now considering the decimal integers 12 and 8, we note that for the number 12 represented by the binary number 1100, the x_2 literal may be factored out by writing $12 \rightarrow x_2(1-00)$ and for the number 8 represented by 1000, the x'_2 literal may be taken out to indicate by writing $8 \rightarrow x'_2(1-00)$, thereby showing the x_2 and x'_2 residues to be identical.

This equality of the residues of expansion can also be shown directly if we note that the residues of the binary numbers 1100 and 1000 would also remain equal if we would replace the "0" in the x_2 position of 1000 by "1" and expand both of them about the x_2 literal. This replacement of "0" by "1" in the x_2 position

of 1000 is identical with the addition of 2^2 to the binary number 1000 or 4 to its equivalent decimal number. So in the expansion given by

$$F = x_2(4, 6, 12) + x'_2(8)$$

we get, by adding 4 to 8, $x'_2(12)$ in place of $x'_2(8)$, which gives an easy way of identifying whether the x'_2 residue is equal to or contained in the x_2 residue. The presence of the same term 12 in both the x_2 and x'_2 residues proves that when x_2 is factored out of the algebraic or binary equivalent of the number 12 and x'_2 from that of the number 8 (by addition of 4 to which we obtain the second 12 in this case) what remains in the bracket (1-00) is the same in both the cases.

By the application of the above principle, expansion about any number of variables can be obtained, first expanding the function about one of the variables, then expanding the residues of first expansion about another variable and so on and lastly the residues can be modified by adding appropriate decimal numbers to the respective residue groups to test for equality.

Let us now apply this principle of expansion and comparison of residue groups to test the invariance of a switching function under single permutation of two variables.

Example :

The switching function $F(x_0, x_1, x_2, x_3) = \Sigma(1, 2, 5, 6, 8, 11, 12, 15)$ is invariant under the following permutation and permutation and negation operations :

$$(a) x_3 \sim x_1, (b) x'_3 \sim x'_1, (c) x_3 \sim x_0, (d) x'_3 \sim x'_0$$

and (e) $x_1 \sim x_0$, (f) $x'_1 \sim x'_0$ where the sign ' \sim ' means 'interchanged with'. This can be shown from the expansion of the function about these different pairs of variables and comparing the different residue groups as given below.

$$\begin{aligned} F &= x_3(8, 11, 12, 15) + x'_3(1, 2, 5, 6) \\ &= x_3x_1(11, 15) + x_3x'_1(8, 12) + x'_3x_1(2, 6) + x'_3x'_1(1, 5). \end{aligned}$$

On modification, the different residue groups become

$$x_3x_1(11, 15), x_3x'_1(10, 14), x'_3x_1(10, 14), x'_3x'_1(11, 15)$$

which shows that the residual functions associated with $x_3x'_1$ and x'_3x_1 are equal (i.e., $R_1 = R_2$) as well as those associated with x_3x_1 and $x'_3x'_1$ (i.e., $R_0 = R_3$). This means that the function possesses invariance for

$$(a) x_3 \sim x_1 \text{ and } (b) x'_3 \sim x'_1.$$

Similarly, expanding the function about x_3x_0 and x_1x_0 and modifying the residue groups give

$$x_3x_0(11, 15), x_3x'_0(9, 13), x'_3x_0(9, 13), x'_3x'_0(11, 15)$$

$$\text{and } x_1x_0(11, 15), x_1x'_0(3, 7), x'_1x_0(3, 7), x'_1x'_0(11, 15)$$

which show that the function is invariant for (c) $x_3 \sim x_0$ and (d) $x'_3 \sim x'_0$, and (e) $x_1 \sim x_0$ and (f) $x'_1 \sim x'_0$. We shall next discuss some further properties associated with the equality of the residual functions of expansion. The total or partial symmetry of switching functions will be detected on the basis of these results.

If in an n variable switching function $F(x_{n-1}, x_{n-2}, \dots, x_0)$, expansion about the pair of variables x_{n-1}, x_{n-2} and comparison of the residual functions of expansion show that $R_1 = R_2$, it not only means that the function is invariant for x_{n-1} permuted with x_{n-2} but it also means that all the functions derived from the given function by applying $(n-2)!$ 2^{n-2} transformations (negation and permutation operations associated with $n-2$ variables) to the remaining $(n-2)$ variables will also continue to remain invariant. This is because any transformation applied to these $(n-2)$ variables will alter the residual functions identically so that R_1 and R_2 will still remain identical. The same will be the case for x'_{n-1} permuted with x'_{n-2} when $R_0 = R_3$. Further if in the expansion of the switching function about x_{n-1} and x_{n-2} , the residual functions $R_1 = R_2$ this also will not only mean that the function is invariant for $x_{n-1} \sim x_{n-2}$ but also the function derived from the given function by priming both x_{n-1} and x_{n-2} will continue to remain invariant when $x'_{n-1} \sim x'_{n-2}$, and this invariance is unaffected by the application of any transformation to the set of $(n-2)$ residual variables. Likewise, when the residual functions $R_0 = R_3$ it also not only means that the function is invariant for $x'_{n-1} \sim x'_{n-2}$ but also the function obtained from the given function by priming either x_{n-1} or x_{n-2} will also continue to remain invariant when $x'_{n-1} \sim x_{n-2}$ or $x_{n-1} \sim x'_{n-2}$ as the case may be, invariance being of course unaffected by any transformation applied to the group of $(n-2)$ residual variables (Mukhopadhyay, 1962). These results may be summarised thus :

(i) If $R_1 = R_2$,

$$F(x_{n-1}, x_{n-2}, \dots, x_0) \equiv x_{n-1} \sim x_{n-2} \quad \dots \quad (5)$$

$$\text{and } \neg F(x_{n-1}, x_{n-2}, \dots, x_0) \equiv x_{n-1} \sim x_{n-2} \quad \dots \quad (6)$$

$$\text{Also } F(x'_{n-1}, x'_{n-2}, \dots, x_0) \equiv x'_{n-1} \sim x'_{n-2} \quad \dots \quad (7)$$

$$\text{and } \neg F(x'_{n-1}, x'_{n-2}, \dots, x_0) \equiv x'_{n-1} \sim x'_{n-2} \quad \dots \quad (8)$$

(ii) If $R_0 = R_3$,

$$F(x'_{n-1}, x_{n-2}, \dots, x_0) \equiv x'_{n-1} \sim x_{n-2} \quad \dots \quad (9)$$

$$\text{and } \neg F(x'_{n-1}, x_{n-2}, \dots, x_0) \equiv x'_{n-1} \sim x_{n-2} \quad \dots \quad (10)$$

$$\text{and also} \quad F(x_{n-1}, x'_{n-2}, \dots, x_0) \equiv x_{n-1} \sim x'_{n-2} \quad (11)$$

$$\text{and} \quad \Gamma F(x_{n-1}, x'_{n-2}, \dots, x_0) \equiv x_{n-1} \sim x'_{n-2} \quad (12)$$

where in the above

' \equiv ' denotes invariance under transformation,

and ' Γ ' denotes different functions obtained by applying $(n-2)!2^{n-2}$ transformations amongst the $(n-2)$ residual variables.

DETECTION OF TOTAL SYMMETRY

To detect total symmetry of a switching function, it is not necessary to test invariance of the function under every interchange of two variables, it is sufficient to test the invariance of the function for n interchanges of two variables (for an n variable switching function) where the sets of variables form a closed chain. For example, if an n variable switching function $F(x_{n-1}, x_{n-2}, x_{n-3}, \dots, x_1, x_0)$ is invariant under the permutations $x_{n-1} \sim x_{n-2}$, $x_{n-2} \sim x_{n-3}$, \dots , $x_1 \sim x_0$, $x_0 \sim x_{n-1}$ then the function is also invariant for any intermediate permutation $x_p \sim x_q$ ($p \neq q$) and hence totally symmetric because any intermediate permutation can be generated from the above sets of cyclic permutations (Chatterjee, 1957). The aggregate of n expansions about the pairs of variables (x_{n-1}, x_{n-2}) , (x_{n-2}, x_{n-3}) , \dots , (x_1, x_0) , (x_0, x_{n-1}) may be called the set of cyclic expansions and will be utilised to detect total symmetry associated with a switching function as illustrated below.

Example :

To show whether the five variable switching function given by

$$F(x_4, x_3, x_2, x_1, x_0) = \Sigma(0, 1, 3, 4, 6, 7, 8, 10, 11, 14, 17, 20, 21, \\ 23, 24, 25, 27, 28, 30, 31) \quad \dots \quad (13)$$

possesses total symmetry.

Taking the function, it is cyclically expanded. We have (1) from expansion about x_4x_3 ,

$$F = x_4(17, 20, 21, 23, 24, 25, 27, 28, 30, 31) + \\ x'_4(0, 1, 3, 4, 6, 7, 8, 10, 11, 14) \\ = x_4x_3(24, 25, 27, 28, 30, 31) + x_4x'_3(17, 20, 21, 23) + x'_4x_3(8, 10, 11, 14) \\ + x'_4x'_3(0, 1, 3, 4, 6, 7).$$

On modification, the above residues become

$$x_4x_3(24, 25, 27, 28, 30, 31), \quad x_4x'_3(25, 28, 29, 31), \\ x'_4x_3(24, 26, 27, 30), \quad x'_4x'_3(24, 25, 27, 28, 30, 31)$$

wherefrom it appears that $R_0 = R_3$.

$$\therefore F(x'_4, x_3, x_2, x_1, x_0) \equiv x'_4 \sim x_3 \quad \dots (14)$$

$$\text{and} \quad \Upsilon F(x'_4, x_3, x_2, x_1, x_0) \equiv x'_4 \sim x_3 \quad \dots (15)$$

$$\text{Also} \quad F(x_4, x'_3, x_2, x_1, x_0) \equiv x_4 \sim x'_3 \quad \dots (16)$$

$$\text{and} \quad \Upsilon F(x_4, x'_3, x_2, x_1, x_0) \equiv x_4 \sim x'_3 \quad \dots (17)$$

(2) from expansion about x_3x_2 ,

$$F = x_3x_2(14, 28, 30, 31) \vdash x_3x'_2(8, 10, 11, 24, 25, 27) \vdash x'_3x_2(4, 6, 7, 20, 21, 23) \\ \vdash x'_3x'_2(0, 1, 3, 17).$$

On modification, these residues become

$$x_3x_2(14, 28, 30, 31), x_3x'_2(12, 14, 15, 28, 29, 31), x'_3x_2(12, 14, 15, 28, 29, 31), \\ x'_3x'_2(12, 13, 15, 29)$$

wherefrom it appears that $R_1 = R_2$.

$$\text{Hence} \quad \Upsilon F(x_3, x_2, x_4, x_1, x_0) \equiv x_3 \sim x_2 \quad \dots (18)$$

$$\text{and} \quad \Upsilon F(x'_3, x'_2, x_4, x_1, x_0) \equiv x'_3 \sim x'_2 \quad \dots (19)$$

(3) from expansion about x_2x_1 ,

$$F = x_2x_1(6, 7, 14, 23, 30, 31) \vdash x_2x'_1(4, 20, 21, 28) \\ \vdash x'_2x_1(3, 10, 11, 27) \vdash x'_2x'_1(0, 1, 8, 17, 24, 25).$$

Modifying the residues we have

$$x_2x_1(6, 7, 14, 23, 30, 31), x_2x'_1(6, 22, 23, 30),$$

$$x'_2x_1(7, 14, 15, 31), x'_2x'_1(6, 7, 14, 23, 30, 31)$$

which shows that $R_0 = R_3$.

$$\therefore \quad \Upsilon F(x'_2, x_1, x_4, x_3, x_0) \equiv x'_2 \sim x_1 \quad (20)$$

$$\text{and} \quad \Upsilon F(x_2, x'_1, x_4, x_3, x_0) \equiv x_2 \sim x'_1 \quad (21)$$

(4) from expansion about x_1x_0 ,

$$F = x_1x_0(3, 7, 11, 23, 27, 31) + x_1x'_0(6, 10, 14, 30) + x'_1x_0(1, 17, 21, 25) \\ \vdash x'_1x'_0(0, 4, 8, 20, 24, 28).$$

On modification, these residues become

$$x_1x_0(3, 7, 11, 23, 27, 31), \quad x_1x'_0(7, 11, 15, 31), \quad x'_1x_0(3, 19, 23, 27), \\ x'_1x'_0(3, 7, 11, 23, 27, 31)$$

which shows that $R_0 = R_1$.

$$\therefore \quad \Upsilon \quad F(x'_1, x_0, x_4, x_3, x_2) \equiv x'_1 \sim x_0 \quad \dots \quad (22)$$

$$\text{and} \quad \Upsilon \quad F(x_1, x'_0, x_4, x_3, x_2) \equiv x_1 \sim x'_0 \quad \dots \quad (23)$$

(5) and lastly from expansion about x_4x_0 ,

$$F = x_4x_0(17, 21, 23, 25, 27, 31) \vdash x_4x'_0(20, 24, 28, 30) \vdash x'_4x_0(1, 3, 7, 11) \\ \vdash x'_4x'_0(0, 4, 6, 8, 10, 14).$$

On modification, we have

$$x_4x_0(17, 21, 23, 25, 27, 31), \quad x_4x'_0(21, 25, 29, 31), \\ x'_4x_0(17, 19, 23, 27), \quad x'_4x'_0(17, 21, 23, 25, 27, 31)$$

which shows that $R_0 = R_3$.

$$\therefore \quad \Upsilon \quad F(x'_4, x_0, x_3, x_2, x_1) \equiv x'_4 \sim x_0 \quad \dots \quad (24)$$

$$\text{and} \quad \Upsilon \quad F(x_4, x'_0, x_3, x_2, x_1) \equiv x_4 \sim x'_0 \quad \dots \quad (25)$$

Combining equations (17), (19), (20), (23), and (25) we have

$$F(x_4, x'_3, x'_2, x_1, x'_0) \equiv x_4 \sim x'_3, \quad x'_3 \sim x'_2, \quad x'_2 \sim x_1, \quad x_1 \sim x'_0 \quad \text{and} \quad x'_0 \sim x_4$$

So the function is totally symmetric and the variables of symmetry are $x_4, x'_3, x'_2, x_1, x'_0$. α -numbers of the function can be found by writing the function in the Truth Table form and double negating the columns under x_3, x_2 , and x_0 . This matrix must have sufficient row sum occurrences, otherwise the chain of cyclic permutations could not have been complete (M. P. Marcus, 1956).

The above matrix shows that the function can be written as

$$S_{2,3}(x_4, x'_3, x'_2, x_1, x'_0).$$

TABLE 1

x_4	x_3	x_2	x_1	x_0	x_4	x'_3	x'_2	x_1	x'_0	Number of ones
0	0	0	0	0	0	1	1	0	1	3
0	0	0	0	1	0	1	1	0	0	2
0	0	0	1	1	0	1	1	1	0	3
0	0	1	0	0	0	1	0	0	1	2
0	0	1	1	0	0	1	0	1	1	3
0	0	1	1	1	0	1	0	1	0	2
0	1	0	0	0	0	0	1	0	1	2
0	1	0	1	0	0	0	1	1	1	3
0	1	0	1	1	0	0	1	1	0	2
0	1	1	1	0	0	0	0	1	1	2
1	0	0	0	1	1	1	1	0	0	3
1	0	1	0	0	1	1	0	0	1	3
1	0	1	0	1	1	1	0	0	0	2
1	0	1	1	1	1	1	0	1	0	3
1	1	0	0	0	1	0	1	0	1	3
1	1	0	0	1	1	0	1	0	0	2
1	1	0	1	1	1	0	1	1	0	3
1	1	1	0	0	1	0	0	0	1	2
1	1	1	1	0	1	0	0	1	1	3
1	1	1	1	1	1	0	0	1	0	2
Ratio of the number of ones to					10	10	10	10	10	
number of zeros .					10	10	10	10	10	

Similarly, combining the sets of equations (15), (18), (21), (22) and (24) the function can be identified as

$$S_{0,1,4,5}(x'_4, x_3, x_2, x'_1, x_0).$$

To find the variables of symmetry associated with a symmetric switching function from the set of cyclic permutations and hence to find all the alternative representations of symmetries of the given switching function, the general procedure may be outlined by taking the example of equation (13) and using the following sets of relations.

$$R_0 = R_3 \longleftrightarrow x'_4 \sim x_3, \quad x_4 \sim x'$$

$$R_1 = R_2 \longleftrightarrow x_3 \sim x_2, \quad x'_3 \sim x'$$

$$R_0 = R_3 \longleftrightarrow x'_2 \sim x_1, \quad x_2 \sim x'$$

$$R_0 = R_3 \longleftrightarrow x'_1 \sim x_0, \quad x_1 \sim x'$$

$$R_0 = R_3 \longleftrightarrow x'_0 \sim x_4, \quad x_0 \sim x'.$$

To start with we shall take any literal, preferably one with the highest value of the subscript p , both primed and unprimed and then associate them with literals with which they are connected by ' \sim ' signs. In the above case, x_4 and x'_4 are connected with x'_3 and x_3 respectively. Similarly, x'_3 and x_3 are connected with x'_2 and x_2

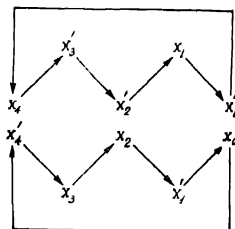


Fig. 1. Possible closed paths indicating possible variables of symmetry.

respectively and so on we proceed until we end on the literals with which we started. The literals that occur in any closed path will give a set of variables of symmetry. Thus, for the above example, there can be traced two and only two closed paths associated with the two possible representations of the functions as given earlier (Fig. 1).

DETECTION OF PARTIAL SYMMETRY

To detect and identify partial symmetry of a switching function, we should look for the invariance of the function under any interchange of the variables belonging to a subset of the set of variables. The chain of cyclic permutations will be complete with these variables of the subset, the variables being either all unprimed, or all primed or of mixed type. Hence, in this case depending on the nature of the problem, complete set of expansions about two variables might be required. Let us take an example to illustrate the method

Example.

Find the partial symmetry associated with the function

$$F(x_3, x_2, x_1, x_0) = \Sigma(0, 1, 3, 4, 6, 7, 9, 10, 12, 15) \quad (26)$$

Taking the function, sets of expansions are done. We have
(i) from expansion about x_3x_2 ,

$$\begin{aligned} F &= x_3(9, 10, 12, 15) + x'_3(0, 1, 3, 4, 6, 7) \\ &= x_3x_2(12, 15) + x_3x'_2(9, 10) + x'_3x_2(4, 6, 7) + x'_3x'_2(0, 1, 3). \end{aligned}$$

The residues, on modification, become

$$x_3x_2(12, 15), x_3x'_2(13, 14), x'_3x_2(12, 14, 15) \text{ and } x'_3x'_2(12, 13, 15)$$

which shows that the residues are not equal.

Similarly, (ii) from expansion about x_3x_1 and on modifying the residue groups, we get

$$x_3x_1(10, 15), x_3x'_1(11, 14), x'_3x_1(11, 14, 15), x'_3x'_1(10, 11, 14)$$

which also shows that the residues are not equal.

Likewise (iii) from expansion about x_3x_0 and on modifying the residue groups, we get

$$x_3x_0(9, 15), x_3x'_0(11, 13), x'_3x_0(9, 11, 15), x'_3x'_0(9, 13, 15)$$

showing the residues to be unequal.

But by (iv) expanding the function about x_2x_1 and modifying the residue groups, we have

$$x_2x_1(6, 7, 15), x_2x'_1(6, 14), x'_2x_1(7, 14), x'_2x'_1(6, 7, 15)$$

which shows that $R_0 = R_3$

$$\therefore F(x'_2, x_1, x_3, x_0) \equiv x'_2 \sim x_1 \quad \dots \quad (27)$$

$$\text{and} \quad F(x_2, x'_1, x_3, x_0) \equiv x_2 \sim x'_1 \quad \dots \quad (28)$$

(v) expanding the function about x_1x_0 and modifying the residue groups, we get

$$x_1x_0(3, 7, 15), x_1x'_0(7, 11), x'_1x_0(3, 11), x'_1x'_0(3, 7, 15)$$

which shows that $R_0 = R_3$.

$$\therefore F(x'_1, x_0, x_3, x_2) \equiv x'_1 \sim x_0 \quad \dots \quad (29)$$

$$\text{and} \quad F(x_1, x'_0, x_3, x_2) \equiv x_1 \sim x'_0 \quad \dots \quad (30)$$

and (vi) lastly expanding about x_2x_0 and modifying, we have the residues

$$x_2x_0(7, 15), x_2x'_0(5, 7, 13), x'_2x_0(5, 7, 13), x'_2x'_0(5, 15)$$

which shows that $R_1 = R_2$.

$$\therefore F(x_2, x_0, x_3, x_1) \equiv x_2 \sim x_0 \quad \dots \quad (31)$$

$$\text{and} \quad F(x'_2, x'_0, x_3, x_1) \equiv x'_2 \sim x'_0 \quad \dots \quad (32)$$

From the above sets of expansions we see that a closed chain of cyclic permutations comprises the variables x_2, x'_1, x_0 and x'_2, x_1, x'_0 so that the function is partially symmetric with respect to these variables. To write the form of the

function, the function should be entered on a matrix and appropriate columns should be double negated. By such operations, the function may be written as

$$x_3 S_0(x_2, x'_1, x_0) + x'_3 S_1(x_2, x'_1, x_0) + (x_3 + x'_3) S_2(x_2, x'_1, x_0) \quad \dots \quad (33)$$

or
$$x'_3 S_2(x'_2, x_1, x'_0) + x_3 S_3(x'_2, x_1, x'_0) + (x_3 + x'_3) S_1(x'_2, x_1, x'_0) \quad \dots \quad (34)$$

The function is also partially symmetric with respect to the subsets of variables of the sets (x_2, x'_1, x_0) and (x'_2, x_1, x'_0)

DISCUSSIONS

In this paper a method has been suggested for the detection of invariance and recognition of the symmetries (both total and partial) of switching functions having variables of symmetry which may be either all primed, all unprimed or of mixed nature. The method of detection of total or partial symmetries of switching functions suggested in this paper by the extension of the principle of the residue test readily gives all the alternative representations of symmetries of functions (total or partial) with their corresponding α -numbers. Importance of detection of total or partial symmetries of switching functions arises principally of the fact that they lead to relay contact networks or electronic circuits which are more economical of elements (diodes, relay contacts, etc.). Hence the knowledge of all these alternative forms of representations of symmetries is considered very important from the actual circuit synthesis point of view. The circuit synthesized from one of these forms may be more desirable than the others from design considerations. Hence when all the forms of representations of symmetries are known, an easy comparison amongst them for economy and simplicity of design can be made. Further, since the different representations of symmetries are associated with different priming operations of the variables of the functions, all the different circuits may also be easily obtained if required, from any one, by appropriately complementing the input variables, when one of them is known.

Lastly, the method is not only exhaustive but also simple and straightforward at the same time.

ACKNOWLEDGMENT

The author wishes to express his indebtedness to Prof. J. N. Bhar, D.Sc., F.N.I., M. Brit. I.R.E., for his guidance and keen interest in the work and to Dr. A. K. Choudhury, M.Sc., D.Phil. for discussions and helpful suggestions throughout the progress of the work. The award of a Senior Research Fellowship by the C. I. S. R. Government of India, is also thankfully acknowledged.

REFERENCES

- Ashenhurst, R. L., 1957, *Proc. International Symposium on the Theory of Switching in the Annals of the Computation Laboratory of Harvard University*, Vol. 29, 74-116.
 Caldwell, S. H., 1954, *Trans. A.I.E.E.*, Vol. 73, Part I, 142-146.

- Caldwell, S. H., 1958, *Switching Circuits and Logical Design*, John Wiley and Sons, Inc., N.Y., 236-270.
- Chatterjee, B. C., 1957, *Abstract Algebra, Part I*, Das Gupta & Co. (Private) Ltd, Calcutta.
- Choudhury, A. K., and Basu, M. S., 1962, *Indian Journal of Physics*, Vol. 36, No. 1, 31-42.
- Epstein, G., 1958, *I.R.E. Transactions on Electronic Computers*, Vol. EC-7, No. 1, 57-60.
- Karnaugh, M., 1953, *Trans. A.I.E.E.*, Vol. 72, Part I, 593-598.
- Keister, W., Ritchie, A. E., and Washburn, S. H., 1951, *The Design of Switching Circuits*, D. Van Nostrand Co. Inc., New York, N. Y.
- Marcus, M. P., 1956, *I.R.E. Transactions on Electronic Computers*, Vol. EC-5, 237-239.
- McCluskey, E. J., Jr., 1956, *Bell System Technical Journal*, Vol. 35, 1445-1453.
- Mukhopadhyay, A., 1962, *Studies on Switching Circuit Theory* (Doctoral Thesis).
- Mullin, A. A., and Kellner, W. G., 1955, "A Residue Test for Boolean Functions", Unpublished teaching Memorandum, Department of Electrical Engineering, M.I.T.
- Shannon, C. E., 1938, *Trans. A.I.E.E.*, Vol. 57, 713-723.
- Shannon, C. E., 1949, *Bell System Technical Journal*, Vol. 28, 59-98.
- Singer, T., 1957, *Proc. International Symposium on the Theory of Switching in the Annals of the Computation Laboratory of Harvard University*, Vol. 29, 125-133.
- Veitch, E. W., 1952, *Proc. of Association for Computing Machinery*, 127-133.
- Washburn, S. H., 1949, *Trans. A.I.E.E.*, Vol. 68, 582-586.

Letters to the Editor

The Board of Editors will not hold itself responsible for opinions expressed in the letters published in this section. The notes containing reports of new work communicated for this section should not contain many figures and should not exceed 500 words in length. The contributions must reach the Assistant Editor not later than the 15th of the second month preceding that of the issue in which the letter is to appear. No proof will be sent to the authors.

2

HYDROGEN BONDING IN N-METHYL FORMAMIDE

K VENKATA RAMIAH AND P. G. PURANIK

DEPARTMENT OF PHYSICS, UNIVERSITY COLLEGE OF SCIENCE,
OSMANIA UNIVERSITY, HYDERABAD

(Received, August 28, 1962)

In our earlier work (1952), we have calculated the shifts in the OH and NH stretching frequencies of alcohols and amides, treating hydrogen bonding as an electrostatic interaction. In these calculations it is assumed that the ionic character of the NH bond diminishes due to intermolecular associations. In this communication, the shift in the NH stretching frequency of N-methyl formamide due to intermolecular associations of the type $\text{N-H}\cdots\text{O}=\text{C}$ is calculated and compared with the experimentally observed value.

The infrared spectra of N-methyl formamide have been recorded with Perkin-Elmer IR Double beam Spectrophotometer Model 21, with NaCl optics. The bonded NH stretching absorption has been recorded by pressing a drop of the liquid between two plates of NaCl so as to form a microfilm of unknown thickness. The free NH stretching frequency of the amide was recorded in dilute solutions of CCl_4 with matched cells of 0.94 mm thickness. The bonded and free NH stretching frequencies, thus recorded are 3290 cm^{-1} and 3484 cm^{-1} .

The bond lengths used in these calculations are (Katz, 1957) $d(\text{N-H}) = 0.995\text{ \AA}$, $d(\text{N-CH}_3) = 1.47\text{ \AA}$, $d(\text{C-N}) = 1.29\text{ \AA}$, $d(\text{C-H}) = 1.094\text{ \AA}$, $d(\text{C=O}) = 1.23\text{ \AA}$ and $d(\text{N-H}\cdots\text{O}) = 2.83\text{ \AA}$. The bond moments of the various linkages are the same as reported earlier (1962).

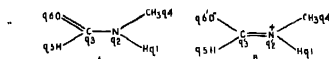


Fig. 1

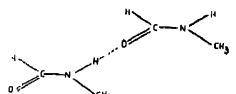


Fig. 2

SIMPLER FORMULAE FOR THE CHAPMAN-COWLING SECOND APPROXIMATION TO THE THERMAL DIFFUSION FACTOR OF BINARY GAS MIXTURES WITH EITHER OF THE COMPONENTS IN TRACE

S. C. SAXENA AND R. K. JOSHI

PHYSICS DEPARTMENT, RAJASTHAN UNIVERSITY, JAIPUR, INDIA.

(Received November 6, 1962)

Saxena and Dave (1961) have derived simpler formulae for the thermal diffusion factor of a binary gas mixture when the heavier component is in trace. Recently they (1963a, 1963b) also gave the formulae when the lighter component is in trace. Formulae were derived both according to the Chapman-Cowling and Kihara approximation schemes and numerical results were tabulated for the Ar-Xe and He-Xe systems. A critical examination of their work shows that the Chapman-Cowling second approximation formula for thermal diffusion factor, $[\alpha_T]_2$, becomes less accurate as the ratio of the mass of the lighter component to the heavier component increases. In this note we report accurate formulae for such systems.

The new formulae reported here are obtained by applying the following two criteria in expanding the Chapman-Cowling determinants

(i) All the terms in the expansion of the various determinants which contain the product of two diagonal elements of the Chapman-Cowling determinant, $A^{(2)}$, are retained.

(ii) In this expansion those terms are also retained which explicitly contain the power of M upto 2. $M = M_2/M_1$ where M_2 and M_1 are the molecular weights of the lighter and heavier components respectively.

Based on these considerations we get the following expression for $[\alpha_T]_2$ when the heavier component is in trace instead of Eq. (7) of Saxena and Dave (1961).

$$\begin{aligned}
 [\alpha_T]_2 = & (5/2\sqrt{2})(1+M)\{(a_{10}/a'_{11}) + M^{-1}\{(a'_{11}a'_{22} - a'^2_{12}) \\
 & (a''_{-2-2} a''_{-1-1} - a''^2_{-1-2})\}^{-1}(a'_{11} a'_{22} - a'^2_{12})(a_{-10} a''_{-2-2} - a_{-20} a''_{-1-2}) \\
 & + a_{10}a'_{22}(a''_{-1-2} a_{-21} - a''_{-2-2} a_{-11}) - a''_{-2-2} a_{02} a_{-12} a'_{11}\}. \quad \dots \quad (1)
 \end{aligned}$$

Similarly when the lighter component is in trace the following formula is obtained instead of Eq. (6) of Saxena and Dave (1963b) :

$$[\alpha_T]_2 = (5/2\sqrt{2})(1 + M)^{\frac{1}{2}} \left[a_{10} a''_{22} (a''_{11} a''_{22} - a''_{12}{}^2)^{-1} + \{(a'_{-1-1} a'_{-2-2} - a'^2_{-1-2}) a'^2_{-1-2} \right. \\ (a''_{11} a''_{22} - a''_{12}{}^2)^{-1} \{ (a_{1-1} a''_{22} - a''_{12} a_{2-1}) (a_{-20} a'_{-1-2} - a_{-10} a'_{-2-2}) \\ + (a_{1-2} a''_{22} - a''_{12} a_{2-2}) (a_{-10} a'_{-1-2} - a_{-20} a'_{-1-1}) \} \\ \left. + M^{-1} (a_{-10} a'_{-1-1}) \left(1 - \frac{a_{-20} a'_{-1-2}}{a_{-10} a'_{-2-2}} \right) \left(1 - \frac{a'^2_{-1-2}}{a'_{-1-1} a'_{-2-2}} \right)^{-1} \right]. \quad \dots (2)$$

In both these formulae the various terms have their usual meaning.

TABLE I

Chapman-Cowling calculated values of $[\alpha_T]_2$ for Xe-Ar system, Xe being in trace

T °K	Rigorous*	S.D.	S.J.
100	-0.0377	-0.0428	-0.0377
300	0.150	0.147	0.156
500	0.275	0.280	0.276
700	0.320	0.317	0.320
900	0.396	0.359	0.399

TABLE II

Chapman-Cowling calculated values of $[\alpha_T]_2$ for Xe-Ar system, Ar in trace

T °K	Rigorous*	S.D.	S.J.
100	-0.0234	-0.0181	-0.0234
300	0.0894	0.0977	0.0894
500	0.165	0.200	0.165
700	0.202	0.238	0.202
900	0.212	0.248	0.212

*These values are calculated afresh and some differ from those reported earlier by Saxena and Dave.

Computed values of $[\alpha_T]_2$ according to Eqs. 1 and 2 for the Ar-Xe system as a function of temperature are recorded in the last column (S.J.) of Tables I and II respectively. Also included in these tables are the previously reported rigorous (column 2) and approximate (S.D., Column 3) $[\alpha_T]_2$ values. An inspection of these tables reveals that the new formulae given in this note are almost as accurate as the rigorous formulae and are much better than the simpler formulae given earlier by Saxena and Davo (1961, 1963a, and 1963b). These new formulae will be extremely useful for predicting the $[\alpha_T]_2$ values or in determining the inter-molecular forces if α_T experimental data are available for those systems where M is not quite small.

It may be pointed out that this method of approximating the Chapman-Cowling determinants has proved very successful for the general case of α_T where both the components are present in appreciable proportions, (Saxena, Dave and Pardeshi 1962, Saxena and Joshi 1963a) and also in the formulation of the second approximation to the binary viscosity (Saxena and Joshi, 1963b).

REFERENCES

- Saxena, S. C. and Dave, S. M., 1961, *Revs Mod Phys*, **33**, 148.
Saxena, S. C. and Dave, S. M., 1963a, *Mol. Phys.*, **6**, 61.
Saxena, S. C. and Dave, S. M., 1963b, *Ind. J. Phys.*, **37**, 111.
Saxena, S. C., Dave, S. M., and Pardeshi, P. A., 1962, *Canadian J. Phys.*, **40**, 1608.
Saxena, S. C. and Joshi, R. K., 1963a, *J. Phys. Soc. Japan*, In press.
Saxena, S. C. and Joshi, R. K., 1963b, to be published.

COHESIVE ENERGIES OF ALKALI HALIDES

R. V. GOPALA RAO, H. V. KEER AND C. DEENADAS

NATIONAL CHEMICAL LABORATORY, POONA-8 (INDIA)

(Received June 22, 1962, Resubmitted Dec 17, 1962)

The principal interactions in ionic lattices which are Coulomb interaction, van der Waals' interaction and overlap force, are two body forces. In the case of simple ions possessing spherical symmetry and rare gas structures, the cohesive energy can be represented as a function of their distance apart. For the ionic crystals a number of observable properties can be calculated using a bi-reciprocal Lennard-Jones potential function coupled with a coulombic term. Recently the cohesive energies of ionic crystals have been calculated (Sharma and Madan, 1961) using a (12 · 6) potential function. It was pointed out that the discrepancy with the experimental data was more pronounced for lighter alkali halides. Hence the authors presently aim to propose an appropriate (9:6) potential function for such alkali halides. This is reasonable in the light of the fact that the values of the repulsion constant 'n' obtained by Pauling's rules (1927, 1928) derived from a theoretical treatment of the interaction of closed shell electronic configurations, lie in the vicinity of 9 (Sherman, 1932).

Hence the energy per cell is represented by

$$\phi_{(r)} = -\frac{\alpha e^2}{r} + \frac{B}{r^9} - \frac{C}{r^6} + \epsilon_0 \quad \dots (1)$$

where α is the Madelung's constant, e is the electron charge, r is the distance between closest ion centres and ϵ_0 is the zero point energy. B and C are the coefficients for repulsive and van der Waals terms.

Here interactions between dipole-quadrupole and other than the nearest neighbours are neglected as their contribution is very small.

By the use of thermodynamic relations it can be easily shown that first and second derivatives of lattice energy can be expressed in terms of directly observable quantities. The equations are :

$$\frac{d\phi_{(r)}}{dr} = \frac{3vT}{r\beta} \left(\frac{1}{V} \cdot \frac{\partial V}{\partial T} \right)_P \quad \dots (2)$$

$$\frac{d^2\phi_{(r)}}{dr^2} = \frac{9v}{r^2\beta} \left[1 + \frac{T}{\beta} \left\{ \left(\frac{\partial \beta}{\partial T} \right)_P + \frac{1}{V} \left(\frac{\partial V}{\partial T} \right)_P \frac{1}{\beta} \left(\frac{\partial \beta}{\partial P} \right)_T \right\} + \frac{2T}{3V} \left(\frac{\partial V}{\partial T} \right)_P \right] \dots (3)$$

TABLE I
Cohesive energy in K. Cal/mole

Compound	Repulsion constant	Experimental	Calculated (present work)	Calculated (12 : 6)	
LiF	6.0	246 ^a	264.6	273.1	246.8
NaF	7.0	218 ^a	227.3	236.6	218.7
LiCl	7.0	201.5 ^b	199.8	212.6	202.0
LiBr	7.5	191.5 ^b	189.9	200.0	190.7
NaCl	8.0	184.0 ^a	182.8	192.8	185.9
KF	8.0	193.0 ^a	195.8	205.8	194.4
LiI	8.5	180.0 ^a	174.8	184.3	176.8
NaBr	8.5	176.1 ^b	172.1	182.1	176.7
RbF	8.5	—	177.9	191.6	185.9
KCl	9.0	167.8 ^a	163.8	174.1	169.4
NaI	9.5	166.0 ^a	159.3	168.8	165.4
KBr	9.5	160.0 ^a	154.8	164.8	162.4
RbCl	9.5	162.0 ^a	155.8	166.8	164.0
RbBr	10.0	157.0 ^a	149.6	159.1	157.5
KI	10.5	152.0 ^a	145.0	155.0	153.0
<hr/>					
a. Plondl (1961)	b. Born and Huang (1954)		c. Cubicciotti (1961)		

Using Equation (3) the repulsive parameter B can be evaluated and hence the cohesive energy. The experimental data used have been taken from Huggins (1937), Seitz (1940) and Spangenberg (1956), Spangenberg *et al.* (1957). The values of cohesive energy are compared with the observed values and also with other determinations. The values calculated with (12 : 6) potential function are also given. All values are listed in Table I.

In the case of lighter halides, the ' n ' value is less than the assumed value of 9. Thus for the lightest one, namely LiF, the ' n ' value is around 6 (Sherman, 1932) and hence cohesive energy is higher. Better agreement can be obtained using the value of ' n ' as 7. As we go down the group of alkali halides the agreement becomes better. This is explicable since in all these cases, the ' n ' values are either 9 or very near 9. For heavier crystals, the calculated values are lower and the discrepancy increases as we proceed towards still heavier compounds. Incidentally the ' n ' value increases to 10.5 and (12 : 6) potential function becomes more appropriate.

The authors are grateful to Dr. A. B. Biswas for his interest in this work and one of us (C. Deenadas) to the Council of Scientific and Industrial Research, New Delhi for the award of a Junior Research Fellowship.

REFERENCES

- Born and Huang, 1954, *Dynamical Theory of Crystal Lattices*, 26
Cubicecotta, D., 1961, *J. Chem. Phys.*, **34**, 2189.
Huggins, M. L., 1937, *J. Chem. Phys.*, **5**, 143
Pauling, L., 1927, *Proc. Roy. Soc.*, **114**, 181.
1927, *J. Am. Chem. Soc.*, **49**, 765.
1928, *Z. Krist.*, **67**, 377.
Plendl, J. N., 1961, *Phys. Rev.*, **123**, 1174.
Seitz, F., 1940, *The Modern Theory of Solids*, 88.
Sharma, M. N. and Madan, M. P., 1961, *Ind. J. Phys.*, **35**, 596.
Sherman, J., 1932, *Chem. Rev.*, **11**, 93.
Spangenberg, K., 1956, *Naturwissenschaften.*, **43**, 394.
Spangenberg, K. and Haussuhl S., 1957, *Z. Krist.*, **109**, 422.

CONTENTS

Indian Journal of Physics

Vol. 37, No. 4

April, 1963.

PAGE

19. Effect of Ionic Currents on Heat-Transfer—S. C. Bhand, M. S. Gaur and D. V. Gogate	185
20. A Study on the Discharge of Condenser Using A Transistorized Blocking Oscillator—R. R. Dutta Gupta	191
21. Gamma-Gamma Coincidences in Pd^{106} —R. Bhattacharyya	209
22. A Circuit for a Self-Strobed Reading Method in Magnetic Drum Digital Stores—D. Dutta Majumdar and R. Biswas	215
23. Detection of Invariance, Total Symmetry and Partial Symmetry of Switching Functions—Sunil Ranjan Das	214

LETTER TO THE EDITOR :

2. Hydrogen Bonding in N-Methyl Formamide—K. Venkata Ramiah and P. G. Puranik	233
3. Simpler Formulae for the Chapman-Cowling Second Approximation to the Thermal Diffusion Factor of Binary Gas Mixtures with either of the Components in Trace—S. C. Saxena and R. K. Joshi	235
4. Cohesive Energies of Alkali Halides—R. V. Gopala Rao, H. V. Keer and C. Deenadas	238

Regd. No. C-3911

VOL. 37

INDIAN JOURNAL OF PHYSICS

No. 5

(Published in collaboration with the Indian Physical Society)

AND

VOL. 48

PROCEEDINGS

No. 5

OF THE

**INDIAN ASSOCIATION FOR THE
CULTIVATION OF SCIENCE**

MAY 1963

**PUBLISHED BY THE
INDIAN ASSOCIATION FOR THE CULTIVATION OF SCIENCE**

JADAVPUR, CALCUTTA 35

BOARD OF EDITORS

K. BANERJEE	D. S. KOTIARI
D. M. BOSE	S. K. MITRA
S. N. BOSE	B. D. NAG CHAUDHURI
S. D. CHATTERJEE	K. R. RAO
P. S. GILL	D. B. SINHA
S. R. KHASTGIR	S. C. SIRKAR (Secretary)
B. N. SRIVASTAVA	

EDITORIAL COLLABORATORS

PROF. R. K. ASUNDI, Ph.D., F.N.I.
 PROF. D. BASU, Ph.D.
 PROF. J. N. BHAB, D.Sc., F.N.I.
 PROF. V. G. BHIDE, Ph.D.(Nag), Ph.D.(Lond).
 PROF. A. BÖSE, D.Sc., F.N.I.
 PROF. S. K. CHAKRABARTY, D.Sc., F.N.I.
 DR. J. S. CHATTERJEE
 DR. K. DAS GUPTA, Ph.D.
 PROF. N. N. DAS GUPTA, Ph.D., F.N.I.
 DR. J. DEAR, D.Phil (So)
 PROF. A. K. DUTTA, D.Sc., F.N.I.
 PROF. C. S. GHOSH, M.Sc., S.M., F.N.I.,
 M.I.E.E.
 PROF. S. GHOSH, D.Sc., F.N.I.
 PROF. S. N. GHOSH, D.Sc.
 PROF. S. GUPTA, M.Sc., F.N.I.
 PROF. D. N. KUNDU, Ph.D., F.N.I.
 PROF. R. C. MAJUMDER, Ph.D., F.N.I.
 PRINCIPAL Y. G. NAIK, Ph.D.
 PROF. S. R. PALIT, D.Sc., F.R.I.C., F.N.I.
 PROF. H. RAKSHIT, D.Sc., F.N.I.
 PROF. A. SAHA, D.Sc., F.N.I.
 DR. VIKRAM A. SARABHAI, M.A., Ph.D., F.N.I.
 DR. A. K. SENGUPTA, D.Sc.
 PROF. NAND LAL SINGH, D.Sc.
 DR. M. S. SINHA, D.Sc., F.N.I.
 PROF. N. R. TAWDE, Ph.D., F.N.I.
 DR. P. VENKATESWARLU

NOTICE

TO INTENDING AUTHORS

Manuscripts for publication should be sent to the Assistant Editor, Indian Journal of Physics, Jadavpur, Calcutta-32.

The manuscripts submitted must be type-written with double space on thick foolscap paper with sufficient margin on the left and at the top. The original, and not the carbon copy, should be submitted. Each paper must contain an abstract at the beginning.

All references should be given in the text by quoting the surname of author, followed by year of publication, e.g., (Ghosh, 1954). The full reference should be given in a list at the arranged alphabetically, as Ghosh, D. K., 1954, *Ind. J.* 485.

Line diagrams should be drawn on white Bristol board or tracing paper with black India ink, and letters and numbers inside the diagrams should be written neatly in capital type with India ink. The size of the diagrams submitted and the lettering inside should be large enough so that it is legible after reduction to one-third the original size. A simple style of lettering such as gothic, with its uniform line width and no serifs should be used, e.g.,

A·B·E·F·G·M·P·T·W·

Photographs submitted for publication should be printed on glossy paper with somewhat more contrast than that desired in the reproduction, and should, if possible, be mounted on thick white paper.

Captions to all figures should be typed in a separate sheet and attached at the end of the paper.

The mathematical expressions should be written carefully by hand. Care should be taken to distinguish between capital and small letters and superscripts and subscripts. Repetition of a complex expression should be avoided by representing it by a symbol. Green letters and unusual symbols should be identified in the margin. Fractional exponents should be used instead of root signs.

Annual Subscription

Inland Rs. 25.00

Foreign £ 2-10-0 or \$ 7.00

BENGAL CHEMICAL & PHARMACEUTICAL WORKS LD.

Pioneer Indian Manufacturers of Pharmaceuticals & Chemicals.

Manufacturers of:

Pharmaceutical Chemicals:

Nicotinic Acid, B.P., Nicotinamide, B.P., Caffeine and its salts, Strychnine Hydrochlor, Strychnine Sulphate, Brucine Sulphate, Potassium Citrate B.P., I.P., Sodium Citrate B.P., I.P., Potassium Acetate B.P., I.P., Potassium Iodide B.P., I.P., Sodium Iodide B.P., I.P., Ferri et Ammon Citrate B.P., I.P., and various other Pharmaceutical Chemicals.

Heavy & Reagent Quality Fine Chemicals:

Alum, Alum Sulphate (Iron Free), Ferro Alum, Zinc Chloride Tech. Naphthalene Pure, Sodium Citrate A.R., Potassium Citrate A.R., Magnesium Sulphate A.R., Sodium Sulphate Anhydrous A.R., Potassium Iodide A.R., Sodium Chloride A.R., Zinc Sulphate A.R., etc.

Please refer your enquiries for the above items and other chemicals in the line to :—

BENGAL CHEMICAL

6, GANESH CHUNDER AVENUE,
CALCUTTA-13, INDIA.

B O R O S I L**LABORATORY GLASSWARE**

such as

FLASKS, BEAKERS, CONDENSERS, MEASURING FLASKS, MEASURING CYLINDERS,
PIPETTES & ANY SPECIAL APPARATUS MADE TO DESIGN

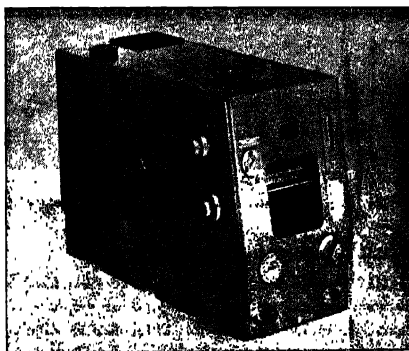
and

PENICILIN VIALS, VACCINE BULBS—WHITE & AMBER

•
ALL OTHER APPARATUS & EQUIPMENT MANUFACTURED TO CLIENT'S DESIGN

**INDUSTRIAL & ENGINEERING APPARATUS CO.
PRIVATE LIMITED**

CHOTANI ESTATES, PROCTOR ROAD, GRANT ROAD, BOMBAY 7

ZEISS Mirror Monochromator "SPM 2"

- * Represents a high quality new development in the field of optophysical measuring instruments.
- * It combines versatility of application with simplicity of operation.
- * It can be used for the production of monochromatic radiation in the wavelength region from 0.193 to 40 microns by using interchangeable prisms and diffraction grating.
- * The respective wavelength scale can be read in projection.



VEB Carl Zeiss JENA
(German Democratic Republic)

Sole Agents in India :

GORDHANDAS DESAI PRIVATE LIMITED

PHEROZSHAH MEHTA ROAD, BOMBAY 1

Branches at :

**22, Linghi Chetty Street,
MADRAS 1.**

**F/7, Mission Row Extension,
CALCUTTA 1.**

**4/2B, Asaf Ali Road,
NEW DELHI 1.**



Our systems for gathering and processing measuring data and for automatic process control permit the full automation of metallurgical processes provided that the process control system is compatible with future automation

Progressive Process Control for Soak-Pit Furnaces

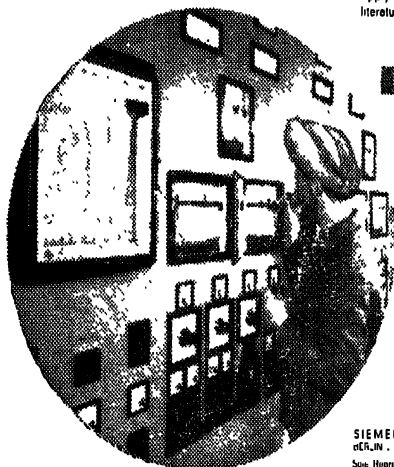
prevents irregular heating and excessive scaling of blooms and ingots. Our electrically operating TELEPERM process control system

has long proved its value in all process problems connected with soak-pit furnaces

Control of chamber temperature, fuel air ratio, chamber pressure

Accommodated in a metal-clad cabinet, the equipment is immune to changes in temperature, power supply fluctuations, frequency deviations, impact, furnace dust and moisture

Apply to our nearest branch or agency for detailed literature and consultation



SIEMENS & HALSKE AKTIENGESellschaft
G.R.M. - MÜNCHEN

Sole Representatives
SIEMENS ENGINEERING & MANUFACTURING
CO. OF INDIA LTD

Bombay . Calcutta . New Delhi . Madras . Bangalore
Visakhapatnam . Ahmedabad . Lucknow . Nagpur
Hyderabad . Trivandrum . Rourkela . Patna

HARSHAW MATCHED WINDOW LINES SINTILLATION DETECTOR



The HARSHAW MATCHED WINDOW LINE thallium activated Sodium iodide crystal assembly is a Scintillation Detector using 3" diameter photomultiplier tubes to view crystals 4" diameter and larger. The advantages of this assembly are : Better energy resolution through improved optical design of the detector system ; System performance is guaranteed since the tubes used are specified ; Elimination of optical coupling problem ; light-tight and ready for plug-in operation ; keeps absorption and scattering to a minimum ; Phototubes are replaceable in the field.

For further details, please write to :

The Sole Distributors :



THE SCIENTIFIC INSTRUMENT COMPANY, LIMITED.

6, Tej Bahadur Sapru Road,
ALIAHABAD

B-7, Ajmere Gate Extn.
NEW DELHI-1

240, Dr. D. Naoroji Road,
BOMBAY

11, Esplanade East,
CALCUTTA

30, Mount Road,
MADRAS

A FOUR-POINT PROBE FOR RESISTIVITY MEASUREMENTS OF SEMICONDUCTORS

J. K. D. VERMA

SAHA INSTITUTE OF NUCLEAR PHYSICS, CALCUTTA

(Received August 20, 1962)

ABSTRACT. The constructional details of a four-point probe for resistivity determination of semi-conductors are given. The method for electrolytic pointing of tungsten wires used in the probe is also described.

INTRODUCTION

The knowledge of resistivity of semiconductors is essential in determining their suitability for fabricating semiconductor devices and hence the need arises for making accurate measurement of resistivity. The rectifying nature of the contacts and the minority carrier injection by one of the current contacts are some of the faults generally encountered in the conventional methods. Valdes (1954) has described a method in which these difficulties have been overcome and offers in addition several other advantages. The one principal advantage is that one does not require any special specimen geometry and permits measurement of resistivity of small volumes within bigger bulk semiconducting material.

The method consists in placing four sharp metal points in a line on a flat surface of the semiconducting material to be measured, passing a current, I (amp), through the two outer electrodes and measuring the voltage, V (volts), across the two inner ones (Fig. 1). Valdes (1954) has discussed the various modes of place-

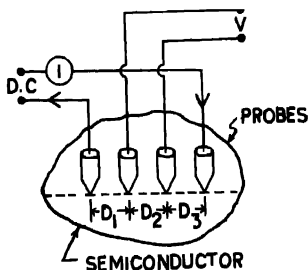


Fig. 1. Arrangement for four probe resistivity measurement

ment of probes and has shown that with certain assumptions, the resistivity in the case of a large sample is given by

$$\rho = \frac{V}{I} \cdot \frac{2\pi}{\left(\frac{1}{D_1} + \frac{1}{D_3} - \frac{1}{D_1 + D_3} - \frac{1}{D_2 + D_4} \right)} \quad \dots (1)$$

where ρ = resistivity, in ohm-cm.

D_1, D_2, D_3 = point spacing, in cm.

When the probe spacing is equal, that is $D_1 = D_2 = D_3$, the above equation simplifies to

$$\rho = 2\pi D \cdot \frac{V}{I} \quad \dots (2)$$

THE PROBE UNIT

Because of the frequent need for making resistivity measurements, the probe unit should be so designed as to permit making quick measurements and, furthermore, the whole unit should be simple in construction. Such a unit has been constructed in this institute and the details are reported here (Fig. 2). The unit is similar to one reported by MacDonald *et al*, (1953) but differs in the method of varying the contact pressure of the metallic points against the semiconductor.

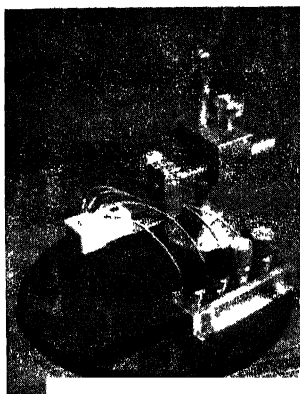


Fig. 2 Photograph of four-probe resistivity measuring instrument.

The unit consists of two parts : (i) A head which supports the tungsten wires and (ii) a pivotal arrangement by means of which pressure contacts on the semiconductor surface is achieved.

The head is made of Teflon because of its high resistance, low humidity absorption, low coefficient of friction, and excellent machining properties. It has four equally spaced holes into which tight fitting 20 mil (0.020 inch) tungsten wire have been inserted. The spacing between the tungsten points is 1.630 ± 0.015 mm.

The head is mounted on an arm which is hinged at the opposite end (Fig. 3). A smooth and regular variation of contact pressure of tungsten wires against the semiconductor surface is manipulated by means of a screw head. MacDonald

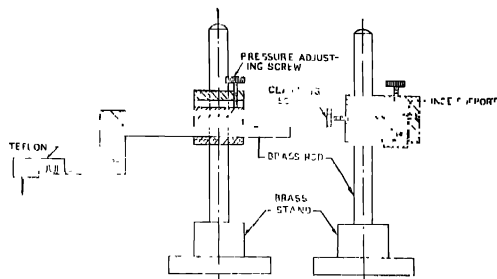


Fig. 3. Line diagram of the probe unit.

et al (1953) have used in their instrument a sliding weight on the hinged arm to vary the contact pressure. The arm supporting the head is in turn mounted on and can slide along a vertical supporting rod. This arrangement facilitates working with samples of different sizes.

ELECTROPOINTING OF WIRES

The tungsten wires in the Teflon head are to be provided with conical points. To obtain wires of equal length and sharpness, an electrolytic technique for pointing, described by Pfann (1947), is employed. By this method it is possible to produce points of any desired degree of sharpness on tungsten and, furthermore by a suitable choice of electrolytes, cathode materials and working voltages, the method can be extended to a variety of metals. The electropointing circuit is shown in Fig. 4, which is self explanatory.

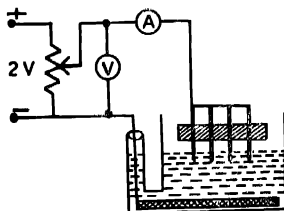


Fig. 4. Electropointing circuit.

The electrolyte is an aqueous solution of potassium hydroxide. While the concentration of potassium hydroxide is not critical and can be varied between 10% and 50%, a 38% concentration has been used in the present work.

The pointing time and the shut off current are only affected by the concentration, the pointing time being smaller for higher composition. The volume of the electrolyte is also immaterial in this particular case. A small quantity of copper in the form of cupric chloride is added to the electrolyte. The quantity of cupric chloride is also variable but the copper content should not exceed 1.1 mg per cc. The purpose of adding copper is two fold. Firstly, it makes the meniscus cling firmly to the wire in position which could otherwise be disturbed due to slightest vibration and secondly, to help in reforming the cathode coating rapidly which is depleted during pointing action.

The cathode is a copper sheet which is previously aged for several days in the electrolyte to form an appreciable coating of copper oxide, so as to make the cathode self-depolarizing. This is desirable to prevent gassing during pointing which may otherwise disturb the menisci, as is usually the case with clean copper cathode. To conserve the cathode coating, it is necessary to maintain an upper current limit. This is done by keeping the ratio of wetted tungsten area to cathode area below 0.01.

The arm holding the Teflon head is lowered until the wires are immersed in the electrolyte to a depth of about 5 mm. The positioning of the vessel containing electrolyte is essential to obtain wires of same length after pointing.

ACKNOWLEDGMENTS

It is a pleasure to thank Dr. B. D. Nag Chaudhuri, Director of the Institute for his keen interest. Thanks are also due to Mr. B. C. Purakayastha for his helpful suggestions regarding electropointing of tungsten wires.

REFERENCES

- MacDonald, A. L., Soled, J. and Stearns, C. A., 1953, *Rev. Sci. Instrum.*, **24**, 884.
- Pfann, W. G., 1947, *Metals Technol.*, **14**, 606.
- Valdes, L. B., 1954, *Proc. IRE*, **42**, 420.

ON THE SELECTIVITY OF A RESISTANCE CAPACITANCE NETWORK

S. C. DUTTA ROY*

ELECTRONICS SECTION, RIVER RESEARCH INSTITUTE, WEST BENGAL

(Received June, 1961; Resubmitted April 17, 1962)

ABSTRACT. A resistance capacitance network, used in circuits for generation (Wien bridge oscillator) and measurement (Wien bridge) of low frequencies, has been analysed for the maximum selectivity condition by defining a design parameter n . It has been shown that a lower value of n gives (i) a more selective response and as such, a purer waveform in the oscillator circuit and a sharper null point in the Wien bridge circuit and (ii) a more favourable condition of operation of the active device in the oscillator circuit. The effect of cascading such networks on the selectivity of the resultant transfer characteristic has been discussed. The effect of interchanging the series and the shunt arms of the network has been considered. It has been shown that if n is high, the resulting network has a characteristic similar to that of a Wien bridge and is superior to the latter in some respects.

INTRODUCTION

The RC network shown in Fig. 1(a) is used in a vacuum tube oscillator circuit for generation and in the Wien bridge circuit for measurement of low frequencies while its current dual shown in Fig. 1(b) is used in a low frequency transistor oscillator. In such applications, it has been conventional to use $R_1 = R_2$ and $C_1 = C_2$; under these conditions, the network has a Q (Morris, 1954) equal to 0.33 only. In this paper, the effect of unequal elements on the selectivity of the transfer characteristic has been investigated. By defining a design parameter n as $n = (R_2/R_1)^{1/2} = (C_1/C_2)^{1/2}$, it has been found that the increase in Q is of the order of 50 % for very small values of n . Thus using a small n , a purer waveform can be obtained in the oscillator circuit and a sharper null point in the Wien bridge circuit. It is also found that using a small value of n ensures a better operating condition for the active device in the oscillator circuit.

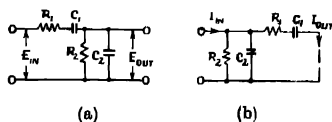


Fig. 1.—The RC networks under consideration. The network (b) is the current dual of the network (a).

It is known that properly cascading two selective networks having the same resonance frequency yields a response characteristic that is more selective than

* Present address: Department of Physics, University of Kalyani, Haringhata, P.O. Mohanpur, Dist. Nadia, West Bengal.

the response of either network. Thus a still better waveform can be obtained in the Wien bridge oscillator if a cascade of two or more RC networks of the form of Fig. 1 is used as the frequency selective network. The conditions and effects of proper cascading are discussed in this paper.

Finally, the networks obtained by interchanging the series and shunt arms of the networks of Fig. 1 have been studied. It has been found that by properly choosing n , these networks have a characteristic similar to that of a Wien bridge and that in some respects, they possess some advantages over the Wien bridge.

ANALYSIS OF THE RC NETWORK

Driven by an ideal voltage generator and working into an open circuited load, the network of Fig. 1(a) has a voltage transfer function given by

$$\beta = \frac{1}{1 + \frac{C_1 R_1 + C_2 R_2}{C_1 R_2} + p C_2 R_1 + \frac{1}{p C_1 R_2}} \quad \dots (1)$$

where $p = j\omega$, ω being the frequency in radians/sec. The above expression also represents the current transfer function of the network of Fig. 1(b) when an ideal current generator is connected across the input terminals and the output terminals are short circuited. From (1), the resonance frequency is given by

$$\omega_0^2 = \frac{1}{C_1 C_2 R_1 R_2} \quad \dots (2)$$

Let us define a design parameter n as follows

$$n = (R_2/R_1)^{1/2} = (C_1/C_2)^{1/2}$$

Then the components of the networks of Fig. 1 can be expressed in terms of a resistance parameter R , a capacitance parameter C and n as follows :

$$R_1 = R/n, \quad R_2 = nR, \quad C_1 = nC \quad \text{and} \quad C_2 = C/n \quad \dots (3)$$

From (2) and (3), we have $\omega_0 = 1/(RC)$. Thus a variation of n will have no effect on ω_0 . Also from (1) and (3), we have,

$$\beta = \frac{1}{1 + (2 + n^2)u + u^2} \quad \dots (4)$$

where $u = pCR$. Applying Morris' definition of Q , we have from (4),

$$Q = \frac{1}{n^2 + 2} \quad \dots (5)$$

For the conventional circuit, $n = 1$ so that $Q = 0.33$. Expression (5) shows that Q can be increased above this value by decreasing n , a maximum value of

0.50 being reached when n tends to zero. At the resonance frequency, $u = j$ so that from (4), the resonant response is given by

$$\beta_0 = \frac{n^2}{n^2 + 2} \quad \dots (6)$$

At $n = 1$, $\beta_0 = 1/3$; as n decreases, β_0 also decreases and tends to zero when n tends to zero. This is not, however, very important because it only means that the gain (open loop voltage gain or the short circuit current gain according as the network of Fig. 1(a) or (b) is used) of the oscillator circuit has to be increased by the proper amount. Thus at $n = 0.30$, $\beta_0 = 0.04$; if this network is used in an oscillator, the minimum gain required for oscillations to occur is 25, a value which is not at all difficult to be realised with two stages of amplification as used in such oscillators. The improvement in Q is however as much as 45%. Fig. 2 shows the variations of Q and β_0 with n .

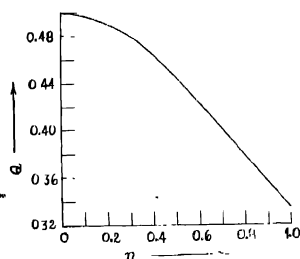


Fig. 2. (a) Showing the variation of Q with n

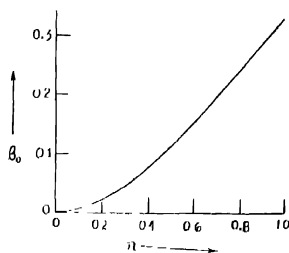


Fig. 2. (b) Showing the variation of β_0 with n

In a vacuum tube Wien bridge oscillator, the input terminals of the network of Fig. 1(a) are connected across the plate to cathode of the second valve while the output terminals are connected across the grid to cathode of the first valve of a two stage RC coupled amplifier. It is thus desirable that the output impedance of the second valve should be negligible compared with the input impedance of the network and the input impedance of the first valve should be very high compared with the output impedance of the network. Since the grid to cathode impedance of a vacuum tube is normally very high, the second condition is usually satisfied in practical circuits. But, with the conventional RC network ($n = 1$), the first condition cannot always be satisfied. This results in (i) loading of the second valve and therefore, reduction of the available gain from this stage and (ii) a deviation of the frequency from the design value $1/(RC)$. In a precision variable frequency oscillator, it is highly desirable that the frequency should be controlled by the elements of the RC network only so that the latter effect has

to be annulled by the use of a compensating resistance placed between the cathodes of the two valves (Davidson, 1952).

The input impedance of the RC network of Fig. 1(a) with the elements given by equations (3), is

$$Z_{in} = R \frac{(u+1)^2 + n^2 u}{nu(u+1)} \quad \dots (7)$$

For the conventional network, $n = 1$ so that

$$Z_{i1} = R \frac{(u+1)^2 + u}{u(u+1)}$$

Therefore,

$$r = \frac{Z_{in}}{Z_{i1}} = \frac{(u+1)^2 + n^2 u}{n\{(u+1)^2 + u\}}$$

At the resonance frequency, $u = j$ so that

$$r_0 = \frac{n^2 + 2}{3n} \quad \dots (8)$$

Equation (8) shows that r_0 increases as n decreases. If $n = 0.1$ then $r_0 = 6.7$; this increased input impedance ensures a better operating condition of the second valve and a less deviation of the frequency from the value $1/(RC)$. If a sufficiently small n can be used, then the use of a compensating resistance can be avoided.

In a transistor oscillator using the network of Fig. 1(b) the network will, in general, reduce the available current gain of the second transistor and will cause a departure of the frequency from the value $1/(RC)$. This latter effect is more important as the transistor parameters vary considerably with the various d.c. voltages and with frequency. It is thus desirable that the input impedance of the network should be small compared with the output impedance of the second transistor and the output impedance of the network should be large compared with the input impedance of the first transistor.

With the elements given by equations (3), the input impedance of the network of Fig. 1(b) is

$$Z'_{in} = R \frac{n(u+1)}{n^2 u + (u+1)^2}$$

For the conventional network,

$$Z'_{i1} = R \frac{(u+1)}{u + (u+1)^2}$$

so that

$$r' = \frac{Z'_{in}}{Z'_{i1}} = \frac{n\{u + (u+1)^2\}}{n^2u + (u+1)^2}$$

and at resonance,

$$r'_0 = \frac{3n}{n^2 + 2}$$

Thus r'_0 decreases with decreasing n and approaches zero as n tends to zero. At $n = 0.1$, r'_0 has a value 0.149. Also Z'_{n0} , the output impedance of the network of Fig. 1(b) is the same as Z_n given by equation (7). Thus at resonance, the ratio Z'_{on}/Z'_{o1} will be the same as r_0 given by equation (8), which increases with decreasing n .

Thus we conclude that a lower value of n gives a higher selectivity and a more favourable operation of the oscillator circuit with either vacuum tubes or transistors as the active elements. This improvement is obtained at the cost of an increased gain of the active elements.

USE IN THE WIEN BRIDGE

Fig. 3 shows the network of Fig. 1(a) with elements given by equations (3), inserted in the two arms of a Wheatstone's bridge the other arms of which are formed by resistances whose values are so chosen that null occurs at a frequency $1/(CR)$. The transfer function of the bridge is given by

$$\begin{aligned} i &= \frac{n^2}{n^2+2} - \frac{n^2}{(n^2+2) + u + 1/u} \\ &= \frac{n^2}{n^2+2} \cdot \frac{u^2 - 1}{u^2 + (n^2+2)u + 1} \end{aligned}$$

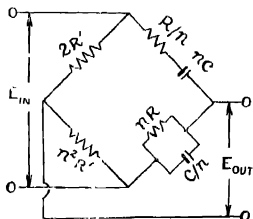


Fig. 3. The Wien bridge.

Thus Q of the network is the same as that given by equation (5). The maximum response of the network occurs at $u = 0$ and at $u = \infty$ and is given by equation

(6). Thus a small value of n gives a sharper null point, but since the maximum response of the network is reduced, the amplifier in the detector circuit has to be more sensitive or the input voltage is to be raised by the proper amount.

EFFECT OF CASCADING

For the construction of a fixed frequency oscillator, if the available gain of the amplifier is considerably greater than the required value, it will be convenient to use a cascade of two or more RC networks of the form of Fig. 1. The resulting circuit will give a better waveform than that obtained with a single network. Cascading of more than two sections will not however be practical as the output will then be heavily attenuated. For a proper cascading of the networks of the form of Fig. 1(a), the output impedance of the first network should be small compared to the input impedance of the second network, while if the networks are of the form of Fig. 1(b), the reverse should be true. The following analysis shows that in a cascade of two networks of the form of Fig. 1(a) or (b) with the same values of n and ω_0 , the above conditions are satisfied if n is less than 0.5.

The transfer function of the cascaded network is

$$\beta_2 = \frac{Z_2^2}{Z_1 Z_2 + (Z_1 + Z_2)^2} = \frac{\beta^2}{1 + \Delta}$$

where β is the transfer function of a single network given by equation (4), Z_1 and Z_2 are the impedances of the series and the shunt arms of a single network and $\Delta = Z_1 Z_2 / (Z_1 + Z_2)^2$ is a measure of the loading of the first stage by the second. Now,

$$\Delta = \frac{Z_1 Z_2}{(Z_1 + Z_2)^2} = \frac{Z_1}{Z_2} \beta^2 = \frac{(u+1)^2}{n^2 u} \beta^2$$

At a frequency given by $u = j$,

$$\Delta = \frac{2n^2}{(n^2 + 2)^2}$$

At $n = 0.5$, $\Delta = 0.099$ so that for $n < 0.5$, $\beta_2 \simeq \beta^2$. Combining this with (4) gives

$$\beta_2 \simeq \frac{\{n^2/(n^2 + 2)\}^2}{\{1 + j(x - 1/x)/(2 + n^2)\}^2} \quad \dots (9)$$

where $x = \omega CR = \omega/\omega_0$ is the normalised frequency. The response at resonance is given by $\beta_{20} = \{n^2/(n^2 + 2)\}^2$. Morris' definition is not applicable here. However, for a resonance curve the definition of Morris gives the same value of Q as that obtained from the conventional definition, viz., $Q = \omega_0/(\omega_1 - \omega_2) = 1/(x_1 - x_2)$, where ω_1 and ω_2 are the frequencies at which the response is 70.7% of that at

resonance. Applying this definition to (9), it can be shown that Q of the cascaded network is given by

$$Q_2 = \frac{1.53}{n^2 + 2} = 1.53Q$$

If $n = 0.1$, then $Q_2 = 0.76$ which is nearly equal to its maximum value 0.765.

EFFECT OF INTERCHANGING THE ARMS

If the series and the shunt arms of the networks of Fig. 1 are interchanged, the transfer function of the resulting network will be given by

$$\beta' = \frac{Z_1}{Z_1 + Z_2} = \frac{n^2 + 2n + 1}{n^2 + (2 + n^2)n + 1}$$

Thus again, $Q = 1/(2 + n^2)$. In terms of the normalised frequency,

$$\beta' = \frac{(1 - x^2) + 2jx}{(1 - x^2) + (2 + n^2)jx}$$

This shows that β' has a maximum value of unity at both $x = 0$ and $x = \infty$ and a minimum value of $2/(2 + n^2)$ at $x = 1$. Thus the network characteristic is similar to that of a Wien bridge excepting that the minimum response is not zero. β' can be made to approach zero by using a large value of n , but then the selectivity will be poor. If a compromise is made between the two, then the network can be used for measurement of low frequencies. With a high impedance detector (e.g. a vacuum tube amplifier-rectifier arrangement), the network of Fig. 1(a) with interchanged arms will be suitable for measuring the frequency of a low impedance source (e.g. a vacuum tube oscillator). With a low impedance detector (e.g. a transistor amplifier-rectifier arrangement), the network of Fig. 1(b) with interchanged arms will be suitable for measuring the frequency of a high impedance source (e.g. a transistor oscillator). In this application, the networks under consideration have the advantages over a Wien bridge of (i) requiring a less number of components, (ii) possessing a common input and output terminal thus avoiding the necessity of using a balance to unbalance transformer, and (iii) a simpler layout.

ACKNOWLEDGMENTS

The author is indebted to Dr. A. K. Choudhury, M.Sc., D.Phil. for his kind help and guidance. The paper is published with the kind permission of the Director, River Research Institute, West Bengal.

REFERENCES

- Davidson, J. A. B., 1952, *Proc. I.E.E.*, **40**, 1124
 Morris, D., 1954, *Electronic Engineering*, **26**, 306.

SINGLET→TRIPLET ABSORPTION IN FROZEN *p*-BROMOTOLUENE

A. R. PAUL AND S. C. SIRKAR,

OPTICS DEPARTMENT

INDIAN ASSOCIATION FOR THE CULTIVATION OF SCIENCE,
CALCUTTA-32.

(Received January 7, 1963)

ABSTRACT. The absorption spectra in the near ultraviolet region of a frozen transparent mass of *p*-bromotoluene of thickness 7.0 mm and of a frozen 12% solution of the compound in methyl cyclohexane at -180°C of thickness 45 mm have been investigated. In each case three sharp bands at 4045 Å, 3812 Å and 3603 Å have been observed. By comparing this spectrum with the luminescence spectrum of the substance at -180°C it has been shown that in absorption the transition from the ground singlet state to the triplet state coupled to an excited vibration state is predominant and that the data lead to the values 1590 cm^{-1} and 1516 cm^{-1} respectively for the ground state and triplet state vibration frequencies of the molecule. It is pointed out that in the luminescence spectrum of the substance at -40°C the 0,0 transition is absent and that the vibration mentioned above is coupled to the transition in the luminescence.

INTRODUCTION

It was observed by Sanyal (1953) while studying the Raman spectra of ortho- and para-chlorotoluene that these compounds in the solid state at -180°C produce strong luminescence bands in the visible region. Biswas (1956a, 1956b) repeated the investigation and also extended it to ortho- and para-bromotoluene, using mainly the 3650 Å group of mercury lines as the exciting radiation. He observed a large number of bands in each case, but the separation of successive bands could not be explained satisfactorily by him. He further showed (Biswas, 1958) that the luminescence is actually an afterglow of short duration. Later, Roy (1959) showed that the luminescence of *p*-chlorotoluene disappears when the wavelength of the exciting radiation becomes greater than 3750 Å. It was, therefore, concluded that the luminescence was produced by absorption of radiation by transition from the singlet to the triplet state and then by re-emission of the absorbed energy. He further tried to find out whether there was discrete absorption bands in the near ultraviolet region in the absorption spectra of these compounds in the liquid state and observed (Roy, 1960) that in the liquid state *m*-fluorotoluene, *p*-chlorotoluene and *o*-bromotoluene show only continuous absorption on the longer wavelength side of the region near 3300 Å, where the absorption in benzene is very weak and that the region of absorption shifts towards longer wavelengths as the atomic weight of the substituent halogen atom

increases. In order to find out whether this continuous absorption was a property of the liquid state of the compounds Sirkar and Roy (1960) studied the absorption spectra of benzene and *o*-bromotoluene in the vapour state with a path length of 18.90 metres at pressures of about 120 mm and 55 mm of Hg respectively and in the liquid state having equivalent path lengths. They observed that even in the vapour state with a path length equivalent to 7 mm of the liquid, *o*-bromotoluene exhibits continuous absorption in the region from 3400 Å to 3500 Å and that the strength of this absorption due to an equivalent thickness of the liquid is much larger than that in the vapour. Benzene on the other hand shows very little absorption in this region and not much difference is observed between the spectra due to the liquid and equivalent path length of the vapour. Roy (1961) observed similar continuous absorption in this region in the case of almost all the isomeric monohalogen-substituted toluenes in the liquid and vapour states.

As already mentioned, the luminescence spectra of all the halogen substituted toluenes in the solid state at -180°C consist of bands while the liquids show continuous absorption in the region on the longer wavelength side of 3400 Å. It can be inferred that the substances in the solid state at low temperatures might exhibit discrete absorption bands instead of continuous absorption in the region mentioned above. As the absorption is extremely weak, a thick layer is to be used to study such absorption and it is difficult to obtain transparent thick layers of the substances in the frozen state. In the present investigation an attempt was made to obtain thick transparent masses of *para* bromotoluene both in the crystalline state and in the frozen solution in methyl cyclohexane and to study the absorption spectra in the near ultraviolet region. The results are discussed in the following sections.

EXPERIMENTAL

The liquid of pure quality supplied by B.D.H of London was further purified by distillation under reduced pressure. The solvent methyl cyclohexane was supplied by Fisher Scientific Co. of U.S.A. and it was also purified similarly. A nearly transparent frozen mass of *p*-bromotoluene at -15°C was obtained in a Pyrex glass cell of special design and having a thickness of 7 mm by cooling the liquid contained in the cell slowly from its lower portions. The method was similar to that for obtaining metallic crystals, the only difference being that in the temperature. This method was used when it had been found that the frozen mass obtained by immersing the cell in liquid oxygen was completely opaque. A 12 percent solution of the substance in methyl cyclohexane in a Pyrex glass cell of thickness 45 mm was held in a brass frame. When the lower portion of the frame was immersed in liquid oxygen contained in a transparent Dewar vessel the solution was frozen and a translucent mass at about -175°C was obtained. The absorption spectra of these two solid masses were photographed using a hydrogen tube as the source of continuum and an

Adam Hilger E 1 quartz spectrograph giving a dispersion of about 10 Å/mm in the region of 3500 Å. Iron arc comparison spectrum was photographed on each of the spectrograms. After drawing a sharp line along the line 4191 Å of the iron arc spectrum with a razor blade and producing it to cut across the absorption spectrum, microphotometric records of the two spectra on each spectrogram were taken. The wavelengths on the absorption spectrum at any point was determined by finding the distance of the point from the mark due to the line 4191 Å and the corresponding wave-length on the record due to the iron arc spectrum.

RESULTS AND DISCUSSION

The microphotometric records due to the spectrograms are reproduced in Figs. 1(a) and 1(b). It can be seen from the records that there are at least three sharp absorption peaks in the spectra due to both the pure crystal and the

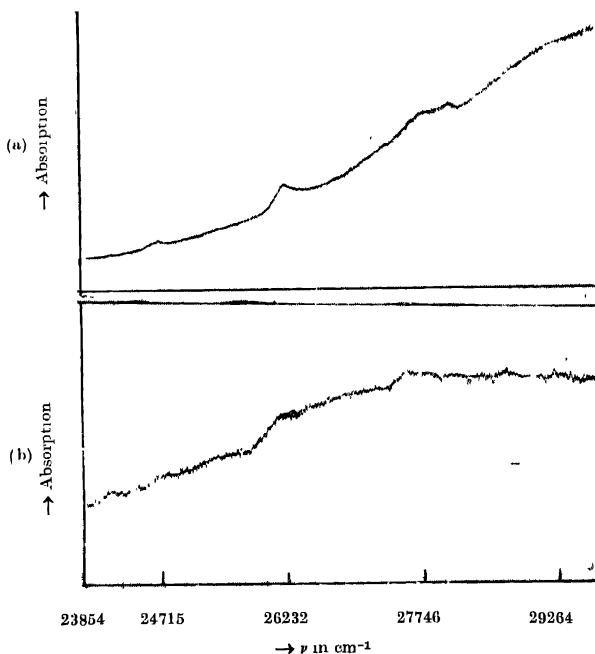


Fig. 1. Microphotometric records of absorption spectra.

(a) *p*-bromotoluene at -15°C .

(b) Solid solution of *p*-bromotoluene in methyl cyclohexane at -180°C .

frozen mixture. The wave numbers and strength of the absorption are given in Table I. A broad fourth band is also included.

TABLE I
Absorption bands of thick layer of *p*-bromotoluene

Pure crystals at -15°C		12% frozen solution in methyl cyclohexane at -180°C	
Positions	Separation	Positions	Separation
21715 m	—	21715 w	—
—	1517	—	1517
26232 s	—	—	—
—	1514	26232 s	—
27746 mb	—	—	1514
—	1518	27746 mb	—
29261 wb	—	—	—

It can be seen from Table I that both the pure crystal and the frozen solution show absorption peaks of the same wavelengths and that the second peak is the strongest in each case. It is found that the mean separation between the successive bands is about 1516 cm^{-1} . This represents the frequency of some mode of vibration of the molecule in the triplet state. In order to identify the mode the luminescence spectrum of the compound reported by Biswas (1956c) is to be compared with the absorption spectrum. It is found that he observed a separation of 1717 cm^{-1} between the first two broad luminescence bands on the shorter wavelength side and the first band is at 4337 Å , i.e., at 23051 cm^{-1} . The first absorption band observed in the present investigation, however, is at 24715 cm^{-1} . If the latter band be identified with the 0, 0 band in the singlet→triplet transition it is found that the 0, 0 band is absent in the luminescence spectrum. Denoting the vibration frequencies in the singlet and triplet states by ν_S and ν_T respectively, we assume that the first band in the luminescence spectrum on the shorter wavelength side is due to a transition from the first excited vibrational state coupled to the triplet state to the second excited vibrational state in the singlet state of the molecule as shown in Fig. 2.

Then we get

$$2\nu_S - \nu_T = 1664$$

$$\text{or } 2\nu_S - 1517 = 1664$$

$$\text{or } \nu_S = 1590\text{ cm}^{-1}.$$

This agrees with the frequency of mode 8A of benzene (Pitzer and Scott, 1943).

The second band in the fluorescence spectrum reproduced by Biswas (1956c) is at 4686 Å, but it is very wide and its strongest portion seems to be at about

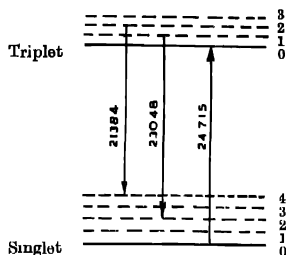


Fig 2. Schematic energy level diagram showing transitions between the Triplet→Singlet states.

4675 Å, which is at a distance of 1667 cm^{-1} from the first band. This may be due to the transition from the second excited vibrational state in the triplet state to the fourth excited vibrational state in the singlet state. The transition from the first excited upper vibrational state to the third lower excited vibrational state would give a band at a distance of 1590 cm^{-1} from the band at 23051 cm^{-1} and there seems to be some intensity in this region in the luminescence spectrum reproduced by Biswas (1956c). Thus, the luminescence bands are broadened by the superposition of the different transitions mentioned above. For an accurate analysis of the luminescence spectrum using the triplet state vibrational frequency found in the present investigation, a careful study of the structure of the luminescence bands is necessary.

It is thus concluded that somehow the mode No. 8A is responsible for the re-emission of the energy absorbed by singlet→triplet absorption which seems to be feebly allowed in the case of halogen substituted toluenes.

REFERENCES

- Biswas, D. C., 1956a, *Ind. J. Phys.*, **30**, 143.
 „ „ 1956b, *Ind. J. Phys.*, **30**, 565.
 „ „ 1956c, *Ind. J. Phys.*, **30**, 407.
 „ „ 1958, *Ind. J. Phys.*, **32**, 301.
 Pitzer, K. S. and Scott, D. W., 1943, *J. Amer. Chem. Soc.*, **65**, 805.
 Roy, J. K., 1959, *Ind. J. Phys.*, **33**, 209.
 „ „ 1960, *Ind. J. Phys.*, **34**, 331.
 „ „ 1961, *Ind. J. Phys.*, **35**, 628.
 Sanyal, S. B., 1953, *Ind. J. Phys.*, **27**, 447.
 Sirkar, S. C. and Roy, J. K., 1960, *Ind. J. Phys.*, **34**, 581.

LOCALIZATION OF EMPTY $4p$ ORBITALS IN CERTAIN TRANSITION METAL COMPOUNDS*

K. P. SINHA

NATIONAL CHEMICAL LABORATORY, POONA-8

AND

CHINTAMANI MANDE

DEPARTMENT OF PHYSICS, POONA UNIVERSITY, POONA-7

(Received November 5, 1962)

ABSTRACT. The splitting of the K x-ray absorption edge of certain transition metal ion compounds with a tetrahedral co-ordination is explained on the basis of ligand field theory. It is pointed out that in the tetrahedral configuration the empty $4p$ orbitals of the metal ion are localised whereas in octahedral surroundings these form strong bonding and antibonding molecular orbitals with the appropriate combination of ligand orbitals. The antibonding empty orbital (t^*_{1u}) to which the first x-ray transition takes place is delocalised

These conclusions are consistent with observations.

INTRODUCTION

The existence of localized empty orbitals in solids is expected to play an important role in several physical processes such as optical absorption, electrical properties, and magnetic exchange interactions (Sinha 1961). X-ray absorption spectroscopy provides a powerful method of studying the nature of empty orbitals in solids (Cauchois, 1948; Mande, 1960). Several workers have investigated the K absorption spectra of transition metal ions in their various physico-chemical states (See Wilkinson and Cotton, 1959 for details).

Recently, van Nordstrand (1960) has reported a large number of K absorption curves of transition metal ions in different types of solids. He classifies these curves in four categories, namely, type I spectra, associated with an octahedral coordination in the common salts, hydrates, complexes and oxides; type II, associated with octahedral coordination shell constituted of linear ligands such as CN or CO; type III characteristic of metals and metallic phases; and type IV, associated with tetrahedral configurations (e.g. KMnO_4). These four typical spectral curves are shown in Fig. 1.

Of these, the type IV curve alone shows the splitting of the principal absorption edge. Collet (1959) has also reported a similar splitting in NiK absorption in the complex $\text{K}_2[\text{Ni}(\text{CN})_4]$, where the ligands form a square planar configuration.

* Communication No. 516 from the National Chemical Laboratory, Poona-8 (India).

The first maximum in the principal absorption edge (in type IV) may be interpreted as a transition of a $1s$ electron towards an empty $4p$ orbital.

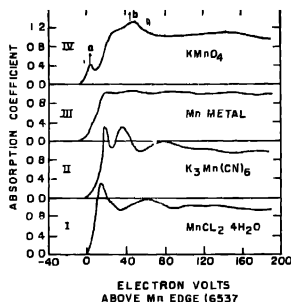


Fig. 1. Four different types of K absorption spectra of manganese in varying chemical states as given by R. A. Van Nordstrand. The markings 'a' and 'b' are by the present authors. 'a' represents the x-ray transition $1s \rightarrow 4p$, and 'b' $1s \rightarrow p$ limit.

The purpose of this note is to point out and interpret theoretically the occurrence of localized $4p$ levels in certain compounds with tetrahedral configuration around the transition metal ion, which in turn, is responsible for the splitting of the absorption edge. We also explain the absence of the same in octahedral systems. A purely electrostatic crystal field calculations by Cotton and Ballhausen (1956) lead to somewhat different conclusions.

THEORETICAL CONCEPTS AND DISCUSSION

In this section, we discuss results of our theoretical calculations for KMnO_4 , which is a typical example of a transition metal ion in tetrahedral configuration i.e. $(\text{MnO}_4)^-$. In formulating the electronic configuration of the tetrahedron, we also include the electrostatic crystal field effects of the surrounding nearest K^+ ions. For the $(\text{MnO}_4)^-$ tetrahedron itself, we follow the molecular orbital approach. The results obtained would apply equally well to other similar systems.

The position of the K^+ ions were taken from the crystallographic data of Mooney (1931) on KMnO_4 . The effective crystal field potential can be expressed, following the general method due to Bethe (1929), as

$$V(6K^+) = C_0^0 Y_0^0 + C_2^0 r^2 Y_2^0 + C_2^{-2} r^2 (Y_2^{-2} + Y_2^{-2}) + \dots \quad (1)$$

where C 's are the coefficients, Y 's the spherical harmonics and r the radial co-ordinate. Since we are concerned with the splitting of the $4p$ levels only terms upto second order spherical harmonics have been included in (1).

The calculation shows that the term $C_0^0 Y_0^0$ gives a constant depression of all the energy levels of Mn by about 20 eV. For an electron in $4p$ orbitals, the other

terms in (1) give rise to a splitting of p_x, p_y, p_z orbitals by approximately 0.2 eV which is comparatively small.

In order to study the influence of the inner oxygen atoms on Mn in $(\text{MnO}_4)^-$, we treat the inner $(1s^2 2s^2 2p^6 3s^2 3p^6)$ electrons of Mn as constituting the ion core and only $3d^5 4s^2$ electrons are supposed to be involved in covalency. The appropriate orbitals to be considered for covalency are, however, $3d, 4s$ and $4p$. Likewise, for oxygen we take the $1s^2 2s^2$ electrons as forming the ion core and the remaining $2p^4$ electrons participate in bonding. The three oxygen p orbitals are p_σ, π_1 and π_2 the former pointing towards the central ion. We classify the central ion valence orbitals and the linear combination of oxygen ion p orbitals, which interact strongly according to the point symmetry group T_h , following Wolfsberg and Helmholz (1952). The metal ion orbitals span the irreducible representation (given in brackets) as indicated: i.e. $s(A_1); d_\gamma: d_{z^2}, d(x^2-y^2) (E); p_x, p_y, p_z; d_c; d_{yz}, d_{zx}, d_{xy}, (T_2)$. The linear combinations of the ligand p_z orbitals span the representations $(\sigma_1 + \sigma_2 + \sigma_3 + \sigma_4)/2: A_1; (\sigma_1 + \sigma_2 - \sigma_3 - \sigma_4)/2, (\sigma_1 - \sigma_2 + \sigma_3 - \sigma_4)/2, (\sigma_1 - \sigma_2 - \sigma_3 + \sigma_4)/2: T_2$. Likewise, there will be combinations of π orbitals belonging to different representations. The strength of the bonding and antibonding molecular orbitals formed between the metal ion and the ligand orbitals is determined from symmetry, relative energies and overlap considerations. It is seen that s, d_γ and d_c form strong bonding and antibonding orbitals with the appropriate anion molecular orbitals. The bonding with the $4p$ orbitals is not strong as can be visualized from overlap considerations and that d_c orbitals also compete strongly for the same purpose. Thus in effect the $4p$ orbitals of the metal ion remain more or less of the atomic type and remain empty along with other antibonding orbitals. The x-ray absorption at ' α ' in Fig. 1 is interpreted as $1s$ to $4p$ transition with the latter remaining localized.

Let us now consider the transition metal ion in octahedral configuration i.e. the metal ion surrounded by six ligands (e.g. O^{2-} or CN). The point symmetry group is O_h . The metal ion orbitals outside the closed shell configuration are again $3d, 4s, 4p$ and span the irreducible representations as indicated i.e. $4s(A_{1g}), 3d_e (T_{2g}), 3d_\gamma (E_g)$ and $4p(T_{1u})$. The appropriate linear combinations of the six ligand p_σ orbitals span the representations A_g, E_g, T_{1u} (Orgel 1960). Here too, we disregard the effect of π orbitals. Thus the strong bonding and antibonding orbitals are due to the mixing of $3d_\gamma, 4s$ and $4p$ orbitals of the metal ion with the appropriate combinations of the p_σ orbitals of the ligands. In contrast to the tetrahedral case, the $4p$ orbitals in the octahedral configuration are subjected to a strong end on overlap with ligand p_σ orbitals. Thus the antibonding combination t_{1u}^* , which is invariably empty in most systems, is extensively delocalized in octahedral configurations. Also, in the octahedral case there is no set of $3d_e$ type orbitals of the central ion belonging to T_{1u} symmetry to compete with $4p$ orbitals of the same. In the tetrahedral case, it was shown that the d_c orbitals

were strongly bonded with the ligand orbitals and this competition also favoured in rendering the $4p$ orbitals localized.

We visualize that in octahedral systems the x -ray transition is from $1s$ to t_{2g}^* , the later being delocalized as well as pushed upwards in energy scale. This would be consistent with the observed spectra in octahedral system where there is no splitting of the principal absorption edge. The effect of the positive ions (e.g. K^+) around the octahedron would be similar to the tetrahedral case; however, the magnitude of the constant depression and splitting of the energy levels would depend on the distances and dispositions of these ions. In complex systems such as Mn_3O_4 (distorted spinel structure) where there are two octahedrally surrounded and one tetrahedrally surrounded metal ions, the effect of the tetrahedron is probably diluted owing to the preponderance of the octahedral ions.

CONCLUDING REMARKS

In the foregoing section, we have made tentative suggestions as to why $4p$ empty orbitals of transition metal ions become localized in tetrahedral systems and delocalized in octahedral surroundings. The above conclusion correlates well with the observed K X-ray absorption spectra in such systems. Detailed theoretical calculations and extensive experimental work are in progress and their results will be reported later.

ACKNOWLEDGMENTS

We are grateful to Dr. L. M. Pant for helpful discussions. Our thanks are also due to Dr. A. B. Biswas and Dr. M. W. Chiplonkar for their interest in the work.

REFERENCES

- Bethe, H. A., 1929, *Ann. der Phys.*, **3**, 181.
- Cauchois, Y., 1948, *Les Spectres de rayons x et la structure electronique de la matiere*, Gauthier—Villars, Paris.
- Collet, V., 1959, *Thesis, Paris*, Gauthier—Villars.
- Cotton, F. A. and Ballhansen, C. J., 1956, *J. Chem. Phys.*, **25**, 617.
- Mande, C., 1960, *Ann. de Phys. (Paris)*, **6**, 1559.
- Mooney, R. C. L., 1931, *Phys. Rev.*, **37**, 1306.
- Orgel, L. E., 1960, *An Introduction to Transition Metal Chemistry*, Methuen, London.
- Sinha, K. P., 1961, *Ind. J. Phys*, **35**, 484.
- Von Nordstrand, R. A., 1960, *Conf. Non-crystalline solids*, John Wiley and Sons, New York.
- Van Nordstrand, R. A., 1960, *Advances in Catalysis*, Vol. **12**, Academic Press, New York.
- Wilkinson, G. and Cotton, F. A., 1959, *Progress in Inorganic Chemistry*, Vol. **I**, Interscience, New York.
- Wolfsberg, M. and Helmholz, L., 1952, *J. Chem. Phys.*, **20**, 837.

ON NUCLEAR QUADRUPOLE COUPLING CONSTANTS OF CHLORINE ISOTOPES AND DIPOLE MOMENT OF BrCl MOLECULE*

K. L. NARAYANA AND C. SANTHAMMA

DEPARTMENT OF PHYSICS, ANDHRA UNIVERSITY, WALTAIR

(Received December 12, 1962)

ABSTRACT. A theoretical estimate of chlorine nuclear quadrupole coupling constant in BrCl molecule has been made for the two isotopic substitutions (Cl^{35} and Cl^{37}) of chlorine on the basis of the theory developed by Townes and Dailey. The dependence of the chlorine nuclear quadrupole coupling constant and dipole moment on the chemical bonding state of BrCl molecule has been investigated. Neither the amount of the hybridization nor the ionicity of the bond could be uniquely determined. However, fixing a probable percentage ionicity of the bond (10% obtained from the electro-negativity considerations) it is found impossible to explain the observed coupling constant without the introduction of $s\%$ whereas the observed dipole moment cannot be explained without the introduction of $d\%$.

The change in quadrupole coupling constant for the isotopic substitution of chlorine is found predominantly due to the change in the corresponding nuclear quadrupole moments.

INTRODUCTION

One of the fundamental quantities determined by pure quadrupole resonance, microwave and molecular spectroscopic observations is the value of eqQ which is a measure of the orientation energy of the nucleus in an asymmetric electric field and is known as the nuclear quadrupole coupling constant. Here Q is the nuclear quadrupole moment, an inherent property of the nucleus and q is the field gradient at the nucleus due to the various charges outside the nucleus. A theoretical estimate of coupling constant is possible only when both Q and q can be exactly determined. Of these Q may be estimated assuming a suitable model and potential function and the evaluation of q may, in certain simple cases be deduced, by a method due to Townes and Dailey (1949).

In the case of atoms, the field gradient ' q ' can be evaluated from the hyperfine structure data. But it is slightly altered when the atom is bonded to another atom, through a single or multiple bond. Townes and Dailey (1955) suggested, the relation

$$q_{\text{mol}} = f \cdot q_{\text{atom}}$$

f , being a function dependent on the molecular electronic structure and explained in terms of (i) Bonding state of the molecule and (ii) Ionicity of the bond. Schatz

*Communicated by Prof. A. K. Saha.

(1954) made use of this relation to study the nature of 'f' in the chlorine π coupling constant in the case of HCl and CH_3Cl molecules where both H-Cl and C-Cl bonds were assumed to have a small ionic contribution and also the chlorine bonding wave function was supposed to be an s - p - d hybrid. An attempt was made by Schatz to evaluate a number of parameters such as percentage s , p , d in the bonding and non-bonding chlorine functions and ionicity of the molecular bond from the observed dipole moment of the molecules. Though there was an ambiguity in fixing up the chemical bonding state of the molecule to explain the observed chlorine eqQ , the hydrogen-like Slater or Morse-Hydrogen-like wave functions could qualitatively explain the nature of the variation of eqQ with different s - p - d hybridizations. A study of I_2 molecule by D. V. G. L. N. Rao (1959) on these lines indicated 10% s -character.

In the present investigation, BrCl molecule is chosen for a similar study in view of its low ionicity (Gordy *et al.*, 1953) and the feature that the chlorine bonding state is a hybrid one. The study is extended to both the isotopic molecules $\text{Br}^{79}\text{Cl}^{35}$ and $\text{Br}^{79}\text{Cl}^{37}$ with a view to determine the change in coupling constants through (i) difference in Q values of nuclear isotopes Cl^{35} and Cl^{37} and (ii) change in 'q' arising out of the difference in internuclear distance i.e. through overlap and moment integrals.

The procedure has been to study the relationship between the chemical bonding state and the quadrupole coupling constant on one hand and dipole moment on the other. An approximate quantitative estimation of the hybridization is found possible only when one can fix the % ionicity of the bond, as that obtained from the electro negativity considerations (Gordy *et al.*, 1953).

CALCULATIONS

The bromine and chlorine atoms have the ground state configurations $4s^2 4p^5$ and $3s^2 3p^5$ respectively for their outermost electrons. The actual state of the BrCl molecule can be described as resonating between the two possible electronic structures Br-Cl, the covalent extreme and Br^+Cl^- , the ionic extreme. A third possible structure $\text{Br}-\text{Cl}^+$ is neglected since the chlorine (3.1) is more electronegative than Bromine (2.9).

The bonding wave function representing the state of the molecule is taken as predominantly covalent with partial ionic character, the contribution of the two being given by 1 and λ (< 1)

$$\psi_b \sim \psi_{\text{Br}; \text{Cl}} + \lambda \psi_{\text{Br}^+; \text{Cl}^-}$$

$$\psi_b = A[\psi_{cl}(1)\psi_{Br}(2) + \psi_{cl}(2)\psi_{Br}(1) + \lambda \psi_{cl}(1)\psi_{cl}(2)]$$

where A is the normalization factor. In order to realize a strong molecular bond, the bonding electrons are assumed to be moving in admixtures of s , p_z and d_{zz} atomic orbitals. Thus

$$\psi_{cl} = a\psi_{3s} + b\psi_{3p_z} + c\psi_{3d_{zz}}$$

where a^2 , b^2 and c^2 represent the percentage s - p - d hybridizations. and $a^2+b^2+c^2=1$.

The ortho-normal non-bonding wave function is of the form

$$\psi_{nb} = a'\psi_{3s} + b'\psi_{3p_z} + c'\psi_{3d_{zz}}$$

satisfying the conditions that $aa'+bb'+cc'=0$ and $a'^2+b'^2+c'^2=1$. In the actual calculations, the contribution of d -orbital in the non-bonding wave function has been taken as zero, since the calculations are insensitive to the magnitude of the parameter (Schatz, 1954).

The total expression for the chlorine nuclear quadrupole coupling can be deduced by analyzing separately the contributions to the field gradient 'q' from the following sources.

(i) The electron-pair forming the molecular bond, (ii) the pairs of $3p_x$ and $3p_y$ electrons which remain unpolarized (iii) the non-bonding lone pair electrons which make a contribution whenever a and c are not zero. (iv) Electrons constituting the inner shells of the chlorine atom and (v) the nucleus of the Bromine atom along with its surrounding electrons except the one involved in the molecular bond.

The inner shells of the chlorine atom will be generally spherically symmetric and any change in the field gradient resulting through the perturbation destroying such spherical symmetry of the inner shells (Sternheimer effect) by both the quadrupole moment and valence electrons is only of a minor order (Das and Hahn, 1958) since we used the experimental quadrupole coupling constants for both the atom and molecule and hence is considered as negligible. The effect of the Bromine atom may be regarded as equivalent to that of a unit +ve charge placed at the position of the Bromine nucleus. The contribution of the bonding electrons is

$$eq_bQ = eQ \left[\frac{(1+\lambda^2+2\lambda S)q_{ClCl} + q_{BrBr} + 2(S+\lambda)q_{BrCl}}{1+S^2+2\lambda S+\lambda^2/2} \right]$$

where

$$q_{BrCl} = \int \psi_{Br}(1) \frac{3 \cos^2 \theta_a - 1}{r_a^3} \psi_{Cl}(1) d\tau(1)$$

r_a and θ_a are the parameters as shown in Fig. 1. q_{ClCl} and q_{BrBr} have similar expressions. The total overlap

$S = aS_{4p3s} + bS_{4p3p} + cS_{4p3d}$ and S_{4p3s} ; S_{4p3p} and S_{4p3d} are the overlap integrals between the suffixed orbitals.

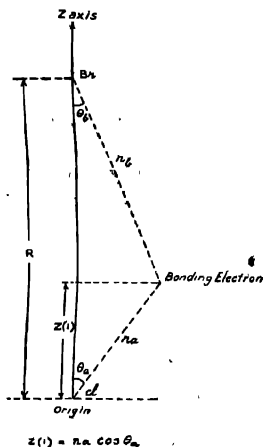


Fig. 1. Co-ordinate system.

Each pair of $3p_x$ and $3p_y$ electrons contribute an amount $-q_{3p_x} 3p_z$ to the field gradient and the total expression for the coupling constant together with the contribution from the Cl non-bonding electron pair (given as $eq_{nb}Q$) is

$$eqQ = eQ(q_b - 2q_{3p_x} 3p_z + q_{nb})$$

This expression is further simplified as follows. The q integrals $q_{3p_x} 3p_z$; $q_{3p_x} 3p_x$ and $q_{3p_y} 3d_{zz}$ vanish due to their angular parts. The rest of the cross-integrals of the type $q_{4p} 3p_z$ can be neglected as a first approximation. Thus

$$eqQ = eQ \left[\frac{(1 + \lambda^2 + 2\lambda S)b^2}{1 + S^2 + 2\lambda S + \lambda^2/2} - 2(1 - b'^2) \right] q_{3p_x} 3p_z \quad (1)$$

The experimentally determined atomic quadrupole coupling constants (Davis *et al.*, 1948) -110.4 Mc/Sec and -86.2 Mc/Sec, were used for Cl^{35} and Cl^{37} nuclei respectively.

The expression for the dipole moment (Robinson, 1949) of the molecule is

$$\mu = e(R - 2\bar{Z}_{nb} - 2\bar{Z}_b) \quad \dots (2)$$

where \bar{Z}_b is the average value of the Z -co-ordinate of a bonding electron and \bar{Z}_{nb} is the same quantity for a non-bonding electron, e is the electronics charge and R is the internuclear distance and

$$\bar{Z}_b = \frac{M(1 + \lambda^2 + 2\lambda S) + R/2 + (S + \lambda)P}{1 + S^2 + 2\lambda S + \lambda^2/2}$$

$$\bar{Z}_{nb} = 2a'b' M_{3p_x} 3d_{xz} + 2b'c' M_{3p_x} 3d_{yz} + 2c'a' M_{3p_x} 3d_{zx}$$

where S is the total overlap and

$$P = a M_{4p3s} + b M_{4p3p_z} + c M_{4p3d_{zz}}$$

$$M = ab M_{3s3p_z} + bc M_{3p_z3d_{zz}} + cd M_{3s3d_{zz}}$$

The various overlap and moment integrals such as

$$S_{4p3s} = \int \psi_{4p}(1) \psi_{3s}(1) d\tau(1); \quad M_{4p3s} = \int \psi_{4p}(1) Z(1) \psi_{3s}(1) d\tau(1)$$

are evaluated (Appendix I) for the isotopic substitutions $\text{Br}^{79} \text{Cl}^{35}$ and $\text{Br}^{79} \text{Cl}^{37}$ employing the inter-nuclear distances 2.13866 Å and 2.11464 Å respectively.

Hydrogen-like wave functions (Pauling and Wilson, 1935) for chlorine $3s$, $3p_z$ and $3d_{zz}$ states and Bromine $4p_z$ state with screening constants (Pauling and Sherman, 1932) ($z_{3s} = 8.26$, $z_{3p} = 6.54$, $z_{3d} = 3.63$ and $z_{4p} = 8.84$) are used. The structural parameters are taken from the microwave observations reported by Smith D. F. (1950) *et al.* ($\mu = 0.57$ Debye units).

The numerical values of the various overlap and moment integrals for the two isotopic substitutions are given in Table I.

TABLE I

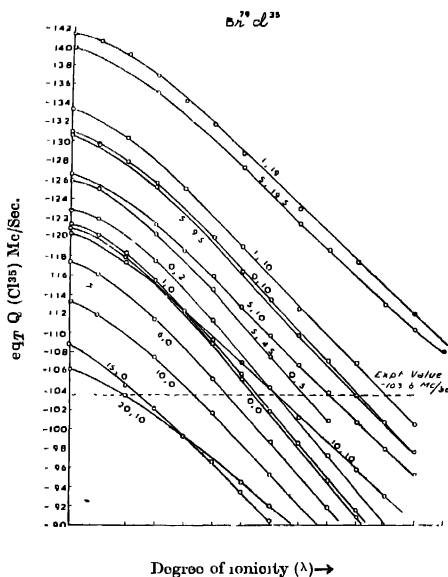
	Values of overlap integrals			Values of moment integrals	
	$\text{Br}^{79} \text{Cl}^{35}$	$\text{Br}^{79} \text{Cl}^{37}$		$\text{Br}^{79} \text{Cl}^{35}$	$\text{Br}^{79} \text{Cl}^{37}$
S_{4p3s}	0.3097	0.3249	M_{3s3p_z}	0.5135	0.5135
S_{4p3p_z}	0.3217	0.3651	$M_{3p_z3d_{zz}}$	0.5199	0.5199
$S_{4p3d_{zz}}$	0.04775	0.03525	$M_{3s3d_{zz}}$	0	0
			M_{4p3s}	0.1809	0.1836
			M_{4p3p_z}	0.2036	0.3263
			$M_{4p3d_{zz}}$	0.01868	0.004423

RESULTS AND DISCUSSION

Graphs drawn (Appendix II) using equations 1 and 2 representing the dependence of the dipole moment as well as quadrupole coupling constant on the amount of ionicity of the molecular bond and various percentage of s - p - d hybridization are given in figures 2, 3, 4 and 5. The dotted lines across the curves in the figures are the experimentally determined values and the numbers on the curves indicate respectively the s and d percentage hybridizations.

Dependence of eqQ

Neglecting overlap effects, the observed eqQ can be obtained only when the bond assumes 30% ionicity in case of Cl^{35} and 33% in case of Cl^{37} which are very



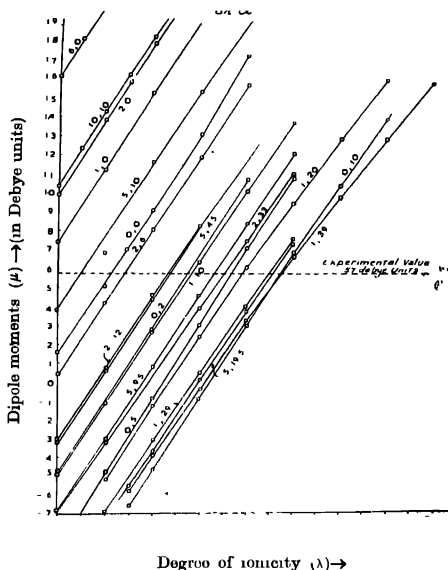


Fig. 4. Variation of dipole moment with ionicity and hybridization for $\text{Br}^{79}\text{Cl}^{35}$.

large compared to the value 10% obtained on the basis of electro-negativity consideration and hence there is a necessity to decrease the ionicity of the bond. However a change in the electro-negativity of the atom can be produced, if the chemical bonding state of the atom is changed, thus leading to a change in the ionic character of the bond i.e. treating the chlorine bonding wave function as not a pure $3p$ state but as an admixture of both $3s$ and $3d$ states. We note (see Fig. 2, 3) for any s - p - d hybridization eqQ decreases with increasing, λ .

The effects of $s\%$ on the eqQ is studied assuming two possible hybridized chlorine bonding wave functions and three ionic characters 0% ($\lambda = 0$); 10% ($\lambda = 0.33$) and 20% ($\lambda = 0.5$) and results are graphically represented in Fig. 6. It can be inferred that eqQ attains a maximum value for $s\%$ ranging from 0% to 2% and for any value of $s\%$, $|eqQ|$ decreases as λ increases and it is also true that as $d\%$ increases the corresponding maximum is lifted up.

If the bond is a pure covalent ($\lambda = 0$) introduction of 15% to 20% s -character without d -hybridization can explain the observed value with an increase of s -percentage (approximately between 20-25%). If the bond were to assume 10% ionic-character ($\lambda = 0.33$) still a smaller $s\%$ (10 to 15) can explain the observed eqQ . Here also it is observed that $s\%$ should be increased when $d\%$ assumes

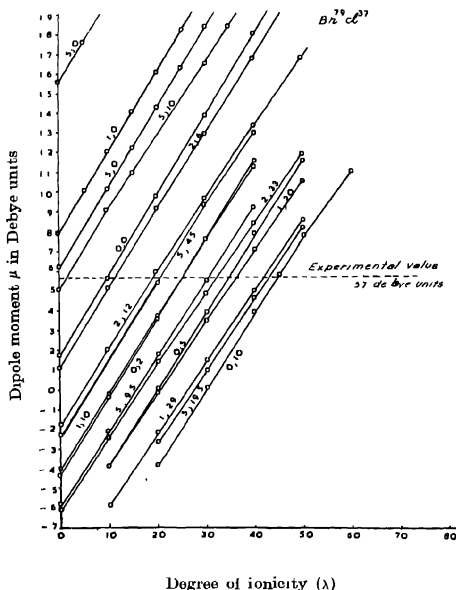


Fig. 5 Variation of dipole moment with ionicity and hybridization for $\text{Br}^{70}\text{Cl}^{30}$.

10 in order to realize the experimentally observed eqQ . Similar behaviour is seen when the ionic character is further increased to 20% ($\lambda = 0.5$).

In all the above cases it is seen that $s\%$ exceeds $d\%$ and the amount by which it exceeds decreases with increasing λ . This is not in agreement with rough estimates made by Whitehead and Jaffe (1961) who stated that a small $d\%$ without $s\%$ can explain the observed eqQ .

On the other hand it is found impossible from the results to explain the observed eqQ without the introduction of $s\%$. This is in agreement with Townes (1958) rule that in the case of bonding Cl, Br and I a 15% s -hybridization is possible if they were bonded to more electropositive atom by 0.25. Further $d\%$ in these cases appears to be negligible as far as 'q' is concerned, in conformity with the rule.

For Cl^{35} in $\text{Br}^{70}\text{Cl}^{35}$ the experimentally observed quadrupole coupling constant can be obtained with 10% ionic character of the bond i.e. ($\lambda = 0.33$) when $d = 0\%$ and $s = 13\%$ and also when $d = 10\%$; $s = 19\%$. It can be concluded in view of the Townes rule that a 13% s with no d -hybridization is perhaps more reasonable if a 10% ionicity is fixed. This estimate of s -hybridization differs

from that made by Gordy (1951, 1955). For $\text{Br}^{79}\text{Cl}^{37}$ the observed coupling constant (-81.14 Mc/Sec) is explained fixing $\lambda = 0.33$ when $d = 0\%$ and $s = 14\%$ and also $d = 10\%$ $s = 19\%$. From the above data, the isotopic substitution of Cl does not effect the hybridization in spite of changes in the values of overlap and moment integrals which are functions of the inter-nuclear distances.

TABLE II

	Observed coupling	s%	d%	λ	Difference
Cl^{35}	-103.6 Mc/Sec.	15	0	0.24	} 0.07
Cl^{37}	-81.14 Mc/Sec	15	0	0.31	
Cl^{45}		10	0	0.433	} 0.054
Cl^{37}		10	0	0.487	
Cl^{35}		0	0	0.647	} 0.046
Cl^{37}		0	0	0.693	

Further, from the data in Table II in the case of the isotopic substitution the difference in percentage ionicity of the bond (3 to 4%), though small, increases with increasing s% hybridization. A change of 0.07 in λ will produce a change in the eqQ by 2 to 3 Mc/Sec.

In view of the above discussion it can be inferred that the large change in the observed quadrupole coupling constant (-103.6 Mc/Sec in Cl^{45} and -81.14 Mc/Sec in Cl^{37}) is mainly due to change in the Q values. In other words, roughly the same field gradient is experienced by each Cl isotope in the compound. This has been experimentally demonstrated, in general in a number of compounds by Livingston and also by Wang (1952). However, a negligibly small contribution to the field gradient 'q' can be expected through changes in the inter nuclear distance and ionicity of the bond for the two isotopic species.

Dependence of dipole moment

As regards the dipole moment, neglecting the overlap effects, it is seen from the observed value that the bond assumes $\lambda = 0.116$ leading to 1.3% ionic character in $\text{Br}^{79}\text{Cl}^{35}$ and 0.99% ionic character in $\text{Br}^{79}\text{Cl}^{37}$ which are much smaller than those obtained from the corresponding observed eqQ value (30% ionic character for $\text{Br}^{79}\text{Cl}^{35}$ 33% ionic character for $\text{Br}^{79}\text{Cl}^{37}$) and also that obtained by electro-negativity considerations. However, for any s - p - d hybridization the dipole moment increases with increasing λ .

For a pure covalent structure ($\lambda = 0$) a 0.7% s -hybridization without any $d\%$ can explain the observed dipole moment if the bond were to assume 0.99% ionic character. But if the bond has 10% ionic character, the observed dipole moment cannot be explained unless a $d\%$ -hybridization is introduced ($s = 0.7\%$; $\lambda = 10\%$ $d = 10\%$).

$eqQ \sim \langle 1/r^3 \rangle$ and $\mu \sim \langle Z_{cl} \rangle$ and thus a change in electron distribution near $\text{Cl}^{35,37}$ will effect eqQ considerably, whereas μ will be affected for change in electron-distribution away from $\text{Cl}^{35,37}$. So with a given value of λ and $s\%$, the increase in $d\%$ will increase eqQ because of non-sphericity of d_{zz} , but the $\%$ change would not be large since d_{zz} extends away from chlorine nucleus.

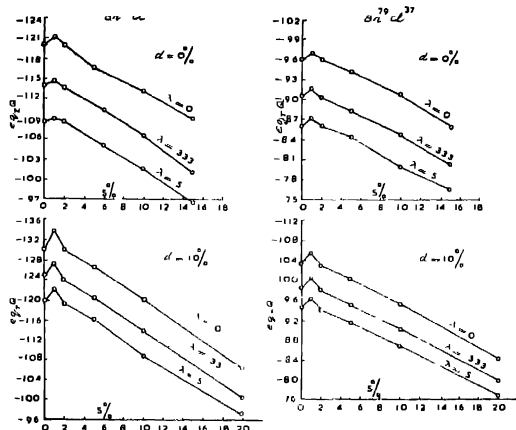


Fig. 6. Variation of quadrupole coupling constant with $s\%$ —hybridization for different λ values and two different $d\%$ —hybridizations for both isotopic substitutions.

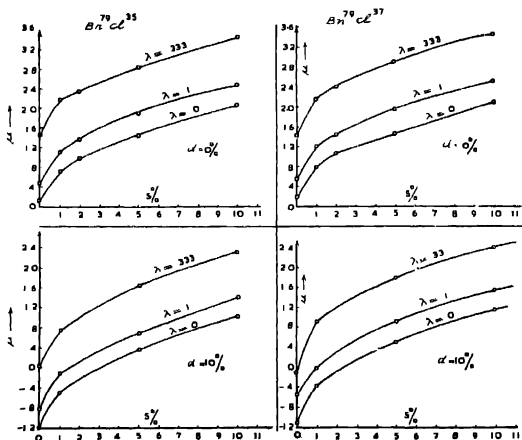


Fig. 7. Variation of dipole moment with $s\%$ —hybridization for different λ values and two different $d\%$ —hybridizations.

Again since d_{zz} hybridization has the effect of spreading out the charge in the molecule, μ will decrease as $d\%$ increases and the % change will be considerably larger because d_{zz} extends away from $\text{Cl}^{35,37}$.

This is also shown up in the data in figures 6 and 7. For $\lambda = 0.33$ $s\% = 10$, eqQ changes by $\sim 6\%$ when $d\%$ changes from 10 to 0. For μ , this change is $\sim 40\%$ and if $\lambda = 0.33$, $d\% = 10$, eqQ changes by 10% when $s\%$ changes from 10 to 2, the corresponding change in μ being $\sim 70\%$.

This shows, that with a reasonable value of λ , it would not be possible to fit both eqQ and μ with the same hybridization.

TABLE III

Relative s and d percentage hybridizations at 10% ionicity

$s\%$	$d\%$	Ionicity	(Cl ³⁵)	$s\%$	$d\%$	Ionicity	(Cl ³⁷)
1	39	10%	0.04	2	33	10%	0.50
1	20	10%	0.35	2	12	10%	0.91
1	10	10%	0.75	2	6	10%	1.30

It is also clear (see Table III) that d -percentage exceeds that of s -percentage to explain the observed dipole moment for both the isotopic substitutions. But the $s\%$ should exceed $d\%$ to explain the observed coupling constant, with percentage ionicity fixed at 10.

CONCLUSIONS

From the above discussion it is noted that the amount of s - d hybridization which explains the observed coupling constant with 10% ionic character fixed from electronegativity considerations, fails to account for the observed dipole moment. A simultaneous explanation of both the observed quantities with roughly the same hybridization can be achieved by suitably adjusting the ionic character. However in such case, one must assume unreasonably high values of ionicity compared to the estimate from the electronegativity data.

Previously Schatz has attempted for a simultaneous explanation of coupling constant and dipole moment in case of CH_3Cl by deducing the ionic character from the dipole moment without success. This inconsistency of the hybridization (and ionic character) contributing differently to the two physical properties may probably be due to the adoption of the same wave functions Dailey, and Townes, 1955) or due to the neglect of polarisation effects and the contributions of lone pair electrons of Br atom in the evaluation of dipole moment (Robinson, 1959).

ACKNOWLEDGMENTS

The authors are deeply indebted to Prof. K. R. Rao for his interest in the work and constant encouragement. The authors also wish to express their sincere

thanks to Prof. A. K. Saha for his comments and help in preparing the final manuscript. They are thankful to the Council of Scientific and Industrial Research for the award of the C.S.I.R. Scheme to C. S. and Junior Research Fellowship to K. L. N.

APPENDIX I

METHOD OF EVALUATION OF OVERLAP AND MOMENT INTEGRALS

The Overlap Integrals :

An overlap integral of the type S_{4p3s} is defined as

$$\int \psi_{4p} \psi_{3s} d\tau \quad \dots \quad (I)$$

and $d\tau = r_a^2 \sin \theta_a d\theta_a d\phi_a dr_a$ is the volume element

$$\begin{aligned} \psi_{4p} = \left(\frac{Z_{4p}}{a_0} \right)^{3/2} \frac{1}{32\sqrt{15}} \frac{2Z_{4p}}{4a_0} \frac{\sqrt{6}}{2} r_b \cos \theta_b \left\{ 20 - \frac{20Z_{4p}}{4a_0} r_b \right. \\ \left. + \frac{4Z_{4p}^2}{16a_0^2} r_b^2 \right\} e^{-\frac{Z_{4p}r_b}{4a_0}} \frac{Z_{4p}r_b}{\sqrt{2\pi}} \\ \psi_{3s} = \left(\frac{z_{3s}}{a_0} \right)^{3/2} \frac{1}{9\sqrt{3}} \left(6 - \frac{12z_{3s}}{a_0} r_a + \frac{4z_{3s}^2}{9a_0^2} r_a^2 \right) \frac{\sqrt{2}}{2} e^{-\frac{Z_{3s}r_a}{3a_0}} \frac{Z_{3s}r_a}{\sqrt{2\pi}} \quad \dots \quad (II) \end{aligned}$$

The parameters R , r_a , θ_a , r_b and θ_b are those indicated in the Figure 1 and a_0 is the Bohr radius. The values of z_{4p} and z_{3s} are given in the body.

The integral (I) with the substitutions of (II) can be evaluated in terms of spheroidal-coordinates ξ , η and ϕ . We have,

$$\xi = \frac{r_a + r_b}{R} ; \eta = \frac{r_a - r_b}{R} ; d\tau = \frac{R^3}{8} (\xi^2 - \eta^2) d\xi d\eta d\phi$$

This transformation of coordinates allows us to express the integrals (I) in terms of $A_m(\alpha)$ and $B_m(\alpha\beta)$ where

$$A_m(\alpha) = \int \xi^m e^{-\alpha\xi} d\xi$$

$$B_m(\alpha\beta) = \int_{-1}^1 \eta e^{-(\alpha\beta)\eta} d\eta \text{ but}$$

$$B_m(0) = \frac{2}{m+1} \text{ for } m \text{ even and}$$

$$= 0 \text{ for } m \text{ odd.}$$

The values of $A_m(\alpha)$ and $B_m(\alpha\beta)$ for the required values of

$$\alpha = \frac{1}{2} - \frac{z'_{4p} + z'_{3s}}{a_0} R \text{ and } \beta = \frac{z'_{4p} - z'_{3s}}{z'_{4p} + z'_{3s}}$$

with

$$z'_{4p} = z_{4p}/4 \text{ and } z'_{3s} = z_{3s}/3$$

can be obtained by interpolation from a tabulation of values of these integrals by Kotani *et al.* (1955).

The moment Integrals

The moment integral is given by

$$M_{4p,3s} = \int \psi_{4p} Z(1) \psi_{3s} dr \quad \dots \quad (\text{III})$$

where $Z(1)$ is the z -coordinate of the electron and is equal to $r_a \cos \theta_a$. ψ_{4p} and ψ_{3s} have the same expressions as given in (II). Again, we can express the integral (III) in terms of $A_m(\alpha)$ and $B_m(\alpha\beta)$ by the use of spheroidal coordinates which allows a straightforward computation of the numerical value given in table (Ib)

APPENDIX II

For any two given s and d percentage hybridizations, the values of eqQ and μ for various Λ -values can be obtained by evaluating S , P , M , b^2 , a'^2 , b'^2 and c'^2 . The expressions for S , P and M are given in the text, and a'^2 , b'^2 can be determined from the orthonormality conditions of bonding and non-bonding wave-functions. The contribution of the d -orbital in the non-bonding wave function has been taken as zero, in the actual calculations for the reasons stated previously.

The equation (1) representing the quadrupole coupling constant contains the total overlap S , which includes the percentage of d -hybridization.

REFERENCES

- Das, T. P. and Hahn, E. L., 1958. *Nuclear Quadrupole resonance Spectroscopy, Solid State Physics, Supplement 1* Academic Press, Inc. New York, 130 and 134-135.
- Davis, L. Jr, Feld, B. T., Zabel, C. W. and Zacharias, J. R. 1948. *Phys. Rev.*, **73**, 525-6.
- Dailey, B. P. and Townes, C. H., 1955. *Disc. Faraday Soc.* **19**, 274.
- Gordy, Walter, 1951. *J. Chem. Phys.*, **19**, 792. Also 1955. *Discussions Faraday Soc.*, **19**, 14.
- Gordy, W., Smith and Trambarulo, 1953. *Microwave Spectroscopy*, New York, Wiley.
- Kotani, M., Ameruya, A., Ishiguro, E., and Kumura, Junsaku. *Tables of Molecular integrals.* (Maruzen Co., Ltd., Tokyo, Japan, 1955).

- Livingston, R , 1953 *J. Phys. Chem* , **57**, 496. Wang, T. C., Townes, C. H., Schawlow, A. L. and Holden, A. N , 1952 *Phys Rev.*, **86**, 809.
- Pauling, L. and Wilson, E. B. Jr., 1935. '*Introduction to Quantum Mechanics*', McGraw Hill Book Company Inc.
- Pauling, L. and Shermann, J. 1932. *Z. Krist.*, **81**, 1.
- Rao, D. V. G. L. N., 1959. *Ind. J. Phys.*, **33**, 103.
- Robinson, David J. 1949. *J. Chem. Phys.*, **17**, 1022.
- Schatz, Paul N. 1954. *J. Chem. Phys.*, **22**, 695, 755, 1974.
- Smith, D. F , Tidwell and Williams, 1950. *Phys Rev.*, **79**, 1007L.
- Townes, C. H. and Schawlow, A L 1955 *Microwave spectroscopy*, New York-Toronto-London : McGraw Hill Book Company.
- Townes, C. H. and Dailey, B P. 1949. *J Chem Phys.*, **17**, 782.
- Townes, C. H 1958 *Handbuch Der Physik.*, Bd XXXVIII/1, 377.
- Whitehead, M. A. and Jaffe, H. H. 1961. *J. Chem. Phys.*, **34**, 2204.

INVESTIGATION ON HYDROGEN BONDING IN PURE CHLORO- AND NITRO ANILINES AND THEIR SOLUTIONS IN POLAR SOLVENTS

K. C. MEDHI AND G. S. KASTHA

OPTICS DEPARTMENT,

INDIAN ASSOCIATION FOR THE CULTIVATION OF SCIENCE,
CALCUTTA-32.

(Received January 22, 1963)

ABSTRACT The changes in the frequencies of infrared absorption bands due to N-H stretching vibrations in pure ortho-, meta-, para-chloro- and nitro aniline and in their solutions in different polar solvents with respect to the values in solutions in carbon tetrachloride have been measured. It has been observed that the reduction in the N-H stretching force constant in different solvents with respect to its value in carbon tetrachloride solution bears a linear relationship with the sum of the shifts of the two frequencies. It has been found that there is no systematic dependence of the total shifts either on the dielectric constants of the solvents or on the dipole moments of the molecules of the solvents.

INTRODUCTION

Recently, Krueger (1962) has elaborately discussed the variations of the N-H stretching force constant and the interbond HNH angle of the NH_2 group of a large number of substituted anilines in solution in carbon tetrachloride with the variation of the Hammett σ -factor of the substituent atom or group of atoms and also with the state of hybridisation of the N-H bonds. Earlier, Bryson and Werner (1960) had shown that information regarding the existence of intramolecular hydrogen bonds in some nitrosubstituted anilines and naphthylamines can be obtained from a study on the change in the N-H stretching force constant of the NH_2 group in the molecules of these compounds with a change of the solvent from carbon tetrachloride to pyridine. More recently, Medhi and Kasta (1963) have concluded that the shifts in the N-H stretching frequencies of aniline and a number of methoxy- and ethoxy-anilines in the liquid state and in solution in some polar solvents relative to the frequencies in solutions in dilute carbon tetrachloride depend on the electronic nature in substituent groups, the relative positions of substitution and on the nature of the solvents. In the present work the investigation has been extended to the chloro- and nitro- derivatives of aniline and the results obtained have been discussed in the following paragraphs.

EXPERIMENTAL

The substances investigated are *o*-, *m*- and *p*-chloroaniline and *o*-, *m*- and *p*-nitroanilines. Chemically pure samples of these compounds were obtained

from reputed firms of U.K. and West Germany. The chloroanilines were fractionated and the solid samples of the nitroanilines were crystallised from suitable solvents. All the compounds were then distilled under reduced pressure. The solvents used were purified and carefully dried. The infrared absorption spectra of the pure compounds and their solutions in different solvents were recorded on a Perkin-Elmer Model 21 double beam instrument provided with rock salt optics under conditions described in an earlier paper (Bancrjee and Kastha, 1962). In order to complete the investigation infrared absorption in nitroanilines in the solid state at the room temperature was also studied. The melting point of the nitroanilines being high, the spectra of the melts of these compounds could not be recorded, and instead, the spectra due to the compounds milled in paraffin oil were obtained. The absorption bands due to N-H stretching vibrational frequencies of aniline in dilute solution in carbon tetrachloride were recorded from time to time throughout the investigation to check the reproducibility of the recorded spectra.

RESULTS AND DISCUSSION

The symmetric and asymmetric N-H stretching vibrational frequencies in cm^{-1} (denoted by ν_s and ν_a respectively) of the pure compounds and of their solutions in different solvents are given in Table I. The values of the sum of the shifts in the N-H vibrational frequencies in cm^{-1} ($\Delta\nu_s + \Delta\nu_a$) of each of the compounds in the different environments relative to the frequencies of the compound in dilute solution in carbon tetrachloride have been entered in Table II which also contains some data obtained in previous investigations for the sake of comparison. The Hammett σ -factors for the various substituents and the pK_a values of the bases, all taken from a paper of Whetsel (1961) have been included in both the Tables.

It is seen from Table I that the N-H stretching frequencies of the pure compounds and of their solutions in polar solvents are lower than those of the respective compounds in solution in carbon tetrachloride. This lowering of the vibrational frequencies is attributable to the formation of intermolecular hydrogen bonds as suggested in an earlier paper (Medhi and Kastha, 1963). If the N-H bonds are not greatly weakened due to the formation of the hydrogen bonds, the decrease in the N-H stretching force constant in dynes cm^{-1} is approximately given by $\Delta f = 5.52 \times 10^{-2}(\nu_s \Delta\nu_s + \nu_a \Delta\nu_a)$ where ν_s and ν_a are the vibrational frequencies in cm^{-1} of the molecule in solution in carbon tetrachloride and $\Delta\nu_s$ and $\Delta\nu_a$ denote respectively the decrease in the values of the symmetric and asymmetric frequencies in passing from CCl_4 solution to the medium in which hydrogen bonding takes place. Remembering that $\nu_a \approx \nu_s(1 + \delta)$ where δ is a small fraction and that $\nu_s \approx 3400 \text{ cm}^{-1}$, we find $\Delta f \approx 188(\Delta\nu_s + \Delta\nu_a)$. This shows that to a first approximation the reduction in the value of the N-H stretching force constant is proportional to the sum of the shifts in the two N-H stretching fre-

quencies. The values of the N-H stretching force constant of the compounds in the liquid state and in solution in carbon tetrachloride and the polar solvents have been calculated and the decrease in the force constant (Δf) with respect to that of the respective compounds in solution in CCl_4 has been obtained in

TABLE I
N-H stretching frequencies ν_s and ν_a in cm^{-1}

Name of the compound and Hammett σ pK_a	Pure		Solution in					
	Solid	Liquid	CCl_4	CHCl_3	$(\text{CH}_3)_2\text{CO}$	$(\text{C}_2\text{H}_5)_2\text{O}$	$(\text{CH}_2)_4\text{O}$	$\text{C}_6\text{H}_5\text{N}$
<i>o</i> -Chloro aniline 2.79		3380	3406	3400	3379	3367	3358	3330
		3453	3485	3480	3444	3462	3445	3442
<i>m</i> -Chloro aniline 0.373 3.52		3373	3408	3400	3383	3372	3362	3340
		3438	3485	3473	3443	3450	3436	3430
<i>p</i> -Chloro aniline 0.227 4.05		3380	3405	3403	3383	3377	3365	3342
		3443	3480	3468	3449	3450	3430	3439
<i>o</i> -Nitro aniline -0.05	3337		3410	3410	3372	3360	3340	3305
	3465		3520	3516	3482	3480	3474	3465
<i>m</i> -Nitro aniline 0.710 2.52	3319		3411	3411	3386	3377	3368	3344
	3406		3493	3493	3467	3462	3433	3345
<i>p</i> -Nitro aniline 1.270 0.99	3360		3421	3420	3384	3370	3360	3340
	3478		3503	3505	3455	3443	3428	3467
Aniline - 0.00 4.68		3300	3402	3398	3380	3376	3364	3340
		3420	3476	3460	3450	3448	3438	3430

TABLE II

Total shift in N-H stretching frequencies ($\Delta\nu_s + \Delta\nu_a$) in cm^{-1}

Compound Hammett σ pK_a	Pure		Solution in				
	Solid	Liquid	CHCl_3	$(\text{CH}_3)_2\text{CO}$	$(\text{C}_2\text{H}_5)_2\text{O}$	$(\text{CH}_2)_4\text{O}$	$\text{C}_5\text{H}_5\text{N}$
<i>o</i> -Chloro aniline 2.79		58	11	68	62	88	110
<i>m</i> -Chloro aniline 0.373 3.52		82	20	67	71	95	123
<i>p</i> -Chloro aniline 0.227 4.05		62	14	53	58	90	104
<i>o</i> -Nitro aniline -0.05	128		4	76	90	116	160
<i>n</i> -Nitro aniline 0.710 2.52	179		0	61	65	103	115
<i>p</i> -Nitro aniline 1.27 0.99	86		-1	85	111	136	117
Anilino 0.00 4.68		98	20	48	54	76	108
<i>o</i> -Anisidino 4.59		53	32	46	35	55	117
<i>m</i> -Anisidino 0.115 4.32		75	24	51	54	76	108
<i>p</i> -Anisidino -0.268 5.40	162	82	32	40	49	54	88
<i>o</i> -Phenetidine 4.47		62	38	51	40	66	123
<i>m</i> -Phenetidine 0.150 4.17		80	29	50	58	77	108
<i>o</i> -Toluidine 4.53		59	24	45	42	76	86
<i>m</i> -Toluidine -0.069 4.81		78	27	36	45	75	80
<i>p</i> -Toluidine -0.170 5.15	80	74	33	52	55	78	82

each case. The plots of the total shifts ($\Delta\nu_s + \Delta\nu_a$) against Δf for some of the compounds shown in Figs. 1(a) and 1(b) are found to be straight lines, as expected.

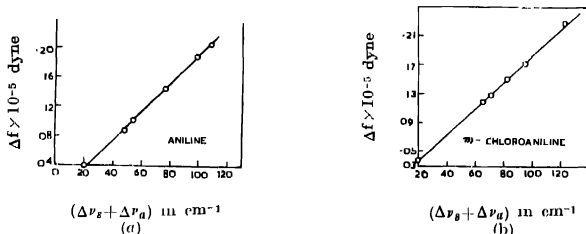


Fig. 1. Relation between the total solvent shifts ($\Delta\nu_s + \Delta\nu_a$) in cm^{-1} and decrease in N-H stretching force constant (Δf) of (a) aniline, (b) m-chloroaniline.

In a previous paper (Medhi and Kastha, 1963) it has been pointed out that the plots of the mean solvent shifts i.e., $\frac{1}{2}(\Delta\nu_s + \Delta\nu_a)$ of aniline in different environments against the corresponding quantities for some substituted anilines under similar conditions are straight lines with slopes different for the different compounds. In the present investigation similar graphs have been plotted for the compounds studied and some of them are shown in Figs. 2(a), (b) and (c). All the graphs are straight lines having different slopes. The values of the

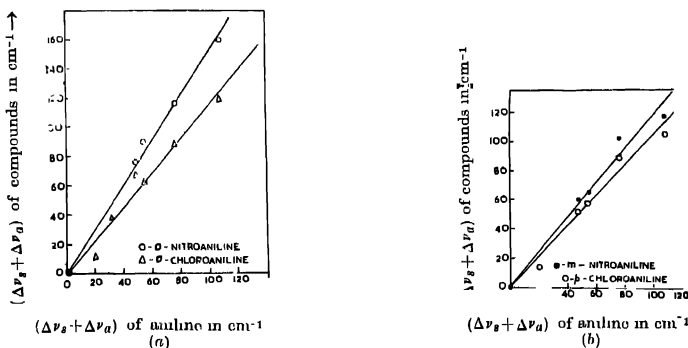


Fig. 2. Plot of total solvent shifts ($\Delta\nu_s + \Delta\nu_a$) in cm^{-1} of (a) o-nitroaniline and o-chloroaniline (b) m-nitroaniline and p-chloroaniline

slopes (denoted by S) obtained in the present investigation and also from data due to compounds investigated earlier, have been plotted against the corresponding pK_a values of the bases in Fig. 3 and the two quantities are found to be linearly related. This indicates that the S-values of the compounds may be taken as a measure of their pK_a values i.e., the proton donating capacities of the different bases with respect to aniline itself.

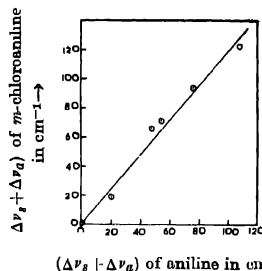


Fig. 2(c). Plot of total solvent shifts ($\Delta\nu_s + \Delta\nu_a$) in cm^{-1} of *m*-Chloroaniline against those of aniline

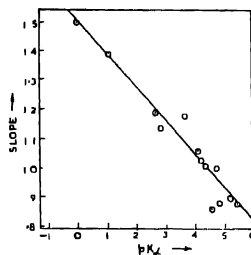


Fig. 3. Dependence of slopes (S) of pK_a values of compounds.

It is seen from Table II that in the case of the solution of the compounds in chloroform, the total solvent shifts for compounds having negative σ -values are greater while for compounds which have positive σ -factors the shifts are smaller than that for aniline. This may be due to the fact that for positive σ -factor, the positive charge on the N-atom of the NH_2 group in the molecules increases and consequently the strength of the hydrogen bonds formed between the N-atom and the hydrogen atom of the solvent molecule (cf. Moritz, 1961 ; Whetsel, 1961) decreases.

The situation, on the otherhand, is just the reverse in the cases of proton-acceptor solvents such as, acetone, ether, tetrahydrofuran and pyridine. For any of the aniline compounds, the shifts are largest in the case of its solution in pyridine and of the three isomers of a given compound the lowering in the N-H frequencies due to a change of the solvent from CCl_4 to pyridine is maximum for the ortho-isomer. This fact is in disagreement with the results reported by Bryson and Werner (1960). This discrepancy may be due to incorrect values of the two N-H frequencies due to the meta- and para-nitro anilines used by them.

It is observed that for aniline and substituted meta- and para-compounds of aniline the magnitude of the solvent shifts increases as the solvent is changed

successively from acetone to ether, tetrahydrofuran and pyridine. The ortho-compounds, however, behave differently, the shifts in solution in ether being less than that in solution in acetone. This may be due to the steric effect as suggested earlier (Medhi and Kastha, 1963).

The effect of steric hindrance on the strength of intermolecular hydrogen bonds is also discernible from an examination of the data on shifts in the N-H frequencies of some of the pure aniline compounds in the liquid state with respect to the values for the solutions in CCl_4 as given in Table II. It is seen that the shifts for the ortho-compounds are less than those for the meta- and para-compounds. However, in all the cases the total shifts are less than that observed in the case of the parent compound aniline, which probably indicates that the relative charge difference on the N-atom and the H-atom in the virtual bond of the N-H...N bridge is less in the substituted anilines than in aniline itself.

Finally, it would be of interest to find out whether there is any systematic dependence of the total solvent shifts in the various polar solvents on the dielectric constant of the solvents and on the dipole moments of their molecules. For this purpose the data have been collected from Landolt-Börnstein and International Critical Tables and are given in Table III.

TABLE III

Solvent	Chloroform	Acetone	Ether	Tetrahydrofuran	Pyridine
Dipole moment in Debye unit	1.10	2.71	1.04	1.71	2.26
Dielectric constant	5.05	21.40	1.335	—	12.5
Solvent shift of aniline in cm^{-1}	20	48	54	76	108

It is seen from the table that there is no systematic relation between the total solvent shifts and the values of the two constants.

ACKNOWLEDGMENT

The authors' sincere thanks are due to Professor S. C. Sirkar, D.Sc., F.N.I. for his helpful criticisms and for his kind interest in the work.

REFERENCES

- Banerjee, S. B. and Kastha, G. S., 1962, *Ind. J. Phys.*, **36**, 163
 Bryson, A. and Werner, R. L., 1960, *Aus. J. Chem.*, **13**, 450
 Krueger, P. J., 1962, *Can. J. Chem.*, **40**, 2300
 Medhi, K. C. and Kastha, G. S., 1963, *Ind. J. Phys.*, **37**, 139.
 Moritz, A. G., 1961, *Spectrochim. Acta.*, **17**, 365.
 Whetsel, K. B., 1961, *Spectrochim. Acta.*, **17**, 614.

AN X-RAY STUDY OF THE ϵ -CuCd₃ PHASE

B. N. DEY AND M. A. QUADER*

DEPARTMENT OF GENERAL PHYSICS AND X-RAYS, INDIAN ASSOCIATION FOR THE CULTIVATION OF SCIENCE, CALCUTTA-32

(Received March 15, 1963)

ABSTRACT. An X-ray study of the ϵ -CuCd₃ phase has been made. The powder diffraction pattern of the phase has been indexed on the basis of a hexagonal unit cell with $a = 8.10\text{\AA}$, $c = 8.76\text{\AA}$.

INTRODUCTION

The present paper reports the preliminary crystallographic data of the ϵ -CuCd₃ phase on the basis of its X-ray powder diffraction pattern. Earlier X-ray study indicated a very complex pattern for this phase and no attempt either to interpret this pattern or to determine the crystal structure appears to have been made (Owen and Pickup, 1933). During the progress of the present work, Borg (1961) reported only the unit cell dimensions of the ϵ -phase from single crystal rotation photographs.

EXPERIMENTAL DETAILS

According to the phase diagram published in Metals Handbook (1948) the ϵ -phase occurs exactly at the composition CuCd₃, and is represented by a vertical line. On the low concentration side of this composition the alloy is a mixture of ϵ -phase and δ -phase with γ -brass type structure, the high cadmium side being a mixture of ϵ -phase and η -phase of cadmium lattice. The alloy investigated was made from spectroscopically pure Mathey Copper and Cadmium to the composition CuCd₃, the weight loss on melting the elements in an evacuated pyrex tube being negligible. However, slightly excess of Cadmium was used to compensate the loss of cadmium by sublimation, if any, and also to avoid the occurrence of the complex δ -phase. The alloy was homogenized at 300°C for a few days after which filings were obtained with a No. 1 file. The powder was annealed in an evacuated pyrex tube at 250°C for 4 hours and then air-cooled. Powder X-ray diffraction photographs were taken on a straumanis-type Debye-Scherrer camera of 114.6 mm. diameter using CuK α radiation. Two alloys with slightly higher and lower cadmium concentration than the composition CuCd₃ were also prepared and their diffraction patterns were recorded. A comparison of the films showed that the alloy under investigation contained very small amount of η -phase and

*Present Address :—National Metallurgical Laboratory, Jamshedpur, India.

the few weak η -lines were eliminated. A difference diagram (Lapson, 1949) was plotted by taking the $\sin^2\theta$ values of the first 20 low angle lines.

INTERPRETATION OF DIFFRACTION PATTERN

It was found that the lines could be indexed either on a tetragonal unit cell with $a = 16.23\text{\AA}$ and $c = 11.76\text{\AA}$, or on an orthorhombic unit cell with $a = 14.08\text{\AA}$, $b = 12.20\text{\AA}$ and $c = 11.76\text{\AA}$ taking wave lengths $^{\lambda}K_{\alpha_1} = 1.54051\text{\AA}$ and $^{\lambda}K_{\alpha_2} = 1.54433\text{\AA}$ for copper radiations.

It was however noted that the different axes bear the ratio

$$a_{tetra}/a_{ortho} = a_{ortho}/b_{ortho} = 2/\sqrt{3} = 1.154,$$

a value, which suggested the possibility of a hexagonal unit cell. The lines were then indexed (Quader, 1962) on the basis of a hexagonal unit cell with $a = 16.23\text{\AA}$ and $c = 16.04\text{\AA}$. However, the indexing was not very probable, although the agreement between observed and calculated values were very satisfactory. A further attempt with accurate diffractometric measurements has been made to obtain a smaller unit cell for the ϵ -phase. Finally, the powder diffraction pattern could be indexed on the basis of a smaller hexagonal unit cell with

$$a = 8.10\text{\AA}, \quad c = 8.76\text{\AA} \quad \text{and} \quad c/a = 1.08$$

which is approximately one-eighth of the previous hexagonal unit.

The powder diffraction data are given in Table I.

TABLE I
Powder diffraction data for ϵ -CuCd₃; CuK $_{\alpha}$ radiation

hkl	$\sin^2\theta$ (calculated)	$\sin^2\theta$ (observed)	Intensity
20 2	.0794	.0805	m
10 3	.0823	.0829	m
21.1	.0923	.0929	vw
30.1	.1165	.1174	s
00.4	.1261	.1260	m
30.2	.1400	.1416	vw
22.0	.1450	.1460	m
31.0	.1570	.1556	vw
22.2	.1762	.1780	vvw

			Intensity
31.2	.1882	.1890	vw
40.0	.1933	.1940	vw
10 5	.2074	.2079	vvw
32.0	.2205	.2280	vw
11.5	.2316	.2300	vw
30.4	.2338	.2340	vw
32.1	.2373	.2380	vw
20.5	.2437	.2440	vw
40 3	.2636	.2623	w
22.4	.2701	.2700	w
00.6	.2814		
10 6	.2934	.2811	w
32.3	.2998	.2935	vw
30.5	.3042	.3000	s
50.1	.3099	.3057	s
33.0	.3262	.3114	vw
33.1	.3340	.3270	w
42.1	.3461	.3335	s
30.6	.3900	.3450	vvw
10.7	.3950	.3890	w
32.5	.4249	.3942	vw
20.7	.4313	.4242	w
60.1	.4428	.4295	vw
33.4	.4513	.4445	w
52.0	.4712	.4515	w (diffuse)
52.1	.4790	.4723	vw
00.8	.5004	.4795	w
51 5	.5698	.4984	vw
		.5698	vw

hkl	$\sin^2\theta$ (calculated)	$\sin^2\theta$ (observed)	Intensity
44 0	.580	.5820	
The following lines correspond into $K\alpha_1$			
30 8	.6066	.5060	w
32.7	.7000	.6097	w
70.2	.6215	.6209	w
60 5	.6278	.6270	w
73.3	.6596		
70 3	.6596	.6600	m
52 5	.6639	.6632	m
71.0	.6859	.6863	w
71 2	.7170	.7137	vw
32 8	.7269	.7248	vw
30 9	.7392	.7360	vw
63 1	.7655	.7645	m
70 6	.7840	.7820	w
72 1	.8139	.8128	w
80 3	.8400	.8391	m
63.4	.8826	.8804	vw
64.0	.9144	.9124	vw
81.3	.9484	.9460	vw
73.0	.9506	.9498	m
80 5	.9647	.9632	w
42.9	.9675	.9674	m
52.3	.9724	.9721	m
11.11	.9782	.9762	vw

According to Borg (1961) the dimensions of the hexagonal unit are

$$a = 8.11 \text{ \AA}, \quad c = 8.76 \text{ \AA}$$

with which our results agree well. Final values of a and c were obtained by adjusting the constants from the observations of the systematic deviations.

The density of the alloy measured by means of a density bottle is 8.004 gms/cc. and hence the number of molecules per unit cell, $M = 6$.

The following systematic absence of reflections were observed :

for $hk \cdot l$, no condition

for $oo \cdot l$, $l = 2n$.

The extinction conditions are consistent with space groups

$$P6_322, P6_{3m}$$

However, a large number of extremely weak lines could not be measured and so the extinction condition, and hence the space group, as mentioned above, may not be correct.

ACKNOWLEDGMENTS

The authors are thankful to Prof. B. N. Srivastava, D.Sc , F N I., for his interest in the work. One of the authors (B.N.D) is thankful to C.S.I.R. (New Delhi) for financial assistance.

REFERENCES

- Borg, R. 1961, *Trans. Met. Soc. (A.I.M.M.E.)*, **221**, 527.
 Lipson, H., 1949, *Acta Cryst.*, **2**, 43
 Metals Handbook, 1948, *Am. Soc. for Metals*.
 Owen, E. A. and Pickup, L., 1933, *Proc. Roy. Soc.*, **A139**, 526.
 Quader, M. A., 1962, *Doctoral dissertation (University of Calcutta)*

Letters to the Editor

The Board of Editors will not hold itself responsible for opinions expressed in the letters published in this section. The notes containing reports of new work communicated for this section should not contain many figures and should not exceed 500 words in length. The contributions must reach the Assistant Editor not later than the 15th of the second month preceding that of the issue in which the letter is to appear. No proof will be sent to the authors

5

HIGH FIELD CONDUCTIVITY OF InAs

B. R. NAG, P. DAS, H. PARIA AND S. K. ROY

INSTITUTE OF RADIO PHYSICS AND ELECTRONICS, UNIVERSITY OF CALCUTTA

(Received February 5, 1963)

Experimental investigations made by Prior (1958), Kanai (1958a, 1958b), Chikksman and Steele (1959, 1960) have shown that both in *n*-type and in *p*-type InSb electrical breakdown occurs before any significant reduction in conductivity due to the applied electric field can be detected. The occurrence of breakdown without showing any reduction in conductivity is in sharp contrast to the high field conductivity characteristics of group IV semiconductors, Ge and Si. It has been suggested (Kanai, 1958) that this contrast may be due to predominance of polar optical scattering in InSb. If this supposition is correct it would be expected that the above characteristic of InSb is typical of III-V semiconductors. Experimental study of other III-V semiconductors, therefore, assume importance. Steele (1959) has reported some results of his studies on polycrystalline *n*-type InAs samples having an initial electron concentration $\sim 5 \times 10^{19}/\text{cm}^3$. It was found that the conductivity characteristics are similar to those of InSb. In this note the experimental results obtained for a *p*-type InAs sample are presented.

The experimental samples were prepared from polycrystalline ingots having a conductivity of 3.5 mho/cm at room temperature. It was estimated from Hall constant data that the sample had a hole concentration $\sim 10^{17}/\text{cm}^3$ and a hole to electron concentration ratio $\sim 10^4$.

High field conductivity characteristics were obtained using rectangular filaments having the dimensions 0.1 cm \times 0.1 cm \times 0.7 cm and a total resistance of 20 ohms at room temperature. The contacts to the samples were soldered using tin and stannous chloride. The current density for different electric fields were obtained using pulses of 1.5 μ sec duration and 0.5 c/s repetition rate. Experimental curves giving the normalised conductivity for different electric fields are shown in Fig. 1.

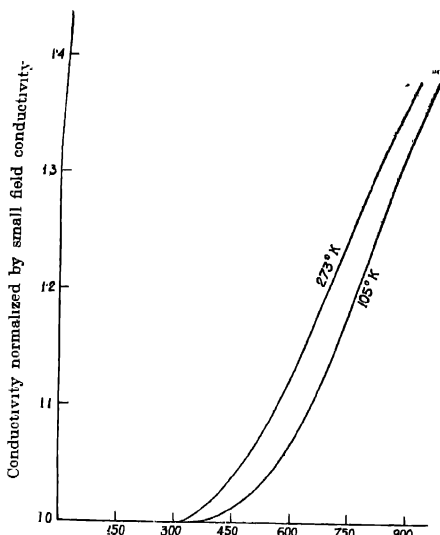


Fig. 1. Electric field in volts/centimeter

Fig. 1. Normalised conductivity characteristic of *p*-type polycrystalline InAs at high fields.

A study of the experimental curves shows that the conductivity characteristics are not much affected by the lattice temperature in the range of 105°K-273°K. No significant reduction in conductivity is found before breakdown, which occurs at an electric field ~ 800 v/cm. It may thus be concluded that the conductivity characteristics of *p*-type InAs also have the same general features as those of InSb. It should also be noted that in view of the nearly spherical constant energy surfaces of InAs, the above observation is likely to be applicable to single crystals of InAs.

The authors wish to express their indebtedness to Prof. J. N. Bhar, D.Sc. F.N.I., for his kind supervision of the present study. Thanks are also due to Messrs. Siemens Schuckertwerke AG., Erlangen through whose courtesy the InAs samples were received.

REFERENCES

- Glicksman, M. and Steele, M. C., 1958, *Phys. Rev.*, **110**, 1204.
- Kanai, Y., (1958a), *J. Phys. Soc. Japan*, **13**, 967.
- Kanai, Y., (1958b), *J. Phys. Soc. Japan*, **13**, 1065.
- Prior, A. C., 1958, *J. Electronics and Control*, **4**, 165.
- Steele, M. C., 1959, *Bull. Amer. Phys. Soc.*, **4**, 28.
- Steele, M. C. and Glicksman, M., 1960, *Phys. Rev.*, **118**, 474.

A NOTE ON GRAVITATIONAL INSTABILITY

J. M. GANDHI AND P. V. BAKORE

DEPARTMENT OF PHYSICS, UNIVERSITY OF RAJASTHAN, JAIPUR

(Received, December 4, 1962)

The purpose of this note is to show that Jeans' criterion for gravitational instability remains unmodified when the viscosity of the medium is assumed to be variable.

Consider an extended viscous and thermally conducting homogeneous medium. The fluctuations in density $\delta\rho$, pressure δp , temperature δT and gravitational potential δv are governed by the following set of equations.

$$\begin{aligned} \rho \frac{\partial \bar{u}}{\partial t} = & -\text{grad } \delta p + \rho \text{ grad } \delta v + \frac{1}{3}\mu \text{ grad div } \bar{u} + \mu \nabla^2 \bar{u} \\ & + (\text{grad } \mu \cdot \text{grad}) \bar{u} + \text{grad } \mu \cdot \text{grad } \bar{u} - \frac{2}{3}(\text{div } \bar{u}) \text{grad } \mu \dots \\ & \frac{d}{dt} \delta \rho = -\rho \text{ div } \bar{u} \\ & \nabla^2 \delta v = -4\pi G \delta \rho \end{aligned} \quad \dots \quad (1)$$

$$\rho c_v \frac{d}{dt} (\delta T) - \frac{d}{dt} \delta p = K \nabla^2 \delta T$$

and
$$\frac{\delta p}{\rho} = \frac{\delta \rho}{\rho} + \frac{\delta T}{T}$$

We shall seek the solutions which correspond to the propagation of plane waves in the z direction. Then these equations break up into three independent modes.

$$\rho \frac{du_x}{dt} = \mu \frac{d^2 u_x}{dz^2} + \frac{du_x}{dz} \frac{d\mu}{dz} \quad \dots \quad (2)$$

$$\rho \frac{du_y}{dt} = \mu \frac{d^2 u_y}{dz^2} + \frac{du_y}{dz} \frac{d\mu}{dz} \quad \dots \quad (3)$$

and

$$\begin{aligned} \rho \frac{du_z}{dt} = & -\frac{d}{dz} \delta p + \rho \frac{d}{dz} \delta v + \frac{4}{3} \mu \frac{d^2 u_z}{dz^2} + \frac{4}{3} \frac{du_z}{dz} \frac{d\mu}{dz}; \\ \frac{d}{dt} \delta \rho = & -\rho \frac{du_z}{dz}; \quad \frac{d^2}{dz^2} (\delta v) = -4\pi G \delta \rho \end{aligned} \quad \dots \quad (4)$$

$$\frac{d}{dt} (\delta p - c^2 \delta \rho) = \frac{K}{\rho c_v} \frac{d^2}{dz^2} (\delta p - c^2 \delta \rho)$$

where c , c' denote the adiabatic and isothermal velocity of sound and K the thermal conductivity. Two modes of wave propagation given by equations (2) and (3) are trivial and unaffected by gravity, compressibility and conductivity as expected. For a solution of equation (4) we write

$$\frac{d}{dt} = i\omega \quad \text{and} \quad \frac{d}{dz} = -ik \quad (5)$$

where ω denotes the frequency and k the wave number. Substitute equation (5) in equation (4), we obtain a system of linear homogeneous equations which can be written in the matrix notation in the form

$$\begin{vmatrix} i\rho\omega + \frac{8}{3}\mu k^2 & i\rho k & -ik & 0 \\ -i\rho k & 0 & 0 & i\omega \\ 0 & -k^2 & 0 & 4\pi G \\ 0 & 0 & \left(i\omega + \frac{K}{\rho c_v} k^2\right) - \left(i\omega c^2 + \frac{K}{\rho c_u} c'^2\right) \end{vmatrix} \begin{vmatrix} u_z \\ \delta v \\ \delta p \\ \delta \rho \end{vmatrix} = 0 \quad \dots \quad (6)$$

This is identical with that obtained by Kato and Kumar (1960) except that the coefficient of μk^2 in the first term of the first column is $8/3$, instead of $4/3$. Hence it can be concluded that there will be no modification of Jeans' Criterion for gravitational instability, when the viscosity of the medium is assumed to be variable.

The authors express their gratitude to Prof. D. S. Kothari and to Prof. F. C. Auluck for their guidance and encouragement.

REFERENCES

- Chandrasekhar, S., "Hydrodynamic and Hydromagnetic Stability" (1961), Oxford (Clarendon Press), (Chap. XIII).
 Jeans, J. H., 1929, *Astronomy and Cosmogony*, Cambridge University Press, pp. 345-347
 Kato, S. and Kumar, S. S., 1960, *Pub. of the Astron. Soc. of Japan* **12**, 255

BOOK REVIEW

GROUP THEORY AND ITS APPLICATIONS TO PHYSICAL PROBLEMS—

By Morton Hamermesh. Pp. 509+xi. Pergamon Press, Oxford, London, New York. 1962. Price £5. 5s. net.

This book has been written with the main object of making the application of abstract group theory to physical problems understandable to physicists. As mentioned by the author in the Preface no previous knowledge of group theory is needed, but the reader should know quantum mechanics.

In the first chapter the elements of the group theory have been discussed with the help of suitable examples. The symmetry groups and their properties have been described in detail in Chapter 2. The third chapter deals with group representations. The methods of finding the irreducible representation of abelian and non-abelian groups are discussed in Chapter 4 and character tables of crystal pointgroups are given in this chapter. Miscellaneous operations with group representations, such as obtaining Kronecker products, complex conjugate representation, real representation, etc. are discussed in Chapter 5.

Taking the case of an atomic system, the application of properties of group representations to solution of physical problems has been discussed in Chapter 6. The properties of symmetry group and different methods for finding the characters of such groups are discussed in great detail in Chapter 7. The next chapter deals with properties of continuous groups and includes discussions on Lie groups, one-parameter groups, Lie algebras, etc. Chapter 9 deals with properties of groups having axial and spherical symmetry. As examples of applications of the properties of such groups the problems of splitting of atomic energy levels in crystalline fields have been discussed in detail. Chapter 10 deals with linear groups in n -dimensional space and methods of constructing irreducible representations of general linear group and its sub-groups, and of orthogonal groups. Applications of the properties of such groups to problems in atomic and nuclear physics have been illustrated in Chapter 11. The last chapter deals with the properties of ray representations and little groups. Finally, the author has given a bibliography and notes including the references of all the journals and books from which the deductions given in the book have been taken. This will be extremely useful to readers who are interested in studying the subject exhaustively.

The book appears to be a valuable text book for students or research workers who are interested in applying the methods of group theory to physical problems. The get-up is excellent.

S. C. S.

BOOK REVIEW

PULSE CIRCUITS—by B. Chatterjee : Pp 159. Asia Publishing House, 1963.
Price Rs. 10.00.

This is a small book presumably meant for advance students of communication engineering specialising in Television and Radio Aids to Navigation. The subject matter is divided into eleven chapters. Two appendices on Laplace Transform cover about one-fifth of the book. The author claims that unnecessary details have been avoided as far as possible and stress has been given only on the fundamental principles.

Chapter one deals with Introduction of Pulse characteristics. To the reviewer it seems better to delete "Introduction of". Chapter two is devoted to pulse-shaping circuits. Chapter three is on delay lines. Chapter four discusses pulse-amplifiers. Chapter five describes the blocking oscillator. Chapter six deals with trigger circuits. Chapter seven describes counter circuits. Chapter eight deals with multivibrators and chapter nine with sweep circuits. Chapter ten is devoted to radar indicators. Chapter eleven discusses pulse measurements and wave-form synthesis.

As expressed by the author in the preface, the book is aimed at discussing the basic principles of ordinary pulse circuits. The reviewer feels that this book is a sketchy outline and many important aspects of the subject are dismissed with the briefest mention. The book is written in a manner similar to the concise note, a lecturer prepares and the remaining gaps are filled up by him in accordance with the needs of his students in the class room. As this book is meant for advanced students it would be a great mistake to mask what is really needed in an attempt to be brief.

It is unfortunate that so many printing and other errors have passed unnoticed. Meanings of the symbols used in some formulae are not given. There are some loose statements like "nonsinusoidal waveforms like rectangular, sawtooth, triangular etc. are known as pulses", "Pulse amplifiers are used in their linear ranges of operations". A diagram on ringing circuits is a conspicuous omission. The book needs a thorough and careful revision. The reviewer would welcome in a new edition a fuller treatment of the chapters with greater care in defining terms more clearly and precisely so that students may not have to consult other books for proper understanding of the topics dealt with in the book itself.

A. K. S.

PUBLICATIONS OF THE INDIAN ASSOCIATION FOR THE CULTIVATION OF SCIENCE

		Rs. nP
1. RUSSELL, E. J.	Methods in Scientific Research ..	0.37
2. JEANS, J. H.	The Origin of the Planets ..	0.37
3. ASTON, F. W.	Separation of Isotopes ..	0.37
4. LENNARD-JONES, J. E.	Interatomic Forces ..	1.50
5. HILL, A. W.	The Royal Botanic Gardens, Kew ..	1.50
6. MILLIKAN, R. A.	The Educational Aims and Practices of the California Institute of Technology ..	0.37
7. MITRA, S. K.	Active Nitrogen—A New Theory ..	2.50
8. WADIA, D. N.	Petroleum Resources of India ..	2.50
9. RAY, P.	The Theory of Valency and the Structure of Chemical Compounds ..	3.00
10. MUKHERJEE, J. N.	The Role of the Electrical Double Layer in the Electro-Chemistry of Colloids ..	1.75
11. ROBINSON, R.	Distribution of Anthocyanins ..	1.25
12. CHAPMAN, S.	The Earth's Magnetism and its Changes ..	1.00
13. MARK, H.	Catalysts in Polymerization Reactions ..	1.50
14. AMALDI, E.	Diffraction Effects in the Scattering of Neutrons, Mesons and Electrons by Nuclei ..	1.50
15. FIESER, L. F.	Lapinone, A New Antimalarial ..	1.00
16. BOSE, N. K.	Fluid Dynamics ..	1.25
17. VENKATARAMAN, K.	Constitutional Problems Concerning Vat Dyes ..	1.00
18. ROY, J. N.	The Chemical Basis of Some Physiological Actions ..	1.00
19. SHOENBERG, D.	Superconductivity ..	1.00
20. PALIT, S. R.	Non-Aqueous Titration ..	3.00
21. KRISHNAN, M. S.	Iron Ores of India ..	5.00
22. SEN, S. N.	Bijzonder Itihas ; Vol. I ..	10.50
	Vol. II ..	12.00
23. SESHADRI, T. R.	An Investigation of Plant Drugs and Insecticide ..	1.00
24. BOWEN, E. G.	The Formation of Natural and Artificial Rain ..	1.50
25. BANERJI, S. K.	Earthquakes in the Himalayan Region ..	3.00
26. MAGNETISM :	Report of the Symposium on Magnetism ..	7.00
27. WESTPHAL, Dr. Ing. E.	The Freight Tube Float ..	8.00
28. HIRSCHFELDER, J. O.	Molecular Physics and Intermolecular Forces ..	1.25
29. SEN, N. R.	The Modern Theory of Turbulence ..	2.00
30. DOUGLAS, A. E.	Some Recent Development in Molecular Spectroscopy ..	1.00
31. SHOENBERG, E.	Experimental Determination of the Electronic Structure of Metal ..	1.00

CONTENTS

Indian Journal of Physics

Vol. 37, No. 5

May, 1963

PAGE

24. A Four-Point Probe for Resistivity Measurements of Semiconductors—J. K. D. Verma ... 241
25. On the Selectivity of a Resistance Capacitance Network—S. C. Dutta Roy ... 245
26. Singlet→Triplet Absorption in Frozen *p*-Bromotoluene—A. R. Paul and S. C. Sirkar ... 252
27. Localization of Empty 4p Orbitals in Certain Transition Metal Compounds—K. P. Sinha and Chintamani Mande ... 257
28. On Nuclear Quadrupole Coupling Constants of Chlorine Isotopes and Dipole Moment of BrCl Molecule—K. L. Narayana and C. Santhamma ... 261
29. Investigation on Hydrogen Bonding in Pure Chloro- and Nitro Anilines and their Solutions in Polar Solvents—K. C. Medhi and G. S. Kastha ... 275
30. An X-ray Study of the ϵ -CuCd₃ Phase—B. N. Dey and M. A. Quader ... 282

LETTERS TO THE EDITOR :

5. High Field Conductivity of InAs—B. R. Nag, P. Das, H. Paria and S. K. Roy ... 287
6. A Note on Gravitational Instability—J. M. Gandhi and P. V. Bakore ... 289
- BOOK REVIEWS ... 291

PRINTED BY KALIPADA MUKHERJEE, EKA PRESS, 204/, B. T. ROAD, CALCUTTA-31
 PUBLISHED BY THE REGISTRAR, INDIAN ASSOCIATION FOR THE CULTIVATION OF SCIENCE
 2 & 3, LADEWILLINGTON ROAD, CALCUTTA-32

Regd. No. C-3911

VOL. 37 **INDIAN JOURNAL OF PHYSICS** No. 6
(Published in collaboration with the Indian Physical Society)

AND

VOL. 46 **PROCEEDINGS** No. 6

OF THE

**INDIAN ASSOCIATION FOR THE
CULTIVATION OF SCIENCE**

JUNE 1963

**PUBLISHED BY THE
INDIAN ASSOCIATION FOR THE CULTIVATION OF SCIENCE
JADAVPUR, CALCUTTA 32**

BOARD OF EDITORS

K. BANERJEE	D. S. KOTHARI
D. M. BOSE	S. K. MITRA
S. N. BOSE	B. D. NAG CHAUDHURI
S. D. CHATTERJEE	K. R. RAO
P. S. GILL	D. B. SINHA
S. R. KHASTGIR	S. C. SIKKAR (<i>Secretary</i>)
B. N. SRIVASTAVA	

EDITORIAL COLLABORATORS

PROF. R. K. ASUNDI, Ph.D., F.N.I.
PROF. D. BASU, Ph.D.
PROF. J. N. BHAR, D.Sc., F.N.I.
PROF. V. G. BHIDE, Ph.D.(Nag), Ph.D.(Lond).
PROF. A. BOSE, D.Sc., F.N.I.
PROF. S. K. CHAKRABARTY, D.Sc., F.N.I.
DR. J. S. CHATTERJEE
DR. K. DAS GUPTA, Ph.D.
PROF. N. N. DAS GUPTA, Ph.D., F.N.I.
DR. J. DHAR, D.Phil (So)
PROF. A. K. DUTTA, D.Sc., F.N.I.
PROF. C. S. GHOSH, M.Sc., S.M., F.N.I., M.I.E.E.
PROF. S. GHOSH, D.Sc., F.N.I.
PROF. S. N. GHOSH, D.Sc.
PROF. S. GUPTA, M.Sc., F.N.I.
PROF. D. N. KUNDU, Ph.D., F.N.I.
PROF. R. C. MAJUMDER, Ph.D., F.N.I.
PRINCIPAL Y. G. NAIK, Ph.D.
PROF. S. K. PALIT, D.Sc., F.R.I.C., F.N.I.
PROF. H. RAKSHIT, D.Sc., F.N.I.
PROF. A. SAHA, D.Sc., F.N.I.
DR. VIKRAM A. SARABHAI, M.A., Ph.D., F.N.I.
DR. A. K. SENGUPTA, D.Sc.
PROF. NAND LAL SINGH, D.Sc.
DR. M. S. SINHA, D.Sc., F.N.I.
PROF. N. R. TAWDE, Ph.D., F.N.I.
DR. P. VENKATESWARLU

Annual Subscription—

Inland Rs. 25.00

Foreign £ 2-10-0 or \$ 7.00

NOTICE

TO INTENDING AUTHORS

Manuscripts for publication should be sent to the Assistant Editor, Indian Journal of Physics, Jadavpur, Calcutta-32.

The manuscripts submitted must be type-written with double space on thick foolscap paper with sufficient margin on the left and at the top. The original copy, and not the carbon copy, should be submitted. Each paper must contain an abstract at the beginning.

All references should be given in the text by quoting the surname of the author, followed by year of publication, e.g., (Ghosh, 1954). The full reference should be given in a list at the end, arranged alphabetically, as follows; Ghosh, D. K., 1954, *Ind. J. Phys.*, 28, 485.

Line diagrams should be drawn on white Bristol board or tracing paper with black India ink, and letters and numbers inside the diagrams should be written neatly in capital type with India ink. The size of the diagrams submitted and the lettering inside should be large enough so that it is legible after reduction to one-third the original size. A simple style of lettering such as gothic, with its uniform line width and no serifs should be used, e.g.,

A·B·E·F·G·M·P·T·W·

Photographs submitted for publication should be printed on glossy paper with somewhat more contrast than that desired in the reproduction, and should, if possible, be mounted on thick white paper.

Captions to all figures should be typed in a separate sheet and attached at the end of the paper.

The mathematical expressions should be written carefully by hand. Care should be taken to distinguish between capital and small letters and superscripts and subscripts. Repetition of a complex expression should be avoided by representing it by a symbol. Green letters and unusual symbols should be identified in the margin. Fractional exponents should be used instead of root signs.

BENGAL CHEMICAL & PHARMACEUTICAL WORKS LD.

Pioneer Indian Manufacturers of Pharmaceuticals & Chemicals.

Manufacturers of:

Pharmaceutical Chemicals:

Caffeine and its salts, Strychnine Hydrochlor, Strychnine Sulphate, Brucine Sulphate, Nicotinic Acid, B.P., Nicotinamide, B.P., Potassium Citrate B.P., I.P., Sodium Citrate B.P., I.P., Potassium Acetate B.P., I.P., Potassium Iodide B.P., I.P., Sodium Iodide B.P., I.P., Ferri et Ammon Citrate B.P., I.P., and various other Pharmaceutical Chemicals.

Heavy & Reagent Quality Fine Chemicals:

Alum, Alum Sulphate (Iron Free), Ferro Alum, Zinc Chloride Tech. Naphthalene Pure, Sodium Citrate A.R., Potassium Citrate A.R., Magnesium Sulphate A.R., Sodium Sulphate Anhydrous A.R., Potassium Iodide A.R., Sodium Chloride A.R., Zinc Sulphate A.R., etc.

Please refer your enquiries for the above items and other chemicals in the line to :—

BENGAL CHEMICAL

6, GANESH CHUNDER AVENUE,
CALCUTTA-13, INDIA.

NON-AQUEOUS TITRATION

A monograph on acid-base titrations in organic solvents

By

PROF. SANTI R. PALIT, D.Sc., F.R.I.C., F.N.I.

DR. MIHIR NATH DAS, D.Phil.

AND

MR. G. R. SOMAYAJULU, M.Sc.

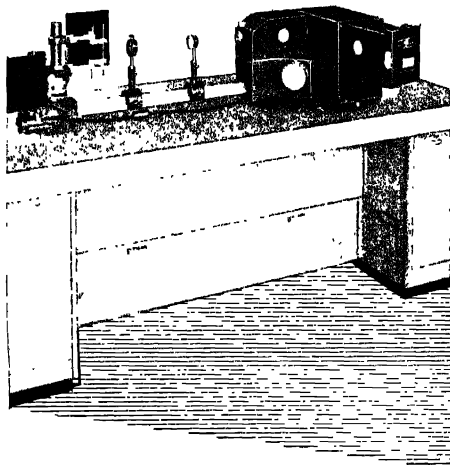
This book is a comprehensive survey of the recently developed methods of acid-base titrations in non-aqueous solvents. Acid-base concept, as developed by Lowry-Brönsted and Lewis is succinctly presented in this slender volume. The subject is divided into two classes, viz. titration of weak bases and titration of weak acids. The method of 'glycolic titration' is described at a great length as also the method of 'acetic titration' including its recent modifications for the estimation of weak bases. Various methods for the titration of weak acids are duly described. A reference list of all pertinent publications is included in this book.

122 pages with 23 diagrams (1954)

Inland Rs. 3 only. Foreign (including postage) \$ 1.00 or 5s.

Published by

INDIAN ASSOCIATION FOR THE CULTIVATION OF SCIENCE
JADAVPUR, CALCUTTA-32, INDIA



ZEISS THREE-PRISM SPECTROGRAPH

A glass-type spectrograph with Foresterling set of prisms of high-power and resolving capacity, large dispersion and excellent definition of lines, self-contained construction.

Equipment with 3 cameras : Camera $f = 12$ cm $F/2.4$ and camera $f = 27$ cm $F/5.4$ for feeble-light phenomena (Raman effect, fluorescence of flame-spectra, etc.)

Autocollimation camera $f = 130$ cm $F/26$ for taking complex emission spectra in the visible region (special type steel, rare earth etc.)

Solves all spectra-chemical problems of organic and inorganic nature.

VEB Carl Zeiss JENA

SOLE AGENTS IN INDIA :

GORDHANDAS DESAI PRIVATE, LTD.

PHEROZSHAH MEHTA, ROAD, BOMBAY 1.

Branches :

4/2B Asaf Ali Road
NEW DELHI.

22, Linghi Chetty Street
MADRAS-1.

P-7, Mission Row Extension
CALCUTTA-1.

New Model 421 high-resolution SPECTROPHOTOMETER offers uninterrupted scan from 2.5 to 18 microns

Highest grating resolution and greatest flexibility over an extended wavelength range—
with no gaps or overlaps—the new Perkin-Elmer Model 421's performance means these advantages:

More accurate identifications: significant absorption bands differing only slightly in frequency can be easily separated by the outstanding resolution of the Model 421's grating dispersion system.

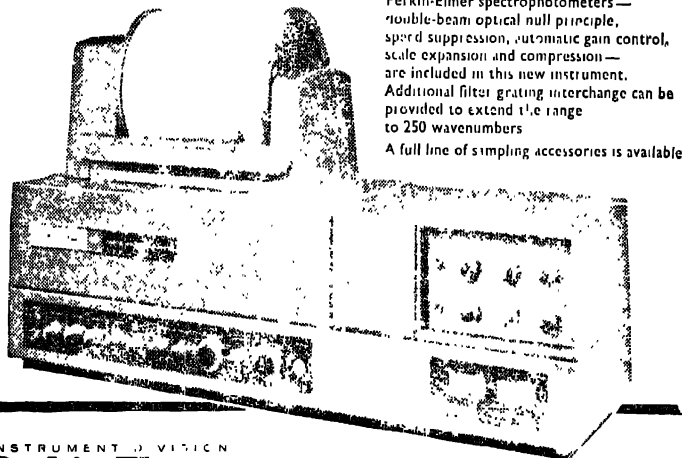
Uninterrupted scan: automatic filter switching as scan proceeds does not interrupt spectral record; the Model 421 presents a continuous, complete grating scan.

Extended wavelength range: the Model 421 operates from 4000 to 550 wavenumbers—
from 2.5 to more than 18 microns—routinely

More precise quantitative measurements: high spectral purity afforded by the Model 421's resolution means close conformity of bands to classical absorption Intensity laws

All the outstanding instrumental operating features of other Perkin-Elmer spectrophotometers—double-beam optical null principle, speed suppression, automatic gain control, scale expansion and compression—are included in this new instrument. Additional filter grating interchange can be provided to extend the range to 250 wavenumbers

A full line of simpling accessories is available,



6885-PE 17, 61

INSTRUMENT DIVISION
Perkin-Elmer Corporation
NORWALK CONNECTICUT

Sold and serviced in India exclusively by

BLUE STAR

**BLUE STAR ENGINEERING
CO. (Calcutta) PRIVATE LTD.**
7 HARE STREET, CALCUTTA 1
Also at: BOMBAY • DELHI
MADRAS • JAMSHEDPUR

PUBLICATIONS OF THE INDIAN ASSOCIATION FOR THE CULTIVATION OF SCIENCE

		Rs. nP
1. RUSSELL, E. J.	.. Methods in Scientific Research . . .	0 37
2. JEANS, J. H.	. The Origin of the Planets . . .	0 37
3. ASTON, F. W.	.. Separation of Isotopes . . .	0.37
4. LENNARD-JONES, J. E.	Interatomic Forces . . .	1.50
5. HILL, A. W.	. The Royal Botanic Gardens, Kew . . .	1.50
6. MILLIKAN, R. A.	. The Educational Aims and Practices of the California Institute of Technology . . .	0 37
7. MITRA, S. K.	.. Active Nitrogen—A New Theory . . .	2 50
8. WADIA, D. N.	.. Petroleum Resources of India . . .	2 50
9. RAY, P.	. The Theory of Valency and the Structure of Chemical Compounds . . .	3 00
10. MUKHERJEE, J. N.	.. The Role of the Electrical Double Layer in the Electro-Chemistry of Colloids . . .	1 75
11. ROBINSON, R.	. Distribution of Anthocyanins . . .	1 25
12. CHAPMAN, S.	.. The Earth's Magnetism and its Changes . . .	1.00
13. MARK, H.	Catalysts in Polymerization Reactions . . .	1 50
14. AMALDI, E.	.. Diffraction Effects in the Scattering of Neutrons, Mesons and Electrons by Nuclei . . .	1.50
15. FIESER, L. F.	.. Lapinone, A New Antimalarial . . .	1.00
16. BOSE, N. K.	.. Fluid Dynamics . . .	1.25
17. VENKATARAMAN, K.	.. Constitutional Problems Concerning Vat Dyes . . .	1.00
18. ROY, J. N.	.. The Chemical Basis of Some Physiological Actions . . .	1.00
19. SHOENBERG, D.	.. Superconductivity . . .	1 00
20. PALIT, S. R.	.. Non-Aqueous Titration . . .	3.00
21. KRISHNAN, M. S.	.. Iron Ores of India . . .	5 00
22. SEN, S. N.	.. Bijzonder Itihas ; Vol. I . . .	10.50
	Vol. II . . .	12.00
23. SESHADRI, T. R.	.. An Investigation of Plant Drugs and Insecticide . . .	1.00
24. BOWEN, E. G.	.. The Formation of Natural and Artificial Rain . . .	1.50
25. BANERJI, S. K.	.. Earthquakes in the Himalayan Region . . .	3.00
26. MAGNETISM :	.. Report of the Symposium on Magnetism . . .	7 00
27. WESTPHAL, DR. ING. E.	.. The Freight Tube Float . . .	8.00
28. HIRSCHFELDER, J. O.	.. Molecular Physics and Intermolecular Forces . . .	1.25
29. SEN, N. R.	.. The Modern Theory of Turbulence . . .	2.00
30. DOUGLAS, A. E.	.. Some Recent Development in Molecular Spectroscopy . . .	1 00
31. SHOENBERG, E.	.. Experimental Determination of the Electronic Structure of Metal . . .	1.00



Our systems for gathering and processing measuring data and for automatic process control permit the full automation of metallurgical processes provided that the process control system is compatible with future automation.

Progressive Process Control for Converters

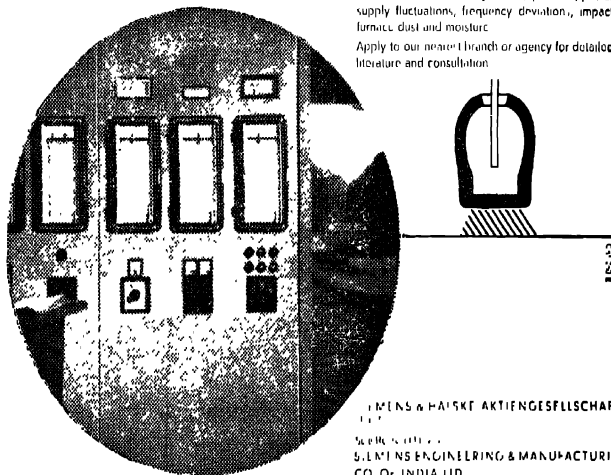
shortens blowing periods and improves the quality of recovered steel. Our electric, pneumatic and combined electro-pneumatic TELFERM TELEPNEU standard process control system

has long proved its value in all process control problems connected with converters.

Control of blast-O₂ ratio during blow operation with mixed oxygen and O₂ flow control during blow operation with pure oxygen.

Accommodated in a metal-clad cabinet, the equipment is immune to changes in temperature, power supply fluctuations, frequency deviation, impact, furnace dust and moisture.

Apply to our nearest branch or agency for detailed literature and consultation.



SIEMENS & HANSEATISCHE AKTIENGESELLSCHAFT

SIEMENS ENGINEERING & MANUFACTURING
CO. OF INDIA LTD.

Bombay Calcutta New Delhi Madras Bangalore Visakhapatnam
Ahmedabad Lucknow Nagpur Hyderabad Tiruvandrum Rourkela
Patna

CENCO LAB — JACK



This stable lab support
can be continuously
elevated to 26 Cm.,
yet will rigidly hold
over 45 Kilos.

While synthesizing carbon-14 and carbon-13 labelled pheynylalanine from similarly labeled Benzene and methyl iodide, Dr. Lerner of Yale University, U. S. A., found it necessary to quickly remove a hot oil bath from the reaction vessel, before adding a reagent to the reaction mixture. Whenever the awkward bath was lowered suddenly, some of the hot oil spilled on the hand of the operator. A simple mechanical method of quickly positioning the heavy bath was required and so that idea of Lab-Jack was conceived.

For further details, please write to :

The Sole Distributors :

**THE SCIENTIFIC INSTRUMENT
COMPANY, LIMITED.**

ALLAHABAD BOMBAY CALCUTTA MADRAS
NEW DELHI

Head Office : 6, Tej Bahadur Sapru Road, Allahabad



THERMAL EXPANSION OF SOME ALKALI FLUORIDES AND MAGNESIUM OXIDE BY X-RAY DIFFRACTION

P. D. PATHAK, N. V. PANDYA AND M. P. GHADIALI

PHYSICS DEPARTMENT, GUJARAT UNIVERSITY, AHMEDABAD

(Received June 23, 1962; Resubmitted September 24, 1962)

ABSTRACT In this paper high temperature X-ray data on the thermal expansion of LiF, NaF and MgO are reported for the first time. The results are compared with the macroscopic observations wherever available. The role of lattice defects is examined and the applicability of Debye-Grüneisen equation to explain the observed variation of thermal expansion with temperature is discussed.

INTRODUCTION

The coefficient of thermal expansion α of almost all ionic crystals increases with temperature. Lawson (1950) assumed that α should be constant for a perfect crystal lattice and deduced that in such a crystal defects do play a part and contribute to the thermal expansion. He succeeded in proving his point in the case of silver bromide but not for silver chloride. It was pointed out in our previous communication (Pathak and Pandya, 1960 (b)) that in the case of ionic crystals Schottky defects shall predominate and that if defects did contribute to the thermal expansion of a crystal, the value of α determined by macroscopic methods should be greater than that measured by the X-ray method. On searching the literature it was found that the high temperature X-ray data for the salts examined in the present experiments were not available.

Lithium fluoride has been studied by Adenstedt (1936) in the low temperature region upto about -225°C . It has also been studied by Eucken and Dannöhl (1934) by the heterodyne beat method and by Sharma (1950) by an interferometric method.

Sodium fluoride has been investigated at low temperatures by Henglein (1925) by the pycnometer method. Room temperature values are quoted by Megaw (1939) and Wooster (1949). It has been recently investigated upto 254°C by Deshpande (1961)

The thermal expansion of magnesium oxide was studied by Fizeau (1867), Goodwin and Mailey (1909) from 120°C to 270°C and Merrit (1926). It has been systematically examined by optical or interferometric methods by Thulenius and Holzmann (1930) upto 1200°C , Austin (1931) upto 800°C , Durand (1936) upto 85°C and Sharma (1950) upto about 700°C . No systematic high temperature X-ray data on this salt are available in the literature.

The observations in the present work were taken by employing a diffractometer, Geiger counter and a ratemeter. The diffractometer had a diameter of 500 mm. and was calibrated in degrees (2θ , each degree divided into four parts). The position of the Geiger counter could be read upto one minute of arc and by estimation upto $\frac{1}{2}$ minute. The error in the measurement of the cell constant a_t is estimated to be less than ± 0.002 .

OBSERVATIONS AND RESULTS

The same small furnace (Pathak and Pandya, 1959) was used in this work which was employed in the earlier measurements on NaCl (Pathak and Pandya, 1959), CsI (Pathak and Pandya, 1960a) and KBr, KI and CsBr (Pathak and Pandya, 1960b). The results of the present measurements are shown in Figs. 1, 2, 3 and Table I.

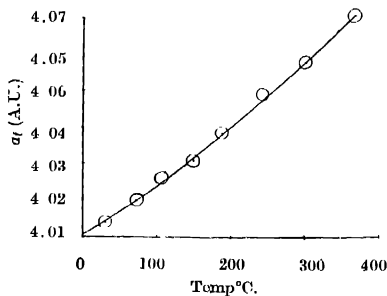
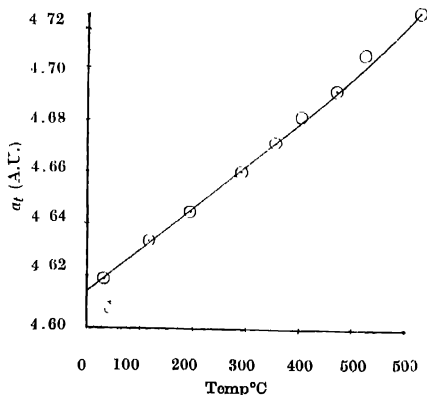
Fig. 1. LaF₃.

Fig. 2. NaF.

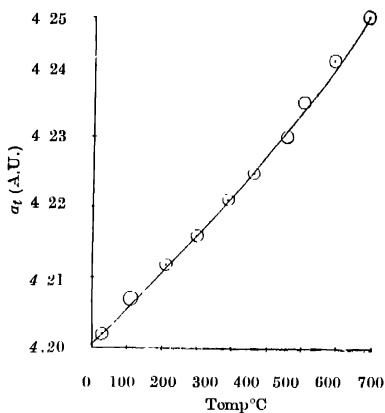


Fig. 3. MgO.

The equations satisfying the smooth curves drawn from the observed points are given below :

$$\text{LiF} \cdot \quad a_t = 4.0102 + 1.312 \times 10^{-4}t + 9.160 \times 10^{-8}t^2$$

$$\text{NaF} \cdot \quad a_t = 4.614 + 1.452 \times 10^{-4}t + 5.595 \times 10^{-8}t^2$$

$$\text{MgO} \cdot \quad a_t = 4.2015 + 4.625 \times 10^{-5}t + 1.392 \times 10^{-8}t^2$$

The coefficient of expansion α was calculated from the equation $\alpha = \frac{1}{a_t} \cdot \frac{da_t}{dt}$.

The comparison of our results with those of others is shown in Tables II, III and IV.

TABLE I

LiF		NaF		MgO	
Temperature degree C	$\alpha \times 10^6$	Temperature degree C	$\alpha \times 10^6$	Temperature degree C	$\alpha \times 10^6$
30	34.1	30	32.2	27	11.2
72	35.9	72	33.1	208	12.3
150	39.4	116	34.2	386	13.5
187	41.0	195	35.9	552	14.6
242	43.3	288	38.1	691	15.4
301	45.9	351	39.5	788	16.0
307	48.7	400	40.6		
		467	42.1		
		520	43.2		
		625	45.5		

TABLE II
Lithium fluoride

Temperature degree C	$\alpha \times 10^6$		
	Authors	Sharma	Eucken and Dannohl
0	32.7	33.8	32.2
30	34.1	34.4	33.4
72	35.9	35.5	35.2
150	39.4	37.9	38.4
187	41.0	38.9	40.0
242	43.3	41.6	42.2
301	45.9	44.4	44.6
367	48.7	47.8	47.4

TABLE III
Sodium fluoride

Temperature degree C	$\alpha \times 10^6$	
	Deshpande	Authors
30	34.0	32.2
72	35.2	33.1
116	36.5	34.2
195	38.8	35.9
288	41.5	38.1

DISCUSSION OF THE RESULTS

X-ray data on LiF at high temperatures are not available and hence it is not possible to compare our results with those of other workers. In Table II, however, comparison with the macroscopic data of Sharma (1950) and those of Eucken and Dannöhl (1934) is shown and it is seen that the agreement is fairly good.

Our results on NaF are compared with the X-ray data of Deshpande (1961) in Table III. Our results are slightly lower. Our α at 0°C viz. 31.5×10^{-6} may also be compared with that of Henglein between -79°C and 0°C viz. 33.0×10^{-6} .

Comparison of our X-ray data on MgO with the macroscopic observations of other workers is shown in Table IV. Our results agree excellently well with those of Sharma (1950). They also agree fairly well with those of Thilenius and Holzmann (1930). Austin's (1931) results are too erratic in the low temperature range but agree well with our results at high temperatures.

TABLE IV
Magnesium oxide

Temperature degree	$\alpha \times 10^6$		
	Literature	Sharma	Authors
40	10.4 ¹	11.2	11.3
120-270	12.1 ²	12.2	12.3
25-800	13.4 ³	13.7	13.6
63.7	11.2 ⁴	11.4	11.4
153	11.9 ⁴	11.9	12.0
246.3	12.8 ⁴	12.5	12.6
348.2	13.8 ⁴	13.1	13.2
448.4	14.1 ⁴	13.8	13.9
546.1	14.6 ⁴	14.5	14.5
645.8	12.2 ⁴	15.2	15.2
745.5	15.7 ⁴	16.0	15.8
20-55	6.7 ⁵	11.2	11.3
20-100	9.1 ⁵	11.3	11.4
20-150	10.4 ⁵	11.5	11.6
20-200	10.9 ⁵	11.6	11.7
20-300	11.6 ⁵	12.0	12.0
20-400	12.1 ⁵	12.3	12.4
20-600	13.0 ⁵	13.0	13.0
20-800	13.5 ⁵	13.7	13.5

1 Fizeau (1867)

2 Goodwin and Mailey (1909)

3 Merritt (1928)

4 Thilonius and Holzmam (1930)

5 Austin (1931)

It can be seen from the above discussion that comparison with macroscopic results are possible only in the case of lithium fluoride and magnesium oxide. In the case of the former the X-ray expansions are greater than the macroscopic ones. If lattice defects played any part the reverse should have happened. In

TABLE V
Gruneisen parameters

Substance	$Q/2R \times 10^3$	$3p$	References
Lithium	29.01	12.01	Present values
fluoride	29.4	11.5	Eucken and Dannohl
	26.2	—	Equation (2)
Sodium	29.54	8.0	Present values
fluoride	29.25	—	Equation (2)
Magnesium	61.15	15.10	Present values
oxide	61.76	—	Equation (2)

the case of magnesium oxide the X-ray data and the macroscopic data agree perfectly. The defects, if any, therefore, affect the X-ray and the macroscopic expansions equally or their contribution to the thermal expansion is negligible.

It can be shown (Pathak and Pandya, 1960b) from the Debye-Grüneisen theory that

$$\frac{a_0}{a_T - a_0} = \frac{Q}{2R} \cdot \frac{1}{TD(\theta/T)} - 3p \quad \dots (1)$$

Where a_0 and a_T are the cell constants at 0°K. and T°K. respectively, $D(\theta/T)$ the Debye function and $Q/2R$ and $3p$ are constants called the Grüneisen's parameters. The above equation shows that for a crystal obeying Grüneisen's law the graph of $a_0/a_T - a_0$ against $1/TD(\theta/T)$ should be a straight line. In the case of substances examined in the present experiments such graphs are found to be straight lines. The Grüneisen's parameters determined from these graphs are compiled in Table V. The value of Q can also be determined from the relation

$$Q = V_0/\gamma K_0 \quad \dots (2)$$

where K_0 and V_0 are the compressibility and molar volume at 0°K. The values of $Q/2R$ calculated from this equation are also given in Table V for comparison, the values of V_0 and γ being taken from Born and Huang (1954).

REFERENCES

- Adenstedt, H., 1936, *Ann. der Physik*, **26**, 69.
 Austin, 1931, *Jour. Am. Cer. Soc.*, **14**, 795.
 Born, M. and Huang, K., *Dynamical Theory of Crystal Lattices*, pp. 52-54, Clarendon Press, Oxford.
 Deshpande, V. T., 1961, *Acta Cryst.*, **14**, 794.
 Durand, M. A., 1936, *Physics*, **7**, 297.
 Eucken, A. and Dannehl, W., 1934, *Z. Electrochem.*, **40**, 814.
 Fizeau, 1867, *Ann. der Physik*, **132**, 292.
 Goodwin and Mailey, 1909, *Phys. Rev.*, **28**, 1.
 Hongleim, F. A., 1925, *Z. Phys. Chem.*, a **115**, 91.
 Lawson, A. W., 1950, *Phys. Rev.*, **78**, 185.
 Mogaw, H. D., 1939, *Z. Kristallogr.*, **100**, 58.
 Merritt, 1926, *Trans. Amer. Electrochem. Soc.*, **50**, 165.
 Pathak, P. D. and Pandya, N. V., 1959, *Curr. Sc.*, **28**, 320.
 Pathak, P. D. and Pandya, N. V., 1960, (a) *Ibid.*, **29**, 14.
 Pathak, P. D. and Pandya, N. V., 1960, (b), *Ind. Jonr. Phys.*, **34**, 416.
 Sharma, S. S., 1950, *Proc. Ind. Acad. Sci.*, **32**, 268.
 Thielems and Holzmänn, 1930, *Z. f. Anorg. Allg. Chem.*, **189**, 381.
 Wooster, W. A., 1949, *A Text Book of Crystal Physics*, p. 33, Cambridge University Press.

THE ELECTRONIC SPECTRA OF SOME TRISUBSTITUTED BENZENES IN DIFFERENT STATES. II

T. N. MISRA

OPTICS DEPARTMENT,

INDIAN ASSOCIATION FOR THE CULTIVATION OF SCIENCE,
CALCUTTA-32

(Received February 12, 1963)

ABSTRACT. The near ultraviolet absorption spectra of 1,2,4-trimethylbenzene and 3,4-dichlorotoluene have been investigated in different states. In the case of these two 1,2,4-trisubstituted benzenes, the allowed transition is of type $A' \rightarrow A'$ and the 0,0 bands appear strongly in the spectra of the substances in the vapour state, but the spectrum of each of the compounds in the solid state at -180°C is very weak compared to the spectra due to the vapour and liquid states. The 0,0 band at -180°C is also displaced towards high energy region with respect to its position in the case of the liquid. It is suggested that the observed bands may represent only one of the two components into which the bands are split up in the crystals at -180°C .

It has been pointed out that the interaction of permanent dipoles of neighbouring molecules on the transition moment of the molecules in the lattice might be partly responsible for this large splitting.

INTRODUCTION

The ultraviolet absorption spectra of some trisubstituted benzene compounds have recently been investigated in this laboratory to study the influence of intermolecular forces on the position and structure of absorption bands in the liquid and solid states. Recently, it has been proposed by Srikar (1962, 63) that the interaction of permanent electric moments of the neighbouring molecules on the transition moments of the molecules in the lattice might be partly responsible for the large splitting observed in the spectra of some crystals of polar molecules at -180°C .

In a previous communication (Misra, 1963) it has been pointed out that in 1, 2, 3-trisubstituted benzenes, the transition which is forbidden in free molecules due to cancellation of three migrational moment vectors, becomes allowed at -180°C , but no large splitting of bands could be detected. Since the magnitude of transition moment is very small in these cases, the interaction with the permanent dipoles of neighbouring molecules is expected to be weak. It was therefore, thought worthwhile to extend the investigation to some other polar molecules having a large value of transition moment and 1, 2, 4-trimethylbenzene and 3, 4-dichlorotoluene were selected for the purpose.

EXPERIMENTAL

The experimental set up was the same as described in an earlier paper (Misra 1960). (Chemically pure samples of 1, 2, 4-trimethylbenzene and 3, 4-dichlorotoluene supplied by Eastman Kodak Co., and Fisher Scientific Co., U.S.A. respectively were used after fractional and repeated vacuum distillation. For studying the absorption spectrum of 3, 4-dichlorotoluene in the vapour state, a 75 cm long absorption tube provided with quartz windows and a bulb attached to a side tube for containing the liquid was used.

Thin films of the substances of thickness of the order of a few microns were used to produce bands in the liquid and solid states. The spectrograms were taken on Agfa Isopan films with a Hilger E 1 spectrograph having a dispersion of about 3A per mm. in the 2600 A region. Microphotometric records were taken with a Kipp and Zonen type Moll microphotometer and absorption spectra were calibrated with the help of a microphotometric record of iron arc spectrum photographed on each spectrogram as explained in a previous paper (Sirkar and Misra, 1959).

RESULTS AND DISCUSSION

The microphotometric records of the absorption spectra of 1, 2, 4-trimethylbenzene and 3, 4-dichlorotoluene are reproduced in Figs. 1 and 2. The wave numbers of the bands with their approximate intensities and probable assignments are given in Tables I and II respectively.

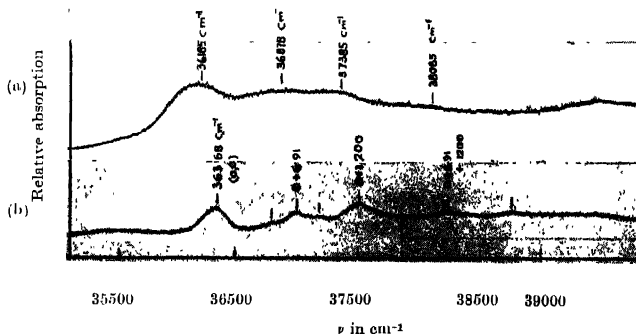


Fig. 1. Microphotometric records of the ultraviolet absorption spectra of 1,2,4-trimethylbenzene in different states.

- (a) In the liquid states at 32°C.
- (b) In the solid states at -180°C.

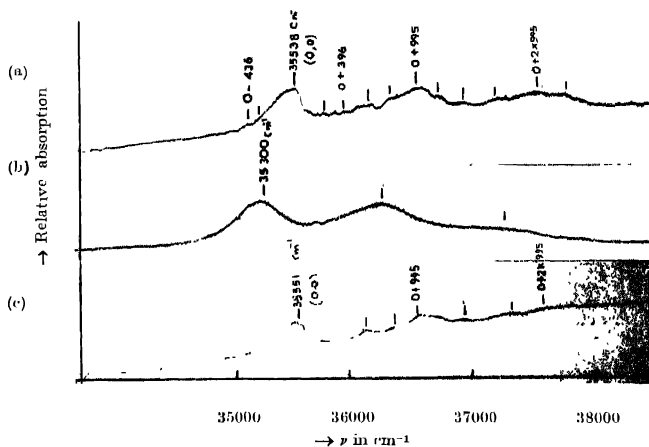


Fig. 2. Microphotometric records of the ultraviolet absorption spectra of 3, 4-dichlorotoluene in different states
(a) Vapour state. (b) Liquid state at 22°C (c) Solid state at - 180°C.

1, 2, 4-Trimethylbenzene

The near ultraviolet absorption spectrum of 1, 2, 4-trimethyl benzene in the vapour state was studied by Sreeramamurty (1951). Assuming the methyl group to behave as a single atom, this molecule has the lowest symmetry C_s among the substituted benzenes and the A_{1g} B_{2u} transition in benzene becomes $A'-A'$ transition in this case. This transition is an allowed one and the 0,0 band appears strongly in the spectrum. The data for the spectrum in the vapour state as reported by Sreeramamurty (1951) have been included in the table for comparison.

In the vapour state, the spectrum of 1, 2, 4-trimethylbenzene (Sreeramamurty, 1951) shows a strong 0,0 bands at 36900 cm^{-1} and a large number of bands involving different vibrational frequencies. In the liquid state, the compound yields four broad bands with the positions of maximum absorption at 36185 , 36878 , 37385 and 38085 cm^{-1} respectively (Fig. 1, Table I). The bands due to the liquid are broad probably due to thermal motion of molecules and merging of $v \rightarrow v'$ transitions into one another. The approximate position of the centre of the strong band on the long wavelength side at 36185 cm^{-1} is taken as the position of the 0, 0 band. Then it is found that on liquefaction of the vapour, the 0, 0 band shifts towards red by 715 cm^{-1} . The other bands are at distances 693, 1200 and 1900 cm^{-1} respectively from the 0,0 band.

With the solidification of the liquid and cooling to -180°C , some more bands are observed. The strongest band on the long wavelength side is at 36368 cm^{-1} and is taken as the 0,0 band of the system. The other bands can then be represented by excited state vibrational frequencies 461, 691, 890 and 1200 cm^{-1} and their combinations. Some of these frequencies agree fairly well with the frequencies 711, 927 and 1180 cm^{-1} reported by Sreeramamurty for the vapour state. The frequency 641 cm^{-1} observed in the spectrum of the crystals

TABLE I

Ultraviolet absorption bands of 1, 2, 4-trimethylbenzene in different states

Vapour (Sreeramamurty, 1951)		Liquid at 32°C		Solid at -180°C	
Wave number (cm^{-1}) and Intensity	Assignment	Wave number (cm^{-1}) and Intensity	Assignment	Wave number (cm^{-1}) and Intensity	Assignment
35977 (vw)	0 - 923				
36351 (vw)	0 - 549				
36683 (vw)	0 - 217				
36900 (vs)	0,0	36185 (s)	0,0	36368 (vs)	0,0
37015 (m)	0 115			36824 (w)	0 + 461
37611 (s)	0 711	36878 (s)	0 693	37059 (s)	0 + 691
37827 (ms)	0 927	37385 (s)	0 1200	37258 (m)	0 + 890
38080 (mw)	0 + 1180			37568 (s)	0 + 1200
		38085 (m)	0 693 1200		
38186 (mw)	0 1286			38268 (m)	0 + 691 + 1200
				38760 (w)	0 + 2 \times 1200

at -180°C was not observed by him in the case of the vapour, but it may be noted that Kohlrausch and Pongratz (Magat, 1936) reported two strong Raman lines 557 cm^{-1} and 474 cm^{-1} . It is seen that when the vapour is liquefied the band system shifts towards red by 715 cm^{-1} and on solidification and subsequent cooling to -180°C , the band system shifts towards shorter wavelength by 183 cm^{-1} . Further, the integrated absorption at each band becomes much smaller when the liquid is frozen and cooled to -180°C .

This decrease in the strength of absorption may be explained by assuming that this band system constitutes one of the two components in which the original band system is split up in the crystal at -180°C and that the other component may be on the short wavelength side. As the crystal structure of the compound

at -180°C is not known it has not been possible to calculate the exact positions of the split components.

3, 4-Dichlorotoluene

As explained above this molecule also has the symmetry C_s and the migrational moment vectors add to give a large value. The transition is allowed and the 0,0 band is expected to appear strongly in the spectrum of free molecules.

Spectrum in the vapour phase.

Three groups of bands degraded towards red, consisting of about fifteen prominent bands (Fig. 2a) have been observed. The very strong sharp band at 35538 cm^{-1} on the long wavelength side has been taken as the 0,0 band of the system. All the other bands can then be assigned in terms of ground state frequencies 363 and 436 cm^{-1} and upper state fundamentals 232, 396, 598, 799, 995, and 1170 their combinations.

TABLE II

Ultraviolet absorption bands of 3, 4-dichlorotoluene in different states

Vapour at 32°C Path length 75 cm		Liquid at 32°C		Solid at -180°C	
Wave number (cm^{-1}) and Intensity	Assignment	Wave number (cm^{-1}) and Intensity	Assignment	Wave number (cm^{-1}) and Intensity	Assignment
35102 (w)	0 - 436				
35175 (w)	0 - 363				
35538 (vs)	0,0	35300 (vs)	0,0	35551 (vs)	0,0
35770 (w)	0 \pm 232	36292 (vs)	0 \pm 992	36123 (m)	0 \pm 572
35934 (w)	0 \pm 396	37284 (m)	0 \pm 2 \times 992	36347 (w)	0 \pm 706
36136 (m)	0 \pm 598			36546 (s)	0 \pm 995
36317 (m)	0 \pm 779			36930 (w)	0 \pm 572 \pm 796
	0 \pm 2 \times 396				
				37302 (m)	0 \pm 995 \pm 796
36533 (vs)	0 \pm 995				
36718 (m-)	0 \pm 1170			37554 (m)	0 \pm 2 \times 995
36925 (m)					
	0 \pm 995 \pm				
	396				
	0 \pm 598 \pm				
	779				
37163 (ms)	0 \pm 1625				
	0 \pm 995 \pm				
	598				
37529 (s)	0 \pm 2 \times 995				
37767 (ms)	0 \pm 2 \times 995				
	\pm 232				

The Raman and infrared spectra of the molecule have recently been reported by Deb and Banerjee (1960). The two ground state fundamentals 363 and 436 cm^{-1} observed as $\nu \rightarrow 0$ transition in the present investigation agrees with the Raman frequencies 368 and 435 cm^{-1} reported by them. The upper state fundamentals 396, 598, 779, 995 and 1170 cm^{-1} satisfactorily correspond to the Raman and infrared frequencies 435, 686, 805, 1030 and 1211 cm^{-1} reported by Deb and Banerjee (1960).

In the liquid state, the substance gives a spectrum consisting of three broad bands. The centres of the first band at 35300 cm^{-1} is taken as the position of the 0, 0 band and other bands are separated from it by 992 cm^{-1} and 2×992 cm^{-1} . Thus on liquefaction of the vapour the band system is shifted towards red by 238 cm^{-1} .

In the solid state at -180°C , the absorption spectrum of the substance consists of about seven prominent but weak bands. The first band at 35551 cm^{-1} is evidently the 0, 0 band of the system. The other bands can then be explained in terms of upper state fundamentals 572, 796 and 995 cm^{-1} . Thus on solidification of the vapour and its subsequent cooling to -180°C , the band system is observed to shift slightly towards higher energies and also the strength of absorption diminishes appreciably.

This decrease in the strength of absorption in the crystals at -180°C may be explained in the same way as in the previous case. It may be noted here that similar shift of one of the split components to the other region of the spectrum has also been observed by Bornstein in the case of bromobenzene as reported by Kasha and Oppenheimer (1962).

ACKNOWLEDGMENT

The author is grateful to Prof. S. C. Sirkar, D.Sc., F.N.I., for his kind interest and guidance in the work.

REFERENCES

- Deb, K. K., and Banerjee, S. B., 1960, *Ind Jour Phys*, **34**, 554.
 Kasha, M., and Oppenheimer, M., 1962, *Theory of molecular Excitons*, Mc Graw Hill Book Company, p. 139.
 Mugat, M., 1936 Numerical Data on Raman Effect, p. 72.
 Misra T. N., 1960, *Ind Jour Phys*, **34**, 381.
 Misra, T. N. 1963, *Ind., Jour. Phys.* **37**, 173.
 Sirkar S. C., and Misra T. N., 1959, *Ind Jour Phys*, **33**, 45.
 Sirkar S. C., 1962, *Proc. Natl Inst Sci of India* **27**, 1, 568.
 Sirkar, S. C., 1963 *Ind Jour. Phys.*, **37**, 101.
 Sreeramamurty, K., 1951, *Proc. Natl. Inst. of Sci. of India*, **17**, 385.

ELECTRONIC TELEPHONE SWITCHES WITH TRANSISTORS

P. N. DAS

ELECTRICAL ENGINEERING DEPARTMENT,
UNIVERSITY OF ROORKEE

(Received September 24, 1962)

ABSTRACT The electro-mechanical switches of usual telephone exchanges are required to perform one or more of the functions of selection under the control of impulses or of automatic hunting or of line finding during the setting up of a telephone connection. Transistorised switches which can perform all the above operations, have been described in the paper. Such switches can, therefore, be utilized with advantage in electronic telephone exchanges.

INTRODUCTION

All the existing automatic telephone systems, whether they be Strowger step-by-step systems or Cross-bar by-path systems or Panel Systems, use electro-mechanical switches and relays and all of them depend on mechanical contacts for establishing connections between different lines or trunks. Due to many disadvantages of these mechanical contacts such as wear due to use, corrosion due to sparks, constant attention required for their adjustments and cleaning etc. and also due to the constant attention required for spring and other mechanical adjustments in the switches and relays, there has been a recent move to replace these mechanical parts by electronic devices and to get what is known as electronic telephone systems. (Flowers, 1950, 1951 and 1952; Heron *et al.*; 1951). The first electronic exchange using gas tubes is already in service at Morris (Chicago) in U.S.A. and the first British electronic exchange is due to be ready for public service this year at the Highgate Wood in London. The former one uses space-division principle and the latter one uses time-division principle for operation. Although these electronic exchanges have been put into service, they are still worked on experimental basis and work is being carried out in U.K., U.S.A. (Harris *et al.*, 1950, Lewis, 1953 and Mathanani, *et al.* 1954) and in other countries (Ortvad, 1960) to find out a more suitable and reliable type of electronic exchange.

All the electro-mechanical systems use space-division principle in which connections are made between different transmission circuits through different switches and different trunks all occupying different positions in space. If the different operations required during setting up of connections by electro-mechanical switches can be performed by some electronic devices, all the electro-mechanical switches of the existing types of exchanges can be dispensed with. In this paper

some transistorised electronic switches which can perform all the above operations have been described and as such can be used in electronic exchanges.

Electronic devices have also made telephonic conversations possible between any two subscribers on other principles such as frequency-division and time-division principles. These principles are more or less based on carrier working and so the system based on them requires complicated apparatus of carrier telephone systems. The system working in U.S.A. uses gas tubes for switching purposes on space-division principle and the system to be worked in U.K. employs time-division principle.

TELEPHONE SWITCHES AND THEIR OPERATIONS

There are many different types of switches used in different types of existing electro-mechanical systems such as uniselectors and two-motion selectors in Strowger system, cross-bar switches in Cross-bar by-path system, motor switches in Panel type system etc. These switches perform following two types of duties.

1. They are used for setting-up the required connections.
2. They are used as connecting paths for carrying out telephonic conversations.

Under the first item these switches are required to perform one or more of the following operations.

1. The desired line or the desired group of multiples are selected under the control of a number of impulses sent. This is called 'Selection' of a desired line or a group.
2. Automatic selection of the calling line is done without being under the control of any impulses when the subscriber takes up his telephone set. This is called 'Line finding' for a calling line.
3. Automatic selection of any free trunk out of a group of trunks is done without being under the control of any impulses. This is called 'Hunting' for a free trunk.

Electronic Switches employing transistors have been described here mentioning how all these different operations can be effected with its help. Connections for speech transmission can be made through other circuit devices which have not been dealt with in the paper.

ELECTRONIC DEVICES FOR SWITCHING

There are the following electronic devices which can be used for switching or getting connections between two lines.

1. Gas tubes.
2. Vacuum tubes.
3. Germanium or silicon diodes,
4. Transistors.

Of these, transistors and semiconductor diodes are most suitable due to their small sizes and small voltages required for their working for the purpose of use

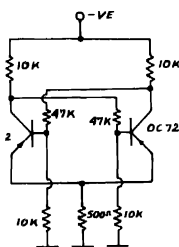


Fig. 1 Bi-stable circuit.

as telephone switches as quite a large number of switches are required in a telephone exchange. The well-known bi-stable circuit with transistors shown in Fig. 1, has been taken as the basic unit for building up such telephone switches. In such circuits with PNP transistors, when one conducts, the base of the other one becomes positive with respect to the emitter and so the other one does not conduct. If, however, a negative pulse is applied to the base of the non-conducting transistor, it becomes conducting and so naturally the base of the other one

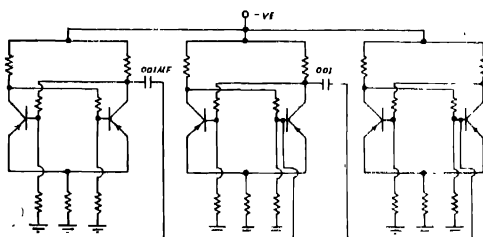


Fig. 2 Switching circuit with bi-stable stage.

becomes positive and so it ceases to conduct. A switching circuit has been developed with the help of such bi-stable circuits three stages of which are shown in Fig. 2.

Different stages of bi-stable circuits are coupled through 0.001 microfarad capacitors connected between collectors of second transistors of previous stages and bases of second transistors of succeeding stages. Suppose that initially the second transistor B_1 of 1st stage is conducting and that the second transistors of all other stages B_2, B_3 etc are not conducting. If a negative pulse is applied to the base of transistor A_1 , it will conduct and B_1 will cease to conduct. So the collector of B_1 becomes suddenly more negative and the negative pulse is applied

through 0.001 microfarad capacitor to the base of B_2 transistor in the second stage and so B_2 transistor becomes conducting and its negative collector voltage is suddenly reduced. A positive pulse is therefore sent to the base of B_3 transistor but as B_1 transistor is already not conducting, this has no effect on it and so the third stage remains unaffected. If a second negative pulse is now applied to the base of transistor A_2 in the second stage, B_2 will become non-conducting and B_3 in the third stage becomes conducting in the same way.

TRANSISTORISED SELECTOR SWITCH

The above arrangement of bi-stable circuits can be used as a telephone selector switch with some modifications. In the case of usual selector switches, they are operated a number of times equal to the number of impulses sent by the dial from their home position where the wipers or moving elements return, as soon as the switch is released. In the present case the bi-stable circuits are so arranged that

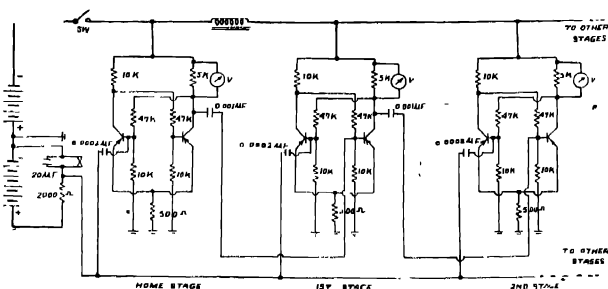


Fig 3. Selector switch.

when the supply voltage is connected to all of them, always the second transistor of the first or home stage conducts and the first transistors of all other stages conduct. This is achieved by connecting slightly different values of resistance in the collector circuits of the two transistors in a stage and by giving the supply to all the subsequent stages except the first one through a suitable choke as shown in Fig 3.

With unsymmetrical bi-stable circuits as shown in the figure if the supply voltage is suddenly applied, the second transistor conducts, but if the supply voltage is applied by gradually increasing its values, it is the first transistor which starts conducting. If the collector supply voltage to all but the first stage is applied through a suitable value of choke as shown in the figure, when switch SW is operated, the second transistor of home stage starts conducting and the first transistors of all the other stages start conducting. This switch SW may be operated by the dial off normal spring contacts of the dial.

The bases of first transistors of all the stages are connected to the dial impulsing contacts through condensers of values of 0.0002 microfarad. When these

spring contacts are operated, negative impulses are sent and applied to the bases of all the first transistors of all the stages. Initially the first transistors of all the stages except the home stage are conducting and so their conditions will not be changed. The first transistor base, however, becomes negative with respect to emitter and it starts conducting and the conditions are changed in the home stage resulting in change in the condition in the first stage only. If another impulse is sent now, the condition of first stage is now changed resulting in a change also in the second stage. Thus if a number of impulses are sent, there will be change in the condition of the bi-stable stage of the corresponding number and its second transistor will be conducting and no other second transistors of any other stage will be conducting. Thus selection is possible among the different stages by dialling any particular number and the entire arrangement can be used as a selector switch.

In order that bi-stable operations are effective, the pulses of voltage or current that are applied, must be very sudden i.e. the rate of change of voltage or current must be very high. In a pulse there is one front edge and one back edge and if both of these edges be equally sharp, the previous initial condition will come back when the entire pulse is sent. In order that one condition is changed only by the sending of one pulse, it is necessary that one edge of the pulse should be sharp and the other edge be gradual. This is achieved by having a suitable high capacitor in series with a suitable resistance across the impulse sending battery and by connecting the dial impulse springs across the capacitor. Initially the capacitor is shorted by dial impulse springs. When these impulse springs break, the condenser is charged through the resistance and a gradually rising front edge of the impulse is obtained and it is so gradual that it can not effect any change in the states of

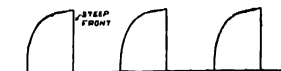


Fig. 4. Nature of wave shape.

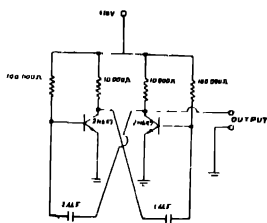


Fig. 5. Astable multivibrator.

any bi-stable stage. When the impulse spring contacts remake, the charged condenser is suddenly shorted and discharged and the back edge of the impulse abruptly

decreases to zero and this is effective in bringing about a change in the state of the home stage initially and of other stages subsequently. The nature of the impulses sent is shown in Fig 4.

TRANSISTORISED LINE FINDER SWITCH

The selector circuit shown in Fig. 3, can be used as a Line Finder circuit if we replace the dial and its associated equipments by an astable multivibrator circuit shown in fig. 5.

N.P.N. transistors type No. OC 647 are used in the multivibrator circuit so that nature of pulses with sharply falling end edges as shown in Fig. 4, are obtained. The values of capacitances and resistances are so chosen that pulses at the rate of 10 per second which can operate the bi-stable circuits without fail are obtained. When the output of such a multivibrator circuit is connected through 0.0002 microfarad capacitors to the bases of first transistors of all bi-stable stages, the states of different stages are changed one after another by the impulses sent from the astable multivibrator and if the last stage is coupled to the first stage by a coupling capacitor, the states go on changing one after another continuously. If now a capacitor of appreciable value, say 0.01 microfarad is connected across the resistance of 10K joined between the base and earth of the first transistor of any stage (Fig 3), as soon as the second transistor of this stage conducts, there cannot be any further change of conditions in any stage and no second transistors of any other stage can be made to conduct afterwards even by the connection of a similar capacitor across similar points in any other stage. Thus the selector switch can be used for line finding action satisfactorily. If the capacitor connection is made by the lines of the subscriber when he takes up his telephone from the cradle, then the second transistor of the bistable circuit corresponding to the line continues conducting and the hunting action stops and if any other subscriber takes up his telephone set subsequently, the transistor of the bistable circuit corresponding to the second line does not conduct also. When a condenser of appreciable value is connected as above, pulses from the multivibrator are bi-passed through it and so they cannot effect any further change of states.

TRANSISTOR HUNTER SWITCH

Bi-stable circuits with slight modifications are used for different stages and the astable multi-vibrator circuit referred to above may be used for driving the switch circuit as shown in Fig. 6.

If a free trunk is indicated by the presence of earth on the emitter of the second transistor of the stage corresponding to the line, then as impulses are sent from the multivibrator, the second transistor of the stage corresponding to the trunk conducts and it continues to conduct so long as earth is present. When the emitter of the second transistor which conducts is earthed, it cannot be made positive with respect to emitter and so hunting action stops. If there is no earth present on the

emitter of the second transistor of any stage, then the bi-stable stage is unaffected by impulses which are by-passed to the next stage. If any trunk is busy, the

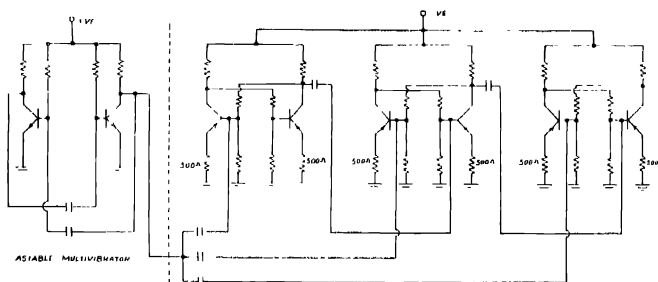


Fig. 6. Multi-switch

purpose is served if there be no earth connected on the emitter of the second transistor corresponding to the trunk. Due to the emitter being given a negative bias, the negative impulse can not produce any change in the state. It is applied, however, through the coupling condenser to the base of the second transistor of the next stage and if earth is present on the emitter of this transistor, the impulse effects a change in the state of this latter stage.

CONCLUSION

These transistorised switches can thus perform all the important functions of usual electro-mechanical switches of telephone exchanges so far as selection of the required line or group of trunks is concerned during setting up of a telephone connection. Therefore, they can be utilised in place of such switches in existing types of exchanges and the complicated circuits required for having electronic exchanges on principle of carrier working or time division system, may be avoided. Speech circuits may be provided by using other transistors or gas tubes or even saturable reactors and they may be operated by the transistorised types of switches described here.

ACKNOWLEDGMENT

The author is very much grateful to Prof. C. S. Ghosh, Head of Electrical Engineering Department, University of Roorkee for his encouragement in carrying out the work.

REFERENCES

- Flowers, T. H., 1950, *Post Office Electrical Engineers' Journal*, vol. 43, 61.
- Flowers, T. H., 1951, *Post Office Electrical Engineers' Journal*, Vol. 43, 177.
- Flowers, T. H., 1951, *Post Office Electrical Engineers' Journal* Vol. 44, 10.

- Flowers, T. H., 1952, *Proc. I.E.E.*, Vol. **99**, Part 1 181.
- Harris, L.R.F., Mann, V.E. and Ward, P.W., 1960. *Proc. I.E.E.*, **107**, Part B, Suppl. No 20
- Heron, K. M., Bakoutt and Benson, D. L., 1951, *Post Office Electrical Engineers Journal*, Vol **44**, 97.
- Lewis, W. D., 1953, *Proc. I.R.E.* Vol, **41**, 1242.
- Mathanor, W. A. and Vanghan, H. E., 1954, *Bell Laboratories*, Record. Vol. **32**, 361.
- Ortved A., 1962, *Proc. I.E.E.*, Vol. **109**, Part B, Number 43.

CORRELATION BETWEEN STRUCTURAL ENERGY AND THE PROPERTIES OF THE NATURALLY RADIOACTIVE NUCLEI

A. K. DUTTA AND B. PAL

PALIT LABORATORY OF PHYSICS, CALCUTTA UNIVERSITY

(Received January 1, 1963)

ABSTRACT. The deviations of the experimentally obtained binding energy of the nuclei from that given by the Bethe-Weizsacker relation have been studied for the α and β active nuclei in the natural radioactive range. In a previous work (Dutta and others, 1962) these deviations have been considered to be the structural energy of the nuclei, according to the generally accepted ideas. It is observed from a graphical representation that the α and β energies, as also their half lives, are intimately connected with the change ' S ', in the structural energy, from the disintegrating to the product nuclei. Suitable relations in terms of the known constituents of the nuclei and the structural energy change ' S ' have been derived for both the α -energy values and the observed β (maximum) energy values. They are given by the relation,

$$E_{\alpha}(\text{obs}) = S - 1704(3Z - N) - 17.61 \text{ Mev.}$$

$$E_{\beta}(\text{obs}) = S \left(1 + 0.25 \frac{dS}{dN} \right) - 0.358(2Z - N) + 12.82 \text{ Mev.}$$

The agreement with observed values are quite satisfactory.

It is known that the α -energy values for different nuclei do not come down lower than a value of the order of 4 Mev. The formation of the α -particle in the radioactive nucleus is also not properly understood. Based on a scheme for the formation of the α -particle, a relation has been obtained to determine the lower limit of α -energy values for different nuclei in the form

$$E_{\alpha}(\text{lm}) = -8 \times (\text{Binding energy of the product nucleus per nucleon}) - 56.6 \text{ Mev.}$$

The observed α -energy values are generally higher than this lower limit, as expected.

Further, the half lives of all the even-even and odd-odd nuclei have been related to a function of E_{α} , Z , N such that they can be calculated with fair agreement. We have for these nuclei,

$$\log \frac{1}{T} = 2.117[N - Z]^3 \{ E_{\alpha}^{1/2} + b_1(90 - Z) \} + C_1(50 - \overline{N - Z}) - 69.54$$

where $b = 0.18$ for even-even nuclei, 0.09 for odd-odd nuclei, C_1 is of the order of 1.7 . It gives fair agreement between calculated and observed values.

INTRODUCTION

In a previous paper (Dutta and *et al.*, 1962) we have studied the deviations of the binding energy of all stable nuclei, calculated by the Bethe-Weizsacker relation, from the experimentally determined values, as tabulated by Everling

and others (1960). The significant findings have been discussed there. We have now extended this study beyond the stable nuclei of lead and bismuth, to cover the naturally radioactive group, as also the artificially radioactive nuclei in this region. The complete series $4n$, $4n+1$, $4n+2$ and $4n+3$, as shown in the schematic representation, in Fig. 1, where the full lines indicate naturally radioactive series, as also a large number of other artificially radioactive nuclei have been covered up in the present study. We have covered in all, about 80 α -disintegrat-

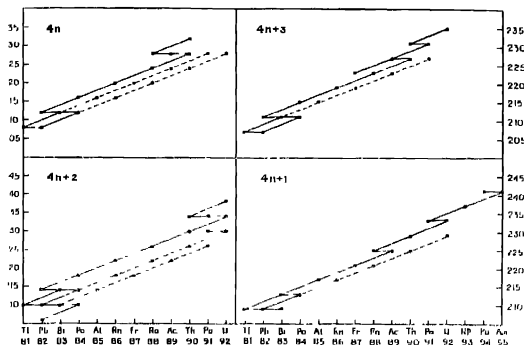


Fig. 1. Schematic representation of the radioactive series.

ing nuclei for which binding energy data are available and 25 β -disintegrating nuclei, for consideration. Their binding energies have been calculated from the Bathe-Weiszacker relation,

$$E = -a_1 A + a_2 A^{2/3} + a_3 Z^2 / A^{1/3} + a_4 (N - Z)^2 / 4A \quad (1)$$

We have utilised the constants as determined by us, and discussed in our previous paper. They are tabulated again, along with those by Green (1954) in Table 1.

TABLE I
Constants for the Betho-Weiszacker relation

	a_1	a_2	a_3	a_4
Dutta and others	16.719	18.505	0.751	96.856
Green	16.918	19.120	0.763	101.78

The deviations of the experimental binding energy values as tabulated by Everling, from those calculated by the Betho-Weiszacker relation, have been calculated for all these nuclei. We have plotted and connected them through α -disintegration processes for the natural radioactive series only, in Fig. 2, in order to avoid confusion by the intersection of lines due to different series. The

nature and characteristics of the curves due to other disintegration series have been found to be similar, in all respects. We have plotted in the curve the ΔE values for α -disintegrating nuclei against mass numbers, as followed in the previous paper. To bring out the β -disintegration characteristics to better relief, one should plot the ΔE values against neutron numbers, as we have done later.

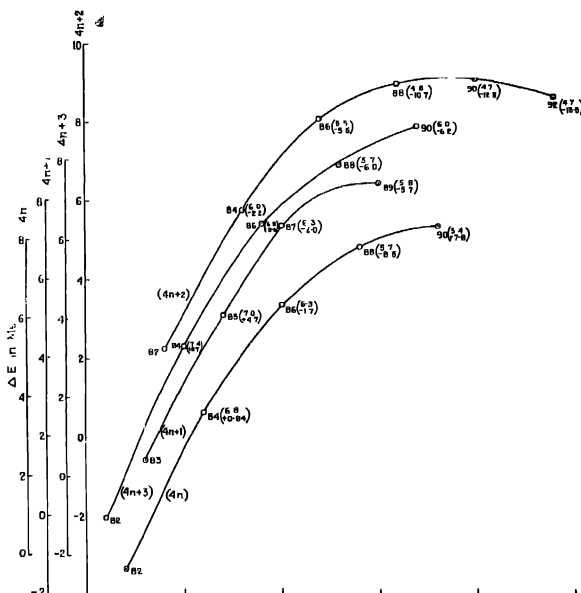


Fig. 2 ΔE Vs. mass numbers of the α -disintegrating nuclei of the four radioactive series

It will be observed from the graph that the change in the ΔE values from one nucleus to its disintegration product, which we prefer to call as S , the structural energy change, varies with the α -energy as also with the half lives τ in a very regular way. The structural energy change, S , is, thus, intimately related with the energy of the α -particles and through it to the half lives of disintegration.

In the α -disintegration chain, in a particular series, the values of S change from a small negative value, through a nearly vanishing magnitude, to a comparatively large positive value. The α -energy values and the half lives, correspondingly suffer a systematic change, starting from apparently arbitrary positive values. This is true for all the different series, although the magnitude of the

energy and half life values, in relation to the structural energy change S , varies with the series.

In the case of the β -energies, the maximum energies observed and the structural energy change S , do not appear to be immediately correlated. We will, however, take up the problem of observed β -energy maximum, in relation to the structural energy change, in a later section. We have utilised the data for the α -energies and the maximum β -energies given in the National Bureau of Standard, Circular No. 499, 1950 and in the Table by Strominger and others (1958).

ANALYSIS OF α -PARTICLE ENERGY

To analyse the data, one observes that in the case of almost all the α -disintegrating nuclei, the energy of the α -particle satisfies a simple relation namely,

$$E' - E'' = E_\alpha + (B.E)_\alpha + \text{recoil energy} \quad \dots (2)$$

Here E' and E'' are the experimental binding energies of the disintegrating and the product nuclei, obtained from Everling's table and the binding energy of the α -particle is taken to be 28.3 Mev. The recoil energy comes to a magnitude of the order of 0.1 mev., and may be neglected generally. For different associated α -energies or energy spectrum for one nucleus, one should have different binding energies, for which, unfortunately, the binding energy data are not available yet. We have associated the binding energy data with the most abundant process of disintegration of a particular nucleus. The above relation originates from the fundamental mass and energy balance principle. Thus :

$$E' = M' - \Sigma(m'_n + m'_p); \quad E'' = M'' - \Sigma(m''_n + m''_p) \\ (B.E)_\alpha = M_\alpha - \Sigma(m_n, m_p)_\alpha$$

giving us, from relation (2),

$$M' = M'' + M_\alpha + E_\alpha + \text{recoil energy of } E_\alpha \text{ product nucleus, } \dots (2a)$$

the energy balance equation. The α -particle energies, thus, satisfy the fundamental energy principle rigidly. It is determined by the binding energies of the disintegrating and the product nuclei, which remain completely arbitrary, so far.

To proceed to understand the energy relationship more explicitly, we may put E' and E'' in terms of the Bethe-Weizsacker binding energies E'_B and E''_B along with the structural energies $\Delta E'$ and $\Delta E''$. It gives us

$$E' - E'' = S + E'_B - E''_B$$

where ' S ' is the structural energy change $\Delta E'_B - \Delta E''_B$, measured in mev., from the disintegrating to the product nuclei. Thus, in view of relation (2), we may put the α -energy relation, in the form,

$$E_\alpha = S + E'_B - E''_B - (B.E)_\alpha + \text{recoil energy} \quad \dots (2c)$$

The involved terms, beside the structural energy change S , is rather complicated to be interpreted in terms of simple nuclear characteristics. One may proceed to find a more easily understandable relation by tabulating the composition characteristics of the complete set of different α -disintegrating series, separately, along with their $(E_\alpha - S)$ values. It becomes evident that the $(E_\alpha - S)$ values for a particular series, with the fixed value of $(N - Z)$, increase with $(N + Z)$ or the nucleon number of the disintegrating nucleus and for different series, with any fixed value of $(N + Z)$, $(E_\alpha - S)$ values, similarly, decreases regularly with $(N - Z)$ values. These observations may be put in a general form of relationship, covering all the α -disintegrating nuclei, as

$$E_\alpha = S + 1704(N - Z - 2N - Z) - 17.61 \text{ Mev.} \quad \dots (3)$$

$$\text{or} \quad E_\alpha = S - 1704(3Z - N) - 17.61 \text{ Mev.}$$

The contribution of Bethe-Weiszacker binding energy etc. to the α -energy, then, reduces to be proportional to the difference between the mass number and double the excess-neutron content of the disintegrating nucleus, together with a constant.

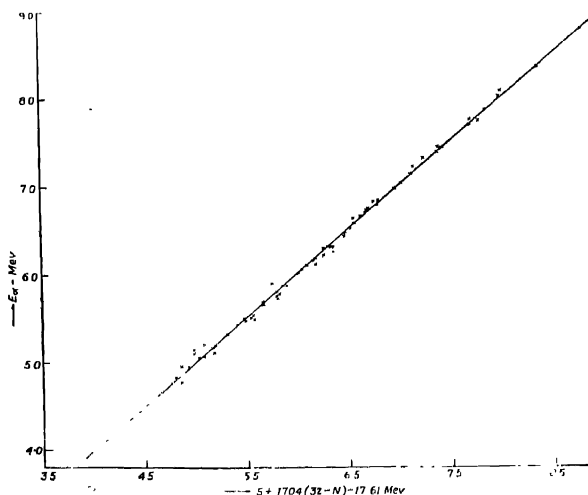


Fig. 3 α -Decay energy- experimental vs. calculated.

The agreement between the relation and the observed α -energies is remarkably well, as will be evident from the graphical representation in Fig. 3, where we have plotted the experimental E_α values against the right hand expression for the corresponding disintegrating nuclei, having particular N and Z values and the structural energy change S , as obtained, from $(E' - E'')$. The calculated

and observed values of E_α along with the calculated S values, are also tabulated in Table II with the observed and calculated values of $\log 1/T$ for some nuclei, discussed later on. There is a slight irregularity of the order of 0.1 Mev, for nuclei with low neutron content, like the polonium isotopes ($Z = 84$, $N = 126$, plotted in Fig. 3 on the lower regions of the graph), which may be due to experimental error in the determination of binding energy or the α -energy, or might be due to some other factor not taken into consideration for these low neutron content nuclei.

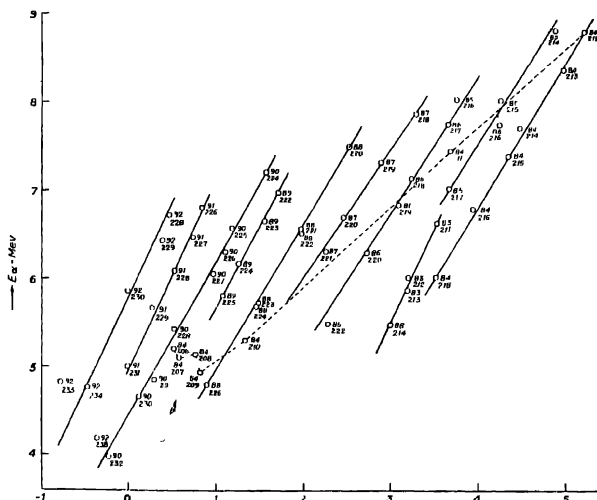


Fig. 4. α -Decay energy against change in ΔE , i.e. 'S' joined through radioactive isotopes.

It is further observed that for any particular element, characterised by the charge value, S increases with the decrease of the neutron number N in the nuclei more or less linearly and for the different elements they are displaced laterally, with some changes in the inclinations of the lines, as will be observed from Fig. 4. For the isotopes with a comparatively small number of neutrons, particularly, for the element polonium ($Z = 84$), the plot of the points give an irregular fall and a rise. The whole character of the diagram is very similar to the well-known α -energy mass number plot of Perlman and others (Perlman, Ghiorso and Seaborg, 1950). A plot of E_α against S or against mass number is, therefore, not very helpful in elucidation of the determining factor of α -energy. It shows, however, that for the isotopes of an element, the α -energy values increase regularly with the structural energy change S , which increases with gradually lower neutron content of the isotopes except for the very low neutron content elements of the

polonium nuclei The plot of Perlman and others moreover shows that a particular value of Z , E_α varies irregularly with the neutron number and for different values of Z the nature of irregularity varies without any possibility of smooth correlationship. It indicates that E_α cannot be measured in terms of any smooth function of N and Z , as has been attempted by G. P. Dube and L. S. Lingh (1954), Y. P. Varshni (1956), M. K. Ranaswamy (1956), and Evans (1955).

TABLE II

Observed and calculated characteristic of α -disintegrating nuclei

$N-Z$	$Z:A$	S	Obs E_α	Calc. E_α	Obs $\log q$	Calc. $\log q$	$N-Z$	$Z:A$	S	Obs E_α	Calc. E_α
54	92:238	-0.37	4.18	4.17	-17.15	-17.41	51	95:241	-0.49	5.48	5.58
								94:239	-0.57	5.16	5.16
52	94:240	-0.39	5.10	5.19	-11.28	-11.88		93:237	-0.53	4.77	4.86
	90:232	-0.23	3.98	3.97	-17.70	-17.56		92:235	-0.51	4.56	4.55
50	96:242	-0.42	6.11	6.17	-7.11	-7.07	49	95:239	-0.60	5.77	5.82
	94:238	0.36	5.51	5.54	-9.45	-9.34		93:235	0.66	5.06	5.07
	92:234	-0.47	4.76	4.76	-12.87	-12.76		92:233	-0.50	4.82	4.80
	90:230	0.12	4.66	4.66	-12.50	-12.42		91:231	-0.03	5.00	5.02
	88:226	0.89	4.80	4.75	-10.70	-10.61		90:229	+0.31	5.05	5.02
	86:222	+2.30	5.49	5.48	-5.51	-5.61		89:227	-0.55	4.94	4.92
	84:218	+3.52	6.00	5.99	-2.26	-1.85					
48	96:240	-0.58	6.30	6.35	-6.36	-5.94	47	93:233	-0.52	5.53	5.56
	94:236	-0.44	5.75	5.81	-7.93	-7.73		91:229	0.27	5.66	5.66
	92:232	-0.25	5.31	5.32	-8.98	-9.07		90:227	-0.97	6.05	6.03
	90:228	-0.52	5.42	5.10	-7.78	-7.64		89:225	-1.09	5.80	5.80
	88:224	+1.46	5.68	5.66	-5.50	-5.53		88:223	+1.48	5.72	5.81
	86:220	+2.74	6.28	6.26	-1.74	-1.80		87:221	+2.24	6.30	6.30
	84:216	+3.95	6.77	6.79	-0.84	-1.26		86:219	+3.10	6.82	6.80
								85:217	+3.68	7.02	7.03
								84:215	+4.36	7.36	7.36
46	94:234	-0.33	6.20	6.26	-4.49	-5.09	45	92:229	+0.39	6.42	6.46
	92:230	-0.01	5.86	5.89	-6.26	-5.80		91:227	+0.75	6.46	6.47
	91:228	+0.53	6.09	6.09	-4.90	-4.29		90:225	+1.18	6.57	6.56
	90:226	+1.11	6.30	6.34	-3.27	-3.24		89:223	+1.57	6.64	6.63
	89:224	+1.27	6.17	6.16	-3.56	-3.53		88:221	+1.98	6.71	6.69
	88:222	+1.99	6.51	6.64	-1.58	-1.59		87:219	+2.91	7.30	7.24
	87:220	+2.47	6.69	6.67	-1.40	-1.09		86:217	+3.68	7.74	7.70
	86:218	+3.25	7.12	7.12	-1.72	-1.54		85:215	+4.28	8.00	7.98
	85:216	+4.27	7.72	7.78	+3.52	+3.26		84:213	+5.01	8.34	8.33
	84:214	+4.50	7.68	7.69	+3.83	+4.40					
44	92:228	0.47	6.72	6.71	-2.75	-2.80	43	84:211	+3.71	7.43	7.39
	91:226	-0.85	6.81	6.76	-2.01	-2.00					
	90:224	+1.59	7.20	7.15	-	0	42	84:210	+1.33	5.30	5.19
	89:222	+1.73	6.96	6.96	0.74	-1.17	41	85:211	+1.39	5.89	5.76
	88:220	+2.54	7.49	7.42	+1.52	+1.09		84:209	+0.82	4.95	4.85
	87:218	+3.29	7.85	7.84	+2.30	+2.14	40	86:212	+1.30	6.17	6.18
	86:216	-3.7	8.07	7.99	+4.00	+3.64		85:208	+0.77	5.14	4.97
	85:214	+4.9	8.78	8.78	+5.70	+5.37	39	84:207	+0.59	5.10	4.97
	84:212	+5.25	8.77	8.75	+6.70	+6.46	38	87:212	+0.75	6.25	6.35
								84:206	-0.53	5.20	5.07

We have already noted that the α -particle energies satisfy the relationships (2) and (3) namely, $E' - E'' = E + (B.E)_\alpha$ or

$$E_\alpha = S + .1704(\bar{N} + Z - 2\bar{N} - Z) - 17.61 \text{ Mev.}$$

With the help of these two relations, it is possible to probe into the reason for the limitation of the α -energy magnitude on the low energy side. In obtaining the lower limit of observed α -energy and in attempting to understand the formation of α -particles, we have departed from the idea that the α -particles cross the central potential barrier and considered that the outgoing particle interacts strongly with the rest of the nucleus as was suggested by Chiang (1946) and modified by Preston (1951) and discussed theoretically by Brussaard and Talhoek (1958). It is well known that the energy of the α -particles are limited, on the lower side, to a magnitude of about 4 Mev only. This property should be related to the other emission characteristics of the nuclei. These are the observed facts that some of these nuclei are always α -disintegrating, some β -disintegrating, some are both α - and β -disintegrating and finally, the end products of these disintegrating series are stable. In our attempt to understand these characteristics on some basis, we note that the scope of the validity of the principles should be considered restricted to the region of the heavy nuclei, in the first instance. Appropriate modifications in other ranges of artificial disintegration are likely.

Let us now consider E' to be the binding energy of the 'A' nucleons in the disintegrating nucleus and E'' as the binding energy of the (A-4) nucleons in the product nucleus for an α -disintegration process. The binding energy per nucleon, in this naturally radioactive region is of the order of ~ 7.7 Mev, and it varies from nucleus to nucleus. If the binding energy per nucleon of the disintegrating and the product nucleus obtained the same value as ~ 7.7 Mev, we would have $E' - E'' = -30.8$ Mev. From the expression for E_α , in relation (2), we would have its magnitude as, $E_\alpha = -30.8$ Mev. $-(B/E)_\alpha = (-30.8 + 28.3)$ Mev $= -2.5$ Mev., which is a negative quantity and would restrict the formation and emission of the α -particle. We now modify the binding energy of the disintegrating nucleus in such a way, that compared to the binding energy of the product nucleus, on the basis of ~ 7.7 Mev per nucleon, there is a total shortage of energy amounting to 2.5 Mev., in the disintegrating nucleus. The distribution of nucleons in the disintegrating nucleus would, on occasions, take the form of the product nucleus for (A-1) of the nucleons, with its necessary energy distribution, leaving the shortage of 2.5 Mev. to the remaining 4 nucleons. This is plausible, as the (A-4) nuclear composition is known to have a structural configuration, corresponding to that binding energy, when left to itself. The four nucleons, with a shortage of 2.5 Mev., would be left with -28.3 Mev the amount required for the binding energy of the α -particle in its free state. The α -particle, however, could not be formed under the conditions. The available energy -28.3 Mev., would be distributed among the four nucleons, mutually, as also between these nucleons and the neighbouring nucleons of the main structure. The formation of an α -particle, under the conditions, would require that the binding energy per nucleon of the 4-particle entity, with its neighbouring nucleons in the composite structure, is less than the α -particle integration energy per nucleon, as a separate entity,

amounting to -7.075 Mev., otherwise the formation of the α -particle would not be possible.

To clarify and illustrate let us take the α -particle in the free state, with the binding energy per nucleon amounting to 7.075 Mev. As one of the alternative processes of conjecturing, this amount may be taken to signify the binding energy of any one of the nucleons to one of its neighbours, in a particular sense or direction, each nucleon behaving in a similar way, in a regular order. In the case of a large close packed structure in space, we may proceed to conjecture in a similar way and are forced to associate a larger number of nucleons, simultaneously, to each nucleon, with a similar behaviour for other nucleons also. Such distribution of binding energies for all the nucleons would compose the complete cohesive character of the larger nucleus.

In a three dimensional close packed structure, each nucleon would be linked with six other nucleons, generally, in the three directions of space, whereas, considering only the α -particle entity in the same structure, we would have each nucleon associated with two other nucleons only, along the two directions of space. The associations of a nucleon with the outside nucleons, corresponding to the larger structure and with the inner group to compose finally the α -particle are thus, in the ratio of $2/3$ to $1/3$. Further, in the sense that an isolated α -particle, would have each nucleon associated with one other nucleon, in a regular way, we would have in the composite structure, each nucleon associated with three other nucleons in a regular way, to build up the complete cohesive structure. Thus, we may consider, for the possibility of integration of the α -particle as a separate entity from a composite structure, the necessary relationship to be satisfied as,

$$2/3(B.E.)_{p,n} + 1/3(B.E.)_{\alpha,n} \geq 7.075 \text{ Mev}$$

Here, $(B.E.)_{p,n}$ signifies the $(B.E.)$ of the product nucleus per nucleon $(B.E.)_{\alpha,n}$ is the binding energy available to each of the four nucleons which would form the α -particle and \geq signifies that the left hand side expression is more positive or weaker in strength. The amount -7.075 Mev. measures the binding energy per nucleon of the α -particle, to be formed finally. As an example, when we have $(B.E.)_{p,n} = -7.7$ Mev and $(B.E.)_{\alpha,n} = -\frac{28.3}{4}$ Mev, we have the left hand expression amounting to -7.49 Mev. which is much stronger than α -integration energy. The particle, thus, cannot be formed.

We consider here the process already envisaged, that except for the four nucleons to form the α -particle, finally, $(A-4)$ nucleons of the disintegrating nucleus takes the structural form for the product nucleus and the energy difference $E' - E''$ are associated with the four nucleons only, so that,

$$\frac{1}{4}(B.E.)_{\alpha,n} = 1/12 (E' - E'').$$

When we put $E' - E'' = E_\alpha + (B.E)_\alpha = E_\alpha - 28.3 \text{ Mev}$,

according to relation (2), we have

$$E_\alpha(\text{lim}) = -8(B.E)_{p, n} - 56.6 \text{ Mev.} \quad \dots (4)$$

where $E_\alpha(\text{lim})$ is determined by the equality relation.

Thus, the lower limit of the emitted α -particle energy may be obtained, on the basis of 3 bonds per nucleon, when the binding energy of the product nucleus is known. Calculated on this basis, the lower limit of the emitted α -energy comes out according to expectation, generally, except for nuclei with lower neutron content, where the number of neutrons is equal to or less than 1.5 times the proton number and also for the nucleus (90.232). In these cases the calculated lower limit of the α -energy is higher than the observed energy. It is expected that the number of bonds per nucleon should depend in some way on neutron-proton ratio. We find that the limiting values become adjusted to the proper magnitude, when the bonds per nucleon in these cases of low neutron content nuclei are taken as 2.5 in place of 3, considered for other nuclei. The reasons for disagreement in case of the element (90.232) remain unexplained. It is, however, not unlikely that the number of bonds to be associated per nucleon should be gradually adjusted, according to the proportion of neutrons and protons in the nuclei, and thus, the lower limit of the α -particle energy also should be further adjusted by corresponding modifications in the relation (4) above.

When there is no α -disintegration in a nucleus and there is no known nucleus corresponding to the product nucleus composition, we may estimate the expected limiting value of the α -energy from a modified and approximate relationship, which immediately follows from the relation (4) above. Thus, we may put,

$$E_\alpha(\text{lim}) = -\frac{8}{A-4} \cdot [(B.E)_D - \delta E] - 56.6 \text{ Mev.} \quad \dots (4a)$$

where $(B.E)_D$ is the binding energy of the disintegrating nucleus and δE is the energy difference in the concerned range, between other nuclear set (Z, A) and $(Z-2, A-4)$, such that $(B.E)_D - \delta E$ correspond to an approximate value of the binding energy of the product nucleus, making relation (4a) identical with (4). The values of δE are obtainable from binding energy tables.

In Table III below, we have compared the calculated limiting values of the α -energy with the observed energy values for α -disintegrating nucleus or with relation (3), in the form,

$$E_\alpha = S + .1704(\overline{N+Z} - 2N - Z) - 17.61 \text{ Mev.},$$

which has been found to determine all α -energy values satisfactorily. The limiting α -energy values for all the nuclei, where the neutron number is more than 1.5

TABLE III

Limiting α -energy values and calculated or observed α -energies of various types of heavy nuclei.

Disintegration character of the nucleus	Nucleus	$E_\alpha(\text{lm})$	$E_\alpha(\text{obs})$ or (calc.)	Remarks
α -disintegrating $N > 1.5Z$	92,238	4.18	4.2	$E_\alpha(\text{obs. or calc.})$ $> E_\alpha(\text{lm.})$
	92,234	4.43	4.76	
	91,231	4.59	5.0	
	90,227	4.88	6.05	"
	90,228	4.84	5.42	
	86,222	5.26	5.49	
	86,220	5.47	6.28	"
	86,219	5.55	6.88	
	85,217	5.74	7.02	
	84,218	5.59	6.0	"
	84,216	5.84	6.77	
	84,215	5.93	7.36	
	84,214	6.06	7.68	"
	84,213	6.19	8.34	
	84,212	6.34	8.78	
α -disintegrating $N \leq 1.5Z$	84,211	6.35	7.43	$E_\alpha \text{ obs.} < E_\alpha(\text{lm.})$
	90,232	4.53	3.98	
	87,212	5.9	6.25	
	86,212	4.43	6.17	$E_\alpha(\text{lm.})$ with 3 and 2.5 bonds per nucleon.
		4.57		
	85,211	6.21	5.89	Upper values with 3 bonds.
		4.68		
	84,210	6.39	5.30	"
		4.80		
	84,209	6.38	4.95	"
		4.79		
	84,208	6.42	5.14	"
		4.83		
	84,207	6.42	5.10	"
		4.83		
	84,206	6.45	5.20	
α and β disintegrating	83,214	6.10	6.07	E_α (calc. or obs.) $\cong E_\alpha(\text{lm.})$.
	83,213	6.32	6.62	
	83,212	5.90	5.56	
	83,211	6.07	6.00	
β -disintegrating	91,234	4.43	$S \pm 4.49$	E_α calculated, except S S values $-m$, small in the range
	90,234	4.48	$S \pm 3.80$	
	89,228	4.79	$S \pm 4.15$	
	89,227	4.86	$S \pm 4.31$	
	88,228	4.81	$S \pm 3.47$	
	83,210	6.48	$S \pm 3.13$	E_α calculated, except S . $S \cong 3.5$ in the range.
	82,214	5.96	$S \pm 1.77$	
	82,212	6.18	$S \pm 2.11$	
	82,211	6.31	$S \pm 2.27$	
	82,210	6.40	$S \pm 2.45$	
Stable	83,209	6.40	$S \pm 3.3$	Upper values E_α calculated. Lower values E_β calculated. S values strongly negative for both.
			$S - 3.3$	
	82,208	6.48	$S \pm 2.8$	
			$S - 1.6$	
	82,207	6.50	$S \pm 2.97$	
	82,206	6.57	$S \pm 3.13$	
			$S - 3.3$	

times the proton number, have been calculated on the basis of 3 cohesional bonds for each of the nucleus as discussed before. For nuclei with the neutron number 1.5 times or less than the proton number, the limiting α -energy values have been calculated with the cohesional bond number per nucleon as 3 and 2.5 also. The observed α -energy values are in agreement with the limiting values calculated with 2.5 cohesional bonds, as against 3 cohesional bonds required for other nuclei. It shows the necessity of change in bond characteristics with the change in neutron proton proportion.

For the β -disintegrating particles, we may compare the expected α -energy values calculated from the relation (3), with the limiting α -energy values obtainable from the relation (4a), where the S values have to be estimated. It is found in these cases, that the expected α -energy values for such nuclei are lower than the limiting α -energy values. It tends to indicate why these nuclei are not of the α -disintegrating type. For those nuclei which have both α and β disintegrating characteristics, it is observed that the limiting α -energy values and the calculated ones are nearly equal. For stable nuclei the limiting α -energy values are much higher than the expected ones, calculated by the α -energy relationship. For these nuclei as also for the β -disintegrating nuclei, α -disintegration is debarred by the limiting energy condition.

PRINCIPLES OF α -AND β -DISINTEGRATION,

This brings us to the problem of β -disintegration. We limit ourselves, in our consideration, to the study of the maximum β -energy of the nuclei, in the naturally radioactive range, along with the artificially radioactive nuclei in the same range. We do not involve ourselves with the continuous character of the β -emission. As in the case of α -energy values, the expected β -emission energy may be calculated by a relation, based on fundamental energy principle, namely,

$$E' - E'' = E_{\beta} + E_{n,p} \quad \dots (5)$$

where E' and E'' are the binding energies of the disintegrating and the product nuclei and $E_{n,p}$ is the neutron-proton exchange energy, amounting to .78 Mev. As a matter of fact these expected β -energy maxima values have been tabulated by Everling in his table, on the basis of the above relationship. By a process similar to that followed to derive the α -energy expression (3), in terms of N , Z and S , we may find and replace the equation to determine the expected maximum β -energy by the relationship,

$$\left. \begin{aligned} E_{\beta} &= S - 0.179\{(N+Z) - 3(N-Z)\} + 12.28 \text{ Mev.} \\ &= S - 0.358(2z - N) + 12.28 \text{ Mev.,} \end{aligned} \right\} \quad \dots (6)$$

where S is the structural energy change for β -disintegration. The relation covers all the calculated E_{β} values in this range quite satisfactorily. There is, however, no limiting value of E_{β} , on the low energy side, as it obtains in the case of E_{α} ,

according to observation. An allowed E_β value in this range is, therefore, given by any positive value for E_β in the expression (6). If we calculate the expected E_β values for the four stable nuclei tabulated in Table II and consider the fact that the expected S values for all of them are negative, they being in the positions of minima for the $\Delta E-A$ curves, we have their expected E_β values strongly negative, indicating stability. The calculated values of E_β are also incorporated in Table III.

We may thus infer the following underlying principles. When the neutron-proton content of a nucleus, along with the structural energy change for a possible disintegration, obtains a value of E_α calculated by relation (3), which is larger than $E_\alpha(\text{lim})$ calculated by relations (4a) or its modified form for the nuclei, with a lower percentage of neutron, we expect an α -particle emission. For the nuclei on the border line having $E_\alpha(\text{Calc}) = E_\alpha(\text{lim})$, we obtain both α and β emission. For $E_\alpha(\text{Calc})$ values definitely less than $E_\alpha(\text{lim})$, we have β -emission only and its maximum possible energy can be calculated by relation (6). When the calculated E_β value becomes negative, the nuclei would belong to the stable category.

RELATION FOR E_β -MAXIMUM

The observed E_β maximum values are not always equal to the values expected from energy consideration, and calculated by the above relations (5) or (6). About fifty percent of the observed values, in this range, agree with the calculated ones, and in some of these cases, there are more than one maximum for one nucleus. Other observed values are generally some fraction of the expected values and in few cases the observed maxima values are definitely larger than the expected ones, on energy consideration. The observed values of β -energy maxima, in this range varies from a vanishingly small magnitude to a value of the order of nearly 4 Mev. To understand the discrepancy between the calculated and the observed β -energy maxima, we may plot the ΔE values from the Bethe-Weiszacker relation against neutron numbers, for all the β -active nuclei, in this range, along with the associated α -energy changes, as shown in the figure (5), by full and dotted lines. It would be observed that about 12 β -active nuclei, which have at least one observed value of the same magnitude as the calculated ones, lie on the maxima or minima of the ΔE versus N -graph, which gives us, from the course of the curves, S against N values. These nuclei are, therefore, in stationary states with regard to structural energy change and satisfy the criterion $dS/dN = 0$. The remaining ten nuclei have their observed E_β values as different fractional magnitudes of the calculated ones, while two nuclei have definitely higher observed values. Corresponding to the large or small variations of the observed and calculated values, they lie on a steeply or slowly changing regions of the curves, as will be observed in the figure, having both positive and negative values of dS/dN . These nuclei are on nonstationary states of structure. The large drop in the observed values from the calculated ones for the element 81(*Tl*), with 127, 128 and 129 neutrons

is closely related with their positions in steep regions of the curves $\Delta E-N$. Those nuclei are on rapidly changing states of structure. It is implied that the β -dis-

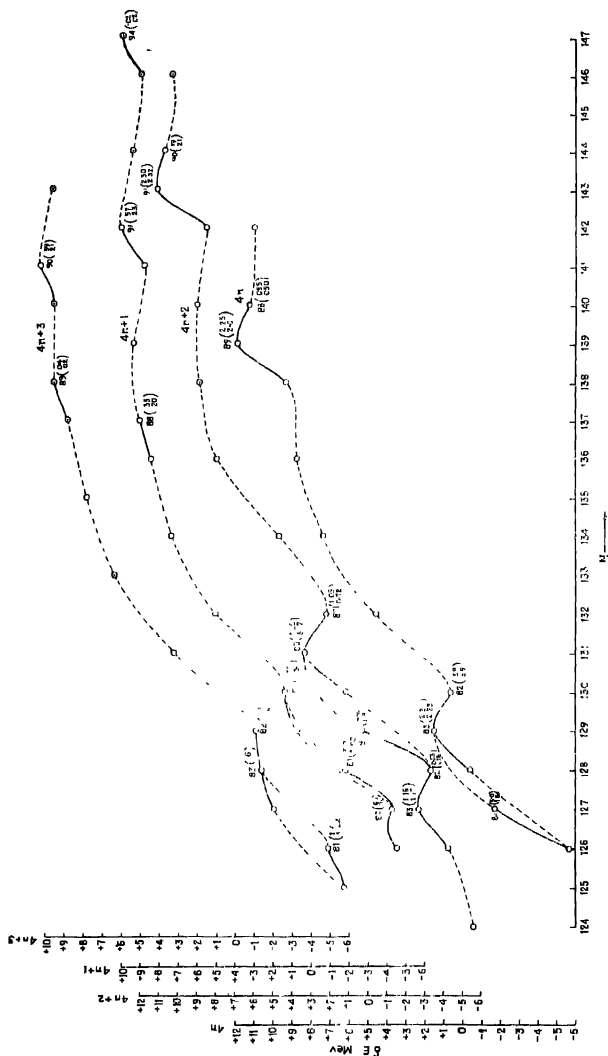


Fig. 5. ΔE Vs. neutron number for α and β -disintegrating nuclei.

integrating nuclei, on such sloping regions of the curve, have not attained the structure required by their constitution fully and should have their structural energy term ' S ' in relation (6), accordingly modified. It may be noted that from our relationship for S with reference to the curve, dS/dN is negative for a downward slope of the curve in the direction of decreasing N . This indicates the criterion for positive dS/dN values also.

We, therefore, replace the structural energy term ' S ' in relation (6), by a more suitable term for the observed β -energy values, in accordance with the observations, just made and replace S by $S \left(1 + K \frac{dS}{dN} \right)$, in the relation, for the observed β -energy. A constant value of $K = 0.25$, satisfies the observed β -energy, values of the nuclei, on the basis of the curves as drawn in Fig. (5). We may thus, modify the relation (6), for observed β -energy in form,

$$E_{\beta}(\text{observed maxima}) = S \left(1 + 0.25 \frac{dS}{dN} \right) = 0.358(2Z - N) + 12.82 \text{ Mev.}, \dots (6a)$$

which obtains all the observed values satisfactorily, including those with observed values higher than the expected or calculated ones. Previous attempts by Glueckauf (1948), Süss and Jensen (1952) and Way and Wood (1954) to systematise the β -energy maxima either observed or expected in this region of heavy nuclei do not suggest definite relationship to calculate the values. It may be noted, however, that there is a scope of adjusting the curvatures of the curves to suit the observed values. This scope of adjustment of the curves gives us also a range of the possible β -energy values in a continuous way, which is significant. It also limits the flexibility in drawing the curves in view of the limitations of the range of observed values for a nucleus.

We may further remark that the observed multiple valued β -energies should correspond to multiple valued binding energies. We have, however, till now, only single binding energies for disintegrating nuclei, and presumably that for the more stationary states, corresponding to the largest of the observed values, with which the curves have been fitted.

It brings us back to the case of calculated α -energies by relation (3), where we have not modified the term S in the expression for E_{α} , to get good agreement between observed and calculated values, although the nuclei lie on as steep curves as in the case of β -disintegration. This implies that the structural change required by the ΔE curve, for α -disintegration is generally established. The structure evidently should be automatically adjusted to the constitution, as, in such emission the product nucleus is already formed within the disintegrating nucleus, according to our observations in connection with the limiting value of α -particle energies.

HALF LIFE -- α -ENERGY RELATIONSHIP

We conclude our work with a study of the interrelation between the half lives and energy of the α -disintegrating nuclei. Quite a lot of work has been done on this line, beginning with Geiger and Nuttall's work (1911), and elaborated initially by Perlman, Glirosio and Seaborg (1950). A more comprehensive up-to-date information is compiled by Preston (1962). The Geiger Nuttall law connecting the ranges of the α -particles with the decay constant λ , came into difficulties because of misfits, and this difficulty has not been removed till now. It has been noted by us that as a guiding principle for all α -disintegrating nuclei, one may take $\log 1/\tau$, as roughly proportional to $E^{1/2}$, for a definite amount of excess neutrons. The slopes are proportional to the reciprocal of the cubes of the excess neutron amount and the displacements along the $E^{1/2}$ scale are also measurable in terms of $(N-Z)$. There are, however, quite a number of large or small deviations.

It is, however, possible to adjust the deviations from a smooth linear course, by suitable terms depending on the nuclear charge, particularly, for all the even-even and odd-odd nuclei. As an example we may refer to the plot of points, in Fig. (6), corresponding to an excess neutron content, amounting to 50, where $\log 1/\tau$ values are plotted against $E^{1/2}$ values, initially. The points lie scattered in the field, as would be noted on a perusal. If, however, we plot $\log 1/\tau$ against $E_{\alpha}^{1/2} + 0.018(90-Z)$, for these even-even nuclei, the points move over to a straight line, as has been indicated in the same figure. It is interesting to note that in the

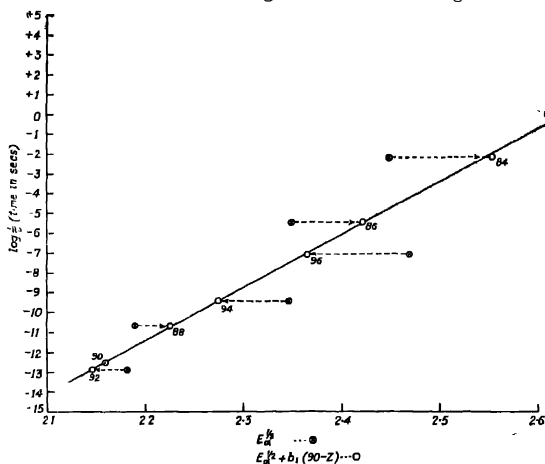


Fig. 6. $\log_{10} 1/\tau$ Vs. $f(E_{\alpha}^{1/2})$ for $(N-Z)=50$.

case of all the even-even and odd-odd nuclei, excepting for the five low neutron content nuclei with $N \leq 1.5Z$, an almost identical relation will bring the points

corresponding to different $(N-Z)$ values, on different straight lines. Their inclinations are made to correspond, when the slopes are multiplied by the cubes of the respective $(N-Z)$ values. The displacement along the x -axis are measurable in terms of magnitudes which are nearly proportional to the $(N-Z)$ values, for all the different disintegration series. It puts all the available even-even and odd-odd nuclei excepting the low-neutron-content ones, into a simple linear relationship, to correlate the half lives with the α -energy and the neutron-proton content of the nucleus. In all, we have taken into consideration, now, thirty α -disintegrating nuclei, of which twenty-five are of the even-even type and five of the odd-odd type, whose data are complete. Their half lives are determined by the relation.

$$\log \frac{1}{\tau} = 2.117[(N-Z)^3\{E_\alpha - b_1(90 - Z)\} + C', (50 - N - Z)] \times 10^{-1} \quad (7)$$

where $b_1 = 0.18$ or 0.09 for even-even and odd-odd nuclei, $C' = 1.750$, for $(N-Z)$ values from 54 to 48, which reduces to 1.725 and 1.625 for $(N-Z)$ as 46 and 44. τ is measured in seconds and E_α in Mev units. We have plotted in Fig. (7) the observed values of $\log 1/\tau$ against the function,

$$f(E_\alpha, N, Z) = \frac{(N-Z)^3}{50^3} [E_\alpha - b_1(90 - Z)] + C', (50 - N - Z) \quad [7a]$$

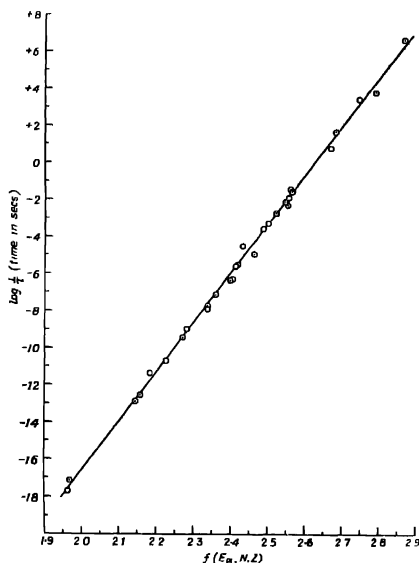


Fig. 7. $\text{Log}_{10} 1/\tau$ against calculated values of $f(E_\alpha, N-Z)$ given by relation (7a).

where b_i 's obtain the same values as before and C_i 's are 0.14, 0.138 and 0.130 in place of the above set of values for C_i . As a matter of fact, the identity relation has been put on the basis of the graphical representation after the slope has been determined. The calculated values of $\log 1/\tau$ for the 30 nuclei, have been tabulated in Table II, along with the observed $\log 1/\tau$ values and other relevant data.

The relations indicate clearly that, for a particular value of $(N-Z)$, the half lives of these nuclei decrease with increasing B_α values and with decreasing proton number. For a particular B_α value, with the same proton number, however, the half life or $\log 1/\tau$ remains nearly balanced with increasing or decreasing excess neutron amount. The additive term involving $(N-Z)$ almost balances the effect of the multiplying factor. Thus the more important factor in determining the half life is the α -energy amount and less predominantly, the proton number in the nucleus. The increase in magnitude of the excess neutron would tend to decrease the half lives when the α -energy is high with a reverse effect when the α -energy is low. The half lives of these nuclei are dependent on the structural energy change ' S ' only through the B_α -expression.

We hope to analyse the half-life data of the remaining even-odd and odd-even α -disintegrating nuclei as also of the low neutron content ones in a future work.

REFERENCES

- Brussard, P. J. and Thalhock, H. A., 1958, *Physica*, **24**, 263.
 Chang, W. Y., 1946, *Phys. Rev.*, **69**, 60 and 70, 632.
 Dube, G. P. and Singh, L. S., 1954, *Ind. J. Phys.*, **28**, 177.
 Dutta, A., Pal, B., Dasgupta, A. and Chaudhury, N., 1962, *Ind. J. Phys.*, **36**, 497.
 Evans, R. D., 1955, *The Atomic Nucleus*, McGraw Hill Book Co. Inc. p. 529.
 Everling, F., Konig, L. A., Mattauch, J. H. and Wapstra, A. H., 1960, *Nuclear Physics*, **18**, 519.
 Fermi, E., 1951, *Nuclear Physics* (Chicago University Press), p. 7.
 Geiger, H. and Nuttal, J. M., 1911, *Phil. Mag.*, **22**, 613.
 Glueckauf, E., 1948, *Proc. Phys. Soc. (Lond.)*, **61**, 25.
 Green, A. E. S., 1954, *Phys. Rev.*, **95**, 1006.
 Perlman, I., Ghiorso, A. and Seaborg, G. T., 1950, *Phys. Rev.*, **77**, 26.
 Preston, M. A., 1951, *Phys. Rev.*, **82**, 515.
 Preston, M. A., 1962, *Physics of the Nucleus* (Addison Wesley Publishing Co.), p. 340.
 Ramaswamy, M. K., 1956, *Nuovo Cimento*, **4**, 1570.
 Strominger, D., Hollandar, J. N. and Seaborg, G. T., 1958, *Rev. mod. Phys.*, **30**, 585.
 Suess, H. E. and Jensen, J. H. D., 1952, *Arkiv F. Fysik*, **3**, 577.
 Varshni, Y. P., 1956, *Nuovo Cimento*, **3**, 1148.
 Way, K. and Wood, M., 1954, *Phys. Rev.*, **94**, 119.

DISPERSION OF ULTRASONIC WAVE IN DIATOMIC GASES AT LOW PRESSURE

K. SAMAL*

PHYSICS DEPARTMENT, UNIVERSITY OF ALBERTA, EDMONTON, CANADA*

(Received May 2, 1962)

ABSTRACT. The quadratic equation resulted from the direct combination of Navier-Stokes equation with rotational relaxation was solved by neglecting the terms containing higher than the second power of viscosity and thermal conductivity. This leads to an approximate expression for V_0/T . Two sets of values for V_0/T have been calculated for different pressures by taking static and complex values of C_p in Eucken's formula for the ratio of thermal conductivity to viscosity. They agree quite well with the experimental result of Boyer and Greenspan, within the limits involved in the original equation and the substituted value of C_p in Eucken's formula. Greenspan's calculation based on the Burnett's theory and the approximation of Becker gas, has been also shown for comparison.

INTRODUCTION

It has been observed by Boyer (1951) that for diatomic gases like O_2 and N_2 the velocity of sound varies significantly as the wave length of the sound approaches the mean free-path of the molecules. Recently Greenspan (1954, 1959) tried to explain the variation from his own experimental result by combining the Herzfeld, Rice and Keesom's theory (1951) of thermal relaxation with the help of Burnett's theory and the approximation of Becker (1922) gas. The disagreement found out in the comparison is not trivial and is attributed to the nature of approximation involved in the Burnett's theory, a single relaxation number for the rotational relaxation process and the way of combining the two processes.

An attempt is made here to combine in the direct possible way the Navier-Stokes equation and the rotational character of the molecule through the complex nature of the specific heat value. This leads to a quadratic equation which has been solved with a view to retain only upto the significant terms containing the second power of viscosity and heat conductivity. It has been shown that the approximation explains quite satisfactorily the experimental results obtained by

Boyer and Greenspan so long as $\frac{\eta}{\rho_0} \frac{\omega}{V_0^2} < 1$

* Present address—Physics Department, Ravenshaw College, Cuttack-3, India.

- where η —Coefficient of viscosity
 ρ_0 —density of the gas not disturbed by sound waves.
 V_0 —sound velocity with very low frequency.
 $\omega = 2\pi f$ f = frequency of the sound wave.

T H E O R Y

After eliminating the flow velocity and condensation (Herzfeld and Litovitz, 1959) from the combination of the equation of motion and equation of continuity the combined form of the equation becomes

$$\left(\frac{k}{\omega}\right)^2 = - \frac{\left(\frac{\partial p}{\partial \rho}\right)^{-1}}{\left[1 + \frac{4}{3} i \omega \frac{\eta}{\rho_0} \left(\frac{\partial p}{\partial \rho}\right)^{-1}\right]}$$

k —propagation constant.

From the thermodynamical consideration specific heat values are suitably modified in the energy relation after taking into account thermal conductivity and relaxation. Substituting these modified specific heat values in the equation of state one can get

$$\left(\frac{\partial p}{\partial \rho}\right)^{-1} = \frac{\rho_0}{B_T} \frac{C_e + C_j(1 + i\omega\tau)^{-1} - iWk^2}{R + C_e + C_j(1 + i\omega\tau)^{-1} - iWk^2} \quad \dots (2)$$

here B_T —Isothermal bulk modulus

C_e —molar specific heat due to translational degrees of freedom.

C_j —molar specific heat value due to internal degrees of freedom.

R —gas constant

τ —rotational relaxation time.

χ —thermal conductivity.

$W = \frac{\chi M}{\rho_0 \omega}$ M —molecular weight of the gas.

It has been assumed that at low pressure O_2 and N_2 behave almost like a perfect gas. Substituting eqn. (2) in eqn. (1) one can get

$$\begin{aligned} \left(\frac{k}{\omega}\right)^4 \frac{\rho_0}{B_T} \frac{W^2 R \omega^4}{C_p^3} - \left(\frac{k}{\omega}\right)^2 \left[1 + \frac{\rho_0}{B_T} \frac{i W R \omega^2}{C_p^3} - \frac{8}{3} \omega^2 \frac{\eta}{\rho_0} \left(\frac{\rho_0}{B_T}\right)^2 \left(\frac{W R^2}{C_p^3} - \frac{W R}{C_p^2}\right)\right] \\ + \frac{\rho_0}{B_T} \left[\frac{1}{\gamma} - 4i\omega \frac{\eta}{\rho_0} \frac{\rho_0}{B_T} \frac{1}{\gamma^3} - \frac{16}{9} \omega^2 \left(\frac{\eta}{\rho_0}\right)^2 \left(\frac{\rho_0}{B_T}\right)^2 \frac{1}{\gamma^3}\right] \quad \dots (3) \end{aligned}$$

$$\text{where } C_p = C_e + R + \frac{C_j}{1 + i\omega\tau}$$

$$C_v = C_e + \frac{C_j}{1 + i\omega\tau}, \quad \gamma = C_p/C_v$$

To get the above form it is assumed that the real parts of $\frac{4}{3} i\omega \frac{\eta}{\rho_0} \left(\frac{\partial p}{\partial \rho} \right)^{-1}$ and $\frac{iWk^2}{C}$ are each less than one.

Solving the eqn (3) for the physically possible root for the propagation of sound waves and neglecting terms containing higher than the second power of viscosity and heat conductivity, one gets

$$\begin{aligned} \left(\frac{k}{\omega} \right)^2 = & \left[\frac{\rho_0}{B_T \gamma} - 4\omega^3 \frac{\eta}{\rho_0} \left(\frac{\rho_0}{B_T \gamma} \right)^3 \frac{WR}{C_p C_v} - i\omega^2 \left(\frac{\rho_0}{B_T \gamma} \right)^2 \frac{WR}{C_p C_v} \right. \\ & + \frac{4}{3} i\omega \left(\frac{\rho_0}{B_T \gamma} \right)^2 \frac{\eta}{\rho_0} - \frac{16}{9} \omega^2 \left(\frac{\eta}{\rho_0} \right)^2 \left(\frac{\rho_0}{B_T \gamma} \right)^3 \\ & \left. + \left(\frac{\rho_0}{B_T \gamma} \right)^3 \omega^4 \frac{W^2 R}{C_v C_p^2} - \left(\frac{\rho_0}{B_T \gamma} \right)^3 \omega^4 \frac{W^2 R^2}{C_v^2 C_p^2} \right] \quad \dots \quad (4) \end{aligned}$$

From Eucken (1952) approach one can write

$$M\chi = \frac{1}{4} (9\gamma - 5)\eta C_v = (\alpha - i\beta)\eta$$

$$\text{where } \alpha = (9.5 + 7.5\omega^2\tau^2)/(1 + \omega^2\tau^2)$$

$$\text{and } \beta = \frac{2\omega\tau}{(1 + \omega^2\tau^2)}$$

For convenience let us write for the real part of $\left(\frac{k}{\omega} \right)^2 = \frac{\mathcal{V}}{V_0^2}$ and for the imaginary

$$\text{part of } \left(\frac{k}{\omega} \right)^2 = \frac{I}{V_0^2}$$

$$\text{and } a = \frac{RC_j}{C_0(C_0 + R)}, \quad C_0 = C_e + C_j, \quad d = \frac{C_0}{(C_0 + R)}$$

$$b = \frac{C_e + R}{C_0 + R}, \quad e = 1 + (b\omega\tau)^2, \quad A = 1 - \frac{ab\omega^2\tau^2}{e}$$

It is seen $\left(\frac{\omega\tau a}{c}\right)^2 \ll A$ (almost 1 in 1000 at best) for the experimental range of Greenspan and Boyer. Thus neglecting the higher than the first power of $\frac{\omega\tau a}{c}$, real and imaginary parts can be separated from (4) as follows.

$$\begin{aligned} \mathcal{A} = & A - \frac{8}{3} \frac{\eta}{\rho_0} \frac{\omega}{V_0^2} \frac{\omega\tau a}{c} A - \frac{16}{9} \left(\frac{\eta}{\rho_0}\right)^2 \left(\frac{\omega}{V_0^2}\right)^2 A^3 \\ & - 4 \left(\frac{\eta}{\rho_0}\right)^2 \frac{\alpha}{R} \left(\frac{\omega}{V_0^2}\right)^2 \frac{A^2}{d} (1-dA)^2 + \frac{\eta}{\rho_0} \frac{\alpha}{R} \frac{\omega}{V_0^2} \frac{\omega\tau a}{c} \left(\frac{1}{d} - A\right) (5-3dA) \\ & + \left(\frac{\eta}{\rho_0}\right)^2 \frac{\alpha^2 - \beta^2}{R^2} \left(\frac{\omega}{V_0^2}\right)^2 \frac{A}{d} (1-dA)^2 \left(2A - \frac{1}{d}\right) - \frac{\eta}{\rho_0} \frac{\beta}{R} \frac{\omega}{V_0^2} \frac{A}{d} (1-dA)^2 \\ & - 8 \left(\frac{\eta}{\rho_0}\right)^2 \frac{\beta}{R} \left(\frac{\omega}{V_0^2}\right)^2 \frac{\omega\tau a}{c} A (1-dA) \left(2A - \frac{1}{d}\right) \\ & - 2 \frac{\alpha\beta}{R^2} \left(\frac{\eta}{\rho_0}\right)^2 \left(\frac{\omega}{V_0^2}\right)^2 \frac{\omega\tau a}{c} \left(A - \frac{1}{d}\right)^2 (8Ad - 4A^2d^2 - 1) \quad \dots \quad (5) \end{aligned}$$

$$\begin{aligned} I = & - \left[\frac{\omega\tau a}{c} + \frac{4}{3} \frac{\eta}{\rho_0} \frac{\omega}{V_0^2} A^2 + \frac{16}{3} \left(\frac{\eta}{\rho_0}\right)^2 \left(\frac{\omega}{V_0^2}\right)^2 \frac{\omega\tau a}{c} A^2 + \frac{\eta}{\rho_0} \frac{\alpha}{R} \frac{\omega}{V_0^2} \frac{A}{d} (1-dA)^2 \right. \\ & + 8 \left(\frac{\eta}{\rho_0}\right)^2 \frac{\alpha}{R} \left(\frac{\omega}{V_0^2}\right)^2 \frac{\omega\tau a}{c} A (1-dA) \left(2A - \frac{1}{d}\right) \\ & + \left(\frac{\eta}{\rho_0}\right)^2 \frac{\alpha^2 - \beta^2}{R^2} \left(\frac{\omega}{V_0^2}\right)^2 \frac{\omega\tau a}{c} \left(A - \frac{1}{d}\right)^2 (8Ad - 4A^2d^2 - 1) \\ & - 4 \left(\frac{\eta}{\rho_0}\right)^2 \frac{\beta}{R} \left(\frac{\omega}{V_0^2}\right)^2 \frac{A^2}{d} (1-dA)^2 + \frac{\eta}{\rho_0} \frac{\beta}{R} \frac{\omega}{V_0^2} \frac{\omega\tau a}{c} \left(\frac{1}{d} - A\right) (5-3dA) \\ & \left. + \frac{2\alpha\beta}{R^2} \left(\frac{\eta}{\rho_0}\right)^2 \left(\frac{\omega}{V_0^2}\right)^2 \frac{A}{d} (1-dA)^2 \left(2A - \frac{1}{d}\right) \right] \quad \dots \quad (6) \end{aligned}$$

If one neglects the frequency dependent terms in Eucken formula $\alpha = M\chi/\eta$ and $\beta = 0$ i.e. by taking the static value of C_v and γ in $\frac{1}{2}(9\gamma-5)C_v$, equations (5) and (6) are simplified as follows.

$$\begin{aligned} \mathcal{A} = & A - \frac{8}{3} \frac{\eta}{\rho_0} \frac{\omega}{V_0^2} \frac{\omega \tau \alpha}{e} A - \frac{16}{9} \left(\frac{\eta}{\rho_0} \right)^2 \left(\frac{\omega}{V_0^2} \right)^2 A^3 - 4 \frac{\eta}{\rho_0} \frac{\chi M}{R \rho_0} \left(\frac{\omega}{V_0^2} \right)^2 \frac{A^2}{d} (1-dA)^2 \\ & + \frac{\chi M}{R \rho_0} \frac{\omega}{V_0^2} \frac{\omega \tau \alpha}{e} \left(\frac{1}{d} - A \right) (5-3dA) + \left(\frac{\chi M}{R \rho_0} \right)^2 \left(\frac{\omega}{V_0^2} \right)^2 \frac{A}{d} (1-dA)^3 \left(\frac{2A-1}{d} \right) \end{aligned} \quad \dots (7)$$

$$\begin{aligned} I = & - \left[\frac{\omega \tau \alpha}{e} + \frac{4}{3} \frac{\eta}{\rho_0} \frac{\omega}{V_0^2} A^2 + \frac{16}{3} \left(\frac{\eta}{\rho_0} \right)^2 \left(\frac{\omega}{V_0^2} \right)^2 \frac{\omega \tau \alpha}{e} A^2 + \frac{\chi M}{R \rho_0} \frac{\omega}{V_0^2} \frac{A}{d} (1-dA)^2 \right. \\ & + 8 \frac{\eta}{\rho_0} \frac{\chi M}{R \rho_0} \left(\frac{\omega}{V_0^2} \right)^2 \frac{\omega \tau \alpha}{e} A (1-dA) \left(\frac{2A-1}{d} \right) \\ & \left. + \left(\frac{\chi M}{R \rho_0} \right)^2 \left(\frac{\omega}{V_0^2} \right)^2 \frac{\omega \tau \alpha}{e} \left(\frac{1}{d} - A \right)^2 (8Ad - 4A^2d^2 - 1) \right] \end{aligned} \quad \dots (8)$$

writing $k = k_1 + ik_2$ where $\frac{k}{\omega} = \frac{1}{V}$ and $k_2 =$ amplitude absorption coefficient,

$V =$ phase velocity. One can readily show

$$\left\{ \left(\frac{k_1}{\omega} \right)^2 - \left(\frac{k_2}{\omega} \right)^2 \right\} V_0^2 = \mathcal{A} \quad \text{and} \quad \frac{2k_1 k_2 V_0^2}{\omega^2} = I$$

Then $(V_0/V)^2 = \frac{\mathcal{A} + (\mathcal{A}^2 + I)^{\frac{1}{2}}}{2} \quad \dots (9)$

and $k_2^2 = \left(\frac{\omega}{V_0^2} \right)^2 \frac{(\mathcal{A}^2 + I)^{\frac{1}{2}} - \mathcal{A}}{2} \quad \dots (10)$

VERIFICATION OF EXPERIMENTAL RESULT

Just to verify the result of Boyer, A and I are calculated from the preceding two sets of equations for N_2 and O_2 taking different pressure values. The constant values used are given below.

Density of N_2 at N.T.P. = $1.25 \times 10^{-3} \text{ gm/cm}^3$

Density of O_2 at N.T.P. = $1.429 \times 10^{-3} \text{ gm/cm}^3$

Coefficient of viscosity for N_2 at $10.9^\circ C = 170.7$ micropoise converted to $0^\circ C$ by Keelson's formula (1942) as 166.3 micropoise. Viscosity of O_2 at $0^\circ C = 189.0$ micropoise.

The collision number for N_2 is taken to be 5.28 as adopted by Greenspan whereas other workers (1959) have taken it to be 6. This difference does not introduce any appreciable deviation in the comparison. But for O_2 this number is taken to be 20 as found out by many workers (1959) and roughly estimated from Boyer's result.

TABLE I

Comparison with Boyer's result 970.68 kc/sec. Temperature $0^\circ C$.

(a) For nitrogen

$\frac{p}{\eta\omega} = r$	Pr. in cms of Hg	(V_o/V) expt.	(V_o/V) cal $C_p = C_o$	(V_o/V) cal $\chi = f(\omega)$
22.6	1.72	0.994	0.999	0.996
8.42	0.64	0.974	0.980	0.977
6.05	0.46	0.966	0.967	0.950
3.16	0.24	0.955	0.950	0.928
1.84	0.14	0.87	0.878	0.816

(b) For oxygen

$\frac{p}{\eta\omega} = r$	Pr. in cms of Hg.	(V_o/V) expt.	(V_o/V) cal $C_p = C_o$	(V_o/V) cal $\chi = f(\omega)$
31.3	2.70	0.990	0.987	0.987
22.6	1.95	0.987	0.977	0.972
18.0	1.55	0.985	0.967	0.962
13.3	1.15	0.978	0.950	0.946
11.6	1.00	0.970	0.940	0.925
6.38	0.55	0.880	0.850	0.870
2.90	0.25	0.835	0.815	0.826

TABLE II

Comparison with Greenspan's result for nitrogen $f=11$ Mc/sec
Temperature 0°C

$\frac{p}{\eta\omega}$	Pr in cms of Hg.	(V_o/V) expt.	(V_o/V) cal. C_o C_o	(V_o/V) cal $\chi = f(\omega)$	Greenspan (V_o/V) cal
0.214	0.185	0.542	0.670	0.585	0.297
0.573	0.496	0.641	0.708	0.640	0.510
0.920	0.797	0.700	0.765	0.678	0.650
1.720	1.480	0.800	0.785	0.757	0.780
2.230	1.930	0.865	0.840	0.820	0.820
3.00	2.600	0.900	0.935	0.850	0.870
5.00	4.330	0.949	0.950	0.940	0.950

In Greenspan's paper frequency being 11Mc/sec., $\frac{\eta}{\rho_0} \frac{\omega}{V_0^2}$ is nearly unity for N_2 at the pressure of 0.835 cms. of Hg. i.e. when $r = \frac{p}{\eta\omega} \simeq 1$. In Table II. a comparison is made between Greenspan's result and the calculated values when $r < 1$. Greenspan's experimental values and his calculated values were estimated from his graph. The agreement is better towards the greater r values as expected from the theory. But the agreement with experiment for r less than unity is rather surprising since the approximation used in this paper are invalid for these r . What should be the exact value of χ/η can only be obtained from the detailed kinetic theory treatment. That's why for comparison two sets of calculated values are incorporated by substituting the static values of C_o in Eucken's formula. As against such uncertainties in the values of χ/η and rotational collision number it is not desirable to reject the Navier-Stokes equation when the agreement with the theoretical result based on the Burnett's theory is not fully satisfactory for diatomic gases.

ACKNOWLEDGMENT

The author is grateful to Prof. A. B. Bhatia for suggesting the problem and helpful discussion and to Dr. Martin Greenspan for sending the reprints of his papers and for suggesting in his comments to use the complex value of C in the calculation. He is also thankful to the Government of Canada for awarding a Commonwealth scholarship and to the University of Alberta where the work was carried out.

REFERENCES

- Boyer, R. A , 1951, *J. Acoust. Soc. Am.*, **23**, 176.
Greenspan, M., 1954, *J. Acoust. Soc. Am.*, **26**, 70 ;
Greenspan, M , 1959, *J. Acoust. Soc. Am.*, **31**, 155.
Herzfeld, Rice and Kneser's theory given in
Markham, Boyer and Lindsay, 1951, *Rev. Mod. Phys.*, **23**, 353.
Becker, R., 1922, *Z. Physik*, **8**, 321
Herzfeld and Litovitz, 1959, "Absorption and Dispersion of Ultrasonic waves" *Academic Press Newyork*, p 25-40, p. 239
Keesom, W. H., 1942, Helium, *Elsevier Press Inc. Amsterdam*, p. 107.
Eucken approach. Chapman and Cowling, 1952, *The Mathematical theory of Nonuniform Gases*, *Cambridge Univ. Press*, p. 237.

ON THE RAMAN SPECTRUM OF ALLYL CYANIDE IN THE SOLID STATE*

K. K. DEB AND D. K. MUKHERJEE

OPTICS DEPARTMENT,

INDIAN ASSOCIATION FOR THE CULTIVATION OF SCIENCE,
CALCUTTA-32.

(Received March, 15, 1963)

Plate V

ABSTRACT The results of investigation on the Raman spectra of allyl cyanide in the liquid state and in the solid state at -180°C have been discussed. Changes in some of the intramolecular oscillations are found to take place with the solidification of the liquid. It has been concluded from the results that the molecules of the compound are associated (through H-atoms and the $\text{C} \equiv \text{N}$ group) when the liquid is solidified and cooled to -180°C .

INTRODUCTION

The Raman spectra of a few organic nitriles in the solid state at -180°C were studied earlier (Bishui, 1948, Deb, 1961). It was concluded from the results that the lines due to $\text{C} \equiv \text{N}$ vibrations in each case undergo changes and a few low-frequency Raman lines appear in the spectra with the solidification of the liquid at low temperatures. In the present work similar investigation has been extended to the case of allyl cyanide.

EXPERIMENTAL

Allyl cyanide supplied by Eastman Kodak Co., U.S.A., was of chemically pure quality and it was further purified by distillation under reduced pressure. The arrangements for recording the Raman spectra in the solid state at -180°C and for studying the state of polarisation of the Raman lines in the liquid state were the same as those used earlier (Deb, 1960; Mukherjee, 1960). The spectra were recorded on Ilford Zenith plates with the help of a Fuess glass spectrograph having a dispersion of about 11 \AA/mm in the region of 4047 \AA .

RESULTS AND DISCUSSION

The Raman spectra of the compound in the liquid state and in the solid state at -180°C are shown in Figs. 1(a) and 1(b), Plate V. The observed Raman shifts of the molecule in the liquid and solid states are tabulated in Table I. The Raman frequencies of the liquid reported by previous workers are also included

*Communicated by Prof. S. C. Sirkar.

in the Table. The states of polarisation of the Raman lines of the liquid are indicated by the letters 'P' and 'D' which mean partially polarised and totally depolarised respectively.

It can be seen from Figs. 1(a), 1(b) and 1(c) and also from Table I that when allyl cyanide is solidified and cooled to -180°C , the line 168 cm^{-1} representing probably the bending of $\text{C}\equiv\text{N}$ bond appears to be replaced by three new Raman lines of shifts 85, 101 and 187 cm^{-1} respectively. The change may be due to the formation of weak molecular association of different strengths in the crystal lattice at low temperature. Further, in the solid state at -180°C the line 1413 cm^{-1} due to C-H bending oscillation shifts to 1394 cm^{-1} and the line 2257 cm^{-1} due to $\text{C}\equiv\text{N}$ stretching oscillation shifts to 2252 cm^{-1} . Also the line 2919 cm^{-1}

TABLE I
Raman spectra of allyl cyanide $\Delta\nu$ in cm^{-1}

Raman shifts Kohlrausch and Stockmair (1935)	Solid at -180°C Present authors	
		85 (5)
		101 (0)
174 (6)	168 (6b) D	187 (3Vb)
205 (4)	212 (1) D	209 (1)
359 (5)	361 (2) D	
404 (5)	407 (2b) P	
	457 (2) P	
555 (2)	558 (0b)	
625 (1)		
804 (5)	806 (6) P	874 (6)
900 (1)		
938 (3)	940 (0)	
1108 (0)		
1221 (4)	1220 (2) P	1220 (2)
1209 (7)	1301 (6) P	1298 (5)
1321 (4)	1322 (2) D	1323 (5)
1410 (7)	1413 (6b) P	1394 (6)
1642 (9)	1645 (10) P	1643 (8)
2245 (-)	2257 (12b) P	2252 (8)
2668 (2)		
2814 ($\frac{1}{2}$)		
2919 (12)	2919 (12b) P	2920 (8)
		2938 (3)
2989 (8)	2990 (4) P	2987 (2)
3030 (8)	3030 (6) P	3027 (6)
3092 (3)	3094 (3) P	3094 (3)

representing the C-H stretching oscillation appears to be split up into two lines 2920 and 2938 cm^{-1} respectively and the intensity of the line 1322 cm^{-1} due to

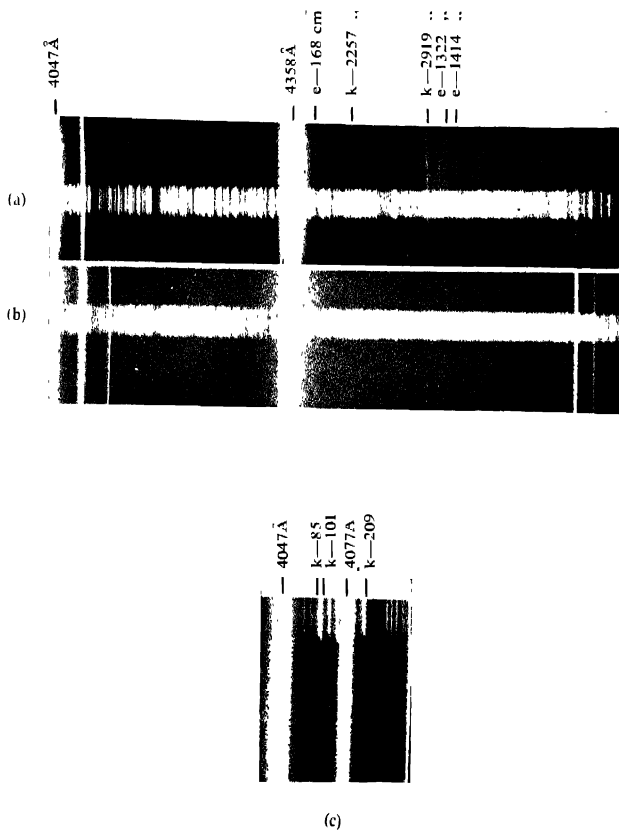


Fig 1. (a) Raman spectrum of allyl cyanide, liquid at 30°C
 (b) " " " " " " solid at -180°C
 (c) Low frequency Raman lines of allyl cyanide, solid at -180°C

C-H deformation oscillation increases while that of the line 1301 cm^{-1} remains unaffected when the compound is solidified and cooled to -180°C . All the results indicate that the molecules are associated through H-atoms and the C-N group when the liquid is solidified and cooled to -180°C . These results agree with those observed in the cases of other nitriles (Bishui, 1948, Deb, 1961).

ACKNOWLEDGMENT

The authors are highly indebted to Professor S. C. Sarkar, D.Sc., F.N.I., for his kind interest throughout the progress of the work.

REFERENCES

- Bishui, B. M., 1948, *Ind. J. Phys.*, **22**, 167.
Deb, K. K., 1960, *Ind. J. Phys.*, **34**, 247.
,, ,, 1961, *Ind. J. Phys.*, **35**, 16.
Kohlrausch, K. W. F. und Stockmayer, W., 1935, *Z. Physik, Chem.* Band **29B**, 297.
Mukherjee, D. K., 1960, *Ind. J. Phys.*, **44**, 402.

DEPENDENCE OF THE INTENSITY OF THE FIRST ORDER DIFFRACTION ON THE LENGTH OF THE SOUND FIELD

C RAGHUPATHI RAO

DEPARTMENT OF PHYSICS, NIZAM COLLEGE, OSMANIA UNIVERSITY, HYDERABAD-7

(Received November 13, 1961 ; Resubmitted November 3, 1962)

ABSTRACT. The dependence of the intensity of the first order diffraction on the length of the sound field at normal incidence of the light beam is studied and the positions of intensity maxima and minima are located with the help of a photo-tube. The positions of maxima are observed for the first time and agree fairly well with the values calculated from Raman and Nath's theory.

The nature of increase of $I_{\pm 1}$ with the length of the sound field at oblique incidence is found to be in good agreement with David's expression obtained from Brillouin's theory.

INTRODUCTION

Bir (1933) was the first to show the changes produced in the diffraction of light by a change of the length of the sound field. He produced photographs which clearly show that a variation of the length of the sound field produces a wandering of intensity similar to that observed by a change in the acoustical power of the crystal. Korff (1936) studied this phenomenon in air at a frequency of 4.28 Mc/s. Newmann (1939), using white light, studied the dependence of the total intensity of diffracted light on the length of the sound wave at 10 Mc/s, using the photo-cell for intensity measurements. Rao (1948) studied this phenomenon using the diffraction of light at 35 Mc/s and all the intensities were visually estimated by him. Except for these qualitative observations, no systematic quantitative intensity measurements were available in the literature on high frequency diffraction orders.

In this investigation, the intensity of the first order diffraction with the length of the sound field is quantitatively measured using an R.C.A. 931-A photo-multiplier tube and some of the interesting results obtained are presented here.

THEORY

All the existing theories of diffraction phenomenon clearly show that the length of the sound field forms an important parameter in all the intensity expressions obtained for diffraction orders. Nath (1938), using the generalised theory

of Raman and Nath with suitable modifications, obtained for I_{+1} , the intensity of the first order diffraction, the following expression

$$I_{+1} = \frac{4}{\rho^2 + 8} \sin^2 \left\{ \sqrt{\frac{\rho^2 + 8}{4}} \xi \right\} \quad \dots \quad (1)$$

where

$$\rho = \frac{\lambda^2}{\mu \mu_0 \lambda^{*2}} \text{ and } \xi = \frac{2\pi\mu L}{\lambda}$$

Thus the length of the sound field L enters in the parameter ' ξ ' showing that the effect of variation of the length of the sound field is analogous to the variation of μ , the maximum change in the refractive index of the liquid medium, which is proportional to the power input to the crystal. The above expression clearly shows that the intensity of the first order goes through successive maxima and minima periodically, the condition for the maximum intensity being

$$\sqrt{\frac{\rho^2 + 8}{4}} \xi = n \cdot \pi/2 \text{ where } n \text{ is any odd integer;}$$

which gives for the length of the sound field the expression

$$L = \sqrt{\left(\frac{\lambda}{\mu_0 \lambda^{*2}} \right)^2 + 8 \left(\frac{\mu}{\lambda} \right)^2} \cdot \frac{n}{2\pi} \quad \dots \quad (2)$$

The condition for minimum of zero intensity is given by $\sqrt{\frac{\rho^2 + 8}{4}} \xi = n\pi$ where n is any integer, which gives for the length of the sound field the expression

$$L = \sqrt{\left(\frac{\lambda}{\mu_0 \lambda^{*2}} \right)^2 + 8 \left(\frac{\mu}{\lambda} \right)^2} \cdot n \quad \dots \quad (3)$$

The expressions (2) and (3) are very important in that they give specific values to L for the intensity of the diffraction order to attain its maximum and minimum respectively. At high frequencies beyond 23 Mc/s, the second term in expressions 2 and 3 within the root becomes negligible when compared to the first. Its contribution is about 1.4% of the first at 23 Mc/s for water, and becomes still less at higher frequencies and for liquids of low ultrasonic velocity. As such, neglecting the second term, the expressions 2 and 3 can be simplified and written as

$$L = \frac{n \mu_0 \lambda^{*2}}{\lambda}, \text{ where } n \text{ is any odd integer} \quad \dots \quad (4)$$

and $L = 2n \cdot \frac{\mu_0 \lambda^{*2}}{\lambda}, \text{ where } n \text{ is any integer} \quad \dots \quad (5)$

respectively. These expressions (4) and (5) predict the intensity maximum and minimum of the diffraction order for definite lengths of the sound field. The same result has been obtained by Rytov (1936) and David (1937).

The intensity of the first order diffraction attains its maximum at regular intervals as given by expression (4) and passes through minima or becomes zero at regular intervals as given by expression (5), when the length of the crystal is gradually increased. These positions of maxima and minima of the diffraction order could easily be detected with the help of the photo-tube. The positions of maxima have not been so far observed by any of the investigators.

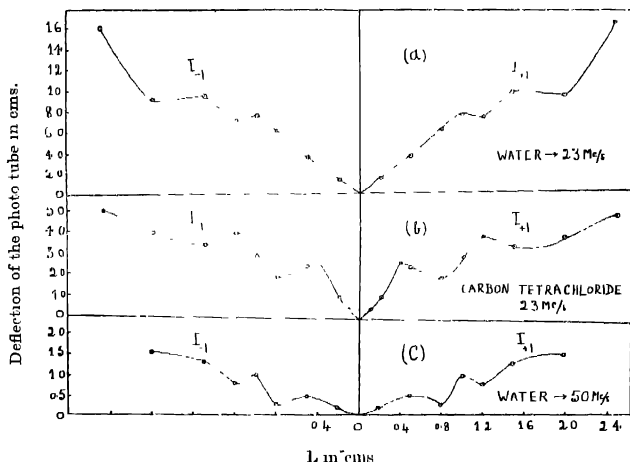


Fig. 1.—Intensity variation of $I_{\pm 1}$ at normal incidence with the length of the sound field.

EXPERIMENTAL RESULTS AND DISCUSSION

Intense first order diffraction lines are produced at 23.0 and 50.0 Mc/s and using the photo-tube, observations are made on the intensity of the first order diffraction at normal incidence of the light beam, varying the length of the sound field. A suitable choice of the liquid medium and the sound frequency facilitates observation of several intensity maxima and minima in a given length of the sound field as the parameter ' L ' depends upon the square of λ^* —the sound wave length in the medium. A one inch square X-cut quartz plate with a fundamental of 1.2 Mc/s is used to generate ultrasonics.

The positions of maxima and minima are located by the photo-tube using water as the seat of ultrasonics. These positions are regularly spaced and are closer at 50 Mc/s than at 23 Mc/s shown in Fig. 1(C and a). Fig. 1(b) shows the curve obtained by the photo-tube at 23 Mc/s in carbon-tetrachloride. The

positions of maxima and minima are closer in carbon-tetrachloride than the corresponding positions in water.

The experimentally located positions of maxima and minima agree fairly well with the theoretical values of ' L ' calculated from expressions (4) and (5) and show clearly their dependence on the square of λ^2 , the sound wave length in the medium.

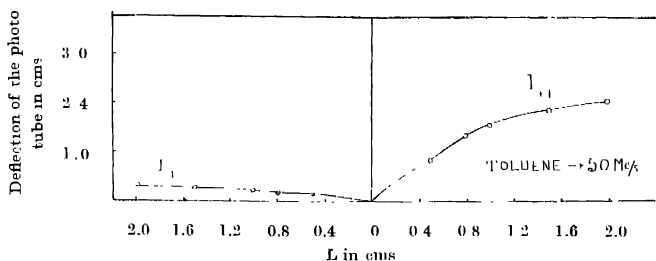


Fig 2—Intensity variation of $I_{\pm 1}$ at oblique incidence with the length of the sound field.

The behaviour of I_{+1} and I_{-1} with the length of the sound field in the oblique incidence position is shown in Fig. 2 for toluene at 50 Mc/s. The intensity of both the diffraction orders increases parabolically with L , though the increase of I_{+1} is far more rapid than that of I_{-1} . This experimental result is in good agreement with the David's expression for $I_m = (\pi\mu L)^2/\lambda^2$ showing that the maximum intensity of the first order diffraction depends upon the square of the length of the sound field.

In conclusion, my thanks are due to Prof S. Bhagavantam for his kind interest in this work.

REFERENCES

- Bar, R., 1933, *Helv. Phys. Acta.*, **6**, 570.
 David, E., 1937, *Physik. Zeitschr.*, **38**, 587.
 Karff, W., 1936, *Physik. Zeitschr.*, **37**, 708
 Nagendra Nath, N. S., 1938, *Proc. Ind. Acad. Sci.*, **8A**, 499
 Newmann, E. A., 1939, *Proc. Phys. Soc.*, **51**, 794
 Rao, B. R., 1948, Thesis presented to the Andhra University.
 Rytov, S., 1936, *C. R. Doklady*, **26**, 229.

BOOK REVIEW

PROBABILITY AND EXPERIMENTAL ERRORS IN SCIENCE—By Lyman G. Parratt. Pp. 255+ 1-xv John Wiley and Sons Inc., New York. 1961. Price \$7.25.

The author has indicated in the Preface that the book was specially intended for explaining the theory of probability to the undergraduate students but "the book is patterned to be a base from which the teacher may go on to discuss further aspects especially these aspects, that deepen and broaden the understanding of science".

After discussing the meaning of probability, the author discusses Classical *a priori* probability and Experimental *a posteriori* probability in the first chapter. Different formulae used for determining probability distributions have also been discussed in this chapter. The second chapter deals with Measurements in science. The methods of finding errors, significant figures, frequency distributions, precision indices, etc. have been discussed in this chapter. The next chapter deals with Statistics of measurements in functional relationships and includes discussions on maximum likelihood, propagation of errors, consistency tests, curve fitting, etc. Chapter 4 is devoted to Normal probability of errors and the fifth chapter deals with Poisson probability distribution. Numerous problems have been included at the end of each chapter.

The presentations of the topics are lucid and the illustrations included in the discussions are helpful. The book is useful not only to students who want to be introduced to the theory of probability but also to all research workers who are engaged in experimental investigations in physics.

S. C. S.

CONTENTS

Indian Journal of Physics

Vol. 37, No. 6

June, 1963

	PAGE
31. Thermal Expansion of some Alkali Fluorides and Magnesium Oxide by X-Ray Diffraction—P. D. Pathak, N. N. Pandya and M. P. Ghadiali ...	293
32. The Electronic Spectra of some Trisubstituted Benzenes in Different States. II—T. N. Misra ...	299
33. Electronic Telephone Switches with Transistors—P. N. Das ...	305
34. Correlation between Structural Energy and the Properties of the Naturally Radioactive Nuclei—A. K. Dutta and B. Pal ...	313
35. Dispersion of Ultrasonic wave in Diatomic Gases at low Pressure—K. Samal ...	331
36. On the Raman Spectrum of Allyl Cyanide in the Solid States—K. K. Deb and D. K. Mukherjee ...	339
37. Dependence of the Intensity of the first order Diffraction on the Length of the Sound field—C. Raghupathi Rao ...	342
BOOK REVIEW	346

Regd. No. G-3911

VOL. 37 **INDIAN JOURNAL OF PHYSICS** No. 7
(Published in collaboration with the Indian Physical Society)

AND

VOL. 46 **PROCEEDINGS** No. 7
OF THE
INDIAN ASSOCIATION FOR THE
CULTIVATION OF SCIENCE

JULY 1963

PUBLISHED BY THE
INDIAN ASSOCIATION FOR THE CULTIVATION OF SCIENCE
JADAVPUR, CALCUTTA 32

BOARD OF EDITORS

K. BANERJEE	D. S. KOTHARI
D. M. BOSE	S. K. MITRA
S. N. BOSE	B. D. NAG CHAUDHURI
S. D. CHATTERJEE	K. R. RAO
P. S. GILL	D. B. SINHA
S. R. KHASTGIR	S. C. SIKKAR (<i>Secretary</i>)
B. N. SRIVASTAVA	

EDITORIAL COLLABORATORS

PROF. R. K. ASUNDI, Ph.D., F.N.I.
PROF. D. BASU, Ph.D.
PROF. J. N. BHAR, D.Sc., F.N.I.
PROF. V. G. BHIDE, Ph.D.(Nag), Ph.D.(Lond).
PROF. A. BOSE, D.Sc., F.N.I.
PROF. S. K. CHAKRABARTY, D.Sc., F.N.I.
DR. J. S. CHATTERJEE
DR. K. DAS GUPTA, Ph.D.
PROF. N. N. DAS GUPTA, Ph.D., F.N.I.
DR. J. DHAR, D.Phil (So)
PROF. A. K. DUTTA, D.Sc., F.N.I.
PROF. C. S. GHOSH, M.Sc., S.M., F.N.I., M.I.E.E.
PROF. S. GHOSH, D.Sc., F.N.I.
PROF. S. N. GHOSH, D.Sc.
PROF. S. GUPTA, M.Sc., F.N.I.
PROF. D. N. KUNDU, Ph.D., F.N.I.
PROF. R. C. MAJUMDER, Ph.D., F.N.I.
PRINCIPAL Y. G. NAIK, Ph.D.
PROF. S. R. PALIT, D.Sc., F.R.I.C., F.N.I.
PROF. H. RAKSHIT, D.Sc., F.N.I.
PROF. A. SAHA, D.Sc., F.N.I.
DR. VIKRAM A. SARABHAI, M.A., Ph.D., F.N.I.
DR. A. K. SENGUPTA, D.Sc.
PROF. NAND LAL SINGH, D.Sc.
DR. M. S. SINHA, D.Sc., F.N.I.
PROF. N. R. TAYLOR, Ph.D., F.N.I.
DR. P. VENKATESWARLU

Annual Subscription—

Inland Rs. 25.00

Foreign £ 2-10-0 or \$ 7.00

NOTICE

TO INTENDING AUTHORS

Manuscripts for publication should be sent to the Assistant Editor, Indian Journal of Physics, Jadavpur, Calcutta-32.

The manuscripts submitted must be type-written with double space on thick foolscap paper with sufficient margin on the left and at the top. The original copy, and not the carbon copy, should be submitted. Each paper must contain an abstract at the beginning.

All references should be given in the text by quoting the surname of the author, followed by year of publication, e.g., (Ghosh, 1954). The full reference should be given in a list at the end, arranged alphabetically, as follows; Ghosh, D. K., 1954, *Ind. J. Phys.*, 28, 485.

Line diagrams should be drawn on white Bristol board or tracing paper with black India ink, and letters and numbers inside the diagrams should be written neatly in capital type with India ink. The size of the diagrams submitted and the lettering inside should be large enough so that it is legible after reduction to one-third the original size. A simple style of lettering such as gothic, with its uniform line width and no serifs should be used, e.g.,

A·B·E·F·G·M·P·T·W·

Photographs submitted for publication should be printed on glossy paper with somewhat more contrast than that desired in the reproduction, and should, if possible, be mounted on thick white paper.

Captions to all figures should be typed in a separate sheet and attached at the end of the paper.

The mathematical expressions should be written carefully by hand. Care should be taken to distinguish between capital and small letters and superscripts and subscripts. Repetition of a complex expression should be avoided by representing it by a symbol. Green letters and unusual symbols should be identified in the margin. Fractional exponents should be used instead of root

BENGAL CHEMICAL & PHARMACEUTICAL WORKS LD.

Pioneer Indian Manufacturers of Pharmaceuticals & Chemicals.

Manufacturers of:

Pharmaceutical Chemicals:

Caffeine and its salts, Strychnine Hydrochlor. Strychnine Sulphate, Brucine Sulphate, Nicotinic Acid, B.P., Nicotinamide, B.P., Potassium Citrate B.P., I.P., Sodium Citrate B.P., I.P., Potassium Acetate B.P., I.P., Potassium Iodide B.P., I.P., Sodium Iodide B.P., I.P., Ferri et Ammon Citrate B.P., I.P., and various other Pharmaceutical Chemicals.

Heavy & Reagent Quality Fine Chemicals:

Alum, Alum Sulphate (Iron Free), Ferro Alum, Zinc Chloride Tech. Naphthalene Pure, Sodium Citrate A.R., Potassium Citrate A.R., Magnesium Sulphate A.R., Sodium Sulphate Anhydrous A.R., Potassium Iodide A.R., Sodium Chloride A.R., Zinc Sulphate A.R., and various other reagent quality analytical chemicals.

Please refer your enquiries for the above items and other chemicals in the line to :—

BENGAL CHEMICAL

6, GANESH CHUNDER AVENUE,
CALCUTTA-13, INDIA.

NON-AQUEOUS TITRATION

A monograph on acid-base titrations in organic solvents

By

PROF. SANTI R. PALIT, D.Sc., F.R.I.C., F.N.I.

DR. MIHIR NATH DAS, D.Phil.

AND

MR. G. R. SOMAYAJULU, M.Sc.

This book is a comprehensive survey of the recently developed methods on acid-base titrations in non-aqueous solvents. Acid-base concept, as developed by Lowry-Brönsted and Lewis is succinctly presented in this slender volume. The subject is divided into two classes, viz. titration of weak bases and titration of weak acids. The method of 'glycolic titration' is described at a great length as also the method of 'acetous titration' including its recent modifications for the estimation of weak bases. Various methods for the titration of weak acids are duly described. A reference list of all pertinent publications is included in this book.

122 pages with 23 diagrams (1964)

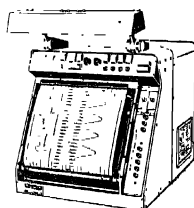
Inland Rs. 3 only. Foreign (including postage) \$ 1.00 or 5s.

Published by

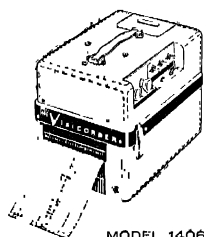
INDIAN ASSOCIATION FOR THE CULTIVATION OF SCIENCE
JADAVPUR, CALCUTTA-32, INDIA

HONEYWELL VISICORDER OSCILLOSCOPE

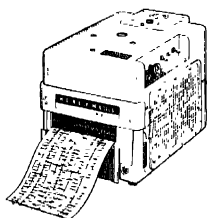
world's most versatile instrument
for the simultaneous recording of
a number of fast changing variables



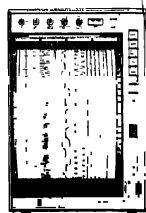
MODEL 1012



MODEL 1406

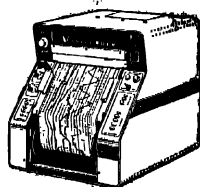


MODEL 906

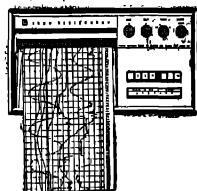


MODEL 1612

Available in several models, from 6 to 36 channels, DC to 5000 c/s response, over 50,000"/sec writing speed. The 36-channel 1012 & the 1612 are the most sophisticated instruments in the line. The 1108 is a highly capable 24-channel model. The 1508 is a compact 24-channel instrument that takes only 7" of vertical space in a relay rack and is also suitable for bench use. The 906 handles either 8 or 14 channels and the 1406 provides up to 6 channels at the lowest cost per channel.



MODEL 1108



MODEL 1508

Honeywell

Sold and serviced in India exclusively by

BLUE STAR

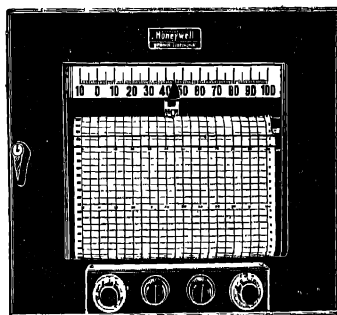
Get complete details from **BLUE STAR** offices at:

7 Hare Street, Calcutta 1
Sukh Sagar, Sandhurst Bridge, Bombay 7
1/23B Asaf Ali Road, New Delhi 1
23/24 Second Line Beach, Madras 1
1B Kaiser Bungalow, Dindli Road, Jamshedpur

It's a dozen test instruments in one!

—the Adjustable Span

Elektronik Recorder



HERE'S a recording potentiometer that is a real jack-of-all-trades (and master of each one) in any development or test laboratory. Just turn the dials, and in seconds, you can set it up for the exact range and sensitivity you want. You don't have to do any rewiring or changing of calibrating circuits.

50-to-1 span adjustment. Millivolt span of the recorder is continuously variable over as much as a 50:1 range. Span adjustment is independent of zero setting.

Variable zero suppression. Coarse and fine adjustment dials let you move the electrical zero point up and down scale, to concentrate recording on only the part of the span in which you're interested. Zero adjustment does *not* affect span setting.

Sensitivity adjustment makes it easy to get the recording characteristics you want to match the span being used.

Many optional features: you can choose from recording speeds of $\frac{1}{4}$, 1, 2, 4 $\frac{1}{2}$, 12 or 24 seconds full scale. . . fully automatic, push-button, or solenoid-actuated remote or locally controlled standardization.

Sold and serviced in India exclusively by

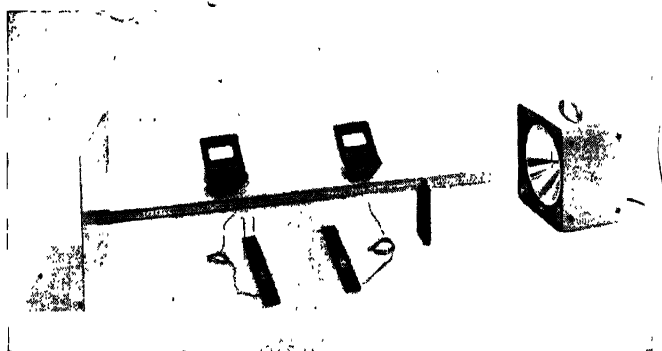
Honeywell

H First in Control

BLUE STAR

**BLUE STAR ENGINEERING
CO. (Calcutta) PRIVATE LTD.**
7 HARE STREET, CALCUTTA I
Also at BOMBAY • DELHI
MADRAS • JAMSHEDPUR

CENCO
MICROWAVE MEASURING EQUIPMENT



Model : 80422 with Model : 80423 probes and accessories

With the Microwave optics Equipment many striking demonstrations may be performed by exploring the radiation field with the receiver or a dipole antenna connected to an audio amplifier and a loud speaker. Reflection, standing waves refraction, polarization, and diffraction can be clearly shown on a scale measured in inches or centimeters and visible from a considerable distance. Many experiments that are difficult with visible light are easily performed in a lighted room before large groups of people.

For further details, please write to :

The Sole Distributors :

**THE SCIENTIFIC INSTRUMENT
COMPANY, LIMITED.**

**ALLAHABAD BOMBAY CALCUTTA MADRAS
NEW DELHI**

Head Office : 6, Tej Bahadur Sapru Road, Allahabad



FLOW OF A CONDUCTING FLUID PAST A ROTATING CONDUCTING CYLINDER

B. B. CHAKRABORTY

DEPARTMENT OF APPLIED MATHEMATICS, INDIAN INSTITUTE OF SCIENCE, BANGALORE-12

(Received April 3, 1962)

ABSTRACT The problem of finding the drag and torque on a cylinder immersed in an inviscid liquid and steadily rotating about its axis (z -axis) is discussed when both the liquid and the cylinder are conducting and the magnetic field and the streaming motion at infinity are uniform and parallel to the z -axis. The magnetic Reynolds number R_M is assumed small and the first order effect of the conductivity (R_M) is studied. Explicit expressions for the coefficients of drag and torque and the vorticity are obtained. It is found that the Maxwell stresses do not contribute to the drag coefficient, but make non-zero contribution to the torque. The variation of the vorticity on circles concentric to the circular section of the cylinder has been shown graphically when the radii of the circles are 1.05, 1.20, 1.40, 1.60 times the radius of the cylinder.

INTRODUCTION

The problem of estimating the effect of a uniform external magnetic field on a flow past a sphere or a body of revolution which at infinity, along with the magnetic field, is parallel to the axis of symmetry, has been discussed by Chester (1957, 1961) under various assumptions. Ludford and Murray (1960) have discussed the flow of an inviscid and finitely conducting liquid past a magnetized sphere for small values of the dimensionless parameter β representing the ratio of some standard magnetic pressure to the free stream dynamic pressure. Recently, Murray and Chi (1960) have considered the corresponding problem for the case of a magnetized cylinder placed in a uniformly streaming fluid whose direction at infinity is normal to the axis of the cylinder.

In the present note we have studied the flow characteristic of a conducting fluid past a conducting rotating cylinder under the assumption that the flow and magnetic field at infinity are uniform and normal to the axis of the cylinder. In particular, we have found expressions for the drag and torque coefficients of the cylinder and the distribution of vorticity in the case when the magnetic Reynolds number is small. We find that (i) the Maxwell stresses do not contribute to the drag though the perturbed pressure makes a non-zero contribution, (ii) the Maxwell stresses produce a torque proportional to the angular velocity Ω and tend to oppose the motion, (iii) the vorticity vanishes on the axis of symmetry drawn upstream and (iv) the conductivity of the rotating cylinder affects the flow characteristics.

The analysis is carried out allowing for the difference in the conductivities of the liquid and the cylinder, though the magnetic Reynolds number for the liquid and the cylinder have been assumed to be of the same order of magnitudes.

BASIC EQUATIONS

We consider the steady two dimensional flow of an incompressible inviscid and electrically conducting liquid. The basic equations in the usual notation are*

$$(\text{curl } \underline{q}) \times \underline{q} = -\text{grad } (p/\rho + \frac{1}{2}q^2) + \frac{\mu}{\rho} (\text{curl } \underline{H}) \times \underline{H}, \quad \dots (1)$$

$$\text{div } \underline{q} = 0, \quad \dots (2)$$

$$\underline{J} = \text{curl } \underline{H} = \sigma[\underline{E} + \mu \underline{q} \times \underline{H}], \quad \dots (3)$$

$$\text{curl } \underline{E} = 0, \quad \text{div } \underline{E} = 0 \quad \dots (4, 5)$$

$$\text{div } \underline{H} = 0. \quad \dots (6)$$

We shall take the axis of the cylinder as z -axis and the undisturbed direction of flow and the external magnetic field as the x -axis. We can neglect (5) from our discussion as it is identically satisfied in view of (3) and the fact that $\underline{q} \times \underline{H}$ is along the z -axis. From (4) and (5) we find that \underline{E} vanishes identically.

Using the radius a of the cylinder, the uniform velocity U at infinity and the magnitude h of the magnetic field at infinity as the standard quantities, the equations (1)-(6) reduce to the following dimensionless forms (retaining the same symbols for the dimensionless quantities as for the nondimensionless ones.)

$$(\text{curl } \underline{q}) \times \underline{q} = -\text{grad } P + \beta (\text{curl } \underline{H}) \times \underline{H}, \quad \dots (7)$$

$$\text{div } \underline{q} = 0 \quad \dots (8)$$

$$\text{curl } \underline{H} = R_M \underline{q} \times \underline{H}, \quad \text{div } \underline{H} = 0, \quad \dots (9, 10)$$

where

$$\beta = \frac{\mu h^2}{\rho U^2}, \quad P = p + \frac{1}{2}q^2, \quad R_M = \mu \sigma a U.$$

We shall assume that the magnetic permeabilities of the cylinder and the liquid are the same and equal to μ . When the liquid is non-conducting i.e. $R_M = 0$, the flow outside the cylinder is the familiar potential flow defined by

$$\underline{q}_0 = \left[\left(1 - \frac{1}{r^2} \right) \cos \theta, \quad - \left(1 + \frac{1}{r^2} \right) \sin \theta, \quad 0 \right] \quad \dots (11)$$

in the cylindrical coordinates (r, θ, z) .

*Throughout the paper m.k.s. system has been used.

When R_M is non-zero but small we expand p, q and H in powers of R_M :

$$\begin{aligned} p &= p_0 + R_M p_1 + R_M^2 p_2 + \dots, \\ q &= q_0 + R_M q_1 + R_M^2 q_2 + \dots, \\ H &= H_0 + R_M H_1 + R_M^2 H_2 + \dots, \end{aligned} \quad \dots \quad (12)$$

where H_0 is obviously the magnetic field at infinity.

SOLUTION OF THE FIRST ORDER PERTURBATION EQUATION

The first order perturbations p_1, q_1, H_1 are determined by the following equations .

$$(\text{curl } \underline{q}_1) \times \underline{q}_0 = -\text{grad } P_1 + \beta (\text{curl } \underline{H}_1) \times \underline{H}_0, \quad \dots \quad (13)$$

$$\text{div } \underline{q}_1 = 0, \quad \dots \quad (14)$$

$$\text{curl } \underline{H}_1 = q_0 \underline{H}_0; \quad \text{div } \underline{H}_1 = 0. \quad \dots \quad (15, 16)$$

The equations (15) and (16) also hold for inside the cylinder if we take $q_0 = (0, \Omega r, 0)$.

In view of (16) we take

$$\underline{H}_1 = \left(\frac{1}{r}, \quad \frac{\partial A}{\partial \theta}, \quad -\frac{\partial A}{\partial r}, \quad 0 \right). \quad \dots \quad (17)$$

and then (15) reduces to

$$\nabla^2 A = -H_0 \sin 2\theta \quad \dots \quad (18)$$

Since we have taken h as the standard magnetic field, $|H_0| = 1$ in dimensionless form. The solution of (18) which vanishes at infinity is given by

$$A = \sum_{m=1}^{\infty} r^{-m} (C_m \cos m\theta + D_m \sin m\theta) + \frac{H_0 \sin 2\theta}{4}. \quad \dots \quad (19)$$

Defining the magnetic vector potential inside the cylinder by $(0, 0, \bar{A})$, we have

$$\bar{A} = \sum_{m=1}^{\infty} r^m (A_m \cos m\theta + B_m \sin m\theta) + \frac{\Omega' H_0 r^3 \cos \theta}{8}, \quad \dots \quad (20)$$

where

$$\Omega' = \sigma' \Omega$$

σ' being the conductivity of the cylinder. Continuity of the normal and tangential components of the magnetic fields on the surface ($r = 1$) of the cylinder gives

$$\left. \begin{aligned} A_m = B_m = C_m = D_m = 0 \quad (m \neq 1, 2) \\ B_1 = D_1 = A_2 = C_2 = 0, \end{aligned} \right\} \quad \dots \quad (21)$$

and

$$\begin{aligned} A_1 = -\frac{\Omega' H_0}{4}, \quad C_1 = -\frac{\Omega' H_0}{8}, \\ B_2 = \frac{H_0}{8}, \quad D_2 = -\frac{H_0}{8} \end{aligned} \quad \dots \quad (22)$$

Thus

$$A = -\frac{\Omega' H_0 \cos \theta}{8r} + \frac{H_0 \sin 2\theta}{4} \left(1 - \frac{r^{-2}}{2} \right), \quad \dots \quad (23)$$

and

$$\bar{A} = -\frac{\Omega' H_0}{4} \left(r - \frac{r^3}{2} \right) \cos \theta + \frac{H_0 r^2 \sin^2 \theta}{8}, \quad \dots \quad (24)$$

The equations (23) and (24) determine the magnetic field completely.

CHARACTERIZATION OF THE FLOW

Taking the curl of (13) and using (14) we have

$$\left(1 - \frac{1}{r^2} \right) \cos \theta \frac{\partial \xi}{\partial r} - \frac{1}{r} \left(1 + \frac{1}{r^2} \right) \sin \theta \frac{\partial \xi}{\partial \theta} = -\frac{2H_0^2 \beta \sin 3\theta}{r^3} \quad \dots \quad (25)$$

where

$$\text{curl } \underline{q}_1 = \xi e_z, \quad \dots \quad (26)$$

is the vorticity vector.

For the potential flow ($R_M = 0$), the velocity potential ϕ_0 and the stream function ψ_0 are given by

$$\phi_0 = \left(r + \frac{1}{r} \right) \cos \theta, \quad \psi_0 = \left(r - \frac{1}{r} \right) \sin \theta. \quad \dots \quad (27)$$

In view of (27), (25) reduces to

$$q_0^2 \frac{\partial \xi}{\partial \phi_0} = -\frac{2H_0^2 \beta \sin 3\theta}{r^3}, \quad \dots \quad (28)$$

so that

$$\xi = -2H_0^2 \beta \int_{-\infty}^{\phi_0(P)} \frac{\sin 3\theta}{q_0^2 r^2} d\phi_0, \quad \dots \quad (29)$$

as the vorticity vanishes upstream as $r \rightarrow \infty$ and the integration is carried out along a stream line $\psi_0 = \text{constant}$ and $\phi_0(P)$ is the velocity potential at the point P .

Along a stream line $\psi_0 = \text{constant}$, we have from (27)

$$\left(1 + \frac{1}{r^2}\right) \sin \theta \, dr + \left(r - \frac{1}{r}\right) \cos \theta \, d\theta = 0.$$

Also

$$\begin{aligned} d\phi_0 &= \left(1 - \frac{1}{r^2}\right) \cos \theta \, dr - \left(r + \frac{1}{r}\right) \sin \theta \, d\theta \\ &\quad - \frac{rq_0^2 d\theta}{1 + \frac{1}{r^2}} \sin \theta \end{aligned} \quad (30)$$

along a streamline on using the last equation, hence from (29) we have

$$\xi = 2H_0^2 \beta \int_{\phi_0(P)}^{\phi_0(P)} \frac{\sin \alpha}{(1 + r^2) \sin \alpha} d\alpha \quad \dots \quad (31)$$

From (27) we obtain

$$\psi_0 = \pm \frac{\sqrt{\psi_0^2 + 4 \sin^2 \theta}}{2 \sin \theta} \quad \dots \quad (32)$$

If $0 < \theta < \pi$, ψ_0 is positive and we take the positive sign in (32). When $-\pi < \theta < 0$, the negative sign has to be taken in (32). Hence

$$\xi = 8H_0^2 \beta \int_{\theta = \pi}^{\theta} \frac{\sin \alpha \sin 3\alpha \, d\alpha}{[4 \sin^2 \alpha + \{\psi_0 + \sqrt{\psi_0^2 + 4 \sin^2 \alpha}\}^2]} \quad \dots \quad (33)$$

for a point on a streamline for which $y > 0$ and similarly for a point on a streamline for which $y < 0$

$$\xi = 8H_0^2 \beta \int_{\theta = -\pi}^{\theta} \frac{\sin \alpha \sin 3\alpha \, d\alpha}{[4 \sin^2 \alpha + \{\psi_0 - \sqrt{\psi_0^2 + 4 \sin^2 \alpha}\}^2]} \quad \dots \quad (34)$$

The boundedness of vorticity can easily be established from (33) and (34). From (33) we have

$$|\xi| \leq \frac{2H_0^2 \beta (\pi - \theta)}{\psi_0^2} \quad \dots \quad (35)$$

and from (34)

$$|\xi| \leq \frac{2H_0^2 \beta (\pi + \theta)}{\psi_0^2} \quad \dots \quad (35)$$

Putting $\psi_0 = 0$ in (33) and (34) and performing the integration we have

$$|\xi| \leq 6H_0^2\beta(\pi - \theta), \quad \text{when } y > 0, \quad \dots \quad (36)$$

and

$$|\xi| \leq 6H_0^2\beta(\pi + \theta), \quad \text{when } y < 0.$$

When ψ_0 is large,

$$\xi \simeq \frac{2H_0^2\beta}{\psi_0^2} \left[\frac{\sin 2\theta}{4} - \frac{\sin 4\theta}{8} \right]$$

Equations (33) and (34) show that at two points (r, θ) and $(r, -\theta)$, vorticity has same magnitude but opposite sign.

In terms of the elliptic integrals of the first and second kind, from (33) we have

$$\begin{aligned} \xi = H_0^2\beta \cdot & \left[(\theta - \pi + \sin 2\theta) - \psi_0 \left\{ \frac{2\psi_0}{k'} E(\pi/2, k) - \frac{\psi_0}{k'} \left(E(\psi, k) - \frac{k^2 \sin \psi \cos \psi}{\sqrt{1-k^2 \sin^2 \psi}} \right) \right. \right. \\ & \left. \left. + (3 + \psi_0^2) \left(-\frac{2k' F(\pi/2, k)}{\psi_0} + \frac{1}{\psi_0} [k' F(\psi, k)] \right) \right\} \right] \end{aligned} \quad (37)$$

for

$$0 \leq \theta \leq \pi/2 \quad \text{and}$$

$$\begin{aligned} \xi = H_0^2\beta \cdot & \left[(\theta - \pi + \sin 2\theta) - \psi_0 \left\{ \frac{\psi_0}{k'} E(\gamma, k) - \frac{\psi_0 k^2}{k'} \frac{\sin \psi \cos \psi}{\sqrt{1-k^2 \sin^2 \psi}} \right. \right. \\ & \left. \left. - (3 + \psi_0^2) \frac{k'}{\psi_0} F(\psi, k) \right\} \right] \end{aligned} \quad (38)$$

when

$$\pi/2 \leq \theta < \pi, \quad \text{and where}$$

$$n = \frac{2}{\psi_0}, \quad \sin \psi = \frac{\sqrt{1+n^2} \sin \theta}{\sqrt{1+n^2 \sin^2 \theta}}, \quad k^2 = \frac{4}{\psi_0^2 + 4}$$

and

$$k' = \sqrt{1-k^2}. \quad (39)$$

We plot in Fig. 1 the variation of ξ with θ for various values of r . We find that on a circle concentric with the cross-section of the cylinder the vorticity shows a considerable variation.

Since ξ is an odd function of θ we assume

$$\xi = \sum_{n=1}^{\infty} \xi_n(r) \sin n\theta. \quad \dots \quad (40)$$

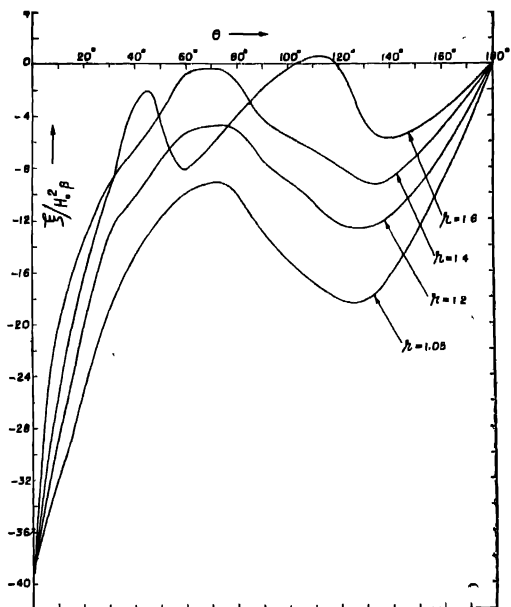


Fig. 1.

Substituting for ξ from (40) in (25) we get

$$\left(r - \frac{1}{r}\right) \frac{d\xi_{n+2}}{dr} + (n+2) \left(1 + \frac{1}{r^2}\right) \xi_{n+2} = - \left(r - \frac{1}{r}\right) \frac{d\xi_n}{dr} + n \left(1 + \frac{1}{r^2}\right) \xi_n, \quad (41)$$

when $n \neq 2$, and when $n = 2$, we have

$$\left(r - \frac{1}{r}\right) \frac{d\xi_4}{dr} + 4 \left(1 + \frac{1}{r^2}\right) \xi_4 = - \frac{4H_0^2\beta}{r^2}, \quad \dots (42)$$

as we can show that $\xi_2 = 0$.

On integrating (41) we have

$$\left(r - \frac{1}{r}\right)^{n+2} \xi_{n+2} = \int_1^r \left[- \left(r - \frac{1}{r}\right)^{n+2} \frac{d\xi_n}{dr} + n \left(r - \frac{1}{r}\right)^{n+1} \left\{1 + \frac{1}{r^2}\right\} \xi_n \right] dr \quad \dots (43)$$

Integrating (42) we get ξ_4 explicitly in terms of r :

$$\xi_4 = - \frac{H_0^2\beta(2r^6 + 3r^4 - 6r^2 + 1 - 12(\log r)r^4)}{(r^2 - 1)^4}, \quad \dots (44)$$

We can evaluate ξ_6, ξ_8, \dots similarly.

ξ_1 cannot be fixed up from this consideration, the recurrence relation (43) is of no use to evaluate $\xi_3, \xi_5, \dots, \xi_{2n+1}, \dots$. However, the odd Fourier coefficients of ξ in (40) can be computed numerically from the expression for ξ , given by equations (37) and (38). Table I gives the values of $\xi_1/8H_0^2\beta$ for $r = 1.05, 1.20, 1.40$ and 1.60 .

TABLE I

$\frac{\xi_1}{8H_0^2\beta}$	- 0.544	- 0.242
-----------------------------	---------	---------

The perturbed velocity q_1 is determined by the stream function ψ

$$q_1 = \left(\frac{1}{r} \frac{\partial \psi}{\partial \theta}, -\frac{\partial \psi}{\partial r}, 0 \right). \quad \dots (45)$$

where ψ is determined by

$$\frac{\partial^2 \psi}{\partial r^2} + \frac{1}{r} \frac{\partial \psi}{\partial r} + \frac{1}{r^2} \frac{\partial^2 \psi}{\partial \theta^2} = -\xi. \quad \dots (46)$$

Assuming
$$\psi = \sum_{n=1} \psi_n(r) \sin n\theta$$

we have

$$\frac{d^2 \psi_n}{dr^2} + \frac{1}{r} \frac{d\psi_n}{dr} - \frac{n^2}{r^2} \psi_n = -\xi_n. \quad \dots (47)$$

In evaluating the drag coefficient we shall require only $\psi_2(r)$. We note that $\xi_2 = 0$ and $\frac{\partial \psi}{\partial r}, \frac{\partial \psi}{\partial \theta}$ have to be regular at infinity. The only admissible solution of (47) when $n = 2$ is $\psi_2 = 0$.

When $n = 4$,

$$\begin{aligned} \psi_4 = Ar^{-4} + H_0^2\beta \left[-\frac{1}{8} - \frac{5}{4}r^{-2} - \frac{5}{4}r^{-6} + \dots \right. \\ \left. + (\log r)(r^{-2} - \frac{5}{2}r^{-4} - 6r^{-6} + \dots) + 3r^{-4}(\log r)^2 \right] \quad \dots (48) \end{aligned}$$

Since the normal component of velocity on the cylinder should vanish, we get $\psi_4 = 0$ at $r = 1$. This condition determines A . Similarly $\psi_6, \psi_8 \dots$ are determined.

DRAG AND TORQUE ON THE CYLINDER

The force on the cylinder is composed of two parts, one due to the fluid pressure and the other due to the Maxwell stresses. The θ -component of (13) gives, on integrating w.r.t. θ ,

$$P_1 = -\frac{\beta H_0^2 \cos 3\theta}{6} - \frac{\beta H_0^2 \cos \theta}{2} + a_0 \quad (49)$$

at $r = 1$ where a_0 is a constant.

But

$$P_1 = p_1 + q_0 \cdot \underline{q}_1 \quad (50)$$

and \underline{q}_0 on the cylinder is $(0, -2 \sin \theta, 0)$.

We have

$$q_{1\theta} = - \sum \frac{d\psi_n}{dr} \sin n\theta \quad (51)$$

for the θ -component of \underline{q}_1 . The drag coefficient, D_p , due to the pressure is given by

$$\begin{aligned} D_p &= -R \int_{\theta=0}^{\pi} p_1 \cos \theta \, d\theta \\ &= \frac{\pi H_0^2 R_M \beta}{2} \dots \end{aligned} \quad (52)$$

The drag and torque on the cylinder due to the Maxwell stresses $T_{ij} = \mu H_i H_j - \frac{1}{2} \mu H^2 \delta_{ij}$, which provides a force on the cylinder with components,

$$\mu \left\{ \frac{1}{2} (H_r^2 - H_\theta^2), H_r H_\theta, 0 \right\}$$

The drag on the cylinder is given in terms of the non-dimensional parameter

$$D = \mu R \int_0^{2\pi} \{ (H_{r0} H_{r1} - H_{\theta 0} H_{\theta 1}) \cos \theta - (H_{r0} H_{\theta 1} + H_{r1} H_{\theta 0}) \sin \theta \} d\theta = 0. \dots \quad (53)$$

In (53) H_{r0} , $H_{\theta 0}$ are the r - and θ -components of \underline{H}_0 and $R_M H_{r1}$ and $R_M H_{\theta 1}$ are the corresponding components of the perturbed magnetic field.

The Maxwell torque is given in terms of the dimensionless parameter T_m where

$$\begin{aligned} T_m &= \mu R_M \int_0^{2\pi} (H_{r0} H_{\theta 1} + H_{r1} H_{\theta 0}) d\theta \\ &= - \frac{\pi \mu \Omega' H_0^2 R_M}{4} \dots \end{aligned} \quad (54)$$

The negative sign shows that the torque tends to oppose the motion of the cylinder.

ACKNOWLEDGMENT

The author records with great pleasure his indebtedness to Prof. P. L. Bhatnagar for his kind guidance and help during the preparation of this paper.

REFERENCES

- Chester, W., 1957, *J. Fluid Mech.*, **3**, 304.
Chester, W., 1961, *J. Fluid Mech.*, **10**, 459.
Ludford, G. S. S. and Murry, J. D., 1960, *J. Fluid Mech*, **7**, 516.
Murray, J. D. and Lan-Kehchi, 1960, *Mathematika*, **7**, 64

E2-M1 MIXING IN THE 100 KEV TRANSITION IN Pr^{144}

R. BHATTACHARYYA AND S. SHASTRY

SARA INSTITUTE OF NUCLEAR PHYSICS, CALCUTTA

(Received November 30, 1962)

ABSTRACT. γ - γ directional angular correlation has been measured for the 34-100 keV cascade of Pr^{144} . The results show a pure 100 keV transition in a $0(2)2(1)1$ cascade decay from the 134 keV level.

INTRODUCTION

The level scheme of Pr^{144} has been studied by many authors (Nuclear Data Sheets). It can be seen from the work of Geiger *et al.* (1960) that all the γ -transitions are pure in character, except, perhaps, the 100 keV one. Geiger *et al.* pointed out that one can fit the internal conversion data with the theoretical values if an M1 admixture of 25% in the 100 keV E2 transition is assumed. Such an assumption demands a non-zero spin-value for the ground state of Pr^{144} . However, the zero spin assignment to the ground state has been established convincingly (Geiger *et al.* 1962). In the present work we have made a measurement on this possible multipole mixing, and hence, the spin of the states involved, by measuring the γ - γ directional angular correlation between the 34 and 100 keV γ -rays.

EXPERIMENT AND RESULTS

The experiment was carried out with a slow-fast coincidence assembly using two RCA 6810A photomultipliers coupled to two $1\frac{1}{2}$ " dia \times $1\frac{1}{2}$ " thick NaI(Tl) phosphors. The coincidence resolving time was 20 ns.

The source was obtained from the Radiochemical centre, Amersham, in the form of CeCl_3 in HCl solution. A small drop (~ 1 mm in diameter) of this evaporated on a thin mylar film (thickness ~ 1 mg/cm²) served as the source for this investigation. The source diameter being very small compared to the size and distance of the phosphors, no geometry correction due to finite size of the source was done.

For measuring the angular correlation of the 34-100 keV cascade, a narrow portion on the low energy half of the 34 keV peak was selected in one channel. The 100 keV peak was selected in the other channel by placing the pulse height analyser on the high energy side of the peak (100 keV peak has a measurable area under it in the coincidence spectrum). This reduced the contribution of the 80 keV γ -ray to a very small value. The distance of both the counters were kept at 7 cms from the source. Slow rate of coincidence did not permit recording of

data at more than four angles from 90° to 180° . The total time for recording these data and the random coincidence was over 50 hours.

The correlation function obtained by least square fit of the data (Rose, 1953) and then corrected for finite geometry of the detectors is given by

$W(\theta) = 1 - (0.226 \pm 0.030)P_2 \cos \theta + (0.018 \pm 0.030)P_4 \cos \theta$. Fig. 1 shows a plot of $W(\theta)$ against θ .

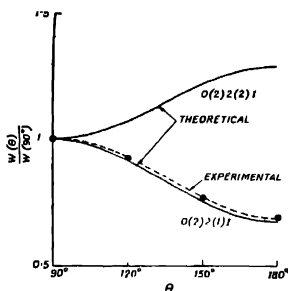


Fig. 1. The theoretical and experimental curves for angular correlation of the 34-100 keV cascade of Pr^{144} . The theoretical values of a_2 are -0.250 for a $0(2)2(2)1$ and -0.244 for $0(1)1(1)1$ and $0(1)1(2)1$ cascades. The value of a_4 is zero for all these cascades.

The theoretical $W(\theta)$ vs θ curves for a few cascades are also given in the same figure for comparison. The cascade that can be compared are $0(2)2(1)1$, $0(1)1(1)1$ and $0(1)1(2)1$, having very nearly the same theoretical values for a_2 . That the a_4 term in the experimental $W(\theta)$ does not contribute anything significantly, can be shown from the F -test as outlined in Klema's work. (Klema 1956, Goulden 1952). Different other cascades with assumed non-zero spins of the ground state were tried but only the above three could be fitted. This fact and the closeness of the theoretical and experimental curves of Fig. 1 excludes any multipole admixture in the 100 keV transition. Referring to Geiger *et al's* internal conversion data, 100 keV can now be accepted as pure E2. Since the angular correlation data show a maximum of 1% E2 admixture in the 34 keV M1 transition, one can conclude that $0(2)2(1)1$ is the only possible mode of decay for the 34-100 keV cascade.

ACKNOWLEDGEMENT

The authors are grateful to Prof. A. K. Saha and Dr. S. Chatterjee for their interest in the work.

REFERENCES

- Geiger, J. S., Graham R. L and Ewan G. T., 1960, 1. *Nuclear Physics* **16**,
 Goulden, C. H., 1952, *Methods of statistical Analysis*, 446.
 Klema, R. D., 1956, *Phys. Rev.* **102**, 449.
Nuclear Data sheets, National Academy of Sciences, National Research Council, Washing-
 ton D. C.
 Rose, M. E., 1953, *Phys. Rev.* **91**, 610.

COMPRESSIBILITIES, HYDRATION AND ACOUSTIC PROPERTIES OF AQUEOUS SOLUTIONS OF SOME METALLIC SULPHATES

M. SATYANARAYANA MURTY AND Bh KRISHNAMURTY

PHYSICS DEPARTMENT, ANDHRA UNIVERSITY, WALTAIR

(Received November 17 1962)

ABSTRACT Using a fixed path interferometer, ultrasonic velocities have been determined at a frequency of about 1.4 Mc/sec and hence adiabatic and apparent molar compressibilities, acoustic impedance, molar sound velocities and hydration numbers have been calculated in the case of aqueous solutions of sulphates of nine metals at a good number of concentrations upto 3 moles and at the temperature of 28°C. The velocity-variation with concentration, adiabatic compressibility-variation with concentration are found to show a dependence on the atomic weight and the radius of the metallic ion respectively. The apparent molar compressibility, the acoustic impedance and the molar sound velocity are found to vary linearly with square root of concentration, concentration and molar fraction of the solute respectively, and the gradients of the straight lines of these three properties are found to exhibit a general dependence on the molecular weight of the salt. The adiabatic compressibility variation with concentration is observed to be dependent inversely on hydration numbers.

INTRODUCTION

The study of the compressibilities and other related properties of aqueous solutions of salts has proved to be very useful in obtaining information regarding the state of affairs that obtain in a solution. A good amount of work has been recently done in this field by different workers (Subrahmanyam, *et al.* 1960). An examination of the literature on the subject reveals however that the work is not extensive and the results of the different authors are contradictory in certain aspects. As an example it is found that the nature of dependence of the ultrasonic velocities and compressibilities on concentration are ascribed to different factors like the atomic weight of the metallic ion, the ionic radius of the metallic ion, molecular weight of the salt, ionic strength etc. Such an ambiguity is probably because certain salts show dependence of their velocity or compressibility variation on atomic weight of the metallic ion and certain other salts on the ionic radius or on the molecular weight of the salt.

The present paper reports results in ultrasonic velocity, the molar sound velocity, the adiabatic and apparent molar compressibilities and the acoustic impedance in aqueous solutions of 9 metallic sulphates, and the different properties

have been discussed in regard to their variation with concentration as dependent on one or the other of the factors suggested above.

EXPERIMENTAL

A fixed path interferometer (Rao and Rao, 1957) working at a frequency of 1.4 Mc/sec has been employed for the determination of ultrasonic velocities. Though this method involves the velocity determination by altering the frequency of the ultrasonic wave around 1.4 Mc/sec. (which is the fundamental frequency of the crystal) the possibility of dispersion can be ignored in view of the very little changes in the frequency of the order of 0.3 Mc/sec. The other related properties are calculated from the velocities by means of the following relations :

$$\beta = \frac{1}{v^2 \rho} \quad \dots (1)$$

Where β is the adiabatic compressibility v is the velocity and ρ the density of the solution.

$$\phi = \frac{1000\beta}{C} - \frac{\beta_1}{\rho_1} \left[\frac{1000\rho}{C} - M_2 \right] \quad \dots (2)$$

ϕ is the apparent molar compressibility

where β and ρ are the compressibility and density of the solution at the concentration C and β_1 and ρ_1 are those of the pure solvent and M_2 the molecular weight of the solute.

$$Z = P v \quad \dots (3)$$

where Z is the specific acoustic impedance.

$$R = \frac{\bar{M}}{\rho} v^{1/3} \quad \dots (4)$$

where R is the molar sound velocity, \bar{M} is average molecular weight calculated from the relation,

$$\bar{M} = \frac{n_1 M_1 + n_2 M_2}{n_1 + n_2}$$

where n_1 is the number of gram moles of the solute, M_1 molecular weight of the solute, n_2 the number of gram moles of the solvent, M_2 molecular weight of the solvent.

$$\lim_{C \rightarrow 0} \phi = -\beta_1 V_n \quad \dots (5)$$

where V_n is the volume of primary water of hydration for mole of the electrolyte. The limiting value of ϕ is obtained by extrapolating ϕ versus \sqrt{C} graph to zero concentration. V_n is then divided by molar volume of the solvent molecules in the primary hydration sheath which gives primary hydration number.

RESULTS AND DISCUSSIONS

Ultrasonic velocity: For all salts chosen in this study the ultrasonic velocity is found to increase with increasing concentration, relatively slower at lower concentrations, say, up to 0.5 mole, and more rapidly beyond that concentration. The curves indicate that the variation approximates to being linear between 0.5 and 2 or 2.5 moles. The gradients of the approximately straight portions of the velocity curves are calculated. It is rather interesting to find that in the case of six sulphates of the metals, lithium, magnesium, iron (ic), nickel, cobalt and cadmium out of the nine taken up the gradients are found to decrease with increasing atomic weight of the metallic ion. Since the sulphate ion is common for all these salts, the decrease in the gradients (the gradient indicating the rate of variation of velocity with concentration) must reasonably be attributed to the increase in the atomic weights of the metallic ions. A logical extension of this idea means that for salts with metallic ions of higher and higher atomic weights,

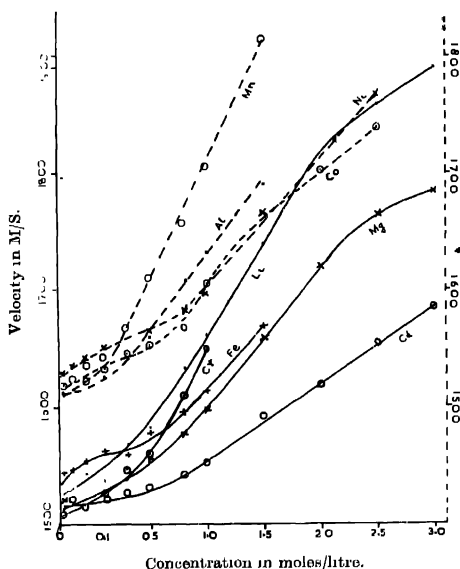


Fig. 1. Variation of ultrasonic velocity with concentration.

the rate of variation of velocity goes on decreasing and for salts with heavy metallic ions the velocity may decrease with increasing concentration. This expectation is corroborated by the results in certain heavy metallic salts reported earlier by the authors, wherein it was shown that in the case of six heavy metallic salts the velocity decreased with concentration.

Adiabatic compressibility : The adiabatic compressibility has decreased with concentration for all salts. Between 0.1 and 2 moles the rate of variation approximates to being linear the gradient being very nearly the same for a majority of the salts worked. When an attempt is made to study the dependence of the variation of β with concentration on the ionic radius of the metallic ion it is found that in the case of the salts of the metals manganese, chromium, iron(II), nickel, cobalt, cadmium which are in the order of increasing ionic radius of the metal

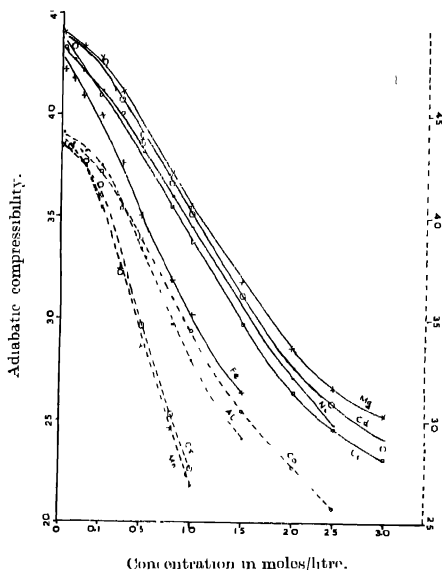


Fig. 2. Variation of adiabatic compressibilities with concentration

ion, the β concentration curves are displaced up, which means that at corresponding concentrations the β values increase for salts with metallic ions of increasing radius. This contradicts the findings of an earlier author (Marks, 1959) where in the reverse dependence was reported. But as his result has been confined to quite a few salts the correctness of the result is open to question.

Apparent molar compressibility :—The apparent molar compressibility ϕ is found to increase linearly with \sqrt{C} only at higher concentrations, say, beyond 0.5 mole and not at the lower concentrations. This result is in conformity with similar findings of the authors (Satyanarayanamurty and Krishnamurty, 1962) in the case of nitrate solutions. An attempt is made to study the dependence of the gradients of the ϕ to \sqrt{C} straight lines on the molecular weights of the salts. A similar study was done in the case of the salts of the nitrates as reported in an earlier publication (Satyanarayanamurty and Krishnamurty, 1962) wherein

a general, though not exactly linear, dependence between the gradients of ϕ to \sqrt{C} straight lines and molecular weights was found in the case of 10 salts. The molecular weights of the salts of the present investigation and their respective gradients are also found to exhibit the general dependence.

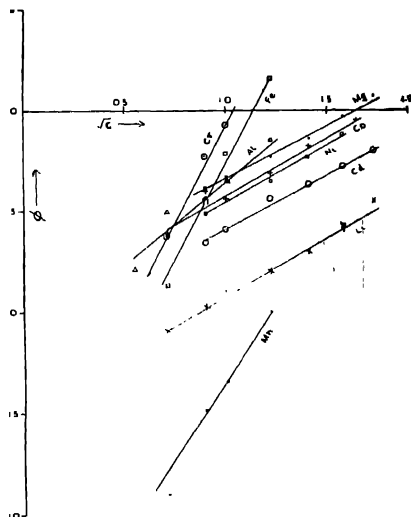


Fig. 3 Variation of " ϕ " with " \sqrt{C} "

Acoustic impedance The acoustic impedance Z depends linearly on the concentration for all the salts taken up here as can be seen from Fig. 4. This confirms Marks findings in the case of some salt solutions. It is also interesting to observe the gradients of the $Z-C$ straight lines show an increase with increasing molecular weight for five salts namely those of Li, Cd, Al, iron(ic) and Cr. Also in the case of other salts of the present investigation there is a general dependence between the two, as for instance, the values of the gradients are almost the same for salts of Cd, Ni and Co whose molecular weights are also almost the same.

However according to equation proposed by Prakash and Srivastava (1958), $(\rho/\beta)^{1/4}$ that is Z^4 , is expected to be linearly dependent on the ionic strength μ and the gradients for various salts have to be the same. But when we have plotted \sqrt{Z} versus μ (Fig. 5) for the salts of the present study, it can be seen that only at lower ionic strengths the relation can be called as being reasonably linear. Also the gradients are found to be by no means the same for all salts.

Molar sound velocity R . As can be seen from Figs. 6 and 7 the molar sound velocity R is found to vary linearly with the molar fraction of the solute

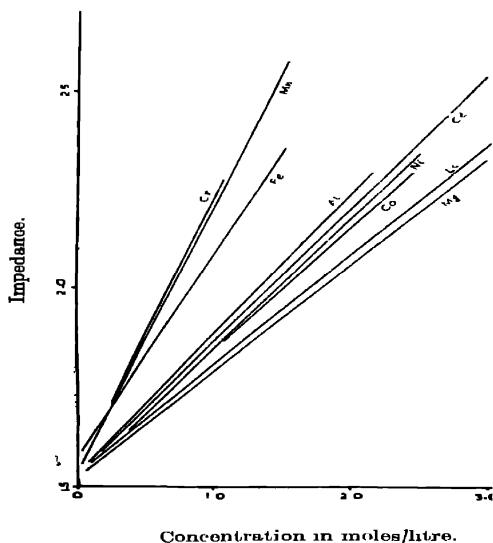


Fig. 4. Variation of acoustic impedance with concentration.

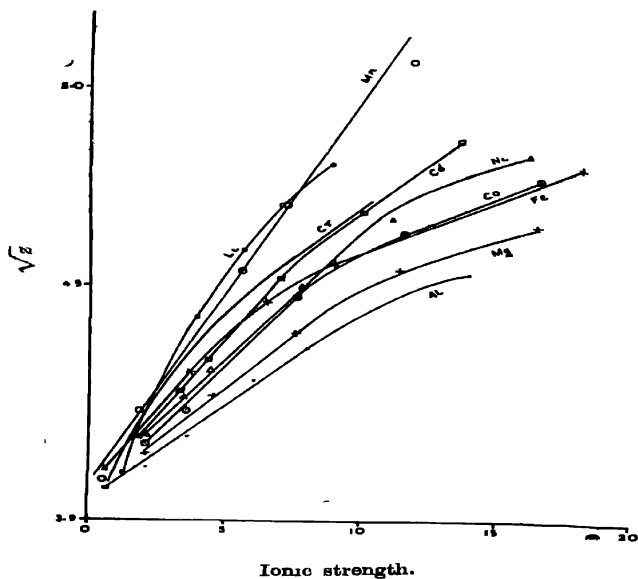


Fig. 5. Variation of " \sqrt{z} " with ionic strength.

as is already suggested by earlier authors (Padmini and Rao, 1960). The gradients of these straight lines (see Table 1) are found to show a general dependence on

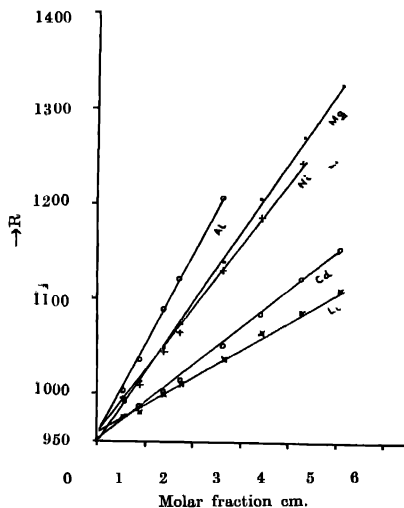


Fig. 6. Variation of molar sound velocity with molar fraction.

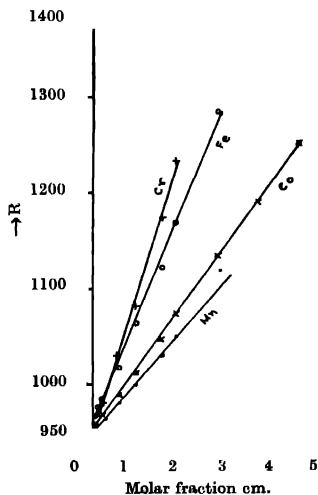


Fig. 7. Variation of molar sound velocity with molar fraction.

TABLE I

Salt sulphate	Molecular weight	Atomic weight of the metallic ion	Radius of the metallic ion	Gradient of V versus C graph	Gradients $\phi - \sqrt{C}$ graph	Gradients of Z-C lines $\times 10^3$	Gradient of cm - R lines	ϕ C-0	Hydation numbers
1. Lithium Li ₂ SO ₄ H ₂ O.	127.96	6.94	0.6	166.6	5.8	27.65	29.36	-15	18.68
2. Magnesium MgSO ₄ . 7H ₂ O.	246.5	24.32	0.65	112.7	5.16	26.83	73.98	-8.5	10.59
3. Cadmium Cd SO ₄ . 7H ₂ O	280.59	112.41	0.97	65.43	5.4	33.43	39.70	-11.3	14.08
4. Nickel NiSO ₄ . 7H ₂ O	280.71	58.71	0.69	108	5.72	32.87	66.01	-10.2	12.71
5. Cobalt CoSO ₄ . 7H ₂ O.	281	58.94	0.72	80	5.8	31.18	69.13	-10	12.46
6. Aluminium Al ₂ (SO ₄) ₃	342.2	26.98	0.54	105.9	8.4	35.16	95.66	-11.8	14.70
7. Manganic Mn ₂ (SO ₄) ₃ .	398.1	54.93	0.51	204	15.67	66.94	8.06	-29	36.13
8. Ferric Fe ₂ (SO ₄) ₃ 9H ₂ O.	562	55.85	0.67	106	18.20	50.94	93.42	-21	26.16
9. Chromium Cr ₃ (SO ₄) ₃ . 18H ₂ O.	716.5	52.01	0.65	175	18.75	68.95	157.40	-19.6	24.42

the molecular weight of the salt by way of increasing for salts with increasing molecular weights. It can be seen that the gradients and the molecular weights increase for the salts of Li, Cd Ni, Co, Fe, Cr.

It has been so far pointed out that the variation of the apparent molar compressibility, acoustic impedance, and the molar sound velocity with concentration shows a general but definite dependence on the molecular weight of the salt. The authors therefore suggest that the important properties of an aqueous solution dependent to a larger extent on the molecular weight of the solute rather than other factors like weight, radius and valence of the cation.

Hydration numbers : A few earlier workers have commented on the effect of hydration on β . One suggestion was that the dependence of variation of β with concentration on cationic radius is influenced by hydration. In the present case, it is found that for salts with decreasing hydration numbers the corresponding β - c curves are displaced up. It happens in the case of the salts of Mn, Fe, Al, Ni, Co, Mg. This means that at any chosen concentration the β depends inversely on hydration number.

It has already been noted that the β - c curves are displaced up for salts of metals with increasing cationic radius. This result coupled with the inverse dependence β - c variation and hydration numbers implies that as the cationic radius increases the hydration number of the salt decreases. This corroborated by the fact (Suryanarayana, 1962) that in the case of monovalent ions that the hydration numbers decrease in the order of $\text{Li} > \text{Na} > \text{K} > \text{Rb} > \text{Cs}$, and in the case of divalent cations in the order $\text{Mg}^{++} > \text{Ca}^{++} > \text{Sr}^{++} > \text{Ba}^{++}$, in both the cases the metals being put in the order of their increasing ionic radius.

ACKNOWLEDGMENT

The authors express their grateful thanks to the C.S.I.R. for giving financial assistance for this work in the form of a scheme.

REFERENCES

- Herbert S. Harnad and Beuton B. Owen 1950, "The Physical Chemistry of Electronic solutions," Reinhold Publishing Corporation.
Krishnamurty Bh. 1951, *J. Sci. Ind. Res.* **10B**, 149.
Marks, G. W., 1959, *Jour. Acous. Soc., America*, **31**, 936.
Padmini, P. R. K. L. and Rao B. R., 1960, *Ind. Jour. Phys.*, **43**, 565.
Prakash, S. and Srivastava, S. C., 1962, *Ind. Jour. Phys.*, **32**, 62.
Rao, K. S. and Rao B. R., 1957, *J. Sci. Ind. Res.*, **16B**, 483.
Satyanarayana Murty, M. Krishnamurty, Bh. 1958, *J. Sci. Ind. Res.* **17B**, 216.
M. Satyanarayanamurty, and Bh. Krishnamurty. 1962, *Jour. Sci. Ind. Res.* **21B**, 590.
-do- (in press).
Subrahmanyam S. V. and Bhimasenachar 1960, *J. Acous Soc America*, **32**, 835.
Suryanarayana, M. 1962, *J. Sci. Ind. Res.* **17B**, 57

NEW BAND SYSTEMS OF Ag_2 MOLECULE IN THE FAR ULTRA-VIOLET REGION

R. C. MAHESHWARI*

PHYSICS DEPARTMENT, ALLAHABAD UNIVERSITY, ALLAHABAD

(Received, November 5, 1962)

Plate VI

ABSTRACT. The absorption spectrum of silver vapours reveals the existence of two new band systems in the regions (i) $\lambda\lambda 2690-2630$ and (ii) $\lambda\lambda 2550-2460$. All these bands are degraded to longer wavelength side. They have been analysed and designated as *C* and *D* systems respectively. The band-heads of these systems can be represented fairly well by the following equations.

C ← — *X* system

$$\begin{aligned} \nu &= 37631.8 + 170.6(v' + \frac{1}{2}) - 0.60(v' + \frac{1}{2})^2 \\ &\quad - 192.2(v'' + \frac{1}{2}) + 0.62(v'' + \frac{1}{2})^2 \end{aligned}$$

D ← — *X* system

$$\begin{aligned} \nu &= 40163.4 + 141.0(v' + \frac{1}{2}) - 0.01(v' + \frac{1}{2})^2 \\ &\quad - 192.2(v'' + \frac{1}{2}) + 0.62(v'' + \frac{1}{2})^2 \end{aligned}$$

INTRODUCTION

A study of the band spectra of diatomic molecules of IB group of elements has been the subject of numerous investigations in recent years. It was Ruamps (1954) who first studied the spectra of these elements in emission from the King's Furnace. The molecules which he actually studied were Cu_2 , Ag_2 , Au_2 and CuAu . Later, Kleman and Lindkvist (1955) observed and analysed the spectra of Cu_2 , Ag_2 and Au_2 molecules appearing in the visible region. They could also resolve the isotope shift which confirmed the identity of the emitters. In view of the fact that these investigations were made in thermal emission, the lower states involved in these transitions were identified as the ground states of these molecules. The spectroscopic constants of these molecules do not show much regularity.

Because self-reversal was only observed in the emission spectrum of Ag_2 , the same was photographed in absorption also. Its spectrum consists of red degraded bands stretching from 5200 to 4000-Å, which have been grouped into

* Now at Department of Chemical Physics, University of Copenhagen, Copenhagen, Denmark.

one system (A—X) by Kleman and Lindkvist. Recent studies by Joshi (1958) on the absorption spectrum of Ag₂ molecule have revealed the existence of a new band system in the region $\lambda\lambda 2940-2750$. All the bands of this system (B—X) are degraded to longer wavelength side.

In the course of investigations on the molecular spectra of AgTe and AgSe, the author photographed the absorption spectrum of silver vapours heated to 1800°C. The following results have been obtained.

(a) The band system between 5200-4000 Å analysed by Kleman and Lindkvist.

(b) A band system between 2940-2750 Å observed and analysed by Joshi.

(c) Two new systems of red degraded bands one between 2690-2630 Å and the other between 2550-2460 Å. The present paper reports the vibrational analysis of these two new systems attributed to Ag₂ molecule.

EXPERIMENTAL

The procedure followed in obtaining the present spectra is the same as in previous studies of AgTe and AgSe molecules. A small quantity of spec. pure silver metal was vapourised in the graphite tube 14 cm long and .5 cm in internal diameter. After evacuation the furnace chamber was filled with nitrogen at a pressure of about 55 cm Hg. Observations were made at different temperatures ranging from 1400°C to 2000°C. It was found that the bands developed best at about 1800°C. The temperature was measured with the help of an optical pyrometer.

A quartz hydrogen discharge lamp manufactured by Thermal Syndicate Ltd., England was used as the source of ultraviolet continuum. Copper arc served as the comparison spectrum. Exposures ranging from 10 to 20 minutes were found sufficient to record the spectrum on Kodak 103-0 spectroscopic plates, using a Hilger large quartz spectrograph, which has an average reciprocal dispersion of about 3 Å nm^{-1} in the region studied.

It would be worthwhile to mention here that these new bands and also those reported by previous workers i.e. A—X and B—X systems, appeared unfailingly when any of the silver halides (AgCl, AgBr and AgI) was heated in the furnace. No silver halide is known to have spectrum in the region where these new bands occur. Also these bands together with $A \longleftrightarrow X$ and $B \longleftrightarrow X$ system of Ag₂ made their appearance when only spect.-pure silver metal was heated to 1800°C. Further the experiments were performed in vacuum i.e. without filling the furnace chamber with nitrogen gas, even then these bands could be photographed. The only difference marked was the diminution in the intensity of the bands. This was due to the rapid effusion of the silver vapours from the open ends of the absorption tube.

RESULTS

The bands obtained in the present investigation occur in two different regions of the spectrum i.e. (i) $\lambda\lambda$ 2690—2630 and (ii) $\lambda\lambda$ 2550—2460. These are designated here as C and D systems respectively. Reproduction of their spectra are shown in Fig. I (Plate) (a) and (b).

C←—X system ($\lambda\lambda$ 2690—2630)

The bands belonging to this system are narrow and all are degraded to longer wavelength side. The intensity is concentrated in $\Delta v = 0$ sequence, falling off rapidly towards $+1$ and -1 sequences. Quantum numbers have been allocated by a study of intensity distribution. The most intense band at $\nu = 37621 \text{ cm}^{-1}$ has been taken as $(0, 0)$ band. To a fair degree of accuracy the wavenumbers of the band-heads of this system can be represented by the following formula.

$$\begin{aligned} \nu = 37631.8 + 170.6(v' + \tfrac{1}{2}) - 0.60(v' + \tfrac{1}{2})^2 \\ - 192.2(v'' + \tfrac{1}{2}) + 0.62(v'' + \tfrac{1}{2})^2 \quad \dots \quad (1) \end{aligned}$$

Besides the classified heads, about five line-like heads remain unclassified in the $\Delta v = 0$ sequence. It is assumed that the band-heads which can be represented by the above formula are Q heads and the unclassified bands which belong to the same system are R heads. However, this assignment is tentative on account of the fact that separations between the Q and R heads cannot be calculated accurately, since these values of rotational constants are not available for this or related molecules.

The measured wavelengths, visual estimates of their intensities on a scale of 10, wavenumbers both observed and calculated and assigned values of the quantum numbers are included in Table I. Table II gives the vibrational scheme suggested for these bands. Table III gives their intensity distribution in the system. In view of the nearly equal values of the upper and ground state vibrational frequencies, the intensity distribution is compatible with the Franck Condon Principle.

D←—X system ($\lambda\lambda$ 2550—2460)

The bands of this system are weak in intensity as compared to the bands of C←—X system. They resemble in appearance to the B system observed by Joshi and to the A system of Kleman. The following equation was found to represent all the observed bands of this system fairly well.

$$\begin{aligned} \nu = 40163.4 + 141.0(v' + \tfrac{1}{2}) - 0.01(v' + \tfrac{1}{2})^2 \\ - 192.2(v'' + \tfrac{1}{2}) + 0.62(v'' + \tfrac{1}{2})^2 \quad \dots \quad (2) \end{aligned}$$

Band-head data, Deslandres scheme and intensity distribution is given in Tables IV, V and VI respectively.

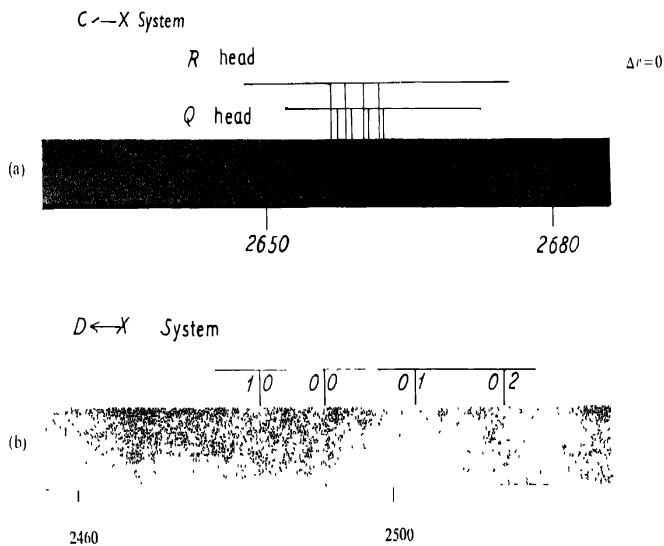


Fig 1 Absorption spectra of Ag_2 molecule

TABLE I

Band head data for the C←—X system of Ag₂ molecule³

λ air Å	Intensity	ν_{obs} (cm ⁻¹)		Analysis (ν' , ν'')
		obs.	calc	
2675.3	1	37368	37369	3, 4 Q
2673.7	1	37390	37389	2, 3 Q
2672.3	2	37410	37410	1, 2 Q
2670.8	4	37430	37430	0, 1 Q
2668.3	5	37465	37471	7, 7 Q
2666.8	5	37487	37492	6, 6 Q
2665.1	6	37511	37514	5, 5 Q
2663.5	7	37533	37535	4, 4 Q
2663.2	4	37537		4, 4 R
2661.9	7	37556	37556	3, 3 Q
2661.5	5	37561		3, 3 R
2660.2	8	37579	37578	2, 2 Q
2659.8	6	37585		2, 2 R
2658.7	9	37601	37599	1, 1 Q
2658.2	8	37608		1, 1 R
2657.3	10	37621	37621	0, 0 Q
2656.7	8	37629		0, 0 R
2653.5	3	37674	37677	6, 5 Q
2651.9	3	37697	37700	5, 4 Q
2650.2	2	37721	37722	4, 3 Q
2648.6	1	37744	37745	3, 2 Q
2646.9	1	37769	37768	2, 1 Q
2645.3	1	37791	37790	1, 0 Q

TABLE II

Deslandres arrangement for the C←—X system of Ag₂ molecule

$v' \ v''$	0	1	2	3	4	5	6	7	8
0	37621	37430							
1	37791	37601	37410						
2		37769	37579	37390					
3			37744	37556	37368				
4				37721	37533				
5					37697	37511			
6						37674	37487		
7								37465	

TABLE III

Intensity distribution for the C←—X system of Ag₂ molecule

$v' \ v''$	0	1	2	3	4	5	6	7	8
0	10	4							
1	1	9	2						
2		1	8	1					
3			1	7	1				
4				2	7				
5					3	6			
6						3	5		
7								5	

TABLE IV

Band head data for the D←—X system of Ag₂ molecule

λ air Å	Intensity	ν vac. (cm. ⁻¹)		Analysis (v', v'')
		obs.	calc.	
2520.6	1	39661	39663	2, 4
2517.8	1	39705	39710	1, 3
2514.5	2	39757	39757	0, 2
2511.6	2	39803	39804	3, 4
2508.6	3	39850	39851	2, 3
2505.6	4	39898	39898	1, 2
2502.6	5	39946	39947	0, 1
2496.8	2	40039	40039	2, 2
2493.7	4	40088	40088	1, 1
2490.6	6	40138	40138	0, 0
2488.1	5	40179	40180	3, 2
2485.0	6	40229	40229	2, 1
2481.9	4	40279	40279	1, 0
2476.4	2	40369	40370	3, 1

TABLE V

Deslandres arrangement for the $\text{D} \leftarrow \text{X}$ system of Ag_2 molecule

v' v''	0	1	2	3	4
0	40138	39946	39757		
1	40279	40088	39898	39705	
2		40229	40039	39850	39661
3		40360	40179		39803

TABLE VI

Intensity distribution for the $\text{D} \leftarrow \text{X}$ system of Ag_2 molecule

v' v''	0	1	2	3	4
0	6	5	2		
1	4	4	4	1	
2		6	2	3	1
3		2	5		2

DISCUSSION

The observations made and the facts recorded thereto under the experimental section indicate that these bands are due to silver.

The vibrational analysis of these bands grouped into two different systems i.e. $\text{C} \leftarrow \text{X}$ and $\text{D} \leftarrow \text{X}$ gives the ground state vibrational frequency 192.2 cm^{-1} , which has already been established as the ground state vib. frequency for the Ag_2 molecule by the studies of Kleeman ($\text{A} \rightarrow \rightarrow \text{X}$ system) and of Joshi ($\text{B} \leftarrow \text{X}$ system). Further these new bands should not be confused with a nitride, a hydride, a carbide and an oxide of silver. In all such cases the molecules are comparatively too light and, therefore, cannot have ground state vib. frequency of the order of 190 cm^{-1} . Thus it is fairly conclusive that these bands are due to diatomic silver molecule. The possibility of formations of polyatomic molecule can be ruled out, in view of the simplicity of the structure of the bands and also the temperature at which they appear. The possibility that these bands may form part of the known systems can safely be ruled out in view of the facts that (a) They occur in different region. (b) They do not fit in the formula suggested for $\text{B} \leftarrow \text{X}$ or $\text{A} \leftarrow \rightarrow \text{X}$ systems and (c) They form well defined sequences and progressions of which the (0, 0) band could easily be recognised.

The confirmation with a study of isotope effect could not be carried out on account of the insufficient resolving power of the spectrograph. Of course, the heads of the bands which are away from the system origin are not so sharp. That

is why there is a slight disagreement between the observed and calculated position for these bands. The reason for the lack of sharpness of these bands can be the presence of isotopic heads. (As for these bands, the isotopic shift will be comparatively large.)

From the photograph of the $C \leftarrow X$ system (Plate VI) it is clear that the (0, 0), (1, 1), (2, 2), (3, 3) and (4, 4) bands are accompanied with a line like band on the shorter wavelength side, which do not fit in the formula and have been classified provisionally as R heads (cf. line like R heads in the u.v. system of $AlCl$ molecule). Their appearance first suggested them to be the lines of silver atom. A comparison of their wavelengths with the extensive M I T Wavelength Table showed that they are neither due to Ag atom nor due to any other impurity. Thus it is almost definite that they are associated with these bands. Their separations from the accompanying bands change in a regular manner i.e. from (0, 0), (1, 1), (2, 2), (3, 3) and (4, 4) band it is 8, 7, 5 and 4 cm^{-1} respectively. The general appearance of these bands, accompanied with the line like bands whose separation decreases uniformly as one proceeds from one band to another in $\Delta v = 0$ sequence suggests them to be R heads. It will be seen that the differences for the Q heads are very uniform, proving that the measured positions of the Q heads are very close to the respective band origins. The corresponding differences of the R heads as is expected show no such uniformity on account of varying distances of the R heads from their band origins.

The analysis of the $D \leftarrow X$ system presented no difficulty as it forms well-developed sequences and progressions. The (0, 0) band was easily recognised. Nearly all the bands observed fit well with the proposed formula for this system.

ACKNOWLEDGMENTS

The author wishes to record his thanks to Prof. D. Sharma, Head of the Department of Physics, University of Gorakhpur, for his guidance in this problem and to the C.S.I.R., New Delhi, for financial support.

REFERENCES

- Bahaduri, B. N. and Fowler, A., 1934, *Proc. Roy. Soc. A.*, **145**, 321.
 Harrison, G. R., M I T Wavelength Table
 Joshi, M. M., 1958, D Phil. Thesis, Allahabad University.
 Kleman, B. and Landqvist, S., 1955, *Ark. Fys.*, 9 paper **26**, 385
 Ruamps, J., 1954, *C.R. Acad. Sci.*, **238**, 1489
 Ruamps, J., 1959, *Ann. Phys. (Paris)*, Ser. 13, **4**, no 9—10, 1111.

LIGHT ABSORPTION IN PARAMAGNETIC IONS IN STATE OF SOLUTION

Part IV- Co^{+2} ions

A. MOOKHERJEE AND N. S. CHHONKAR

PHYSICS LABORATORIES, AGRA COLLEGE, AGRA

(Received December 8, 1962)

ABSTRACT. Light absorption in Co^{+2} ion salts is studied by a Hilger's "UVISPEK" spectrophotometer in the range 3,900 Å. The results are discussed in the light of crystalline electric field theory.

It is observed that the overall crystal field splitting ($\sim 19,550 \text{ cm}^{-1}$) is more than that for Ni^{+2} ion salt but less than that of Cr^{+3} ion salts.

The term separation as deduced comes out smaller than the free ion value. From this lowering, the covalency factor f^2 was evaluated. f^2 tends to a value .95 pointing to the fact that in Co^{+2} ion salts the σ - and π - orbitals overlap is negligible and the water cluster about the Co^{+2} ion is more susceptible to secondary distortions due to distant atoms than that of Cu^{+2} and Cr^{+3} ions.

I N T R O D U C T I O N

In the third part of this paper (Mookherji and Chhonkar 1961) which we shall refer as Part III hereafter, a systematic optical investigation of the consequences of the crystalline electric field on the optical and magnetic behaviour of Cr^{+3} ion salts in aqueous solution has been reported. A number of interesting results that have been obtained are

1. The overall cubic field splitting is much larger in Cr^{+3} ion salts as compared to Cu^{+2} and Ni^{+2} ion salts.
2. The covalency factor f^2 arises out of σ - and π -orbital overlap.
3. The effect of the long range fields on the water cluster about Cr^{+3} ion is negligible.

The ground state of free Co^{+2} ion is an F-state ($3d^7 \ ^4F$) like Cr^{+3} ion ($3d^3 \ ^4F$) and Ni^{+2} ion ($3d^8 \ ^3F$). But unlike octahedrally coordinated Ni^{+2} ion or Cr^{+3} ion an orbitally degenerate triplet Γ_4 lies lowest in the stark pattern for Co^{+2} ion with similar coordination. Naturally the optical and magnetic behaviour will differ considerably from that of Ni^{+2} ion or Cr^{+3} ions.

As the triplet lies lowest there will be a large orbital contribution to the magnetic moment in ordinary pink cobalt salts. Consequently secondary distortions from distant atoms will be quite appreciable (Bose *et al.* 1952).

* Now at Burdwan University, Burdwan

Dreisch *et al.* (1937) working on the selective absorption spectra of Co^{++} ion salts observed band heads approximately at 8,000, 12,982 and 19,418 cm^{-1} while Holmes *et al.* (1957) observed band heads at 8,350, 19,800 cm^{-1} . Dreisch *et al.* (1937) found fine structures for the infrared band but Holmes *et al.* (1957) with much higher resolving power instruments failed to observe any fine structure for that band.

Jorgensen (1954) tried to explain these bands on the assumption of a purely cubic field acting on the Co^{++} ion and came to the conclusion that for a correct explanation the influence of a tetragonal field should also be taken into account. Indeed Abragam and Pryce (1951) could explain the PMR data on Co^{++} ion salts on the assumption of a small anisotropic field having tetragonal symmetry comparable to spin-orbit coupling superimposed upon a predominant cubic field acting on Co^{++} ion. On the basis of the same theory Bose *et al.* (1961) explained satisfactorily the experimental magnetic susceptibility data of Co^{++} ions in crystals.

The present communication deals with the measurements of absorption spectra of about a dozen of Co^{++} ion salts in aqueous solutions. The results of measurements are discussed in the light of crystalline electric field theory.

EXPERIMENTAL

The spectra of solutions were obtained with Hilger's UVISPEK spectrophotometer using the same procedure as in Part I. (Mookherji and Chhonkar 1959). Chemicals used were of Merck's gravimetric reagent quality. Triple distilled water was used for making solutions.

The measurements centred round 27°C. No observable change of the position of the absorption bands was noted for small room temperature changes.

RESULTS

Results of measurements are collected in Table I. The location of the maximum of the absorption band for various salts are given in wave numbers. The variation of absorption in different salt solutions are shown graphically in Figs. 2 to 12. Just like the cupric salts (Part, I) nickel salts (Part II) and chromic salts (Part III) progressive dilution from that concentration at which the prominent peak is obtained does not change the position of the absorption peak.

DISCUSSION

(a) The absorption spectra

The spectrogram of absorption spectra of Co^{++} ion in about a dozen of salts in aqueous solution show a single band at about 19,550 cm^{-1} and two discernable bands at about 20900 cm^{-1} and 21,800 cm^{-1} within the range of our studies. These bands are assigned the transitions ($C-a$), (C_1-p_1) and (C_2-p_2) and will be designated by ΔE_a , ΔE_{p_1} and ΔE_{p_2} respectively as shown in Fig. 1. The other band which is in the infrared ($\sim 8350 \text{ cm}^{-1}$) will be called as ΔE_b .

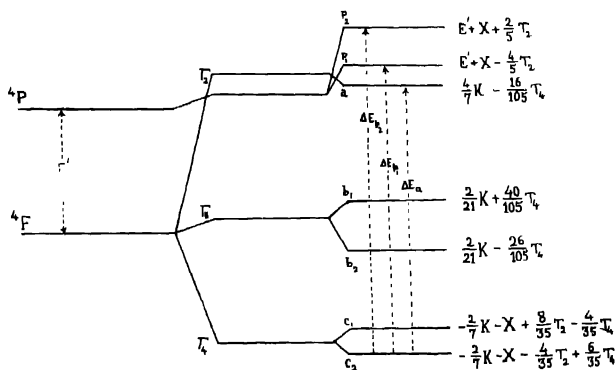


Fig. 1. Stark splitting of the ground state of Co^{++} ion.

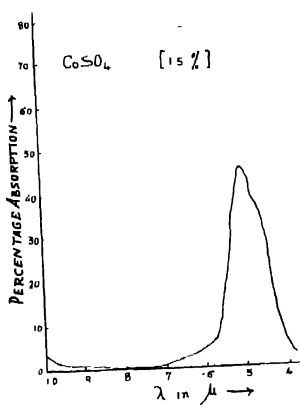


Fig. 2. Absorption curve of CoSO_4 1.5 % solution.

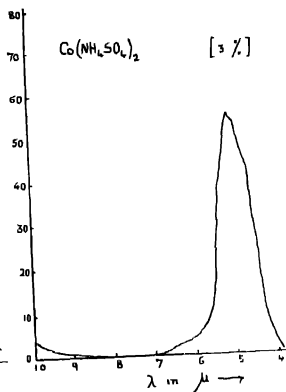


Fig. 3. Absorption curve of $\text{Co}(\text{NH}_4\text{SO}_4)_2$ 3 % solution.

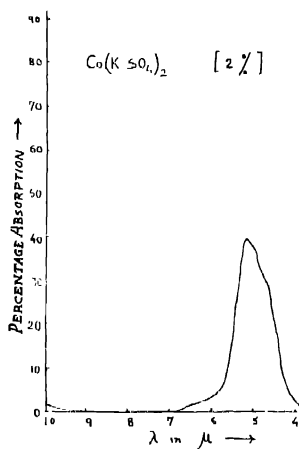


Fig. 4. Absorption curve of $\text{Co}(\text{K}_2\text{SO}_4)_2$
2 % solution.

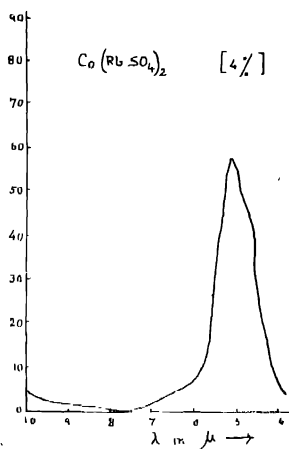


Fig. 5. Absorption curve of $\text{Co}(\text{Rb}_2\text{SO}_4)_2$
4% solution.

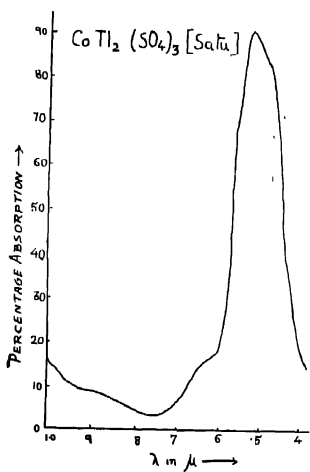


Fig. 6. Absorption curve of $\text{Co}(\text{TlSO}_4)_2$
saturated solution.

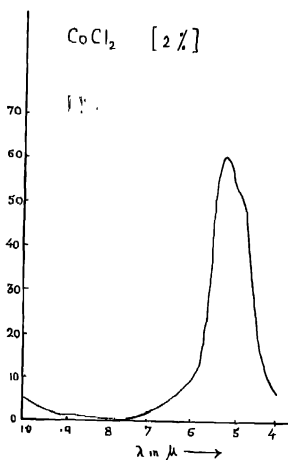


Fig. 7. Absorption curve of CoCl_2
2% solution.

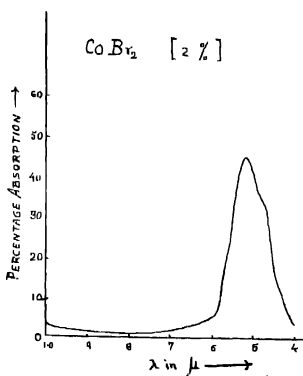


Fig. 8. Absorption curve of CoBr_2 2 % solution.

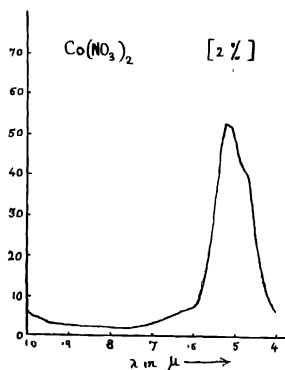


Fig. 9. Absorption curve of $\text{Co}(\text{NO}_3)_2$ 2 % solution.

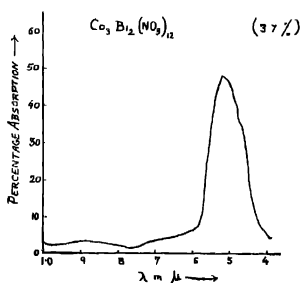


Fig. 10. Absorption curve of $\text{Co}_3 \text{Bi}(\text{NO}_3)_{12}$ 3.7 % solution.

(7) *The crystal field and energy level*

The ground state of Co^{+1} ion is $3d^7 {}^4F$ and the term of the same multiplicity lies about $15,400 \text{ cm}^{-1}$ (Moore 1952) above it. The type of complex ions with which we will be dealing in this paper have the Co^{++} ion at the centre of an elongated octahedron of water dipoles.

The electric field potential near about Co^{++} ion is of the form as given by Eq. 1 of Part II. This field splits the ground state of Co^{++} ion into energy levels as shown in Fig. 1.

According to Owen (1955) the energy levels will be approximately given by the expressions as given in Fig. 1.

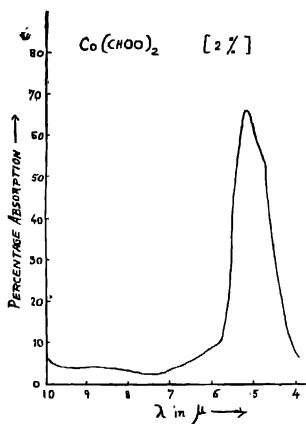


Fig. 11. Absorption curve of $\text{Co}(\text{CHOO})_2$
2 % solution.

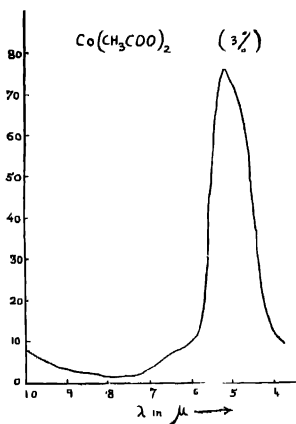


Fig. 12 Absorption curve of $\text{Co}(\text{CH}_3\text{COO})_2$
3 % solution.

TABLE I

Salt	Concentration %	Position of maximum absorption ν in cm^{-1}	$K \text{ cm}^{-1}$	E'	f^2
Co SO_4	1.5	19,610	22,890	14,630	.950
$\text{Co}(\text{NH}_4.\text{SO}_4)_2$	3.0	19,530	22,785	14,650	.951
$\text{Co}(\text{K}.\text{SO}_4)_2$	2.0	19,530	22,785	14,650	.951
$\text{Co}(\text{Rb}.\text{SO}_4)_2$	4.0	19,530	22,830	14,650	.951
$\text{Co}(\text{Tl}.\text{SO}_4)_2$	Saturated	19,570	23,100	14,640	.951
CoCl_2	2.0	19,800	22,785	14,560	.946
Co Br_2	2.0	19,530	22,830	14,650	.951
$\text{Co}(\text{NO}_3)_2$	2.0	19,570	22,785	14,650	.951
$\text{Co}_3\text{B}_{12}(\text{NO}_3)_{12}$	4.0	19,530	22,785	14,650	.951
$\text{Co}(\text{CHOO})_2$	2.0	18,530	22,785	14,665	.952
$\text{Co}(\text{CH}_3\text{COO})_2$	3.0	19,490	22,350	14,650	.951

It is evident from the expressions of energy levels as given in Fig. 1 that we should expect not less than six absorption bands in the visible region, but actually we have observed only three. The occurrence of three bands instead of six can be explained in the following manner.

From the expressions of energy separation it is evident that the energy difference between $(C_2 - p_2)$ and $(C_1 - p_1)$ is $(\frac{19}{35} T_2 - 10/35 T_4)$. This is also the case with the transitions from C_1 and C_2 to a_1 and p_1 respectively.

The two terms in the expression, $(12/35 T_2 - \frac{19}{35} T_4)$ are of opposite sign and of comparable magnitude ($12 T_2 \approx 10 T_4$). So for fitting optical data one can treat C_1 and C_2 levels as a singlet in state of solution. Consequently the absorption bands will be limited to only three as observed. This view is also supported by the theoretical findings that the tetragonal splitting in case of single crystal $Cu(K_2SO_4) \cdot 6H_2O$ is $\approx 280 \text{ cm}^{-1}$ (Chakravorty *et al.* 1959). Moreover, even at ordinary temperatures C_1 is appreciably less populated than C_2 so that the transition from C_1 would be weaker.

(c) Calculation of the cubic field coefficient (K)

We have stated earlier that we can treat the lowest levels C_1 and C_2 as a single level. The approximate energy levels under the condition will be given by Eq. 3 taking the lowest as zero.

$$\begin{aligned}
 {}_4a - J & \quad P_2 \quad E' + X + \frac{2}{7}K + \frac{9}{35}T_4 \\
 & \quad P_1 \quad E' + X + \frac{2}{7}K - \frac{26}{35}T_4 \\
 & \quad \left\{ \begin{array}{l} a \quad 6/7K + X - 24/105T_4 \\ b_1 \quad 8/21K + X + 36/105T_4 \\ b_2 \quad 8/21K + X - 40/105T_4 \\ c \quad 0 \end{array} \right.
 \end{aligned}$$

Thus

$$\begin{aligned}
 \Delta E_a &= 6/7K + X - \frac{24}{105}T_4 \\
 \Delta E_{p_1} &= E' + 2X + 2/7K - 26/35T_4 \\
 \Delta E_{p_2} &= E' + 2X + 2/7K + 9/35T_4
 \end{aligned}$$

From these assignments it is possible to estimate T_4 from the measured band ΔE_{p_1} and ΔE_{p_2} , which comes out $\approx 900 \text{ cm}^{-1}$.

Holmes *et al.* (1957) found that the infrared band is a single one, suggesting that the terms $\frac{24}{105}T_4$ and $\frac{36}{105}T_4$ are quite small, compared to $\Delta E_y \sim 8350 \text{ cm}^{-1}$. Our evaluated value of T_4 also points to the same. Thus taking the levels b_1 and b_2 as single we get $X \approx 200 \text{ cm}^{-1}$. Consequently in the expression for ΔE_a ,

Eq. 2, we are justified to drop the contribution of $X - \left(\frac{24}{105}\right) T_4$. As a result we get $E_a = 6/7 K$ and hence K can be evaluated from the measured ΔE_a -values for the different salts. These are included in Table I.

(d) *Evaluation of the Spectroscopic term separation (E')*

For Co^{++} ions in which ${}^4\text{F}$ state lies lowest the term separation E' can be evaluated from 1st and 2nd expressions of Eq. 3 by eliminating X . Thus we have

$$E' = E_{p1} - 2\Delta E_a + \frac{10}{7} K + \frac{30}{105} T_4.$$

On substituting the observed values of ΔE_{p1} and ΔE_a and the calculated values of K and T_4 we have evaluated E' for the various salts. These are also included in Table I.

It is seen that there is a lowering of the term separation E' from the free ion value. Following Owen (1955) this lowering is attributed to the covalency factor f^2 arising from the partial overlap of 3d-orbitals with σ - and π -orbitals of the surrounding atoms. Hence $E'/E = f^2$, where $f^2 = f_{\pi}^2 f_{\sigma}^2$.

We have thus calculated f^2 taking $E = 15,400 \text{ cm}^{-1}$ (Moore 1952). * These are also included in Table I.

It is interesting to note that these f^2 values are almost unity suggesting that in octahedrally coordinated Co^{++} ions salts the partial overlap of 3d-orbitals with σ - and π - orbitals of their surroundings is negligible. This is in complete agreement with the findings of Chakravarty and Chatterji (1959) and Bose *et al.* (1960). Incidentally this also justifies our assumption that X and $\frac{24}{105} T_4$ cancel each other.

Primarily this covalency factor should not be different for the similarly coordinated salts of Co^{++} ion, but there might be an appreciable change in it due to the distant atoms. In state of solution distant atom effect will be negligible and hence covalency factor should not vary appreciably. This is what has been observed.

f^2 -values give a measure of the covalent character of the ions. In case of Co^{++} ion salts this is almost unity hence the stabilising energy is small compared to Cu^{++} , Cr^{+++} and Ni^{++} ion salts. As a result the secondary distortions due to the distant atoms on the water cluster will be very pronounced. This is also the conclusion arrived at by Bose and Mitra (1952) from their survey of the comparative influence of short and long range fields on the magnetic behaviour of the salts of iron group.

ACKNOWLEDGMENTS

The work was carried out at the Physics Laboratories of Agra College, Agra. We wish to express our sincere thanks to University Grants Commission whose generous grants enabled us to carry out this piece of work.

REFERENCES

- Abragam, A and Pryce, M. H. L., 1951, *Proc. Roy. Soc. A.*, **206**, 175.
Bose, A., Chakravarty, A. S. and Chatterjee, R., 1961, *Proc. Roy. Soc. A.*, **261**, 43.
Bose, A. and Mitra, S. C., 1952, *Ind. Jour. Phys.*, **26**, 543.
Chakravarty, A. S. and Chatterjee, R., 1959, *Ind. Jour. Phys.*, **42**, 153.
Dreish, T. 1927, *Zeits f. Phys.*, **17**, 714.
Holmes, O. G. and M. C. Chubb. D. S., 1957, *Chem. Phys.*, **26**, 1686.
Jorgensen, C. K., 1954, *Acta. Chem.*, **8**, 1502.
Mookerji, A. and Chhonkar, N. S., 1959, *Ind. Jour. Phys.*, **33**, 74.
Mookerji, A. and Chhonkar, N. S., 1960, *Ind. Jour. Phys.*, **34**, 363.
Mookerji, A. and Chhonkar, N. S., 1961, *Ind. Jour. Phys.*, **35**, 437.
Moore, C. E., 1952, *Nat. Bur. Stand. Cir.*, **52**, 467.
Owen, J., 1955, *Proc. Roy. Soc. A.*, **227**, 183.

AN EMPIRICAL RELATION FOR ALPHA DISINTEGRATION ENERGIES FOR MEDIUM-HEAVY ELEMENTS

M. RAMA RAO

SAHA INSTITUTE OF NUCLEAR PHYSICS, CALCUTTA, INDIA

(Received, December 27, 1962)

ABSTRACT It has been observed that for elements with $N > 82$ and $Z < 82$, the function $(Q - 0.624Z)$ has a regular variation with mass number A , where Q is the alpha disintegration energy MeV. A plot of $(Q - 0.624Z)$ vs. mass number A is found to yield a linear graph which takes up the form $(Q - 0.624Z) = -0.21A - 5.5$. This equation has been utilised in calculating the decay energies of alpha emitters of the medium-heavy elements. The agreement between observed values and those calculated with the help of this formula lies within an average of ± 5 per cent.

INTRODUCTION

To the experimentalist engaged in the search for new alpha activities, a beforehand knowledge of the decay energy of such alpha emitters is a desirable thing. This information together with a reasonable estimate of the half-lives of the unknown alpha emitters as can be deduced from Bethe equation [cf. Segrè (1959)] relating half-life T to the decay energy E and charge number Z , is quite useful and serves as a checkup on the discrepancies in experimental results.

Bethe-Weizsäcker (1936) semi-empirical mass formula derived on the basis of the liquid drop model of the nucleus has been used by a number of workers in the calculation of the alpha-decay energies.

Pryce (1950) calculated the alpha-decay energies from Bethe-Weizsäcker formula and found that for nuclei $Z \geq 84$, $N \geq 128$, the difference between experimental and calculated values of the energy is a smoothly varying function of the mass number A and is expressed by the relation .

$$Q(\text{obs}) - Q(\text{calc}) = 4\epsilon - 4a(A - 210.5) \quad \dots (1)$$

where ϵ and a are constants and A is the mass number. Das (1950) has also calculated the alpha-decay energies and showed that it satisfactorily described the observed trend in alpha-decay energies as a function of mass number.

Bethe-Weizsäcker mass formula has been refined by Stern (1949) who by adding a correction term could obtain more correct values of energies for nuclei $A \geq 208$. Jha and Dube (1952) calculated the alpha-decay energies for isotopes $Z = 83, 84$ and 85 with the help of B-W formula after accounting for the Stern correction factor and found satisfactory results. Dube and Singh (1945) have

suggested other types of correction terms to the mass formula to close up the differences between the observed and calculated energy values.

Another Semi-empirical formula, which included among other refinements, empirical corrections in binding energy due to shell effects has been presented by Cameron (1957). Alpha-decay energies were calculated using this formula by Macfarlane (1959) for elements between Sn and Pb and compared with the values obtained from mass data and in a number of cases the disagreement between observed and calculated values is very large.

When the alpha decay energy of heavy elements was closely observed it was found that for mass numbers except in the neighbourhood of $Z = 82$, where the closed shell effects come in, there exists a systematic dependence of the alpha decay energy on the number of neutrons and protons. Roger (1955) has suggested a formula

$$Q \text{ (in Mev)} = 9 - \frac{N-128}{6} \cdot \frac{102-Z}{6} \quad \dots (2)$$

for nuclei beyond $Z = 84$ and $N = 128$.

Utilising the same observation Varshni (1956) developed an empirical relation relating the number of protons and neutrons to the alpha decay energy for heavy elements.

$$Q \text{ (in Mev)} = 0.4Z - 1.795(N-132)^2 - 26.208 \quad \dots (3)$$

for nuclei $N > 128$.

Varshni found that the energies calculated with the help of this formula agreed with the observed values to within an average of ± 3.6 per cent for the heavy elements.

In so far as it has been mentioned in the earlier paragraphs a brief outline has been given regarding the systematics of alpha-decay energies in relation to the heavier elements. Prior to 1947 not much was known about alpha radioactive decay nuclides with mass numbers below 210. In the following years several investigations were reported in the rare earth region with light nuclides of the elements from Cerium to Holmium ($Z = 58-67$).

Using the same formula as proposed by Varshni, Ramaswamy (1956) has redetermined the empirical constants and established a similar equation for the rare earth alpha emitters :

$$Q = 0.36Z - 1.19(N-82)^2 - 17.89 \quad \dots (4)$$

for $N > 82$, $Z < 82$.

The energies calculated with the help of this formula agreed with the observed values to within an average of ± 5.3 per cent for 15 nuclides in the rare earth region.

More recently Varshni and Bhargava (1961) starting from a different approach have suggested another empirical formula valid for the region $Z \geq 84$ and $N \geq 128$.

TABLE I

Nuclide	Z	A	Q(obs) (Mev)	Ref.	Q(calc) (Mev)	Q(obs) -Q(calc)	Percentage error
Nd	60	144	1.90	a	1.70	0.20	+10.0
		147	1.04	a	1.07	0.03	-2.8
Pm	61	146	2.31	b	2.11	0.20	+9.0
		147	1.56	a	1.69	0.13	-8.0
Sm	62	146	2.62	c	2.52	0.10	+3.8
		147	2.26	a	2.31	0.05	-2.2
		148	2.22	d	2.10	0.12	+5.4
		149	1.90	d	1.89	0.01	+0.5
Eu	63	147	3.00	e	2.94	0.06	+2.0
Gd	64	148	3.27	a	3.35	0.08	-2.1
		149	3.10	a	3.14	0.04	-1.3
		150	2.80	a	2.93	0.13	-4.6
		152	2.21	c	2.51	0.30	-13.0
Tb	65	149	4.08	a	3.77	0.31	+5.0
		151	3.56	a	3.35	0.21	+5.9
Dy	66	150	4.35	a	4.18	0.17	+3.9
		151	4.20	a	3.97	0.23	+5.7
		152	3.73	a	3.76	0.03	-0.8
		153	3.57	c	3.55	0.02	+0.6
		154	3.44	e	3.34	0.10	+3.0
Ho	67	151	4.60	f	4.59	0.01	+0.2
		152	4.52	f	4.38	0.14	+3.1
		153	4.45	f	4.17	0.28	+6.3
		154	4.23	f	4.04	0.19	+4.5
		155	4.05	f	3.75	0.30	+7.4
Hf	72	174	2.56	c	2.88	0.32	-12.5
W(?)	74	178	3.15	g	3.19	0.04	-1.3
Pt	78	190	3.2	c	3.27	0.07	-2.2
		192	2.66	h	2.85	0.19	-7.1

a—Ramaswamy (1956); b—Nurmia (1962); c—Taagepera and Nurmia (1961); d—Karras, M., (1960); e—Toth and Rasmussen (1960); f—Macfarlane and Griffioen (1961); g—Porschen and Riezler (1953); h—Porschen and Riezler (1956).

It has been shown that $(Q-0.625Z)$ is a smooth function of the mass number A , where Q is the alpha disintegration energy. A reasonable representation of the plot between $(Q-0.625Z)$ and mass number is incorporated in the analytical expression of the form .

$$(Q-0.625Z) = -364.1233 + 0.8025944A + 6779630/A^2$$

... [5]

for $Z \geq 84$ and $N \geq 128$.

Using this formula, the agreement between observed and calculated values is within an average per cent error of ± 2.45 .

RESULTS

In the present work an empirical formula is presented for the alpha disintegration energies for the medium-heavy elements. The formula is as follows :

$$Q \text{ (in Mev)} = 0.624Z - 0.21A - 5.5$$

... (6)

for $N > 82$, $Z < 82$,

where Q = the disintegration energy in Mev,

A = the mass number,

Z = the charge number.

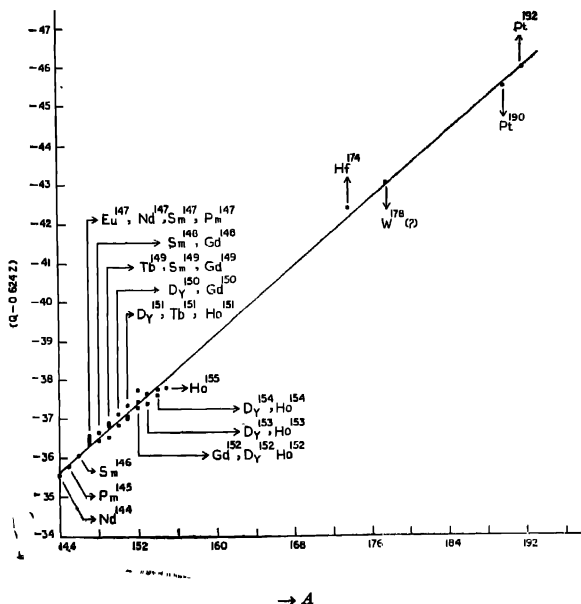


Fig. 1. The function $(Q-0.624Z)$ vs. the mass number A .

This is derived from the simple consideration that the function $(Q-0.624Z)$ has a regular variation with mass number A showing that $(Q-0.624Z)$ decreases in a linear fashion with increasing mass number A . A plot of the points between $(Q-0.624Z)$ and mass number A for all available data between $Z = 60$ (Nd) and $Z = 78$ (Pt) yields a straight line graph and is represented by an equation of the form

$$(Q-0.624Z) = -0.21A - 5.5$$

The data used and their sources are presented in Table I.

DISCUSSIONS

The average per-cent error is ± 4.6 . The agreement between observed values and those calculated by the present formula can be considered satisfactory. Whereas the present formula works quite well in the region of rare earth elements, its scope is extended to include other medium—heavy elements like Hf^{173} , W^{184} , Pt^{190} and Pt^{192} .

ACKNOWLEDGMENTS

The author is thankful to Prof. B. D. Nagechaudhuri, Director of the Institute and Prof. D. N. Kundu for their keen interest and valuable suggestions.

REFERENCES

- Bothe, A. H. and Bacher, R. F., 1936, *Rev. Mod. Phys.*, **8**, 82.
 Cameron, A. G. W., 1957, *Can. J. Phys.*, **35**, 1021.
 Das, R. K., 1950, *Ind. J. Phys.*, **24**, 523.
 Dube, G. P. and Singh, L. S., 1954, *Ind. J. Phys.*, **28**, 177.
 Jha, S. and Dube, G. P., 1952, *Ind. J. Phys.*, **26**, 15.
 Karias, M., 1960, *Ann. Acad. Scient. Fen. A.*, **6**, 65.
 Macfarlane, R. D., (1959) Thesis (Unpublished), Carnegie Institute of Technology, Pittsburg, U S A.
 Macfarlane, R. D. and Griffioen, R. D., 1961, *Bull. Am. Phys. Soc. Ser. II*, **6**, 287.
 Nurmia, M., 1962, *Phys. Rev.*, **127**, 943.
 Porschen, W. and Riezler, W., 1953, *Zeit. f. Naturf.*, **8a**, 502.
 Porschen, W. and Riezler, Z., 1956, *Z. Naturforsch.*, **11a**, 143.
 Pryce, M. H. L., 1950, *Proc. Phys. Soc.*, **63**, 692.
 Ramaswamy, M. K., 1956, *Nuovo cimento*, **3**, 1148.
 Roger, F., 1955, *Compt. Rend. Acad. Sci.*, **240**, 858.
 Segre, E., 1959, *Experimental Nuclear Physics*, III, Sec 2 B 2, John Wiley & Sons.
 Stern, M. O., 1949, *Rev. Mod. Phys.*, **21**, 316.
 Taagopere, R. and Nurmia, M., 1961, *Ann. Acad. Scient. Fen. A.*, **6**, 78.
 Toth, K. S. and Rasmussen, J. O., 1960, *Nuclear Physics*, **16**, 474.
 Varshni, Y. P., 1956, *Nuovo Cimento*, **3**, 1148.
 Varshni, Y. P. and Bhargava, R. N., 1961, *Nuovo Cimento*, **22**, 450.

SCATTERING OF LOW ENERGY NEUTRONS BY CARBON

CHHAYA GANGULY AND N. C. SIL

DEPARTMENT OF THEORETICAL PHYSICS, INDIAN ASSOCIATION FOR THE CULTIVATION OF
SCIENCE, JADAVPUR, CALCUTTA-32

(Received March 26, 1963)

ABSTRACT. The cross sections of scattering of low energy neutrons by carbon have been calculated by the phase shift method, the complex nuclear potential is taken as of Woods-Saxon form and the phases are calculated with the help of a relation given by Brysk. The theoretical values of the differential cross sections for 2.7 and 4.1 Mev neutrons agree fairly well compared with the experimental findings for the same given by Little *et al.*, and Wult & Boyster respectively.

INTRODUCTION

A number of investigations (Feshbach *et al.* 1954; Feshbach, 1958) on neutron—nucleus interaction have been carried out with considerable success in terms of an optical model of the nucleus. In this model the interaction due to the target nucleus consisting of many individual nucleons is replaced by an average potential well of complex nature which can be used to determine the differential cross section for elastic scattering, its imaginary portion takes care of the absorption due to the formation of the compound nucleus. Most of the calculations of this type have been done with a square well potential which, though, has the advantage of mathematical simplicity and of giving fairly reasonable result, is however unsatisfactory in predicting much larger values of scattering cross section for larger angles than what are experimentally found. The cause of the discrepancy is due to the sharp edge of the potential well and as such the model has been modified by Woods-Saxon (1954) who has replaced the sharp edge by a diffuse one. Various results obtained with this model having a smoothly rounded edge agree reasonably well with experimental findings.

The object of the present paper is to calculate by the phase-shift method the cross section of scattering of low energy neutrons by carbon; the complex nuclear potential is taken to be of Woods-Saxon (1954) type and the phases are calculated with the help of a relation given by Brysk (1962). Brysk's formula differs from the Born's relation by a factor in the denominator which for high energy becomes 1. The claim of Brysk is that his relation gives more exact values of phase angles for energies lower than those where Born method is valid. At low energy of the incident particle the contribution to the scattering cross section will come mostly from the first few phase-shifts. The calculation of phase shift is generally

difficult and analytical solutions can be obtained only in few special cases. It is doubtful whether the Born approximation is valid for energies below 100 Mev, the method of calculating the individual phases by the Born method may push the limit of validity a little lower than 100 Mev. But Brysk claims that the calculation of the phase angles by his method brings down the limit of validity to as low as 5 Mev particle energy for spherical well potential with range of the order of \hbar/mv i.e. $\lambda/2\pi$. His method is not very useful for long range potential—a limitation imposed by certain approximations introduced in his calculations. The Woods-Saxon potential being of short range nature will not offer any difficulty in Brysk method.

RESULTS AND DISCUSSIONS

The scattering amplitude is expressed by

$$f(\theta) = (2ik)^{-1} \sum_{l=0}^{\infty} (2l+1)(e^{2i\delta_l} - 1)P_l(\cos \theta) \quad \dots (1)$$

We calculate the phases δ_l by Brysk's relation

$$\tan \delta_l = \frac{-\frac{2\mu k}{\hbar^2} \int_0^{\infty} r^2 dr j_l^2(kr) V(r)}{1 - \frac{2\mu k}{\hbar^2} \int_0^{\infty} r^2 dr j_l(kr) y_l(kr) V(r)}$$

where j_l, y_l are spherical Bessel and Neumann functions respectively,

$$k = \frac{\sqrt{2\mu E}}{\hbar}$$

μ being the reduced mass and E , the energy in the centre of mass system, the nuclear potential $V(r)$ is of the form as given by Woods and Saxon viz.,

$$V(r) = - \frac{(V+iW)}{1 + e^{(r-R)/a}} \quad \dots (3)$$

where R is the nuclear radius and a is the diffusivity parameter.

The integrals for s -wave phase-shift have been calculated analytically. With the substitution $x = \frac{r-R}{a}$ the integral in the numerator of the right hand side of eqn. (2)

$$\int_0^{\infty} \frac{\sin^2 kr}{1 + e^{(r-R)/a}} dr$$

takes the form $1/2 [L(0) - L(2k)]$

$$\text{where } L(p) = a \int_{-R/a}^0 \frac{\cos p(R+ax)}{1+e^x} dx + a \int_0^\infty \frac{\cos p(R+ax)}{1+e^x} dx$$

$$\text{Now } \frac{1}{1+e^x} = \sum_{n=1}^{\infty} e^{-nx} (-1)^{n+1} \text{ for } x < 0$$

$$\text{and } \frac{1}{1+e^x} = \sum_{n=1}^{\infty} e^{-nx} (-1)^n \text{ for } x > 0$$

$$\begin{aligned} \text{Hence } L(p) &= a \sum_{n=1}^{\infty} (-1)^{n+1} \int_{-R/a}^0 \cos p(R+ax) e^{-nx} dx \\ &\quad + a \sum_{n=1}^{\infty} (-1)^n \int_0^\infty \cos p(R+ax) e^{-nx} dx \end{aligned}$$

The integrals are elementary and can be evaluated easily.

Making use of the relation (c.f. Bromwich, 1947)

$$1 + 2a^2 \sum_{n=1}^{\infty} \frac{(-1)^n}{n^2 + a^2} = \frac{a\pi}{\sin ha\pi}$$

we may finally write

$$L(p) = \frac{2 \sin pR}{p} - \frac{a\pi \sin pR}{\sin ha\pi} - a \sum_{n=1}^{\infty} \frac{(-1)^n n e^{-nR/a}}{n^2 + p^2 a^2}$$

Similarly, the integral in the denominator can be evaluated and we have

$$\int_0^\infty \frac{\sin 2kr}{1+e^{(r-R)/a}} dr = -\frac{\cos 2kR}{k} + \frac{1}{2k} + \frac{a\pi \cos 2kR}{\sin h 2ka\pi} + a \sum_{n=1}^{\infty} \frac{(-1)^n 2ake^{-nR/a}}{n^2 + 4k^2 a^2}$$

The infinite integrals for p -wave and d -wave phase-shifts in the numerator have been split up as

$$\int_0^R r^2 dr j_l^2(kr) + \int_R^\infty \left(1 - \frac{1}{1+e^{(r-R)/a}}\right) j_l^2(kr) r^2 dr + \int_0^\infty \frac{1}{1+e^{(r-R)/a}} j_l^2(kr) r^2 dr$$

The first integral is evaluated analytically and last two integrals have been calculated numerically. The integrals in the denominator have been calculated in a similar way.

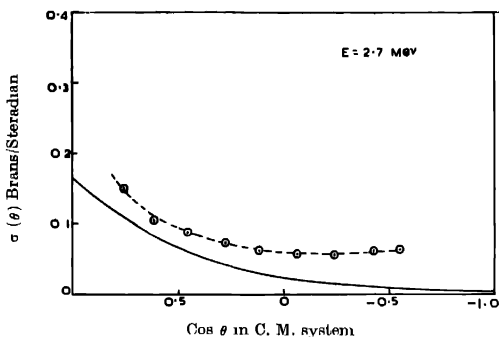


Fig. 1 Differential cross section of scattering of 2.7 Mev neutrons by carbon
 ----- experimental curve
 ————— theoretical curve

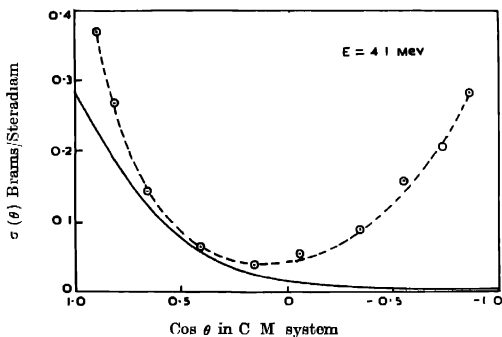


Fig. 2 Differential cross section of scattering of 4.1 Mev neutrons by carbon
 ----- experimental curve
 ————— theoretical curve

We have to calculate the differential cross sections in the c.m. system for the incident neutron energies corresponding to 2.7 Mev and 4.1 Mev in the laboratory system. We use the values of the parameters as given by Feshbach *et al.* (1958)

$$R = (1.15A^{1/3} - 1.4) \times 10^{-13} \text{ cm}$$

$$a = 0.57 \times 10^{-13}$$

$$V = 52 \text{ Mev}$$

$$W = 3.12 \text{ Mev.}$$

Results of our calculation for $\tan \delta_i$ in the c.m. system have been given in the following Table for the elastic scattering of 2.7 Mev and 4.1 Mev neutrons by carbon. The differential cross sections for these incident energies have been compared with the experimental values given by R. N. Little *et al* (1955) and Walt and Beyster (1955) respectively.

Energy in lab system	$\tan \delta_0$	$\tan \delta_1$	$\tan \delta_2$
2.7 Mev	$-0.6930 + 0.0059 i$	$-0.2194 + 0.0033 i$	$-0.0340 + 0.0012 i$
4.1 Mev	$-0.9838 + 0.0099 i$	$-0.3736 + 0.0061 i$	$-0.1092 + 0.0036 i$

It is found that the experimental values of scattering cross sections for 2.7 Mev particles show a decrease with increasing angle till 90° and after that a little tendency to increase, whereas for 4.1 Mev particles the cross section decreases with angle upto 90° and thereafter goes on increasing, the experimental curve for the differential cross section of 4.1 Mev particles is almost symmetric about 90° . Our theoretical values agree fairly well with the experimental results upto 90° but after that the theory fails to show the increase which is presumably due to the preponderance of d scattering brought in by the deformation of the nucleus. In the energy region considered we have appreciable compound elastic scattering and it is very difficult to separate this from the total elastic scattering observed experimentally. The theoretical curves which give only the shape elastic part of the elastic scattering are necessarily below the experimental ones which include both the shape elastic and the compound elastic scattering.

ACKNOWLEDGMENTS

We wish to thank Professor D. Basu, for his kind interest in the problem and for many helpful discussions during the progress of the work.

REFERENCES

- Bromwich, 1947, *Introduction to the theory of Infinite Series*, 2nd Edition.
 Brysk, Henry, 1962, *Phys. Rev.*, **126**, No. 4, 1589.
 Feshbach, H., Porter, C. E. and Weisskopf, V. F., 1954, *Phys. Rev.*, **96**, 448.
 Feshbach, H., 1958, *Annual Rev. of Nuclear Science*, **8**, 88.
 Little, R. N., Jr., Leonard, B. P., Jr., Prud'homme, J. T., and Vincent, L. D., 1955, *Phys. Rev.*, **98**, 634.
 Walt, M. and Beyster, J. R., 1955, *Phys. Rev.*, **98**, 677.
 Woods, R. D. and Saxon, D. S., 1954, *Phys. Rev.*, **95**, 577.

SPUTTERING OF SILVER BY IONS OF NOBLE GASES

A. V. NARASINHAM AND S. B. KARMOHAPATRO

SAHA INSTITUTE OF NUCLEAR PHYSICS, CALCUTTA-9

(Received December 17 1962)

ABSTRACT. Sputtering yields of silver in collision with the ions of noble gases at energies from 3-7 Kev were determined by tracer method. Angular distribution of the sputtered atoms of silver was measured. Results are discussed and compared with the existing theories.

INTRODUCTION

The studies of the phenomena of sputtering of the solid surfaces are of current interest, since it gives some ideas of the mechanism of the surface collision processes by energetic ions. Such studies of the metal surfaces are important for optimising the ion retention condition of a collector in an electromagnetic isotope separator and the use of the ions of noble gases gives informations about the improvement of the method of preparation of the gaseous isotopic targets, required in the experiments of nuclear physics.

Wehner (1955) has reviewed the results of the experiments on the sputtering by low energy ions. Moore *et al.* (1957), Brian *et al.* (1958), Grönlund *et al.* (1960), Rol *et al.* (1960), Yonts *et al.* (1960) and Wehner (1960) have given the results on the sputtering yield for energies below 100 kev and some of them present the angular distribution of the sputtered material. Ahnen and Bruce (1961) have investigated various aspects of sputtering of metal by ions of noble gases as well as other ions in the light of the collection problems of the isotopes.

In the present paper, we have presented some preliminary results of the measurement of the sputtering yields of silver along with the angular distribution of the sputtered materials for ions of helium, neon, krypton and xenon at energies from 3-7 Kev.

EXPERIMENTAL METHOD

The system employed in the present experiment consists of a magnetic oscillation type arc discharge ion source with radial extraction arrangements with a 3/16" diameter hole for extraction of the ions. The electronic circuits used in the experiment, are power supplies for the arc, filament and the accelerating voltage previously described by Karmohapatro (1960). The sputtering chamber with the silver-110m target and the ion source are shown in Fig. 1. 99-100% pure gases are introduced to the ion source. The number of ions, on the target,

considered to be all as singly charged, was estimated by a current indicator and integrator. For each experiment with the different gases, the ion current was fixed at $\sim 10\mu\text{A}$ by varying the arc condition, to avoid unequal heating of the target, which might cause variations in the total yield. The sputtering chamber was kept at a pressure $\sim 10^{-5}\text{mm Hg}$ in course of bombardment with the aid of a differential pumping arrangement.

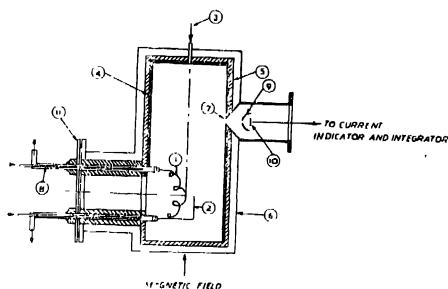


Fig 1. Schematic diagram of the ion source and the sputtering chamber, (1) 40 mil dia tungsten filament, (2) molybdenum plate, (3) gas inlet and electrical load for anode, (4) graphite anode, (5) electrical insulation (Eigan), (6) metal casing, (7) ion exit slit, (8) water cooling tubes, (9) collector of the sputtered atoms, (10) silver-110m target, (11) insulated flange for filament holders.

The total activity in the collector cup was measured with a $1\frac{1}{2}$ " diameter NaI crystal scintillation spectrometer. The counts for each collector give the relative sputtering yield for ions of different energy and mass. The sputtering yield, S , (atom per ion) at 5 Kev for neon ions, found by Grønlund *et al.* (1960) as 5.5, was normalised to that estimated by the radioactivity in our experiment. This value of S at 5 Kev is reasonable, when compared to 1.98 found by Laegried and Wehner (1961) at 600 ev. With respect to this absolute value, S was estimated for different ions of the noble gases of various energies in collision with silver surface.

The angular distribution was measured by the activity, with a Geiger counter, of the small pieces ($1/16$ " dia) of the collector cup, cut uniformly in the radial direction.

In all cases, the target was bombarded by normally incident ions and after each bombardment the target was properly cleaned.

Since the sputtering chamber was within the magnetic field of the ion source itself, the number of the secondary electrons from the target was assumed to be negligible.

RESULTS

Fig. 2 shows the sputtering yield S as a function of the mass number of the noble gas ions in collision with silver. Figs. 3 and 4 show the energy versus yield curve for krypton and xenon ions respectively. Fig. 5 is the polar diagram showing the angular distribution of the sputtered atoms for different ion masses at 5 Kev. Figs. 6 and 7 are the polar diagrams showing the angular distribution of the materials sputtered by different energy ions.

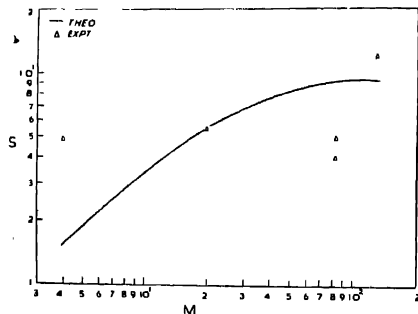


Fig. 2. Sputtering yield, S , as a function of mass of ion for normally incident 5 Kev ions on silver-110 m target.

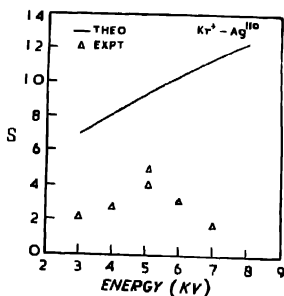


Fig. 3. Sputtering yield as a function of ion energy for krypton ions normally incident on silver-110 m target.

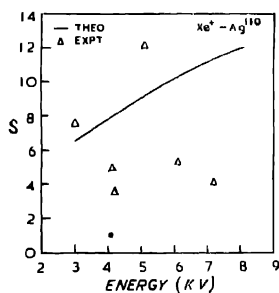


Fig. 4. Sputtering yield as a function of ion energy for xenon ions normally incident on silver-110 m target.

DISCUSSION

The theoretical models, explaining the sputtering process are mainly (1) the theory of evaporation and the (2) momentum transfer process.

The velocity of the sputtered atoms, determined by Wehner (1959), mass dependence of the sputtering yields found by many authors and in the present work, the ejection patterns of the sputtered atoms in the preferential direction of a monocrystal observed by Wehner (1955) and some other experimental results related to the sputtering phenomena cannot be explained by the evaporation theory.

The angular distribution of the sputtered materials measured by Seeliger and Sommermeyer (1935), Brian *et al* (1958) and Grönlund *et al* (1960) seems to follow cosine law, so that the evaporation theory is supported.

The results of our measurements of the angular distribution of the sputtered material with the ion energy and mass are presented in Figs. 5, 6 and 7. The polar diagrams are drawn such that the enclosed areas in each diagram are propor-

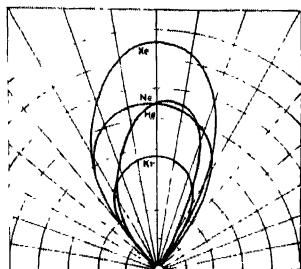


Fig 5 Polar diagram of material sputtered from silver-110 m by normally incident 5 Kev ions of helium, neon, krypton and xenon

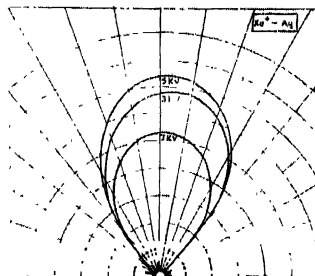


Fig. 6. Polar diagram of material sputtered from silver-110 m by normally incident krypton ions of different energies.

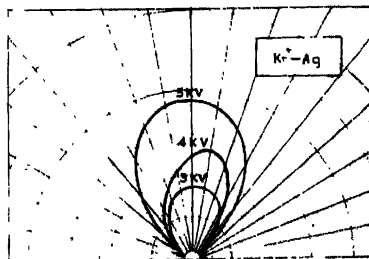


Fig. 7. Polar diagram of material sputtered from silver-110 m by normally incident xenon ions of different energies.

tional to the relative sputtering yields. The slight asymmetry with the normal in some of these curves is probably for deviation from the perpendicular incidence due to some mechanical misalignment of the collector

All the diagrams show that the angular distribution seems to be over-cosine in this energy range. This is in agreement with that found by Rol *et al.* (1960) for 20 Kv ions in copper or by Holmstron and Knight (1961) for argon ions in silver. For low energy ions the angular distribution is under-cosine, observed by Wehner *et al.* (1960). From all these findings it seems that depending on the energy and masses of the ions and the targets along with the orientations of a polycrystalline target, the angular distribution is influenced, since in case of a monocrystal, the sputtering prefers a closed packed direction of the crystal plane. However, considering all the observations the evaporation theory cannot explain the nature of change in the angular distribution of the sputtered materials.

It is difficult to compare the experimental results on the total sputtering yield S with the theoretical expectations, since the momentum theory, based on different assumptions and subject to modifications for different cases, cannot be applied in one form, but it indicates the nature of its dependence on the different parameters like mass, energy etc. In the light of the hard sphere collision model worked out by Keywell (1955), Thommen (1958), Pease (1958), Goldman *et al.* (1958), the mass dependence of the sputtering yield can be explained

Following the treatment of Rol *et al.* (1960), the sputtering yield is given by

$$S = K \cdot \frac{1}{\lambda} \cdot \frac{M_1 M_2 E}{(M_1 + M_2)^2}$$

where K is a constant, M_1, M_2 are masses of the incident ion and the target, E is the energy of the incident ions. The mean free path

$$\lambda = \frac{1}{\pi R^2 n_0}$$

where n_0 is the number of lattice atoms per unit volume and the collision radius

$$R = C \cdot \frac{\alpha_0}{(z_1^{2/3} + z_2^{2/3})^{1/2}} \ln \frac{z_1 z_2 e^2 (M_1 + M_2)}{\epsilon_0 R E M_1}$$

as given by Seitz *et al.* (1956), where C is a constant, ϵ_0 , the dielectric constant in vacuum, α_0 , the first Bohr radius in hydrogen atom, e , the elementary charge, z_1 and z_2 are the atomic numbers of the incident ion and the target.

With a simple assumption that the sputtering happens in the first collision, the above expression is worked out. Assuming this model to be valid for the present

energy range, we calculated the values of S for ions of different masses and energies. In calculating the theoretical values of S the value of K was chosen to give the best agreement with the experimental value ($= 5.5$) for 5Kv neon in silver, found by Grønlund *et al.* (1960). With this value of K , the values of the sputtering yields of silver, bombarded with ions of noble gases as a function of energy and masses of ions are shown in Figs. 2, 3 and 4. The comparison shows that the agreement is better for Xe^+ than Kr^+ in silver. The general discrepancy may be due to (1) a multiple collision process instead of the single collision approximation used in the theory, (2) the deviation of the value of K as shown by Almen and Bruce (1961) from a constant one, approximated in the above theory. The major disagreement between the experimental results and the theoretical expectations lies in the fact that the value of S for krypton ions is relatively lower than that for neon ions, secondly, the maximum near 5 Kev in the sputtering yield versus ion energy for krypton and xenon ions cannot be explained with this model. The maximum near 5Kv with silver bombarded by helium and neon ions, observed by Grønlund *et al.* (1960) is similar to our observations for xenon and krypton ions. For nitrogen and neon in collision with copper, Rol *et al.* (1960) have found a maximum for S near 15 Kev. The maximum may be explained by the two opposite effects of the increasing energy, one of which increases the probability and the other increases the mean free path, thus reducing the probability of collision. Then the nature and position of such maximum will depend upon the target material and the bombarding ion. From the few experimental results observed so far, such dependence cannot be uniquely established. The lower value of S for krypton ions as compared with neon ions in collision with silver surface also cannot be explained with the theory discussed above. Further examinations of more such data may be helpful for understanding the process in more detail.

ACKNOWLEDGMENTS

Authors are thankful to Prof. D. N. Kundu for his keen interest in this work and to Prof. B. D. Nagechowdhury, Director, for the facilities to carry out this work. Thanks are also due to Mr S. Guha for his technical assistance in course of the experiment.

REFERENCES

- Almen, C., and Bruce, G., 1961 *Nuclear Instruments and Methods*, **11**, 257, 259.
Brian, C. D., Lindner, A., and Moore, W. J., 1958, *Jour. Chem. Phys.*, **29**, 3.
Goldman, D. T. and Simon, A., 1958, *Phys. Rev.*, **111**, 383.
Grønlund, F. and Moore, W. J., 1960, *Jour. Chem. Phys.*, **32**, 1540.
Holmström, F. E. and Knight, R. D., 1961, *Bull. Am. Phys. Soc. Ser II*, **6** Abs. **2**, 168.
Karmohapatro, S. B., 1960, *Ind. Jour. Phys.*, **34**, 407.
Keywell, F., 1955, *Phys. Rev.*, **97**, 67.
Laegreid, N. and Wehner, G. K., 1961, *Jour. App. Phys.*, **32**, 365.

- Moore, W. J., Brian, C. D. O. and Lindner, A., 1957, *Ann. New York Acad. Sci.*, **67**, 600.
Pense, R. S., 1955, *Rept. Prog. Phys.*, **18**, 1.
Rol, P. K., Flut, J. M. and Kistemaker, J., 1960, *Physica*, **26**, 1000, 1009.
Seeliger, R. and Sommermeyer, K., 1935, **93**, 692.
Sextz, F. and Koehler, J. S., 1956, *Solid State Physics*, Acad. Press, New York, Vol. 2, p. 329.
Thommen, K., 1958, *Z. Phys.*, **151**, 144.
Wehner, G. K., 1955, *Advances in Electronics and Electron Physics*, **7**, 239.
Wehner, G. K., 1959, *Phys. Rev.*, **114**, 1270.
Wehner, G. K. and Rosenberg, D., 1960, *Jour. App. Phys.*, **31**, 177.
Youts, O. C., Normand, C. E. and Harrison, D. E., 1960, *Jour. App. Phys.*, **31**, 447.

Letters to the Editor

The Board of Editors will not hold itself responsible for opinions expressed in the letters published in this section. The notes containing reports of new work communicated for this section should not contain more figures and should not exceed 500 words in length. The contributions must reach the Assistant Editor not later than the 15th of the second month preceding that of the issue in which the letter is to appear. No proof will be sent to the authors.

7

ON THE WING OF RAYLEIGH LINE DUE TO CARBON-DISULPHIDE AT DIFFERENT TEMPERATURES

K. V. RAMACHANDRA

OPTICS DEPARTMENT, INDIAN ASSOCIATION FOR THE CULTIVATION OF SCIENCE, CALCUTTA-32

(Received April 27, 1963)

Majumder (1949) while studying the Raman spectra of carbon disulphide in liquid and solid states at different temperatures, observed a broad band at a dis-

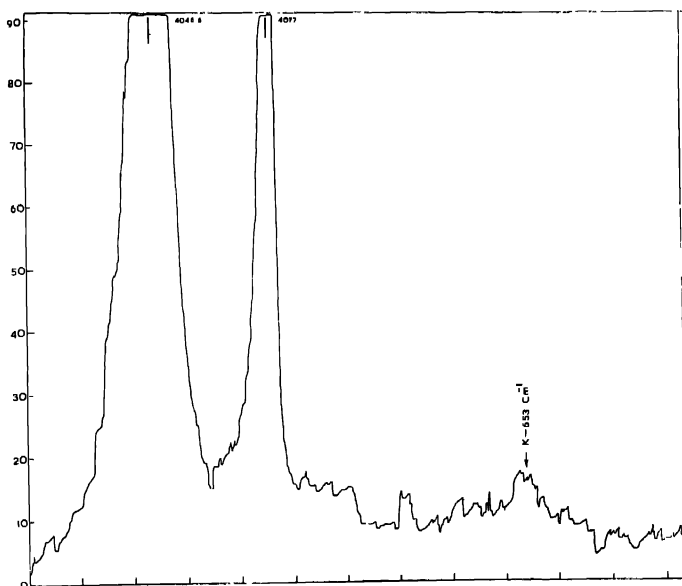


Fig. 1(a). Raman spectrum of carbon disulphide at 28°C.

tance of 45 cm^{-1} from centre of the Rayleigh line due to the liquid at -100°C . It was also observed by him that when the liquid was solidified and cooled to -125°C , the band was replaced by two discrete lines at 59 cm^{-1} and 70 cm^{-1} respectively. On further lowering the temperature of the solidified mass to -183°C , he found the lines to shift to 69 cm^{-1} and 80 cm^{-1} respectively. From these results he concluded that the band at 45 cm^{-1} due to the liquid at -100°C originates from vibration in dimers formed in the liquid at low temperatures and that the band splits up into two lines with the solidification of the liquid. The mean of the frequency shifts of the two lines due to the solid, however, is found to be much greater than 45 cm^{-1} deduced from the inflexion in the microphotometric record of the spectrogram due to the liquid. Recently, Sirkar *et al.* (1961) used a self-recording grating spectrophotometer for studying the wing accompanying the Rayleigh lines due to liquids and showed that the disadvantage due to scattering by grains in the photographic emulsion in the photographic method mentioned above can be avoided if a recording spectrophotometer is used. It was, therefore, thought worthwhile to investigate the wing of the Rayleigh line scattered by carbon disulphide at different temperatures with the recording spectrophotometer

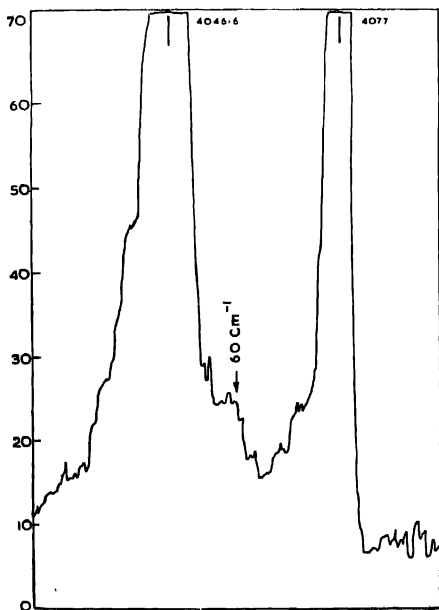


Fig. 1(b). Wing due to carbon disulphide at -80°C .

used by Sirkar *et al.* (1961) and to determine the position of the band mentioned above more accurately.

The arrangement used to record the spectrum of the light scattered by purified carbon disulphide at 28°C and -80°C was similar to that used by Sirkar *et al.* (1961) to record the wing due to benzene, but to cool the liquid to the desired low temperatures mixtures of alcohol and liquid oxygen in appropriate proportions were used as the coolant. The records of the Raman spectra are reproduced in Figs. 1(a) and 1(b) respectively.

It is seen from Fig. 1(a) that inspite of fluctuations in the background intensity the Raman line at 653 cm^{-1} due to carbon disulphide excited by the Hg line 4047Å has been clearly recorded and the distribution of intensity in the wing of the Rayleigh line does not show any maximum. Fig. 1(b), on the other hand, shows a broad band at about 60 cm^{-1} in the wing, the sharp peak on its left side being due to fluctuation in the intensity of the background. The band was found to appear at the same place in several records taken for the liquid at the low temperature. Thus the appearance of the broad band is definitely established, but its Raman shift is 60 cm^{-1} instead of 45 cm^{-1} observed by Majumder (1949) and the origin of the band seems to be a mode a vibration in dimers as postulated by him.

The author is indebted to Professor S. C. Sirkar, D.Sc., F.N.I., for his constant guidance during the progress of the work.

REFERENCES

- Majumder, N. C., 1949, *Ind. J. Phys.*, **23**, 253
Sirkar, S. C., Roy, S. B. and Ghosh, D. K., 1961, *Ind. J. Phys.*, **35**, 377.

BOOK REVIEW

INTRODUCTION TO THERMODYNAMICS OF IRREVERSIBLE PROCESSES by I. Prigogine. Pp. xi + 119. Interscience Publishers Inc., New York 1962, Second Revised Edition. Price \$ 5.00

It is well known that most of the phenomena studied in different subjects are irreversible and cannot be treated accurately by the classical thermodynamics based on the assumption of reversible processes and true equilibrium states. As a consequence, the subject of the thermodynamics of irreversible processes has recently been receiving considerable attention from scientific workers. This monograph written by one of the foremost authorities on the subject represents a very concise and elegant introduction to irreversible thermodynamics.

In chapters I-IV the basic ideas of the irreversible thermodynamics have been discussed and explained. The departure from the classical thermodynamics have very clearly been pointed out. Chapters V-VII deal with a few selected applications of irreversible thermodynamics to physico-chemical problems. The only addition made in this second edition is the last chapter dealing with the non-linear problems which will be of particular interest to research workers.

This book will be of immense value to students and scientific workers who wish to have a brief introduction to the subject of irreversible thermodynamics. It is excellently bound but the price is somewhat high.

(B. N. Srivastava)

CONTENTS

Indian Journal of Physics

Vol. 37, No. 7

July, 1969

	PAGE
38. Flow of a Conducting Fluid Past a Rotating Conducting Cylinder—B. B. Chakraborty	347
39. E2-M1 Mixing in the 100 Kev Transition in Pr^{144} —R. Bhattacharyya and S. Shastri	357
40. Compressibilities, Hydration and Acoustic Properties of Aqueous Solutions of some Metallic Sulphates—M. Satyanarayana Murty and Bh. Krishnamurty	359
41. New Band Systems of Ag_2 Molecule in the Far Ultra-Violet Region—R. C. Maheshwari	368
42. Light Absorption in Paramagnetic Ions in State of Solution Part IV— Co^{++} Ions—A. Mookherji and N. S. Chhonkar	375
43. An Empirical Relation for Alpha Disintegration Energies for Medium-Heavy Elements—M. Rama Rao	384
44. Scattering of Low Energy Neutrons by Carbon—Chhaya Ganguly and N. C. Sil	389
45. Sputtering of Silver by Ions of Noble Gases—A. V. Narasimham and S. B. Karmohapatro	394
LETTER TO THE EDITOR :	
7. On the Wing of Rayleigh Line Due to Carbon-disulphide at Different Temperatures—K. V. Ramachandra	401
BOOK REVIEW	404

Regd. No. C-3911

VOL. 37

INDIAN JOURNAL OF PHYSICS

No. 8

(Published in collaboration with the Indian Physical Society)

AND

VOL. 46

PROCEEDINGS

No. 8

OF THE

**INDIAN ASSOCIATION FOR THE
CULTIVATION OF SCIENCE**

AUGUST 1963

PUBLISHED BY THE
INDIAN ASSOCIATION FOR THE CULTIVATION OF SCIENCE
JADAVPUR, CALCUTTA 34

BOARD OF EDITORS

K. BANERJEE	D. S. KOTHARI
D. M. BOSE	B. D. NAG CHAUDHURI
S. N. BOSE	K. R. RAO
S. D. CHATTERJEE	D. B. SINHA
P. S. GILL	S. C. SIKHAR (Secretary)
S. R. KHASTGIR	B. N. SRIVASTAVA

EDITORIAL COLLABORATORS

PROF. R. K. ASUNDI, Ph.D., F.N.I.
PROF. D. BASU, Ph.D.
PROF. J. N. BHAR, D.Sc., F.N.I.
PROF. V. G. BHIDE, Ph.D.(Nag), Ph.D.(Lond).
PROF. A. BOSE, D.Sc., F.N.I.
PROF. S. K. CHAKRABARTY, D.Sc., F.N.I.
DR. J. S. CHATTERJEE
DR. K. DAS GUPTA, Ph.D.
PROF. N. N. DAS GUPTA, Ph.D., F.N.I.
DR. J. DHAR, D.Phil (So)
PROF. A. K. DUTTA, D.Sc., F.N.I.
PROF. C. S. GHOSH, M.Sc., S.M., F.N.I., M.I.E.E.
PROF. S. GHOSH, D.Sc., F.N.I.
PROF. S. N. GHOSH, D.Sc.
PROF. S. GUPTA, M.Sc., F.N.I.
PROF. D. N. KUNDU, Ph.D., F.N.I.
PROF. R. C. MAJUMDER, Ph.D., F.N.I.
PRINCIPAL Y. G. NAIK, Ph.D.
PROF. S. R. PALIT, D.Sc., F.R.I.C., F.N.I.
PROF. H. RAKSHIT, D.Sc., F.N.I.
PROF. A. SAHA, D.Sc., F.N.I.
DR. VIKRAM A. SARABHAI, M.A., Ph.D., F.N.I.
DR. A. K. SENGUPTA, D.Sc.
PROF. NAND LAL SINGH, D.Sc.
DR. M. S. SINHA, D.Sc., F.N.I.
PROF. N. R. TAWDE, Ph.D., F.N.I.
DR. P. VENKATESWARLU

NOTICE

TO INTENDING AUTHORS

Manuscripts for publication should be sent to the Assistant Editor, Indian Journal of Physics, Jadavpur, Calcutta-32.

The manuscripts submitted must be type-written with double space on thick foolscap paper with sufficient margin on the left and at the top. The original copy, and not the carbon copy, should be submitted. Each paper must contain an abstract at the beginning.

All references should be given in the text by quoting the surname of the author, followed by year of publication, e.g., (Ghosh, 1954). The full reference should be given in a list at the end, arranged alphabetically, as follows; Ghosh, D. K., 1954, *Ind. J. Phys.*, 28, 485.

Line diagrams should be drawn on white Bristol board or tracing paper with black India ink, and letters and numbers inside the diagrams should be written neatly in capital type with India ink. The size of the diagrams submitted and the lettering inside should be large enough so that it is legible after reduction to one-third the original size. A simple style of lettering such as gothic, with its uniform line width and no serifs should be used, e.g.,

A·B·E·F·G·M·P·T·W·

Photographs submitted for publication should be printed on glossy paper with somewhat more contrast than that desired in the reproduction, and should, if possible, be mounted on thick white paper.

Captions to all figures should be typed in a separate sheet and attached at the end of the paper.

The mathematical expressions should be written carefully by hand. Care should be taken to distinguish between capital and small letters and superscripts and subscripts. Repetition of a complex expression should be avoided by representing it by a symbol. Greek letters and unusual symbols should be identified in the margin. Fractional exponents should be used instead of root signs.

Annual Subscription—

Inland Rs. 25.00.

Foreign £ 2-10-0 or \$ 7.00

BENGAL CHEMICAL & PHARMACEUTICAL WORKS LD.

Pioneer Indian Manufacturers of Pharmaceuticals & Chemicals.

Manufacturers of:

Pharmaceutical Chemicals:

Caffeine and its salts, Strychnine Hydrochlor, Strychnine Sulphate, Brucine Sulphate, Nicotinic Acid, B.P., Nicotinamide, B.P., Potassium Citrate B.P., I.P., Sodium Citrate B.P., I.P., Potassium Acetate B.P., I.P., Potassium Iodide B.P., I.P., Sodium Iodide B.P., I.P., Ferri et Ammon Citrate B.P., I.P., and various other Pharmaceutical Chemicals.

Heavy & Reagent Quality Fine Chemicals:

Alum, Alum Sulphate (Iron Free), Ferro Alum, Zinc Chloride Tech. Naphthalene Pure, Sodium Citrate A.R., Potassium Citrate A.R., Magnesium Sulphate A.R., Sodium Sulphate Anhydrous A.R., Potassium Iodide A.R., Sodium Chloride A.R., Zinc Sulphate A.R., and various other reagent quality analytical chemicals.

Please refer your enquiries for the above items and other chemicals in the line to :—

BENGAL CHEMICAL

6, GANESH CHUNDER AVENUE,
CALCUTTA-13, INDIA.

We design and supply

VARIOUS TYPES OF

ELECTRONIC EQUIPMENT

such as

STABILIZED POWER SUPPLY UNITS

BATTERY CHARGERS FOR HOME, GARAGE AND GENERAL PURPOSE

NEON SIGN TRANSFORMERS

CONSTANT VOLTAGE, BOOSTING GLOW DISCHARGE, STEP-UP, STEP-DOWN
TRANSFORMERS

BATTERY ELIMINATORS, METAL RECTIFIERS, WAVE-BAND SWITCHES, ETC., ETC.

FOR ANY DESIRED SPECIFICATIONS

*We have been designing and supplying to the market various
Electrical and Electronic Equipment for over 15 years past.*

Guaranteed Performance !

Prompt Attention !

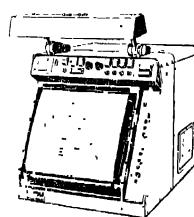
RADIO ELECTRIC (PRIVATE) LTD.

2R LAMINGTON CHAMBERS, LAMINGTON ROAD, BOMBAY—4

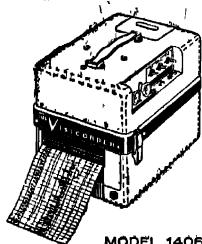
SP/RE/3

HONEYWELL VISICORDER OSCILLOGRAPH

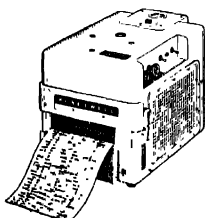
world's most versatile instrument
for the simultaneous recording of
a number of fast changing variables



MODEL 1012



MODEL 1406

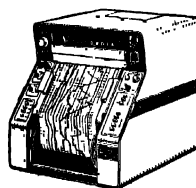


MODEL 906

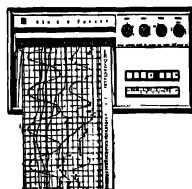


MODEL 1612

Available in several models, from 6 to 36 channels, DC to 5,000 c/s response, over 50,000"/sec writing speed. The 36-channel 1012 & the 1612 are the most sophisticated instruments in the line. The 1108 is a highly capable 24-channel model. The 1508 is a compact 24-channel instrument that takes only 7" of vertical space in a relay rack and is also suitable for bench use. The 906 handles either 8 or 14 channels and the 1406 provides upto 6 channels at the lowest cost per channel.



MODEL 1108



MODEL 1508

Honeywell

Sold and serviced in India exclusively by

BLUE STAR **STAR**

Get complete details from **BLUE STAR** offices at:

7 Hare Street, Calcutta 1
Sukh Sagar, Sandhurst Bridge, Bombay 7
1/23B Asaf Ali Road, New Delhi 1
23/24 Second Line Beach, Madras 1
1B Kaiser Bungalow, Dindli Road, Jamshedpur

**Measure
and plot changes
in variables
as they occur...
with**

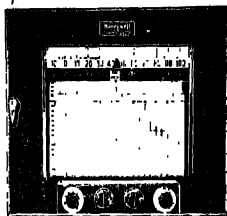
Electronik

instruments for research

Here's an exceptional group of instruments to measure and record your research findings swiftly, surely, conveniently. These Electronik instruments for research can speed completion of your projects by eliminating many of the tedious time-consuming details of test work.

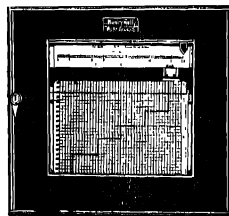
Electronik

ADJUSTABLE SPAN RECORDER measures spans and magnitudes of a variety of emf's. Instrument calibration can be in terms of any variable reducible to d.c. voltage. Can be used with thermocouples, strain gauges, tachometers and other transducers.



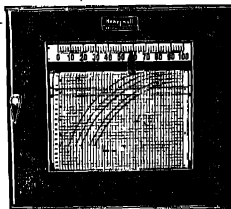
Electronik

EXTENDED RANGE RECORDER facilitates measurement of any linear variable whose values change over a wide range, and where precise evaluation and good resolution are important. This instrument is particularly suited to the measurement of forces in conjunction with a strain gauge bridge.



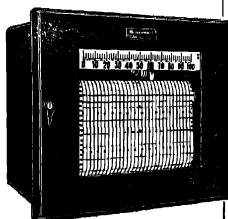
Electronik

FUNCTION PLOTTER automatically and continuously plots a curve which shows the relationship of one variable to another. Typical uses: speed versus torque, stress versus strain, temperature versus pressure, plate voltage versus plate current (and other electron tube characteristics), and many other variable relationships.



Electronik

NARROW SPAN RECORDERS accurately measure d.c. potentials as low as 0.1 microvolt and spans as narrow as 100 microvolts. Available as a precision indicator, circular chart recorder and strip chart recorder. Useful (with appropriate primary measuring elements) for measuring differential temperatures and slight variations in the temperatures of small objects through the use of radiation pyrometry.



P181-122/63

Honeywell

First in Control
SINCE 1906

Sold and serviced in India exclusively by

BLUE STAR

**BLUE STAR ENGINEERING
CO. (Calcutta) PRIVATE LTD.**
7 HARE STREET, CALCUTTA
Also at BOMBAY • DELHI
MADRAS • JAMSHEDPUR


SIEMENS
MEASURING
INSTRUMENTS

Our systems for gathering and processing measuring data and for automatic process control permit the full automation of metallurgical processes provided that the process control system is compatible with future automation

Progressive Process Control for Converters

shortens blowing periods and improves the quality of recovered steel. Our electric, pneumatic and combined electropneumatic

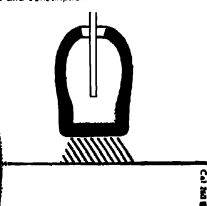
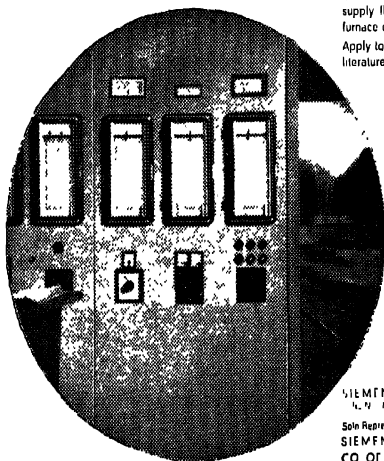
TELEPERM-TELEPNEU standard process control system

has long proved its value in all process control problems connected with converters

Control of blast- O_2 ratio during blow operation with mixed oxygen and O_2 -flow control during blow operation with pure oxygen

Accommodated in a metal-clad cabinet, the equipment is immune to changes in temperature, power supply fluctuations, frequency deviations, impact, furnace dust and moisture

Apply to our nearest branch or agency for detailed literature and consultation



SIEMENS & HALSKE AKTIENGESELLSCHAFT
100 00 MUNICH

Sole Representatives

SIEMENS ENGINEERING & MANUFACTURING
CO OF INDIA LTD.

Bombay • Calcutta • New Delhi • Madras • Bangalore • Visakhapatnam
Ahmedabad • Lucknow • Nagpur • Hyderabad • Trivandrum • Rourkela
Pune

PUBLICATIONS OF THE INDIAN ASSOCIATION FOR THE CULTIVATION OF SCIENCE

		Rs. nP
1. RUSSELL, E. J.	. Methods in Scientific Research ..	0 37
2. JEANS, J. H.	. The Origin of the Planets	0.37
3. ASTON, F. W.	. Separation of Isotopes	0.37
4. LENNARD-JONES, J. E.	. Interatomic Forces . ..	1 50
5. HILL, A. W.	. The Royal Botanic Gardens, Kew ..	1.50
6. MILLIKAN, R. A.	. The Educational Aims and Practices of the California Institute of Technology . ..	0.37
7. MITRA, S. K.	. Active Nitrogen—A New Theory ..	2.50
8. WADIA, D. N.	. Petroleum Resources of India ..	2 50
9. RAY, P.	. The Theory of Valency and the Structure of Chemical Compounds	3.00
10. MUKHERJEE, J. N.	. The Role of the Electrical Double Layer in the Electro-Chemistry of Colloids ..	1.75
11. ROBINSON, R.	. Distribution of Anthocyanins	1.25
12. CHAPMAN, S.	. The Earth's Magnetism and its Changes ..	1.00
13. MARK, H.	. Catalysts in Polymerization Reactions ..	1 50
14. AMALDI, E.	. Diffraction Effects in the Scattering of Neutrons, Mesons and Electrons by Nuclei	1.50
15. FIESER, L. F.	. Lapinone, A New Antimalarial	1.00
16. BOSE, N. K.	. Fluid Dynamics	1.25
17. VENKATARAMAN, K.	. Constitutional Problems Concerning Vat Dyes ..	1.00
18. ROY, J. N.	. The Chemical Basis of Some Physiological Actions ..	1.00
19. SHOENBERG, D.	. Superconductivity	1.00
20. PALIT, S. R.	. Non-Aqueous Titration	3.00
21. KRISHNAN, M. S.	. Iron Ores of India	5.00
22. SEN, S. N.	. Bijnaner Itihas ; Vol. I	10.50
	Vol. II	12.00
23. SESHADRI, T. R.	. An Investigation of Plant Drugs and Insecticide ..	1.00
24. HOWEN, E. G.	. The Formation of Natural and Artificial Rain ..	1.50
25. BANERJI, S. K.	. Earthquakes in the Himalayan Region ..	3.00
26. MAGNETISM :	. Report of the Symposium on Magnetism ..	7.00
27. WESTPHAL, DR. ING. E.	. The Freight Tube Float . ..	8.00
28. HIRSCHFELDER, J. O.	. Molecular Physics and Intermolecular Forces ..	1.25
29. SEN, N. R.	. The Modern Theory of Turbulence	2.00
30. DOUGLAS, A. E.	. Some Recent Development in Molecular Spectroscopy ..	1.00
31. SHOENBERG, E.	. Experimental Determination of the Electronic Structure of Metal	1.00

HEWLETT PACKARD

NEW NO - PARALLAX 120B OSCILLOSCOPE
EASIEST - to - use SUREST READING 450 KC



Those, who have tested the new 120 B feel it is perhaps the easiest to use, most widely versatile, and highest value commercial 450 KC scope ever offered.

The new h/p 120B Oscilloscope combines probably more actual measuring help and desirable features than any 450 KC scope ever produced.

Not only is reading error from parallax ended and not only are distracting reflections eliminated ; but you also have a genuinely unique array of electrical and convenience features for measurements from dc to 450 KC.

For further details, please write to :

The Sole Distributors :

**THE SCIENTIFIC INSTRUMENT
COMPANY, LIMITED.**

ALLAHABAD BOMBAY CALCUTTA MADRAS
NEW DELHI

Head Office : 6, Tej Bahadur Sapru Road, Allahabad



$\pi^* \leftarrow \pi$ SYSTEMS IN THE ELECTRONIC SPECTRA OF ORTHO AND PARA FLUOROBENZALDEHYDES

KAILASH CHANDRA and D. SHARMA

DEPARTMENT OF PHYSICS, UNIVERSITY OF GORAKHPUR, GORAKHPUR

(Received, November 3, 1962, resubmitted April 24, 1963)

Plate—VII

ABSTRACT. The near ultraviolet absorption spectra of ortho and para fluorobenzaldehydes have been recorded for the first time and vibrational assignments have been proposed. The bands at 34331 and 35981 cm^{-1} have been assigned as 0,0 bands of the longest wavelength $\pi^* \leftarrow \pi$ systems of ortho and para fluorobenzaldehydes respectively. The ground and excited state fundamentals observed in these spectra have been correlated with the lower and upper state fundamentals of other mono-derivatives of benzaldehydes.

INTRODUCTION

The ultraviolet absorption spectra of benzaldehyde in vapour phase have been investigated by Garg (1953), who has also reviewed the earlier literature. Among the derivatives of benzaldehyde, the hydroxy benzaldehydes and chlorobenzaldehydes have drawn the attention of several workers. Morton and Stubbs (1941), who have studied the absorption spectra of *o*-, *m*- and *p*-hydroxy benzaldehydes in vapour as well as solution phases, have shown that in the case of the longest wavelength $\pi^* \leftarrow \pi$ systems of these isomers the order of the shift to longer wavelength side is $o > m > p$. Later Lemov (1947), Buraway and Chamberlain (1952), and Rao and Rao (1960) have extended the work of Morton and Stubbs (1941). Chlorobenzaldehydes have been studied by Patel (1959) Achyuta Rao (1961) and Pandhyc and Viladkar (1960, 1961). But a number of substituted benzaldehydes in vapour phase still require systematic study. It was, therefore, considered desirable to study the ultraviolet absorption spectra of fluorinated benzaldehydes.

Investigations of the near ultraviolet absorption spectra of ortho fluorobenzaldehyde and parafluorobenzaldehyde have shown bands in the regions 3900-3200Å, 2990-2630Å, 2450-2310Å, in the case of the former and 3950-3250Å, 2900-2550Å in the case of the later isomer. The present paper deals with the study of the longest wavelength $\pi^* \leftarrow \pi$ system (corresponding to $B_{2u} \leftarrow A_{1g}$ transition of benzene) of each isomer.

EXPERIMENTAL

The near ultraviolet absorption spectra of ortho and para fluorobenzaldehydes were recorded on Hilger medium quartz spectrograph at temperatures varying

from 20° to 100°C. The spectrum of ortho fluorobenzaldehyde was also photographed on large quartz spectrograph. Path-lengths varying from 5 to 250 cm were used. The spectra were recorded on Ilford N-30 and N-40 plates. Details of absorption cells used are described below. Slit widths of about 20 microns were used. A hydrogen arc lamp served as the source of continuous radiation. Times of exposure varied from 10 minutes to 4 hours. Iron arc comparison spectrum provided the standard wavelengths. Measurements were made on four different plates, twice on each, with the help of Hilger comparator having a least count of 0.0001 cm. Calculations were made with Hartmann dispersion formula and weighted mean values of wavelengths were taken. Band heads were measured in the case of sharp bands and centres in the case of diffuse ones. The former are accurate upto $\pm 4 \text{ cm}^{-1}$ and the later to $\pm 10 \text{ cm}^{-1}$. The chemicals, supplied by Messrs L. Light and Co U. K., were purified by repeated distillations before use.

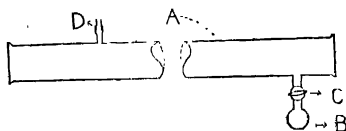


Fig 1. Schematic diagram of absorption tube.

Figure 1 gives a schematic diagram of the absorption cells used. Tube A, with quartz windows sealed at the two ends, served as the main cell. The bulb B, serving as a container, was connected to A with the help of the stop-cock C and the system could be evacuated through the side tube D. The vapour pressure of the substance was adjusted with the help of the stop-cock. In some cases the absorption cell was also used at atmospheric pressure without evacuation. An alternative method of adjusting the vapour in the cell was also tried by introducing drops of liquid into the main cell through the side tube D with the help of a fine dropper. In this case the tube was not evacuated and the container B was kept out of contact with the absorption column. Some times this method was found more convenient.

RESULTS

The values of wavelengths and wave numbers together with visually estimated intensities, separations from 0, 0 band and the proposed assignments are given in Tables I and II for ortho and para fluoro-benzaldehydes. Fig. 2, Plate VII gives enlarged reproductions of the spectra obtained in the region of this system for (a) ortho and (b) para isomers. The experimental conditions and the general disposition differ for each isomer and hence these are discussed individually.

*Ortho*fluorobenzaldehyde :

Bands lying in the range 2990-2630A represent the longest wavelength $\pi^* \leftarrow \pi$ system of this isomer (Chandra and Sharma, 1962). These bands are

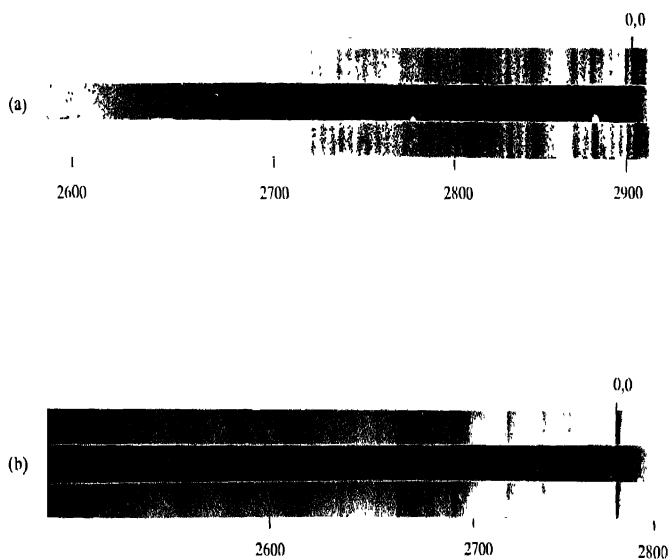


Fig. 2. Absorption spectra of $\pi^* \leftarrow \pi$ system of (a) ortho fluorobenzaldehyde and (b) para fluorobenzaldehyde. In (a) all the three spectra have been obtained under similar conditions except the amount of vapour which was larger in the case of the central strip. In (b) the central spectrum is at 100 cm pathlength and reduced pressure while the upper and lower parts are with 50 cm. pathlength and atmospheric pressure

sharp and degraded to red. The general absorption in this region takes place even at room temperatures and 25 cm pathlength at reduced pressure. The amount of vapour in the absorption column was adjusted as described earlier and spectrograms, using path lengths of 10, 25, 50, 100 and 150 cm, were taken at temperatures of 20° and 80°C. Fig. 2(a) is the spectrum of ortho fluorobenzaldehyde using a path length of 25 cm at room temperature ($\sim 20^\circ\text{C}$) and atmospheric pressure. The central strip is with 3 drops of the liquid in the absorption cell, while the lower and the upper strips were photographed with 1 drop.

Para fluorobenzaldehyde

The bands lying in the region 2880-2550 Å represent the corresponding system of this isomer. These bands are rather sharp and are degraded to red, but they are weak as compared with those of ortho fluorobenzaldehyde. The spectra were photographed at different path-lengths varying from 10 to 150 cm, at room temperatures and under normal as well as reduced pressures. It was observed that the maximum number of bands to shorter wavelength side of the 0, 0 band were recorded using 50 cm pathlength at room temperature and normal pressure (upper and lower strips, Fig. 2(b)) whereas a pathlength of 100 cm at reduced pressure was required for the bands to longer wavelength side of the 0, 0 band (central strip).

ANALYSIS AND DISCUSSION

The ortho fluorobenzaldehyde molecule belongs to the symmetry class C_s , the only symmetry element being the molecular plane containing all the atoms. Hence there are only two types of electronic and vibrational levels, those symmetrical and those antisymmetrical to the molecular plane. The electronic transition involved in the spectrum is of the allowed type $A' \leftarrow A'$. The transition moment lies in the plane of the molecule. It is to be expected that the 0, 0 band (the pure electronic transition) should be present in the first group of bands towards longer wavelengths, and the strongest band at 34331 cm^{-1} is assigned as the 0, 0 band. The separations 135, 202, 340, 505 and 846 cm^{-1} respectively of prominent bands (with visually estimated intensities 5, 3, 1, 0, 0 respectively) from the 0, 0 band towards longer wavelength side have been assigned as ground state fundamentals. It may be remarked that some of these frequencies have also been observed in the less developed 2450-2310 Å system of this molecule. One observes towards the violet side of the 0, 0 band a number of strong bands with intensities 4, 4, 6, 5, 6, 5, 5, 5 and 6 respectively. The separations of these bands from the 0, 0 band give the frequencies of vibration in the upper electronic state of the molecule. These are 121, 189, 325, 468, 776, 962, 1101, 1166 and 1242 cm^{-1} . As can be seen from Fig. 2(a), the overtones of these fundamentals have got the intensities in decreasing order as expected. Table I gives the interpretation of all the bands in terms of the fundamentals in the upper and lower states.

TABLE I
Ultraviolet absorption bands of *o*-fluorobenzaldehyde

Wave number (ν) cm ⁻¹	Relative Intensity				Shift from 0,0 band ($\Delta\nu$) cm ⁻¹	Assignment
	Path-length	25 cm	25 cm	25 cm		
	Temperature Liquid	23°C 1 drop	20°C 3 drops	80°C 1 drop		
33485			1		- 846	0-846
33533			0.5		- 798	0-846+56
33679			0		- 652	0-505-2(71)
33757			0.5		- 574	0-505-71
33826		0	1	0.5	- 505	0-505
33924		1	2	1	- 407	0-2(202)
33991		1	4	2	- 340	0-2(172); 0-340
34055		2	2d	1	- 276	0-202-71
34129		3		2b	- 202	0-202
34159		5		-	- 172	0-135-38
34196		5		4b	- 135	0-135
34260		7		-	- 71	0-846+776
34293		-		2d	- 38	0-505+468
34331		10		10	0	0,0
34387		5		8	+ 56	0+189-135
34452		4		4	+ 121	0+121
34520		4		5	+ 189	0+189
34596		4b		4b	+ 265	0+468-202
34656		6		8	+ 325	0+325
34713		4d		2d	+ 382	0+325+56; 0+2(189)
34763		4		-	+ 432	0+468-38
34799		5		5	+ 468	0+468
34856		2b		4b	+ 525	0+468+56
34923		2b		3b	+ 592	0+468+325-202
34978		2b		3b	+ 647	0+2(325)
35040		3b		4b	+ 709	0+776-71
35107		6		7b	+ 776	0+776
35163		3		5b	+ 832	0+776+56

TABLE I (contd.)

Ultraviolet absorption bands of *o*-fluorobenzaldehyde

Wave number (ν) cm ⁻¹	Relative Intensity				Shift from 0,0 band ($\Delta\nu$) cm ⁻¹	Assignment
	Path-length Temperature Liquid	25 cm 23°C	25 cm 20°C	25 cm 80°C		
		1 drop	3 drops	1 drop		
35225		3b		4b	+ 894	0 + 962 - 71; 0 - 1242 - 340; 0 - 2 (408) - 38
35293		5		7	+ 962	0 + 962
35361		3		-	+ 1030	0 + 1101 - 71
35432		5			+ 1101	0 + 1101
35497		5			+ 1166	0 + 1166
35573		6			+ 1242	0 + 1242
35626		4			+ 1295	0 + 1242 + 56
35694		3			+ 1363	0 + 1242 + 121
35763		3			+ 1432	0 + 962 + 468
35824		3b			+ 1493	0 + 1166 + 325
35897		5			+ 1566	0 + 1242 + 325; 0 + 2 (776)
35959		0.5			+ 1628	0 + 56 + 1242 + 325
35997		0.5			+ 1666	0 + 2 (776 + 56)
36014		0.5			+ 1683	0 + 1242 + 121 + 325
36071		3		4	+ 1740	0 + 2 (776) + 189
36173				1b	+ 1806	0 + 2 (962) - 135 - 38 + 56
36205		0.5		1b	+ 1874	0 + 1242 + 325 + 121 + 189; 0 + 2 (1101) - 340
36276		1		5	+ 1945	0 + 1242 + 2 (189) + 325
36350		1		3	+ 2019	0 + 2 (776) + 468
36405		1		3b	+ 2074	0 + 2 (776) + 468 + 56
36464		1		3b	+ 2133	0 + 2 (1101) - 71
36538		4		5b	+ 2207	0 + 2 (1101)
36600		1		4b	+ 2269	0 + 1101 + 1166
36674		1		4b	+ 2343	0 + 2 (1166); 0 - 1242 + 776 - 1242; 0 + 3 (776)
36739		1		4b	+ 2408	0 + 2 (1242) - 71
36807		0		4b	+ 2476	0 + 2 (1242)
36866		0		5	+ 2535	0 + 2 (1242) + 56

TABLE I (contd.)
Ultraviolet absorption bands of *o*-fluorobenzaldehyde

Wave number (ν) cm^{-1}	Path-length Temperature Liquid	Relative Intensity			Shift from 0,0 band ($\Delta\nu$) cm^{-1}	Assignment
		25 cm 23°C	25 cm 20°C	25 cm 80°C		
36933		0		0.5	-2602	0 + 2 (1212) + 121
37005				1	-2674	0 + 1242 + 325 + 1101
37060				2	-2729	0 + 2 (1242) + 2 (121)
37133				2	-2802	0 + 3 (776) + 468
37186				1	-2855	0 + 3 (776) + 468 + 56
37247				1	+2916	0 + 3 (776) + 468 + 189 - 71, 0 + 3 (776) + 168 + 121
37320				2	-2989	0 + 3 (776) + 468 + 189
37373				1	-3042	0 + 3 (776) + 468 + 189 + 56
37139				1b	+3108	0 + 4 (776)
37508				2	-3177	0 + 2 (1242 + 325) + 121 - 71
37581				1b	+3250	0 + 2 (1242 + 325) + 121
37639				1	+3308	0 + 3 (1101)
37705				1	+3374	0 + 2 (1242 + 121 + 325); 0 + 1 (776) + 468 - 202
37770				1	+3439	0 + 2 (1242 + 121 + 325) + 56
37832				1	+3501	0 + 3 (1166)
37899				1	+3568	0 + 3 (1101) + 468 - 202

b--broad, d--diffuse, bd--broad and diffuse

To a first approximation para fluorobenzaldehyde molecule reduces to C_{2v} symmetry from D_{6h} of benzene. Under the reduced symmetry the transition $B_{2g} \leftarrow A_{1g}$, with the transition moment in the plane (YZ) of the molecule and corresponding to the forbidden transition $B_{2u} \leftarrow A_{1g}$ of benzene, becomes allowed. It is thus expected that the spectra of this isomer should show the characteristics of an allowed transition. The strongest band at 35981 cm^{-1} is consequently identified as the 0,0 band. The shifts 190, 344, 389, 541, 796, 1141, 1191, 1230 and 1492 cm^{-1} of the prominent bands (with intensities 4, 5, 5, 5, 6, 4, 8, 5 and 8 respectively) towards shorter wavelength side of the 0,0 band are easily identified as the upper state fundamentals. The separations 140, 193, 375, 416, 636, 856 and 1161 cm^{-1} of bands (with intensities 5, 5, 1, 2, 1, 1, and 0.5 respectively) towards longer wavelength side have been taken as the fundamentals of the ground state for this molecule. A satisfactory explanation of all the bands, which is plausibly

consistent with the intensities, is given in Table II using the above values of the fundamentals.

It is interesting to observe (vide Tables I and II) that the intensities of ν bands go on decreasing as one goes to longer wavelength side of the 0,0 bands in each of the two spectra under investigation. This variation is as expected because the bands should show a decrease in intensity in view of the Boltzmann factor since quanta of higher energy in the ground state are involved in absorption. On examining the bands to the shorter wavelength side of the 0,0, bands one observes that the bands involving fundamentals or overtones in the excited state are very much stronger than combination bands. These observations show that the assignments are correct.

Table III gives a comparison of the fundamentals of ortho and para fluorobenzaldehydes with the fundamental frequencies of other substituted benzaldehydes. The modes of vibration of these fundamentals have also been suggested. One observes that the values obtained for *o*- and *p*-fluorobenzaldehydes are of the correct order of magnitude. Of these fundamentals, the excited state fundamentals 1242 and 1230 cm^{-1} of *o*- and *p*-fluorobenzaldehydes respectively are of particular interest. They are medium strong prominent frequencies combining with a number of other fundamentals in explaining the bands. The frequency 1242 cm^{-1} gives its overtone. These frequencies in view of their appearance and combining power, seem to be totally symmetric. As can be seen from Table III, they can be assigned as --C--C stretching vibration corresponding to b_{2u} 1310 cm^{-1} of benzene. This benzene vibration however reduces to totally symmetric vibration in the case of C_u symmetry and nontotally symmetric vibration in the case of C_{2v} symmetry. Hence bands corresponding to 1230 cm^{-1} of para fluorobenzaldehyde (C_{2v} symmetry) should be weak rather than medium strong. The absence of frequency corresponding to it in the case of *p*-chlorobenzaldehyde thus seems to be justified. Rao and Sponer (1957) have given 1320 and 1335 cm^{-1} as lower state frequencies corresponding to --C--F stretching vibrations in the case of 1,2,4, trifluorobenzene and 1,2,4,5 tetrafluorobenzene. The corresponding excited state fundamental is 1274 cm^{-1} for 1,2,4 trifluorobenzene. We expect a frequency of this order in the present case and consequently the excited state frequencies 1242 and 1230 cm^{-1} of ortho- and para-fluorobenzaldehydes respectively can also be interpreted as the --C--F stretching vibration. This equality of the --C--C stretching and --C--F stretching frequencies explains the medium strong intensity of the bands corresponding to 1230 cm^{-1} in para fluorobenzaldehyde which should be weak if they are assigned to --C--C stretching vibration alone. This explanation is plausible in view of the fact that the --C--F stretching frequencies in other derivatives of benzene are of the same order—*p*-fluoroanisole 1280; *m*- and *p*-difluorobenzene 1269 and 1250 respectively; *o*-, *m*-, and *p*-fluorotoluenes 1230, 1261 and 1229 respectively; and *o*-fluorochlorobenzene 1249 cm^{-1} .

TABLE II
Ultraviolet absorption bands of *p*-fluorobenzaldehyde

Wave number (ν) cm ⁻¹	Relative Intensity		Shift from 0,0 band ($\Delta\nu$) cm ⁻¹	Assignment
	Path-length Pressure	100 cm Reduced	50 cm Normal	
34820		0.5		-1161 0-1161
35025		0.5		-956 0-416-859 344-33
35122		1		-859 0-859
35210		0.5		-771 0-636-140
35345		1		-636 0-636
35380		1		-592 0-4 (140)-33; 0-375-140-
35469		0.5		-512 0-375-140, 0-859 344
35565		2		-416 0-416; 0-3 (140)
35606		1		-375 0-375
35631		0.5		-350 0-280-78, 0-859 541-33
35664		1		-317 0-375+51, 0-859 541
35701		5		-280 0-2 (140)
35750		5		-231 0-2 (140) 51
35788		5		-193 0-193
35841		5bd	0.5	-140 0-140
35903		6bd	1	-78 0-78; 0-416 344
35948		6b	-	-33 0-375+344
35981		10	10	0 0,0
36032		4	-	+51 0+190-140
36063		5	0.5d	82 0 344 231-33
36171		7	4	190 0-190
36251		4	0.5	270 0 190+82
36325		4	5	+344 0 344
36370		4	5	+389 0 389; 0 2 (190)
36522			5	+541 0 541
36576			0.5d	+595 0+541+51
36736		2	+	755 0+344+389+51-33
36777		6	+	796 0+796
36832		2	+	851 0+796 51

TABLE II (contd.)
Ultraviolet absorption bands of *p*-fluorobenzaldehyde.

Wave number (ν) cm ⁻¹	Relative Intensity		Shift from 0,0 band ($\Delta\nu$) cm ⁻¹	Assignment
	Path-length Pressure	100 cm Reduced	50 cm Normal	
36933			2	+ 952
36967			2	+ 986
36977			1	+ 996
37030			0.5	+1049
37087			4	+1106
37122			4	+1141
37172			8	+1191
37211			5	+1230
37260			4	+1288
37354			6d	+1373
37473			8	+1492
37519			4	+1538
37562			6	+1581
37710			2	+1729
37755			1	+1774
37815			2	+1834
37863			1	+1882
37909			1	+1928
37964			2	+1983
38009			2	+2028
38212			2	+2231
38265			4	+2281
38310			3	+2329
38354			4	+2373
38404			2	+2423
38605			2	+2624
38661			2	+2680
38705			3	+2724
38745			2	+2764
38789			1	+2808
38943			1	+2962
39054			2d	+3073
				0 + 1141 - 193
				0 + 796 + 190
				0 + 1141 - 140; 0 + 996
				0 + 996 + 51
				0 + 1141 - 33
				0 + 1141
				0 + 1191
				0 + 1230
				0 + 1492 - 140 - 2 (33)
				0 + 1191 + 190
				0 + 1492
				0 + 1492 + 51
				0 + 1191 + 389
				0 + 1492 + 190 + 51
				0 + 1230 + 541
				0 + 1492 + 344
				0 + 1492 + 344 + 51
				0 + 1191 + 344 + 389
				0 + 1191 + 796
				0 + 1230 + 796
				0 + 1230 + 996
				0 + 2 (1141)
				0 + 1141 + 1191
				0 + 2 (796 + 389); 0 + 1230 + 1141
				0 + 2 (796 + 389) + 51; 0 + 1230 + 1141 + 51
				0 + 2 (1230) + 190 - 78 + 51
				0 + 1492 + 1191
				0 + 1230 + 1492
				0 + 2 (1191 + 190)
				0 + 2 (1230) + 344
				0 + 2 (796 + 389) + 541 + 51
				0 + 1492 + 1191 + 389

b—broad; d—diffuse; bd—broad and diffuse.

TABLE III
Fundamental frequencies of ground and excited state of monoderivatives of benzaldehyde.

Ground state frequencies				Excited state frequencies												
Ortho hydroxy (benzal dehyde)	Ortho fluoro benzal dehyde	Orthochloro- benzaldehyde			Ortho bromo benzal dehyde	Ortho hydroxy benzal dehyde	Para chloro benzal dehyde	Para fluoro benzal dehyde	Ortho bromo benzal dehyde	Ortho hydroxy benzal dehyde	Para fluoro benzal dehyde	Para chloro benzal dehyde	Vibra- tion mode			
		A. Rao	Padhye and Viladkar	Orthochloro- benzaldehyde												
—	135	—	183	126	—	140	120	—	121	—	111	117	—	—	γC-H	
—	202	—	184	167	—	193	185	—	159	—	174	164	174	190	180	γC-X
269	—	262	285	269	—	—	301	263	—	292	283	249	—	—	—	γC-X
—	340	—	—	—	394	375	—	—	325	—	—	312	326	344	—	βC-C
426	—	414	—	—	—	416	—	410	—	388	—	—	—	389	—	βC-X
558	505	—	—	472	635	636	—	523	468	469	—	453	529	541	—	βC-C
—	—	—	—	—	—	—	—	671	—	—	654	—	—	—	667	γC-X
776	846	—	—	—	861	859	—	763	776	711	717	675	787	796	798	γC-C breathing
—	—	—	—	—	—	—	—	937	968	978	975	977	996	—	—	βC-C
—	—	—	—	—	—	1161	—	1013	1101	1068	1059	1039	1142	1141	1071	βC-H
1232	—	—	—	—	—	—	—	1201	1166	1188	1185	1181	1181	1191	1198	γC-CHO
—	—	—	—	—	—	—	—	—	1242	1257	1256	1242	1267	1230	—	γC-C
—	—	—	—	—	—	—	—	1503	—	—	1475	—	—	1492	1397	γC-C

γ —out of plane bending vibration.

β —in plane bending vibration.

ν —stretching vibration.

TABLE IV

Shift of 0,0 band towards longer wavelength side of monoderivatives of benzaldehyde with respect to 0,0 band of benzene

Isomer	Ortho	Meta	Para
Molecule	cm ⁻¹	cm ⁻¹	cm ⁻¹
Fluoro-benzaldehyde	3758		2108
Chloro-benzaldehyde	4621	4298	2968
Bromo-benzaldehyde	4767	4120	3066
Hydroxy-benzaldehyde	9829	5757	2838

In the end it will not be out of place if something is said about the shift of the 0,0 bands of *o*-, *m*- and *p*-isomers of derivatives of benzaldehyde with respect to the 0,0 band of benzene. It shows that the shift from ortho to para in the case of fluoro-benzaldehydes is in keeping with the observations of other workers in case of other derivatives of benzaldehyde. This shift is *o* \rightarrow *m* \rightarrow *p* as expected for the derivatives of benzene having one substituent as ortho-para directing and the other as meta directing group. It has been observed for a number of *p*-fluoro substituted benzenes that if the spectral shift produced by a first substituent is ortho-para directing then a red shift is produced by the para-substituted fluorine (Cooper 1953). On the other hand if the spectral shift produced by a first substituent is meta directing then a violet shift should be produced by the para substituted fluorine, for example, the shift in the 0,0 band of *p*-fluorobenzonitrile with respect to the 0,0 band of benzonitrile is 100 cm⁻¹ towards the violet. In the present investigations this shift of the 0,0 band (35981 cm⁻¹) of *p*-fluorobenzaldehyde with respect to the 0,0 band (35201 cm⁻¹) of benzaldehyde is 780 cm⁻¹ towards the shorter wavelength side.

ACKNOWLEDGMENTS

The authors are grateful to Dr R. C. Maheshwari and Mr. N. K. Sanyal for useful discussions. They are also thankful to Sri Raj Magal Prasad Jaiswal for supplying the fundamental frequencies of ortho bromobenzaldehyde before publication. The authors express their gratefulness to C.S.I.R. for financial assistance and award of a fellowship to one of them (K.C.S.).

We have been informed that recently a paper by Padhye and Viladkar on the spectra of fluorobenzaldehydes has appeared in the Indian Journal of Pure and Applied Physics, 1963.

REFERENCES

- Buraway, A. and Chamberlain, J. T., 1952, *J. Chem. Soc.*, 2310.
 Chandra, K. and Sharma, D., 1962, *J. Sci. Industr. Res.*, **21B**, 330.
 Cooper, C. D., 1953, *J. Chem. Phys.*, **21**, 379.

- Garg, S. N., 1953-54, *J. Sci. Res. Banaras Hindu University*, **4**, 42.
Lemov, H. W., 1947, *J. Amer. Chem. Soc.*, **67**, 2998.
Morton, R. A. and Stubbs, A. L., 1941, *J. Chem. Soc.*, 1347.
Padhye, M. R. and Viladkar, B. G., 1960, *J. Sci. Industr. Res.*, **19B**, 45.
Padhye, M. R. and Viladkar, B. G., 1961, *J. Sci. Industr. Res.*, **20B**, 530.
Patel, J. C., 1959, *J. Sci. Industr. Res.*, **18B**, 265.
Rao, I. A. and Rao, V. R., 1960, *Ind. J. Phys.*, **34**, 196.
Rao, I. A., 1961, *J. Sci. Industr. Res.*, **20B**, 523.
Rao, K. N. and Spomer, H., 1957, *Canad. J. Phys.*, **35**, 332.
Sklar, A. L., 1939, *J. Chem. Phys.*, **7**, 984.
Sklar, A. L., 1942, *J. Chem. Phys.*, **10**, 135, *Rev. Mod. Phys.* **14**, 232.

INDIRECT SPIN COUPLING IN NiAs TYPE MAGNETIC COMPOUNDS*

K. P. SINHA, M. K. SINHA[†] AND U. N. UPADHYAYA[†]

NATIONAL CHEMICAL LABORATORY, POONA-8

(Received, December 20, 1962; Resubmitted on April 16, 1963)

ABSTRACT. A theoretical study of the spin coupling in the magnetic compounds crystallizing with NiAs structure is made following the spin polarization mechanism developed earlier. For this purpose, a seven centre unit of the crystal, i.e., a trigonal prism with the six magnetic ions at the corners and the anion at the centre, is chosen. Since this mechanism operates through the empty orbitals of the system, crystal field calculations for the empty orbitals on the central ion (excitation model) and empty orbitals on the metal ions (charge transfer model), are carried out. A semi-quantitative estimate of the A-O-B, A-O-C and A-O-D interactions (where A, B, C, D represent the magnetic ions at the various corners of the trigonal prism and O stands for the anion at the centre) on this mechanism gives results in general agreement with the observed magnetic behaviour of the systems.

INTRODUCTION

Magnetic compounds crystallizing with NiAs structure present a difficult system for theoretical studies of magnetic indirect exchange interaction (Kramers 1934). While some compounds are antiferromagnetic (e.g. CrS , CrSe , MnTe , CrSb , etc.) others exhibit ferromagnetic ordering (e.g. CrTe , MnAs , MnSb) (Lotgering and Gorter 1957). The previous predictions (Anderson 1950) that cations having less than half filled d shells will couple ferromagnetically via the anion do not fit with the above systems (e.g. CrS and CrTe assuming that in both Cr has d^4 configuration). Similar difficulties are encountered when one attempts to rationalize such systems with the help of some recent suggestions (Anderson 1959, Wollen 1960.).

In what follows, we study the spin coupling in these systems on the basis of mechanisms recently developed by one of the authors and co-workers (Koide and Sinha 1959, Koide, Sinha and Tanabe 1959) and applied to different types of structures (Sinha and Koide 1960, Sinha 1961, Sinha and Sinha 1962). In essence, the mechanism takes into account the spin polarization of the anion electrons and the delocalization of the cation electrons operating through the agency of an ortho-normalized set of empty orbitals for the unit chosen with respect to the occupied anion and cation orbitals. For actual calculations, however, only a few

* Communication No. 521 from the National Chemical Laboratory, Poona-8 (India).

† C.S.I.R. Research Fellows.

excited low lying orbitals are considered in that others will not be important because of large energy denominators.

CHOICE OF THEORETICAL MODEL

For this purpose, first a brief description of NiAs type structure is in order. The structure is hexagonal ($P6_3/mmc$ or D_{6h}^4) with each type of atom surrounded by six of the other. The anion or metalloid (e.g. S, Te or As) is surrounded by six metal ions (e.g. Cr^{2+} or Mn^{2+}) at apices of a trigonal prism. The metal ion, on the other hand, is surrounded octahedrally by six anions which are the immediate neighbours with two metal ions which are relatively closer than other metal ions.

The appropriate unit for describing the cation-cation and cation-anion-cation interactions for this system seems to be one trigonal prism with the metal ions at the corners and the anion at the centre. The unit chosen is shown in Fig. 1. The point symmetry group of this unit is D_{3h} . Likewise for the cation, the point symmetry group is a superposition of octahedral (due to six anions octahedrally co-ordinated) and the axial symmetry (owing to the presence of two cations one above and the other below lying on the $\langle III \rangle$ axis of the octahedron defined by the anions). In classifying the atomic orbitals of the anion and cations we shall make use of the crystal field pertaining to the appropriate point symmetry groups as described above (Fig. 2 for cation surrounding)

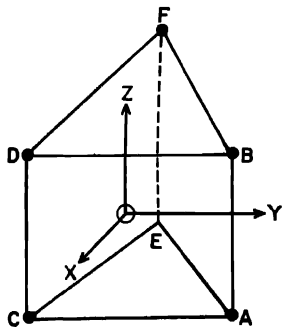


Fig. 1. Geometry of the model chosen. Open circle represents anion or metalloid and full circle a metal ion.

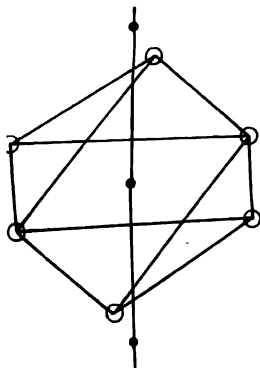


Fig. 2. Disposition of the anion octahedron and the two nearest neighbour metal ions around the central ion.

For the classification of anion orbitals (e.g. Te, Se, S) in the appropriate surrounding the outermost shell is taken into consideration i.e. $ns^2 np^6$ (the orbitals in $(n-1)$ shells downwards will be treated as constituting the ion core). The

s^2p^6 description is not convenient for the present unit and hence we have to take into account the hybridisation of sp orbitals. If we consider the z axis as the line passing through the anion 0 and normal to the planes defined by the three cations above and below, then the following choice of orbitals seems appropriate: p_z and the three trigonal orbitals $\sigma_1, \sigma_2, \sigma_3$, given by,

$$\sigma_1 = \sqrt{\frac{1}{3}} s + \sqrt{\frac{2}{3}} p_x \quad \dots (1)$$

$$\sigma_2 = \sqrt{\frac{1}{3}} s - \sqrt{\frac{1}{6}} p_x + \sqrt{\frac{1}{2}} p_y \quad \dots (2)$$

$$\sigma_3 = \sqrt{\frac{1}{3}} s - \sqrt{\frac{1}{6}} p_x - \sqrt{\frac{1}{2}} p_y \quad \dots (3)$$

The advantage of the above choice is that each of the σ 's points mid-way towards the two cations lying on the vertical edges of the trigonal prism (e.g. AB) with p_z passing through the principal axis of symmetry. Thus the outer electronic configuration considered here amounts to $p_z^2 \sigma_1^2 \sigma_2^2 \sigma_3^2$. In view of the equivalence of σ_1, σ_2 and σ_3 , we shall choose only one of these orbitals along with p_z i.e. the configuration $np_z^2 n\sigma_1^2$ for describing the spin coupling in the subsequent calculations.

We now consider excited orbitals for an electron centred on the anion and moving in its field as well as the field of the cations at the corners of the trigonal prism. For this purpose, one electron of the anion is assumed to be promoted to excited orbitals, the energies of the various orbitals being calculated as in an atom under the influence of the crystal field. To fix ideas, let us first consider the possible excited orbital configurations for the ions S^{2-} , Se^{2-} and Te^{2-} . For S^{2-} the occupied outer shell configuration is $3s^2 3p^6$ and hence the low lying excited orbitals to be considered on this ion are $4s$ and $3d$. Likewise, for Se^{2-} , with outermost filled shell structure $4s^2 4p^6$ the possible empty orbitals are $5s$ and $4d$. On the other hand, for Te^{2-} with $5s^2 5p^6$ the possible excited empty orbitals will be $6s, 4f$. Of these, the d and f orbitals will undergo splitting under the influence of the trigonal crystal field. A rough estimate of this will be given now.

For the point group D_{3h} , the expression of the crystal field is given by (Low 1960)

$$V_{D_{3h}} = A_0^0 Y^0 + A_2^0 Y_2^0 + A_4^0 Y_4^0 + A_6^0 Y_6^0 + B_6(Y_6^6 + Y_6^{-6}) + \dots \quad \dots (4)$$

where A 's and B 's are the coefficients and Y 's are the normalized spherical harmonics. The coefficients for each system were determined by evaluating the expression given by Low (1960), the cations at the corners being treated as positive point charges. The effect of the first term in (4) is to give a constant shift of all the orbital levels. The other terms do not effect the s orbitals. The orbitals which

are most effected are the d and f . The splitting of empty d orbitals for S^{2-} and Se^{2-} is shown in Fig. 3. A similar calculation for $4f$ empty orbitals on Te^{2-} yields the level scheme as shown in Fig. 4.

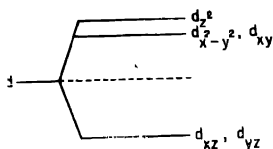


Fig. 3. Level scheme for a $3d$ electron in crystal field with D_{3h} symmetry.

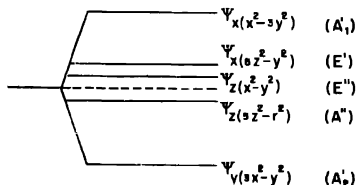


Fig. 4. Level scheme for an f electron in $V_{D_{3h}}$.

The splitting of the cation occupied and empty orbitals (e.g. for Cr^{2+} or Mn^{2+}) are determined for an octahedral field due to six anions and an axial field due to two cations lying on $\langle 111 \rangle$ axis (i.e. z) one above and the other below. The crystal field is expressed as

$$V = V_c + V_a \quad \dots (5)$$

$$= A_0^0 Y_0^0 + A_2^0 Y_2^0 + A_4^0 Y_4^0 + D_4^0 \left[Y_{-4}^0 \sqrt{\frac{10}{7}} \left((Y_4^3 + Y_4^{-3}) \right) \right] + \dots (6)$$

For the case of d^4 type ions (e.g. Cr^{2+} or Mn^{2+}) one can calculate the splitting for a positive d electron hole in d^5 configuration. The level scheme calculated on this basis turns out to be as shown in Fig. 5.

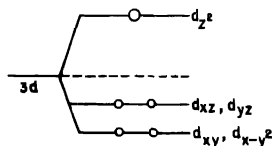


Fig. 5. Level scheme for d electron of a d^4 ion placed in the crystal field of symmetry of Fig. 2.

Thus for a weak field case the four electrons of d^4 type ion will be distributed in the low lying orbitals d_{xy} , $d_{x^2-y^2}$, d_{xz} , d_{yz} and the hole will exist in the upper d_{z^2} orbital. For d^5 ion (i.e. Mn^{2+}), all the orbitals will be singly occupied.

Further among the low lying empty orbitals for d^6 (e.g. Mn^{2+}) ion i.e. $4s$ and $4p$, calculations based on the potential given by eq. (5) shows that the p_z orbital is depressed whereas p_x and p_y are pushed up, the s orbital being unaffected by the axial field.

As suggested before (Koide, Sinha and Tanabe 1959, Sinha 1961), the excited orbitals which are involved in the electron transition in the present mechanism

are selected both on the 'excitation model' as well as 'charge transfer model'. The orbitals on the anions which are made available as a result of crystal field depressions constitute the orbitals according to the excitation model.

In the charge transfer model, we take such linear combinations of the empty cation orbitals (e.g. d_{z^2} , s , etc. on d^1 type ions and p_z , s etc. on d^5 type ions) which belong to the various irreducible representations of the point symmetry group of the unit chosen. For the bigger seven centre system (see Fig. 1) one has to classify such orbitals based on the point group D_{3h} . However, the calculations for a ten electron system for this unit (i.e. four electrons from the central ion and one each from the cations) will become unwieldy. We shall, therefore, study the interactions between the various ions separately, namely, A-B, A-C and A-D via the central ion (see Fig. 1). We shall classify such orbitals for each dicationic unit according to the relevant symmetry element present.

In the case of systems such as CrS, CrSe, CrTe, the empty orbitals on the metal ions are of even symmetry namely, $3d_{z^2}$ and will be denoted by d_k where k stands for (a, b, c, d , etc.). The appropriate molecular orbitals formed for each di-cationic unit will be orthogonalized with respect to the $p_0(=p_z)$ and $\sigma_0(-\sigma_z)$ orbitals of the central ion.

Thus for A-B unit we have

$$\phi_g(d) = (d_a + d_b - 2s_{ag}\sigma_0)/\sqrt{2(1 - 2s_{ag}^2)} \quad \dots (7)$$

$$\phi_u(d) = (d_a - d_b - 2s_{ag}p_0)/\sqrt{2(1 - 2s_{ap}^2)} \quad \dots (8)$$

where the symmetry element is taken to be the reflection in the xy plane passing through the central ion; g and u stand for even and odd respectively and

$$S_{ag}\sigma = \langle d_a | \sigma_0 \rangle, \quad S_{ap} = \langle d_a | p_0 \rangle \quad \dots (9)$$

are the overlap integrals. Owing to overlap considerations, the role of σ_0 orbital is not expected to be important in the study of A-C and A-D interactions. These interactions will therefore be considered through the p_0 orbital of the central ion. The molecular orbitals for other units can be expressed in the same manner.

In what follows, we first present the formal theory and then consider the specific cases in the subsequent sections.

FORMULATION OF INTERACTION MECHANISM

For each type of interaction under study, we choose a "three centre and a six electron" system represented by M_1OM_2 . Of these, four electrons belong to the central ion and are assumed to exist in the configuration $p_z^2\sigma_z^2$. Further, we consider one representative electron from each magnetic ion M_1 and M_2 and the respective orbitals are denoted by u_1 and u_2 . The orbitals may be taken to be

either $d_{x^2-y^2}$, d_{xy} or d_{yz} , d_{zx} . Two possibilities might exist; under reflection in the plane bisecting normally the line joining the two metal ions or any appropriate rotation by 180° we may have

$$\begin{array}{ccc} R & & R \\ u_1 \longleftrightarrow u_2, \text{ or } & u_1 \longleftrightarrow -u_2 & \dots \quad (10) \end{array}$$

with R standing for the appropriate symmetry operation. The set of excited orbitals are formally denoted by ϕ_g, ϕ_u . With the above definition in mmd, the wave functions of the total system which constitute the eigenstates of the S^2 operator are written below.

Ground State

Triplet :

$$|{}^3\psi_0\rangle_{od} = {}^3\{{}^1(u_1 u_2){}^1(p_0)^2 {}^1(\sigma_0)^2\} \quad \dots \quad (11)$$

Singlet :

$$|{}^1\psi_0\rangle = {}^1\{{}^1(u_1 u_2){}^1(p_0)^2 {}^1(\sigma_0)^2\} \quad \dots \quad (12)$$

Excited States - involving one electron transition from p_0 orbital.

Triplets

$$|{}^3\psi_1(g, u)\rangle_{od, ev} = {}^3\{{}^1(u_1 u_2) {}^3(p_0 \phi_g, u) {}^1(\sigma_0)^2\} \quad \dots \quad (13)$$

$$|{}^3\psi_2(g, u)\rangle_{ev, od} = {}^3\{{}^3(u_1 u_2) {}^3(p_0 \phi_g, u) {}^1(\sigma_0)^2\} \quad \dots \quad (14)$$

Singlets

$$|{}^1\psi_1(g, u)\rangle_{ev, od} = {}^1\{{}^3(u_1 u_2) {}^3(p_0 \phi_g, u) {}^1(\sigma_0)^2\} \quad \dots \quad (15)$$

For one electron transitions from the σ_0 orbital, we shall have similar expressions as above except that the role of p_0 and σ_0 is interchanged. The notations ev , od denote the symmetry of the total wave function under the appropriate symmetry operation.

The matrix elements of the Hamiltonian (in atomic units $c = \hbar = m = 1$)

$$H = \sum_i H_i + \sum_{i < j} \frac{1}{r_{ij}} \quad \dots \quad (16)$$

within the manifold given above are easily obtained following the methods of earlier papers (Sinha *et al.* 1959 to 1962).

The energies of the ground triplet and singlet states are given respectively as

$${}^3E_0 = E_0 - J(u_1 u_2) \quad \text{and} \quad {}^1E_0 = E_0 + J(u_1 u_2)$$

their mean being E_0 . Likewise, for the energies of the various excited triplet and singlet states we shall take a mean $E_m = Q_{g, u}$ neglecting the relatively small

exchange integrals compared to coulomb and one electron terms contained $Q_{\theta u}$. The singlet or triplet depressions, other than those due to direct exchange $J(u_1 u_2)$ can be expressed in the second order perturbation of the various zeroth order ground states as a result of interaction with the excited states (Sinha *et al*)

$$\delta E(2S+1) = \sum_m \frac{\langle S_{p,\sigma} = 0 | H | S_{p,\sigma} = 1 \rangle \langle S_{p,\sigma} = 1 | H | S_{p,\sigma} = 0 \rangle}{E_m - E_0} \quad (17)$$

Thus the splitting of energies between the triplet and singlet can be expressed as

$$\begin{aligned} 2J_{ff} - 3E - 1E \\ = \left\{ \sum_g \frac{4}{E_g - E_0} \left| \langle u_1 \phi_g | u_1 \phi_0 \rangle \right|^2 - \sum_u \frac{4}{E_u - E_0} \left| \langle u_1 \phi_u | u_1 p_0 \rangle \right|^2 \right\} \\ + \left\{ \sum_g \frac{4}{E_g - E_0} \left| \langle u_1 \phi_g | u_1 \sigma_0 \rangle \right|^2 - \sum_u \frac{4}{E_u - E_0} \left| \langle u_1 \phi_u | u_1 \sigma_0 \rangle \right|^2 \right\} \\ - 2J(u_1 u_2) \end{aligned} \quad (18)$$

If we were to disregard the effect of the direct exchange for the time being, the coupling due to the spin polarization mechanism (i.e. terms in the curly brackets) is dependent on the relative symmetry of ground and excited orbitals as well as their energy difference. Transitions between orbitals having the same symmetry stabilize the triplet state and those between orbitals of different symmetry stabilize the singlet state. When the excited orbitals $\phi_{\theta,u}$ are centred on the anion, they are automatically orthogonal to the ground state atomic orbitals p_0 or σ_0 . However, for the molecular orbitals constituted as in (7) to (8) from the cation empty orbitals the overlap integrals such as S_{ap} , S_{au} will be important. Thus for the choice of orbitals as in (7) and (8), the hybrid exchange integrals of the type $\langle u_1 u_{p,n} | u_1 \phi_{gu} \rangle$ take the following specific forms.

$$\langle u_1 \phi_p | u_1 p_0 \rangle = \{ \langle u_1 d_a | u_1 p_0 \rangle + \langle u_1 d_b | u_1 p_0 \rangle - 2s_{au} \langle u_1 \sigma_0 | u_1 p_0 \rangle \} / \sqrt{2(1 - 2S_{au}^2)} \quad \dots \quad (19)$$

$$\langle u_1 \phi_u | u_1 p_0 \rangle = \{ \langle u_1 d_a | u_1 p_0 \rangle - \langle u_1 d_b | u_1 p_0 \rangle - 2s_{ap} \langle u_1 p_0 | u_1 p_0 \rangle \} / \sqrt{2(1 - 2S_{ap}^2)} \quad \dots \quad (20)$$

$$\langle u_1 \phi_u | u_1 \sigma_0 \rangle = \{ \langle u_1 d_a | u_1 \sigma_0 \rangle - \langle u_1 d_b | u_1 \sigma_0 \rangle - 2S_{ap} \langle u_1 p_0 | u_1 \sigma_0 \rangle \} / \sqrt{2(1 - 2S_{ap}^2)} \quad \dots \quad (21)$$

$$\langle u_1 \phi_p | u_1 \sigma_0 \rangle = \{ \langle u_1 d_a | u_1 \sigma_0 \rangle + \langle u_1 d_b | u_1 \sigma_0 \rangle - 2S_{au} \langle u_1 \sigma_0 | u_1 \sigma_0 \rangle \} / \sqrt{2(1 - 2S_{au}^2)} \quad \dots \quad (22)$$

The integrals of the type $\langle ab/cd \rangle$ represent the coulomb interaction $(1/r_{12})$ between the two charge densities $a^*(1)$ $b(1)$ and $c^*(2)$ $d(2)$. The magnitude of the integrals occurring on the left hand side of (19) to (22) will depend on the sign and magnitude of the various integrals on the right hand side. The integrals of the

type $\langle u_1 d_b | u_1 p_0 \rangle$, $\langle u_1 d_b | u_1 \sigma_0 \rangle$ and $S \langle u_1 \sigma_0 | u_1 p_0 \rangle$ are expected to be negligible owing to their disposition and overlap considerations.

We shall now discuss the specific interactions namely, AOB, AOC and AOD based on the concepts developed above.

APPLICATION TO SPECIFIC CASES

First, we consider the A-B interaction in the unit A-O-B. The symmetry element is reflection in the xy plane passing through O and bisecting normally the line AB. The anion orbitals σ_0 and p_0 (p_z) have already been described (cf. equations (1) to (3)). For the singly occupied cation orbitals u_1 and u_2 in the case of CrS, CrSe, CrTe, we choose d_{yz} (d_{zx}) which has the maximum overlap with the anion orbitals. In the case of MnTe like systems, d_{z^2} type orbitals will be chosen to represent u_1 and u_2 .

The choice of empty orbitals on the anion and cations is guided by crystal field depressions of the next shell orbitals. For CrS, CrSe, the empty orbitals on the anion centre are taken to be d_{yz} , d_{zx} (cf. Fig. 3) both odd under the above operation and for CrTe, the lowest is $\psi_g(3x^2 - y^2)$ being an even orbital, the others lying appreciably higher up. For empty orbitals on cations, $3d_{z^2}$ is taken for $\text{Cr}^{2+}\text{X}^{2-}$ system and $4p_z$ for $\text{Mn}^{2+}\text{X}^{2-}$ systems. These orbitals have been chosen both from energy as well as overlap considerations.

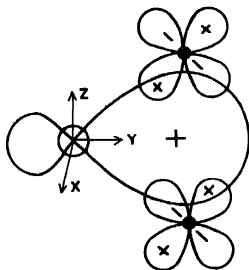


Fig. 6 Schematic representation of the σ_0 and d_{yz} orbitals for AOB interaction.

It may be remarked that the cations are closest in AOB unit compared to other units. Further from overlap considerations the occupied orbital of the anion which partakes more strongly in the indirect exchange interaction is σ_0 rather than p_0 (See Fig. 6). The effective exchange integral for this unit can be written for CrS, CrSe (with d_{e_1} standing for d_{yz} , or d_{zx} on anion and ϕ_θ or ϕ_u as given by (7) and (8) d_u being d_{z^2}) as

$$2J_{eff} = \left\{ \frac{4}{\Delta E_{e_1}} |\langle u_1 d_{e_1} | u_1 \sigma_0 \rangle|^2 + \frac{4}{\Delta E_u} |\langle u_1 \phi_u | u_1 \sigma_0 \rangle|^2 - \frac{4}{\Delta E_\theta} |\langle u_1 \phi_\theta | u_1 \sigma_0 \rangle|^2 \right\} - 2J(u_1 u_2) \quad (23)$$

Since optical experiments on similar systems indicate that anions effectively shield the metal ions from one another (Casselman and Keffer 1960), the direct exchange is expected to be very feeble. We, therefore, neglect $J_T(u_1u_2)$. The terms in (23) owing to the excitation model i.e. $\sum_i 4 | \langle u_1 d_{\epsilon_i} | u_1 \sigma_0 \rangle |^2 / \Delta E_{\epsilon_i}$, stabilize the singlet state. The terms due to charge transfer are better understood on expanding the integrals in atomic orbitals.

$$4 | \langle u_1 \phi_u | u_1 \sigma_0 \rangle |^2 \approx \frac{4 | \langle u_1 d_u | u_1 \sigma_0 \rangle |^2}{\Delta E_u [2(1 - 2S_{au}^2)]} \quad (24)$$

$$\frac{4 | \langle u_1 \phi_y | u_1 \sigma_0 \rangle |^2}{\Delta E_y} \approx 4 | \{ \langle u_1 d_u | u_1 \sigma_0 \rangle - 2S_{au} \langle u_1 \sigma_0 | u_1 \sigma_0 \rangle \} |^2 \dots \quad (25)$$

Using Mulliken's approximation (Mulliken 1953), we can write

$$\langle u_1 d_a | u_1 \sigma_0 \rangle = \frac{1}{2} S_{1a} \{ \langle u_1 d_a | u_1 u_1 \rangle + \langle u_1 d_a | \sigma_0 \sigma_0 \rangle \} \quad \dots \quad (26)$$

where $S_{1a} = \langle u_1 | \sigma \rangle$. The integral of the type centred at one cation, will be zero unless the azimuthal quantum numbers of the orbitals satisfy (Condon and Shortley 1953)

$$m_l(u_1) + m_l(d_a) = m_l(u_1) + m_l(u_1) \quad \dots \quad (27)$$

This will have finite value only when the orbitals involved are of the type d_z^2 , p_z , etc. For the present case when u is d_{yz} or d_{xy} and $d = d_z^2$, this integral vanishes. Thus to a rough approximation

$$2J_{eff}(CrSe, CrS) \approx 4 \left\{ \sum_i \frac{| \langle u_1 d_{\epsilon_i} | u_1 \sigma_0 \rangle |^2}{\Delta E_{\epsilon_i}} - \frac{2S_{au}^2 | \langle u_1 \sigma_0 | u_1 \sigma_0 \rangle |^2}{\Delta E_u (1 - 2S_{au}^2)} \right\} \quad (28)$$

In view of the S_{au}^2 factor and the overlap of $u_1 \sigma_0$ which is expected to be smaller when $u_1 = d_{yz}$ than when it is d_z^2 , the last term in (29) will be relatively small compared to first terms. Thus the singlet state is likely to be more stabilized and the coupling in CrSe, CrS will be antiferromagnetic. For CrTe where the excitation orbitals is $f_a - \psi_y (3x^2 - y^2)$ we get

$$2J_{eff}(CrTe) \approx 4 \left\{ - \frac{| \langle u_1 f_a | u_1 \sigma_0 \rangle |^2}{\Delta E_a} - \frac{2S_{au}^2 | \langle u_1 \sigma_0 | u_1 \sigma_0 \rangle |^2}{\Delta E_u (1 - 2S_{au}^2)} \right\} \quad \dots \quad (29)$$

The above, of course, always stabilises the triplet state and the coupling will be ferromagnetic. While considering the case of MnTe, we recapitulate that $u_1 = d_z^2$ and $d_a = p_z$ and hence the integral $\langle u_1 d_a | u_1 u_1 \rangle$ is quite appreciable. (Koide, Sinha and Tanabe 1959). Further the overlap density $u_1 \sigma_0$ is expected to be quite appreciable. However, as shown before, the first and second terms in

(25) nearly cancel each other and accordingly the effective exchange integral for MnTe can be written as

$$2J_{eff}(\text{MnTe}) = 4 \left\{ \frac{|\langle u_1 \phi_u | u_1 \sigma_0 \rangle|^2}{\Delta E_u} - \frac{|\langle u_1 f_d | u_1 \sigma_0 \rangle|^2}{\Delta E_d} \right\} \dots \quad (30)$$

In view of the large overlap of d_{z^2} , p_z with σ_0 and smaller energy denomination it is expected that the charge transfer model will be more important in the present case and hence the second term in (30) will be of smaller magnitude. Therefore (30) would stabilize the singlet state.

For MnAs, MnSb also, the charge transfer model will be more important owing to a high degree of covalency but the choice of orbitals for u_1 and d_u is the same as CrTe and accordingly the coupling is expected to be ferromagnetic. In the case of CrSb, the metal ion ground state configuration will be d^3 , with d_{z^2} , d_{yz} , d_{xy} being pushed down and $d_{x^2-y^2}$, d_{xz} pushed up. For the excited orbital however, p_z is pushed down owing to crystal field effects. Thus the choice of u_1 and d_u is the same as MnTe and the charge transfer model would lead to a stabilization of the singlet state.

Study of AOC Interaction

As indicated before, the role of σ_0 orbital of the central ion will not be of importance for the present unit as compared to the p_0 orbitals. Further, using the criterion of maximum overlap (in Fig. 7), the choice of u_1 for d^4 ions is $d_{x^2-y^2}$, (d_{xy}). On the same basis it can be seen that the excited orbital such as d_{yz} (d_{xz}) on the excitation model on S, Se, Te, etc. will have lesser significance than the s orbital to a certain extent. Thus for A-C interaction, we discuss the charge transfer model and the s -orbital effect for the excitation model. Now $p_0 (= p_z)$ is an even orbital under reflection in XZ plane. Hence for d^4 type ions (CrS, CrSe, CrTe, MnAs, MnSb) with $u_1 = d_{x^2-y^2}$, $d_u = d_{z^2}$ the effective interaction can be written as

$$2J_{eff} = -4 \left\{ \frac{2S_{ap}^2 |\langle u_1 p_0 | u_1 p_0 \rangle|^2}{\Delta E_u(1-2S_{ap}^2)} - \frac{|\langle u_1 s | u_1 p_0 \rangle|^2}{\Delta E_s} \right\} \dots \quad (31)$$

which would always favour parallel coupling between A and C . The above is also true for CrSb except that $u_1 = d_{z^2}$ and $d_u = d_{x^2-y^2}$. In the case of systems such as MnTe, CrSb with $d_u = p_z$ and noting that S_{ap} is likely to be negative (See Fig. 7), we have

$$2J_{eff} = 2 \left\{ \frac{|\langle u_1 d_u | u_1 p_0 \rangle|^2}{\Delta E_d} - \frac{|\langle u_1 d_u | u_1 p_0 \rangle + 2 |S_{ap}| |\langle u_1 p_0 | u_1 p_0 \rangle|^2}{\Delta E_u(1-2S_{ap}^2)} \right\} \dots \quad (32)$$

which assuming that ΔE_d and $\Delta E_u(1-2S_{ap}^2)$ are comparable would be negative in sign and hence the parallel case is again favoured. One can, therefore, conclude

that A-C interaction is ferromagnetic in all cases although the strength of the interaction will be weaker compared to A-B interaction.

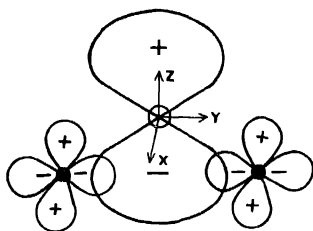


Fig. 7 Schematic representation of the p_0 and d_{32-y^2} orbitals for AOC interaction

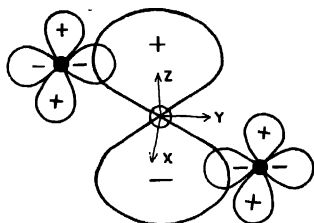


Fig. 8 Same as Fig. 7, for AOD interaction.

Study of AOD Interaction.

In this situation also the effective anion orbital would be p_0 which is odd under rotation by 180° around x -axis. With $u_1 = d_{x^2-y^2}$, $d_a = d_{z^2}$ and excitation orbital s , the effective exchange integral for CrS, CrSe, where excitation model is more important is given by

$$2J_{eff} = | \langle u_1 s | u_1 p_0 \rangle |^2 / \Delta E'_s \quad (33)$$

and for the systems CrTe, MnAs, JnSb where the charge transfer mechanism is expected to be important (cf. § 6) it is

$$2J_{eff} = -2 | \langle u_1 d_a | u_1 p_0 \rangle |^2 / \Delta E_d \quad (34)$$

The former (cf. eq. 33) favours antiferromagnetic stabilization and the latter (cf. eq. 34) ferromagnetic. For the systems MnTe, CrSb, with $u_1 = d_{z^2}$, $d_a = p_z$ the charge transfer process gives

$$2J_{eff} = 2 | \langle u_1 d_a | u_1 p_0 \rangle |^2 / \Delta E_d \quad (35)$$

favouring antiferromagnetic coupling between A and D. It may be noted that the weaker AOD interaction is acting in the same direction as the A-B interaction for the said systems.

GENERAL CONCLUSIONS

The foregoing analysis shows that in the NiAs type magnetic compounds the spin-polarization mechanism provides a reasonable explanation of the observed spin coupling. It shows that the strongest interaction based on this mechanism is A-O-B i.e. between the closest magnetic ions via the σ_0 orbital of the anion. The A-O-C and A-O-D interactions are feeble, the former always giving rise to parallel alignment, the latter strengthening A.O.B interaction.

The details of these interactions can be classified under two headings, namely: (1) Coupling via excited orbitals belonging to the central ion (excitation model) and (2) Coupling via excited cationic orbitals (charge transfer model).

In deciding as to which of the two models plays a dominant role in specific cases, we are guided by a rough idea of the energy denominators as well as the hybrid exchange integrals occurring in the numerators (c.f. eq. (22)). Further, we now briefly assess the energy denominators. On the excitation model, the foregoing analysis tacitly assumes that only those excited empty orbitals on the central ion constitute a semilocalized bound state, which are depressed owing to the crystal field perturbations. In addition to the constant shift of all the levels, the splitting of *p*, *d* or *f* levels will be of the order of 2 to 5 eV, as the estimate made here and in earlier work shows (Sinha *et al.* 1962). Further the energy denominators occurring in equation (18) can be taken to be equal to the excitation energy to the appropriate excited orbital (atomic or molecular). For the orbitals on the excitation model we estimate this from atomic energy states for the free ions (e.g. *S*) (Watson 1958) plus $2|e|$ well. Thus S^{2-} ion in a crystal would be approximately equivalent to argon atom along with additional corrections due to crystal field splittings. For the charge transfer model, we estimate the energy denominators as approximately equal to the energy involved in transferring one electron from the anion to cation which in turn is roughly derived from the appropriate ionization potential of the metal ion and the electron affinity of the anions. (Koide, Sinha and Tanabe 1959). The tentative estimates are indicated below:

<i>Substance</i>	$\Delta E(\text{excitation})$	$\Delta E(\text{charge transfer})$
CrS, CrSe	10 ev.	> 20 ev.
CrTe	~15 ev.	~15 ev.
MnTe	~15 ev.	< 15 ev.

From the above, it appears that in compounds such as CrS, CrSe or generally $M^{2+}X^{2-}$ (*X* being S and Se), the excitation model dominates and leads to antiferromagnetic coupling. For *MX* where *X* is Te, As, Sb it seems that, in general, the charge transfer model will dominate the excitation mechanism. In CrTe, both may be equally important but they act in the same direction. This is quite consistent with the stronger covalency in MTe, MAs, MSb etc. We have already discussed before as to which of the hybrid exchange integrals are likely to be important. A numerical estimate for the various exchange and overlap integrals is not attempted keeping in mind the hopelessly difficult job of having an accurate knowledge of the various orbitals involved in such systems. No Hartree-Fock calculations are available except for some free transition metal ions. It is hoped that a better knowledge of electronic orbitals in crystals in future will render it possible to make quantitative estimates.

REFERENCES

- Anderson, P. W., 1950, *Phys. Rev.*, **79**, 350.
Anderson, P. W., 1959, *Phys. Rev.*, **115**, 2
Cusack, T. N. and Keller, F., 1960, *Phys. Rev. Letters*, **4**, 498
Condon, E. U. and Shortley, G. H., 1953. *Theory of Atomic Spectra* (Cambridge).
Koride, S. and Sinha, K. P., 1959, *Bussanri Kenkyu* (January Issue) in Japanese.
Koride, S., Sinha, K. P. and Tanabe, Y., 1959, *Progr. Theoret. Phys.*, **22**, 617.
Kramers, H. A., 1934, *Physica*, **1**, 182.
Lotgering, F. K. and Gorter, E. W., 1957, *J. Phys. Chem. Solids*, **3**, 238.
Low, W., 1960, *Solid state physics*, supplement 2, Edited by F. Seitz and D. Turnbull (Academic Press).
Mulliken, R. S., 1953, *J. Chem. Phys.*, **21**, 466
Sinha, K. P. and Koride, S., 1960 *Sci. Pap. coll. Gen. Edu. University of Tokyo*, **10**, 195.
Sinha, K. P., 1961, *Ind. J. Phys.*, **35**, 111, 481.
Sinha, K. P. and Sinha, M. K., 1962, *Ind. J. Phys.*, **36**, 439
Watson, R. E., 1958, *Phys. Rev.*, **111**, 1108.
Wollan, E. O., 1960, *Phys. Rev.*, **117**, 387.

THEORETICAL POLARISATIONS OF HIGH FREQUENCY RADIO WAVES AT A LOW LATITUDE STATION

C. ABHIRAMA REDDY

IONOSPHERIC RESEARCH LABORATORIES, ANDHRA UNIVERSITY, WALTAIR.

(Received, November 3, 1962)

ABSTRACT. The polarisations of vertically propagated high frequency radio waves have been evaluated from the Appleton-Hartree formula for the latitude of Waltair (Geomagnetic Lat. 7.4°N , Dip angle 20°) by the rigorous computational method. The variations of the axial ratio and the tilt angle of the polarisation ellipse with electron density, collisional frequency and wave frequency are directly delineated so as to make possible a ready comparison with experimentally measured values of the above parameters.

INTRODUCTION

There are two principal methods of numerically evaluating the theoretical polarisations of ionospherically propagated radio waves from the Appleton-Hartree formula. One is the graphical method developed by Bailey (1934) and another is the computational method, which was also outlined by Bailey (1938). Both of these methods have been used by many workers for obtaining the general curves of polarisation parameters for a variety of propagation conditions (Martyn 1935, Murthy and Khastgir 1960; Ghosh 1938; Singh and Murthy 1958; Scott 1950; Taylor 1933; 1934; Snyder and Hellivell 1952 and Ratcliffe 1959).

It is the purpose of the present communication to describe the results obtained from an extensive series of calculations of polarisation parameters for vertical propagation conditions at Waltair, which is a low latitude station (Geomag. Lat. 7.4°N , Dip angle 20°).

DESCRIPTION OF THE METHOD

The magneto-ionic equation for the complex polarisation (R) of the radio waves can be written in the form .

$$R = i[(\eta + i\xi) \pm \{(\eta + i\xi)^2 + 1\}^{1/2}] \quad \dots (1)$$

where

$$\eta = X/(X^2 + Y^2) ; \xi = Y/(X^2 + Y^2)$$

$$X = \frac{(1-x)p}{v_c} ; Y = v/v_c$$

*Communicated by Prof B. Ramachandra Rao.

$$x = \frac{4\pi N e^2}{m p^2} \quad z = v/p$$

$$v_e = \left| \frac{P_H \sin^2 \theta}{2 \cos \theta} \right|$$

$$P_H = \frac{H e}{m c} = \text{angular gyrofrequency of electrons}$$

H = Strength of the earth's magnetic field

θ_p = Angle between the direction of propagation and the direction of the magnetic field.

p = Angular frequency of the wave

v = Collisional frequency of electrons

e, m = Charge and mass of an electron.

c = Velocity of e.m. waves in free space.

N = Number density of electrons.

Following the procedure outlined by Bailey (1938) eq. (1) can be transformed into the form :

$$R = r + is = i \left[(\eta + i\xi) \mp \left\{ \left(\frac{C+A}{2} \right)^{\frac{1}{2}} + i \left(\frac{C-A}{2} \right)^{\frac{1}{2}} \right\} \right] \quad \dots (2)$$

where

$$A = \eta^2 - \xi^2 + 1.$$

$$B = 2\xi\eta$$

$$C = [(A^2 + B^2)^{\frac{1}{2}}]$$

From a detailed analysis it can be shown that the upper negative sign in eq. (1) and (2) refers to the ordinary magneto-ionic component while the lower positive sign refers to the extraordinary component. Thus, denoting the ordinary wave polarisation by R_0 , we can write .

$$R_0 = r_0 + is_0 \quad \dots (3)$$

where

$$\left. \begin{aligned} r_0 &= - \left(\xi - \sqrt{\frac{C-A}{2}} \right) \\ s_0 &= \left(\eta - \sqrt{\frac{C+A}{2}} \right) \end{aligned} \right\} \quad \dots (4)$$

Using the positive sign before the radical in eq. (2) and proceeding as above we obtain for the extraordinary wave

$$R_e = r_x + isx$$

where

$$\left. \begin{aligned} r_x &= -\left(\xi + \sqrt{\frac{C-A}{2}}\right) \\ s_x &= \left(\eta + \sqrt{\frac{C+A}{2}}\right) \end{aligned} \right\} \dots \quad (5)$$

Thus, starting from a pair of values of ξ and η , the polarisation parameters, r and s , of either characteristic wave can be calculated through A , B , C and equations (4) and (5). From the known values of r and s , the tilt angle (ψ) and the axial ratio (ϵ) of the polarisation ellipse can be calculated from the following set of equations:

$$r^2 + s^2 = \rho^2 \quad (6)$$

$$\tan^{-1}(s/r) = \phi \quad (7)$$

$$\tan 2\psi = \frac{2\rho \cos \phi}{\rho^2 - 1} \quad (8)$$

$$\epsilon^2 = \tan^2 \theta = \frac{\rho^2 + 1 - \sqrt{(\rho^2 - 1)^2 + 4\rho^2 \cos^2 \phi}}{\rho^2 + 1 + \sqrt{(\rho^2 - 1)^2 + 4\rho^2 \cos^2 \phi}} \quad (9)$$

$$\epsilon = \frac{\text{semi-minor axis}}{\text{semi-major axis}}$$

ψ = the angle between the major axis of the ellipse and the magnetic north direction.

The electric vector is considered in all the above equations.

But, the above method of obtaining ψ and ϵ corresponding to a set of r and s values is rather laborious, and a simpler graphical method, which gives the parameters ψ and ϵ to an accuracy sufficient for comparison with experimental values, is used. This method is based on the analysis given by Booker (1934) of the complex polarisation R which is represented in a complex plane. He had shown that all possible polarisations can be known from points in the first quadrant of a unit circle in the complex R -plane, by using proper signs and inversions depending upon the signs of X and Y . Therefore, if a chart is prepared containing lines of constant ψ and constant θ in this first quadrant, then the values of ψ and θ corresponding to any particular set of r and s values can be read directly from this chart. The following

two equations, relating r and s to the parameters ψ and θ , can be derived from equations (8) and (9).

$$\left(r - \frac{1}{\tan 2\psi}\right)^2 + s^2 = 1/\sin^2(2\psi) \quad \dots (10)$$

$$\left(s \pm \frac{1}{\sin 2\theta}\right)^2 + r^2 = 1/\tan^2(2\theta) \quad \dots (11)$$

Each of the above is an equation for a circle. Thus, the curves of constant ψ are circles with centres at $(1/\tan 2\psi, 0)$ and with radii, $(1/\sin 2\psi)$, the curves of constant θ are circles with centres at $(0, \pm 1/\sin 2\theta)$ and radii $(1/\tan 2\theta)$. A chart of 20 cm \times 20 cm size with 1 mm divisions has been used for obtaining ψ and θ by the above method.

Each of the parameters ξ and η involves four variables namely, the electronic density, the collisional frequency, the wave frequency and the critical collisional frequency. For vertical propagation, the critical collisional frequency ν_c , which is determined by the strength and inclination of earth's magnetic field with respect to the direction of propagation, is uniquely fixed at any one place if its height variation in the ionosphere is neglected. Therefore, the value of X is determined by x and p and that of Y by ν . By assigning the desired values to p , x and ν , sets of values of X and Y can be tabulated and the corresponding values of r and s evaluated.

Computations have been made starting with discrete values of X and Y the possible ranges of which have been determined from the chosen ranges of wave frequency and the collisional frequency. The chosen wave frequency range is from 1 to 6 Mc/s. The critical collisional frequency for the latitude of Waltair being 8.63 Mc/s, the value of X varies from zero to a maximum of 4.37 in the above wave frequency range if propagation within the x -range of 0–1.0 is considered. The collision frequency (ν) of electrons varies from about 5×10^6 /s at the lower fringe of the E -region to about 10^9 /s in the region of maximum ionization in the F -layer (Ratcliffe 1960, Nicolet 1959). For the wave frequencies chosen, this range of collisional frequency values is relevant under different possible conditions of ionospheric propagation. Therefore, ten values of $Y (= 2\nu/\nu_c)$ in the range of 0 to 2.0 have been used in the computations.

It may be mentioned that the quantities X and Y above are the same as the X and Z , respectively, in Snyder and Hellwell's graphs (Snyder and Hellwell 1952), and the $(-\xi)$ and $|\nu/w|$ in Ratcliffe's curves (Ratcliffe, 1959, p. 72).

RESULTS AND DISCUSSION

The results of theoretical calculations for the ordinary wave are presented graphically in figures 1 to 4. It is usual to represent the variation of polarisation with electron density by means of $\theta-N$ and $\psi-N$ curves. Such representation

has the advantage that both the sets of curves can be shown in the same graph in a compact form. But, with a view to facilitate a direct comparison of the theoretical and experimental values of polarisation parameters that are actually measured, curves have been drawn showing the variation of the axial ratio (ϵ or $\tan \theta$) and the tilt angle (ψ) with the electronic density for different fixed values of collisional frequency. Fig. 1 shows the variation of ϵ with x for a fixed wave

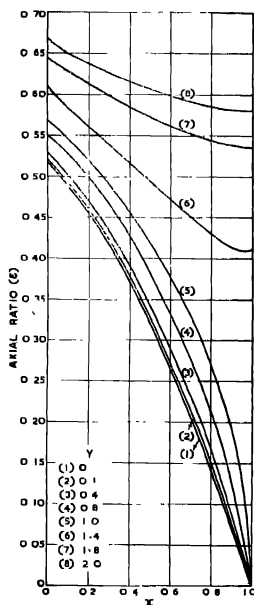


Fig. 1 Variation of axial ratio with electron density.

frequency of $2Mc/s$ and for eight different values of Y in the range of 0 to 2. The important conclusions that can be drawn from these curves are as follows:

(i) There is a marked variation with electronic density in the ellipticity for all values of collisional frequency.

(ii) The rate of variation of ϵ with x over the x -range of 0 to 1 increases slowly at first with collisional frequency upto $\nu = \nu_c$, but for values of $\nu > \nu_c$, there is a sharp reduction in the variation of ϵ with x ; the variation becomes very small for $\nu \gg \nu_c$.

(iii) The effect of increased collisional frequency at any value of x is to increase the axial ratio, the effect being more marked at larger values of x .

(iv) The most important feature of practical interest is the negligibly small change in ϵ , at any value of x , as Y changes from 0 to 0.1 corresponding to a collisional frequency change of zero to 8.63×10^5 C/s. The effect of collisions on the axial ratio becomes appreciable only when Y is about 0.5 or larger.

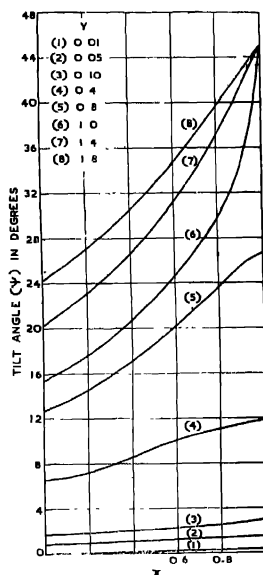


Fig. 2 Variation of tilt angle with electron density

The variation of the tilt angle (ψ) with x is shown in Fig. 2. The important features of this variation are as follows:

(i) The variation of ψ with x has a maximum range for $\nu = \nu_c$ and gets smaller as ν decrease below or increases above the value of ν_c .

(ii) For values of Y smaller than about 0.01, the variation of ψ with x is negligibly small.

(iii) The effect of collisional frequency on the tilt angle is much larger than the effect on axial ratios; thus, as Y changes from 0 to 0.1, ψ changes from 0 to 2° , which is a measurable change, while the corresponding change in ϵ is seen to be negligible.

(iv) The value of ψ changes appreciably with the collisional frequency for values of $Y > 0.10$.

From the above features, it may be concluded that the axial ratio is, in

general, more sensitive to changes in electron density while the tilt angle is more sensitive to changes in collisional frequency.

One important feature observable in both the Figs. 1 and 2 is the marked difference in the shape of the curves as Y increases through unity. The axial ratio becomes zero at $x = 1$ for all values of $\nu < \nu_c$, while it has different values at $x = 1$ for different values of $\nu > \nu_c$. On the other hand, the tilt angle has different values at $x = 1$ for different values of $\nu < \nu_c$, while it shows the same maximum value of 45° for all values of $\nu > \nu_c$. It is to be noted, however, that this difference in the behaviour of the polarisation characteristics for $\nu > \nu_c$ and $\nu < \nu_c$ is absent for lower values of x , notably at $x = 0$, and the variations of ϵ and ψ are gradual.

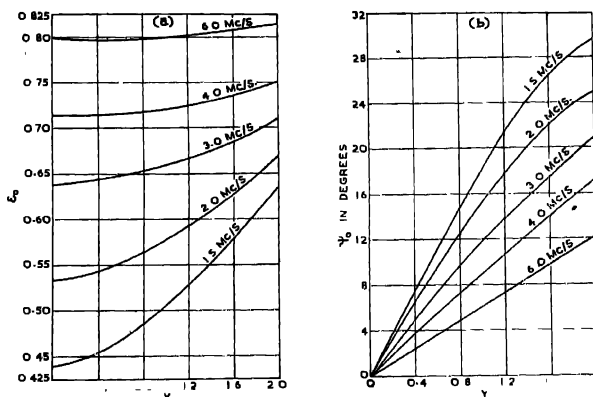


Fig. 3 Variation of ϵ_0 and ψ_0 with collision frequency

The variations of ϵ and ψ with electron density are shown for a single frequency of 2 Mc/s; these curves are typical for the high frequency range and the general conclusions given above hold good for frequencies higher than 2 Mc/s. The theoretical values of particular interest are those of the axial ratio and tilt angle at $x = 0$. These are the values that are experimentally measured when the radio waves, emerging out of the ionosphere, reach the ground. Some doubt has been expressed regarding the validity of the assumption that the final polarisation of the radio waves leaving the ionosphere corresponds to the level where $x = 0$ (Roy and Verma 1955). A detailed quantitative study of the limiting polarisation of radio waves has shown clearly that, in case of high frequency radio waves coming down vertically, the final limiting polarisation is acquired at a level in the ionosphere where the value of x does not differ significantly from zero. Therefore, these limiting values, ϵ_0 and ψ_0 , of the axial ratio and tilt angle, respectively, at $x = 0$ are shown graphically in Fig. 3 and 4. Fig. 3(a) shows the

variation of ϵ_0 with collisional frequency for five fixed wave frequencies. The following points of practical interest emerge from a study of these curves.

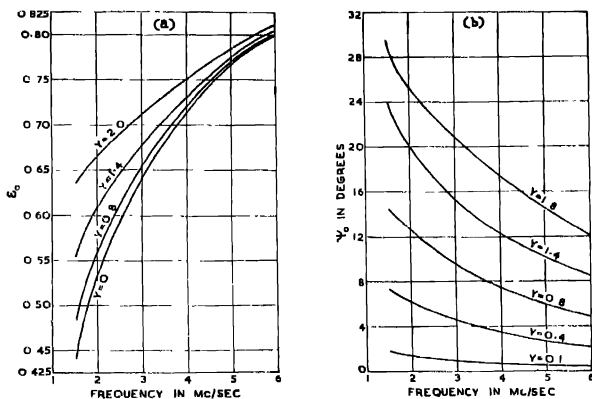


Fig. 4 Variation of ϵ_0 and ψ_0 with wave frequency.

(i) At frequencies of 2Mc/s and higher, the axial ratio of the limiting polarisation ellipse for all values of $\nu \leq 0.5\nu_c$ differs by less than 1 per cent from the zero collisional frequency value.

(ii) The effect of collisional frequency on ϵ_0 diminishes rapidly as the wave frequency increases above 2Mc/s, the increase in ϵ_0 even at $\nu = 2\nu_c$ over that at $\nu = 0$ being less than one per cent at the wave frequency of 6Mc/s.

The importance of the above theoretical facts becomes obvious when it is remembered that the collisional frequencies in the 'limiting region' where the downcoming waves in the frequency range of 2Mc/s and above acquire their final polarisation are not likely to be greater than $0.5\nu_c$ under normal ionospheric conditions. As such, the observed axial ratios in this frequency range should practically be the same as predicted by the magneto-ionic theory for the case of no collisions.

Fig. 3(b) shows the variations of ψ_0 with Y for the same five fixed frequencies as in (a). The effect of collisional frequency is significant in this case, especially at frequencies 3Mc/s and below. A collisional frequency of $0.1\nu_c$, which is likely to obtain in the 'limiting region' when it is situated at the lower fringe of the (mid-day) *E*-region, causes a radio wave of 2Mc/s to have a tilt angle of nearly 1.5° which is at the lower limit of measurable values of tilt angle. For lower values of ν , the tilt angle is too small to be measured accurately.

The variations of ϵ_0 and ψ_0 with the wave frequency are shown in Fig. 4, for fixed values of Y , to bring out clearly the dependence of the limiting polarisation

sation on the wave frequency. The important points of interest to be noted from the curves are as follows.

(i) There is a marked variation of the axial ratio with frequency in the range of 1.5 to 6.0 Mc/s, the rate of variation being larger at lower wave frequencies and at smaller collisional frequencies.

(ii) The variation in tilt angle with wave frequency gets smaller for smaller values of collisional frequency and the variation is negligibly small in the practical range of ($Y \leq 0.10$) collisional frequency values when the wave frequency varies from 2 to 6 Mc/s.

(iii) The larger the wave frequency, the smaller is the effect of collisional frequency on the tilt angle of the limiting polarisation ellipse.

All the above results and discussions refer to the ordinary magneto-ionic component. It is well known that the ordinary and extraordinary wave polarisations are related to each other in a well defined way at each level of the ionosphere. As such the extraordinary wave polarisation is not discussed separately.

CONCLUSIONS

The detailed investigation of theoretical polarisations of radio waves at this low latitude station (Waltair) has shown that the experimental measurements on polarisation at low latitude stations in the frequency range of 1 to 6 Mc/s, should show a clear increase in the measured axial ratios with frequency and that the measured tilt angles should be rather too small to observe their variations with frequency. The results of the above study are in general agreement with those of the many previous workers referred to in the Introduction, with the exception of Mary Taylor's results. The conclusion of Mary Taylor (1933, 1934) that the limiting polarisation is always circular is found to be at variance with the results of all subsequent workers on polarisation and it lacks a theoretical basis.

ACKNOWLEDGMENTS

The author is indebted to Prof B. Ramachandra Rao, D.Sc., M. Brit. I.R.E., Sr. M.I.R.E., F.P.S. (Lond), for his keen interest and valuable guidance throughout this investigation. Thanks are also due to the Ministry of Education, Government of India, for the award of a Senior Research Scholarship to the author during the period of the above investigation.

REFERENCES

- Bailey, V. A., 1934, *Phil. Mag.*, **18**, 516.
 Bailey, V. A., 1938, *Ibid.*, **26**, 425.
 Booker, H. G., 1934, *Proc. Roy. Soc. A.*, **147**, 352.
 Ghosh, S. P., 1938, *Ind. Jour. Phys.*, **12**, 341.
 Martyn, D. F., 1935, *Phil. Mag.*, **19**, 376.

- Murthy, Y S N and Khastgir, S R , 1960, *J Sci Indust Res* , **19B**, No 8, 281
- Nicolet, M , 1959, *Physics of Fluids*, **2**, 95.
- Ratcliffe, J. A , 1959, "The Magneto-ionic Theory and Its Applications to the Ionosphere" (Cambridge University Press)
- Ratcliffe, J. A , 1960, "Physics of the Upper Atmosphere" (Academic Press, London).
- Roy, R and Volma, J K D , 1955, *J. Geophys. Res* , **60**, 457.
- Scott, J. C. W , 1950, *Proc I R E* , **38**, 1057.
- Singh, R N. and Murthy, Y S N., 1958, *Current Science*, **27**, No 5, 1961.
- Snyder, W. and Helliwell, R. A., 1952, *J. Geophys Res* , **57**, 73.
- Taylor, M , 1933, *Proc Phys Soc* **45**, 245.
- Taylor, M , 1934. *ibid* , **46**, 408

ON THE RAMAN SPECTRA OF MONOMERIC ACRYLONITRILE IN LIQUID AND SOLID STATES AND INFRARED SPECTRA OF THE POLYMER

N. K. ROY*

INDIAN ASSOCIATION FOR THE CULTIVATION OF SCIENCE, CALCUTTA-32

(Received, June 7, 1963)

Plate VIII

ABSTRACT The Raman spectrum of monomeric acrylonitrile solidified and cooled down to -180°C has been recorded and compared with that obtained for the substance at room temperature and the spectra of the monomer in liquid and solid states have been compared to the infrared spectra of the monomer and the polymer. It is found that when the monomer is solidified and cooled to -180°C all the frequencies due to stretching vibrations of the molecule remain unchanged but most of the frequencies corresponding to deformation vibrations shift to longer wave numbers. Further, four new low frequency lines at 51, 81, 96 and 128 cm^{-1} appear in the Raman spectrum of the frozen monomer at -186°C .

It is pointed out that the frequencies 86 and 128 cm^{-1} appear also in the infrared spectrum of the polymer with reversed intensity ratio and it is concluded that these lines and bands are due to oscillations in the molecules associated to each other through N-H bond. It is further pointed out that the increase in the frequencies of vibrations involving bending of the C-H bonds in the frozen monomer as well as in the polymer further corroborates such a hypothesis.

The appearance of the infrared bands at 1612 , 1656 and 2030 cm^{-1} are attributed to the formation of both linear and bent $\text{C}=\text{C}=\text{N}$ chains in the polymer.

INTRODUCTION

The Raman and infrared spectra of monomeric acrylonitrile have been investigated by many workers (Timm and Mecke, 1935; Kohlrausch *et al.*, 1937; Rietz *et al.*, 1938; Thomson and Torkington, 1944; Halverson *et al.* 1948) and some of them (Thomson and Torkington, 1944; Halverson *et al.*, 1948) have assigned the observed Raman shifts and infrared absorption bands to different modes of vibration of the molecule. Liang and Krimm (1958) studied the infrared spectrum of a thin sheet of polyacrylonitrile and made assignments of the observed infrared absorption bands to the different modes of vibration of the constituent groups in the structural unit of the polymer. Recently, Chen *et al.* (1960) obtained polyacrylonitrile by X-ray irradiation of acrylonitrile at 78.5°C and studied the infrared spectrum of the polymer. They reported a new band at

* Present address: Assistant Professor of Physical Chemistry, National Dairy Research Institute, Karnal, Punjab.

2030 cm^{-1} and attributed it to the formation of ketenimine groups $\text{C}=\text{C}=\text{N}$ during polymerisation. They also reported other bands at 1525, 1630, 1675 cm^{-1} the origin of which could not be explained by them. Likewise, Deichert and Tobin (1961) studied the infrared spectrum of polyacrylonitrile formed by passing electric discharge (20000 volts, 60 cycles) through liquid acrylonitrile and observed a band at 2019 cm^{-1} which was attributed to the presence of ketenimine group in the polymer. On the other hand, Liang and Krimm (1958) did not observe any a band either at 2019 cm^{-1} or at 2030 cm^{-1} . It would therefore, be of interest to polymerise the monomer under known conditions and to find out whether the $\text{C}=\text{C}=\text{N}$ chain is formed in the polymer under such conditions.

In two earlier communications (Roy, 1953, 1954) it was pointed out that the changes observed in some of the vibrational frequencies of the monomers with solidification and cooling down to -180°C were to some extent parallel to the changes observed with polymerisation of the monomer. It was, therefore, thought worthwhile to make a comparative study of the changes in the vibrational frequencies of monomeric acrylonitrile with solidification and with polymerisation. With this object the Raman spectra of monomeric acrylonitrile in the solid state at -180°C and the infrared spectrum of the polymer in *nujol* mull have been studied and compared with the spectra of the monomer in the liquid state. The results obtained have been discussed in the present paper.

EXPERIMENTAL

A sample of monomeric acrylonitrile supplied by the National Chemical Laboratory of India was purified by a method described earlier (Roy, 1953). The purified liquid was fractionated and the distillate obtained at $77.3^{\circ}\pm 0.5^{\circ}\text{C}$ was redistilled in pyrex double bulbs under reduced pressure. The Raman spectrum of the purified monomer in the liquid state was studied in the usual way and in the case of the monomer in solid state at -180°C the method used earlier (Roy, 1953) was adopted. A Fuess glass spectrograph having a dispersion of 11 \AA./mm in the 4046 \AA region was used to photograph all the Raman spectra and on each spectrogram iron arc spectrum was photographed for comparison. After each exposure proper test for the detection of the presence of polymer in the monomer was applied and by trial the spectrogram of the specimen showing no trace of polymer after exposure was obtained.

Polymeric acrylonitrile was prepared in the laboratory from the purified sample of the monomer. About 0.1% of benzoyl peroxide was used as a catalyst in one sample. This sample was heated in an electric oven at 100°C for about 24 hours when the polymer was obtained as a white powder. Another sample was prepared with a redox catalyst of potassium permanganate and oxalic acid in aqueous suspension of acrylonitrile. The resulting polymer was washed several times with hot water and dried thoroughly by heating under vacuum at

40°C and subsequently in a vacuum desiccator. The samples obtained by these two methods were opaque and consequently their Raman spectra could not be studied. Infrared spectra of the polymer in nujol mull were recorded with and without compensation cell in the reference beam. The former spectrum was used to correctly identify the bands due to the polymer in the regions where nujol has its own absorption bands and in the latter case a thicker film was used to record very weak absorption bands of the polymer in the region where nujol has no band of its own. A 0.022 mm thick cell obtained between two rock salt plates was used to record the infrared spectra of the monomer. A Perkin-Elmer Model 21 infrared spectrophotometer provided with rock salt optics was used for recording the infrared spectra of the samples of monomeric and polymeric acrylonitrile.

RESULTS

The Raman shifts of monomeric acrylonitrile in the liquid and solid states together with the wave numbers (in cm^{-1}) of the infrared bands are given in Table I which also contains the Raman shifts along with their assignments given by Halverson *et al.* (1948). In Table II the frequencies of the infrared absorption

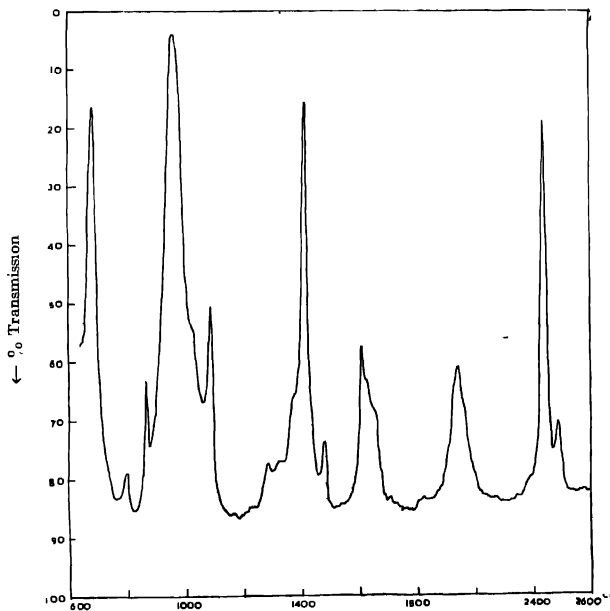


Fig. 2. Infrared spectrum of acrylonitrile monomer (liquid at 27°C)

bands of the polymer obtained after necessary corrections from calibration chart have been tabulated and a probable assignment of the frequencies have been given. Some of the important infrared bands of thin sheet of polyacrylonitrile reported by Liang *et al.* (1958) have also been included in Table II.

Some of the Raman spectra of the monomer are reproduced in Fig. 1, Plate VIII, while the infrared curves of the monomer and the polymer are shown in Figs. 2 and 3.

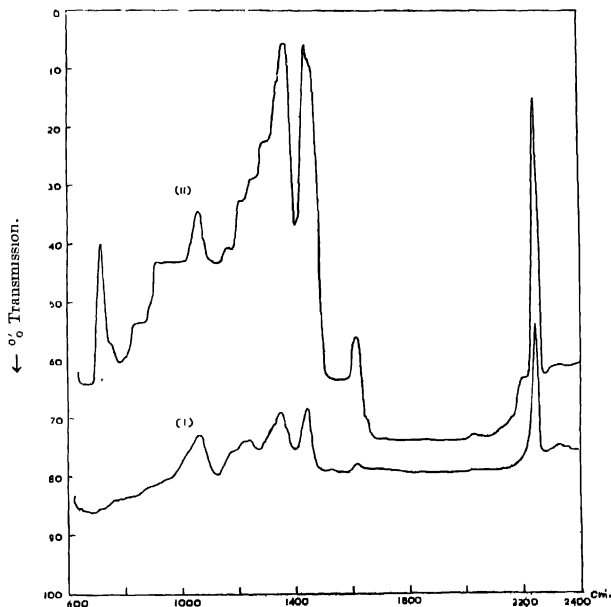


Fig. 3. Infrared spectra of polyacrylonitrile in nujol mull
(i) With compensation (ii) Without compensation.

DISCUSSION

(a) Raman and infrared spectra of monomeric acrylonitrile

It can be seen from Table I that out of the fifteen vibrational frequencies expected from the molecule of monomeric acrylonitrile thirteen have been observed in the Raman spectrum of the liquid. Previous workers variously reported a weak Raman line in the region 305 cm^{-1} — 384 cm^{-1} , but no such line has been observed in the present investigation. When the monomer is solidified and cooled to -180°C all the frequencies due to various stretching vibrations remain unchanged

TABLE 1
Raman shifts and infrared frequencies of acrylonitrile

Infrared frequencies ν , cm^{-1} Liquid at 25°C Present author	Raman shifts $\Delta\nu$, cm^{-1}			Probable assignments Halverson <i>et al.</i> (1948)
	Liquid at 30°C	Solid at -180°C	Liquid Halverson <i>et al.</i> (1948)	
		51 (0)		
	A wing upto 100 cm^{-1} from the Rayleigh line	81 (3b)		
		96 (4b)		
		128 (0)		
	241 (6b)	247 (5)	P 242 (16)	C-C \equiv N bend, α'
			302	C-C \equiv N bend, α''
	568 (1)	568 (0)	P 570 (4.1)	C = C-C bend, α'
682 vs	689 (0)	694 (1)	D 688 (3.0)	C = C torsion, α'
745 w (h)				
800 w				
868 m	874 (1)	874 (1)	P 871 (4.7)	C-C stretch, α'
962 vs				
972 vs (h)	970 (0,vb)	976 (0)	D 970 (2.8)	H ₂ C = C wag, α''
		996 (1)		HRC = C wag, α''
1030 m (h)				
1092 m	1093 (0,vb)	1093 (0)	D 1094 (2.8)	CH ₂ rock, α' (in plane wag)
1283 m	1287 (2)	1300 (2b)	P 1286 (14)	CH rock, α' (in-plane wag)
1325 wv				
1375 w (h)				
1419 vs	1415 (5)	1426 (4)	P 1412 (20)	CH ₂ def, α'
1608 ms	1608 (9)	1608 (8)	P 1607 (36)	C = C stretch, α'
1625 m				682 + 962*
1653 m				682 + 972
1940 m				962 + 972
2230 vs	2228 (10)	2228 (10)	P 2228 (100)	C \equiv N stretch, α'
2277 w				868 + 1416
	2989 (1)	2989 (1)	P 2989	
	3031 (6)	3031 (6)	P 3032 (45)	C-H stretch, α'
			3068 (7.5)	C-H stretch, α'
	3117 (3)	3117 (3)	P 3116 (14)	C-H stretch, α'

P = Polarised; D = Depolarised

* Assignment proposed now.

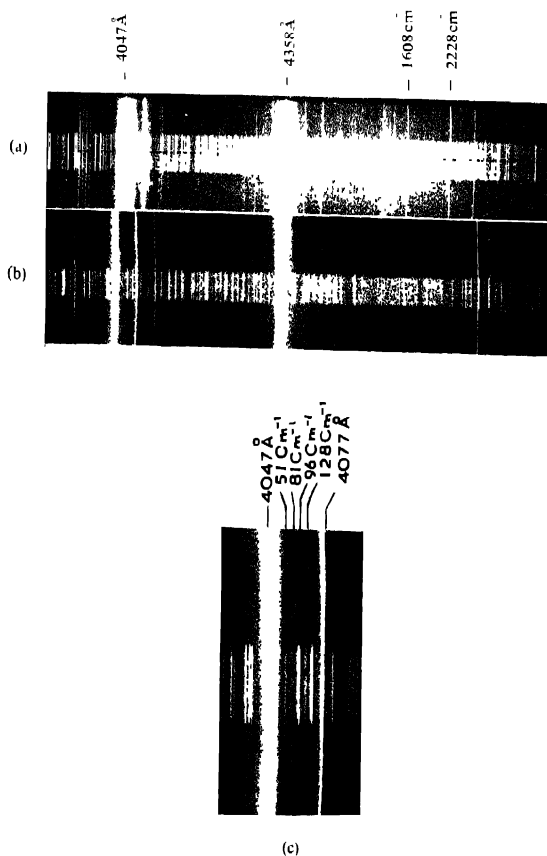


Fig. 1. Raman spectra of acrylonitrile monomer

- (a) Liquid at 30°C
- (b) Solid at -180°C
- (c) Solid at -180°C (showing low frequency lines)

TABLE II

Infrared frequencies (ν , cm^{-1}) of polyacrylonitrile in nujol mull

Of thin film, Liang and Krimm (1958)	In nujol mull	Probable assignment
86 mw		
127 vs		
259 ms		
430 w		
532 m		
675 w		
778 m	760 m (h)	
862 vw	825- 872 m (vvb)	
1041 f (sh)	905-1020 ms (vvb)	
1073 s	1058 s	} C-C-C skeleton vibration of polymer chain
1115 (sh)	1080 ms (h)	
1175 (sh)	1170 ms (b)	
1227 mw	1205 s (b)	C-H bending in the polymer chain
1247 s	1242 s	
1310 w	1310 s (b)	C-H rock
1359 ms	1350 vs (h)	C-H bending in the polymer chain
1375 (sh)	1362 vs	
1447 vs	1440 vs	CH ₂ def.
1613 m	1612 m	Symmetric stretching vibration in bent C = C = N group
1678 w	1656 w (h)	Antisymmetric stretching vibra- tion in bent C = C = N group
	2030 vvw	Linear C = C = N stretch
2185 vw	2196 m (bh)	1242+954
2237 vs	2245 vs	C \equiv N stretch
2510 vw		
2810 vw	The bands due to C-H stretching vibrations are overlapped by those due to nujol.	
2870 m		
2940 vs		
2985 (sh)		

but most of the frequencies corresponding to deformation vibrations undergo changes. For instance, the Raman line 970 cm^{-1} of the liquid is split up into two components in the case of the solid at 976 and 996 cm^{-1} respectively. This line is due to wagging of CH_2 and CH groups (Halverson, 1948). The medium strong Raman line 241 cm^{-1} probably due to $\text{C}-\text{R}$ bending, where R represents $\text{C} \equiv \text{N}$, shifts to 247 cm^{-1} . Also, the frequency of the Raman line 689 cm^{-1} (682 cm^{-1} in the infrared spectrum) assigned to $\text{C}-\text{C}$ torsional vibration increases to 694 cm^{-1} , whereas the line 1287 cm^{-1} due to $\text{C}-\text{H}$ rocking motion shifts to 1300 cm^{-1} . Similarly, the Raman line due to scissoring deformation of the CH_2 group has a frequency of 1415 cm^{-1} in the liquid but increases to 1426 cm^{-1} in the case of the solid. The weak Raman lines 568 and 1093 cm^{-1} do not show any shift although these lines are assigned to $\text{C}=\text{C}-\text{C}$ bending and CH_2 rocking motions respectively. The changes mentioned above may be due to formation of a weak linkage between the H atom of the CH_2 groups and the N atom of the neighbouring molecule. Probably this $\text{N}\cdots\text{H}$ bond lies in the plane containing the $\text{C}-\text{N}$ and $\text{H}-\text{C}$ bonds so that any bending of the $\text{C}-\text{H}$ group at right angles to the plane results in the bending of the weak linkage and it affects very little the frequency of the CH_2 rocking vibration. Similarly, the weak linkage does not alter the bending oscillation frequency of the $\text{C}=\text{C}-\text{C}$ group.

It is observed that in the present case the $\text{C}=\text{C}$ stretching vibration frequency, 1608 cm^{-1} , is lower than that in ethylene (Herzberg, 1945), styrene (Roy, 1954) or methyl methacrylate (Roy, 1953). Also the $\text{C} \equiv \text{N}$ frequency, 2228 cm^{-1} , is lower than that observed in the spectra of other simple nitriles, e.g., succinonitrile, methyl cyanide, etc. (Herzberg, 1945). The conjugation between $\text{C}=\text{C}$ and CN bonds in the structure, $\text{C}=\text{C}-\text{C} \equiv \text{N}$, of acrylonitrile molecule seems to be responsible for the lowering of both the frequencies. This will also increase the electronic charge on the terminal C and N atoms and facilitate the formation of intermolecular $\text{N}\cdots\text{H}$ bonds mentioned earlier.

Besides the changes discussed above, other characteristic changes also occur in the Raman spectrum with solidification. Four new Raman lines of frequency shifts 51 , 81 , 96 and 128 cm^{-1} are observed in the spectrum of the solid at -180°C . Of these, the two Raman lines at 81 and 96 cm^{-1} are fairly intense, while the other two lines are weaker. These lines are evidently not due to intramolecular vibrations.

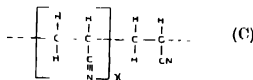
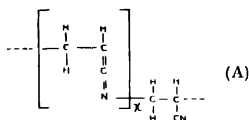
It may be pointed out that although two bands at 86 and 127 cm^{-1} were observed by Liang and Krimm (1958) in the infrared spectrum of polyacrylonitrile there are no corresponding lines in the Raman spectrum of the liquid monomer, because the intensity of the wing present upto 100 cm^{-1} the Rayleigh line in the Raman spectrum of the liquid monomer is very feeble in the above two regions. The strong new Raman lines 81 and 96 cm^{-1} observed in the case of frozen monomer

may correspond to the feeble infrared band at 86 cm^{-1} and the Raman line 128 cm^{-1} may correspond to the infrared band at 127 cm^{-1} . Thus it appears that in the polymer also the weak N...H bond is formed and the vibration of low frequencies observed in the case of the frozen monomer occurs also in the polymer. Liang and Krimm (1958), however, concluded that no hydrogen bonding takes place in the polymer, but they seem to have overlooked the fact that the $\text{C} \equiv \text{N}$ stretching frequency may not be affected even if the N...H bond is formed, as pointed out earlier. The assignment of the two frequencies 86 and 127 cm^{-1} made by them may not therefore be correct.

The number of new low frequency lines is generally large in substituted ethylene when at least one of the substituents has non-bonding electrons or a resonance structure as in benzene. In the present case there may be more than one molecule in the unit cell and the strengths of the N...H bonds formed between neighbours at different distances may be different. The assignment of the low frequency lines to oscillation of N...H groups is supported by the facts that in the case of tetrachloroethylene at -180°C no new low frequency Raman line is observed, while frozen trichloroethylene shows one such line at 62 cm^{-1} (Sanyal, 1950).

Infrared spectrum of polyacrylonitrile

It is seen from Table II that in the infrared spectrum of polyacrylonitrile in nujol mull there are extra bands at 1058, 1170, 1205, 1242, 1350, 1656, 2030 and 2196 cm^{-1} which are not represented in the infrared spectrum of the monomer. In order to account for these bands one has to explain first the appearance of two frequencies 1612 and 1656 cm^{-1} in the spectrum of the polymer. Evidently, although in the usual process of polymerisation the $\text{C} = \text{C}$ bond should be replaced by the $\text{C}-\text{C}$, in this case in some percentage of the polymer the $\text{C} = \text{C}$ reappears, and therefore, an alternative process takes place. The formation of the ketenimine group has been suggested by Chen *et al* (1960). The characteristic frequency of linear $\text{C} = \text{C} = \text{NH}$ group is 2030 cm^{-1} , but when the angle between $\text{C} = \text{C}$ and $\text{C} = \text{N}$ is about 90° the group may have the two frequencies 1612 and 1656 cm^{-1} respectively due to the symmetric and antisymmetric vibrations. As all the three frequencies have been observed in the present case it is evident that in certain percentage of the polymer the ketenimine chain is linear, in some it is bent and in the rest no ketenimine chain is formed. The three cases are illustrated by the formulae (A), (B) and (C). It may be pointed out here that Chen *et al*. (1960) observed the bands 1630 and 1675 cm^{-1} but overlooked this plausible explanation of their origin. On the other hand, Liang and Krimm (1958) observed only the two bands 1613 and 1678 cm^{-1} but not the band 2030 cm^{-1} . Hence in their polymer also the bent group $\text{C} = \text{C} = \text{N}$ was formed but the linear ketenimine chain was not formed. The bands observed by them was due to this configuration of the polymer and not due to impurities as assumed by them,



Of the remaining extra bands the bands 1058 and 1170 cm^{-1} can now be assigned to the vibration of the chain $\text{C}-\text{C}-\text{C}$ in the predominant configuration of the polymer and the bands 1205 , 1242 and 1350 cm^{-1} may be due to vibration of the $\text{C}-\text{H}$ groups in the chain involving $\text{C}-\text{H}$ bond.

It may be pointed out that the infrared bands 1310 and 1440 cm^{-1} of the polymer correspond to the bands at 1283 and 1416 cm^{-1} respectively of the monomer and the increase in the values indicates formation of $\text{N}\cdots\text{H}$ bonds in the polymer. The band 2196 cm^{-1} is rather weak and it may be due to the combination of the frequencies 1242 and 954 cm^{-1} .

As mentioned earlier, the frequency 86 cm^{-1} observed in the infrared spectrum of the polymer is replaced by two frequencies 81 and 96 cm^{-1} in the Raman spectrum of the frozen monomer, while the frequency 128 cm^{-1} appears in the Raman spectrum of the frozen monomer as well as in the infrared spectrum of the polymer. The intensities are however reversed in the two spectra, which shows that these are due to some fundamental vibrations in which the selection rule is operative so that the Raman lines 81 and 96 cm^{-1} are very intense while the infrared band 86 cm^{-1} is weak. These Raman lines have been assigned to vibrations in molecules of the frozen monomer associated to each other through $\text{N}\cdots\text{H}$ bonds. Evidently, in the polymer also such hydrogen bonding takes place. The low frequency Raman lines are therefore not produced by the crystal lattice because in the polymer there is no such regular arrangement.

It may be pointed out that the unusual properties of polyacrylonitrile, viz., that the polymer is an opaque powder while polystyrene and polymethylmethacrylate are transparent, that polyacrylonitrile is infusible even upto a temperature of 250°C , that it is insoluble in common polymer solvents, but dissolves only in some special solvents, e.g., succinonitrile, dimethylformamide etc., may be due to the abnormal ketonimine type of linkage at least in some percentage as well as $\text{N}\cdots\text{H}$ type of linkage present in the polymer as discussed above.

ACKNOWLEDGMENTS

The work was done partly in the Optics Department of the Indian Association for the Cultivation of Science during 1962 and was completed later. The author's sincerest thanks are due to Prof S C Sirkar, D.Sc., F.N.I. for his guidance during the progress of the work and to the authorities of the I.A.C.S. for providing facilities in the laboratories of the Association.

REFERENCES

- Chen, C. S. H., Colthup, N., Deichert, W. and Well, R. L., 1960, *J. Poly. Sci.*, **45**, 247.
Deichert, W. G. and Tobin, M. C., 1961, *J. Poly. Sci.*, **54**, 539.
Halverson, F., Stamm, R. F. and Whalen, J. J., 1948, *J. Chem. Phys.*, **16**, 808.
Herzberg, G., *Infrared and Raman Spectra of Polyatomic Molecules*, Van Nostrand, New York, 1945.
Kohlrausch, K. and Skrabal, R., 1937, *S.B. Akad. Wiss. Wien*, **146**, 44 & 377.
Luong, C. Y. and Kimm, S., 1958, *J. Poly. Sci.*, **31**, 513.
Reitz, A. W. and Sabathy, R., 1938, *S.B. Akad. Wiss. Wien*, **146** (11b), 577.
Roy, N. K., 1953, *Ind. J. Phys.*, **27**, 167.
Roy, N. K., 1954, *Ind. J. Phys.*, **28**, 365.
Sanyal, S. B., 1950, *Ind. J. Phys.*, **24**, 151.
Thomson, H. W. and Torkington, P., 1944, *J. Chem. Soc.*, 595 and 597.
Timm, B. and Mecke, R., 1935, *Z. Physik*, **97**, 221.

EVAPORATION OF FREELY SUSPENDED AND CHARGED WATER DROPLETS

NARAYAN R. GOKHALE*

STATE UNIVERSITY OF NEW YORK, ALBANY, N.Y.

(Received, January 16, 1963)

ABSTRACT. Experimental data for the evaporation of water droplets of 1μ size, evaporating in humid air, are obtained. These droplets are charged and are freely suspended in air. After adequate correction for the cooling of droplets due to evaporation, $r \, dr/dt$ is found to be proportional to $\{\rho_v(s) - \rho_v\}$, over a considerable range. However, at very low values of $\{\rho_v(s) - \rho_v\}$, a departure from such a trend is indicated. In every case, the rate of evaporation for charged droplets of 1μ size, is found to be considerably less than that calculated from Fuchs' theory for uncharged droplets.

INTRODUCTION

The evaporation of organic liquid droplets evaporating in air, has been the subject of extensive experimental observations. The variation of the rate of evaporation with droplet radius, temperature and pressure has been observed. Such evaporation rates have been noted for attached, as well as, unattached droplets of several such liquids.

The evaporation of water droplets in gaseous media and the reverse process of droplet growth by condensation, are extremely important in nature. The cycle of water proceeds via the condensation of water vapor on hygroscopic particles in the troposphere, with the formation of cloud droplets. Such droplets either evaporate, depending on the turbulence and the environmental conditions, or form bigger rain drops. It is also well-known that charge is present in a cloud. Thus the study of evaporation rates of small charged water droplets, under controlled conditions, is extremely important in the relatively new field, cloud physics.

THEORETICAL AND EXPERIMENTAL BACKGROUND

The basis of the theory of evaporation of droplets in gaseous medium was laid by Maxwell. Considering purely diffusion control of evaporation, Maxwell arrived at the following equation, for the rate of decrease of droplet radius

$$\frac{dr}{dt} = - \frac{D}{\rho_L r} \{\rho_v(s) - \rho_v\} \quad \dots \quad (1)$$

* This work was carried out in Institute of Science, Bombay.

where, r is the drop radius, D the diffusion coefficient of water vapour in air $\rho_v(s)$, ρ_v are respectively the vapour densities at the surface of the drop and in the distant environment, and ρ_L is the density of liquid water.

But it soon became evident that, when the droplet radius is comparable to the mean free path of a diffusing vapour molecule, Maxwell's expression does not hold good. Fuchs (1934) derived theoretically a more adequate expression for such an evaporation rate, which is given by

$$\frac{dr}{dt} = - \frac{\alpha v}{\rho_L \left(1 + \frac{\alpha v r}{D} \right)} \{ \rho_v(s) - \rho_v \} \quad \dots \quad (2)$$

where α is the condensation coefficient and $v = (kT/2\pi m)^{1/2}$ in the usual notation.

Frisch and Collins (1952) derived the same expression as that of Fuchs by more analytical methods based on stochastics. Monchick and Reiss (1954), on the other hand, have developed a theoretical formalism using non-Maxwellian distribution functions. They have concluded that, except for small modifications in the constants, Fuchs expression is correct to the first order in their perturbation theory.

Woodland and Mack (1933), Shereshevsky and Steckler (1936), Bradley, Evans and Whytlaw-Gray (1946), Birks and Bradley (1949) as well as Monchick and Reiss (1954) have experimentally observed the evaporation rates for droplets of organic liquids under different conditions of pressure and temperature. They have all confirmed Fuchs expression for the evaporation rates of such droplets of organic liquids, evaporating in dry air.

Gudris and Kulikova (1924) measured the rate of evaporation of charged water droplets, with an aqueous solution in the chamber, with vapor pressure 2.5mm (i.e., approx. 15%) lower than that of the saturated vapour. In this case, initial radius decreased steadily for 40 minutes from 0.64 to 0.49 μ . This rate was many times less than the theoretical. It was thought desirable therefore, to check the evaporation rates for 1 μ size water drops which are freely suspended and charged, under more exact conditions of pressure, temperature and relative humidity, inside a chamber.

EXPERIMENTAL TECHNIQUE AND PROCEDURE

The Millikan's oil-drop apparatus of 'CENCO' design has been used for the observation of water droplets in the present experimental investigation. The plate separation was adjustable to either 0.53cm or 0.7 cm. The 400V D.C supply required for these observations, was obtained by connecting nine 45V batteries in series. The illumination of the droplets was provided by converging a beam of light. Adequate precautions were taken to avoid any significant drift of the droplet due to uneven heating. The smallest division of the tele-microscope, used for observing the droplet transit, measured 0.081 cm.

To measure accurately the relative humidity of the air, inside the small chamber of Millikan's apparatus, a special form of the dew-point hygrometer was developed. In this apparatus, the dew was formed on the end of a narrow silver tube, inserted inside the chamber, by cooling the tube with the help of a controlled flow through it of pre-cooled ethyl ether. The temperature of the surface, where dew is formed, was noted accurately with the help of a thermo-couple. Only a small portion of the tube was exposed, as the rest was covered by rubber tubing. This hygrometer allowed the determination of relative humidity within the small chamber, quite accurately as described by N.R. Gokhale and K. M. Gatha (1959).

In the present series of experiments a set of observations was characterised by some constant values for pressure, temperature and relative humidity. The same selected droplet freely suspended between the two plates was repeatedly observed in such a set of observations. This was accomplished by bringing the droplet which was charged due to friction while spraying, to its original position everytime, by applying the electric field. In this manner, the free fall under gravity was observed for the same droplet at various epochal times ' t '. At every epochal time ' t ' the time t_g for the free fall of the droplet through one division of the tele-microscope was noted. The time t_g was small as compared to the time interval between two successive epochs. The velocity V_g , of free fall under gravity was thus obtained from t_g , for each value of t . Next, for each ' t ' the droplet radius r was calculated with the help of the equation

$$r = \left\{ \frac{9\eta V_g}{2g(\rho - \rho_a)} \right\}^{\frac{1}{3}} \quad (3)$$

where $\eta = 183.2 \times 10^{-6}$ dynes per sq. cm, is the coefficient of viscosity for air, $\rho_L = 0.996$ gm cm $^{-3}$ is the density of water, $\rho_a = 0.00129$ gm cm $^{-3}$ is the density of air, while g is the acceleration due to gravity.

The above expression for r in terms of V_g is based upon Stokes' law. However, it is known that this law needs correction when the droplet-radius is comparable to the mean free path of air molecules. According to Millikan (1923), the corrected value of V_g is

$$V_g^1 = V_g \left(1 + A \frac{l}{r} \right)^{-1} \quad \dots \quad (4)$$

where $l = 9.6 \times 10^{-6}$ cm, is the mean free path for air molecules at room temperature and atmospheric pressure, while A is the correction constant to be determined empirically. Millikan has shown that A depends upon the droplet-liquid and the medium through which the droplet falls.

To determine the constant A , which is not known, for water droplets falling through air, a special experiment was performed. The procedure was similar to that used by Millikan. However, the evaporation rate for water droplets in air

is rather large. Hence, special precautions were necessary to prevent any significant change in the droplet radius during the time of each observation. This was accomplished by reducing the time of observation and by saturating the air by placing water-boats inside the chamber. This experiment, gives $A = 0.701$ for water droplets falling through air, as described by N. R. Gokhale and K. M. Gadhia (1958).

By inserting the corrected velocity Vg' into Eqn. (3), the corrected droplet radius was calculated for each value of t' . The evaporation rate dr/dt was next calculated from the above set of values of r and t .

RESULTS

The evaporation rate for water droplets, evaporating in humid air, is expected to depend upon pressure, temperature, the droplet radius and the relative humidity of air. All observations reported herein have been carried out at atmospheric pressure equal to 76 cm of *Hg* and temperature 28°C approximately. The present series of experiments consist of over seventy sets of observations.

The principal purpose of the present investigation has been to observe the dependence of the evaporation rate on relative humidity. Thus, these sets of observations correspond to the droplet radius equal to $(10 \pm 2) \times 10^{-5}$ cm, while the temperature was kept at 28°C approximately. On the other hand, the relative humidity was systematically varied from 0.20 to 0.85. The corrected droplet radius was plotted against t for each set of observations. It was found that the experimental points fell on a straight line for each such set of observations with relative humidity greater than 0.3. The evaporation rate (dr/dt) was calculated, for each such set, from the slope of the corresponding straight line. Four such sample plots are shown in Fig. 1. On the other hand, the experimental plots indicated small curvatures for those sets of observations, where the relative humidity was less than 0.3. Four such sample plots are illustrated in Fig. 2. The evaporation rate (dr/dt), in such cases, was calculated from the slope of the tangent to the curve at some value of r , lying within the above range.

Further eight sets of observations at room temperature were taken with the droplet radius varying from 5×10^{-5} cm to 17×10^{-5} cm. The experimental values of r plotted against t , in each case, fall on a curve. The evaporation rate was next calculated at the two end points of the curve for each set. It was found that in every case the evaporation rate increased with the decrease in the droplet radius as expected from Maxwell's and Fuchs' equations. However, the relative humidity being different for different sets, significantly affected the evaporation rates.

A plot of rdr/dt against $\{\rho_v(s) - \rho_v\}$ failed to produce a linear relationship if $\rho_v(s)$ is assumed to be the saturation vapour density at the temperature of the en-

vironment. It was noted however, that a correction for the fall in temperature of the droplet caused by evaporation, was necessary. Kinzer and Gunn (1951)

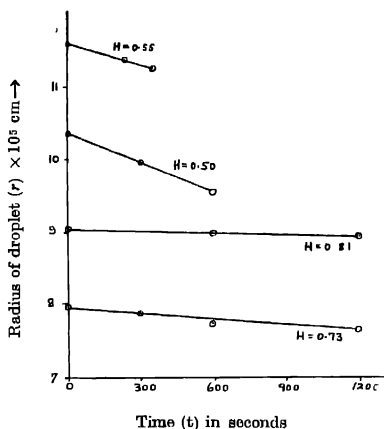


Fig. 1. Variation of radius of droplet with time

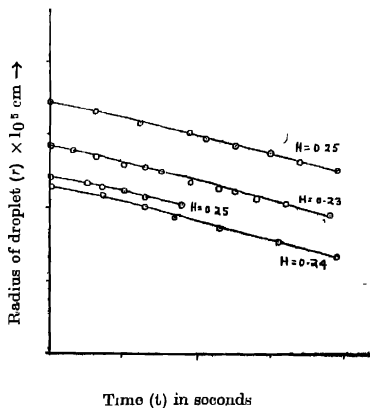


Fig. 2. Variation of radius of droplet with time

determined the temperature of freely-falling drops and showed that this temperature and that of a ventilated wet-bulb thermometer are very close. Hence, $\rho_v(s)$ was assumed to be the saturation vapour density appropriate to the surface temperature of the drop, treated as a wet-bulb thermometer. With this correction rdr/dt was found to be proportional to $\{\rho_v(s) - \rho_v\}$ over a certain range, as shown

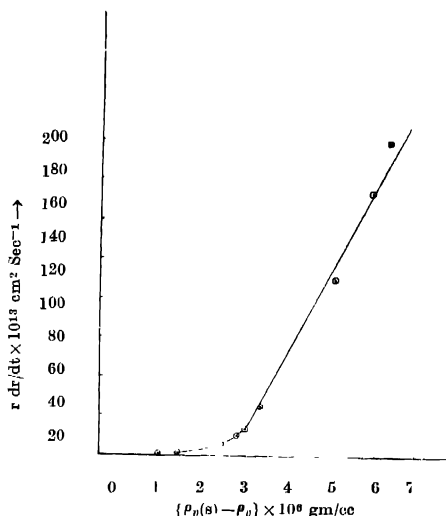


Fig. 3. Variation of $r \frac{dr}{dt}$ with humidity

in Fig. 3. Each point plotted for this graph is a mean value of three to four similar observations. For low values of $\{p_v(s) - p_v\}$ however, slight departure from this trend, is indicated.

DISCUSSION OF THE RESULTS

Using Maxwell's expression for the evaporation rate given in equation 1, one finds that the value of dr/dt is equal to $3.8 \times 10^{-3} \text{ cm sec}^{-1}$ for $r = 1\mu$, $D = 0.26$, the pressure 76 cm of Hg, temperature 28°C and relative humidity 0.85. Using Fuchs expression given in equation 2, with $\alpha = 0.036$ and all other values as indicated above, one obtains $dr/dt = 6.6 \times 10^{-4} \text{ cm sec}^{-1}$. The experimentally observed value is $7.0 \times 10^{-9} \text{ cm sec}^{-1}$. Thus, it is obvious that these theoretical values are much too large, as compared to that of the observed ones.

It is extremely important however, to note that the experimentally observed values, agree well with the value obtained by Gudris and Kulikowa (1924). Their value for the above case, is $dr/dt = 6.3 \times 10^{-9} \text{ cm sec}^{-1}$. As already stated, their droplets were freely suspended and charged and the rate was many times less than the theoretical. Thus, it is confirmed that the water droplets of one micron size, evaporate considerably slowly, than that calculated from Fuchs expression. The two possibilities which might help in explaining this discrepancy are

- (1) Both the equations, of Maxwell as well as of Fuchs, have not been tested for very small drops of micron size and shown to be true in this range; and
- (2) These equations are derived for drops which are not charged. It is true that the charge has no significant effect for bigger drops of say, 1 mm diameter. However, there is some evidence as stated below to suggest that the charge may be effective for very small droplets, in reducing their evaporation rates.

Careful measurements of freely falling water drops, at 0-40°C and 10-100% relative humidity have been made by Kinzer and Gunn (1951), using refined electronic technique. Drops of diameter ranging from 40μ to 1mm were produced and electrified by dropper. Of exceptional interest are the measurements in the region of very small Reynolds numbers. The results of Kinzer and Gunn indicate that very small droplets, whose motions are controlled largely by viscous forces, evaporate relatively slowly.

Thus the problem of the rate of evaporation of charged water droplets of very small size, can by no means be considered as solved.

ACKNOWLEDGMENTS

The author wishes to thank Dr L. A. Ramdas for suggesting this problem, and Dr. K. M. Gatha for useful discussions and suggestions during this work.

REFERENCES

- Birks, J. and Bradley, R. S., 1949, *Proc. Roy. Soc. (Lond)*, A, **198**, 226.
 Bradley, R. S., Evans, M. G. and Whytlaw-Gray, R. W., 1946, *Proc. Roy. Soc. (Lond)*, A, **186**, 368.
 Frisch, H. L. and Collins, F. C., 1952, *J. Chem. Phys.*, **20**, 1797.
 Fuchs, N., 1934, *Physik. F. Sowjetunion*, **6**, 225.
 Golchale, N. R. and Gatha, K. M., 1958, *Ind. Jour. Phys.*, **32**, 521-24.
 Gokhale, N. R. and Gatha, K. M., 1959, *Ind. Jour. of Met. Geophys.*, **10**, 337-40.
 Gudris, N. and Kulikova, L., 1924, (1) *Z. Physik*, **25**, 121. (2) International Critical Tables, **5**, 54.
 Kinzer, G. D. and Gunn, R., 1951, *J. Met.*, **81**, 71.
 Millikan, R. A., 1920, *Phys. Rev*, **15**, 545; 1923, *Phys. Rev*, **21**, 217; 1923, *Phys. Rev.* **22**, 1.
 Monchick, L. and Reiss, H., 1954, *J. Chem. Phys.*, **22**, No. 5.
 Shereshtotsky, J. L. and Steckler, S., 1936 *J. Chem. Phys.*, **4**, 108.
 Woodland, D. J. and Mack, E., 1933, *J. Am. Chem. Soc.*, **55**, 3149.

NOTICE

No claims will be allowed for copies of journal lost in the mail or otherwise unless such claims are received within 4 months of the date of issue.

RATES OF ADVERTISEMENTS

1. Ordinary pages :

Full page	Rs. 50/- per insertion
Half page	Rs. 28/- per insertion

2. Pages facing 1st inside cover, 2nd inside cover and first and last page of book matter :

Full page	Rs. 55/- per insertion
Half page	Rs. 30/- per insertion

3. Cover pages by negotiation

25% commissions are allowed to *bona fide* publicity agents securing orders for advertisements.

CONTENTS

Indian Journal of Physics

Vol. 37, No. 8

August, 1963

PAGE

46. $\pi^*\leftarrow\pi$ Systems in the Electronic Spectra of Ortho and Para Fluorobenzaldehydes
— Kailash Chandra and D. Sharma ... 405
47. Indirect Spin Coupling in NiAs Type Magnetic Compounds— K. P. Sinha,
M. K. Sinha and U. N. Upadhyaya ... 417
48. Theoretical Polarisation of High Frequency Radio Waves at a Low Latitude
Station— C. Abhirama Reddy ... 430
49. On the Raman Spectra of Monomeric Acrylonitrile in Liquid and Solid States
and Infrared Spectra of the Polymer— N. K. Roy ...
50. Evaporation of Freely Suspended and Charged Water Droplets— Narayan
R. Gokhale ... 450

Regd. No. C-3911

VOL. 37 INDIAN JOURNAL OF PHYSICS

No. 9

(Published in collaboration with the Indian Physical Society)

AND

VOL. 46

PROCEEDINGS

No. 9

OF THE

**INDIAN ASSOCIATION FOR THE
CULTIVATION OF SCIENCE**

SEPTEMBER 1963.

**PUBLISHED BY THE
INDIAN ASSOCIATION FOR THE CULTIVATION OF SCIENCE
JADAVPUR, CALCUTTA 32**

BOARD OF EDITORS

K. BANERJEE	D. S. KOTHARI
D. M. BOSE	B. D. NAG CHAUDHURI
S. N. BOSE	K. R. RAO
S. D. CHATTERJEE	D. B. SINHA
P. S. GILL	S. C. SIKKAR (<i>Secretary</i>)
S. R. KHASTOIR	B. N. SRIVASTAVA

EDITORIAL COLLABORATORS

PROF. R. K. ASUNDI, Ph.D., F.N.I.	
PROF. D. BASU, Ph.D.	
PROF. J. N. BHAR, D.Sc., F.N.I.	
PROF. V. G. BHIDE, Ph.D. (Nag), Ph.D. (Lond).	
PROF. A. BOSE, D.Sc., F.N.I.	
PROF. S. K. CHAKRABARTY, D.Sc., F.N.I.	
DR. J. S. CHATTERJEE	
DR. K. DAS GUPTA, Ph.D.	*
PROF. N. N. DAS GUPTA, Ph.D., F.N.I.	
DR. J. DHAR, D.Phil. (Sc)	
PROF. A. K. DUTTA, D.Sc., F.N.I.	
PROF. C. S. GHOSH, M.Sc., S.M., F.N.I.,	M.I.E.E.
PROF. S. GHOSH, D.Sc., F.N.I.	
PROF. S. N. GHOSH, D.Sc.	
PROF. S. GUPTA, M.Sc., F.N.I.	
PROF. D. N. KUNDU, Ph.D., F.N.I.	
PROF. R. C. MAJUMDER, Ph.D., F.N.I.	
PRINCIPAL Y. G. NAIR, Ph.D.	
PROF. S. R. PALIT, D.Sc., F.R.I.C., F.N.I.	
PROF. H. RAKSHIT, D.Sc., F.N.I.	
PROF. A. SAHA, D.Sc., F.N.I.	
DR. VIKRAM A. SARABHAI, M.A., Ph.D., F.N.I.	
DR. A. K. SENGUPTA, D.Sc.	
PROF. NAND LAL SINGH, D.Sc.	
DR. M. S. SINHA, D.Sc., F.N.I.	
PROF. N. R. TAWDE, Ph.D., F.N.I.	
DR. P. VENKATESWARLU	

Annual Subscription—

Inland Rs. 25.00

Foreign £ 2-10-0 or \$ 7.00

NOTICE

TO INTENDING AUTHORS

Manuscripts for publication should be sent to the Assistant Editor, Indian Journal of Physics, Jadavpur, Calcutta-32.

The manuscripts submitted must be type-written with double space on thick foolscap paper with sufficient margin on the left and at the top. The original copy, and not the carbon copy, should be submitted. Each paper must contain an abstract at the beginning.

All references should be given in the text by quoting the surname of the author, followed by year of publication, e.g., (Ghosh, 1954). The full reference should be given in a list at the end, arranged alphabetically, as follows; Ghosh, D. K., 1954, *Ind. J. Phys.*, 28, 485.

Line diagrams should be drawn on white Bristol board or tracing paper with black India ink, and letters and numbers inside the diagrams should be written neatly in capital type with India ink. The size of the diagrams submitted and the lettering inside should be large enough so that it is legible after reduction to one-third the original size. A simple style of lettering such as gothic, with its uniform line width and no serifs should be used, e.g.,

A·B·E·F·G·M·P·T·W·

Photographs submitted for publication should be printed on glossy paper with somewhat more contrast than that desired in the reproduction, and should, if possible, be mounted on thick white paper.

Captions to all figures should be typed in a separate sheet and attached at the end of the paper.

The mathematical expressions should be written carefully by hand. Care should be taken to distinguish between capital and small letters and superscripts and subscripts. Repetition of a complex expression should be avoided by representing it by a symbol. Greek letters and unusual symbols should be identified in the margin. Fractional exponents should be used instead of root signs.

BENGAL CHEMICAL & PHARMACEUTICAL WORKS LD.

Pioneer Indian Manufacturers of Pharmaceuticals & Chemicals.

Manufacturers of

Pharmaceutical Chemicals:

Caffeine and its salts, Strychnine Hydrochlor, Strychnine Sulphate, Brucine Sulphate, Nicotinic Acid, B.P., Nicotinamide, B.P., Potassium Citrate B.P., I.P., Sodium Citrate B.P., I.P., Potassium Acetate B.P., I.P., Potassium Iodide B.P., I.P., Sodium Iodide B.P., I.P., Ferri et Ammon Citrate B.P., I.P., and various other Pharmaceutical Chemicals.

Heavy & Reagent Quality Fine Chemicals:

Alum, Alum Sulphate (Iron Free), Ferro Alum, Zinc Chloride Tech. Naphthalene Pure, Sodium Citrate A.R., Potassium Citrate A.R., Magnesium Sulphate A.R., Sodium Sulphate Anhydrous A.R., Potassium Iodide A.R., Sodium Chloride A.R., Zinc Sulphate A.R., and various other reagent quality analytical chemicals.

Please refer your enquiries for the above items and other chemicals in the line to :—

BENGAL CHEMICAL

6, GANESH CHUNDER AVENUE,
CALCUTTA-13, INDIA.

(INDIA MADE)

X'RAY DIFFRACTION APPARATUS

Complete with

MACHLETT SHOCKPROOF BERYLLIUM WINDOW SEALED TUBES OF
DIFFERENT TARGET MATERIALS
SINGLE VALVE HALF-WAVE RECTIFIED OR TWO VALVE
FULL-WAVE RECTIFIED

MACHINE already incorporates voltage compensator to compensate plus
or minus 15 volts supply change.

Electro-Magnetic, Electronic, Servo-Mechanical or Chemo-Electric STABILISER
can be added to the filament circuit or

to the entire MACHINE for further STABILISATION.

CAMERAS OF VARIOUS TYPES CAN ALSO BE SUPPLIED

FOR THE MACHINE

ALSO

X'RAY PLANT FOR BIOLOGICAL RESEARCH & INDUSTRIAL RADIOGRAPHY
AND HIGH TENSION TESTING SETS

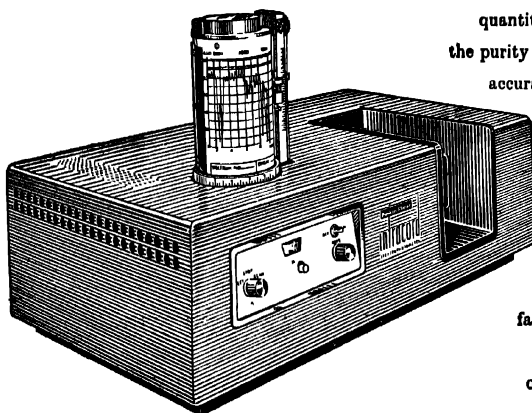
DELIVERY EX-STOCK : : NO LICENCE REQUIRED.

Further details from :—

RADON HOUSE P. LTD.,

7, Sirdar Sankar Road, Calcutta-26.

What the INFRACORD[®] does for the Organic Chemist



*Three models in the
Infracord family covering
various infrared regions
are now available*

The Perkin-Elmer Model 137
double-beam Infracord
Spectrophotometer is the most
compact and inexpensive
infrared instrument available,
featuring utmost simplicity of
operation with excellent resolution.

It identifies unknowns;
performs qualitative and
quantitative analyses, controls
the purity of products with speed,
accuracy and reproducibility.

A large number of
accessories generally
associated with
higher priced
instruments can be
used with the Infracord
family, thereby extending
its utility in every type
of infrared investigation

Model	Range
NaCl INFRACORD	From 2.5 to 15 microns
KBr INFRACORD	From 12.5 to 25 microns
Model 137. G INFRACORD	With two first-order gratings from .83 to 2.55 microns in NIR & from 2.45 to 7.65 microns in fundamental region

Sold and serviced in India exclusively by

INSTRUMENT DIVISION
Perkin-Elmer Corporation

BLUE STAR

**BLUE STAR ENGINEERING
CO. (Calcutta) Private LTD.**
7 HARE STREET, CALCUTTA 1
Also at BOMBAY · DELHI · MADRAS

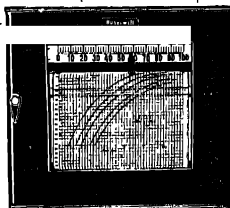
**Measure
and plot changes
in variables
as they occur...
with**

Electronik instruments for research

Here's an exceptional group of instruments to measure and record your research findings swiftly, surely, conveniently. These Electronik instruments for research can speed completion of your projects by eliminating many of the tedious time-consuming details of test work.

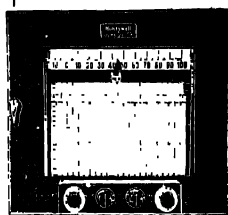
Electronik

FUNCTION PLOTTER automatically and continuously plots a curve which shows the relationship of one variable to another. Typical uses, speed versus torque, stress versus strain, temperature versus pressure, plate voltage versus plate current (and other electron tube characteristics), and many other variable relationships.



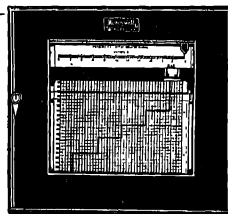
Electronik

ADJUSTABLE SPAN RECORDER measures spans and magnitudes of a variety of emf's. Instrument calibration can be in terms of any variable reducible to d.c. voltage. Can be used with thermocouples, strain gauges, tachometers and other transducers.



Electronik

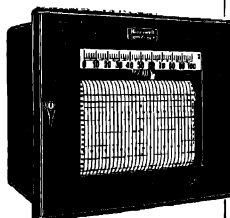
measurement of any variable whose values vary over a wide range, and where precise evaluation and good resolution are important. This instrument is particularly suited to the measurement of forces in conjunction with a strain gauge bridge.



Honeywell
 *First in Control*

Electronik

NARROW SPAN RECORDERS accurately measure d.c. potentials as low as 0.1 micro-volt and spans as narrow as 100 microvolts. Available as a precision indicator, circular chart recorder and strip chart recorder. Useful (with appropriate primary measuring elements) for measuring differential temperatures and slight variations in the temperatures of small objects through the use of radiation pyrometry.



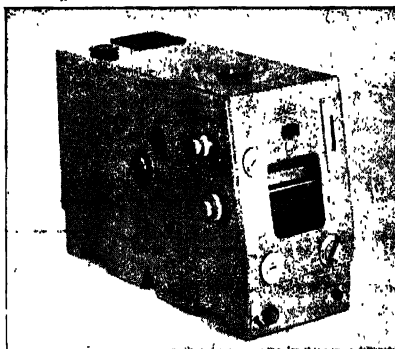
PBS-40233

Sold and serviced in India exclusively by

BLUE STAR

**BLUE STAR ENGINEERING
CO. (Calcutta) PRIVATE LTD.**
7 HARE STREET, CALCUTTA I
Also at BOMBAY • DELHI
MADRAS • JAMSHEDPUR

ZEISS Mirror Monochromator "SPM 2"



- * Represents a high quality new development in the field of optophysical measuring instruments.
- * It combines versatility of application with simplicity of operation.
- * It can be used for the production of monochromatic radiation in the wavelength region from 0.193 to 40 microns by using interchangeable prisms and diffraction grating.
- * The respective wavelength scale can be read in projection.



VEB Carl Zeiss JENA
(German Democratic Republic)

Sole Agents in India :

GORDHANDAS DESAI PRIVATE LIMITED

PHEROZSHAH MEHTA ROAD, BOMBAY 1

Branches at :

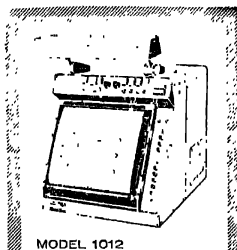
**22, Linghi Chetty Street,
MADRAS 1.**

**P/7, Mission Row Extension,
CALCUTTA 1.**

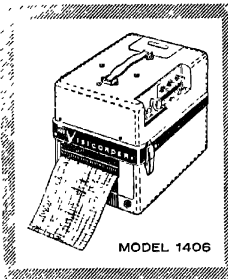
**4/2B, Asaf Ali Road,
NEW DELHI 1.**

HONEYWELL VISICORDER OSCILLOGRAPH

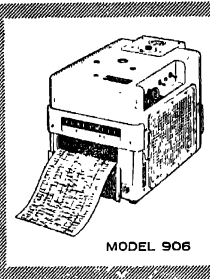
world's most versatile instrument
for the simultaneous recording of
a number of fast changing variables



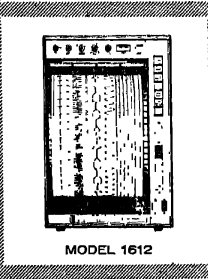
MODEL 1012



MODEL 1406

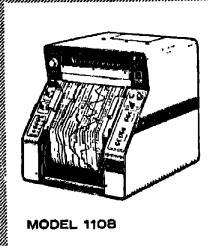


MODEL 906



MODEL 1612

Available in several models, from 6 to 36 channels DC to 5,000 c/s response, over 50,000"/sec writing speed. The 36-channel 1012 & the 1612 are the most sophisticated instruments in the line. The 1108 is a highly capable 24-channel model. The 1508 is a compact 24-channel instrument that takes only 7" of vertical space in a relay rack and is also suitable for bench use. The 906 handles either 8 or 14 channels and the 1406 provides upto 6 channels at the lowest cost per channel.



MODEL 1108

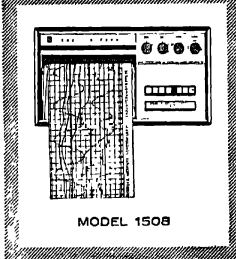
Honeywell

Sold and serviced in India exclusively by



Get complete details from **BLUE STAR** offices at:

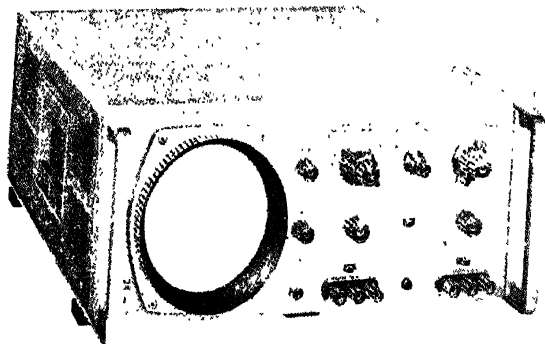
7 Hare Street, Calcutta 1
Sukh Sagar, Sandhurst Bridge, Bombay 7
1/23B Asaf Ali Road, New Delhi 1
23/24 Second Line Beach, Madras 1
1B Kaiser Bungalow, Dindli Road, Jamshedpur



MODEL 1508

HEWLETT PACKARD

NEW NO - PARALLAX 120B OSCILLOSCOPE
EASIEST - to - use SUREST READING 450 KC



Those, who have tested the new 120 B feel it is perhaps the easiest to use, most widely versatile, and highest value commercial 450 KC scope ever offered

The new h/p 120B Oscilloscope combines probably more actual measuring help and desirable features than any 450 KC scope ever produced.

Not only is reading error from parallax ended and not only are distracting reflections eliminated ; but you also have a genuinely unique array of electrical and convenience features for measurements from dc to 450 KC.

For further details, please write to :

The Sole Distributors :

**THE SCIENTIFIC INSTRUMENT
COMPANY, LIMITED.**

ALLAHABAD : BOMBAY · CALCUTTA : MADRAS :
NEW DELHI

Head Office : 6, Tej Bahadur Sapru Road, Allahabad



FRANCK-CONDON FACTORS AND r -CENTROIDS FOR ${}^2\Delta-{}^2\Delta$ SYSTEM OF VO

S. S. Prasad

DEPARTMENT OF PHYSICS, L. S. COLLEGE, MUZAFFARPUR, BIHAR

(Received June 4, 1962; resubmitted May 29, 1963)

ABSTRACT. Franck-Condon factors, $|\int \psi_{v'} \psi_{v''} dr|^2$ and the r -centroids have been reported for the VO ${}^2\Delta-{}^2\Delta$ system. The r -centroid for a given (v', v'') band has been found to increase smoothly with the corresponding wavelength $\lambda_{v',v''} \cdot \Delta \bar{r} = \bar{r}_{v'+1,v''} + 1 - \bar{r}_{v',v''}$ in a sequence remains constant.

INTRODUCTION

The r -centroid, $\bar{r}_{v',v''}$, of a $v' \rightarrow v''$ transition in a diatomic molecular band system has been defined as (Nicholls and Jarman 1956)

$$\bar{r}_{v',v''} = \int \psi_{v'} \bar{r} \psi_{v''} dr / \int \psi_{v'} \psi_{v''} dr. \quad \dots (1)$$

where $\psi_{v'}$ and $\psi_{v''}$ are the vibrational wave functions and r is the internuclear distance. There exists a smooth relationship (Nicholls and Jarman 1956; Nicholls, Robinson, Parkinson and Jarman 1956) between $\bar{r}_{v',v''}$ and $\lambda_{v',v''}$ the wavelength of the corresponding transition. $\bar{r}_{v',v''}$ increases with $\lambda_{v',v''}$ if $r_e' > r_e''$ and vice versa. $\Delta r \equiv (\bar{r}_{v'+1,v''} + 1 - \bar{r}_{v',v''})$ along a sequence remains constant. Furthermore, the r -centroids possess the following important property.

$$\int \psi_{v'} f(r) \psi_{v''} dr = f(\bar{r}_{v',v''}) \int \psi_{v'} \psi_{v''} dr \quad \dots (2)$$

provided (a) $f(r)$ is a polynomial in r , the highest power of r in which does not exceed 10, (b) $\mu \omega_e \sim 10^4$ (c) $0.01 \text{ \AA} < |r_e' - r_e''| < 0.25 \text{ \AA}$. The importance of this property lies in the fact that it enables us to obtain information about the variation of electronic transition moment in any band system provided the experimental vibrational intensity distribution, $\bar{r}_{v',v''}$, and the Franck-Condon factors (i.e. the squares of the overlap integral $\int \psi_{v'} \psi_{v''} dr$) are known (Fraser 1954).

It is in this background that the Franck-Condon factors and r -centroids have been calculated and reported in this paper for the ${}^2\Delta-{}^2\Delta$ band system of an astrophysically important molecule VO. The bands corresponding to this system are very prominent in M -type stars.

* Presently at Department of Applied Mathematics, The Queen's University of Belfast on study leave.

METHOD OF COMPUTATION AND RESULTS

In the present case the Franck-Condon factors have been calculated by approximate analytical method as developed by Fraser and Jarman (1953). The calculations have been checked by the 'remainder formulas' (Fraser and Jarman 1953b). In this method the constants α_1 and α_2 occurring in the Morse potential functions of the two electronic states involved in the transition

$$U_i(r) = D_i \{1 - \exp\{-(\alpha_i - r/r_e)\}\}^2 \quad \dots (3)$$

are replaced by their arithmetic mean value $\alpha = \frac{\alpha_1 + \alpha_2}{2}$. If α_1 and α_2 are not

widely different $\left(\frac{\alpha_1 + \alpha_2}{\alpha_1 + \alpha_2} = 4\%\right)$ this replacement does not involve much distortion of the potential curve and at the same time enables convenient analytical expressions to be developed. If however, α_1 and α_2 differ much, a further correction called 'r_e-shift correction' is needed. In the present case the values of α_1 and α_2 are 1.97484 Å and 1.88119 Å respectively and hence 'r_e-shift correction' was not needed.

The r-centroids have been evaluated in this work by (i) the graphical method and (ii) by quadratic equation method. (i) The quadratic equation method — This method, developed by Nicholls and Jarman (1956) uses the following equation

$$\begin{aligned} E_{v'} - E_{v''} &= D_1 [1 - \exp\{ -\alpha_1(\bar{r}_{v',v''} - r_{e1}) \}]^2 \\ &- D_2 [1 - \exp\{ -\alpha_2(\bar{r}_{v',v''} - r_{e2}) \}]^2 \quad \dots (4) \end{aligned}$$

where $D_i = \omega_{e_i}^2/4\omega_{ex_i}$ and $E = \omega_e(v - \frac{1}{2}) - \omega_{ex}(v + \frac{1}{2})^2$ which can be solved for $\bar{r}_{v',v''}$. If α_1 and α_2 are replaced by the mean α and equivalent adjustment of α -dependent parameters are made the equation (4) becomes

$$\begin{aligned} E_{v'} - E_{v''} &= D'_1 [1 - \exp\{ -\alpha(\bar{r}_{v',v''} - r_{e1}) \}]^2 \\ &- D'_2 [1 - \exp\{ -\alpha(\bar{r}_{v',v''} - r_{e2}) \}]^2 \quad \dots (5) \end{aligned}$$

This equation can be considered to be a quadratic equation in $x = \exp\{ -\alpha(\bar{r}_{v',v''}) \}$. It should be noted that similar approximations and adjustments have been made for obtaining the Franck-Condon factors also by the Fraser and Jarman method. The eq. (5) is equivalent to

$$Px^2 - 2Qx + R_{v',v''} = 0 \quad \dots (6)$$

where

$$\left. \begin{aligned} P &= F_1^2 D'_1 - F_2^2 D'_2 & F_1 &= \exp(\alpha r_{e1}) \\ Q &= F_1 D'_1 - F_2 D'_2 & F_2 &= \exp(\alpha r_{e2}) \\ R_{v',v''} &= D'_1 - D'_2 - (E_{v'} - E_{v''}) & x &= \exp(-\alpha \bar{r}_{v',v''}) \end{aligned} \right\} \quad \dots (7)$$

and the primed quantities D'_1 , D'_2 , $E_{v'}'$, $E_{v''}'$ are the original D_1 , D_2 , $E_{v'}$, $E_{v''}$ adjusted for the mean α . This equation has two roots $-1/\alpha \ln x$. Out of these two roots the physically meaningful root is chosen.

(ii) Graphical method. The right-hand side of the equation (4) can be calculated and plotted as a function of r over the significant range say, at the interval of 0.001 Å. The $E_{v''} - E_{v'}$ can also be found out corresponding to the transition in question. The value of r corresponding to a given $E_{v''} - E_{v'}$ then gives the required $\bar{r}_{v'',v'}$.

The results of the calculations are shown in Table I and II. Table I gives the value of the Franck-Condon factors relative to that of the (0, 0) band as unity (actual value being 0.334). Table II gives the $\bar{r}_{v'',v'}$ values for different bands of the system.

TABLE I
Franck-Condon factors

v''			
v'	0	1	2
0	1.000	1.170	0.595
1	1.000	0.008	0.556
2	0.578	0.341	0.345

TABLE II
 r -Centroids

$v'' \backslash v'$	0	1	2	3	4	5
0	1.631 1.631	1.672 1.672	1.716 1.717	1.762 1.764	1.812 1.815	1.864 1.871
1	1.598 1.598	1.637 1.637	1.679 1.678	1.722 1.723	1.768 1.770	1.817 1.821
2	1.568 1.568	1.605 1.604	1.643 1.643	1.686 1.684	1.728 1.728	1.774 1.776
3	— 1.539	1.574 1.574	1.611 1.610	1.650 1.649	1.692 1.690	1.734 1.734
4	—	—	1.580	1.617	1.656	1.697
5	—	—	1.552	1.587	1.623	1.662

First row : $\bar{r}_{v'',v'}$ by graphical method in angstrom unit

Second row : $\bar{r}_{v'',v'}$ by quadratic equation method in angstrom unit.

TABLE III
Molecular constants

States	ω_e	$\omega_e x_e$	$r_e(\text{\AA})$	$\alpha(\text{\AA}^{-1})$	mean α (\AA^{-1})
$A^2\Delta$	863.5	5.4	1.67	1.97484	
$X^2\Delta$	1012.7	4.9	1.59	1.88119	1.928015

DISCUSSION

In Table III are given the spectroscopic constants and the related constants which have been used in the calculation. The values of r_e are from Lagerquist and Selin (1955) and the rest are from Herzberg (1950). It is clear from the table that in the present case $r_e' > r_e''$ and hence $r_{v',v''}$ should increase with $\lambda_{v',v''}$. In Fig. 1 the corresponding graph is plotted which is in agreement with the above expectation. This is in conformity with the findings of Nicholls and Jarman (1956) and of Nicholls, Robinson, Parkinson and Jarman (1956) on some other band systems.

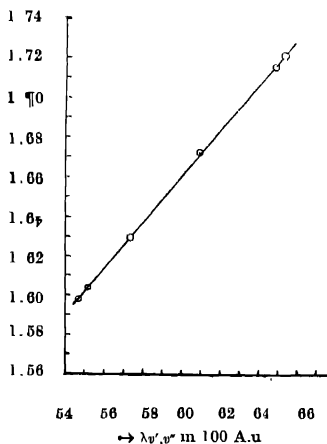


Fig. 1. Variation of \tilde{r} -centroid with wavelength for $^2\Delta$ - Δ^2 system of VO.

These authors have further shown by investigations on some band systems that $\Delta\tilde{r} = (\tilde{r}_{v'+1,v''+1} - \tilde{r}_{v',v''})$ in a sequence remains constant. In the present case of VO $^2\Delta$ - $^2\Delta$ system also the same thing is found to occur as is clear from Table IV which is drawn from values $\tilde{r}_{v',v''}$ for 0, 0 sequence of Table II.

Finally it may be mentioned that the values obtained by the graphical method and the quadratic equation method agree very well.

TABLE IV
 $\Delta \bar{r}$ values of (0, 0) sequence

Bands v', v''	$\bar{r}_{v', v''}$ (in Å)	$(\Delta \bar{r}_{v'+1, v''+1} - \bar{r}_{v', v''})$ (in Å)
0,0	1.631	
1,1	1.637	0.006
2,2	1.643	0.006
3,3	1.650	0.007
4,4	1.656	0.006
5,5	1.662	0.006

REFERENCES

- Fraser, P. A. and Jarman, W. R., 1953, *Proc. Phys. Soc.*, **66A**, 1145.
 Fraser, P. A. and Jarman, W. R., 1953b, *Proc. Phys. Soc.*, **66A**, 1153.
 Fraser, P. A., 1954, *Canad. Jour. Phys.*, **32**, 515.
 Herzberg, G., 1950 *Spectra of Diatomic molecules*, 2nd edition, D. Van Nostrand Co., New York, p. 578.
 Lagerqvist, A. and Selin, L. E., 1955, *Naturwiss.*, **42**, 65 (Sci. Abstract Physics Abs. No. 4517, 1955)
 Nicholls, R. W. and Jarman, W. R., 1956, *Proc. Phys. Soc. (Lond.)*, **69A**, 253
 Nicholls, R. W., Robinson, D., Parkinson, W. and Jarman, W. R., 1956, *Proc. Phys. Soc. (Lond.)*, **69A**, 713

X-RAY DIFFRACTION STUDY OF COPPER AT HIGH TEMPERATURES

G. B. MITRA and S. K. MITRA*

DEPARTMENT OF PHYSICS, INDIAN INSTITUTE OF TECHNOLOGY

KHARAGPUR, INDIA

(Received March 16, 1962)

ABSTRACT. Spectroscopically pure copper was cold worked upon by drawing it in form of a wire and was annealed at 500°C for about eight hours when equilibrium conditions were achieved. X-ray diffraction photographs of the sample at various high temperatures were taken. The lattice parameters as obtained from the photographs gave a nonlinear plot against temperature. The plot of the reciprocal of the volume expansion against the reciprocal of the product of the absolute temperature and the Debye function for energy at that temperature was found to be nonlinear. Similar results have been obtained by analysing the data due to Nix and MacNair. An exponential form of Gruneisen equation has been shown to explain all the above results.

INTRODUCTION

The lattice parameter of pure copper at room temperature has been determined by various authors. A very accurate determination on an extremely pure sample of copper has been carried out by Hume Rothery and Andrews (1942). Before them, Esser, Elander and Bungardt (1938) also determined the same value and claimed great precision in their measurements. Both these groups of workers arrived at the same value, viz., 3.6074 Å.U. at 18°C. These workers had also determined the lattice parameter at various high temperatures. Recently, Eppelsheimer and Penman (1950) have made the same measurements. The values obtained by these various groups of investigators were found to differ from one another. Miller and Russel (1952, 1953) and Eshelby (1953) have shown that lattice defect cause differences in thermal expansion. It is difficult to decide whether this difference is to be attributed to the difference in purity of the samples studied or to the states of strain in them. It was therefore decided to measure the lattice parameters of a sample of copper of known purity and an estimated amount of residual strain.

II. EXPERIMENTAL

(a) Description of the sample

A spectroscopically pure rod of copper supplied by M/s. Johnson Mathey and Co. Ltd., London, was used for preparing the sample. Spectroscopic exami-

*Present address.—Physical Metallurgy section, University of California, Berkeley, California, U.S.A.

nation revealed that it contained an estimated amount of 3 in a million of nickel and lead, of 1 in a million of silicon, iron and lithium, of 0.5 in a million of silver and manganese and less than 1 in a million of sodium, potassium, magnesium and calcium. The copper rod was drawn into a thin wire about 0.5 mm in diameter with the help of a jeweller's die. The cold working consisted of drawing as well as hammering previous to drawing. The sample was then maintained at 500°C for 12 hours and annealed so that room temperature (30°C) was reached after 12 hours. This process was repeated several times till the lattice spacings at 30°C became constant. This indicated that equilibrium conditions were attained. An idea of the defect introduced by cold working was obtained by measuring the resistivity of the sample at room temperature. The specific resistivity of this sample of copper was found to be 1.61×10^{-6} ohms/c.c. as against 1.5106×10^{-6} ohms/c.c. for a single crystal of copper (Metals Handbook).

(b) *X-ray diffraction Technique.*

For determining the lattice parameters of cold worked copper at various temperatures, X-ray powder diffraction technique was used. Nickel filtered copper radiations were used to irradiate the sample mounted on the axis of a 19 cm high-temperature camera. The sample was mounted very carefully on the axis of the camera so as to eliminate the slightest eccentricity. The absence of eccentricity was confirmed by examining the sample through a powerful microscope while the sample was being rotated. The sample was so adjusted that it was found stationary during the rotation for vertical as well as horizontal mount of the microscope. The temperature of the sample was maintained constant with the help of a thermostatic arrangement within $\pm 1^\circ\text{C}$.

The diffraction pattern was calibrated against the powder diffraction pattern of quartz taken with the same camera and under identical experimental conditions. For determining the values of the lattice parameter accurately the well known extrapolation technique developed by Sinclair and Taylor (1945) and by Nelson and Riley (1945) was adopted. For each observed value of the lattice spacing ' d ' the corresponding value of the edge length of the cubic cell ' a ' was calculated and plotted against

$$f(\theta) = \frac{\cos^2 \theta}{\sin \theta} + \frac{\cos^2 \theta}{\theta} \quad \dots (1)$$

where θ is the Bragg angle. The extrapolated value of ' a ' for $f(\theta) = 0$ was accepted to be the true value of the lattice parameter. The accuracy obtained in the measurement of ' a ' was estimated to be $\pm .0001$ A.U.

III RESULTS AND DISCUSSIONS

(a) *Thermal Expansion*

The lattice parameter of copper for various temperatures ranging from 27°C to 527°C are tabulated in Table 1. The change of the lattice parameter with

temperature is shown graphically in Fig. 1. The plot thus obtained is non-linear showing that the rate of change of lattice parameter is not constant. The values of da/dT for different temperatures have been determined from the experimental curve shown in Fig. 1. These have been tabulated in Table II. The experimental results shown in Tables I and II can be summarised by the equation

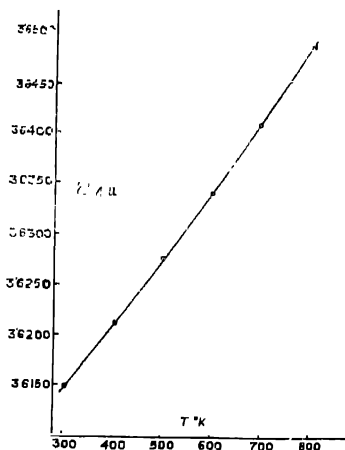


Fig. 1. Lattice dimensions of copper at different temperatures.

$$a_T = 3.61293 + 7.81 \times 10^{-6}T + 3.7 \times 10^{-8}T^2 - 5.2 \times 10^{-11}T^3 \quad (2)$$

where a_T is the lattice constant of copper sample at the temperature $T^\circ\text{K}$.

TABLE I

The variation of lattice constant of copper with temperature (obtained from the present investigation).

Temp. °K	a' A.U.
303	3.6147
403	3.6210
503	3.6276
603	3.6342
703	3.6412
803	3.6486

X-Ray Diffraction Study of Copper at high Temperatures 465

TABLE II

The values of (da/dT) and the coefficient of linear thermal expansion for copper at different temperatures obtained during present investigation

Temp. °K	$(da/dT) \times 10^5$ A.U./°K	Coef. of linear thermal expansion $\times 10^6$
300	6.0	16.60
400	6.2	17.12
500	6.6	18.19
600	6.8	18.71
700	7.2	19.78
750	7.4	20.30

Values of 'a' for copper have been obtained by Hume Rothery and Andrews (1942) at 291°K, 573°K and 773°K respectively. The difference between the values obtained by these authors and the authors of the present investigations may well be due to the changes caused by lattice defects. Vegard and Kloster (1934) reported to have obtained the cell dimensions of copper at 748°K as 3.6589A.U. Nix and MacNair (1942) have also measured the fractional changes in length of copper at various temperatures with respect to its length at 273°K. Their results have been converted into data for lattice parameter at various temperatures with the help of present measurements. Nix and MacNair (1942) have carried out their measurements on a massive polycrystalline annealed sample of copper. Their sample may be taken to be more or less strain free. It is apparent that the lattice dimensions, according to Nix and MacNair (1942) were always less than those of the sample of copper under study. This may very well be attributed to the difference in lattice defect in the two samples due to different residual strains.

Eppelshimer and Penman (1950) have shown that there is no anisotropy in the thermal expansion of copper. A study of the thermal expansion in the various directions of the cold worked copper did not reveal any anisotropy. However, for greater concentration of defects some anisotropy of thermal expansion may be expected.

The thermal expansion of solids has been attributed to the anharmonic vibration of atoms about their mean position. If the potential energy of the atom at a displacement x from their equilibrium separation at 0°K be expressed as

$$U(x) = ax^2 - bx^3 - cx^4$$

where the terms in x^3 represent the asymmetry of the mutual repulsion of the

atoms and the x^4 terms the general 'softening' of the vibration at large amplitudes, the average displacement at temperature $T^\circ K$ can be shown to be (Kittel, 1954).

$$\bar{x} = 3kTb/4a^2$$

where k is the Boltzmann constant. Thus the coefficient of thermal expansion $(1/x_0) dx/dT$ is expected to be independent of temperature. However, as the present experiment reveals, the coefficient of thermal expansion is dependent on temperature. This dependence has been attributed to various types of lattice defects.

(b) *The Gruneisen equation*

Gruneisen (1910) established the relationship connecting the volume expansion $(\partial V/\partial T)$ of a solid with its atomic specific heat C_v given by

$$\left(\frac{\partial V}{\partial T} \right)_p = \gamma K_0 C_v \quad \dots (3)$$

$$\left(\frac{1}{V_0} \frac{\partial V}{\partial T} \right) = \frac{\gamma K_0}{V_0} C_v \quad \dots$$

$$3\alpha = \frac{C_v}{V_0} \quad \dots (4)$$

where Q represents the expression $V_0/\gamma K_0$ where V_0 is the volume of the solid at absolute zero and K_0 is the compressibility at the same temperature. γ is a constant known as Gruneisen constant and α is the coefficient of linear expansion. α is thus proportional to C_v and the variation of α with temperature should be of the same nature as that of C_v .

The above relationship due to Gruneisen can be expressed in various ways Hume Rothery (1945) has discussed the various forms and has recommended the one due to Simon and Vohsen (1928) which states that

$$\frac{V_T - V_0}{V_0} = \frac{E_T}{Q - KE_T} \quad \dots (5)$$

where V_T and V_0 are volumes of the solid at $T^\circ K$ and $0^\circ K$ respectively, E_T the energy imparted to the solid during the change in temperature and Q and K are constants of the substance under investigation. Q in Eq. (5) is identical with that in Eqn. (4). From Eqn. (5), we have

$$\frac{V_0}{V_T - V_0} = \frac{Q}{E_T} - K \quad \dots (6)$$

Putting the Debye expression $9RTD(\theta/T)$ for the energy at $T^\circ K$, where R is the

universal gas constant, $D(\theta/T)$ represent the Debye function for energy θ being the characteristic temperature. We may write

$$\frac{V_0}{V_T - V_0} = \frac{Q}{9RT \cdot D(\theta/T)} - K$$

$$\text{or} \quad \frac{1}{3} \cdot \frac{a_0}{a_T - a_0} = \frac{Q}{9RT \cdot D(\theta/T)} - K \quad \dots (7)$$

Eqn. (7) clearly shows that the plot of $a_0/a_T - a_0$ against $1/T \cdot D(\theta/T)$ should be a straight line. In fact, Fischmeister (1956) actually obtained straight lines representing the variation of $a_0/a_T - a_0$ with $1/T \cdot D(\theta/T)$ for alkali halides. In the present investigations the method used by Fischmeister (1956) for determining the $a_0/(a_T - a_0)$ was adopted. We know

$$(a_T - a_0)/a_0 = (a_T - a_r)/a_r \left(\frac{a_r - a_0}{a_a - a_0} + 1 \right) + \frac{a_r - a_0}{a_a}$$

where a_r represent the lattice constant at the room temperature T_r . Also from Eqns. (4) and (5) with approximation

$$(a_r - a_0)/a_0 = \frac{E_r}{3Q} = \frac{\alpha E_r}{C_v} \quad \dots (8)$$

where E_r is the energy of the solid at room temperature and C_v is the atomic heat at the same temperature a_r , a_r and α are the experimentally determined quantities E_r and C_v were calculated from appropriate Debye expressions and thus $(a_T - a_0)/a_0$ was obtained.

The plot of $a_0/a_T - a_0$ vs $1/T \cdot D(\theta/T)$ is shown in Fig. 2A. It is found to be nonlinear, more or less parabolic, in contradiction to what is expected.

The nonlinearity of the above plot can be attributed to one or more of the following reasons :

- (1) Change in the Debye characteristic temperature due to cold working.
- (2) limitations of the Debye approximation in deriving the expression for energy E_r .
- (3) inaccurate value of α obtained by the extrapolation embodied in Eqn. (7).
- (4) variation with temperature of γ the Gruneisen constant resulting in change of Q with temperature.

Non-linearity in the $a_0/(a_T - a_0)$ vs $1/T \cdot D(\theta/T)$ curves for a number of cubic face centered metals has recently been observed by Mitra and Mitra (1957). In

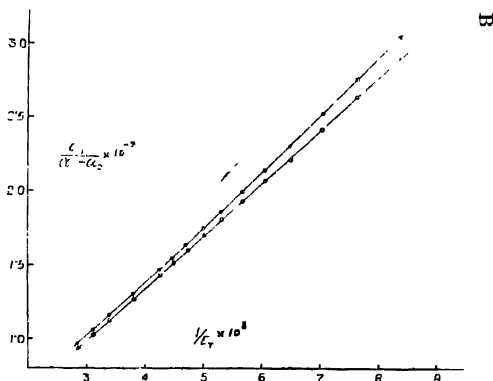


Fig. 2. Plot of $\frac{a_0}{a_T - a_0}$ against $\frac{1}{E_T}$ for copper.

a_0 = lattice constant of copper at 0°K.

a_T = " " " " " " " " T°K.

$$E_T = \int_0^T C_v dT.$$

C_v = atomic heat of copper at constant volume.

A— E_T calculated from Debye formula.

B— E_T calculated from experimentally obtained values of C_v .

order to eliminate uncertainties due to (2) and (3), $E_T = \int_0^T C_v dT$ can be determined from purely experimental values and a_0 can be obtained by extrapolation of a_T vs T curve at very low temperature region.

(c) Extrapolation of a

For the above purpose, it has been found convenient to analyse the data due to Nix and MacNair (1941). Their data have been acclaimed to be extremely accurate and cover a very wide range from 80°K to 800°K. Moreover, the data are for noncoldworked specimen of pure poly-crystalline copper. So the existing specific heat data will be applicable to it. Nix and MacNair (1941) have tabulated the values of $\Delta l/l$ the fractional change in length with temperature, l being the length at 0°C. In order to convert the data due to Nix and MacNair (1941) to that suitable for drawing the a vs T curve, the value of a at 30°C has been taken to be 3.6147 A.U., the value obtained by the present authors. $\Delta a/a_0 = 5.047 \times 10^{-4}$ according to Nix and MacNair (1941). From this a at 0°C has been found to be 3.6129 A.U. Values of a at various temperatures have been determined in a similar way and have been plotted against respective temperatures. This curve is shown in Fig. 3. It will be seen that the curve shows an almost

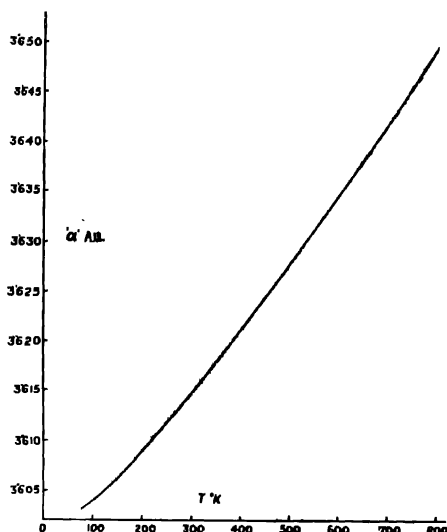


Fig. 3. Plot of lattice constants of copper at different temperatures.
Data due to NiX and Macvair (1941).

linear declination with fall in temperature but shows a sharp bend after 150°K. The curve in the region 80°K to 100°K can be fitted with the equation.

$$a_T = 3.60305 - 1.75 \times 10^{-5}T + 2.6 \times 10^{-7}T^2 \quad \dots (9)$$

from the above equation, the value of a at absolute zero has been found to be 3.60305.

(d) Evaluation of E_T

For the evaluation of $E_T = \int_0^T C_p dT$, values of C_p at various temperatures tabulated by Furukawa and Douglas (1957) were plotted against corresponding temperatures. From this plot required values of C_p have been determined. Values of C_v at various temperatures have been calculated from the thermodynamic relationship.

$$C_p - C_v = \frac{9\alpha_T^2 \cdot K_T \cdot T}{J\rho_T} \quad (10)$$

where α_T is the coefficient of linear expansion at $T^\circ\text{K}$.

K_T is the bulk modulus at $T^\circ\text{K}$.

ρ_T is the density at $T^\circ\text{K}$.

and J is the mechanical equivalent of heat

$\frac{1}{\alpha_0} \frac{d\alpha}{dT}$ was calculated from the graph in Fig. 3 and with the extra-

polated value of α_0 . K_T was taken from the data of Overton and Gaffney (1955). ρ_T was calculated from the experimentally obtained values of α_T and from space group considerations. The values of C_p at various temperatures thus obtained were plotted against the corresponding temperature and the area of the plot enclosed between 0°K to $T^\circ\text{K}$ gave the value of $\int_0^T C_p dT = E_T$ at $T^\circ\text{K}$.

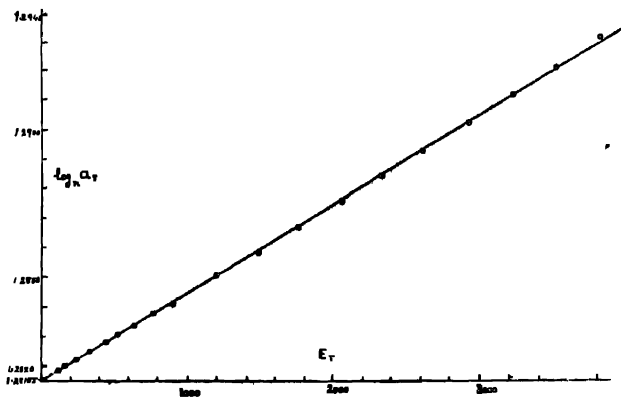


Fig. 4. Plot of logarithm of α_T against E_T . For explanation of symbols see caption of Fig. 2B

With values of α_T , α_0 and E_T thus obtained $\alpha_0/\alpha_T - \alpha_0$ was plotted against $1/E_T$ for various values of T . The resultant curve is shown in Fig. 2B. This is non-linear although with lesser curvature than Fig. 2A.

(e) $\log \alpha_T - E_T$ curves.

In this connection, it is interesting to note that the plot of $\log \alpha_T$ against E_T as shown in Fig. 5 is linear. The intersection of this straight line with the axis of $E_T = 0$ yields the value of $\log \alpha_0$ from which α_0 is found to be 3.6024 A.U. The plot of $\alpha_0/(\alpha_T - \alpha_0)$ against $1/E_T$ from this value of α_0 is observed to be very nearly linear in agreement with the Gruneisen equation. It thus appears to

be evident that the non-linearity in Fig. 3A and Fig. 2B were due to inaccurate values of a_0 . The correct value of a_0 is obtained from the plot in Fig. 4 which suggests the equation.

$$a_T = a_0 e^{CT} \quad \dots (11)$$

C being a constant. C has been calculated from the slope of the straight line in Fig. 4 and is found to be identical with $1/3Q$ where $Q = 120 \times 10$ cal/mol. It is the same value as used by Nix and MacNair (1941) to fit their result with Eqn. (6). Thus from Eqn. (10), we can write

$$\begin{aligned} a_T &= a_0 e^{E_T/Q} \\ &= a_0 \left(1 + \frac{E_T}{3Q} \right) \text{ terms involving higher powers of } E_T/3Q. \\ &= a_0 (1 + E_T/3Q) \text{ where } E_T/3Q \text{ is small.} \\ &= 3Q/E_T \end{aligned} \quad (12)$$

which is the same as Eqn. (6) but for the correction term K can be taken care of by modifying Eq. (11) into $a_T = a_0 e^{E_T/3(Q - KE_T)}$ which reduces to Simon and Vohsen form of Gruneisen equation in the first approximation provided that it thus appears that the correct relationship between a_T and E_T is given by Eq. (13) which reduces to Gruneisen relationship in the first approximation. It is possible that the slight departure from Gruneisen relationship shown by most metals is natural consequence of equation (13) and need not be corrected by assuming fictitious values of either the Debye characteristic temperature as suggested by Nix and MacNair (1941) or for Q as suggested by Hume Rothery (1945). However, Eqn. (12) should be tested at very low temperatures to ascertain whether the value of a_0 obtained from it is correct. We are carrying on investigations on other metals and alloys to find out whether Eqn. (12) holds good to them too.

ACKNOWLEDGMENT

The authors express their grateful thanks to Prof. K. Banerjee and Prof. S. Gupta for their kind interest in the work.

REFERENCES

- Crussard and Aubertin, (1949), *Rev. Metall.*, **46**, 354
 Eppelsheimer and Ponman, 1950, *Physica*, **16**, 792.
 Escholby, 1953, *J. App. Phys.*, **24**, 1249.
 Esser, Eilander and Bungardt, 1938, *Arch. Eisen huttens*, **12**, 157.
 Fischmeister, 1956, *Acta Cryst.*, **9**, 416.

- Furukawa and Douglas, 1957, *Handbook Amer. Instt. of Physics.*, p. 395.
Granoison, 1910, *Ann. Phys. Lpz.*, **33**, 33.
Hume Rothery, and Andrews, 1945, *J Inst Metals*, **68**, 19.
Hume Rothery, 1945, *Proc. Phys. Soc.*, **57**, 209
Kittel, 1954, *Solid State Physics.*, John Wiley.
Lawson, 1950, *Phys. Rev.*, **78**, 185.
Metals Handbook—American Society of Metals (1945)
Miller and Russol, 1953, *J. App Phys.*, **24**, 1248
Mitra and Mitra, 1957, *Nature*, **179**, 1295.
Nelson and Riley, 1945, *Proc. Phys. Soc.*, **57**, 160.
Nix and MacNair, 1941, *Phys. Rev.*, **60**, 597.
Nix and MacNair, 1942, *Phys. Rev.*, **61**, 74.
Ovorton and Gaffnoy, 1955, *Phys. Rev.* **98**, 969.
Seeger, 1955, *Handbuch der Physik*, **7**, 392.
Simon and Vohsen, 1928, *Z. Phys. Chem.*, **133**, 165.
Sinclair and T aylor, 1945, *Proc. Phy. Soc.*, **57**, 108.
Uno, 1951, *Chem. Abs.*, **46**, 6890., *Bussuoron Kenkyu*, **36**, 32.
Vegard and Kloster, 1934, *Z. Krist.*, **89**, 560.

ON THE POLARIZATION OF RADIO-WAVE TRAVELLING THROUGH THE IONOSPHERE

S. K. BANERJEE and S. R. KHASTGIR

UNIVERSITY COLLEGE OF SCIENCE, UNIVERSITY OF CALCUTTA

(Received, June 8, 1963)

ABSTRACT. The limiting polarization as deduced by Baker and Green without taking the usual Appleton-Hartree formulae has been shown to be identical with the limiting polarization deduced directly from the Appleton-Hartree formulae. From Bailey's formulae for the amplitude-ratio of the normal to the abnormal components of the magnetic vector of the radio-wave, the phase-difference between them at any level of the ionosphere has been deduced for $\nu \ll \nu_c$ where ν_c is the critical collisional frequency. It has also been shown that for $\nu \ll \nu_c$, the amplitude ratio is nearly unaffected at any level by electron collisional frequency.

1. *Identity of the expression for the limiting polarization as given by Baker and Green with that deduced directly from the Appleton-Hartree formulae*

Without taking the usual Appleton-Hartree formulae (1927, 1929) it was shown by Baker and Green (1933) that the limiting polarization R_a is given by the roots of the following equation.

$$R_a^2 + \frac{l^2}{n} q' R_a - 1 = 0 \quad (1)$$

where

$$R_a = \frac{E_y}{jE_t}, \quad \frac{l^2}{n} = \frac{\sin^2 \theta}{\cos \theta}, \quad q' = \frac{p_0}{p - j\nu}, \quad p_0 = \frac{eH}{mc} \quad (2)$$

θ = angle between the direction of propagation of the radio-wave and the positive direction of earth's magnetic field.

E_y = component of the electric vector along OY (Fig. 1).

E_t = component of the electric vector along OT (Fig. 1).

H = intensity of earth's magnetic field.

e, m = electronic charge and mass.

ν = electronic collisional frequency.

c = velocity of light in vacuum.

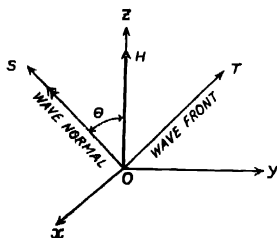


Fig. 1. Co-ordinate system used by Baker and Green. OS —wavenormal
 OT —wavefront
 H —earth's magnetic field

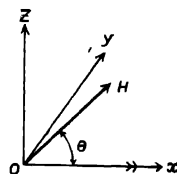


Fig. 2. Right-handed co-ordinate system used by Appleton
 OX —wave normal
 H —earth's magnetic field

When the right-handed co-ordinate system of Fig. 2 is used, where the direction of propagation of the radio-wave has been taken along OX -axis, it can be shown that

$$R_a = \frac{h_y}{jE} = -j \left(\frac{hz}{hy} \right) \quad (3)$$

where

hz = component of the magnetic vector along OZ (Fig. 2).

hy = component of the magnetic vector along OY (Fig. 2).

From Eq. (3)

$$\left(\frac{hz}{hy} \right) = jR_a \quad (3a)$$

Solving Eq. (1), we have

$$R_a = -\frac{l^2}{2n} q' \pm \sqrt{\frac{l^4}{4n^2} q'^2 + 1} \quad (1a)$$

Putting the value of l^2/n and q' from Eq. (2) in Eq. (1a)

$$R_a = -\frac{eH \sin^2 \theta}{2mc \cos \theta (p - j\nu)} \pm \sqrt{\frac{e^2 H^2 \sin^4 \theta}{4m^2 c^2 \cos^2 \theta (p - j\nu)^2} + 1} \quad \dots \quad (1b)$$

Since the critical collisional frequency is

$$\nu_c = \frac{p_H \sin^2 \theta}{2 \cos \theta}, \text{ where } p_H = \frac{eH}{mc}$$

we get

$$R_a = -\frac{\nu_c}{p - j\nu} \pm \sqrt{\frac{\nu_c^2}{(p - j\nu)^2} + 1} \quad (1c)$$

Using (1c) and (3a) :

$$\left(\frac{hz}{hy} \right) = j \left[- \frac{\nu_e}{p - j\nu} \pm \sqrt{1 - \frac{\nu_e^2}{(p - j\nu)^2}} + 1 \right] \quad \dots \quad (1d)$$

This equation can be deduced *directly* from the Appleton-Hartree formula. Appleton used the right-handed co-ordinate system of Fig 2 and the polarization is given by

$$\left(\frac{hz}{hy} \right) = R = - \frac{j}{\gamma_L} \left[- \frac{\gamma_T^2}{2(1 + \alpha + j\beta)} \pm \sqrt{1 - \frac{\gamma_T^4}{4(1 + \alpha + j\beta)^2} + \gamma} \right] \quad \dots \quad (4)$$

Using $\alpha = -p^2/p_0^2$, $\beta = p\nu/p_0^2$, $p_0^2 = 4\pi Ne^2/m$, $\gamma = p_T^2 - p\rho_{LT}/p_0^2$

Eq (4) can be written as

$$R = - \frac{j}{p_L} \left[- \frac{p p_T^2}{2(p_0^2 - p^2 + j p \nu)} \pm \sqrt{1 - \frac{p^2 p_T^2}{4(p_0^2 - p^2 + j p \nu)^2} + p_L^2} \right] \quad \dots \quad (4a)$$

Hence the limiting value is obtained by putting $p_0^2 = 0$ (i.e. $N = 0$) in Eq. (4a)

$$R = \left(\frac{hz}{hy} \right) = j \left[- \frac{\nu_e}{p - j\nu} \pm \sqrt{1 - \frac{\nu_e^2}{(p - j\nu)^2}} + 1 \right] \quad \dots \quad (4b)$$

It is seen that Eqs (1d) and (4b) are identical.

2. *Evaluation of the phase-difference between the normal and the abnormal Components of the magnetic vector of a radio-wave at any level of the ionosphere for $\nu < \nu_e$*

It was shown by Bailey (1934) that the amplitude-ratios of the normal to the abnormal components of magnetic vector are given by

$$\rho_0 = a \left[1 - \frac{d_1}{d_2} \cot \phi_0 \right] \text{ for the } O\text{-mode} . \quad \dots \quad (5a)$$

and

$$\rho_x = a \left[1 + \frac{d_1}{d_2} \cot \phi_0 \right] \text{ for the } X\text{-mode} . \quad \dots \quad (5b)$$

where

$$a = \frac{1}{2} [\sqrt{1 + Y} + \sqrt{1 + Y'}] \\ Y = 2 \frac{d_1 d_2^2}{d_1^2 + d_2^2} + \frac{d_1^3 d_2^2}{d_1^2 + d_2^2} \quad \dots \quad (5c)$$

$$Y' = -2 \frac{d_1 d_2^2}{d_1^2 + d_2^2} + \frac{d_1^2 d_2^2}{d_1^2 + d_2^2}$$

$$d_1 = v_c/v, \quad d_2 = v_c/p', \quad p' = p \left(1 - \frac{p_0^2}{p^2} \right), \quad p_0^2 = \frac{4\pi N e^2}{m}$$

ϕ_0 = phase-difference for the O -mode.

Using Eq. (5c), it can be shown

$$Y = \frac{v_c}{v^2 + p'^2} (2v + v_c) \quad \dots \quad (6a)$$

$$Y' = \frac{v_c}{v^2 + p'^2} (v_c - 2v) \quad \dots \quad (6b)$$

Using Eqs. (5a) and (5b) and the relation, $\rho_0 \rho_x = 1$,

$$\cot \phi_0 = \pm \frac{d_2}{d_1} \sqrt{1 - \frac{1}{a^2}} \quad \dots \quad (7a)$$

When $v < v_c$, we get from (6a), (6b) and (5c),

$$Y = Y' \simeq \frac{v_c^2}{v^2 + p'^2} \quad \dots \quad (6c)$$

$$\text{Hence} \quad a^2 \simeq \frac{p'^2 + v_c^2}{p'^2 + v^2} \quad \dots \quad (6d)$$

Using (6d) and (7a)

$$\tan \phi_0 \simeq \pm \frac{p'}{v} \sqrt{1 + \frac{p'^2}{v_c^2}} \quad \dots \quad (7b)$$

According to Murty and Khastgir (1960), ϕ_0 lies in the first quadrant for the vertically downcoming wave in the northern hemisphere, hence taking the positive sign in (7b), we have

$$\tan \phi_0 \simeq \frac{p'}{v} \sqrt{1 + \frac{p'^2}{v_c^2}} \quad \dots (7c)$$

Similarly, for the vertically downcoming radio wave in the southern hemisphere :

$$\tan \phi_0 \simeq - \frac{p'}{v} \sqrt{1 + \frac{p'^2}{v_c^2}} \quad \dots \quad (7d)$$

From Eq. (7c), we can draw several conclusions .

(a) At the level $p_0^2 = p^2$ (i.e. $p' = 0$), the wave is plane-polarised.

(b) The sense of rotation of the magnetic vector is reversed when the wave crosses the level $p_0^2 = p^2$.

(c) Since at the lower boundary of the ionosphere, $p' = p$ and at the level, $p_0^2 = p^2$, $p' = 0$, the phase-difference gradually increases from zero to a certain value depending on p , v , and v_c as the wave comes down from the level, $p_0^2 = p^2$, to the lower boundary of the ionosphere.

(d) At the level $p_0^2 = p^2 - pp_H$,

$$[\tan \phi_0]_{p_0^2 = p^2 - pp_H} = \frac{p_H}{v} [\cot^2 \theta + \operatorname{cosec}^2 \theta]$$

3. Effect of electron collisional frequency on the amplitude-ratio at any level for $v < v_c$.

It can be shown from the Appleton-Hartree formulae (1927, 1929) that the amplitude-ratio for the ordinary mode for vertically down-coming radio-wave in the northern hemisphere for zero collisional frequency is given by

$$\rho_0 = -\frac{v_0}{p'} + \sqrt{1 + \frac{v_c^2}{p'^2}} \quad (8)$$

where

$$p' = p \left(1 - \frac{p_0^2}{p^2} \right), \quad v_c = p_H \sin^2 \theta / 2 \cos \theta$$

From Eq. (8), it can be shown .

$$\left[\frac{1 + \rho_0^2}{1 - \rho_0^2} \right]_{v=0} = \frac{\sqrt{v_c^2 + p'^2}}{v_c} \quad (9)$$

It has been shown by Murty and Khastgir (1959) that

$$\rho_0 = \frac{a'}{v_c} \left[\frac{v}{\cos \phi_0} - \frac{p'}{\sin \phi_0} \right] \quad (10a)$$

and

$$\rho_x = \frac{a'}{v_c} \left[\frac{v}{\cos \phi_0} + \frac{p'}{\sin \phi_0} \right] \quad (10b)$$

where

$$a' = \frac{v_c}{\sqrt{v^2 + p'^2}}$$

Using $\rho_0 \rho_z = 1$, we have from Eqs. (10a), (10b)

$$\rho_0^2 = \frac{\nu}{\cos \phi_0} \frac{p'}{\sin \phi_0} \quad \dots \quad (10c)$$

Hence from Eq. (10c)

$$\left[\frac{1 + \rho_0^2}{1 - \rho_0^2} \right]_{\nu=0} = \frac{\nu}{p'} \tan \phi_0 \quad \dots \quad (11)$$

Using (11), (7c),

$$\left[\frac{1 + \rho_0^2}{1 - \rho_0^2} \right]_{\nu=0} = \sqrt{\nu_c^2 - 1} p'^2 \quad \dots \quad (11a)$$

and from (11a) and (9)

$$[\rho_0]_{\nu \neq 0} \approx [\rho_0]_{\nu=0}$$

This means that at any level of the ionosphere, the amplitude-ratio for the O -mode is nearly unaffected by electron collisional frequency provided the critical collisional frequency is much larger than electron-collisional frequency. The same conclusion can be drawn for X -mode also.

REFERENCES

- Appleton, E. V., 1927, U.R.S.I. Paper.
 Bailey, V. A., 1934, *Phil. Mag.*, **19**, 376.
 Baker, W. G. and Green, A. L., 1933, *Proc. I.R.E.*, **21**, 1103.
 Hartree, D. R., 1929, *Proc. Camb. Phil. Soc.*, **25**, 47.
 Murty, Y. S. N. and Khastgir, S. R., 1959, *Proc. Nat. Inst. Sci.*, **25A**, No. 5.
 Murty, Y. S. N. and Khastgir, S. R., 1960, *Jour. Geo. Res.*, **65**, May Issue.

THE CHAPMAN-COWLING SECOND APPROXIMATION TO THE VISCOSITY COEFFICIENT OF BINARY GAS MIXTURES

S. C. SAXENA and R. K. JOSHI

DEPARTMENT OF PHYSICS, RAJASTHAN UNIVERSITY, JAIPUR, INDIA

(Received, March 21, 1963)

ABSTRACT The additional bracket integrals needed for the Chapman-Cowling second approximation to the coefficient of viscosity of a binary gas mixture, $[\eta_{mix}]_2$, have been reported. The rigorous $[\eta_{mix}]_2$ expression is further simplified where the approximation $M_1 \gg M_2$ is valid and also for the case where the additional condition $\sigma_{11} > \sigma_{22}$ holds. Numerical calculations for the specific systems as well as for certain ideal cases have been performed to examine and demonstrate the accuracies of the new formulae derived. The maximum contribution of the second approximation for most of the actual systems will be of the order of one per cent.

INTRODUCTION

Recent attempts to measure the transport coefficients to a high degree of precision and their subsequent analysis to determine the intermolecular forces in conjunction with the Chapman-Enskog theory have necessitated the knowledge of more accurate theoretical expressions than were available till a few years back. In the theoretical formulation of Chapman and Cowling (1953) all the transport coefficients are finally represented by an infinite series and the calculation of higher approximations involves only the evaluation of increasing number of terms of this series. In this fashion gaseous diffusion, thermal conductivity and thermal diffusion have already been investigated to some extent, and in the present paper we consider the coefficient of viscosity of a binary mixture, η_{mix} . Only the formulation as given by Chapman and Cowling (1953) will be considered and an alternative treatment according to Kihara (1949) and extended Kihara scheme as given by Mason (1957) will be postponed for the time being till more numerical calculations are performed for the specific systems and its need is realized. It may be pointed out that the accurate determination of viscosity of gaseous mixtures is being pursued in several laboratories and that such data may be used to evaluate the molecular potentials as indicated by Hirschfelder, Taylor, Kihara and Rutherford (1961). Srivastava (1961) has already used some viscosity data to determine the unlike interactions of several gas pairs. For an accurate interpretation of all these works the analysis of higher approximations will be essential. In this paper we give the expression for the second

approximation to η_{mix} and discuss results for the Ar-He and He-Xe systems in detail and a few other cases of interest.

EVALUATION OF BRACKET INTEGRALS

The determination of higher approximations to transport coefficients according to the procedure of Chapman and Cowling (1953) essentially involves the evaluation of a set of bracket integrals. The details of this calculation are given by Chapman and Cowling (1953) and will not be repeated here. Some of these bracket integrals have been evaluated by Chapman and Cowling (1953), and by Mason (1954, 1957). The additional integrals needed for the second approximation to η_{mix} are listed below

$$\left[S_{\frac{5}{2}}^{(1)}(C_1^2) \mathcal{C}_1^0 \mathcal{C}_1, \mathcal{C}_2^0 \mathcal{C}_2 \right]_{12} = - \frac{4M_1 M_2^2}{3(M_1 + M_2)^3} [70\Omega_{12}^{(1,1)} - 28\Omega_{12}^{(1,2)} - 21\Omega_{12}^{(2,2)} + 6\Omega_{12}^{(2,3)}],$$

$$\left[\mathcal{C}_1^0 \mathcal{C}_1, S_{\frac{5}{2}}^{(1)}(C_2^2) \mathcal{C}_2^0 \mathcal{C}_2 \right]_{12} = - \frac{4M_1^2 M_2}{3(M_1 + M_2)^3} [70\Omega_{12}^{(1,1)} - 28\Omega_{12}^{(1,2)} - 21\Omega_{12}^{(2,2)} + 6\Omega_{12}^{(2,3)}],$$

$$\left[S_{\frac{5}{2}}^{(1)}(C_1^2) \mathcal{C}_1^0 \mathcal{C}_1, S_{\frac{5}{2}}^{(1)}(C_2^2) \mathcal{C}_2^0 \mathcal{C}_2 \right]_{12} = - \frac{2M_1^2 M_2^2}{3(M_1 + M_2)^4} [770\Omega_{12}^{(1,1)} - 392\Omega_{12}^{(1,2)} - 301\Omega_{12}^{(2,2)} + 64\Omega_{12}^{(1,3)} + 84\Omega_{12}^{(2,3)} - 12\Omega_{12}^{(2,4)} + 24\Omega_{12}^{(3,3)}],$$

$$\left[S_{\frac{5}{2}}^{(1)}(C_1^2) \mathcal{C}_1^0 \mathcal{C}_1, \mathcal{C}_1^3 \mathcal{C}_1 \right]_{12} = \frac{4M_1^2}{3(M_1 + M_2)^3} [70M_1\Omega_{12}^{(1,1)} - 28M_1\Omega_{12}^{(1,2)} + 21M_2\Omega_{12}^{(2,2)} - 6M_2\Omega_{12}^{(2,3)}],$$

$$\left[S_{\frac{5}{2}}^{(1)}(C_1^2) \mathcal{C}_1^0 \mathcal{C}_1, S_{\frac{5}{2}}^{(1)}(C_2^2) \mathcal{C}_1^0 \mathcal{C}_1 \right]_{12} = \frac{2M_2}{3(M_1 + M_2)^4} [2M_1(140M_1^2 + 245M_2^2)\Omega_{12}^{(1,1)} - 392M_1M_2\Omega_{12}^{(1,2)} + 64M_1M_2\Omega_{12}^{(1,3)} + (154M_1^2M_2 + 147M_2^3)\Omega_{12}^{(2,2)} - 84M_2^2\Omega_{12}^{(2,3)} + 12M_2^3\Omega_{12}^{(2,4)} + 24M_1M_2^2\Omega_{12}^{(3,3)}].$$

Here the bold letters refer to vector quantities, $\Omega_{ij}^{(l,n)}$ are the Chapman-Cowling collision integrals, M_1 and M_2 are the molecular weights of species 1 and 2 respectively, and rest of the quantities are as defined by Chapman and Cowling (1953).

THEORETICAL FORMULAE FOR VISCOSITY

According to Chapman and Cowling (1953) the coefficient of viscosity of a binary gas mixture, η_{mix} , is given by

$$\eta_{mix} = \frac{5}{8}kT \sum_{i,j} \frac{L_{ij} [X_1^2 B_{11}^{(m)} - 2X_1 X_2 B_{1-1}^{(m)} + X_2^2 B_{-1-1}^{(m)}]}{X_1 X_2 B^{(m)}}, \quad \dots \quad (1)$$

where X_i is the mole fraction of the species i , k is the Boltzmann's constant, T is the temperature of the gas mixture, $B^{(m)}$ is a symmetrical determinant of order $2m$, whose general term is b_{ij} , where i and j range from $-m$ to $+m$, excluding zero, the minor of $B^{(m)}$ obtained by suppressing the row and column containing b_{ij} is denoted by $B_{ij}^{(m)}$. The determinant elements b_{ij} necessary for the first approximation, $m = 1$ in Eq. (1) usually denoted by $[\eta_{mix}]_1$, are already given by Chapman and Cowling (1953). Now a days it is more common to use the reduced collision integrals, $\Omega_{ij}^{(l,n)*}$ which are defined as the ratio of $\Omega_{ij}^{(l,n)}$ to its value for the rigid sphere model, Hirschfelder, Curtiss and Bird (1954). In this notation Eq. (1) becomes

$$\eta_{mix} = \frac{RT}{2N\sigma_{12}^2} \left\{ \frac{1}{2\pi} \left(\frac{M_1 M_2}{M_1 + M_2} \right)^{\frac{1}{2}} \frac{L}{\sigma_{12}} [X_1^2 B_{11}^{(m)} - 2X_1 X_2 B_{1-1}^{(m)} + X_2^2 B_{-1-1}^{(m)}] X_1 X_2 B^{(m)} \right\} \quad (2)$$

where N is the Avogadro's number, R is the gas constant per mole, σ_{12} is a distance parameter characteristic of the interaction between two molecules of types 1 and 2, and its exact definition follows from the particular form chosen for the intermolecular potential. $B^{(m)}$ and $B_{ij}^{(m)}$ are again defined in the same fashion as in connection with Eq. (1) except that b_{ij} are now defined differently. The Eq. (2) quoted by Mason (1957) contains a misprint.

The calculation of η_{mix} , according to Eq. (2), requires the knowledge of determinants, $B^{(m)}$, $B_{11}^{(m)}$, $B_{-1-1}^{(m)}$, $B_{-1-1}^{(m)}$ and hence the determinant elements, b_{ij} . The additional b_{ij} needed for the second approximation $m = 2$, in Eqs (1) and (2) usually denoted by $[\eta_{mix}]_2$, have been evaluated by Saxena and Joshi (1963) and will not be reproduced here because of their length.

The formula for $[\eta_{mix}]_2$ can be simplified for certain limiting cases of binary gas mixtures. The systems where either of the components is present in small concentration is not very interesting because then the system reduces to the case of a pure gas for which the contribution of higher approximations is known. The case when $M_1 \gg M_2$, so that higher powers of $M = (M_2/M_1)$ are negligible, is interesting. Much simpler expressions for the four determinants of Eq. (2) are obtained if these determinants are expanded and only those terms are retained which contain the explicit power of M smaller than two. The simpler expressions are

$$B^{(2)} = (b_{11}b_{22} - b_{12}^2)(b_{-1-1}b_{-2-2} - b_{-1-2}^2), \quad (3)$$

$$B_{11}^{(2)} = b_{22}(b_{-1-1}b_{-2-2} - b_{-1-2}^2), \quad (4)$$

$$B_{-1-1}^{(2)} = b_{22}(b_{1-1}b_{-2-2} - b_{1-2}b_{-1-2}), \quad (5)$$

$$B_{-1-1}^{(2)} = b_{-2-2}(b_{11}b_{22} - b_{12}^2). \quad (6)$$

If the additional condition $\sigma_{11} \gg \sigma_{22}$ holds, so that terms containing σ_{22}/σ_{11} are negligible, the above expressions get further simplified. The final results are

$$B^{(2)} = \{(b'_{11} + (X_1/X_2)B''_{11})(b'_{22} + (X_1/X_2)B''_{22}) - (b'_{12} + (X_1/X_2)B''_{12})^2\} \\ (b_{-1-1}b'_{-2-2} - b'^2_{-1-2}), \dots \quad (7)$$

$$B^{(2)}_{11} = (b'_{22} + (X_1/X_2)B''_{22})(b'_{-1-1}b'_{-2-2} - b'^2_{-1-2}), \dots \quad (8)$$

$$B^{(2)}_{1-1} = (b'_{22} + (X_1/X_2)B''_{22})(b'_{-11}b'_{-2-2} - b'^2_{-1-2}b_{-11}), \dots \quad (9)$$

$$B^{(2)}_{-1-1} = b'_{-2-2}\{(b'_{11} + (X_1/X_2)B''_{11})(b'_{22} + (X_1/X_2)B''_{22}) \\ (b'_{12} + (X_1/X_2)B''_{12})^2\} \dots \quad (10)$$

B''_i are obtained from corresponding b_i by substituting $\sigma_{11} = 2\sigma_{12}$

Even for those systems where M is not sufficiently small fairly accurate values of $[\eta_{mix}]_2$ can be obtained from the above equations if Eq. (3) is replaced by the following

$$B^{(2)} = (b_{11}b_{22} - b_{12}^2)(b_{-1-1}b_{-2-2} - b_{-1-2}^2) - b_{22}(b_{-2-2}b_{1-1}^2 \\ + b_{-1-1}b_{1-2}^2) - b_{11}(b_{-2-2}b_{-12}^2 + b_{-1-1}^2b_{2-2}), \dots \quad (11)$$

The additional terms in Eq. (11) arise from those elements of the Chapman-Cowling determinant, $B^{(2)}$, which contain the product of two diagonal terms. Such terms do not occur in Eqs. (4) to (6) which therefore remain unaltered. This procedure has also proved very successful in improving the accuracies of the simpler formulae for the Chapman-Cowling second approximation to the thermal diffusion factor of the binary gas mixtures, Saxena and Joshi (1963a, 1963b).

RESULTS AND DISCUSSION

Sample calculations were first performed to estimate the accuracy of the approximate formulae derived in the previous section. It was found that for values of $M < (1/30)$ the approximate formula, Eq. (2) in conjunction with Eqs. (3) to (6), yield fairly accurate values. Thus, for the He-Xe system the rigorous and approximate second approximation values differ only by 0.037%, while the difference between the values of the first two approximations of η_{mix} is 1.6%. This calculation was done according to the rigid sphere model and it was assumed that $\sigma_{11}/\sigma_{12} = 1.387$ and $X_1/X_2 = 10$. For systems where $M > (1/30)$ it was found essential to replace Eq. (3) by Eq. (11). Computed values of η_{mix} for the specific case of He-Ar are given in the Table I. It is seen that the maximum difference between the approximate and rigorous $[\eta_{mix}]_2$ values is 0.09%. Equation (2) in conjunction with Eqs. (7) to (10) is also quite accurate if $\sigma_{11} \gg \sigma_{22}$. Under this condition and on the rigid sphere model for $M = (1/30)$ the approximate $[\eta_{mix}]_2$ value differs from the rigorous value only by 0.03%, while the second approximation value is 2.8% greater than the first approximation value.

In general, the difference between the first and second approximations to η_{mix} will depend upon the temperature, composition, on the nature of the intermolecular potential and will differ from system to system. For the He-Ar system on the rigid sphere model if it is assumed that $(\sigma_{11}/\sigma_{12}) = 1$ we find that the percentage difference between the first two approximations is 1.2 when $X_1/X_2 = 10$, and 0.9 when $X_1/X_2 = 1$. The calculations reported in the Table I for this system on a realistic modified Buckingham exp-six potential in conjunction with the potential parameters given by Mason (1955), reveal that the maximum contribution of the second approximation is only 0.6%. The contribution of the second approximation will usually reduce as M reduces. Thus, when M is reduced from (1/30) to 10^{-10} the contribution of second approximation falls from 2.8 to 1.5%, for the rigid sphere model and with the assumption that $\sigma_{22} = \sigma_{11}$.

To see the dependence on composition we consider the experimental data of Rietveld, Uiterbeek and Van Den Berg (1953) for He-Ar system at $T = 291^\circ\text{K}$. These data are listed in the Table I and involve the experimental uncertainty of about 1%. It is seen from this table that the difference between the first and second approximations does not vary much with the composition though it exhibits an increase as the proportion of the lighter component increases in the mixture. Thus, though the contribution of the second approximation is comparatively small yet its knowledge is essential in view of the high precision ($\sim 0.1\%$) attainable in the measurements of viscosity, Kestin and Leidenfrost (1959).

Another point to note in Table I is that consideration of higher approximation to η_{mix} mostly improves the agreement between theory and experiment. Further, the theoretical values of η_{mix} according to the exp-six potential are in better agreement with the experiment than the calculated values of Rietveld *et al.* (1953) on the familiar Lennard-Jones (12-6) potential. This again tends to simply confirm the earlier view of Weissman, Saxena and Mason (1960) that the exp-six is a better potential for He-Ar system than L-J (12-6) potential.

It will also be interesting to examine the contribution of the second approximation at still higher temperatures. To investigate this we choose He-Xe system for which Chapman-Enskog theory holds rigorously and the two molecules are widely different. The calculations have been performed according to L-J(12-6) potential and using the Eqs (2) to (6). The potential parameters for He ($\epsilon/k = 10.22^\circ\text{K}$, $\sigma = 2.556\text{\AA}$) as given by Hirschfelder, Curtiss and Bird (1954), and for X_e of Whalley and Schneider (1955) were used. The reason for choosing this particular set for X_e lies in its ability to correlate all the observed properties as shown by Saxena and Joshi (1963c). The parameters for the unlike interaction were computed by the conventional combination rules viz., geometric mean rule for ϵ_{12} and arithmetic mean rule for σ_{12} . The final results are tabulated in Table II. The contribution of the second approximation increases with temperature and also with the increasing percentage of the lighter component.

TABLE I

Experimental and calculated values of η_{mix} in μP for He-Ar system at $T = 291.1^\circ K$ as a function of composition

% He	η_{mix} Exptl	Theoretical	η_{mix} values		Percentage deviation	
		$[\eta_{mix}]_{12}^{T,0}$	$[\eta_{mix}]_{12}^{T,0}$	$[\eta_{mix}]_{12}^{approx}$	Columns 3 and 4	Columns 4 and 5
11.4	222.3	221.48	222.0	222.06	0.2	0.03
13.65	224.3	223.27	223.93	223.98	0.3	0.02
20.1	224.0	223.40	224.05	224.10	0.3	0.02
29.2	228.1	225.32	225.99	226.08	0.3	0.04
38.2	229.4	226.83	227.77	227.66	0.4	0.05
51.0	230.9	228.27	229.27	229.34	0.5	0.03
53.9	231.1	228.45	229.63	229.49	0.5	0.06
59.4	230.4	228.34	229.38	229.40	0.4	0.01
70.2	229.0	226.58	227.62	227.75	0.4	0.06
80.4	222.9	221.56	222.68	222.85	0.5	0.08
89.7	210.1	211.97	213.30	213.51	0.6	0.09

*Values obtained from eqn. (2) in conjunction with eqns. (4) to (6) and (11)

TABLE II

The ratio $[\eta_{mix}]_2/[\eta_{mix}]_1$ for the He-Xe system at various temperatures and composition on L-J(12-6) potential

% Xe	T °K			
		300	600	1000
0.0001		1.0078	1.0077	1.0076
25		1.0067	1.0077	1.0083
50		1.0058	1.0066	1.0077
75		1.0023	1.0058	1.0065
99.9999		1.0002	1.0027	1.0050

REFERENCES

- Chapman, S., and Cowling, T. G., 1933, *The Mathematical Theory of Non-Uniform Gases* (Cambridge University Press).
- Hirschfelder, J. O., Curtiss, C. F., and Bird, R. B., 1954, *Molecular Theory of Gases and Liquids* (New York: John Wiley).
- Hirschfelder, J. O., Taylor, M. H., Kihara, T., and Ruthertford R., 1961, *Phys. Fluids*, **4**, 663
- Kestin, J., and Leidolfrost, W., 1959, *Physica*, **25**, 1033
- Kihara, T., 1949, *Imperfect Gases*, Originally published in Japanese by Asakura Bookstore, Tokyo, Japan, and Translated into English by the U.S. Office of Air Research, Wright-Patterson Air Force Base, See also, 1953, *Rev. Mod. Phys.*, **25**, 831
- Mason, E. A., 1954, *J. Chem. Phys.*, **22**, 169, 1955
- Mason E. A., 1955, *J. Chem. Phys.*, **23**, 49
- Mason, E. A., 1957, *J. Chem. Phys.*, **27**, 75
- Rietveld, A. O., Van Itterbeek, A., and Van Den Berg, G. J., 1963, *Physica*, **19**, 617.
- Saxena, S. C., and Joshi, R. K., 1963, *Physica*, **29**, in press
- Saxena, S. C. and Joshi, R. K., 1963a, *Canadian J. Phys.*, **41**, 207
- Saxena, S. C. and Joshi, R. K., 1963b, *Ind. J. Phys.*, **37**, 235
- Saxena, S. C. and Joshi, R. K., 1963c, *Physica*, **29**, 257
- Srivastava, I. B., 1961, *Ind. J. Phys.*, **35**, 86
- Weissman, S., Saxena, S. C., and Mason, E. A., 1960, *Phys. Fluids*, **3**, 610
- Whalley, E., and Schneider, W. G., 1955, *J. Chem. Phys.*, **23**, 1644.

r -CENTROIDS AND THEIR PROPERTIES OF ($A'\pi \rightarrow X^1\Sigma^+$) SYSTEM OF PN

S. SANKARANARAYANAN

DEPARTMENT OF PHYSICS, INDIAN INSTITUTE OF SCIENCE,
BANGALORE 12, INDIA

(Received, April 3, 1963)

ABSTRACT. The r -centroids of ($A'\pi \rightarrow X^1\Sigma^+$) system of PN have been investigated using a Morse Potential function. The applicability of the Morse potential for the present calculation has been justified from Pekeris relation and by a comparison of the r_{min} and r_{max} obtained from Morse potential with those evaluated from the 'true' potential. The calculated values of the $\bar{r}_{v'v''}$ show that $\bar{r}_{v'v''}$ increases with $\lambda_{v'v''}$, that the potentials are not very anharmonic and are not very broad. The graphical and quadratic equation methods yield values of r -centroids which are in good agreement.

INTRODUCTION

Diatomic molecules of atoms of group V of the periodic table are of special interest because they have nearly the same mass as the heteronuclear molecules derived from atoms belonging to group IV and VI respectively and have the same number of electrons. In fact each molecule of the former type is found to be similar to two molecules of the latter category e.g., PN similar to SiO and CS. The vibrational coefficients of the ground state of these isoelectronic molecules show a similarity in regard to the trend of variation and the order of magnitude. But in the case of the excited states of the 22-electron molecules SiO, CS and PN, numerical similarities of the electronic energies and vibrational constants are noticed only between PN and CS. Recently McGregor, Nicholls and Jarmain (1961) have evaluated the Franck-Condon factors and r -centroids for the $A'\pi - X^1\Sigma^+$ system of SiO. The r -centroid is dependent on both the electronic states involved in the transition and is essential for a study of R_e the electronic transition moment. It was considered desirable therefore to calculate the r -centroids for PN and compare them with those of the corresponding isoelectronic molecule, viz., SiO.

THEORY AND METHODS OF CALCULATION

The r -centroid $\bar{r}_{v'v''}$ of a molecular band ($v' \rightarrow v''$) can be defined as (Nicholls and Jarmain, 1956).

$$\bar{r}_{v'v''} = \int \psi_{v'} r \psi_{v''}^* dr / \int \psi_{v'} \psi_{v''}^* dr \quad \dots (1)$$

and is an average internuclear separation which can be associated with that

particular transition. The ψ 's are the vibrational eigenfunctions and r is the internuclear distance. The square of the overlap integral $\int \psi_{v''} \psi_{v'} dr$ gives the Franck-Condon factor. A knowledge of the r -centroid and the Franck-Condon factors and band intensities will enable the evaluation of the dependence of electronic transition moment B_e on internuclear distance r . The r -centroids for the ${}^1\pi \rightarrow {}^1\Sigma^+$ system of PN have been evaluated by two different computational techniques. As both the methods assume the validity of the Morse potential type of expression for the molecule, one has to first examine if a potential function of the Morse type can reasonably be used to approximate the 'true' potentials of both the electronic states involved in this band system. This was done by determining the 'true' potential curves by the Klein-Dunham-Jarmain method (Jarmain, 1959) using data given by Herzberg (1950) and comparing the corresponding points on the Morse potential curves. The values of r_{min} and r_{max} for the various vibrational levels of the two electronic states are given in Table I.

TABLE I
Ground state of PN(${}^1\Sigma^+$)

v	r_{min}		r_{max}	
	True	Morse	True	Morse
0	1.4424	1.4411	1.5449	1.5436
1	1.4098	1.4058	1.5881	1.5841
2	1.3888	1.3821	1.6199	1.6133
3	1.3724	1.3631	1.6472	1.6379
4	1.3588	1.3469	1.6717	1.6598

Upper state of PN (${}^1\pi$)

0	1.4935	1.4934	1.6064	1.6063
1	1.4584	1.4588	1.6551	1.6547
2	1.4360	1.4354	1.6913	1.6906
3	1.4187	1.4178	1.7225	1.7216
4	1.4045	1.4033	1.7508	1.7496

It is seen from Table I that the Morse potential is a very good approximation of the 'true' potential of the ${}^1\pi$ state as well as that of the ground state ${}^1\Sigma^+$. An additional check on the validity of the assumption of a Morse potential for the molecule was made by calculating the α_e 's from known molecular constants by the Pekeris relation (Pekeris, 1934)

$$\alpha_e = \frac{6B_e^2}{w_e} \left[-1 + \left(\frac{w_e x_e}{B_e} \right)^2 \right] \quad (2)$$

and comparing them with the experimentally observed values of α_e . These are indicated in Table II.

TABLE II

State	Calculated	Observed
$N^1\Sigma^+$	0.00519	0.00557
$A^1\pi$	0.00663	0.00623

The deviation of the observed values of α_e from the values given by (2) serves as an indication of the deviation of the Morse function from the actual potential function (Herzberg, 1950).

(u) *The Graphical Method.* Nicholls and Jarman (1956) have given the following expression for the r -centroid $\bar{r}_{v'v''}$.

$$E_{v'} - E_{v''} = D_1[1 - \exp\{-\alpha_1(\bar{r}_{v'v''} - r_{e1})\}]^2 - D_2[1 - \exp\{-\alpha_2(\bar{r}_{v'v''} - r_{e2})\}]^2 \quad \dots (3)$$

where

$$E_v = \omega_e(v + \frac{1}{2}) - \omega_e x_e(v + \frac{1}{2})^2$$

$$D_i = \frac{\omega_e^2 x_e}{4(\omega_e x_e)_i}$$

$$\alpha_i = 0.243534[\mu_A(\omega_e x_e)_i]^{\frac{1}{2}}$$

in which μ_A is the reduced mass in atomic weight units, r_{ei} = equilibrium internuclear distance in the state i . The values (say y) of the expression on the R.H.S. of the eq. (3) are computed over a suitable range of values for \bar{r} at intervals of 0.02A and the values of $\bar{r}_{v'v''}$ appropriate to the observed values of $y = E_{v'} - E_{v''}$ of the bands are then obtained graphically. The values of $\bar{r}_{v'v''}$ obtained thus are given in Table III.

(ii) *The quadratic equation method.* Alternatively, one may regard (3) as a quadratic equation in $x = \exp\{-\alpha\bar{r}_{v'v''}\}$ after making an approximation which consists in replacing α_1 and α_2 by means of $\alpha = \frac{\alpha_1 + \alpha_2}{2}$ and an equivalent adjustment of all α -dependent parameters. (Nicholls and Jarman, 1956).

Then the approximate equation is of the form

$$E'_{v'} - E'_{v''} = D'_1[1 - \exp\{-\alpha(\bar{r}_{v'v''} - r_{e1})\}]^2 - D'_2[1 - \exp\{-\alpha(\bar{r}_{v'v''} - r_{e2})\}]^2 \quad \dots (5)$$

where the primes over the various quantities indicate that these have been adjusted with respect to the chosen mean value of α .

The expression (5) can be written as

$$Px^2 - 2Qx + R_{v'v''} = 0 \quad \dots (6)$$

where P , Q and R have the same significance as indicated by Nicholls and Jarman. The above equation in x will have two roots given by $\bar{r}_{v'v''} = -1/\alpha \ln x$. Of these two roots, the physically significant one is chosen. The Morse constants employed in the present calculation are

$$\alpha_1 = 2.03270 \text{ } A^{0.1}; \quad \alpha_2 = 1.998783 \text{ } A^{0.1} \\ \alpha = 2.015742 \text{ } A^{0.1}$$

The values of r -centroids by the quadratic equation method have also been included in Table III

TABLE III
r-Centroids (A) and wavelengths (A) of bands of ($A^1\pi-X^1\Sigma^+$)
system of PN

$\begin{smallmatrix} \diagup & v'' \\ v' & \diagdown \end{smallmatrix}$	0	1	2	3	4
0	1 522 1.522 (2518.2)	1 577 1.577 (2605.0)	1 630 1 631 (2696.9)	1 683 1 685	
1	1.475 1 475 (2451.1)	1.532 1.532 (2533.0)	1.586 1.586 (2620.1)	1 630 1 630 (2712.1)	
2	1.426 1.424 (2388.2)	1.486 1.486 (2466.2)	1 542 1.542	1 591 1 595 (2635.2)	1 647 1 648 (2727.5)
3	1 370 1.365	1 439 1.437 (2403.3)	1.497 1.497 (2481.4)	1.551 1.551	1 604 1.604 (2650.9)

First row: $\bar{r}_{v'v''}$ by the graphical method.

Second row: $\bar{r}_{v'v''}$ by the quadratic equation method.

Third row: $\lambda_{v'v''}$ wavelengths of bands indicated in parenthesis (Curry, Herzberg, Herzberg, 1933)

DISCUSSION

When a graph of $\bar{r}_{v'v''}$ against $\lambda_{v'v''}$ of the corresponding band is drawn from from the results given above it is found that all the points lie on a smooth curve

and that $\bar{r}_{v'v''}$ increases with $\lambda_{v'v''}$. This is in good accordance with what one should expect for a case where $r_{e1} > r_{e2}$. Also \bar{r}_{00} is slightly greater than $(r_{e1} + r_{e2})/2$ and enables one to substantiate what is found from the relative magnitudes of ω_e and $\omega_e x_e$, namely that the potentials are not very anharmonic. Further values of the r -centroids for PN follow a pattern not different from the molecules studied by Nicholls and Jarman (1956) and Nicholls, Robinson, Parkinson and Jarman (1956) and $\bar{r}_1 - \bar{r}$ (Nicholls and Jarman, 1956) is practically constant for a given sequence. $\bar{r}_1 - \bar{r}$ is also seen to be less than or equal to 0.01 Å and supports the view that the potentials are not wide. The r -centroids obtained by both the methods compare very favourably for this molecule and are in fact identical for the (0, 0) sequence. But on account of the approximations involved in the quadratic equation method slight departures are noticed in off diagonal sequences and the difference increases as $|\Delta v|$ increases. However, as the maximum deviation is of the order of 0.4% only, the replacement of the Morse constants by a mean α appears to be quite legitimate in the case of $\text{PN}(^1\Pi \rightarrow ^1\Sigma^+)$ system.

When these values of r -centroids are compared with those of SiO reported by McGregor *et al.*, one finds that PN exhibits systematic constant difference $\Delta \bar{r}$ in all the sequences while in SiO these differences are rather erratic. However, along (0, 2) sequence of both, the r -centroid values are identical or nearly the same.

ACKNOWLEDGMENT

It gives me great pleasure in acknowledging with thanks the constant encouragement and guidance I had from Prof. R. S. Krishnan and Dr. P. S. Narayanan.

REFERENCES

- Curry, J., Herzberg, L., and Herzberg, G., 1933, *Zett. f. Phys.*, **86**, 348
 Herzberg, G., 1950, *Spectra of Diatomic Molecules*—2nd Edition, D. Van Nostrand Co., New York, P. 101-102, 108 and 564
 Jarman, W. R., 1959, *J. Chem. Phys.*, **31**, 1137
 McGregor, A. T., Nicholls, R. W., and Jarman, W. R., 1961, *Canad. Jour. Phys.*, **39**, 1215.
 Nicholls, R. W. and Jarman, W. R., 1956, *Proc. Phys. Soc. (Lond.)*, **69A**, 253.
 Nicholls, R. W., Robinson, D., Parkinson, W. and Jarman, W. R., 1956, *Proc. Phys. Soc. Lond.* **69A**, 713
 Pokoris, C. L., 1934, *Phys. Rev.* **45**, 98

POTENTIAL PARAMETERS FOR LIKE AND UNLIKE INTERACTIONS ON MORSE POTENTIAL MODEL

ANIL SARAN

INDIAN ASSOCIATION FOR THE CULTIVATION OF SCIENCE, CALCUTTA-32.

(Received, May 15, 1963)

ABSTRACT. Viscosity data have been utilised to determine the force constants for the Morse potential model for Ar, N₂, He, CO₂ and O₂. These parameters can reproduce the experimental viscosity data more satisfactorily than the parameters determined from the second virial and crystal property data. A set of combination rules for unlike interactions has been proposed and tested in relation to the inter-diffusion coefficients. The results thus obtained show a good agreement with the experimental values available in the literature.

INTRODUCTION

Of the various forms of the inter-molecular potential, the Lennard-Jones (12 : 6) model and Buckingham Exp-six model are quite realistic and are, therefore, invariably used for calculating the transport and equilibrium properties of gases. Recently, Konowalow, Taylor and Hirschfelder (1961a) have calculated the second virial coefficient for the Morse potential and these have been utilised by Konowalow and Hirschfelder (1961b) for determining the potential parameters for some non-polar molecules from the virial coefficients and crystal data. Over a wide range of temperature, the theoretical second virial coefficients determined from the Morse potential agree very well with the experimental data and are quite comparable with those obtained by using Lennard-Jones (12 : 6) and Buckingham Exp-six potential.

Morse potential is written in the form,

$$\phi(r) = c[\exp \{-2(c/\sigma)(r-r_m)\} - 2\exp \{-(c/\sigma)(r-r_m)\}] \quad \dots (1)$$

where $\phi(r)$ is the potential energy of the two molecules separated by a distance r , c is the maximum attraction energy at $r = r_m$, σ is the finite value of r at which $\phi(r) = 0$, and the parameter c is related to the width of the potential well. The quantity c is given by the relation

$$c = \sigma(1 + 1/c \ln 2) \quad (2)$$

Very recently, Lovell and Hirschfelder (1962) have evaluated the collision integrals for the gases obeying the Morse potential and hence the evaluation of the parameters from transport data is also possible. Usually viscosity data are used for this purpose. Very accurate data for the viscosity of Ar, N₂, He, CO₂ and O₂

are available for a wide range of temperature. We have here utilised these data to obtain the potential parameters for these substances.

A set of combination rules has been proposed to determine the unlike molecular interactions from a knowledge of the like interactions. These were so chosen as to fit in with the experimental data on the inter-diffusion coefficients of the systems He-Ar, He-N₂, CO₂-N₂ and CO₂-O₂ given by Walker and Westenberg (1958, 1959 and 1960) and by workers in this laboratory.

CALCULATIONS OF POTENTIAL PARAMETERS FROM VISCOSITY

Various methods can be employed to determine the potential parameters from the experimental viscosity data. In the present paper, we have used the ratio method. The viscosity data for Ar, N₂, He and O₂ in the temperature range 100°K-1000°K and for CO₂ in the temperature range 200°K-1000°K were utilised for this purpose.

On the Chapman-Enskog theory, the coefficient of viscosity η is given to the first approximation as (Hirschfelder *et al.*, 1954).

$$[\eta]_1 \times 10^7 = \frac{266.93 \times \sqrt{T \times M}}{\sigma^2 \Omega^{(2,2)*}[c, T^*]} \quad (3)$$

where T is the absolute temperature, M is the molecular weight of the substance, $\Omega^{(2,2)*}[c, T^*]$ are the collision integrals depending on c and $T^* = T/(\epsilon/k)$ as tabulated by Lovell and Hirschfelder (1962).

Let η_1 and η_2 be the viscosity coefficients at temperatures T_1 and T_2 respectively. Then

$$\left[\frac{\eta_2}{\eta_1} \right] = \left[\frac{T_1}{T_2} \right]^{\frac{1}{2}} \frac{\Omega_1^{(2,2)*}[c, T_1^*]}{\Omega_2^{(2,2)*}[c, T_2^*]} \quad (4)$$

By knowing experimentally the quantities η_1 and η_2 , values of c and c/k can be so adjusted that the right hand side of eqn. (4) becomes equal to the experimental $[\eta_2/\eta_1]$. A particular value of $[\eta_2/\eta_1]$ was chosen and for various values of c , values of c/k were found satisfying the eqn. (4). Thus for one particular value of $[\eta_2/\eta_1]$ we found corresponding values of c and c/k . The values of c were plotted against c/k for various values of $[\eta_2/\eta_1]$ and from the intersection of the curves c and c/k were found. The values of σ was then calculated using eqn. (3) at two or three temperatures and mean taken. Eqn. (2) now determines the value of r_m . The values of the force constants thus obtained are shown in the Table I. For the sake of comparison the values obtained by Konowalow and Hirschfelder (1961b) from virial and crystal data are also included in the table.

It is seen from the table, that the potential parameters determined from viscosity and those from the virial and crystal data are mutually not quite con-

sistent. This type of discrepancy between the potential parameters determined from the non-equilibrium and the equilibrium properties of fluids has been observed in the case of other potential models as well.

TABLE I
Values of the force constants on Morse potential model

Substance	From viscosity				From Virial and crystal data			
	c	$e/l^{\circ}K$	$\sigma \text{\AA}$	$r_m \text{\AA}$	c	$e/l^{\circ}K$	$\sigma \text{\AA}$	$r_m \text{\AA}$
Ar	5.7	120	3.461	3.882	5.0	144.8	3.386	3.855
N ₂	6.1	92	3.697	4.117	5.5	134.4	3.579	4.030
He	6.0	11	2.622	2.925	—	—	—	—
CO ₂	5.1	196	3.968	4.507	—	—	—	—
O ₂	5.9	98	3.544	3.937	—	—	—	—

COMPARISON WITH EXPERIMENT

In order to test the reliability of the force constants thus determined, it is necessary to see how far they reproduce the experimental data over a wide range of temperature.

TABLE II
Experimental and calculated viscosity coefficients for Ar, N₂, He, CO₂ and O₂ at different temperatures

Substance	$T^{\circ}K$	$\eta \times 10^7$ g/cm sec expt	$\eta \times 10^7$ g/cm sec. calculated with force constants from	
			Viscosity	Virial and crystal property data
Ar	100	839 ^a	841	769
	120	993 ^a	1003	921
	140	1146 ^a	1157	1077
	160	1298 ^a	1308	1226
	180	1447 ^a	1457	1377
	200	1594 ^a	1602	1527
	220	1739 ^a	1743	1671
	240	1878 ^a	1878	1813
	260	2014 ^a	2000	1952
	280	2145 ^a	2125	2083

TABLE II—(contd)

Substance	$T^{\circ}K$	$\eta \times 10^7$ g/cm. sec. expt	$\eta \times 10^7$ g/cm. sec. calculated with force constants from	
			Viscosity	Virial and crystal property data
Ar	300	2270 ^a	2254	2209
	800	4621 ^b	4617	4761
	1000	5302 ^b	5380	5593
N ₂	100	698 ^c	705	620
	120	826 ^c	832	737
	140	948 ^c	955	858
	160	1068 ^c	1072	972
	180	1183 ^c	1186	1084
	200	1295 ^c	1290	1194
	220	1403 ^c	1394	1304
	240	1505 ^c	1493	1410
	260	1603 ^c	1588	1510
	280	1696 ^c	1681	1606
	300	1786 ^c	1769	1698
	800	3493 ^b	3504	3563
	1000	4011 ^b	4064	4158
Po	100	947 ^a	941	—
	120	1068 ^a	1062	—
	140	1182 ^a	1178	—
	160	1290 ^a	1288	—
	180	1395 ^a	1393	—
	200	1496 ^a	1495	—
	220	1595 ^a	1594	—
	240	1692 ^a	1688	—
	260	1789 ^a	1783	—
	280	1888 ^a	1875	—
	300	1987 ^a	1963	—
	800	3840 ^d	3861	—
	1000	4455 ^d	4521	—

TABLE II (contd.)

Substance	T °K	$\eta \times 10^7$ g/cm sec expt.	$\eta \times 10^7$ g/cm sec. calculated with force constants from	
			Viscosity	Virial and crystal property data
CO ₂	200	1015 ^a	1015	—
	220	1112 ^a	1111	—
	240	1209 ^a	1212	—
	260	1303 ^a	1307	—
	280	1400 ^a	1405	—
	300	1495 ^a	1499	—
	800	3391 ^b	3383	—
	1000	3935 ^b	3986	—
O ₂	100	768 ^c	794	—
	120	917 ^c	940	—
	140	1061 ^c	1080	—
	160	1202 ^c	1216	—
	180	1341 ^c	1348	—
	200	1476 ^c	1473	—
	220	1604 ^c	1587	—
	240	1728 ^c	1707	—
	260	1845 ^c	1817	—
	280	1958 ^c	1943	—
	300	2071 ^c	2031	—
	800	4115 ^e	4059	—
	1000	4720 ^e	4717	—

^a = Johnston, H. L. and Gilly, E. R., (1942)
^b = Vasilosco, V (1945)
^c = Johnston, H. L., and McCloskey, K. E. (1940)
^d = Trantz, M., and Zink, R., (1930)
^e = Values obtained in from the interpolation of available high temperature viscosity data.

Viscosity

Experimental and calculated viscosity coefficients in the wide range of temperature for Ar, N₂, He, CO₂ and O₂ are given in the Table II. The

calculated values of the viscosity coefficients for Ar and N₂ using the force constants from virial and crystal data are also given in the table for comparison. It can be seen from the table that the experimental viscosity data are much better reproducible with the force constants determined in this paper than with those from virial and crystal property data.

COMBINATION RULES FOR UNLIKE MOLECULAR INTERACTION

The properties of gas mixtures are dependent on the forces between unlike molecules. In principle, these forces can be determined from the accurate experimental data on the transport and equilibrium properties of mixtures. In the absence of accurate experimental data it would be very helpful to be able to predict the interaction for unlike molecules from the known interaction for like molecules. In this way the properties of gas mixtures could be calculated from the data on the pure components. Combining rules for the Morse potential model can be obtained by writing the eqn. (1) in the form

$$\phi(r) = Ae^{-2br} - Be^{-br} \quad \dots (5)$$

Following Zener (1931), we get the parameter b for unlike interaction, as

$$b_{12} = \frac{1}{2}(b_1 + b_2) \quad \dots (6)$$

which, when expressed in terms of the constants of the Morse potential, gives

$$\frac{c_{12}}{\sigma_{12}} = \frac{1}{2} \left[\frac{c_1}{\sigma_1} + \frac{c_2}{\sigma_2} \right] \quad \dots (7)$$

Following the suggestion of Srivastava and Srivastava (1958), the combination rule for the parameter c is taken as

$$c_{12} = [c_1 \times c_2]^{\frac{1}{2}} \quad \dots (8)$$

The usual combination rule for σ , which is exactly valid for the rigid sphere, is given by

$$\sigma_{12} = \frac{1}{2}(\sigma_1 + \sigma_2) \quad \dots (9)$$

The value of c_{12} is fixed by eqs. (7) and (9). The fourth parameter r_m of the Morse potential for the unlike interaction is then

$$(r_m)_{12} = \sigma_{12} \left[1 + \frac{1}{c_{12}} \ln 2 \right] \quad \dots (10)$$

However, it was found that the agreement with the calculated values of the inter-diffusion coefficient from the prescribed combination rules [Eqs. (7)-(10)] and the

experimental values was not satisfactory. Consequently, we have tried the geometric mean rule for σ_{12} , i.e.

$$\sigma_{12} = [\sigma_1 \times \sigma_2]^{\frac{1}{2}} \quad \dots (11)$$

The agreement between the calculated and the experimental values of the inter-diffusion coefficients improve by using the geometric mean rule for σ_{12} . Consequently, we suggest, eqs. (7), (8), (10) and (11) as the combination rules for unlike interactions on the Morse potential. The unlike interaction parameters for the gas pairs He-Ar, He-N₂, CO₂-N₂ and CO₂-O₂ determined by using the like interaction parameters of Table I and the combination rules are given in Table III.

The combination rules for the gas pairs shown in Table III have been tested by comparing with the experimental values of the interdiffusion coefficients. To the first approximation, the inter-diffusion coefficient D_{12} is given as (Hirschfelder *et al*, 1951).

$$[D_{12}]_1 = \frac{0.002628 \sqrt{T^3(M_1 + M_2)/2M_1M_2}}{p \sigma_{12}^2 \Omega_{12}^{(1,1)*} [c_{12} T_{12}^*]} \quad (12)$$

where p is the pressure in atmosphere, M_1 and M_2 are molecular weights of species 1 and 2, T is the absolute temperature, σ_{12} is the collision diameter, $\Omega_{12}^{(1,1)*}$ [c_{12}, T_{12}^*] is the collision integral and T_{12}^* is the reduced temperature equal to kT/ϵ_{12} .

TABLE III
Unlike force constants on Morse potential model.

Gas pairs	ϵ_{12}	$\epsilon_{12}/k^\circ K$	$\sigma_1, \text{\AA}$	$(\epsilon_m)_{12}, \text{\AA}$
He—Ar	5.9	36.3	3.012	3.366
He—N ₂	6.1	31.8	3.113	3.467
CO ₂ —N ₂	5.6	134.3	3.630	4.304
CO ₂ —O ₂	5.5	138.6	3.750	4.223

The experimental and the calculated values of D_{12} over extensive range of temperatures are shown in Table IV. It may be seen that except for the measurements of Srivastava (1959) on the He-Ar system, the agreement between the experimental and the calculated values of D_{12} is only fair. A large part of the discrepancy may be attributed to the uncertainties in the experimental method of Walker and Westenberg (1958, 1959 and 1960). Consequently, till better data are available to provide a more definite answer, the combination rules for the Morse potential as suggested in this paper may be used for calculating unlike interactions.

TABLE IV

Experimental and calculated values of inter-diffusion coefficient for the systems He-Ar, He-N₂, CO₂-N₂ and CO₂-O₂ at 1 atm.

Systems	T °K	D_{12} cm ² /sec expt.	D_{12} cm ² /sec calculated using the combination rules proposed
He—Ar	273	0.640 ^a	0.640
	288	0.701 ^a	0.702
	300	0.726 ^b	0.752
	303	0.760 ^a	0.765
	318	0.825 ^a	0.830
	400	1.247 ^b	1.224
	500	1.831 ^b	1.786
	600	2.557 ^b	2.432
	700	3.347 ^b	3.158
	800	4.202 ^b	3.956
	900	5.149 ^b	4.837
	1000	6.310 ^b	5.782
He—N ₂	243.2	0.477 ^c	0.510
	275.0	0.596 ^c	0.629
	300.0	0.739 ^d	0.728
	303.55	0.719 ^c	0.743
	332.5	0.811 ^c	0.866
	400	1.218 ^d	1.183
	500	1.782 ^d	1.724
	600	2.434 ^d	2.344
	700	3.144 ^d	3.038
	800	3.940 ^d	3.849
	900	4.752 ^d	4.650
	1000	5.652 ^d	5.560
CO ₂ —N ₂	300	0.171 ^d	0.157
	400	0.300 ^d	0.264
	500	0.445 ^d	0.392
	600	0.610 ^d	0.539
	700	0.798 ^d	0.704
	800	0.998 ^d	0.837
	900	1.215 ^d	1.085
	1000	1.468 ^d	1.299

TABLE IV (cont'd.)

Systems	T °K	D_{12} cm ² /sec expt	D_{12} cm ² /sec calculated using the combination rules proposed
CO ₂ —O ₂	300	0.160 ^a	0.156
	400	0.270 ^a	0.203
	500	0.400 ^a	0.391
	600	0.565 ^a	0.538
	700	0.740 ^a	0.705
	800	0.928 ^a	0.887
	900	1.142 ^a	1.086
	1000	1.386 ^a	1.302

^a = Srivastava, K. P. (1959).

^b = Walker, R. E. and Westenberg, A. A., (1959).

^c = Paul, R., and Srivastava, I. B., (1961).

^d = Walker, R. E. and Westenberg, A. A., (1958).

^e = Walker, R. E. and Westenberg, A. A., (1960).

ACKNOWLEDGMENT

The author is grateful to Prof. B. N. Srivastava, D.Sc., F.N.I., for suggesting the problem and for his valuable guidance throughout the progress of the work. Thanks are also due to Mr. P. K. Chakraborti, for some helpful discussions.

REFERENCES

- Hirschfelder, Curtiss and Bird, 1954, *Molecular Theory of Gases and Liquids*, (John Wiley and Sons, Inc., N. Y.)
- Johnston, H. L. and McCloskey, K. E., 1940, *J. Phys. Chem.*, **44**, 1038.
- Johnston, H. L., and Grilly, E. R., 1942, *J. Phys. Chem.*, **46**, 948.
- Konowalow, D. D., Taylor, M. H., and Hirschfelder, J. O., 1961a, *Phys. Fluids*, **4**, 622.
- Konowalow, D. D., and Hirschfelder, J. O., 1961b, *Phys. Fluids*, **4**, 629.
- Lovell, S. E. and Hirschfelder, J. O., 1962, Univ. of Wisconsin, WIS-AF-21.
- Paul, R., and Srivastava, I. B., 1961, *Ind. Jour Phys.*, **35**, 523.
- Srivastava, B. N. and Srivastava, K. P., 1958, *J. Chem. Phys.*, **28**, 543.
- Srivastava, K. P., 1959, *Physica*, **25**, 571.
- Trautz, M., and Zink, R., 1930, *Ann. Physik*, **7**, 427.
- Vasilosco, V., 1945, *Ann. Physique*, **20**, 292.
- Walker, R. E. and Westenberg, A. A., 1958, *J. Chem. Phys.*, **29**, 1139.
- Walker, R. E. and Westenberg, A. A., 1959, *J. Chem. Phys.*, **31**, 519.
- Walker, R. E., and Westenberg, A. A., 1960, *J. Chem. Phys.*, **32**, 436.
- Zener, C., 1931, *Phys. Rev.*, **37**, 556.

Letters to the Editor

The Board of Editors will not hold itself responsible for opinions expressed in the letters published in this section. The notes containing reports of new work communicated for this section should not contain main figures and should not exceed 500 words in length. The contributions must reach the Assistant Editor not later than the 15th of the second month preceding that of the issue in which the letter is to appear. No proof will be sent to the authors.

8

FAVOURSED DURATION OF SUDDEN IONOSPHERIC DISTURBANCE

S. D. DESHPANDE

DEPARTMENT OF PHYSICS, GOVERNMENT POLYTECHNIC, KOLHAPUR.

(Received April 1, 1963)

It is wellknown that the duration, i.e., the interval of time between the earliest indication of sudden ionospheric disturbance and its end, of any individual disturbance may vary from a few minutes to about 100 min. or more in some cases. However, during the present analysis of the data on various ionospheric solar flare effects for 1956-58, it is observed that the duration of SID as noted by the time interval of start and end of a short wave radio fade-out shows a typical behaviour. For a certain period such as a season or a year, though an individual fade-out may have any duration extending from a few minutes to about 100 min. or more, large number of SIDs tend to have a certain favoured duration which closely depends upon solar activity for that period under consideration.

It is observed that during the year 1956 nearly 36% of SIDs have their duration between 11 to 20 min. with a favoured duration of 15 min. This later factor being obtained graphically from a plot of number of fade outs against their duration for the year. For 1958, a year of intense solar activity, 35% of the SIDs show duration between 21 to 30 min. centred round the favoured duration of 26 min. Table I shows the first favoured duration interval and favoured duration along with the annual sunspot numbers for the years 1956 to 1959. Data for a few months for 1957 and 1959 is lacking but the general trend is quite apparent. Data for 1936 (Berkner and Wells, 1937) has been analysed for comparison.—Unfortunately sufficient and continuous data was not available in literature particularly for the low sunspot activity period of 1941-43. Linear dependence of

favoured duration on the corresponding sunspot number of the year may be noted from the Table.

As nearly 35% of the total SIDs have their durations lying in a first favoured duration interval, the next 22% or so of the disturbances have their duration in a second favoured duration interval. Again, maximum number of the disturbances of first favoured duration interval of the year occur in equinoctial months while the large number of SIDs during summer and winter show the duration of the second favoured duration interval.

This concept of favoured duration, if extended to the time of growth and decay of the disturbance, may indicate the most general process underlying the ionization and response of the ionospheric region of the disturbance for a certain average solar activity of that period and each individual SID with its deviation from the general process may be considered as related to the specific solar events.

The period under consideration is that of high solar activity and a large number of fade outs have been reported. It is found that the present analysis of this data does not confirm the observation of McIntosh (1951) that April is the month of greatest frequency of occurrence of short wave radio fade outs. Again in general, the fadeouts occur more frequently in morning than in afternoon as is reported in case of various ionospheric solar flare effects. (McIntosh 1951, Shain and Mitra, 1954). However for some winter and equinoctial months the ratio of number of fadeouts in forenoon to the number in afternoon was much less than one; thus supporting the remarks (Shain and Mitra 1954) that there is no real forenoon bias in occurrence of SIDs and the observed effect may be certainly due to the atmospheric interference.

TABLE I

Year	Annual sunspot number	Favoured duration interval (mm.)	Percentage of SID in favoured duration interval	Favoured duration (mm.)
1930	80	0-10	54%	4
1956	106	11-20	36%	15
1957	171	11-20	35%	20
1958	192	21-30	35%	26
1959	182	21-30	30%	23

REFERENCES

- Berkner, L. V. and Wolls, H. W., 1937, *Terr. Magn. and Atmos. Elect.*, **42**, 183.
 McIntosh, D. H., 1951, *J. Atmos. Terr. Phys.*, **1**, 315.
 Shain, C. A. and Mitra, A. P., 1954, *J. Atmos. Terr. Phys.*, **5**, 316.

SPACE GROUP AND UNIT CELL DIMENSIONS OF ANTHRARUFIN

S. N. GIRI

INDIAN ASSOCIATION FOR THE CULTIVATION OF SCIENCE
JADAVPUR, CALCUTTA-32.

(Received July 20, 1963)

Anthrurufin is 1 : 5 dihydroxyanthraquinone having the following structural formula.

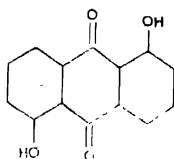


Fig. 1.

No goniometric or crystallographic data of the compound are available.

Single crystals of suitable size can be obtained by slow evaporation of the solution of the substance in benzene or in ether. The crystals obtained from benzene are needle-shaped, whereas plate-like crystals are obtained from ether solution.

From the rotation photograph and zero-and first layer-line Weissenberg photographs along the needle axis, the other two probable crystallographic axes were assigned. Rotation photographs and zero and first layer line Weissenberg photographs along these probable axes were then taken. From these photographs and those along the needle axis, the crystal was found to be monoclinic with the needle axis as the symmetry axis (i.e., *b*-axis). The axial lengths and the monoclinic angle were determined from the high-angle spots for which $\text{Cu-K}\alpha_1$ and $\text{Cu-K}\alpha_2$ were resolved in the Weissenberg photograph. Film shrinkage correction was applied by the method of Srivastava (1959).

The parameters along with the standard deviations, obtained are :

$$a = 15.86 \pm .02 \text{ \AA}$$

$$b = 5.36 \pm .02 \text{ \AA}$$

$$c = 6.03 \pm .01 \text{ \AA}$$

$$\beta = 94^\circ 3' \pm .6'$$

In the zero and higher layer line Weissenberg-photographs, the following extinction conditions are present :

hkl — no condition

hol — $h = 2n+1$ absent

oko — $h = 2n+1$ absent

thereby indicating that the probable space group is $P2_1/a$

Density was determined by floatation method using aqueous solution of potassium iodide as the heavier and water as the lighter liquid. This gives a value of $d = 1.59 \text{ g cm}^{-3}$. The density calculated by considering two molecules in the unit cell is 1.56 g cm^{-3} .

The space group is centrosymmetric having four equivalent points. This presents no difficulty since the molecule itself possesses a symmetry-centre.

Further work is in progress.

The author is indebted to Dr. R. K. Sen, D.Sc. for his kind interest and guid-

REFERENCES

Srivastava, S. N., *Acta Cryst.*, (1959) **12**, 412.

A NEW LIQUID OXYGEN CRYOSTAT

S. MITRA, S. K. DUTTA ROY AND A. BOSE

DEPARTMENT OF MAGNETISM, INDIAN ASSOCIATION FOR THE CULTIVATION OF SCIENCE

(Received, July 24, 1963)

Although the gas flow type cryostats, using liquid oxygen as coolant, constructed by Bose (1947) and by Dutta Roy (1955) are quite simple and efficient, the range of temperature covered with these is about 300°K to 85°K (Bose 1947). The control of the temperatures is not very fine and the measurements at small intervals of temperature cannot be conveniently undertaken. The system is not also economic as much of the cold is wasted.

In view of the above difficulties the present authors have constructed a new liquid oxygen bath type cryostat which provides an extremely fine control of temperature and makes it possible to work between 400°K and 64°K. The cryostat consists of a wide-mouthed silvered glass Dewar vessel carrying the liquid oxygen, with a narrow tail to be accommodated between the pole pieces of an electromagnet. The experimental chamber is a silvered vacuum jacketed pyrex glass tube passing down into the tail. The temperature inside the experimental chamber is accurately maintained by controlling the pressure inside the vacuum jacket and balancing the cold from liquid oxygen with the heat from a small non-inductive electric heater within the chamber. The control is, further, made automatic with the help of a gas-thermometric relay system. The Dewar is connected to a low vacuum pump to boil the contained liquid oxygen at different reduced pressures to obtain temperatures down to 64°K.

It has been observed that the temperature remains very accurately constant for a long time within 0.05°C. These are measured with a calibrated Cu-constantan thermocouple.

Details of the cryostat will be published shortly.

One of the authors (S.M.) is grateful to the Council of Scientific and Industrial Research for the award of a Research Fellowship.

REFERENCES

- Bose, A., 1947, *Ind. Jour. Phys.*, **21**, 277.
 Dutta Roy, S. K., 1955, *Ind. Jour. Phys.*, **29**, 429.

NOTICE

No claims will be allowed for copies of journal lost in the mail or otherwise unless such claims are received within 4 months of the date of issue.

RATES OF ADVERTISEMENTS

1. Ordinary pages :

Full page Rs. 50/- per insertion

Half page Rs. 28/- per insertion

2. Pages facing 1st inside cover, 2nd inside cover and first and last page of book matter :

Full page Rs. 55/- per insertion

Half page Rs. 30/- per insertion

3. Cover pages by negotiation

25% commissions are allowed to *bona fide* publicity agents securing orders for advertisements,

CONTENTS

Indian Journal of Physics

Vol. 37, No. 9

September, 1963

PAGE

51. Frank-Condon Factors and r -Centroids for $^2\Delta-^2\Delta$ System of VO— S. S. Prasad	457
52. X-ray Diffraction Study of Copper at High Temperature— G. B. Mitra and S. K. Mitra	462
53. On the Polarization of Radio-wave Travelling through the Ionosphere— S. K. Banerjee and S. R. Khastgir	473
54. The Chapman-Cowling Second Approximation to the Viscosity Coefficient of Binary Gas Mixtures— S. C. Saxena and R. K. Joshi	479
55. r -Centroids and their Properties of $(A'\pi \rightarrow X^1\Sigma^+)$ System of PN— S. Sankaranarayanan	486
56. Potential Parameters for Like and Unlike Interactions on Morse Potential Model— Anil Saran	491

LETTERS TO THE EDITOR—

8. Favoured Duration of Sudden Ionospheric Disturbance— S. D. Deshpande	500
9. Space Group and Unit Cell Dimensions of Anthrarufin— S. N. Giri	502
10. A New Liquid Oxygen Cryostat— S. Mitra, S. K. Dutta and A. Bose	504

VOL. 37

INDIAN JOURNAL OF PHYSICS

No. 10

(Published in collaboration with the Indian Physical Society)

AND

VOL. 46

PROCEEDINGS

No. 10

OF THE

**INDIAN ASSOCIATION FOR THE
CULTIVATION OF SCIENCE**

OCTOBER 1963

PUBLISHED BY THE
INDIAN ASSOCIATION FOR THE CULTIVATION OF SCIENCE
JADAVPUR, CALCUTTA 32

BOARD OF EDITORS

K. BANERJEE	D. S. KOTHARI
D. M. BOSE	B. D. NAG CHAUDHURI
S. N. BOSE	K. R. RAO
S. D. CHATTERJEE	D. B. SINHA
P. S. GILL	S. C. SIKKAR (Secretary)
S. R. KHASTGIR	B. N. SRIVASTAVA

EDITORIAL COLLABORATORS

PROF. R. K. ASUNDI, Ph.D., F.N.I.
PROF. D. BASU, Ph.D.
PROF. J. N. BHAR, D.Sc., F.N.I.
PROF. V. G. BHIDE, Ph.D.(Nag), Ph.D.(Lond).
PROF. A. BOSE, D.Sc., F.N.I.
PROF. S. K. CHAKRABARTY, D.Sc., F.N.I.
DR. J. S. CHATTERJEE
DR. K. DAS GUPTA, Ph.D.
PROF. N. N. DAS GUPTA, Ph.D., F.N.I.
DR. J. DHAR, D.Phil (So)
PROF. A. K. DUTTA, D.Sc., F.N.I.
PROF. C. S. GHOSH, M.Sc., S.M., F.N.I., M.I.E.E.
PROF. S. GHOSH, D.Sc., F.N.I.
PROF. S. N. GHOSH, D.Sc.
PROF. S. GUPTA, M.Sc., F.N.I.
PROF. D. N. KUNDU, Ph.D., F.N.I.
PROF. R. C. MAJUMDER, Ph.D., F.N.I.
PRINCIPAL Y. G. NAIK, Ph.D.
PROF. S. R. PALIT, D.Sc., F.R.I.C., F.N.I.
PROF. H. RAKSHIT, D.Sc., F.N.I.
PROF. A. SAHA, D.Sc., F.N.I.
DR. VIKRAM A. SARABHAI, M.A., Ph.D., F.N.I.
DR. A. K. SENGUPTA, D.Sc.
PROF. NAND LAL SINGH, D.Sc.
DR. M. S. SINHA, D.Sc., F.N.I.
PROF. N. R. TAWDE, Ph.D., F.N.I.
DR. P. VENKATESWARLU

NOTICE

TO INTENDING AUTHORS

Manuscripts for publication should be sent to the Assistant Editor, Indian Journal of Physics, Jadavpur, Calcutta-32.

The manuscripts submitted must be type-written with double space on thick foolscap paper with sufficient margin on the left and at the top. The original copy, and not the carbon copy, should be submitted. Each paper must contain an abstract at the beginning.

All references should be given in the text by quoting the surname of the author, followed by year of publication, e.g., (Ghosh, 1954). The full reference should be given in a list at the end, arranged alphabetically, as follows; Ghosh, D. K., 1954, *Ind. J. Phys.*, 28, 485.

Line diagrams should be drawn on white Bristol board or tracing paper with black India ink, and letters and numbers inside the diagrams should be written neatly in capital type with India ink. The size of the diagrams submitted and the lettering inside should be large enough so that it is legible after reduction to one-third the original size. A simple style of lettering such as gothic, with its uniform line width and no serifs should be used, e.g.,

A·B·E·F·G·M·P·T·W·

Photographs submitted for publication should be printed on glossy paper with somewhat more contrast than that desired in the reproduction, and should, if possible, be mounted on thick white paper.

Captions to all figures should be typed in a separate sheet and attached at the end of the paper.

The mathematical expressions should be written carefully by hand. Care should be taken to distinguish between capital and small letters and superscripts and subscripts. Repetition of a complex expression should be avoided by representing it by a symbol. Greek letters and unusual symbols should be identified in the margin. Fractional exponents should be used instead of root signs.

Annual Subscription—

Inland Rs. 25.00

Foreign £ 2-10-0 or \$ 7.00

BENGAL CHEMICAL & PHARMACEUTICAL WORKS LD.

Pioneer Indian Manufacturers of Pharmaceuticals & Chemicals.

Manufacturers of:

Pharmaceutical Chemicals:

Caffeine and its salts, Strychnine Hydrochlor. Strychnine Sulphate, Brucine Sulphate, Nicotinic Acid, B.P., Nicotinamide, B.P., Potassium Citrate B.P., I.P., Sodium Citrate B.P., I.P., Potassium Acetate B.P., I.P., Potassium Iodide B.P., I.P., Sodium Iodide B.P., I.P., Ferri Cit Ammon Citrate B.P., I.P., and various other Pharmaceutical Chemicals.

Heavy & Reagent Quality Fine Chemicals:

Alum, Alum Sulphate (Iron Free), Ferro Alum, Zinc Chloride Tech. Naphthalene Pure, Sodium Citrate A.R., Potassium Citrate A.R., Magnesium Sulphate A.R., Sodium Sulphate A.R., Potassium Iodide A.R., Sodium Chloride A.R., Zinc Sulphate A.R., and various other reagent quality analytical chemicals.

Please refer your enquiries for the above items and other chemicals in the line to :

BENGAL CHEMICAL

6, GANESH CHUNDER AVENUE,
CALCUTTA-13, INDIA.

(INDIA MADE)

X'RAY DIFFRACTION APPARATUS

Complete with

MACHLETT SHOCKPROOF BERYLLIUM WINDOW SEALED TUBES OF
DIFFERENT TARGET MATERIALS
SINGLE VALVE HALF-WAVE RECTIFIED OR TWO VALVE
FULL-WAVE RECTIFIED

MACHINE already incorporates voltage compensator to compensate plus
or minus 15 volts supply change.

Electro-Magnetic, Electronic, Servo-Mechanical or Chemo-Electric STABILISER
can be added to the filament circuit or

to the entire MACHINE for further STABILISATION.

CAMERAS OF VARIOUS TYPES CAN ALSO BE SUPPLIED
FOR THE MACHINE.

ALSO

X'RAY PLANT FOR BIOLOGICAL RESEARCH & INDUSTRIAL RADIOGRAPHY
AND HIGH TENSION TESTING SETS.

DELIVERY EX-STOCK : : NO LICENCE REQUIRED.

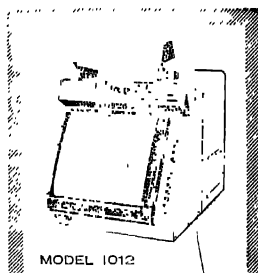
Further details from :-

RADON HOUSE P. LTD.,

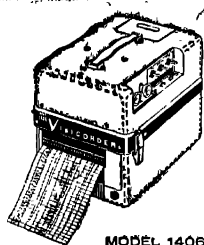
7, Sirdar Sankar Road, Calcutta-26.

HONEYWELL VISICORDER OSCILLOGRAPH

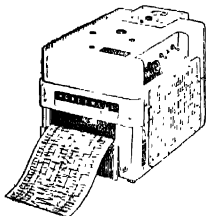
world's most versatile instrument
for the simultaneous recording of
a number of fast changing variables



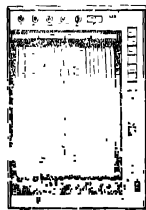
MODEL 1012



MODEL 1406

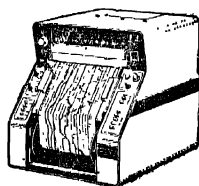


MODEL 906



MODEL 1612

Available in several models, from 6 to 36 channels, DC to 5000 c/s response, over 50,000"/sec writing speed. The 36-channel 1012 & the 1612 are the most sophisticated instruments in the line. The 1108 is a highly capable 24-channel model. The 1508 is a compact 24-channel instrument that takes only 7" of vertical space in a relay rack and is also suitable for bench use. The 906 handles either 8 or 14 channels and the 1406 provides upto 6 channels at the lowest cost per channel.



MODEL 1108

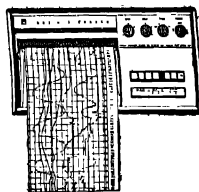
Honeywell

Sold and serviced in India exclusively by

BLUE INSTRUMENTS **STAR**

Get complete details from **BLUE STAR** offices at:

7 Hare Street, Calcutta 1
Sukh Sagar, Sandhurst Bridge, Bombay 7
1/23B Asaf Ali Road, New Delhi 1
23/24 Second Line Beach, Madras 1
1B Kaiser Bungalow, Dindli Road, Jamshedpur

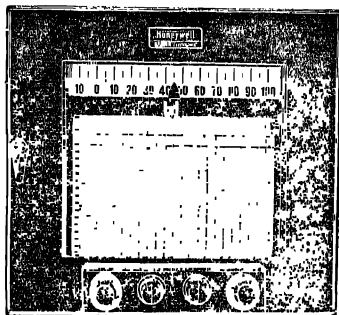


MODEL 1508

It's a dozen test instruments in one!

—the Adjustable Span

***Electronik* Recorder**



HERE'S a recording potentiometer that is a real jack-of-all-trades (and master of each one) in any development or test laboratory. Just turn the dials, and in seconds, you can set it up for the exact range and sensitivity you want. You don't have to do any rewiring or changing of calibrating circuits.

50-to-1 span adjustment. Millivolt span of the recorder is continuously variable over as much as a 50:1 range. Span adjustment is independent of zero setting.

Variable zero suppression. Coarse and fine adjustment dials let you move the electrical zero point up and down scale, to concentrate recording on only the part of the span in which you're interested. Zero adjustment does *not* affect span setting.

Sensitivity adjustment makes it easy to get the recording characteristics you want to match the span being used.

Many optional features : you can choose from recording speeds of $\frac{1}{2}$, 1, 2, $4\frac{1}{2}$, 12 or 24 seconds full scale . . . fully automatic, push-button, or solenoid-actuated remote or locally controlled standardization.

Sold and serviced in India exclusively by

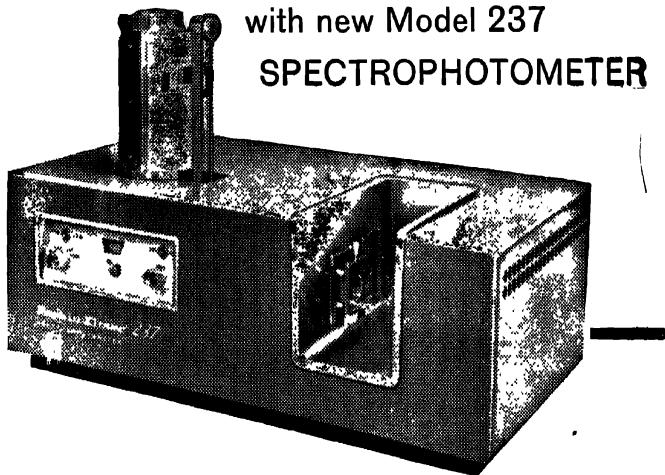
Honeywell

H First in Control

BLUE STAR

**BLUE STAR ENGINEERING
CO. (Calcutta) PRIVATE LTD.**
7 HARE STREET, CALCUTTA 1
Also at BOMBAY • DELHI
MADRAS • JAMSHEDPUR

Now...grating resolution over fundamental IR range with new Model 237 SPECTROPHOTOMETER



You can now have the advantages of high-resolution analysis over the entire Infrared spectral range of fundamental analytical importance—4000 to 625 wavenumbers (2.5 to 16 microns)...even if your budget is limited. The New Perkin-Elmer Model 237 Double-Grating Spectrophotometer, latest in P-E's low-cost Infracord line, makes this possible

Basic to this high performance at low cost is the Model 237's grating-filter design: the dispersing power of gratings, used only in their first orders, is complemented by filters to eliminate higher orders of radiation. The result is outstanding spectral purity achieved with simplicity and dependability of mechanical operation previously not available.

Flexible Presentation. You can specify a Model 237 recording in either linear wavelength or linear wavenumbers, as you prefer. Full wavelength coverage is divided into two ranges: 4000-1300 and 2000-625 wavenumbers; or 2.5-7.7 and 5.0-16 microns. The analyst selects the range he desires by the flick of a panel switch, thus assuring maximum legibility of fine structural detail.

Two scanning rates for each range are available: fast (8 minutes) rate for survey scans or spectra of materials with relatively few narrow spectral bands; slow (24 minutes) rate provides details of very complex spectra. Here, too, a panel switch puts both speeds at the analyst's fingertips.

Optional auxiliary recorders are available to give you continuous spectra at fixed wavelengths or to let you expand or compress ordinate or abscissa. The chart ordinate—a full 15 centimeters—provides maximum accuracy in recording band intensities.

INSTRUMENT DIVISION
Perkin-Elmer *Corporation*
NORWALK, CONNECTICUT

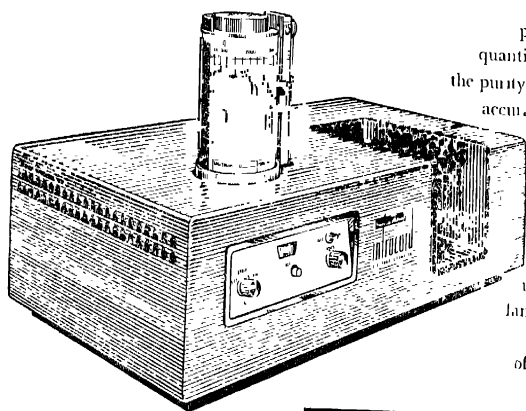
Sold and serviced in India exclusively by

BLUE STAR



**BLUE STAR ENGINEERING
CO. (Calcutta) PRIVATE LTD.**
7 HARE STREET, CALCUTTA I
Also at BOMBAY · DELHI
MADRAS · JAMSHEDPUR

What the INFRACORD[®] does for the Organic Chemist



The Perkin-Elmer
double-beam Infracord
Spectrophotometer is the most
compact and inexpensive
infrared instrument available,
featuring utmost simplicity of
operation with excellent resolution.
It identifies unknowns;
performs qualitative and
quantitative analyses; controls
the purity of products with speed,
accuracy and reproducibility.

A large number of
accessories generally
associated with
higher priced
instruments can be
used with the Infracord
family, thereby extending
its utility in every type
of infrared investigation.

*Four models in the
Infracord family covering
various infrared regions
are now available.*

PERKIN-ELMER DIVISION
Perkin-Elmer Corporation
NORWALK, CONNECTICUT

Sold and serviced in India exclusively by

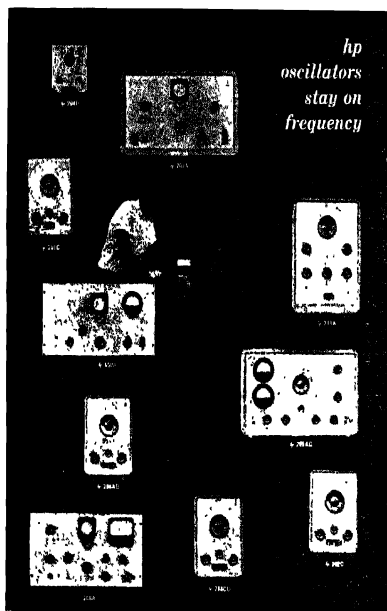
BLUE STAR

**BLUE STAR ENGINEERING
CO. (Calcutta) Private LTD.**
7 HARE STREET, CALCUTTA 1
Also at BOMBAY · DELHI · MADRAS

MODEL	RANGE
INFRACORD	From 2.5 to 15 microns with NaCl prism monochromator and two-speed scanning
237 INFRACORD	From 2.5 to 16 microns in 2 steps (2.5 to 7.7, 5 to 16 microns) Employs first-order double-grating monochromator giving remarkably high resolution Two-speed scanning
137 KBr INFRACORD	1.25 to 25 μ
137-G INFRACORD	With two first-order gratings from 0.83 to 2.55 microns in near infrared and 2.45 to 7.65 microns in fundamental region

HEWLETT PACKARD

ACCURATE TEST SIGNALS 0.008 cps to 10 MC



Model	Frequency Range	Output
200AB	20 cps to 10 KC 4 ranges	1 v alt. (21 v/600 ohms)
200CD	5 cps to 600 KC 5 ranges	60 mw (10 v/600 ohms)
201 C	20 cps to 20 KC 5 ranges	2 watts (12 v/600 ohms)
202 A	0.008 to 1,200 cps, 5 ranges	28 mw (30 v/600 ohms)
211 A	1 cps to 1 MC	7 v p-p/75 ohms 55 v p-p/60 ohms
202 C	1 cps to 100 KC 5 ranges	160 mw (10 v/600 ohms)
204 B	5 cps to 500 KC 5 ranges	16 mw (2.5 v/600 ohms)
205 AG	25 cps to 20 KC 3 ranges	5 watts adjustable 50, 200, 600, 5000
206 A	20 cps to 20 KC 3 ranges	+15 diam/50, 150-200 ohms
650 A	10 cps to 10 MC 6 ranges	15 mw (7 v/600 ohms)

The resistance-capacity oscillator, pioneered and developed by Hewlett-Packard, provides simple operation with high stability and wide frequency range. Just select the signal you want on easy-to-read controls, and you get a dependable output without tedious resetting or adjustment. These oscillators give you low distortion, excellent frequency response and extreme amplitude stability. These instruments can make your test work easier, faster, successful, economical.

For further details, please write to :

The Sole Distributors :

**THE SCIENTIFIC INSTRUMENT
COMPANY, LIMITED.**

ALLAHABAD : BOMBAY CALCUTTA : MADRAS :
NEW DELHI

Head Office : 6, Tej Bahadur Sapru Road, Allahabad



AN ELECTRODYNAMIC BALANCE AND A NEW LIQUID OXYGEN CRYOSTAT FOR MEASUREMENT OF MAGNETIC SUSCEPTIBILITIES BETWEEN 400°K AND 60°K.

A. BOSE, S. K. DUTTA ROY*, P. K. GHOSH** AND S. MITRA

DEPARTMENT OF MAGNETISM & ELECTRICITY

INDIAN ASSOCIATION FOR THE CULTIVATION OF SCIENCE, JADAVPUR, CALCUTTA-32

(Received for publication, September 4, 1963)

ABSTRACT A highly accurate and sensitive electrodynamic balance of robust construction for the measurement of magnetic susceptibilities of single crystals, powdered samples and liquids has been described. The balance uses an electrodynamic compensation of magnetic force and photoelectric magnification of deflection, avoids many sources of errors and troubles and gives an accuracy better than 0.1%. A new cryostat providing an extremely fine control of temperature, with the help of some special devices, is incorporated with the balance to work between 400°K and 63°K, using liquid oxygen as coolant and is described in detail. The calibrations of the balance and the thermo-couple have been compared against the existing Loden and Calcutta measurements on standard paramagnetic substances, e.g., Cr^{+3} alum, Fe^{+3} alum.

INTRODUCTION

In the study and measurement of the principal magnetic susceptibilities of crystals, a number of difficulties such as accurate calibration of field, location and orientation of the crystals, maintenance of steady temperature balancing the magnetic force etc. limits the accuracy of the data to within $\sim 1\%$. To estimate the anisotropies of the crystals of the order of 5 to 30% of the mean susceptibilities with sufficient accuracy, the above limit should be pushed back to about 0.1% or less. The present paper describes a modified Curie-balance of robust construction designed to measure susceptibilities of crystals as well as powders and liquids down to 60°K, and uses a new electrodynamic compensation of the magnetic force and photoelectric magnification of deflection. The temperatures between 400°K and 60°K are maintained accurately using a new cryostat with liquid oxygen as coolant and a vacuum jacket with a heater element as a temperature compensating device.

* Now at the Department of Physics and Meteorology, I.I.T., Kharagpur, India

** Now at Fertilizer Corporation of India Ltd., Sindri, Bihar, India.

A SURVEY OF OLDER METHODS

Most of the usual methods for measuring susceptibilities consist of estimating the translational force on a sample placed in an inhomogeneous magnetic field. For example, in the original Curie method (1895) the horizontal translational magnetic force on a small sample fixed at one end of a balance arm, suspended from the midpoint with a fine fibre, is balanced against the torque of the fibre. In the Gouy Method (1889) the vertical pull on a long sample suspended from one arm of an analytical balance is compensated by weights on the other arm. In the Sucksmith's ring balance (1929), the vertical pull on a small sample is balanced against the bending moment of a phosphor bronze ring from which the sample is suspended. In the Foex-Forrer balance (1936), the horizontal magnetic force on the sample mounted at one end of a horizontal beam, which is suspended with double bifilar strings, is compensated by the electrodynamic force exerted between a current-bearing coil carried on the moving system and a fixed permanent magnet. The quartz fibre torsion microbalance of Bose (1947) with its arrangement of suspending the crystal from one end of the beam with a fine quartz fibre is very delicate, but rather unstable and hence difficult to handle. The Curie-type torsional balance of Dutta Roy (1955) eliminates many sources of errors. But besides powdered and liquid samples, only single crystals of axial symmetry can be measured with it. Moreover, the manual operation of torsion head causes vibration of the system.

All the above balances excepting the Curie types are inherently gravity controlled and hence have low deflection sensitivity in order to be sufficiently stable, and excepting the microbalance type none is suitable for single crystals. Most of these are so delicately suspended that it is a great strain upon the worker to handle them and external disturbing factors and zero shifts often make it impossible to have reproducible values.

Considering all these facts, a balance was constructed, avoiding the defects and utilizing the points of advantages of the earlier instruments as far as possible. To avoid gravity control a Curie method was chosen. For the sake of sensitivity, a null type instrument rather than a deflection type instrument was decided upon. For the sake of ease of manipulation and robust construction, fragile quartz fibre suspension was replaced by metallic strip. Vibrations and consequent uncertainty due to manual operation were eliminated by the technique of remote controlled electrodynamic restitution.

THEORY OF THE METHOD

The l -th component of the force acting on a single crystal of volume v placed in a magnetic field H is given by

$$|F_l| = v \sum_j k'_{lj} H_j \frac{\partial H_j}{\partial x_l} \quad (i, j, l = 1, 2, 3) \quad \dots \quad (1)$$

where $|H_i|$ is the component of field along x_i axis. k'_{ij} is ij th component of the volume susceptibility tensor with reference to any arbitrary set of axes x_1, x_2, x_3 . Expressing the susceptibility tensor in terms of a set of axes X_1, X_2, X_3 fixed in the crystal, conveniently chosen as the principal axes of the susceptibility ellipsoid, we have only three non-vanishing components. The relation between k and k' is given by

$$k'_{ij} = \sum_{\alpha=1}^3 k_{\alpha} \frac{\partial X_{\alpha}}{\partial x_i} \cdot \frac{\partial X_{\alpha}}{\partial x_j} \quad \dots \quad (2)$$

Substituting in equation (1),

$$F_i = v \sum_{\alpha} \sum_{ij} k_{\alpha} \frac{\partial X_{\alpha}}{\partial r_i} \cdot \frac{\partial X_{\alpha}}{\partial x_j} H_i \frac{\partial H_i}{\partial k_i} \quad \dots \quad (3)$$

In our present experimental arrangement, the pole pieces are so shaped as to produce a horizontal field with a horizontal gradient, x_3 being taken as the vertical direction. The single crystal is suspended from a very thin fibre from one arm of a modified Curie balance to be described later, with k_3 vertical, leaving the crystal free to rotate in the horizontal plane. Assuming $k_1 > k_2$, X_1 axis of the crystal will set parallel to the field H , neglecting the very small torsion of the fibre. X_2 and X_3 directions being perpendicular to H , K_2 and K_3 will have no contribution to the force. Now

$$H_1 = H \frac{\partial x_1}{\partial X_1}, H_2 = \frac{\partial x_2}{\partial X_1}, H_3 = 0 \quad \dots \quad (4)$$

or
$$H = H_1 \frac{\partial X_1}{\partial x_1} + H_2 \frac{\partial X_1}{\partial x_2}$$

Therefore denoting the direction of the field gradient as simply x

$$\frac{dH}{dx} = \frac{\partial H_1}{\partial x} \cdot \frac{\partial X_1}{\partial x_1} + \frac{\partial H_2}{\partial x} \cdot \frac{\partial X_1}{\partial x_2} \quad \dots \quad (5)$$

From equations (4) and (5),

$$\sum_j \frac{\partial X_1}{\partial x_j} \cdot \frac{\partial X_1}{\partial x_j} H_i \frac{\partial H_j}{\partial x} = H \frac{dH}{dx} \quad \dots \quad (6)$$

Eq. (3) therefore reduces to

$$F = vk_1 \cdot H \frac{dH}{dx} \quad \dots \quad (7)$$

The derivation clearly indicates that the field direction and the gradient direction need not be exactly perpendicular as required in certain earlier methods. In the experimental arrangement, the force on the sample is exactly balanced by the force exerted on a small vertical coil, rigidly attached to the balance beam, placed close to the sample with its axis as nearly parallel to the field direction as possible, and carrying a suitable electric current C . This force due to the field on the coil

$$F' = nAC \frac{dH}{dx} \cos \theta \quad \dots (8)$$

where,

n = number of turns in the coil

A = mean area of a turn

θ = small angle between the axis of the coil and the field.

For balancing, $F = F'$

$$\text{or} \quad vk_1 \left(H \frac{dH}{dx} \right)_{\text{sample}} = nAC \left(\frac{dH}{dx} \right)_{\text{coil}} \cos \theta \quad \dots (9)$$

In general the suspended system including the coil, the suspension rod the sample holder if any, will experience a pull even in the absence of any magnetic sample. To balance this pull, we must employ an "initial current" C_0 through coil. Also we must take into account the susceptibility k_0 of the surrounding medium. Correcting for these, eq. (9) becomes

$$v(k_1 - k_0) \left(H \frac{dH}{dx} \right)_{\text{sample}} = nA(C - C_0) \left(\frac{dH}{dx} \right)_{\text{coil}} \cdot \cos \theta \quad \dots (10)$$

or, expressing in terms of mass susceptibility

$$m \left(\chi_1 - \frac{K_0}{\rho} \right) \left(H \frac{dH}{dx} \right)_{\text{sample}} = nA(C - C_0) \left(\frac{dH}{dx} \right)_{\text{coil}} \cdot \cos \theta \quad \dots (11)$$

where m is the mass and ρ the density of the sample. For the calibration of the balance a standard substance of known susceptibility is used. If the volume of the standard sample is nearly the same as that of the experimental sample so that

the integrated value of $\left(H \frac{dH}{dx} \right)_{\text{sample}}$ per unit volume is the same for both,

we get :

$$\frac{m(\chi_1 - k_0/\rho)}{m_s(\chi_s - k_0/\rho_s)} = \frac{C - C_0}{C_s - C_0}$$

$$\chi_1 = \frac{C_1 - C_0}{C_s - C_0} \left(\chi_s - \frac{K_0}{\rho_s} \right) \cdot \frac{m_s}{m} \cdot \frac{K_0}{\rho} \quad (12)$$

where the subscript s refers to the standard substance χ_2 and χ_1 can either be calculated from anisotropy data, or they can be measured directly as above. Obviously, similar relation will also hold good in the case of the mean susceptibility $\bar{\chi}$, for a liquid or powder specimen

DESCRIPTION OF THE BALANCE ASSEMBLY

A preliminary note on the balance was earlier published by Ghosh (1961). Several substantial improvements upon that have been made in the present construction. Basically, the instrument is of the Curie-type, the movement of the arm being restricted to a horizontal plane. It consists (Fig. 1) of a horizontal light

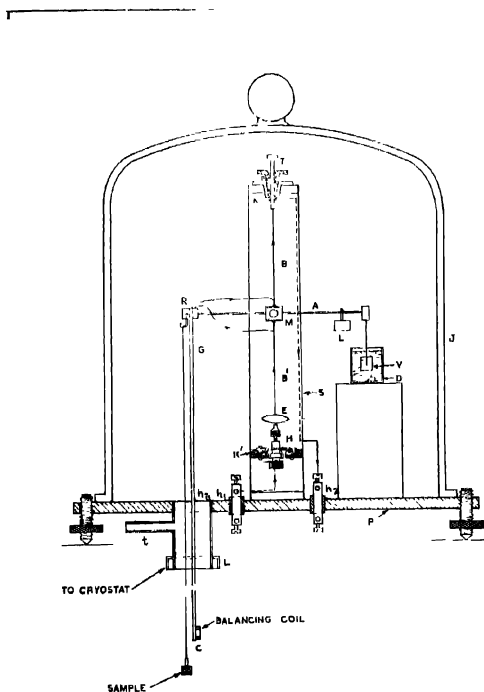


Fig. 1

glass beam *A*, kept tautly suspended at the middle with moderately fine vertically stretched phosphor-bronze strips. The upper strip *B* is soldered to a torsion head *T* used for adjusting the position of the beam, whereas, the lower one *B'* terminates in an elliptic spring *E* secured to a universal adjustable holder *H* which can be rotated, or moved up and down or sidewise so that the torsion on the upper strip can be released, the tension of the suspension can be adjusted or the strips can be lined up vertically. The torsion head and the holder are fixed to chonite blocks *K*, *K'* held in a supporting brass pillar *S*.

A small perspex block *R* has one horizontal hole which fixes it to balance beam, another vertical hole takes a long thin glass tube *G*, at the lower extremity of which is attached the electric balancing coil *c* with its plane vertical and perpendicular to the magnetic field. The attachments are made rigid with araldite cement. The coil comprises of 50 turns of 42 s w g enamelled copper wire wound over a cylindrical thin walled pyrex glass 'former' tube of about 9 mm external diameter and about 2 mm. length and impregnated with araldite cement to give high insulation as also rigidity. The electric lead to the coil pass through the supporting glasstube and are soldered one to each of the phosphor bronze strips. The phosphor bronze strips thus serve a double purpose, they act as suspension wires, as well as electric connections of the coil.

A damping vane *V* made of thin mica sheet, dipping in a dashpot *D* of apiezon diffusion pump oil fixed to the other end of the glass beam effectively damps out all spurious vibrations. The brass upright support *S* that holds the balance assembly, is mounted on a flat circular brass base plate *P*, resting on three levelling screws. A greased ground bell-jar *J* forms a convenient cover for the balance assembly. Three holes are drilled in the base plate. In two of these h_1 , h_2 are two chonite blocks with binding terminals, sealed vacuum tight with araldite, for leading in the coil current. The terminals are connected with the phosphor bronze strips. The third aperture h_3 about 2.5 cm in diameter is fitted with a brass collar *L* taking the glass tube extension of the experimental chamber. Joints of the tube are sealed vacuum tight with picien sealing wax. The glass tube carrying the balance coil and the fine fibre carrying the specimen hang side by side in the experimental tube enclosed in the cryostat, placed between the pole pieces of an electromagnet. A side tube *t* allows the balance chamber and the experimental chamber to be evacuated or filled with dry air through a drying tower system or with any gas as desired.

MOUNTING THE SPECIMEN

The sample is suspended by a fine unspun silk fibre from a hook embedded in the perspex blocks, to which the balancing coil assembly is also attached. If the sample is in powder (or liquid) form it is packed in a small round glass capsule fitted with a miniature ground glass stopper to which the fibre is attached. If

it is a single crystal, a small piece of thin glass rod is fixed to it along one of the principal magnetic axes and the silk fibre attached to the glass rod. When placed in proper position, the sample stands clear of the coil and of the side walls of the chamber, so that it is free to rotate about the vertical axis. The advantage of this method of mounting is obvious for a single crystal specimen, in which two principal susceptibilities are now contained in the horizontal plane and on applying a horizontal magnetic field, the principal axis corresponding to the greater susceptibility value automatically aligns itself parallel to the field direction. Thus one principal susceptibility value can be directly known (cf. Bose, 1947). It is found that in spite of the flexible suspension, there is no appreciable linear motion between the sample and the beam. Even if it is there to a small extent, the maximum direction of susceptibility still sets along the direction of the field, and the magnetic pull being always horizontal, no other restoring force except that due to the rigidity of the phosphor-bronze strip exists.

In the present Curie-balance set up the gradient and hence the motion of the specimen being in the horizontal plane, the restoring force arises only from the torsional rigidity of the suspension strip, so that the sensitivity of deflection can be made large without considerable sacrifice of stability, unlike the micro-balance type in which gravity is the major controlling as well as stabilizing factor. Again here change in the weight of the sample due to deposition of frost or loss of water etc. during measurement will not be recorded as a change in magnetic pull.

The Sucksmith form of pole-pieces (Sucksmith, 1939) is adopted as it is the simplest design to obtain the quantity $H \frac{dH}{dx}$ fairly constant over a considerable volume. This ensures that small differences in the position of the different samples will not affect the accuracy of calibration. The magnet is fed by a highly stabilized 15 KW 220 V D.C. generator. The current is read on an accurate 15 cm. mirror dial ammeter with a magnifying eyepiece. A fine screw rheostat is used to regulate the value of the current and a commutator is provided to reverse the direction of the current several times after each measurement. With a pole gap of 6 cm., required to accommodate the cryostat, the magnet produces a field of 2500 oersteds with a gradient of about 15 oersteds/cm at 1.5 amperes.

DETECTION SYSTEM

The use of phosphor-bronze strip for suspension results in a very small overall deflection of the system. This is desirable in several respects. But on the other hand, this necessitates a very sensitive detection system. In practice, a spot of light from a 36 watt 6 volts lamp, fed from a stabilized D. C. generator after collimation and reflection from a mirror fixed at the centre of the balance beam, illuminates nearly equally a pair of photoelectric cells connected in opposition

by a bridge arrangement through a sensitive galvanometer. When the balance beam is in the null deflection position, the resistance of the bridge is adjusted until there is no deflection of the galvanometer. But, when there is a small deflection of the balance beam, the spot shifts more on one cell, thus destroying the balance and a large deflection of the galvanometer is observed. By this means a magnification of the balance beam deflection of nearly 500 times is easily obtained. It can be increased even further by increasing the intensity of illumination.

The photocells are mounted side by side in a wooden box painted black inside with a small aperture to admit the light, the cells being located at the farthest end of the aperture. A screw motion is provided at the back to shift the position of the photocells slightly, if necessary.

MEASURING SYSTEM

Current to energise the compensating coil is taken by suitably tapping a 200 ohms variable potentiometer type wire-wound resistance connected in series with a six volt lead accumulator of 1.25 ampere hour capacity. The variable tapping is necessary for measuring samples of different orders of susceptibility value. Three variable resistances of 2500 ohms, 500 ohms and 10 ohms connected in series with compensating coil are employed to provide coarse, medium and fine controls of the current, respectively. A switch starts and stops the current while a commutator controls its direction to balance para- or dia-magnetic samples. Three precision wire-wound manganin resistances of 500, 1000 and 1500 ohms with potentialappings are included in series with the coil, the potential drops across any one or more of which can be measured with an accurate potentiometer giving results correct upto 2 microvolts. The same galvanometer which is used with the photocells, can be connected by a throw-over switch to the potentiometer circuit when desired.

In actual measurements, the galvanometer is first connected to the photocells, after the sample is placed in position. The position of the galvanometer light spot is noted. When the magnetic field is switched on, the light spot is observed to move away. Now the current in the balancing coil is started and adjusted first with coarse, then medium and finally with fine controls, till the galvanometer spot comes back to its original position. The galvanometer is then connected to the potentiometer circuit and the potential drop across the desired standard resistance is measured by comparing against a Weston standard cell. The temperature is measured with a calibrated copper-constantan thermocouple using the same potentiometer with a throw-over switch arrangement. The susceptibility is calculated from eqn. (12) by calibrating with a standard substance and knowing the initial current.

REPRODUCIBILITY AND ACCURACY

To test the Reproducibility of the balance the following procedure was adopted. The 'initial' current C_0 was determined. Then a crystal of chromium potassium sulphate alum prepared from Merck's G. R. quality reagent was suspended and balancing current was determined. The same process was repeated with seven crystals of the same substance with different masses. The ratios of the masses and the corresponding potential drops for balancing currents corrected for initial current should be the same provided the temperatures are same. The results, after allowing for small temperature changes during measurements are summed up in the Table I

TABLE I

Serial no. of crystals	Mass of crystal	Potential drop in microvolts corresponding to			Ratio of potential drops	Ratio of masses	Differences
		Initial current	Balancing current	Corrected current			
1	0.10492 gm	-53	4266	$V_1 = 4319$	$V_1 - 1.3693$	$m_1 - 1.3700$	-0.0007
2	0.07658 "	-53	3101	$V_2 = 3154$	$V_2 - 1.6997$	$m_2 - 1.6991$	+0.0006
3	0.06175 "	-52	2489	$V_3 = 2541$	$V_3 - 1.8778$	$m_3 - 1.8799$	-0.0021
4	0.05581 "	-52	2248	$V_4 = 2300$	$V_4 - 2.0905$	$m_4 - 2.0917$	-0.0012
5	0.05016 "	-53	2013	$V_5 = 2066$	$V_5 - 2.4061$	$m_5 - 2.4042$	+0.0019
6	0.04364 "	-54	1795	$V_6 = 1795$	$V_6 - 4.1649$	$m_6 - 4.1635$	+0.0014
7	0.02520 "	-54	0983	$V_7 = 1037$			

It will be seen from above that the reproducibility of the results are better than 0.1%

We adopted the following procedures to check the accuracy of our measurements :

a) A carefully prepared single crystal of Fe^{+3} alum belonging to the cubic class (using E Merck's G.R. quality reagent) was suspended from the balance arm in the usual manner. The balancing current was very accurately measured. The temperature was measured with the thermocouple. The same process was repeated with the Merck's G.R. quality cobalt-free standard NiCl_2 solution of conc = 0.2590 and density = 1.2993 at 305.3°K, the mass susceptibility of which has been measured very accurately by several workers

(Weiss and Bruns, 1926, Brant, 1921; Bose, 1935; Nettleton and Sugden, 1939) and is given by the formula $\chi \times 10^6 = \left(\frac{10160}{T} + 0.7193 - 0.486 \right) c - 0.7193$ where T is the absolute temperature and c is the concentration of NiCl_2 in gms per gm of the solution. The initial current was determined and susceptibility of Fe^{+3} alum was calculated. Any fluctuation in temperature was accounted for. The measurements were made on 3 or 4 crystals of Fe^{+3} alum and the mean value was taken. The value was corrected for diamagnetism and the mean sq. moment was determined by the formula:

$$\mu_f^2 = \frac{3k\chi_M T}{N\beta^2} = 7.995\chi_M T$$

The value of μ_f^2 is found to be 34.78 at 300°K as against earlier values 34.79 by Onnes and Oosterhuis (1926) and 34.80 obtained by Dutta Roy (1955) at 300°K. It has been shown by Van Vleck and Penney (1934) that for Fe^{13} ion which is in the ${}^6S_{5/2}$ state, the mean susceptibility value should obey the Curie law upto $\frac{1}{T^2}$ term at least with a spin only value of the moment. The small difference from the spin only value 35, can not be due to error arising from the shape effect of the single crystal since a spherical powder sample was observed to give the same value. The small departure must then be due to the deviations from the ideal S -state in consequence of configurational coupling or a small departure from Russel-Saunders coupling. However, our results agree with others to within 0.1%.

b) Cr^{+3} alum crystal also belongs to the cubic class. The same procedure was adopted and the μ_f^2 value was obtained taking Fe^{+3} alum as standard

TABLE II
Results on $\text{Ni}(\text{KSO}_4)_2 \cdot 6\text{H}_2\text{O}$

Serial no crystal	Mass in gms.	Potential drop corr. to			Mol. susceptibility			Mean $\chi \times 10^6$	Temp
		Initial current	Balancing current	Corrected current	$\chi_1 \times 10^6$	$\chi_2 \times 10^6$	$\chi_3 \times 10^6$		
1	0.6725	-52	2353	2405	4483	4351	4350	4398	300°K
2	0.5429	-52	1891	1943	4487	4355	4356	4390	300°K
3	0.4670	-53	1616	1669	4482	4350	4349	4393	300°K
Powder	0.8844	-235	2926	3161	—	—	—	4393	300°K
Sample Mean								4395	300°K
Krishnan <i>et al</i> (1933)	—	—	—	—	4306	4140	4152	4251	300°K

The value for Cr^{+3} alum as obtained by us, is 14.89 as against 14.92 by de Haas and Gorter (1932), after correction by Serres, and 14.91 by Dutta Roy (1956), all at 300°K, and is well within the experimental error of these authors.

c) As a last check, we have measured the principal susceptibility values of $\text{Ni}(\text{KSO}_4)_2 \cdot 6\text{H}_2\text{O}$ of monoclinic class. Taking chrome alum as standard, measurements were taken on three different single crystals of $\text{Ni}(\text{KSO}_4)_2 \cdot 6\text{H}_2\text{O}$, suspended with crystallographic *b*-axis vertical. The measurements gave χ_1 for the substance. Employing the accurate anisotropy results of Dutta (1954), χ_2 and χ_3 were calculated. The mean $\bar{\chi}$ for spherical powdered samples was determined. The values are given in Table II. The results of Krishnan (Chakravorty and Banerjee (1933) are given for comparison.

DESCRIPTION OF THE CRYOSTAT

The earlier cryostats used in this laboratory (Bose, 1947; Dutta Roy 1955) were of gas flow type in which liquid oxygen, kept in a separate reservoir, was pumped into the cryostatic chamber, evaporated and made to flow round the experimental chamber, the control of the temperature being effected partly by adjusting the flow of liquid and partly by a gas thermometer relay device. The range of temperature was limited between 300°K. and 82°K. The control of temperature was not very fine and measurements at very small intervals of temperature could not be very conveniently undertaken. Moreover, the consumption of liquid oxygen was quite large as much of the cold was wasted.

In view of the above difficulties, we have constructed a new type of cryostat which avoids the above drawbacks and provides an extremely fine control of temperature. A liquid bath type of cryostat, instead of the flow type, has been chosen, the control of temperature being effected by varying the pressure in the vacuum jacket of the experimental tube. Provisions have been made to boil the oxygen at reduced pressure to reach temperatures below 90°K. A heater has been incorporated to counteract a slight excess of cooling, thus facilitating an extremely fine control of temperature. The system offers a great economy of the liquid oxygen.

The cryostat (Fig. 2) consists of a wide-mouthed (about 10 cm. inner diameter) silvered glass Dewar vessel (*D*) with a narrow tail (about 5.5 cm. outer diameter) to go between the pole pieces of an electromagnet with a pole gap of about 6 cm. The wider part of the Dewar is about 16 cms. long and the narrow tail about 18 cm. long. A suitable brass casing *O* protects the Dewar from accidental breakage. Another brass case (*B*) fits inside the glass Dewar and contains the refrigerant liquid oxygen, preventing breakage of the glass Dewar by direct contact with liquid oxygen refrigerant. The experimental chamber (*A*) is a double-walled silvered cylindrical pyrex glass tube 41 cms. in length, and of 2.6 cms. and 3.8 cms. inner and outer diameter respectively, with an inner lining of copper sheet and

outer wrapping of copper gauze (G) to maintain the temperature uniform. The inter-space of this jacket is connected to a mercury diffusion pump to maintain

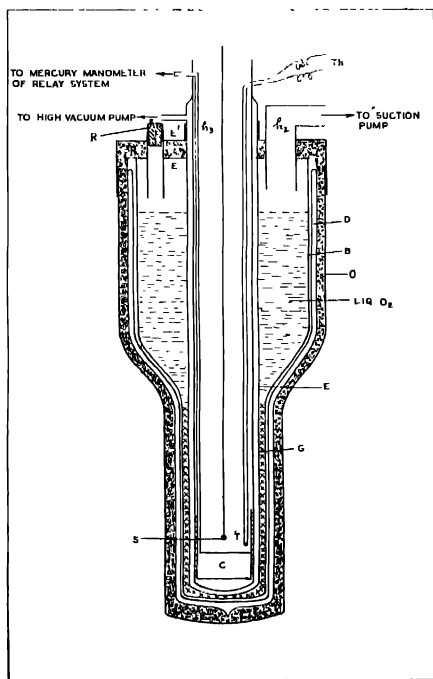


Fig. 2

a high vacuum. The interspace has a controllable leak to the fore vacuum side to control the heat leakage across the vacuum jacket. The top of the cryostat chamber is covered with a brass cap (E) fitting the inner brass casing, to which it is sealed leak tight with Wood's alloy. The outer brass casing has another cap (E') sealed to it with Wood's alloy. Each of the brass caps has three corresponding outlets. The first pair of holes h_1 are connected by a german silver tube through which liquid oxygen can be poured in and the mouth closed leak tight with a rubber stopper. Through the second pair h_2 passes a german silver tube connected to a large capacity suction pump through a pressure stabilizing bottle to make the liquid oxygen boil at reduced pressure. A sensitive differential manometer is introduced in this circuit to record the vapour pressure inside the container. The experimental tube comes out through the third tabular aperture

h_1 at the centre of the cap and is coupled to it leak-tight by a rubber band. The experimental tube then proceeds to the bottom of the balance chamber where it is sealed with picen wax. The space between the outer and inner brass caps is packed with felt and lined with an aluminium reflector to minimize the heat leakage from the top of the cryostat.

A cylindrical copper capsule (c) of about 2.4 cms. diameter and 3 cms. length fitted at the bottom of the experimental space is connected by a stainless steel capillary tube of $\frac{1}{4}$ mm. diameter to a mercury manometer system, and serves as a constant volume air thermometer temperature control unit. Two platinum electrodes fused in the manometer glass tube, one dipping inside the mercury, the other just above the mercury level, are connected to a small magnetic relay system, breaking and making the circuit of a non-inductive cylindrical nichrome 30 watt heater element kept inside the experimental chamber and fed from a 12 volt battery. The heat can be suitably controlled with an external variable loading resistance. Without using liquid oxygen in the Dewar the temperature can safely be raised to any value up to about 400°K.

The thermostatic relay-system is pre-set to any given temperature by adjusting the mass of the air in the gas thermometer. As soon as there is any fall in the temperature, the air contracts and the mercury column in the manometer closes the relay circuit through upper platinum contact which starts the heating current. When the temperature rises above the preset value, the relay circuit is broken off and the heating current stops. In this way, the temperature is controlled automatically and remains constant for sufficiently long time, within 0.01°C. This difference is not observable by changing potentiometer dial of which the least count is 2 microvolts or about 0.05°, but is detectable only with deflection of the galvanometer with no shunt, capable of detecting changes of 0.1 microvolt i.e., about 0.002°.

For temperatures below that of room, the interspace of the glass jacket is evacuated by the mercury diffusion pump until the dark stage in the attached discharge tube is observed. The cryostat chamber is then filled with liquid oxygen and the mouth is closed by the rubber cork. The temperature inside the experimental tube is then found to go down slowly at the rate of about 1° per minute. The fall of temperature can be stopped at any stage and held constant by presetting the relay. To obtain lower and lower temperature, the fine leak to the fore vacuum is opened more and more and then diffusion pump is switched off, only the backing pump is kept running. Finally, for the measurement at liquid oxygen temperature, the backing pump is also shut off and a leak to the atmosphere is introduced.

For measurements in the range of 90°K to 60°K, the liquid oxygen inlet is tightly closed by a rubber cork and the large capacity suction pump connected to the cryostat chamber is started. The pressure is adjusted and read off from

the differential manometer giving the temperature of boiling oxygen, from vapour pressure chart. Different temperatures down to about 62°K are obtained by changing the pressure with the help of a suitable leak valve in the pump circuit and using the heater coil with the help of the relay system.

THEMOCOUPLE CALIBRATION AND TEMPERATURE MEASUREMENT

The temperature in the region occupied by the crystal in the experimental chamber is measured with the help of a copper-constantan thermocouple T (Fig. 2). One of the junction is located close to the crystal where the temperature is appreciably the same and the other junction is kept at the temperature of pure melting ice kept mixed with distilled water in a thermos bottle outside. The two junctions are sheathed by thin walled pyrex glass tube.

The thermocouple was calibrated in the usual manner (Bose, 1947) using a vernier potentiometer reading to 1 microvolt

The temperature — e.m.f. relationship of the thermocouple is given by

$$E = at + bt^2 + ct^3 + dt^4$$

where for our thermocouple,

$$a = 41.101$$

$$b = 0.03977$$

$$c = 1.941 \times 10^{-6}$$

$$d = 4.7905 \times 10^{-7}$$

The calibration of the thermocouple was checked with the Leiden helium gas thermometer scale by comparing Leiden susceptibility measurements of ferric ammonium sulphate alum at the room-temperature, liquid ethylene and liquid nitrogen temperatures with our own. Our room temperature susceptibility is related to those at other temperatures by the formula (Bose, 1947).

$$\frac{F_T}{F_\theta} = \frac{\chi_T}{\chi_\theta} \left[1 + \frac{K_{ag}}{K_\theta} (1 - \gamma\theta) \left(1 - \frac{\theta}{T} \right) \right] \quad \dots (13)$$

where χ_T and χ_θ are the gram molecular susceptibilities of the substance at temperature T and room temperature respectively, F_T and F_θ are the forces acting on the sample at these temperatures, K_{ag} and K_θ are the volume susceptibility of air and that of the substance at room temperature θ , and γ is the coefficient of thermal volume expansion of the sample. So, the measurements of susceptibilities at other temperatures can be easily made by comparing forces on the sample at room temperature and any other temperature.

The results of the low temperature measurements of ferric ammonium alum are given graphically in the form of $\chi^2 - T$ curve (Fig. 3) which shows very close agreement with Leiden and other values.

Since the accuracy of the measurement of the balance has already been checked and can not be doubted, the temperatures at which the susceptibilities are measured fall in very well with the Leiden scale.

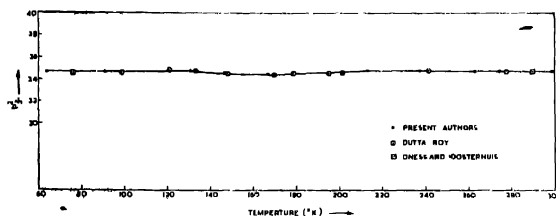


Fig. 3

Our curve for Fe^{+3} alum shows a very interesting deviation from Curie Law which, it is expected, to follow being in a ${}^6S_{5/2}$ ground state. There is a deviation in the linearity of the $\chi^2 - T$ curve with a flat minimum at about 170°K . This deviation is reproducible and exactly reversible. It is already noticeable in Leiden and Dutta Roy's measurements, but no explanation of this has as yet been given.

ACKNOWLEDGMENT

One of us (S M) is grateful to the Council of Scientific and Industrial Research for the award of a Research Fellowship.

REFERENCES

- Bose, A., 1935, *Proc Ind Acad. Sci.*, **1**, 606
 Bose, A., 1947, *Ind. Jour Phys.*, **21**, 277.
 Brant, L., 1921, *Phy. Rev.*, **17**, 678
 Curie, P., 1895, *Jour. de Phys.*, **4**, 197, 163.
 de Haas, W. J. and Gorler, C. J., 1929-31, Comm. Leiden no 208C
 Dutta, S. K., 1954, *Ind. Jour. Phys.*, **28**, 239.
 Dutta Roy, S. K., 1955, *Ind Jour. Phys.*, **29**, 429
 Dutta Roy, S. K., 1956, *Ind. Jour. Phys.*, **30**, 169
 Poex, G. and Forrer, R., 1926, *Jour. de phys.*, **7**, 180.
 Ghose, P. K., 1961, *Ind. Jour. Phys.*, **35**, 319.
 Guoy, L. G., 1889, *C.R. Acad. Sci., Paris*, **109**, 935.
 Krishnan, K. S., Chakravorty, N. C., and Banerjee, S., 1933, *Phil. Trans Roy Soc.*, **232**, 99.
 Nettleton, H. R. and Sugden, D., 1939, *Proc. Roy. Soc.*, **137**, 313
 Omnes, H. K. and Oosterhuis, E., 1926, Comm Leiden, no 139c.
 Serros, A., 1932, *Ann. de Phys.*, **17**, 561.
 Stoner, E. C., *Magnetism and Matter*, (1934, Methuen, London).
 Sucksmith, W., 1939, *Proc. Roy. Soc.*, **17**, 551.
 Van Vleck, J. H., and Penney, W. G., 1934, *Phil. Mag.*, **17**, 901.
 Weiss, P. and Bruns, T. L., 1926, *Proc. Amst. Acad.*, **18**, 246.

A REMOTE CONTROL ELECTRONIC TORQUEMETER

S. C. MUKHERJEE*, AND H. RAKSHIT

INDIAN INSTITUTE OF TECHNOLOGY, Kharagpur

(Received August 9, 1963)

ABSTRACT. The paper gives details of observations on an electronic torquemeter. A rotating shaft transmitting mechanical power undergoes a twist which is measured in terms of time interval and number of revolutions per minute of the shaft. These two quantities can be measured from a remote distance with sufficient accuracy. The torquemeter described is suitable for both high and low speeds and does not impose any appreciable load on the rotating system. The stability of the torquemeter at high speed has been critically studied and details of design explained. The performance in measuring power transmitted by a rotating shaft has also been checked by comparison method.

INTRODUCTION

The various types of instruments that have been developed for measuring torque of a rotating shaft can be broadly classified as follows.

- (i) Mechanical devices based on concentric sleeve and disc displacement,
- (ii) Electrical devices based on the change of inductance and capacitance and resistance of strain gauges,
- (iii) Electronic devices based on the detection of electrical signal produced by changes introduced in the shaft due to torque.

Of these various types of instruments, those based on electronic detection are by far the most sensitive. However, complex electronic instruments which have so far been introduced (Dean and Kilburn 1955, Ainley 1948) have certain disadvantages and limitations, viz (a) they are not suitable for both high and low speeds and (b) there is difficulty in accommodation of the detecting devices. These limitations have been obviated in a sensitive remote control electronic torquemeter designed by the present authors (Rakshit and Mukherjee 1955 and 1958).

As has previously been reported, in the new system two sharp pulses of voltage are produced in two magnetic pick-up coils due to the change in flux caused by two balanced blades of magnetic material fixed at a known separation on the rotating shaft. Initially, when the shaft is running free without any load and there is no twist in the shaft, the positions of the pick-up units are so adjusted that the two pulses occur at the same instant. In practice, the physical positioning does not require to be critically adjusted and the simultaneous occurrence of the

*Lecturer in Communication Engineering, Bengal Engineering College, Howrah.

two pulses at the measuring point is ensured by adjusting to zero the relative delay between the pulses after they have travelled through electrical delay systems. A block schematic of the arrangement is shown in Fig. 1.

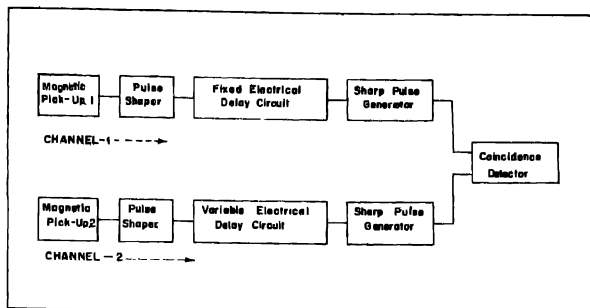


Fig. 1 Block diagram of the torquemeter

When the shaft transmits power, it will undergo a twist and as a result the pulses will be separated by a small interval of time which is dependent upon the angle of twist and the speed of rotation of the shaft. This time interval T is given by

$$T = \frac{\theta}{6N} \text{second,} \quad \dots (1)$$

where N = speed of the shaft (rev./min),

and θ = twist angle in mechanical degree between the two blade positions.

Coincidence is then restored by varying the delay, with the help of an accurately calibrated potentiometer, of one of the pulses with respect to the other. The change in delay is obviously equal to T and this ultimately gives θ .

ACCURACY OF THE MEASURING TECHNIQUE

The main problem in the electronic torquemeter is thus to measure the very small time interval between the two pulses and the number of revolutions per minute which, of course, is relatively quite easy. For example, if $N = 15,000$ rev/min. and $\theta = 0.1^\circ$, which is the permissible full load twist angle per foot of mild steel shaft, $T = 1.1$ microseconds approximately.

It is obvious that once coincidence is established, either in the rotating or in the non-rotating condition of shaft, it has to be maintained in order that the measurements may be reliable. Moreover the accuracy of measurement of a small time interval between two pulses is dependent upon the sharpness and also the duration of the pulses. The resolving time which is half the maximum time separation for which the pulses will remain coincident is obviously a function of the

pulse width. Special care has therefore been taken to develop suitable circuits for generating very sharp and stable pulses. The operation of the system under static condition of shaft which obviously depends only upon the electronic circuits has been found to be very stable. For this purpose the two pulses obtained from the pick-ups under dynamic condition of shaft were simulated by a single reference pulse obtained from (a) 50 cycle mains, as also from (b) 1Kc/s multivibrator. This single pulse excited the two electronic delay channels. The resolving time was found to be 0.02 μ sec; a small amount of jittering could not, however, be avoided.

The stability under rotating condition of the shaft depends upon both the electronic circuits and the rotating mechanical system including the associated magnetic pick-up devices. The present paper gives a detailed account of the dynamic stability at both high and low speeds.

STABILITY TEST

For studying the stability of such an electronic torquemeter a high speed shaft unit was first constructed with two brass discs, 4 inches in diameter and 1/8 inch thick, fixed six inches apart on a 5/8 inch diameter shaft. Two projected and balanced mild steel blades were fixed on the two brass discs (Fig. 2). The shaft

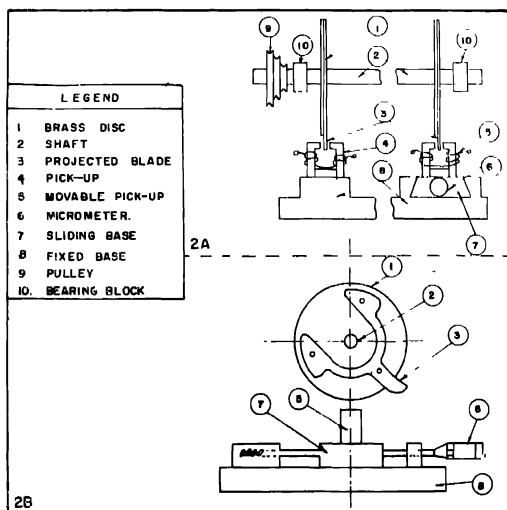


Fig 2 High speed shaft/unit with pick up devices. (A) Mechanical set-up, (B) projected blade and micrometer arrangement.

could be rotated at different speeds by a three phase a.c. motor through a V-belt and sets of pulleys. Initial observations showed that at low speeds the system works quite satisfactorily but at higher speeds considerable jitter is present. This is due to the fact that in addition to the small amount of jitter due to electronic circuits, there are under dynamic conditions three main factors contributing to enhanced jitter. These are :

- (i) Vibration of projected blades due to intermittent resistance experienced by them in the pick-up gaps. This vibration causes relative displacement between the blade and the associated pick-up and thereby increases the jittering.
- (ii) Vibration of the V-belt due to the fact that the periodic air drag on the projected blades when they move through the pick-up air gaps introduces intermittent changes in the tension of the belt. The non-uniform elastic property of the belt material throughout the belt also causes random change in tension of the belt which, in turn, produces non-uniform driving torque to the shaft by the belt and hence causes jittering.
- (iii) Vibration of blade and pick-up due to magnetic interaction resulting from periodic linkage of the projected steel blade and the magnetic field in the pick-up gap.

The design of the bearing block used in the initial stages is shown in Fig. 3. The leading edges of the blades were of course of special form to reduce air friction.

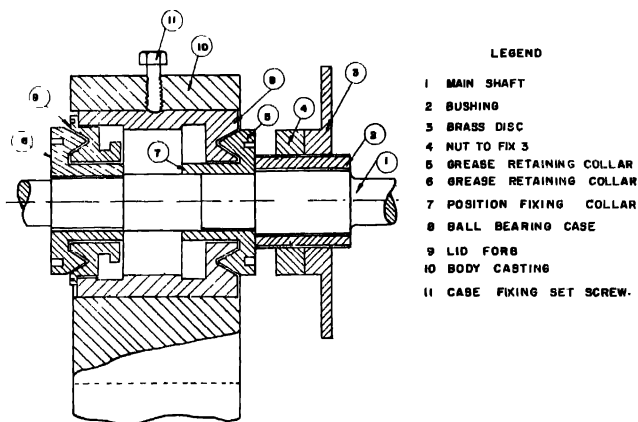


Fig. 3. Bearing block for shaft unit.

The pick-up units were rigidly fixed on a massive base and one pick-up could be moved at right angles to the shaft by micrometer arrangement (Fig. 2B).

Instead of a twist produced in the shaft by load, it was simulated in the following way. The two pick-up units are so positioned that the two pulses occur approximately at the same instant when the shaft is running free. The initial delay in each channel is adjusted to a value near its minimum corresponding to the linear portion of the calibration curve giving delay against potentiometer reading. The delay is controlled by means of a linear Helipot potentiometer fitted with a precision dial. The shaft unit is then rotated without load and the delay in the variable channel so adjusted that the two output pulses occur simultaneously. The movable pick-up is then linearly shifted by 2-circular divisions of the micrometer in a direction opposite to that of the rotational direction of the blade near the pick-up and as a result the coincidence is lost. This shifting of the pick-up produced an equivalent twist θ between the two blades, given by

$$\theta = \frac{180d}{\pi R} \text{ degree,} \quad \dots (2)$$

where d = linear displacement of the pick-up
and R = effective radius of the blades

Coincidence is then restored by increasing the delay in the channel corresponding to the movable pick-up. Owing to finite width of the coinciding pulses and some unavoidable jittering and flutter in the blades it was not possible to realize sharp coincidence with very small resolving time as will be seen from the results given below.

Incidentally, this gives us a method of finding the effective radius R . Thus if the delay potentiometer is calibrated and the delay for one dial division of the potentiometer is K and the change in dial reading for restoring coincidence is A divisions then the delay is KA and from equations (1) and (2) we have

$$R = \frac{30d}{\pi NKA} \quad \dots (3)$$

Results of initial observations

As already pointed out the resolving time was not as small as desired but flickering coincidence was detected over a certain range of the Helipot dial as given in Table I.

It should be noted that the scatter in the coincidence reading, e.g., between 160 and 277 for the initial potentiometer reading for r.p.m. 3060 is partly due to (a) the jittering between the channels (Fig. 1) and resolving time for coincidence, and is largely due to (b) the fluctuation of torque between the two blades and the vibration of the blade and pick-up as explained above. In regard to (a) it is of

TABLE I

 $d = 2$ circular divisions ≈ 0.002 inch, $K \approx 10.4$ nanoseconds/division

Rev/Min	Potentiometer Reading				Difference	Average	θ (degree)	R (inch)
	Initial		Final					
	Range	Mean	Range	Mean				
3000	160	218.5	355	442.5	224	223	0.0426	2.691
	277		530					
	170	226.5	357	448.5	222			
	283		540					
5800	160	212	280	331	119	119	0.0430	2.661
	264		382					
	175	231	293	350	119			
	287		407					
9660	160	210	235	285	75	74.5	0.0449	2.635
	260		335					
	181	226	253	300	74			
	271		347					

the order of $0.02 \mu\text{second}$ as observed when the reference pulse was applied directly to the delay circuits; this increases to $0.03/0.04 \mu\text{second}$ when the two pulse shaping channels are introduced as indicated in Fig. 1. The fluctuation of torque (b) originates from the pulsating "air-drag" and "magnetic drag" jointly in each narrow gap of the pick-up, and is also due to vibration of the V-belt system. The air drag is likely to increase with speed up to a certain limit while the magnetic drag is expected to decrease since the duration of magnetic interaction between blade and pole piece will decrease with increasing speed. On account of the inertia of the rotating disc assembly it is likely that the vibration due to V-belt driving system will be less at higher speeds. The overall jitter at any speed will be given by the resultant effect of all these causes. It will be noticed from Table I that within the range of observation, the scatter in coincidence decreases with increasing speed. Thus, for initial coincidence, the scatter is $115 \pm \frac{1}{2}[(277-160) - (283-170)]$ divisions at 3060 rev/min, 108 divisions at 5800 rev/min and 95 divisions at 9660 rev/min. Although the scatter in coincidence reading decreases, the corresponding flutter $\delta\theta$ in twist angle increases with speed. Thus from equation (1)

$$K = \frac{\delta\theta_1}{A_1 N_1} = \frac{\delta\theta_2}{A_2 N_2} = \frac{\delta\theta_3}{A_3 N_3},$$

where $A_1 = 115$ at $N_1 = 3060$ rev/min
 $A_2 = 108$ at $N_2 = 5800$ rev/min
 $A_3 = 95$ at $N_3 = 9660$ rev/min.

This gives $\delta\theta_1 : \delta\theta_2 : \delta\theta_3 = 3.519 : 6.264 : 9.179$, i.e., $\delta\theta_3 > \delta\theta_2 > \delta\theta_1$, which shows that the pulsating torque increases with speed.

Moreover it has been observed that a considerably larger amount of power is required for driving the shaft with projected blades to overcome the steady frictional resistance due to air when the speed is increased from 3060 to 5800 r.p.m. It has further been noticed that when the projected part of the blade is reduced from 1.5 inch to 1 inch, this extra driving power becomes very small. The design of the rotating discs and the shaft unit had therefore to be modified as described below.

Modified design of rotating disc and shaft unit :

The modified design is given in Fig. 4 and the special features are the following :

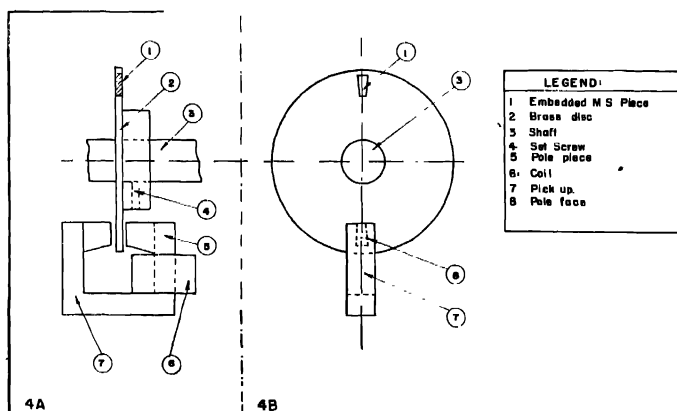


Fig. 4 Modified design of disc and pick-up (A) Front elevation, (B) Side elevation

- (i) *Blade* To avoid air friction on the rotating projected blades and vibrations set up therein due to magnetic interaction in the pick-up pole pieces each blade was replaced by a small mild steel piece ($3/8" \times 3/16" \times 1/8"$ thick) embedded $1/8"$ inside the periphery of the brass disc ($3\frac{1}{4}" \times 1/8"$ thick). The flat surfaces of the discs were highly polished to minimise air friction on the rotating discs.
- (ii) *Pick-up.* The air gap in the pole piece of the pick-up previously used was $\frac{1}{8}$ inch and the intensity of magnetic field in the gap was 5700 gauss. The interaction between the rotating blade and this magnetic field produces vibration not only in the blade but also in the base and body of the pick-up. For better stability of performance, which is very important for high-speed operation, since for the same torque θ the time

interval T decreases with increasing speed, the construction of the pick-up unit is to be more rigid. In the modified design a U -shaped permanent magnet with screwed pole piece has been used. The pole faces are $3/8" \times 3/16"$ with $1/4"$ air gap (Fig. 4A). The intensity of magnetic field in the air gap of the modified pole piece has, however, been much less, about one-tenth of the previous value. The rigid construction of pick-up, the embedded blade system combined with reduction of magnetic field, considerably minimised the vibration problem. The scatter in potentiometer reading for coincidence reduced to about 15 divisions as against over 100 divisions in the previous arrangement.

- (iii) *Pre-amplifier.* With the modified pick-up the amplitude of the pulses produced at a speed of 1500 r.p.m. was only about 1 volt. A two channel pre-amplifier with cathode-follower output has therefore been used to get a negative pulse with flat top and sharp leading edge for driving the main amplifier in the electronic torquemeter at a remote distance. The preamplifier is fed with a stabilised power supply.

Performance test with load

For testing the operation of torquemeter under load, the shaft unit was put in between a d.c. motor and a d.c. generator driven by the motor. The principle of measurement of power transmitted by the shaft is based on Hopkinson's method of back-to-back test of d.c. shunt machines in which the different losses and the efficiencies of the two d.c. machines can be ascertained precisely. It has been checked that during operation the mechanical power transmitted by shaft is equal to the mechanical power received by the generator. The method becomes simpler if the two machines are identical, i.e. of same rating, type and model.

In the experimental arrangement, the two identical d.c. machines were coupled by means of a shaft 0.751 inch diameter and 10.5 inches long, the two discs with embedded blades being fixed $5\frac{1}{16}$ inches apart on the shaft (Fig. 5). The tests were conducted at speeds near about 1500 r.p.m. The transmitted and received powers measured from electrical data gives torque in electrical units. This torque is compared with that estimated from mechanical data involving the twist angle θ measured by the shaft unit.

The diagram of connections of the Hopkinson's method is shown in Fig. 6. The field current I_f of the driven machine working as a generator is so adjusted that at the operating speed the output voltage of generator is equal to that across motor armature. Under this condition the generator output is fed back to the motor armature. Assuming that the shaft unit is not absorbing any power, the mechanical power output of the motor becomes equal to the input to the generator, and the total losses of the two machines, i.e. no-load loss and copper loss, is provided by the supply mains. As shown in Fig. 6, the electrical power supplied to the combination of the two machines running in parallel is W , given by



Fig. 5. Assembly view for performance test

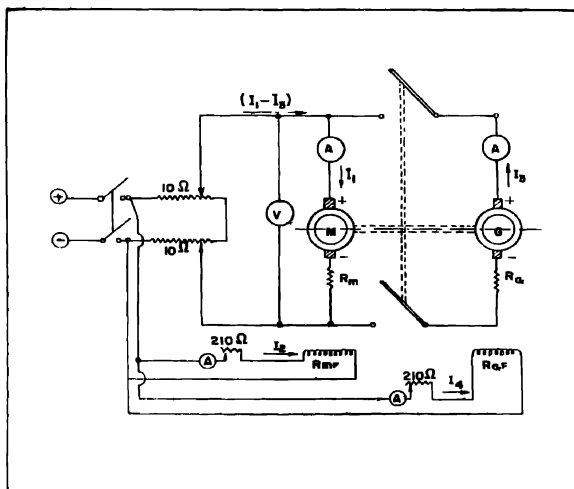


Fig. 6 Connection diagram for performance test.

$$W = (I_1 - I_3)V.$$

This power W consists of :

- (i) No-load loss w of each machine.
- (ii) Motor armature copper loss $w_1 = I_1^2 R_m$
- (iii) Generator armature copper loss $w_2 = I_3^2 R_g$,

where R_m = motor armature resistance and R_g = generator armature resistance. The total no-load loss of the combination, which is equally shared by the two machines = $W - w_1 - w_2$. The no-load loss w per machine is therefore given by $w = \frac{W - w_1 - w_2}{2}$

Now, power transmitted (P) in watts = motor output = generator input. And, motor output = motor input minus its losses, while generator input = generator output plus its losses. Hence

$$P = I_1 V - (w_1 + w) = I_3 V + (w_2 + w) \quad \dots (4)$$

The transmitted power thus estimated from electrical data is also equal to

$$\frac{2\pi T_R N}{12 \times 33,000} \text{ hp,}$$

where T_R = torque produced in inch-pound
and N = rev/min.

$$\text{Hence} \quad T_R = \frac{12 \times 33,000 P}{746 \times 2\pi N} \quad \dots (5)$$

Again, in terms of mechanical data, T_R is given by

$$T_R = \frac{\pi^2 c d^4 \theta}{360 \times 16l} = \frac{\pi^2 c d^4}{5760l} \times 6NKA, \quad \dots (6)$$

where c = rigidity modulus in lbs/inch²,

d = diameter of shaft in inch.

l = length of shaft between the two blades in inches as measured between the two fixing screws,

K = calibration constant = delay for one dial division of potentiometer,

A = change in helipot dial divisions for restoring coincidence.

For any given shaft therefore,

$$T_R = (\text{constant}) \times NA \quad \dots (7)$$

Comparison of T_R as given by equations (5) and (6) enables us to estimate the accuracy of torque measurement by the electronic torquemeter.

MEASUREMENT AND RESULTS

(i) *Rigidity Measurement*.

A shaft from same specimen of mild steel as used in Hopkinson method was tested in one Amsler Torsion Testing machine, to find out the rigidity modulus c , which comes out to be 11.44×10^6 lbs/inch².

(ii) *R.P.M. Measurement* :

Since the blade produces one pulse in one revolution, the r.p.m. is 60 times the recurrence frequency of the pulses per second. A simple method which has given very satisfactory results is shown in Fig. 7. Across the horizontal deflect-

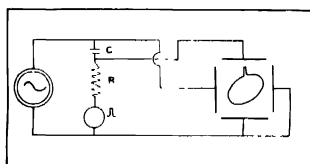


Fig. 7 Arrangement for speed measurement.

ing plates of a cathode ray tube the output of a calibrated audio oscillator is directly applied. Across the vertical deflecting plates we have the phase-shifted oscillator voltage in series with the pulse voltage. Under these conditions we get on the C.R.O. screen an ellipse on which is superimposed the pulse voltage moving round the periphery of the ellipse. When the pulse recurrence frequency is the same as that of the audio oscillator, a single stationary pulse is seen on the ellipse.

A second method, without utilizing a cathode ray tube, has also been used with good results. The recurrent pulses derived from one of the pick-ups and pulses derived from a calibrated oscillator are applied to the grids of two valves having a common anode load resistance. A large output is obtained when the two pulses occur simultaneously. Details of the coincidence technique of measuring r.p.m. have already been described by the authors (Rakshit and Mukherjee 1955/2)

(iii) *Torque Measurement*.

The motor is run at desired speed by regulating the field current I_2 (Fig. 6). By controlling I_4 , the output voltage of the generator is made equal to V and the two machines are put in parallel. The generator output current I_3 is now zero and the motor input current I_1 is used up in the motor armature copper loss w_1 plus the no-load losses $2w$ of the two machines

(a) For torque measurement from electrical data we have to measure, in addition to N and the different currents and voltage V , the values of R_m and R_g . These armature resistances are determined at room temperature and corrections made for rise in temperature under working conditions.

(b) For torque measurement from mechanical data we have to measure, in addition to c, d, l, N and K , the change Δ in delay potentiometer reading between no-load and load conditions. With the shaft unit put in-between the motor and generator we do not get the no-load condition and the change Δ required as per equation (6) is obtained as follows

Initially when I_3 is zero, as stated above, only a very small torque is present in the shaft. The variable delay in the appropriate channel is adjusted for initial coincidence and the Helipot reading is noted. Due to flickering coincidence, two extreme readings are taken to obtain a mean value, say A' . The transmitted power P is then increased by increasing I_3 which, in turn, is obtained by varying I_4 , keeping V and N constant. The new Helipot reading is then noted. This is repeated for different values of transmitted power and also for different values of N .

It will be noted that for a given value of N , the plot of T_R or H.P. transmitted against A will be a straight line passing through the origin. Now if for $N = N_1$, the initial no-load coincidence corresponds to A_0 and the potentiometer reading

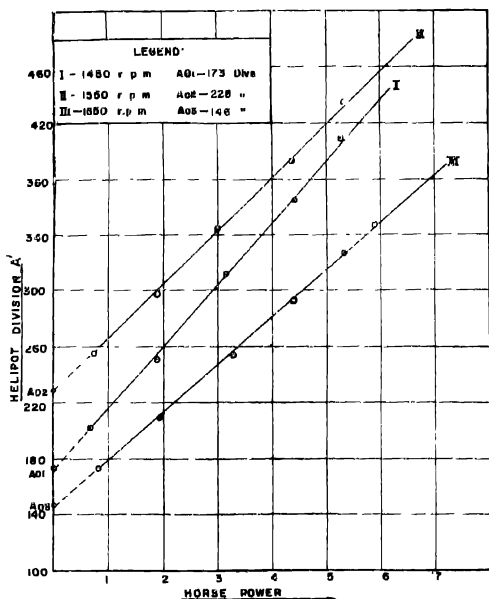


Fig. 8. Graph of transmitted power vs. Helipot division.

under load is A' , the corresponding value of A is $A' - A_0$. Hence the straight line plot of H.P. transmitted T_R against A' will give an intercept A_0 on the A' axis. Fig 8 gives the values of A_0 for different values of N and these are shown in Table II. The values of torque estimated from electrical data as also from mechanical data for different operating conditions are presented in Table II.

TABLE II

$d = 0.751$ inch, $l = 5\frac{9}{16}$ inch; $K = 10.4$ nanoseconds/division, $c = 11.44 \times 10^6$ lbs/inch²

R.P.M.	Transmitted H P.	Torque measured from eqn(5) in Inch-Pound	Helipot Reading A'	A_0 from Fig 8.	Difference $A = (A' - A_0)$	Torque measured from eqn.(6) in Inch-Pound
1650	.0816	3 116	172.5	146	26 5	3.058
	1941	7.410	209 5		63 5	7 328
	3294	12.576	253.0		107 0	12 35
	4392	16.769	292.5		146.5	16.90
	5315	20 293	327.0		181 0	20.88
	5881	22 454	346 5		200.5	23 14
1550	0729	2.963	255 0	228	27.0	2.927
	1887	7.670	297.0		69.0	7 478
	2987	12 141	343 0		115.0	12.47
	4359	17 718	392.0		164.0	17.77
	5333	21.677	434 0		206.0	22.33
1450	.0669	2.906	202 0	173	29.0	2 941
	.1863	8.093	250.5		77.5	7.859
	3149	13.681	311.0		138.0	14 00
	4401	19.121	364.0		191.0	19 360
	5284	22 958	408 0		235.0	23.83

DISCUSSION

The results of observations as given in Table II show that the torque obtained from the torquemeter is in very close agreement with that obtained by the Hopkinson's electrical method. The measurements were unfortunately limited to speeds round about 1500 r.p.m. since the two electrical machines used in the Hopkinson's test were designed for such low speed.

Other torquemeters have some inherent damping and are consequently rather sluggish in operation. They give a fairly steady average value even when the torque is fluctuating, i.e., short time variations in torque go undetected. The present torquemeter can however detect such temporary variations. The electronic circuitry can, of course, be easily modified to measure average torque when necessary. An additional advantage of this torquemeter is that practically no extra load is imposed on the system.

The coincidence has not been very sharp and there is a definite range over which the coincidence takes place. This scatter in coincidence does not depend

upon transmitted power and within the speed range of observation the scatter decreases with increasing speed. This is expected since at higher speeds the impulse given to the vibrating system when the magnetic blade passes through the pick-up is of shorter duration resulting in reduced vibration.

ACKNOWLEDGMENT

The work was started under the auspices of the Council of Scientific and Industrial Research and the authors are grateful to the Council for permission to publish the results. One of the authors (S C M) is also thankful to the Council for grant-in-aid. Thanks are also due to Dr S S Baral and Prof. D Banerjee of Bengal Engineering College, Howrah and Dr. B Karunes of Calcutta University, for helpful suggestions.

REFERENCES

- Ainley, D G, 1948, *Proc I Mech E*, **159**, 240.
Dean, S K. and Kilburn, M A, 1955, *The Engineer*, **200**, 686.
Rakshit, H and Mukherjee, S C, 1955/1, *J. Sci. Industr. Res.*, **14B**, 304.
Rakshit, H and Mukherjee, S. C, 1955/2, *J Inst Telecom Engrs*, **1**, 130.
Rakshit, H. and Mukherjee S C, 1958, *Electronic Engineering*, **30**, 557.

ENERGY STATES AT THE INTERFACE OF TWO SEMI-INFINITE ONE-DIMENSIONAL CRYSTALS

S. K. GHOSH AND A. K. LASKAR

DEPARTMENT OF PHYSICS, INDIAN INSTITUTE OF TECHNOLOGY,
KHARAGPUR

(Received July 10, 1963)

ABSTRACT. Localized energy levels are computed, by the scattering matrix method of Saxon and Hutner (1949), at the interface of two similar semi-infinite crystals with adsorbed gas at the interface. First, the calculations have been made for a clean interface and then for an impurity atom at the interface. The results show the existence of localized states at certain potential strength of the adsorbed gas. Some experimental evidence of the theoretical results are given.

INTRODUCTION

Tamm (1932) showed the existence of localised energy levels at the free surface of a one dimensional semi-infinite crystal. Since then several authors have calculated surface energy levels by various methods. Shockley (1939), and Aerts (1960) calculated surface energy levels on the assumption that the potential of the boundary atom shows a symmetric behaviour. Aerts further extended the case to a surface contaminated by an adsorbed impurity atom. On assuming this kind of potential, the results obtained by Aerts conform to the experimental observations.

In this paper, the electronic energy states localised at the interface of two semi-infinite crystals with adsorbed gas layer at the interface, are computed. Aerts (1960) has shown that the interface between two crystals is a kind of imperfection, which gives rise to energy state and thus plays a great role in its electrical behaviour. It is well established that the electrical conductivity of both semiconducting crystals and films are strongly dependent on the adsorbed gas. When films of a substance are deposited on a substrate, we have adsorbed gas at the interface of two crystallites of identical nature. The presence of an impurity may also be possible at the interface of identical crystallites. We propose to investigate the energy-states in the above mentioned systems. A simple method based on the work of Saxon and Hutner (1949) has been followed.

THE CRYSTAL MODEL AND THEORY

Since the essential features of the problem would remain same, a simplified model of two semi-infinite crystals, of identical nature in contact is considered. The semi-infinite monatomic lattice has the same spacing on both sides. Let

U be the atomic potential. Due to the adsorbed gas at the interface the surface atoms may be assumed to have the potential strength $U + U_1$. Let the interface potential be $U + U_2$. A graphical representation of the crystal model is given in Fig. 1.

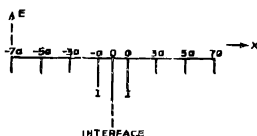


Fig. 1. Graphical representation of the crystal model with adsorbed impurity (U) at the interface.

Choosing the origin of the co-ordinate system at the interface, the atoms of the R.H.S. are localized at the points with abscissa $x = (2n+1)a$ and those of L.H.S. are localised at the points $x = -(2n+1)a$, n being a positive integer.

On the R.H.S. the potential energy is of the form

$$-ev_1 = \left(\frac{au\hbar^2}{m} \right) \sum_0^{\infty} \delta[x - (2n+1)a] + \frac{au_1\hbar^2}{m} \delta(x-a) \quad (1)$$

and on the L.H.S. the potential energy is of the form

$$-ev_2 = \left(\frac{au\hbar^2}{m} \right) \sum_0^{\infty} \delta[x + (2n+1)a] + \frac{au_1\hbar^2}{m} \delta(x+a) \quad (2)$$

The waves propagating from either side will undergo scattering by the combined disturbances, first at the adsorbed impurity atom, then at the interface and again at the adsorbed impurity atom. Following Saxon and Hutner's method, the M -matrix associated with the three combined disturbances may be given by

$$M = (R_2)(Q_2)(R_{21})(Q_1)(R_1) \quad \dots (3)$$

The matrix (R_2) is associated with the adsorbed impurity situated at $x = a$. It is

$$R_2 = \begin{vmatrix} 1 + i \tan \theta & i \tan \theta \\ -i \tan \theta & 1 - i \tan \theta \end{vmatrix} \quad (4)$$

where,

$$\tan \theta = \frac{au_1 \sin 2\mu a}{\chi \sin 2\mu a} \quad (5)$$

where μ is the wave vector and $\chi^2 = \frac{2mE}{\hbar^2}$, E being the electron energy in the crystal.

(Q_2) is the translation matrix for $x = a$ to $x = 0$ and is of the form

$$Q_2 = \begin{vmatrix} e^{i\mu a} & 0 \\ 0 & -e^{i\mu a} \end{vmatrix} \quad \dots \quad (6)$$

The matrix (R_{12}) , associated with the disturbance at the interface potential, is given by

$$R_{12} = \begin{vmatrix} 1 - \frac{iau_2 \sin \chi a}{2x \sin \mu a} & -\frac{iau_2 \sin \chi a}{2\chi \sin \mu a} \\ \frac{au_2 \sin \chi a}{2\chi \sin \mu a} & 1 + \frac{au_2 \sin \chi a}{2\chi \sin \mu a} \end{vmatrix} \quad \dots \quad (7)$$

Q_1 is the translation matrix for $x = 0$ to $x = -a$ and is of the form

$$Q_1 = \begin{vmatrix} e^{i\mu a} & 0 \\ 0 & e^{-i\mu a} \end{vmatrix} \quad \dots \quad (8)$$

The matrix (R_1) is associated with adsorbed impurity situated at $x = -a$ and it is

$$R_1 = \begin{vmatrix} 1 + i \tan \theta & i \tan \theta \\ i \tan \theta & 1 - i \tan \theta \end{vmatrix} \quad \dots \quad (9)$$

Writing $\tan \theta = A$, $e^{i\mu a} = B$ and $\frac{au_2 \sin \chi a}{2\chi \sin \mu a} = C$

and then substituting the values of (R_2) , (Q_2) , (R_{12}) , (Q_1) and R_1 in equation (3), we have

$$M = \begin{vmatrix} [1 + iA - iA + B] & 0 & [1 - iC - iC + B] & 0 & [1 + iA] & iA \\ -iA & [1 + iA + B] & iC & [1 + iC + B] & -iA & [1 - iA] \end{vmatrix} \quad \dots \quad (10)$$

The localized energy levels at the interface are determined by the conditions

$$M_{22} = 0; \mu = \frac{n\pi}{2a} + i\xi, \quad \xi > 0 \quad \dots \quad (11)$$

Using second and third conditions of equation (11), the appropriate Kronig and Penny relation can be written as

$$(-1)^n \cos 2a\xi = \cos 2a\chi + \left(\frac{au}{\chi}\right) \sin 2a\chi \quad \dots \quad (12)$$

The matrix element M_{22} as obtained from equation (10) is given by

$$M_{22} = \tan^2 \theta [2i (\sin \mu a - C \cos \mu a) + C] \\ - 2 \tan \theta [i(1 + iC)e^{-2i\mu a} + C] \\ + (1 + iC)e^{-2i\mu a} \quad \dots \quad (13)$$

Using the first condition of eq. (11), the two values of $\tan \theta$ obtained as a solution of the quadratic Eq. (13), are given by

$$\left(i \sin \mu a - \frac{au_2}{\chi} \tan \chi a \cos \mu a \right) (1 - 2 \cos^2 \mu a - 2i \sin \mu a \cos \mu a)$$

$$\tan \theta = \frac{\frac{u_2}{\chi} \tan \chi a \cos \mu a \pm i \sin \mu a}{2i \left[2i \sin^2 \mu a \cos \mu a - \frac{au_2}{\chi} \tan \chi a \cos \mu a (1 - 2 \sin^2 \mu a) \right.}$$

$$\left. \frac{u_2}{\chi} \tan \chi a \cos \mu a \right] \dots \quad (14)$$

Putting second and third conditions of equation (11) in equation (14) and taking negative sign, we obtain

$$\tan \theta_1 = \frac{i \left[i(1 - ch \, 2a\xi)^{\frac{1}{2}} - \frac{au_2}{\chi} \tan \chi a (1 - ch \, 2a\xi)^{\frac{1}{2}} \right] [(1 - ch \, 2a\xi)^{\frac{1}{2}} + i(1 + ch \, 2a\xi)^{\frac{1}{2}}]}{2 \left(1 + \frac{au_2}{\chi} \tan \chi a \right) (1 + ch \, 2a\xi)} \quad \dots \quad (15)$$

To obtain the energy states within the first forbidden gap we take $n = 1$ in equation (12) and by eliminating ξ between (12) and (15), we get

$$\frac{i}{2} \left[i \left(1 - \frac{aU_2}{\chi} \cot a\chi \right)^{\frac{1}{2}} - \frac{au_2}{\chi} \tan a\chi \left(\cot^2 a\chi + \frac{aU}{\chi} \cot a\chi \right)^{\frac{1}{2}} \right]$$

$$\tan \theta_1 = \frac{\left[\left(\cot^2 a\chi + \frac{aU}{\chi} \cot a\chi \right)^{\frac{1}{2}} + i \left(1 - \frac{aU}{\chi} \cot a\chi \right)^{\frac{1}{2}} \right]}{\left(1 + \frac{aU_2}{\chi} \tan a\chi \right) \left(1 - \frac{aU}{\chi} \cot a\chi \right)} \quad (16)$$

Substituting the value of $\tan \theta_1$ as in equation (5) in (16) we have

$$X_1 = \frac{V \left[1 - \frac{Z^2}{V^2} + \frac{2Z}{V} \cot \pi V \right]^{\frac{1}{2}}}{2 \left[1 + \frac{Y}{V \cot \frac{\pi V}{2}} \right] \left[1 - \frac{Z}{V} \cot \frac{\pi V}{2} \right]}$$

$$\left[i \left(1 - \frac{Z}{V} \cot \frac{\pi V}{2} \right) \left(1 + \frac{Z}{V \cot \frac{\pi V}{2}} \right)^{\frac{1}{2}} \right]$$

$$\left(\cot \frac{\pi V}{2} - \frac{Y}{V} \right) - \frac{Y}{V} \cot \frac{\pi V}{2} \left(1 - \frac{Z}{V \cot \frac{\pi V}{2}} \right)$$

$$- \left(1 - \frac{Z}{V} \cot \frac{\pi V}{2} \right) \quad (17)$$

where $X_1 = \frac{2a^2}{\pi} U_1$, $Y = \frac{2a^2}{\pi} U_2$; $Z = \frac{2a^2}{\pi} U$ and $V = \frac{2a}{\pi} \chi$... (17)

Now taking the positive sign in equation (14) for the second solution of $\tan \theta$, we similarly obtain

$$X_2 = -X_1 + \frac{V}{\sin(\pi V) + \frac{2Y}{V} \sin^2\left(\frac{\pi V}{2}\right)} \quad \dots (18)$$

Equations (17) and (18) are rather involved in V , therefore, it is difficult to calculate the energy values directly for different values of x , i.e. different types of

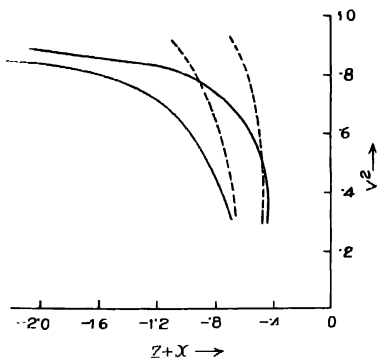


Fig. 2

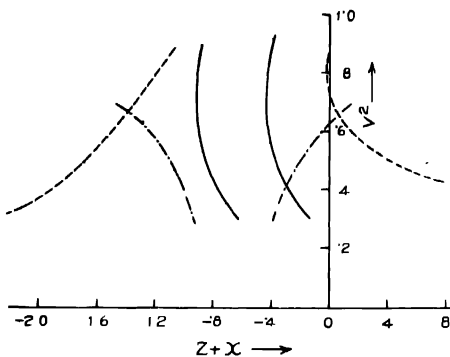


Fig. 3 Solutions of the equations (17) and (18)

————— for $Z = -\frac{1}{2}$, $Y = -1$

..... for $Z = -\frac{1}{2}$, $Y = -\frac{1}{2}$

-o-o-o- for $Z = -\frac{1}{2}$, $Y = 0$

adsorbed gas. Hence, α assuming reasonable values of V , X_1 and X_2 have been calculated with the help of equations (17) and (18). It is thus possible to have same energy for different nature of adsorbed gas.

RESULTS AND DISCUSSION

The plots in Figs. 2 and 3 represent the results of our calculations. It should be mentioned that only the solutions that have a physical meaning are plotted. Fig. 2 represents the solutions for a definite value of atomic potential Z , and positive values of interface potential Y ; Fig. 3 shows the solutions for a definite value of atomic potential Z with zero and negative values of interface potential Y . For positive values of Y one finds the localized energy levels at the interface when there is only adsorbed gas at the clean interface of two crystallites of identical nature and for negative values of Y there are adsorbed gas and also an impurity at the interface. The plots are interrupted at certain values of V because we have restricted the calculations to the first forbidden gap.

The family of curves in Figs. 2 and 3 can in general be explained if we consider that when the potential strength of the adsorbed impurity is smaller than that of the bulk, an electron can escape more easily because it is more loosely bound and there is possibility of larger interaction with the neighbouring atomic potentials. On the contrary when the potential strength of adsorbed impurity is deeper than that of the bulk, the electron is more tightly bound to the impurity and the possibility of interaction with the neighbouring atomic potential decreases. It is, however, not possible to explain every detail of the curves only on the above considerations. It is striking to note that the energy levels move towards the conduction, creating degenerate levels near the conduction band as the impurity potentials become deeper. This means the creation of n -type levels by highly p -type impurities when they are consecutively placed in the atomic lattice or are in close proximity. It was experimentally observed by Ghosh (1960) that there is a possible existence of n -type regions in the films deposited from highly p -type tellurium. The existence of n -type tellurium as such is not found, but it appears from the above discussion that an n -type region is possible in a film deposited from highly p -type materials at places where there is an accumulation of impurity atoms or a highly p -type gas adsorbed at the interface of two crystallites.

REFERENCES

- Aerts, E., 1960, *Physica*, **26**, 1063.
- Ghosh, S. K., (1960) Thesis submitted for the Ph.D degree at the Indian Institute of Technology, Kharagpur.
- Saxon, D. S and Hutner, R. A., 1949, *Philips Res. Rep.* **4**, 81.
- Shockley, W., 1939, *Phys. Rev.*, **56**, 317
- Tamm, I. L., 1932, *Phys. Z. Sowjetunion*, **1**, 733.

ZERO PRESSURE JOULE-THOMSON COEFFICIENT FOR A FEW NON-POLAR GASES ON THE MORSE POTENTIAL

R. S. GAMBHIR AND S. C. SAXENA

PHYSICS DEPARTMENT, RAJASTHAN UNIVERSITY, JAIPUR, INDIA

(Received June 21, 1963)

Recently Konowalow, Taylor and Hirschfelder (1960, 1961) have added the Morse potential to the list of potentials for which detailed computations of various gas properties are possible. This potential is

$$\phi(r) = \epsilon(x^2 - 2x),$$

where

$$x = \exp [-(c/\sigma)(r - r_m)].$$

Here, $\phi(r)$ is the potential energy between two molecules at a separation distance r , ϵ is the depth of the potential minimum at $r = r_m$, σ is that value of r for which $\phi(r) = 0$, and c is a third parameter which governs the curvature at the minimum and the steepness of the repulsive limb. Konowalow and Hirschfelder (1961) have determined the three parameters for a few non-polar gases from crystal and second virial data. They also compared the experimental second virial values with the calculated values according to this potential and the exp-6 and Lennard-Jones (12-6) potentials. This work revealed that most probably the Morse and exp-6 potentials are comparable in accuracy and both are somewhat superior to the 12-6 potential. Saxena and Gambhir (1963) have also investigated the second virial data of a few pure gases over a wider temperature range, and also of a few gas mixtures. They found the Morse potential to be somewhat superior to the other two potentials. Saxena and Bahethi (1963) have calculated the transport properties in conjunction with the potential parameters given by Konowalow and Hirschfelder (1961) and compared the values with the experimental data. They found that the transport properties are not adequately reproduced and have expressed the necessity of redetermination of the parameters for an accurate relative assessment.

To investigate the adequacy of this potential further we consider the experimental data of zero pressure Joule-Thomson coefficient, μ^0 . The theoretical computed values of the reduced μ^0 are given by Konowalow, Taylor and Hirschfelder (1960). The experimental values of $\mu^0 C_p^0$ (C_p^0 being the zero pressure specific heat of the gas at constant pressure) for He, Ar, CH₄, and N₂ have been reported by Lunbeck (1950). In addition to these values we also consider the experimental

data of Budenholzer, Sage and Lacey (1939) for CH_4 ; and of Charnley, Isles and Townley (1953), Roebuck and Osterberg (1935) Gusak (1937), and Collins and Keyes (1939), (as reported by Charnley *et al* 1953) for N_2 . These experimental values are shown plotted in Fig. 1. The computed values both according to the Morse as well as the $L-J$ (12-6) potentials are also shown. The exp-6 potential could not be considered for the theoretical values of the reduced μ^0 are not available. We also do not consider here the $L-J$ (18-6) potential introduced by Saxena and Joshi (1962) because though the reduced μ^0 is known, potential parameters for most of these gases have not been determined as yet. The potential parameters used in calculations are those tabulated by Konowalow and Hirschfelder (1961) except for He. It may be noted that for both the potentials the parameters have been determined from the equilibrium properties only. For He we use the parameters of Bahethi and Saxena (1963) determined from the second virial data. These are $\epsilon = 4$, $\epsilon/k = 14.43^\circ\text{K}$, and $\sigma = 2.976\text{\AA}$.

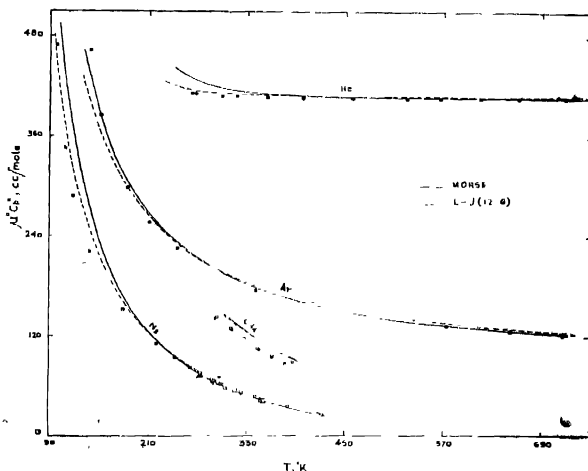


Fig. 1. Plots of $\mu^0 C_p$ as a function of temperature. For Ar ordinates have been displaced by ± 120 units, and for He abscissae and ordinates have been displaced by ± 180 and ± 420 units, respectively. Experimental data: He, Ar, CH_4 , N_2 , \bullet Lumbeck; CH_4 , \circ Budenholzer *et al.*; N_2 , \square Charnley *et al.*, Δ Gusak, ∇ Roebuck and Osterberg, \square Collins and Keyes.

From the figure we find that for Ar the Morse potential is better than the 12-6 potential over the entire temperature range. For N_2 at high temperatures both the potentials are about equally good but the differences are appreciable at low temperatures. The deviations, however, are less for the 12-6 potential. For CH_4 both the potentials yield approximately similar results, with a slight preference

for the 12-6 potential. Some alternative choices for the 12-6 potential parameters are also available for this gas. Schamp *et al.* (1958) have reported the potential parameters for CH_4 ($\epsilon/k = 148.07^\circ\text{K}$, $\sigma = 3.810\text{\AA}$) from the analysis of their virial data. These parameters lead to values which are nearly 4% greater than those plotted in the figure. Similar results are obtained if we consider the potential parameters given by Hamann and Lambert (1954) for CH_4 .

In the case of He the 12-6 potential is definitely superior to the Morse potential in the low temperature range even if the quantum corrections are considered. Bahethi and Saxena (1963) have also noted that for He the above parameters completely fail to reproduce the transport properties. They have determined the Morse potential parameters from viscosity data also. The values are $\epsilon/k = 6$, $\epsilon/k = 8.55^\circ\text{K}$, and $\sigma = 2.687\text{\AA}$. These parameters reproduce the transport properties but fail in the case of second virial coefficient. If we use these parameters to compute $\mu^0 C_p^0$ we get almost the same values at high temperatures but consistently smaller values at low temperatures. This disagreement will further increase if quantum corrections are applied.

The above comparison leads to the conclusion that the $L-J$ (12-6) potential is slightly better than the Morse potential. This conclusion is specially interesting in view of the simplicity of the 12-6 potential. The fact that in the case of He one set of Morse parameters cannot correlate both the equilibrium and non-equilibrium properties implies that the Morse potential is not as good as the other two potentials, viz. 12-6 and ex-6, for this gas.

ACKNOWLEDGMENT

We are thankful to the Council of Scientific and Industrial Research, New Delhi, for financial support. We are also grateful to Prof. J. O. Hirschfelder for sending the reports in advance of their publications.

REFERENCES

- Bahethi, O. P. and Saxena, S. C., 1963, *Phys. Fluids in Press*.
 Budenholzer, R. A., Sage, B. H. and Lucey, W. N., 1939, *Ind. Eng. Chem.*, **31**, 369.
 Charnley, A., Isles, G. L. and Townley, J. R., 1953, *Proc. Roy. Soc. (London)*, **A 218**, 133.
 Collins, S. C. and Keyes, F. G., 1939, *J. Phys. Chem.*, **43**, 5.
 Gusak, I. M., 1937, *Phys. Z. Sowjet*, **11**, 60.
 Hamann, S. D. and Lambert, J. A., 1954, *Australian J. Chem.*, **7**, 1.
 Konowalow, D. D., Taylor, M. H. and Hirschfelder, J. O., 1960, University of Wisconsin Theoretical Chemistry Rept. WIS-AF-16.
 Konowalow, D. D., Taylor, M. H. and Hirschfelder, J. O., 1961, *Phys. Fluids*, **4**, 622.
 Konowalow, D. D. and Hirschfelder, J. O., 1961, *Phys. Fluids*, **4**, 629.
 Lunbeck, R. J., 1950, Doctoral Dissertation, Amsterdam.
 Roebuck, J. R. and Osterberg, H., 1935, *Phys. Rev.*, **48**, 450.
 Saxena, S. C. and Bahethi, O. P., 1963, *Mol. Phys. in Press*.
 Saxena, S. C. and Gambhir, R. S., 1963, *Molecular Physics*, **6**, 577.
 Saxena, S. C. and Joshi, K. M., 1962, *Indian J. Phys.*, **36**, 422.
 Schamp, H. W., Jr., Mason, E. A., Richardson, A. C. B. and Altman, A., 1958, *Phys. Fluids*, **1**, 329.

Letters to the Editor

The Board of Editors will not hold itself responsible for opinions expressed in the letters published in this section. The notes containing reports of new work communicated for this section should not contain main figures and should not exceed 500 words in length. The contributions must reach the Assistant Editor not later than the 15th of the second month preceding that of the issue in which the letter is to appear. No proof will be sent to the authors.

11

ON THE BINDING ENERGIES OF THE MOST STRONGLY BOUND NUCLEI OF DIFFERENT MASS NUMBERS

A. K. DUTTA, B. PAL, P. GANGULY AND D. BANERJEE

UNIVERSITY COLLEGE OF SCIENCE, 92, ACHARYA PRAFULA CHANDRA ROAD,
CALCUTTA-9

(Received, October 4, 1963)

In a previous communication (Dutta, 1963), a relation in the form $E = -9.893A + 9.181 \times 10^{-3} A^2 + 37.0$ Mev., had been put forward, to express the mean course of the nuclear binding energy in relation to mass number. To make the fluctuations symmetrical, the foregoing relationship has been modified for even and odd mass numbers, to the form,

$$E = -9.828A + 8.877 \times 10^{-3} \cdot A^2 + 32.6 \pm 0.4 \text{ mev} \quad \dots (1)$$

according as A is odd or even.

The neutron numbers of the most strongly bound even and odd mass nuclei of different mass numbers have been found to be related to the mass numbers by a nearly linear relationship. A smooth curve through them is expressible as,

$$N_0 = -7.0 + 0.637A + 8.432 \exp - .0267A, \quad \dots (2)$$

indicating a definite relation for the neutron proton ratio. It gives us the optimum neutron number, N_0 , necessary for the most strongly bound condition, for any particular even or odd mass number, and is not necessarily, an integral number. It will enable one to obtain the optimum charge $Z_0 = (A - N_0)$ and the excess neutron $I_0 = (2N_0 - A)$, for any mass number.

The binding energies of the most strongly bound nuclei associated with N_0 values for different mass numbers, deviate from the above relation (1), by a composition of two periodic curves. The independent variables may be considered to be the optimum Z_0 and the I_0 values. The combination of the periodic curves, approximately, measures the deviation of the experimental binding

energies of the most strongly bound nuclei (Konig and others, 1962) of different mass numbers, also. One may express Z_0 and I_0 in terms of A , by relation (2) and, thus, the two periodic curves also, in terms of A .

The two periodic curves are determined by the combination,

$$a_z \sin \pi f(Z) + a_I \sin \pi f(I) \quad \dots (3)$$

or,

$$a_z \sin \pi f(Z) + a_I \sin \pi \{f(Z) - \phi\}.$$

where

$$a_z = 11.3 + (4.15 - .00875A) \sin \pi(.656 + .01875A) \text{ Mev.}$$

$$a_I = 10 - 2.7 \sin \pi(.630 + .009258A) \text{ Mev.}$$

$$f(Z) = 3.14 \sinh .01(A - 160)$$

$$f(I) = [f(Z) - \phi]$$

$$\phi = 96 + 22 \exp -1.7 \times 10^{-3}(A - 148)^2 + \exp -1.55 \times 10^{-2}(A - 217)^2]$$

The two phase relations in terms of A , give us the courses of the periodic curves, against mass number scale, obtained in nuclear growth. The amplitudes and the phases of the two periodic curves are mutually adjustable to a small extent, giving a scope for a closer agreement with experimental results. The phase difference is of the order of π . The values of A at the minima and the maxima of the periodic curves, as also the approximate I_0 and Z_0 values, are tabulated in Table I, where they have been arranged in rows.

TABLE I

	max	min	max	min	max	min	max	min	max	min	max
$A(I_0)$	14	28	44	64	85	115	148	176	208	233	256
(I_0)	5	3.4	4.4	8.4	13	18	26	34	43	50	56
	min	max	min	max	min	max	min	max	min	max	min
$A(Z_0)$	13	27	44	64	87	114	144	176	206	233	256
(Z_0)	6	13	20	28	38	48	59	71	82	92	100

The binding energies of the most strongly bound nuclei would be given by the combination of relations (1) and (3) drawn in Fig. 1, except for a small deviation on account of the shift of the integral neutron numbers from the optimum neutron number of N_0 . They are shown in Table II, for 51 nuclei from carbon to Mendelevium, running through the complete set. The average error is 0.70 mev. A modification of the relations would be necessary to make them correspond to the energy values associated with the optimum neutron numbers, more closely. This would be taken up later.

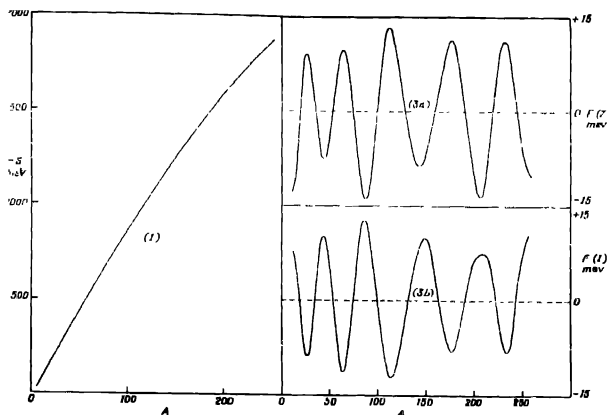


Fig. 2

TABLE II

A	$-B(e_{rp})$ mev.	$-B(C_{al})$ mev.	A	$-B(e_{rp})$ mev.	$-B(C_{al})$ mev.	A	$-B(e_{rp})$ mev.	$-B(C_{al})$ mev.
12	92.2	89.1	90	781.2	782.6	175	1412.3	1412.3
15	115.5	116.2	95	821.7	822.9	180	1446.0	1415.8
16	127.6	126.1	100	863.0	863.3	185	1478.6	1478.2
20	160.6	161.7	105	900.5	901.1	190	1512.6	1513.3
25	205.6	206.8	110	940.8	940.6	195	1545.6	1547.4
30	255.6	254.3	115	979.2	979.0	200	1581.1	1582.9
35	298.8	299.0	120	1020.6	1019.5	205	1615.0	1614.9
40	343.8	344.2	125	1057.3	1058.6	210	1645.6	1645.3
45	388.4	388.7	130	1096.9	1098.4	215	1670.1	1670.2
50	437.8	436.4	135	1134.3	1135.0	220	1697.8	1696.8
55	482.1	482.6	140	1172.8	1171.4	225	1725.3	1725.6
60	526.8	527.8	145	1205.2	1204.9	230	1755.2	1755.7
65	569.2	569.8	150	1239.5	1239.5	235	1783.8	1783.7
70	611.1	611.8	155	1273.6	1273.2	240	1813.3	1813.1
75	652.6	652.6	160	1309.8	1309.4	245	1841.5	1840.9
80	696.8	696.3	165	1344.3	1344.2	250	1869.8	1869.2
85	739.5	739.0	170	1379.0	1379.7	255	1894.8	1895.3

The deviations of the binding energies of weakly bound nuclei from those of the most strongly bound nuclei would be discussed in the next communication

REFERENCES

- Dutta, A. K., 1963, *Ind. J. Phys.*, **37**, 183.
 König, L. A., Mattheuch, J. H., Wapstra, A. H. 1962, *Nuclear Physics*, **31**, 18

CRYSTAL STRUCTURE OF SCANDENIN

K. V. KRISHNA RAO AND P. VENKATESWARA RAO

PHYSICS DEPARTMENT, OSMANIA UNIVERSITY, HYDERABAD-7

(Received for publication, March 25, 1963)

Scandenin ($C_{26}H_{20}O_6$), the major crystalline compound obtained from the roots of *Derris Scandens*, has been studied by many investigators¹⁻³ in view of its pronounced toxic properties. More recently, Rao and Khan⁴ made a detailed chemical and spectroscopic study of the compound and concluded that it is a 2,3-disubstituted benzo- γ -pyranone derivative (Fig. 1). As regards the residue

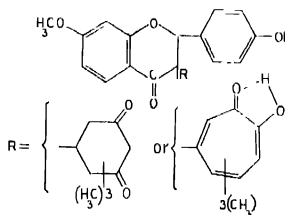


Fig. 1. Molecule of Scandenin

R in position 3, they proposed two alternative structures, namely, a tropolone ring or a dimedone ring. In order to find out which of these two structures is present, the authors have undertaken the structure analysis of scandenin. The present communication describes the results regarding its space group and unit cell dimensions.

The unit cell dimensions have been determined from rotation and zero layer Weissenberg photographs about the three crystallographic axes using $CuK\alpha$ radiation. Accurate values for the cell dimensions have been obtained by the least squares method using the data on the high angle reflections on Weissenberg photographs. The crystal is found to belong to the monoclinic system with the following cell dimensions.

$$a = 18.212 \text{ \AA}, \quad b = 17.446 \text{ \AA}, \quad c = 14.600 \text{ \AA} \quad \text{and} \quad \beta = 96^\circ.$$

Examination of the zero layer and the higher layer equi-inclination Weissenberg photographs showed only two types of systematic absences, *h*0*l* when *l* is odd and *o*k*o* when *k* is odd which are consistent with the space group P_{21}/o .

The density of the crystal is determined by the floatation method using a mixture of nitrobenzene and *o*-dichlorobenzene. The observed density 1.262 is found to be in good agreement with the value 1.246 calculated for 8 molecules per unit cell. The slightly higher value of the observed density may be due to the solvent of crystallisation. We are now trying to introduce a heavy atom into the molecule and solve the structure by the heavy atom technique.

In conclusion, we wish to thank Professor N. V. Subba Rao for providing us with the scandenin crystals used in this investigation. One of us (P.V.R.) is grateful to the authorities of the Osmania University for the award of a research scholarship.

REFERENCES

- Rao, N. V. S. and Seshadri, T. R., 1946, *Proc. Ind. Acad. Sci.*, **24A**, 365.
Clark, E. P., 1943, *J. Org. Chem.*, **8**, 489.
Murty, V. V. S., Rao, N. V. S. and Seshadri, T. R., 1948, *Proc. Ind. Acad. Sci.*, **27A**, 111.
Rao, N. V. S. and Khan, W. A., 1961, *Jour. Sci. Ind. Research*, **20B**, 87.

A SHORT NOTE ON THE ORTHO-RHOMBIC POTENTIAL IN TERMS OF LIGAND MOMENTS AND THEIR DISTANCES IN AN OCTAHEDRAL COMPLEX

U. S. GHOSH

DEPARTMENT OF MAGNETISM, INDIAN ASSOCIATION FOR THE CULTIVATION OF SCIENCE,

JADAVPUR, CALCUTTA-32

(Received July 22, 1963)

Theoretical investigation on the magnetic and optical behaviour of some iron group salts considers the crystalline electric field as having an ortho-rhombic symmetry. The expression for potential near the central ion of an octahedral complex is usually obtained by expanding the potential in terms of spherical harmonics since it satisfies Laplace's equation $\Delta^2 V = 0$. Considering that the symmetry of the field is ortho-rhombic and that the electrons of interest belong to the 3d shell in iron group salts, the expression for potential is given by (Bose *et al.*, 1963).

$$V = D(x^4 + y^4 + z^4 - \frac{3}{5}r^4) + Ax^2 + By^2 + (A+B)z^2 + \alpha x^4 + \beta y^4 + (\alpha + \beta)z^4 - 6\alpha x^2 z^2 - 6\beta y^2 z^2 \quad (1)$$

The form of the potential function must remain unchanged even if we take a purely ionic model of the octahedral complex, but the above expression does not explicitly contain the distances of the co-ordinating ligands from the central ion and their dipole moments, the only thing that can be said is that the co-efficients D , A , B , α and β are related with them. Polder (1942) derived an expression for potential in terms of these quantities considering only a tetragonal distortion of the complex. An expression for ortho-rhombic potential and hence the co-efficients D , A , B , α and β in terms of dipole moments and distances of the ligands might be helpful in some investigations and with a view to this such an expression has been derived

The type of octahedral complex that will be considered here has the paramagnetic ion at the centre which is the origin of our co-ordinate system and dipoles of moment μ_1, μ_2, μ_3 at $(\pm a, 0, 0)$, $(0, \pm b, 0)$, and $(0, 0, \pm c)$ respectively. The

negative ends of the dipoles are pointing inwards and their axes are coinciding with the co-ordinate axes

Potential at a point (x, y, z) near the origin due to the pair of dipoles

$$\begin{aligned} \text{at } (\pm a, 0, 0) = & -\frac{\mu_1(a-x)}{(a^2+r^2-2ax)^{3/2}} - \frac{\mu_1(a+x)}{(a^2+r^2+2ax)^{3/2}} \\ = & -\mu_1 \left[\frac{2}{a^2} - \frac{3r^2}{a^4} + \frac{15}{4} \frac{r^4}{a^6} - \frac{9x}{a^4} + \frac{175}{4} \frac{x^3}{a^6} - \frac{75}{2} \frac{r^2 x^2}{a^6} \right] \end{aligned}$$

(retaining terms upto the fourth power as can be seen from equation (1), higher power terms need not be considered in iron group)

(Considering all the three pairs of dipoles, the total potential at (x, y, z) is

$$\begin{aligned} V = & - \left(\frac{2\mu_1}{a^2} + \frac{2\mu_2}{b^2} + \frac{2\mu_3}{c^2} \right) + 3r^2 \left(\frac{\mu_1}{a^4} + \frac{\mu_2}{b^4} + \frac{\mu_3}{c^4} \right) - \frac{15}{4} r^4 \left(\frac{\mu_1}{a^6} + \frac{\mu_2}{b^6} + \frac{\mu_3}{c^6} \right) \\ & - 9 \left(\frac{x^2\mu_1}{a^4} + \frac{y^2\mu_2}{b^4} + \frac{z^2\mu_3}{c^4} \right) - \frac{175}{4} \left(\frac{x^4\mu_1}{a^6} + \frac{y^4\mu_2}{b^6} + \frac{z^4\mu_3}{c^6} \right) \\ & + \frac{75}{2} r^2 \left(\frac{x^2\mu_1}{a^6} + \frac{y^2\mu_2}{b^6} + \frac{z^2\mu_3}{c^6} \right) \end{aligned}$$

The first term representing potential at the origin is constant and is generally left out of consideration. Remembering that $r^2 = x^2 + y^2 + z^2$ and rearranging the remaining terms the expression can be put into the form given in equation (1) as follows

$$\begin{aligned} V = & 3 \left[\frac{\mu_2}{b^4} + \frac{\mu_3}{c^4} - \frac{2\mu_1}{a^4} \right] x^2 + 3 \left[\frac{\mu_3}{c^4} + \frac{\mu_1}{a^4} - \frac{2\mu_2}{b^4} \right] y^2 + 3 \left[\frac{\mu_1}{a^4} + \frac{\mu_2}{b^4} - \frac{2\mu_3}{c^4} \right] z^2 \\ & - \frac{25}{4} \left[\frac{4\mu_1}{a^6} + \frac{4\mu_2}{b^6} - \frac{\mu_3}{c^6} \right] (x^4 + y^4 + z^4 - \frac{8}{3}r^4) + \frac{25}{4} \left[\frac{\mu_2}{b^6} - \frac{\mu_3}{c^6} \right] x^4 \\ & + \frac{25}{4} \left[\frac{\mu_1}{a^6} - \frac{\mu_3}{c^6} \right] y^4 + \frac{25}{4} \left[\frac{\mu_1}{a^6} + \frac{\mu_2}{b^6} - \frac{2\mu_3}{c^6} \right] z^4 - \frac{75}{2} \left[\frac{\mu_2}{b^6} - \frac{\mu_3}{c^6} \right] x^2 z^2 \\ & - \frac{75}{2} \left[\frac{\mu_1}{a^6} - \frac{\mu_3}{c^6} \right] y^2 z^2 \dots \quad (1) \end{aligned}$$

The form of this expression is identical with that given in equation (1); the coefficients D , A , B , α and β are thus expressed in terms of μ_1, μ_2, μ_3 and, a, b, c as follows.

$$D = -\frac{25}{4} \left[\frac{4\mu_1}{a^6} + \frac{4\mu_2}{b^6} - \frac{\mu_3}{c^6} \right]$$

$$A = 3 \left[\frac{\mu_2}{b^4} + \frac{\mu_3}{c^4} - \frac{2\mu_1}{a^4} \right]$$

$$B = 3 \left[\frac{\mu_3}{c^4} + \frac{\mu_1}{a^4} - \frac{2\mu_2}{b^4} \right]$$

$$\alpha = \frac{25}{4} \left[\frac{\mu_2}{b^6} - \frac{\mu_3}{c^6} \right]$$

$$\beta = \frac{25}{4} \left[\frac{\mu_1}{a^6} - \frac{\mu_3}{c^6} \right]$$

If we put $a = b = c$ and $\mu_1 = \mu_2 = \mu_3$, we get $A = B = \alpha = \beta = 0$ and the expression (2) reduces to the wellknown result for cubic potential as expected in case of a regular octahedron i.e.

$$V = -\frac{175}{4} \frac{\mu_1}{a^6} (x^4 + y^4 + z^4 - \frac{3}{5} r^4)$$

In case of tetragonal distortion along z -axis of the octahedron $a = b \neq c$ and $\mu_1 = \mu_2 \neq \mu_3$, we get $A = B$, $\alpha = \beta$ and the expression (2) reduces to

$$\begin{aligned} V = 3 \left[\frac{\mu_2}{c^4} - \frac{\mu_1}{a^4} \right] (x^2 + y^2 - 2z^2) - \frac{25}{4} \left[\frac{8\mu_1}{a^6} - \frac{\mu_3}{c^6} \right] (x^4 + y^4 + z^4 - \frac{3}{5} r^4) \\ + \frac{25}{4} \left[\frac{\mu_1}{a^6} - \frac{\mu_3}{c^6} \right] (x^4 + y^4 + 2z^4 - 6x^2z^2 - 6y^2z^2) \quad \dots \quad (3) \end{aligned}$$

Expression (3) can be shown to be equal to

$$\begin{aligned} 3 \left[\frac{\mu_3}{c^4} - \frac{\mu_1}{a^4} \right] (x^2 + y^2 - 2z^2) - \frac{25}{4} \left[\frac{4\mu_1}{a^6} + \frac{3\mu_3}{c^6} \right] (x^4 + y^4 + z^4 - \frac{3}{5} r^4) \\ + \frac{25}{4} \left[\frac{\mu_1}{a^6} - \frac{\mu_3}{c^6} \right] (z^4 + 6x^2y^2 - \frac{3}{5} r^4) \end{aligned}$$

This expression exactly agrees with Polder's result for potential under tetragonal distortion of the octahedron. Numerical calculations of the coefficients in the orthorhombic case are presently in progress.

The author is grateful to Prof. A. Bose, D.Sc., F.N.I., for his guidance and helpful criticism of the work

R E F E R E N C E S

- Bose A. and Chatterjee R, 1963, *Proc. Phys. Soc.* , **82**, 23.
Polder, 1942, *Physica* **9**, 709.

AN ELECTRODYNAMIC METHOD OF MEASURING ABSOLUTE MAGNETIC SUSCEPTIBILITIES OF SINGLE CRYSTALS

S. MITRA, P. K. GHOSH AND S. K. DUTTA ROY

DEPARTMENT OF MAGNETISM, INDIAN ASSOCIATION FOR THE CULTIVATION OF SCIENCE,
JADAVPUR, CALCUTTA-32

(Received, July 26, 1963)

In a short communication, Ghosh (1961) has described an electrodynamic method for compensation of magnetic force in a Curie-type magnetic balance. In Ghosh's method, the magnetic sample in powder form packed in a spherical glass ampoule is placed inside a current carrying coil and are together rigidly attached at one end of a horizontal Curie-balance arm (Dutta Roy, 1955). The method was immediately afterwards modified by the present authors to suit single crystals as described herein. Several earlier authors (Fox and Forrer, 1936, Hutchinson and Reekie, 1946 etc.) have used electrodynamic balancing with a Curie or other types of balances. Innovation of the present method lies in suspending a single crystal from one arm of a Curie-balance with a fine unspun silk fibre so that its maximum susceptibility direction in the horizontal plane sets along the horizontal magnetic field and the crystal moves bodily along the horizontal gradient at right angles to the field available with a modified Sucksmith type pole-gap of an electromagnet. A current bearing coil, rigidly suspended from this arm of the balance, with its axis parallel to the field direction, is placed close to the sample, to compensate the magnetic force on the sample, acting ultimately on the balance arm.

For the sake of robustness of the system, the usual single fragile quartz suspension fibre of the balance beam, has been replaced by a pair of thick phosphor bronze strips above and below the beam which also serve as current leads for the compensating coil. This has made the deflection of the balance beam and hence the displacement of sample in the field advantageously small. For accurate compensation of the force on the sample, the small deflection is highly magnified by a balanced photoelectric cell device. A light spot, reflected from a small mirror attached to the centre of the balance beam, falls equally on a pair of photoelectric cells in series, the out-put of which is fed to a sensitive galvanometer, the circuit being adjusted for null deflection. A small deflection of the beam, and hence of the light spot, upsets the balance of the circuit, and a large deflection of the galvanometer is observed. The current in the compensating coil, in the magnetic field, is adjusted until the spot comes back exactly to its original position.

The coil current can be very accurately determined by measuring the potential drop across a standard resistance. With this type of suspension and an oil damping device, effects of all external disturbances on the system are practically eliminated. The balance assembly is covered with a glass bell-jar and the system can be evacuated or filled with any gas.

The overall error in the measurement at room temperature is estimated to be not more than 0.1%, including any difference in the value due to different samples.

The balance has been standardised. The square of the effective moment (corrected for diamagnetism) p_e^2 for ferric ammonium sulphate alum obtained by us is 34.79 as against 34.80 obtained by Dutta Roy (1955) and 34.79 by Onnes and Oosterhuis (1926), all at 290°K. Taking this value as standard, that of chromium potassium sulphate alum is measured to be 14.89 as against 14.91 by Dutta Roy (1956) and 14.92 by de Haas and Gorter (1929) all at 300°K, and that of $\text{NiSO}_4 \cdot 6\text{H}_2\text{O}$ along its tetragonal axis is found to be 9.701 as against 9.687 by Dutta Roy (1955) and 9.656 by Mookerji (1946), all at 307°K.

The details of the balance will be published shortly.

The authors are grateful to Prof. A. Bose, D.Sc., F.N.L., for his guidance in the work. One of us (S.M.) is grateful to the Council of Scientific and Industrial Research for the award of a Research Fellowship.

REFERENCES

- de Haas, W. J. and Gorter, C. J., 1929-31, *Comm. London*, no. 208C.
Dutta Roy, S. K., 1955, *Ind. J. Phys.*, **29**, 429.
Dutta Roy, S. K., 1956, *Ind. J. Phys.*, **30**, 169.
Fox, G. and Forrer, R., 1936, *J. Phys. Rad.*, **7**, 180.
Ghosh, P. K., 1961, *Ind. J. Phys.*, **35**, 319.
Hutchinson, T. S. and Reekie, J., 1940, *J. Sci. Instrum.*, **23**, 209.
Mookerjee, A., 1946, *Ind. J. Phys.*, **20**, 9.
Onnes, H. K. and Oosterhuis, E., 1926, *Comm. London*, no. 139C.

NOTICE

No claims will be allowed for copies of journal lost in the mail or otherwise unless such claims are received within 4 months of the date of issue.

RATES OF ADVERTISEMENTS

1. Ordinary pages :

Full page	Rs. 50/- per insertion
Half page	Rs. 28/- per insertion
2. Pages facing 1st inside cover, 2nd inside cover and first and last page of book matter :

Full page	Rs. 55/- per insertion
Half page	Rs. 30/- per insertion
3. Cover pages by negotiation
25% commissions are allowed to *bona fide* publicity agents securing orders for advertisements.

CONTENTS

Indian Journal of Physics

Vol. 37, No. 10

October, 1963

PAGE

57. An Electrodynanic Balance and a new Liquid Oxygen Cryostat for Measurement of Magnetic Susceptibilities Between 400°K and 60°K— A. Bose, S. K. Dutta Roy, P. K. Ghosh and S. Mitra ... 505
58. A Remote Control Electronic Torquemeter—S. C. Mukherjee and H. Rakshit 520
59. Energy States at the interface of two Semi-infinite one-Dimensional Crystals—S. K. Ghosh and A. K. Laskar ... 534
60. Zero Pressure Joule-Thomson Coefficient for a few non-polar gases on the Morse Potential—R. S. Gambhir and S. C. Saxena ... 540

LETTERS TO THE EDITOR—

11. On the Binding energies of the most strongly bound Nuclei of different Mass Numbers—A. K. Dutta, B. Pal, P. Ganguly and D. Banerjee ... 543
12. Crystal Structure of Scandenin—K. V. Krishna Rao and P. Venkateswara Rao ... 546
13. A short note on the Ortho-rhombic Potential in Terms of Ligand moments and their distances in an Octahedral Complex—U. S. Ghose ... 548
14. An Electrodynanic Method of Measuring Absolute Magnetic Susceptibilities of Single Crystals—S. Mitra, P. K. Ghosh and S. K. Dutta Roy 552

Regd. No. C-3911

VOL. 37 **INDIAN JOURNAL OF PHYSICS** No. 11
(Published in collaboration with the Indian Physical Society)

AND

VOL. 46 **PROCEEDINGS** No. 11

OF THE

**INDIAN ASSOCIATION FOR THE
CULTIVATION OF SCIENCE**

NOVEMBER 1963

**PUBLISHED BY THE
INDIAN ASSOCIATION FOR THE CULTIVATION OF SCIENCE
JADAVPUR, CALCUTTA, 88**

BOARD OF EDITORS

K. BANERJEE	D. S. KOTHARI
D. M. BOSE	B. D. NAG CHAUDHURI
S. N. BOSE	K. R. RAO
S. D. CHATTERJEE	D. B. SINHA
P. S. GILL	S. C. SIKKAR (<i>Secretary</i>)
S. R. KHASTGIR	B. N. SRIVASTAVA

EDITORIAL COLLABORATORS

PROF. R. K. ASUNDI, PH.D., F.N.I.
PROF. D. BASU, PH.D.
PROF. J. N. BHAR, D.Sc., F.N.I.
PROF. V. G. BHIDE, PH.D.(Nag), PH.D.(Lond).
PROF. A. BOSE, D.Sc., F.N.I.
PROF. S. K. CHAKRABARTY, D.Sc., F.N.I.
DR. J. S. CHATTERJEE
DR. K. DAS GUPTA, PH.D.
PROF. N. N. DAS GUPTA, PH.D., F.N.I.
DR. J. DHAR, D.Phil (So)
PROF. A. K. DUTTA, D.Sc., F.N.I.
PROF. C. S. GHOSH, M.Sc., S.M., F.N.I., M.I.E.E.
PROF. S. GHOSH, D.Sc., F.N.I.
PROF. S. N. GHOSH, D.Sc.
PROF. S. GUPTA, M.Sc., F.N.I.
PROF. D. N. KUNDU, PH.D., F.N.I.
PROF. R. C. MAJUMDER, PH.D., F.N.I.
PRINCIPAL Y. G. NAIK, PH.D.
PROF. S. R. PALIT, D.Sc., F.R.I.C., F.N.I.
PROF. H. RAKSHIT, D.Sc., F.N.I.
PROF. A. SAHA, D.Sc., F.N.I.
DR. VIKRAM A. SARABHAI, M.A., PH.D., F.N.I.
DR. A. K. SENGUPTA, D.Sc.
PROF. NAND LAL SINGH, D.Sc.
DR. M. S. SINHA, D.Sc., F.N.I.
PROF. N. R. TAWDE, PH.D., F.N.I.
DR. P. VENKATESWARLU

NOTICE

TO INTENDING AUTHORS

Manuscripts for publication should be sent to the Assistant Editor, Indian Journal of Physics, Jadavpur, Calcutta-32.

The manuscripts submitted must be type-written with double space on thick foolscap paper with sufficient margin on the left and at the top. The original copy, and not the carbon copy, should be submitted. Each paper must contain an abstract at the beginning.

All references should be given in the text by quoting the surname of the author, followed by year of publication, e.g., (Ghosh, 1954). The full reference should be given in a list at the end, arranged alphabetically, as follows; Ghosh, D. K., 1954, *Ind. J. Phys.*, 28, 485.

Line diagrams should be drawn on white Bristol board or tracing paper with black India ink, and letters and numbers inside the diagrams should be written neatly in capital type with India ink. The size of the diagrams submitted and the lettering inside should be large enough so that it is legible after reduction to one-third the original size. A simple style of lettering such as gothic, with its uniform line width and no serifs should be used, e.g.,

A·B·E·F·G·M·P·T·W·

Photographs submitted for publication should be printed on glossy paper with somewhat more contrast than that desired in the reproduction, and should, if possible, be mounted on thick white paper.

Captions to all figures should be typed in a separate sheet and attached at the end of the paper.

The mathematical expressions should be written carefully by hand. Care should be taken to distinguish between capital and small letters and superscripts and subscripts. Repetition of a complex expression should be avoided by representing it by a symbol. Greek letters and unusual symbols should be identified in the margin. Fractional exponents should be used instead of root signs.

Annual Subscription—

Indian Rs. 25.00

Foreign £ 2-10-0 or \$ 7.00

BENGAL CHEMICAL & PHARMACEUTICAL WORKS LD.

Pioneer Indian Manufacturers of Pharmaceuticals & Chemicals.

Manufacturers of:

Pharmaceutical Chemicals:

Caffeine and its salts, Strychnine Hydrochlor, Strychnine Sulphate, Brucine Sulphate, Nicotinic Acid, B.P., Nicotinamide, B.P., Potassium Citrate B.P., I.P., Sodium Citrate B.P., I.P., Potassium Acetate B.P., I.P., Potassium Iodide B.P., I.P., Sodium Iodide B.P., I.P., Ferri et Ammon Citrate B.P., I.P., and various other Pharmaceutical Chemicals.

Heavy & Reagent Quality Fine Chemicals:

Alum, Alum Sulphate (Iron Free), Ferro Alum, Zinc Chloride Tech. Naphthalene Pure, Sodium Citrate A.R., Potassium Citrate A.R., Magnesium Sulphate A.R., Sodium Sulphate Anhydrous A.R., Potassium Iodide A.R., Sodium Chloride A.R., Zinc Sulphate A.R., and various other reagent quality analytical chemicals.

Please refer your enquiries for the above items and other chemicals in the line to :—

BENGAL CHEMICAL

6, GANESH CHUNDER AVENUE,
CALCUTTA-13, INDIA.

(INDIA MADE)

X'RAY DIFFRACTION APPARATUS

Complete with

MACHLETT SHOCKPROOF BERYLLIUM WINDOW SEALED TUBES OF
DIFFERENT TARGET MATERIALS
SINGLE VALVE HALF-WAVE RECTIFIED OR TWO VALVE
FULL-WAVE RECTIFIED

MACHINE already incorporates voltage compensator to compensate plus
or minus 15 volts supply change.

Electro-Magnetic, Electronic, Servo-Mechanical or Chemo-Electric STABILISER
can be added to the filament circuit or
to the entire MACHINE for further STABILISATION.
CAMERAS OF VARIOUS TYPES CAN ALSO BE SUPPLIED

FOR THE MACHINE.

ALSO

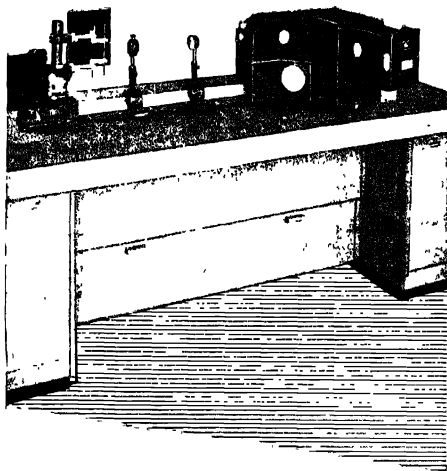
X'RAY PLANT FOR BIOLOGICAL RESEARCH & INDUSTRIAL RADIOGRAPHY
AND HIGH TENSION TESTING SETS.

DELIVERY EX-STOCK : : NO LICENCE REQUIRED.

Further details from :—

RADON HOUSE P. LTD.,

7, Sirdar Sankar Road, Calcutta-26.



ZEISS THREE-PRISM SPECTROGRAPH

A glass-type spectrograph with Foresterling set of prisms of high-power and resolving capacity, large dispersion and excellent definition of lines, self-contained construction.

Equipment with 3 cameras : Camera $f = 12$ cm $F/2.4$ and camera $f = 27$ cm $F/5.4$ for feeble-light phenomena (Raman effect, fluorescence of flame-spectra, etc.)

Autocollimation camera $f = 130$ cm $F/26$ for taking complex emission spectra in the visible region (special type steel, rare earth etc.)

Solves all spectra-chemical problems of organic and inorganic nature.

VEB Carl Zeiss JENA

SOLE AGENTS IN INDIA :

GORDHANDAS DESAI PRIVATE, LTD.

PHEROZSHAH MEHTA, ROAD, BOMBAY 1.

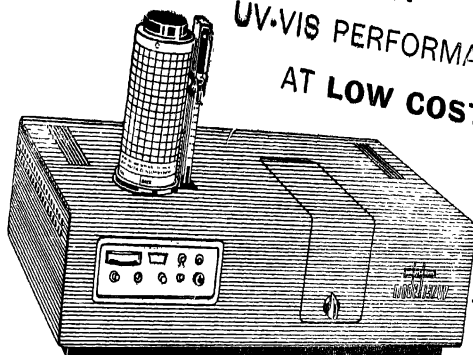
Branches :

4/2B Asaf Ali Road
NEW DELHI.

22, Linghi Chetty Street
MADRAS-1.

P-7, Mission Row Extension
CALCUTTA-1.

NEW SPECTROPHOTOMETER GIVES HIGHEST UV-VIS PERFORMANCE AT LOW COST



A new ultraviolet-visible spectrophotometer—the Perkin-Elmer Model 202—provides photometric and wavelength capabilities you expect from more expensive instruments. Its low price brings it within the range of any lab budget.

The Model 202 covers two regions, 190 to 390 $m\mu$ in the ultraviolet, and 350 to 750 $m\mu$ in the visible. Two scanning speeds—two and eight minutes per scan—are available for survey or precise work.

FEATURES

- **EASE OF OPERATION.** Minimum controls, plus Automatic Gain Control and slit programming, makes the Model 202 easy to run. Records linearly in absorbance units (0-1.5).
- **OPTICAL NULL RECORDING.** For high accuracy in quantitative analysis, plus high reproducibility.
- **AUTOMATIC GAIN CONTROL.** An exclusive feature, automatically increases energy of the system in high absorption areas. Makes the most difficult differential analyses routine.

Notebook-size Chart: Spectra of each range recorded on standard 8 $\frac{1}{2}$ x 11 chart, with large ordinate for accuracy. Linear wavelength presentation. Specifications are:

	ULTRAVIOLET	VISIBLE
Resolution	0.2 $m\mu$ at 250 $m\mu$	1.5 $m\mu$ at 600 $m\mu$
Photometric accuracy in absorbance units	± 0.01	± 0.01
Photometric reproducibility in absorbance units	0.05	0.05
Wavelength accuracy	$\pm 0.5 m\mu$	$\pm 1.0 m\mu$
Wavelength reproducibility	0.3 $m\mu$	0.5 $m\mu$

Perkin-Elmer Corporation
NORWALK, CONNECTICUT

Sold and serviced in India exclusively by

BLUE STAR

**BLUE STAR ENGINEERING
CO. (Calcutta) Private LTD.**
7 HARE STREET, CALCUTTA 1
Also at BOMBAY · DELHI · MADRAS

When you require

MEASURING INSTRUMENTS & PRECISION TEST-GEAR

for different purposes

make it a point to contact us

We Supply : Moving Coil Movements for Voltage or Current Measurements in any range, RF Signal Generators, RC Audio Generators, Mamoni Test Instruments and Other Testing Equipments.

We can also design to your requirements

Oscillographs, Signal Generators, Rectifier Units, Power Supply Units

State your detailed requirements and get our quotations.

*We have been designing and supplying to the market various
Electrical and Electronic Equipment for over 15 years past.*

Guaranteed Service !

Prompt Attention !

RADIO ELECTRIC (PRIVATE) LTD.

2R LAMINGTON CHAMBERS, LAMINGTON ROAD, BOMBAY—4

SP/RE/3

NOTICE

No claims will be allowed for copies of journal lost in the mail or otherwise unless such claims are received within 4 months of the date of issue.

RATES OF ADVERTISEMENTS

1. Ordinary pages :

Full page Rs. 50/- per insertion

Half page Rs. 28/- per insertion

2. Pages facing 1st inside cover, 2nd inside cover and first and last page of book matter :

Full page Rs. 55/- per insertion

Half page Rs. 30/- per insertion

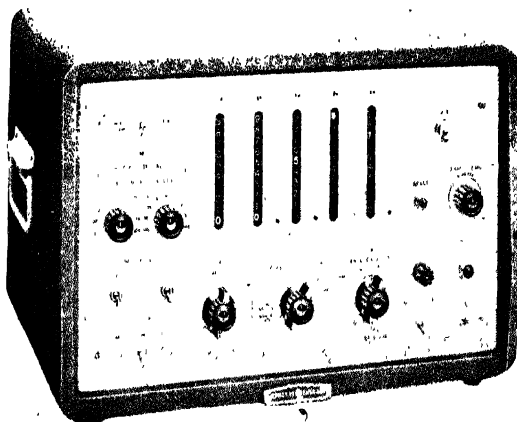
3. Cover pages by negotiation

25% commissions are allowed to *bona fide* publicity agents securing orders for advertisements.

PUBLICATIONS OF THE INDIAN ASSOCIATION FOR THE CULTIVATION OF SCIENCE

		Rs. nP
1. RUSSELL, E. J.	.. Methods in Scientific Research	0.37
2. JEANS, J. H.	. 'The Origin of the Planets'	0.37
3. ASTON, F. W.	.. Separation of Isotopes	0.37
4. LENNARD-JONES, J. E.	Interatomic Forces	1 50
5. JILL, A. W.	.. 'The Royal Botanic Gardens, Kew'	1 50
6. MILLIKAN, R. A.	. 'The Educational Aims and Practices of the California Institute of Technology'	0.37
7. MITRA, S. K.	Active Nitrogen—A New Theory	2 50
8. WAJDA, D. N.	. 'Petroleum Resources of India'	2.50
9. RAY, P.	'The Theory of Valency and the Structure of Chemical Compounds'	3 00
10. MUKHERJEE, J. N.	. 'The Role of the Electrical Double Layer in the Electro-Chemistry of Colloids'	1.75
11. ROBINSON, R.	Distribution of Anthocyanins	1 25
12. CHAPMAN, S.	. 'The Earth's Magnetism and its Changes'	1.00
13. MARK, H.	. 'Catalysts in Polymerization Reactions'	1 50
14. AMALDI, E.	. 'Diffraction Effects in the Scattering of Neutrons, Mesons and Electrons by Nuclei'	1.50
15. FIESER, L. F.	Lapinone, A New Antimalarial	1.00
16. BOSE, N. K.	.. Fluid Dynamics	1.25
17. VENKATARAMAN, K.	. 'Constitutional Problems Concerning Vat Dyes'	1.00
18. ROY, J. N.	.. 'The Chemical Basis of Some Physiological Actions'	1.00
19. SHOENBERG, D.	.. Superconductivity	1.00
20. PALIT, S. R.	.. Non-Aqueous Titration	3.00
21. KRISHNAN, M. S.	.. Iron Ores of India	5.00
22. SEN, S. N.	.. 'Bijnaner Ithas ; Vol. I'	10.50
	Vol. II	12.00
23. SESHADRI, T. R.	.. 'An Investigation of Plant Drugs and Insecticide'	1.00
24. BOWEN, E. G.	. 'The Formation of Natural and Artificial Rain'	1.50
25. BANERJI, S. K.	.. 'Earthquakes in the Himalayan Region'	3.00
26. MAGNETISM :	.. Report of the Symposium on Magnetism	7.00
27. WESTPHAL, DR. ING. E.	.. 'The Freight Tube Float'	8.00
28. HIRSCHFELDER, J. O.	.. Molecular Physics and Intermolecular Forces	1.25
29. SEN, N. R.	.. 'The Modern Theory of Turbulence'	2.00
30. DOUGLAS, A. E.	.. 'Some Recent Development in Molecular Spectroscopy'	1.00
31. SHOENBERG, E.	.. 'Experimental Determination of the Electronic Structure of Metal'	1.00

HEWLETT PACKARD
ELECTRONIC COUNTER
VERSATILE LOWCOST PRECISION COUNTER
COVERS 10 cps to 120 KC



Model: 522B

Range: 10 cps to 120 KC
(220 KC at slight
extra charge)

Accuracy: ± 1 count \pm
time base accu-
racy

Input requirement: 0.2
volt r.m.s. mini-
mum

This all purpose Hewlett Packard counter is used in an ever-increasing variety of manufacturing and research measurements. The 522B counter offers the convenience of frequency, period and time interval measurement over a broad frequency range. Results are displayed automatically in direct reading from either in cps, KC, seconds or multi-seconds. Reliable and accurate readings make measurement quick and convenient, even for unskilled personnel.

For further details, please write to :

Sole Distributors :

**THE SCIENTIFIC INSTRUMENT
COMPANY, LIMITED.**

ALLAHABAD : BOMBAY . CALCUTTA : MADRAS :
NEW DELHI

Head Office : 6, Tej Bahadur Sapru Road, Allahabad



A 1.2 cm E. P. R. SPECTROMETER AND PARAMAGNETIC RESONANCE IN SOME COPPER SALTS

U. S. GHOSH, R. N. BAGCHI AND A. K. PAL

DEPARTMENT OF MAGNETISM, INDIAN ASSOCIATION FOR THE CULTIVATION OF SCIENCE,
CALCUTTA-32

(Received, September 23, 1963)

ABSTRACT. A transmission type e.p.r. spectrometer operating at 1.28 cm wavelength, set up in our laboratory from purchased and constructed components is described in details. Resonance absorption signals at room temperature for some concentrated paramagnets have been obtained with a small noise-to-signal ratio. Orthorhombic g -values and orientations of the tensor ellipsoid of single crystal of $\text{CuK}_2(\text{SO}_4)_2 \cdot 6\text{H}_2\text{O}$ have been determined at room temperature and some features of e.p.r. spectra of two copper salts have been discussed.

INTRODUCTION

If a steady magnetic field H is applied on a paramagnetic substance, the energy levels of the paramagnet (electron, atom, ion, molecule or radical) which were initially degenerate split into the so-called Zeeman levels, the energy separation $E_1 \sim E_2$ between successive Zeeman levels being given by $g\beta H$ where β is the Bohr magneton, and g is the spectroscopic splitting factor. With magnetic fields of a few thousand gauss the energy values of the Zeeman splittings fall in the microwave range of electromagnetic radiation. Thus, microwaves falling upon paramagnets under such static magnetic fields will under certain conditions provide the requisite energy for transitions between the successive Zeeman levels so that on an average the population of the upper levels increases and a net characteristic absorption of microwaves occurs. For the transitions to occur it is evident that the energy of the incident microwave radiation $h\nu$ should be equal to the separation $g\beta H$ of successive Zeeman levels i.e. $h\nu = g\beta H$ and the maximum transition probability is obtained when the microwave field is perpendicular to the static magnetic field.

It very often happens that the internal fields in a paramagnetic crystal splits up the energy states to more or less extent and the introduction of the external static magnetic field only serves to enhance these splittings to an extent just needed to be spanned by a given microwave energy. In this case the relationship between the so-called zero field splitting superposed Zeeman splitting and the microwave energy is more complicated.

DESCRIPTION OF THE COMPLETE 1.2 CM MICRO-WAVE SPECTROMETER

(1) The complete experimental set-up is shown in a block diagram in Fig. 1. A few of the wave guide components, klystron power pack, klystron and other

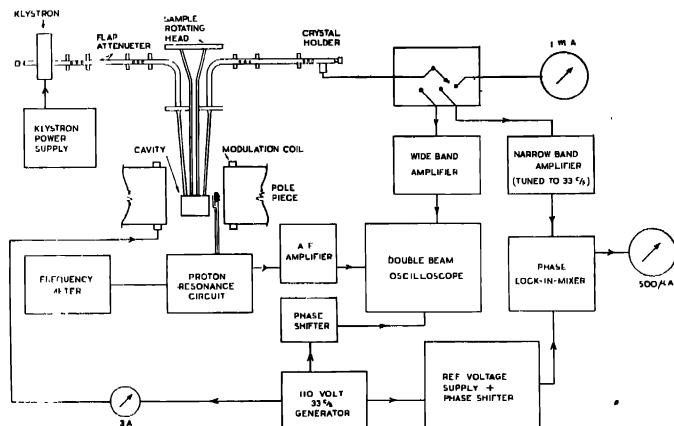


Fig. 1

accessories were purchased as in pieces and others such as flap attenuator, probe tuner, waveguide bends, low temperature distrene filled german silver guides, cavity resonator, crystal holder, modulation coils, phase sensitive detector, proton resonance fluxmeter, low temperature tuning assembly, narrow band amplifier, waveguide couplers, waveguide bench etc. were made in the laboratory.

The 1.2 cm spectrometer employs a 2K33 reflex klystron tube as the source of microwave power. Appropriate stabilized voltages have been supplied to the resonator, reflector and grid of the klystron from an electronically stabilized power pack (P.R.D. type 801 A, universal klystron power supply), the filament being heated by 6 volt a.c. obtained from the same power pack. TE_{10} mode is excited and propagated after proper tuning by the klystron tuner and tuning screws along the 'K' band wave guide ($1.064 \text{ cm} \times 0.432 \text{ cm}$) with suitable attenuation by a flap attenuator. The incident microwave power then passes through an H-bend section (bent in the plane of magnetic lines of force) of the waveguide and is fed into the cavity resonator through a distrene filled thin walled German silver wave guide of appropriate smaller dimension, namely, $6.0 \text{ mm} \times 2.5 \text{ mm}$. A cylindrical brass cavity resonator operated in TE_{111} mode has been used in order to concentrate the microwave field energy in the sample placed inside the cavity. The distrene filled *g.s* guides have been used to minimise the dimension of the

guide and hence the leakage of heat inside the cryostat in which the cavity is placed for low temperature work. The narrow g.s. guide is matched with the *H*-bend of normal size through a tapered g.s. section of length 5.5 cm, and taper-angle of 7° along the broad face. The part of the distrene within this section is oppositely tapered ending as a point where the g.s. guide taper just starts. The internal diameter of the cavity is 1.3 cm and the cavity length can be varied from 4 cm to 12 cm by means of a tuning choke plunger at its bottom running in a fine screw thread and being operated from above through a gear system by a thin stainless steel shaft. Elliptical iris hole ($2.5 \text{ mm} \times 1.5 \text{ mm}$ approximately) at the top surface of the cavity is used to couple the g.s. guide to and feed microwave signal into it. The output signal from the cavity is taken through another similar distrene filled German silver guide coupled to the cavity and an *H*-bend section as before. A long thin stainless steel tube of 5 mm internal bore is coaxially fixed into a hole at the top surface of the cavity. A microwave choke attached to another stainless steel tube of smaller diameter can be easily lowered until the end face of the choke becomes flush with the inside top of the cavity, a graduated circular disc with a vernier scale is fixed at the top of this tube, so that it can be rotated through any desired angle about the cone fitting between the two tubes just below the disc. The face of a single crystal sample in which the measurement is to be taken, is placed flat upon the end face of the choke and fixed to it with a thin layer of vacuum grease. The static magnetic field remains always parallel to the end face of the choke which lies in the region of maximum concentration of microwave field at TE_{111} mode. If the specimen is magnetically isotropic it can also be placed at the centre of the tuning plunger. Tuning screw matching is provided in the wave guide run before and after the input and the output *H*-bend sections respectively. The complete assembly of *H*-bends, German silver guides and the cavity resonator is shown in Figure 2.

The transmitted microwave power from the cavity resonator is detected by a silicon-tungsten crystal, type IN 26, mounted inside the crystal holder section of the guide coupled to the output *H*-bend. The rectified output from the crystal detector is taken off through a co-axial line. For optimum performance of the crystal the rectified crystal current is usually kept near .5 mA by adjusting the attenuator.

(ii) *Magnet* :

The cavity is placed in the central region of the variable gap between the pole faces of a strong electromagnet supplied by Newport Instrument Ltd. (England). The electromagnet is capable of producing a highly homogeneous and constant field of maximum value 9000 oersted with 10 cm diameter pole face and 2.3 cm gap, at a continuous rating of 4 amperes delivered from a 220 volt battery of lead accumulators through a series of rough and fine control rheostats. With a pair of auxiliary coils wound over brass spools with 750 turns of D.C.C. wire (S.W.G.

No 20) in each and mounted round the poles the steady magnetic field can be sinusoidally modulated at 33c/s. 33c/s is obtained from an 110 volt 2 kw alter-

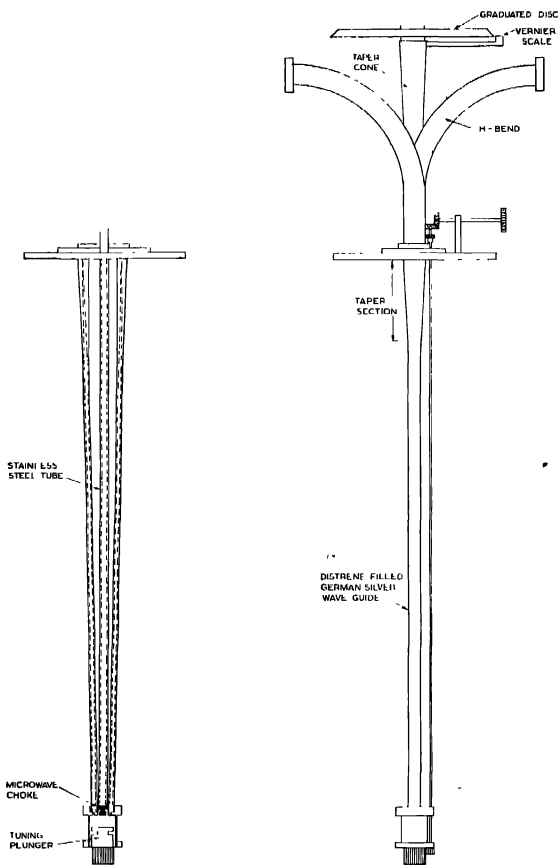


FIG. 2.

nator driven by a D.C. motor, the D C voltage being supplied from a stable 220V, 15 kw D.C generator with a constant voltage transformer at its input. The modulation amplitude of the field can be varied by changing the current given to modulation coils with a variac. The maximum modulation field is found to be nearly 250 gauss.

(iii) *Detection and measuring system*

(a) *Video-detection method* In video-detection system the whole width of an absorption signal is covered by the 33 c/s modulation sweep applied to the steady magnetic field which is brought to the resonance value. The rectified current from the crystal detector will then consist of a function representing the shape of the absorption signal recurring at twice the modulating frequency since absorption of microwaves will occur when the resonance value of magnetic field is attained both during the forward and backward sweep of the modulation. The absorption signal from the crystal detector is fed to a wide band amplifier (by M/s Solartron Ltd, England) having the proper input impedance (600 ohms) required to match the impedance of the detector crystal, of sufficient bandwidth (15 c/s–300 kc/s) to pass almost all the Fourier components of the absorption signal and thus to pass the signal without any distortion of its shape. The output from the amplifier is applied to the Y-plates of Cossor no. 1049 blue trace double beam oscilloscope, the time base being fed at the modulating frequency via a phase shifter, the circuit diagram of which is shown in fig. 3.

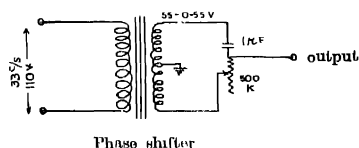
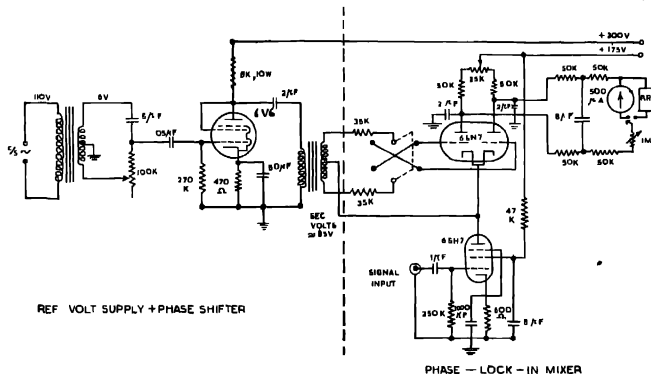


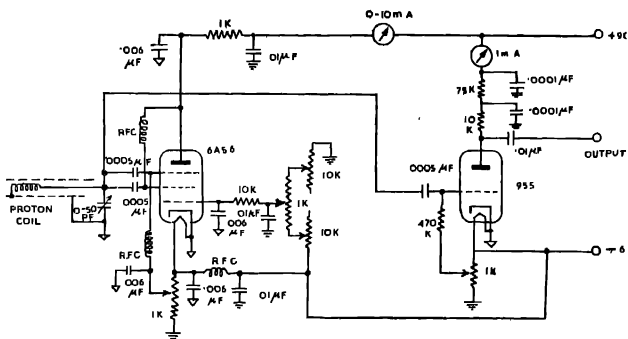
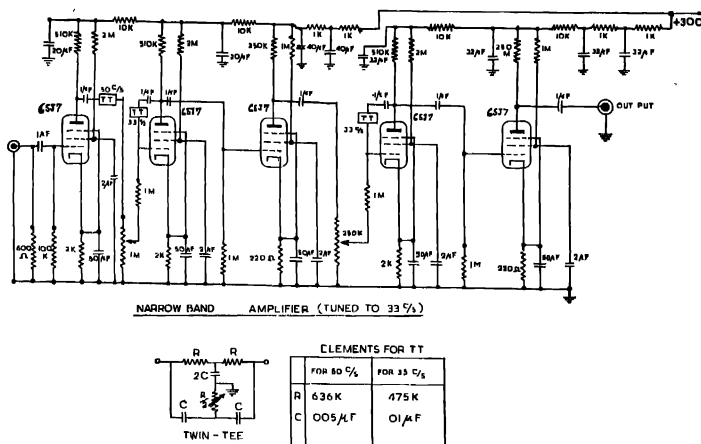
Fig. 3 Out put to External time base of Oscilloscope (cossor)

Two traces of the signal appear on the C.R.O. screen corresponding to the forward and backward sweep, which are brought to coincidence by adjusting the phase shifting circuit. The steady magnetic field is then adjusted to bring the two coincident peaks just at the centre of the horizontal trace of the oscilloscope. This corresponds to the exact resonance value of the steady magnetic field. Although this video-detection method is suitable in the case of narrow lines, it presents many difficulties for a line width of 50 gauss or more, which is very common with the concentrated salts of the iron group we want to study. Apart from the troubles arising out of the unavoidable 50 c/s pick up and crystal and circuit noises, wide lines will introduce additional troubles in requiring large enough depth of modulation and very large bandwidth of the amplifier stage for undistorted display of the signal shape.

(b) *Phase-sensitive detection method*. For wide lines phase sensitive detection (p.s.d.) method has been adopted and the difficulties mentioned above are thus got rid of to a large extent. In this method the steady magnetic field is modulated by a small magnetic field varying sinusoidally at 33c/s and having an amplitude equal to a very small fraction of the total line width. The steady field is then gradually and slowly increased so that each part of the whole absorption



The magnetic field is measured with the help of a proton resonance (p.r.) fluxmeter (Fig. 6) designed mostly after Knoeble and Hahn (1948). 0.12 molar



$\text{Fe}(\text{NO}_3)_3$ solution in a narrow cylindrical capsule of pyrex glass is used as the proton sample. The proton probe is a simple rigid co-axial cable carrying the capsule at one of its ends; a few number of turns of S.W.G No. 30 enamelled copper wire are wound over the capsule with one end connected to the central conductor and the other to the outer shield of the co-axial cable. The proton sample is placed very near the cavity within the central region of the pole faces such that the coil wound over the narrow capsule and the experimental specimen inside the cavity occupy symmetrical position between the pole faces. It has been found that within a range of 1 cm the value of the magnetic field in the central region

remains everywhere the same within 1 part in 10,000 as seen from the unchanged position and shape of the proton resonance (p.r.) signal in the C.R.O.

METHOD OF MEASUREMENT OF THE P.M.R. PEAKS IN SINGLE CRYSTALS

In actual measurement the experimental sample a, single crystal, is placed with a given plane horizontal on the end face of the microwave sample holder choke as explained earlier, a standard sample of the free radical D.P.P.H. (diphenyl picryl hydrazil) is placed at the centre of the tuning plunger of the cavity and the proton probe just outside the cavity in a manner explained above. All these are then within a range of 1 cm and the magnetic field is the same at each of them. The D.P.P.H. sample holder is a very thin and small perspex plate over which few grams of D.P.P.H. are spread and fixed by a thin layer of duro-fix.

In video-detection system the p.m.r. signal is fed to one beam of the double beam C.R.O. via a wideband amplifier and the p.r. signal to the second beam via an audioamplifier. The radio-frequency at which proton resonance occurs can be varied by adjusting a variable condenser in the r.f. oscillator so that the peaks for the two resonance signals coincide at the centre of the C.R.O. for the given static magnetic field at which paramagnetic resonance peak occurs. This p.r. frequency is then measured very accurately correct up to 1 part in 10^4 by a heterodyne frequencymeter (Signal Corps, BC-221-AH) having crystal check points. Measuring the p.r. frequencies at different static magnetic fields corresponding to two P.M.R. signals one for the experimental specimen and the other for the standard D.P.P.H. sample, we can easily calculate the g -values of the specimen along the direction of the applied magnetic field as follows. When the proton signal is made to coincide with the P.M.R. signal for the specimen we will have

$$g\beta H = h\nu \quad \dots (1)$$

$$g_N\beta_N H = h\nu_N \quad \dots (2)$$

where g and g_N are the g -values for the specimen and the proton (nuclear g -factor) respectively, β and β_N are atomic and nuclear Bohr magnetons, and ν and ν_N are the microwave and radio frequency respectively. Similarly, when the proton signal is made to coincide with the P.M.R. signal corresponding to D.P.P.H. occurring at a different magnetic field, the microwave frequency remaining unchanged we will have

$$g_D\beta H' = h\nu \quad \dots (3)$$

$$g_N\beta_N H' = h\nu_N' \quad \dots (4)$$

From equations (1), (2), (3) and (4) we get the g -value of the specimen to be

$$g = g_D \cdot \frac{\nu_N'}{\nu_N} = 2.0023 \frac{\nu_N'}{\nu_N} \quad \dots (5)$$

[g -value for D.P.P.H is accurately known to be 2.0023 (ref. Ingram, 1955)]. It is obvious from above that any variation of the steady magnetic field during the measurement will not affect the result, provided the microwave and r.f. frequencies remain constant.

In the p.s.d. method used in the case of wide lines, the small modulation amplitude is sufficient to sweep through the whole of the proton or D.P.P.H. signal which are both quite narrow. Hence the proton signal can be displayed on the C.R.O. screen, while the steady magnetic field is kept at resonance value for the experimental specimen in a manner explained earlier by observing the zero position of the microammeter in p.s.d. out-put. The p.r. frequency is measured as in the previous case. Equations (1) and (2) will also now hold good. Again making the proton signal to coincide with the P.M.R. signal for D.P.P.H. in the C.R.O. and measuring the p.r. frequency under this condition we will have the conditions of equations (3) and (4) fulfilled. Thus from these two measurements of p.r. frequencies we can calculate the g -value of the specimen with the help of equation (5). Any change in the magnetic field during the measurement of p.r. frequency corresponding to the p.m.r. of the specimen will be indicated by the unbalance of the centre-zero microammeter ($500\mu A$) from its null position.

The line width can also be obtained directly from the separation of the maximum and minimum of the derivative curve in the case of well resolved lines, otherwise the full absorption signal is to be obtained after numerical integration of the derivative curve. This is best done with the help of a pen-recorder. Due to the lack of such an instrument the linewidth has not been quantitatively measured although a qualitative idea can be obtained from the C.R.O. display of the signal or from the derivative response of the centre-zero microammeter.

RESULTS AND DISCUSSION

C.R.O. display of p.r. signal and P.M.R. signals for D.P.P.H, single crystals of $\text{CuSO}_4 \cdot 5\text{H}_2\text{O}$ (trichnic) and $\text{CuK}_2(\text{SO}_4)_2 \cdot 6\text{H}_2\text{O}$ (monochmic) are shown in Figs. (7), (8), (9) and (10) respectively. In the photographs the return trace of the oscilloscope is blacked out.

In the case of $\text{CuSO}_4 \cdot 5\text{H}_2\text{O}$ figure (9) shows the absorption signal, when the magnetic field is applied along a particular direction, parallel to the (110) face of the crystal, in which it is most prominent. The line width shows an angular variation becoming so large in some orientations that the signal gets completely ill-defined for C.R.O. display (c.f. Baguley and Griffiths, 1950). In this case we were unable to resolve the two lines for the two ions in the different planes even with p.s.d. method at 1.2 cms and 300°K and hence the principal ionic g values and their orientations could not be measured. We are trying to do this by setting up a 0.8 cm spectrometer.

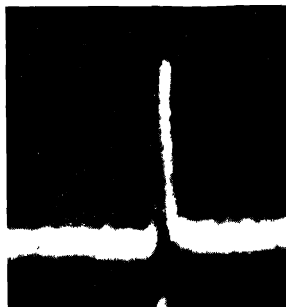


Fig. 7. Proton Signal

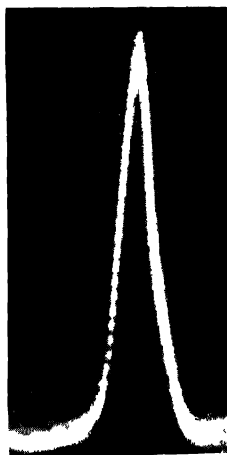
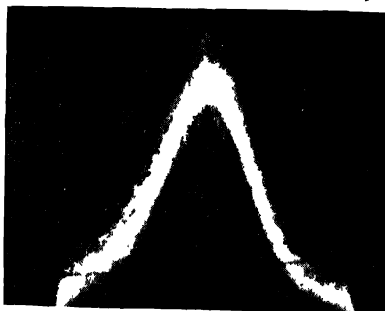


Fig. 8. Signal for D.P.P.H.

Fig. 9.
Signal for $\text{CuSO}_4 \cdot 5\text{H}_2\text{O}$ Fig. 10
Broad Signal for $\text{CuK}_2(\text{SO}_4)_2 \cdot 6\text{H}_2\text{O}$.

In the case of the single crystal of $\text{CuK}_2(\text{SO}_4)_2 \cdot 6\text{H}_2\text{O}$ the absorption signal is too broad to be very faithfully displayed on the C.R.O. screen although the peak could be recognized for all orientations of the crystal. With the p.s.d. method it was possible to determine the positions of the peaks very clearly for the resolved lines. In general for any orientation of the crystal two signals appear due to the two inequivalent ions* in the unit cell obtained from one another by a reflection

* Crystallographically equivalent.

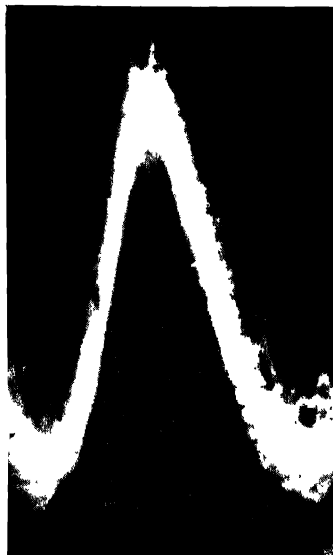


Fig. 11

Narrow Signal for $\text{CuK}_2(\text{SO}_4)_2 \cdot 6\text{H}_2\text{O}$ (Photographs in Fig. 9, 10, 11 taken under identical modulation amplitude).

in the (010) plane. The linewidth also shows angular variation, (cf. Bleaney *et al.*, 1949) the amount of variation being less than in the case of $\text{CuSO}_4 \cdot 5\text{H}_2\text{O}$. From the measurement of g values in different directions along four simple planes of the crystal (mostly natural faces) g values have been calculated directly by a convenient method analogous to the determination of principal susceptibilities in triclinic crystals (Ghosh and Bagchi 1962) developed by us and to be discussed in details in a further communication. The principal ionic g -values in $\text{CuK}_2(\text{SO}_4)_2 \cdot 6\text{H}_2\text{O}$ show that the symmetry of the crystalline electric field is definitely orthorhombic rather than tetragonal (c.f. Bleaney *et al.*, 1949). The principal g values at room temperature (300°K) and their orientations in usual tensor notations, with reference to the crystallographic axes, are shown in Tables I and II respectively.

These values are consistent with the results of Bleaney *et al.* (1949) at 90°K calculated indirectly by trial.

It appears that g values do not differ much for these two temperatures indicating that the crystal field remains almost unaltered in this range of temperatures.

TABLE I

	This paper	Bleaney <i>et al.</i>
G_1	2 16	2.14
G_2	2 05	2 04
G_3	2.38	2 36

TABLE II

c^* is a line normal to ' a ' and ' b ' axes
of the monoclinic crystal

	a		
G_1	54°5'	134°6'	114°24'
G_2	72°50'	106°56'	24°30'
G_3	41°6'	48°59'	92°

The fact that the signals for the two inequivalent ions in the unit cell are resolved in the case of $\text{CuK}_2(\text{SO}_4)_2 \cdot 6\text{H}_2\text{O}$ and in no orientation the line width is small enough to be very faithfully displayed on the C.R.O. screen, unlike the case of single sulphate of copper for which the line width is comparatively much less in some orientations although signals for two inequivalent ions are not resolved, suggests that exchange interaction effects are more prominent in $\text{CuSO}_4 \cdot 5\text{H}_2\text{O}$ than in $\text{CuK}_2(\text{SO}_4)_2 \cdot 6\text{H}_2\text{O}$ (cf. Bleaney *et al.*, 1949).

It is known that magnetic dipole-dipole interaction between paramagnetic neighbours broadens the lines. Exchange interaction between similar ions i.e. ions with the same energy and parallel precessional axes of spin vectors in the applied magnetic field produces a narrowing of the line, while exchange interaction between dissimilar ions adds to the dipolar broadening (Gorter and Van Vleck, 1947). In the second type of exchange, if the interaction energy between two neighbouring ions is less than the separation in energy of the two ions in the applied magnetic field, two lines will appear corresponding to the two ions (Pryce, 1948). Hence the narrow unresolved signal of $\text{CuSO}_4 \cdot 5\text{H}_2\text{O}$ at least qualitatively indicates that both types of exchange forces are much stronger in single sulphate of copper than in copper potassium sulphate. This is expected considering the closer proximity of neighbouring copper ions in $\text{CuSO}_4 \cdot 5\text{H}_2\text{O}$ and agrees with the earlier findings.

Further, it is readily found from the C.R.O. display or from the derivative response that the signal for $\text{CuK}_2(\text{SO}_4)_2 \cdot 6\text{H}_2\text{O}$ in (001) face shows a definite narrowing of the peak to some extent in some orientations (Figs. 10 and 11). This occurs whenever the two signals corresponding to two ions are coincident i.e. whenever the direction of applied magnetic field is equally inclined to the corresponding principal axes of the two ions (the magnetic field is then either along ' a ' or ' b ' axis of the crystal). In such a situation the magnetic energy of the two ions in the applied magnetic field is the same although the spin vectors of the two ions may not precess about parallel axes. Under such condition exchange broadening will be much less and apparent narrowing of the line will result, the degree of such narrowing being much less in this salt than in $\text{CuSO}_4 \cdot 5\text{H}_2\text{O}$ as seen readily from

oscilloscope display or derivative response of the signal. This suggests that in $\text{CuK}_2(\text{SO}_4)_2 \cdot 6\text{H}_2\text{O}$ exchange forces, although weaker in strength, are not negligible.

ACKNOWLEDGMENT

The authors are grateful to Prof. A. Bose, D.Sc., F.N.I., for initiating the problem and guidance throughout the progress of the work. The authors are thankful to our Workshop Superintendent Mr. A. K. Sarkar for constructing a number of microwave components and for other technical assistance, and to Dr. C. R. Kanekar of Tata Institute of Fundamental Research, Bombay, for kindly supplying a freshly prepared sample of D.P.P.H.

REFERENCES

- Bagguley, D. M. S. and Griffiths, J. H. E., 1950, *Proc. Roy. Soc. A.*, **201**, 366.
Bleaney, B., Penrose, R. P., Plumptre, B. I., 1949, *Proc. Roy. Soc. A*, **198**, 406.
Ghosh, U. S. and Bagchi, R. N., 1962, *Ind. Jour. Phys.*, **36**, 538.
Gorter, C. J. and Van Vleck, J. H., 1947, *Phys. Rev.*, **72**, 1128.
Ingram, D. J. E., 1955, *Spectroscopy at radio and microwave frequencies*, London, Butterworths.
Knooble, H. W. and Hahn, E. L., 1951, *Rev. Sci. Instr.*, **22**, No. 12, 904.
Pryce, M. H. L., 1948, *Nature*, **162**, 539.
Schuster, N. A., 1951, *Rev. Sci. Instr.*, **22**, No. 4, 254.

A NOTE ON THE ELECTROSTATIC MODEL OF HYDROGEN BOND APPLIED TO HYDROGEN BONDING IN ANILINE AND SUBSTITUTED ANILINES IN DIFFERENT ENVIRONMENTS

G. S. KASTHA and K. C. MEDHI

OPTICS DEPARTMENT,

INDIAN ASSOCIATION FOR THE CULTIVATION OF SCIENCE,

CALCUTTA-32

(Received September 10, 1963)

ABSTRACT Coggeshall's method of treatment of the electrostatic model of hydrogen bond has been applied to the case of hydrogen bonding in solutions between the molecules of aniline or of substituted anilines and the molecules of some polar solvents and also to the case when such bonds are formed between similar molecules in the liquid state of the pure compounds. It is pointed out that in the case of such a model, the ratio of the values of the sum of the solvent shifts in the frequencies of N-H stretching vibrations of a particular compound in solutions in two different solvents should be independent of the nature of the compounds. In the case of the pure liquids, on the other hand, the ratio of the sum of the frequency shifts to the geometric mean of the frequencies of symmetric and asymmetric N-H stretching vibrations for the different compounds is expected to remain constant. The data reported previously are found to conform to these expectations. Moreover, the experimental fact that the ratio of the sum of the solvent shifts in the frequencies of the two N-H stretching vibrations of a particular compound in a certain solvent to that of aniline in the same solvent is a constant for the compound and is approximately independent of the nature of the solvent, has been satisfactorily accounted for on the basis of the model.

INTRODUCTION

Since Pauling (1928) proposed that the hydrogen bond is electrostatic in nature, many authors (Sack and Prigogine, 1941; Maladère and Magat, 1947; Maladère 1948; Coggeshall, 1950; Shigorin and Dokumikhin, 1955) have calculated the spectroscopic properties of hydrogen bonds using such models. Coggeshall (1950) theoretically investigated the frequency shift, the intensity of absorption and the energy of association of a hydroxyl group which is participant in a hydrogen bonded complex by solving the Schrodinger equation for a hydroxyl group treated as a diatomic molecule with a Morse potential energy function to which the polarisation energy of a hydroxyl group due to electrostatic interaction has been added. He found that the stretching vibrational frequency of the hydrogen-bonded O-H group in benzyl alcohol and catechol calculated by the above method agrees well with the experimentally observed values. Coggeshall also showed that,

for small vibrations, considerations based on partial ionic and covalent characteristics of the hydroxyl group also yield frequencies in fair agreement with experiment. Venkata Ramiah and Puranik (1962a, b) applied the latter method with some modifications to the calculation of the stretching vibrational frequencies of hydrogen bonded N-H bonds in amides and of O-H bonds in acids and alcohols and achieved fair agreement with the observed values. In all these cases the frequency change due to hydrogen bonds formed between similar molecules have been calculated, but no such calculations based on the electrostatic model of hydrogen bonds formed between two dissimilar molecules viz., a solvent and a solute molecule have been made. Medhi and Kastha (1963a, b) have studied hydrogen bonding in aniline and substituted anilines in the liquid state and in solutions in some polar solvents. They have observed that the ratio of the sum of the solvent shifts in the frequencies of symmetric and asymmetric N-H stretching vibrations of a particular aniline compound in a certain solvent to that of aniline in the same solvent is a constant which is almost independent of the nature of the solvent. Moreover, the value of the constant was found to be greater than unity for compounds whose molecules contain electronegative atom or group of atoms (for which Hammett σ factor is positive), while for compounds with molecules containing a electropositive group (Hammett σ factor negative) the value of the ratio is less than unity. It is the purpose of the present paper to find out how far the electrostatic model of hydrogen bonds treated by Coggeshall can explain some of the observed facts qualitatively.

COGGESHALL MODEL APPLIED TO N-H...X BOND

In applying the model of Coggeshall to hydrogen bonds formed between the H-atom in one of the N-H bonds of the molecule of aniline or any substituted aniline and an atom X (where X = O or N) in the molecule of the solvent the following simplifying assumptions have been made.

- (i) The solutions are so dilute that only the interaction between a single molecule of the solute and a molecule of the solvent need be considered.

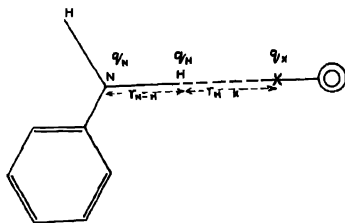


Fig 1.

Linear hydrogen bond N—H...X between a molecule of Phenyl amino and a molecule of a Polar solvent.

(ii) The hydrogen bonds N-H...X are always very nearly linear. (cf. Pimentel and McClellan, 1960) as shown in Fig. 1.

(iii) The distance r_{H-X} is almost the same in the case of solution of aniline and of substituted anilines in the polar solvent whose molecule contains the atom X.

(iv) The bond length r_{N-H} in the molecules of the various phenyl amines is approximately constant.

It is assumed that all these considerations apply to those aniline compounds where the substituent is neither very electronegative nor offers steric hindrances. In the following paragraphs the physical quantities associated with a substituted aniline compound with a definite Hammett σ -factor are designated with a superscript σ .

(a) X representing an atom of nitrogen or of oxygen in the molecule of the solvent

The force constant for the stretching of N-H bond in the various phenyl amines is calculated from the equation $f'' = 2.76 \times 10^{-2} (v_a'' + v_s'')^2$ dynes/cm and is related to the dissociation energy D_0 in K. Cal/mole of the normal covalent N-H bond through the relation $f'' = 2a''^2 D_0$, where a'' is a constant, which is slightly different for different molecules in the series of phenyl amines investigated, in the expression of the vibrational potential function of the Morse type used by Coggeshall (1950). Remembering that $v_a'' = v_s''(1 + \delta)$, where δ is small, we find the total solvent shift $\Delta v_t'' (= \Delta v_a'' + \Delta v_s'')$ is given by $\Delta v_t'' = 6.02 a'' D_0^{-1/2} \Delta D''$.. (1), where $\Delta D'' = D_0 - D''$, D'' being the dissociation energy in K. Cal/mole of the hydrogen bonded N-H bond. According to Coggeshall (1950) $D'' = D_0 \cdot (F_1/F_2)^\sigma \beta$, where D_0 is the dissociation energy in K. Cal/mole of a normal covalent N-H bond and β , also in K. Cal/mole, is the energy due to ionic character of the N-H bond. $(F_1/F_2)^\sigma$ represents the ratio of the electrostatic forces exerted by the unbalanced charges q_X on X and q_N on N respectively on the unbalanced charge q_H on H and is given by,

$$(F_1/F_2)^\sigma = \frac{q_X}{r_{H-X}^2} \bigg/ \frac{q_N}{r_{N-H}^2} \quad \dots (2)$$

It is seen from eqn. (1) that for the same compound dissolved in two different polar solvents whose molecules contain the atoms X_1 and X_2 respectively, the ratio of the total solvent shift in the two solvents is given by, $(\Delta v_t'')_1/(\Delta v_t'')_2 = \frac{D_0 - D_1''}{D_0 - D_2''}$. Substituting the values of D_1'' and D_2'' and using equation (2) we obtain,

$$(\Delta v_t'')_1/(\Delta v_t'')_2 = (F_1/F_2)_1^\sigma / (F_1/F_2)_2^\sigma = \frac{q_{X_1}}{q_{X_2}} \cdot \frac{r_{H-X_2}^2}{r_{H-X_1}^2} \quad \dots (3)$$

Eqn. (3) shows that the value of the above ratio for the different compounds

dissolved in the same pair of solvents is a constant for the particular pair of solvents and is independent of the nature of the compounds. The value of the ratio computed from the total solvent shifts for a number of aniline and substituted anilines in solutions in acetone, ether, tetrahydrofuran and pyridine as obtained by Medhi and Kastha (1963b) are given in Table I. The approximate constancy of the ratio for a pair of solvent is evident.

Now, if we compare the value of the total solvent shift ($\Delta\nu_t^\sigma$) for a substituted aniline compound with that of aniline ($\Delta\nu_t^0$), both in solution in the same solvent, we find from eqn. (1)

$$\Delta\nu_t^\sigma/\Delta\nu_t^0 = \frac{a^\sigma}{a^0} \cdot \frac{D_0 - D^\sigma}{D_n - D^0}$$

TABLE I

Compound	$\frac{(\Delta\nu_t^\sigma)}{(\Delta\nu_t^0)}$ Pyridine Acetone	$\frac{(\Delta\nu_t^\sigma)}{(\Delta\nu_t^0)}$ Tetrahydrofuran Acetone	$\frac{(\Delta\nu_t^\sigma)}{(\Delta\nu_t^0)}$ Ether Acetone
Aniline	2.25	1.58	1.12
<i>m</i> -Phenoldine	2.16	1.54	1.16
<i>m</i> -Anisidine	2.12	1.50	1.06
<i>p</i> -Anisidine	2.20	1.40	1.22
<i>m</i> -Toluidine	2.22	2.10	1.25
<i>o</i> -Nitroaniline	2.10	1.53	1.18

Substitution of the values of D^σ and D^0 and use of eqn. (2) yield

$$\frac{\Delta\nu_t^\sigma}{\Delta\nu_t^0} = \frac{a^\sigma}{a^0} \cdot (F_1/F_2)^\sigma / (F_1/F_2)^0 = \frac{a^\sigma}{a^0} \cdot \frac{q_N^0}{q_N^\sigma} \cdot \left(\frac{r_{N-H}^\sigma}{r_{N-H}^0} \right)^2$$

If we assume $a^\sigma \approx a^0$ and $r_{N-H}^\sigma \approx r_{N-H}^0$ then the value of the above ratio, denoted by S^σ becomes,

$$S^\sigma = \frac{\Delta\nu_t^\sigma}{\Delta\nu_t^0} \approx \frac{q_N^0}{q_N^\sigma}$$

It is seen from the relation that the value of S^σ is a constant for a particular compound and is independent of the nature of the solvent as has been observed by Medhi and Kastha (1963b). The charge q_N^σ on the *N*-atom in the molecule of a substituted aniline compound consists of two parts, a negative unbalanced charge $-Q^\sigma$ originating from the bond moments of the various localised bonds in the molecule and a part $+q_\pi^\sigma$ arising from the migration of charge from the *N*-atom into the delocalised π -orbitals of the molecule. If the values of the first portion

of the unbalanced charge for the various substituted anilines are not much different from that for aniline, then $S^\sigma = \frac{-Q^3 + q_\pi^0}{-Q^2 + q_\pi^0} \approx \frac{-Q + q_\pi^0}{-Q + q_\pi^0}$. The charge q_π^σ will in general be greater or smaller than q_π^0 depending on whether the substituent in the given position in the molecule of the particular compound is electronegative or electropositive respectively in comparison to the H -atom in the same position of the aniline molecule.

Thus for the electronegative groups Cl and NO_2 the value of S^σ is greater than unity, while in the case of the electropositive methyl group the value of S^σ is less than unity. Since the Hammett σ factor for the electronegative atom or group of atoms is positive and that for electropositive group is negative, the foregoing discussion explains the observed facts mentioned in the introduction.

(b) *X*-representing the N -atom in the NH_2 group in the molecule of the phenyl amines.

In the case of aniline and some substituted aniline compounds in the liquid state the hydrogen bonding takes place between the H atom of the NH_2 group of one molecule and the N -atom in the NH_2 group of another molecule as shown in Fig. 2.

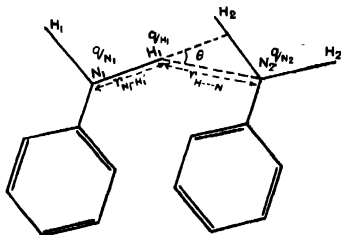


Fig. 2.

Bent hydrogen bond $N-H \cdots N$ between two molecules of aniline in the liquid state.

The $N-H \cdots N$ bridge in the figure is pictured as slightly bent, however, for $\theta = 0$, the linkage becomes linear.

The relation in eqn. (1) can be written in the slightly different form .

$$\Delta v_t^\sigma = (v_a^\sigma v_s^\sigma) \Delta D^\sigma / D_0 \quad (4)$$

Substituting the value of ΔD^σ in eqn. (4) and replacing F_1 by $F_1 \cos \theta$, the component along $N_1 H_1$ of the electrostatic force exerted by the charge q_{N_2} on the N -atom of second molecule on the charge q_{H_1} on the H -atom of the first molecule, we obtain

$$(v_a^\sigma v_s^\sigma) \Delta v_t^\sigma = \frac{\beta}{D_0} \left(\frac{F_1 \cos \theta}{F_2} \right)^\sigma = \left(\frac{r_{N-H}^\sigma}{r_{H \cdots N}} \right)^2 \cdot \frac{\beta}{D_0} \cos \theta \quad \dots (5)$$

If the values of θ , r_{N-H}^o and $r_{H..N}$ are not much different for the various phenyl amines then the values of $(v_a^o v_s^o)^{-1} \Delta v_t^o$ are expected to be almost the same in all the compounds. The values of the quantity computed from the data on Δv_t^o , v_a^o and v_s^o obtained by Medhi and Kastha (1963b) for aniline and some substituted aniline compounds are given in Table II. The value is seen to be approximately the same for the different compounds.

TABLE II

Compound	$(v_a^o v_s^o)^{-1} \Delta v_t^o$
Aniline	.029
<i>m</i> -Chloroaniline	.024
<i>m</i> -Anisidine	.022
<i>p</i> -Anisidine	.024
<i>m</i> -Phenetidine	.023
<i>m</i> -Toluidine	.023
<i>p</i> -Toluidine	.022

From the above discussions it is seen that the electrostatic model of hydrogen bonds treated by Coggeshall fairly explains the observed facts qualitatively.

ACKNOWLEDGMENT

The authors' grateful thanks are due to Professor S. C. Sirkar, D.Sc., F.N.I., for his valuable suggestions.

REFERENCES

- Coggeshall, N. D., 1950, *J. Chem. Phys.*, **18**, 978.
 Maladière, P., 1948, *Compt. Rend.*, **226**, 1600.
 Maladière, P. and Magat, M., 1947, *Compt. Rend.*, **225**, 676.
 Medhi, K. C. and Kastha, G. S., 1963a, *Ind. J. Phys.*, **37**, 139.
 Medhi, K. C. and Kastha, G. S., 1963b, *Ind. J. Phys.*, **37**, 275.
 Pauling, L., 1928, *Proc. Nat'l Acad. U.S.*, **14**, 359.
 Pimentel, G. C. and McClellan, A. L., 1960, *The Hydrogen Bond*, W. H. Freeman and Company.
 Sack, H. S. and Prigogine, I., 1941, *Phys. Rev.*, **59**, 924.
 Shigorin, D. N. and Dokunikhin, N. S., 1955, *Doklady Akad. Nauk, S.S.S.R.*, **100**, 323.
 Venkata Ramiah, K. and Puranik, P. G., 1962a, *Proc. Ind. Acad. Sc.*, **56A**, 96.
 Venkata Ramiah, K. and Puranik, P. G., 1962b, *Proc. Ind. Acad. Sc.*, **56A**, 155.

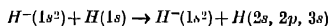
EXCITATION OF HYDROGEN ATOM IN FAST ENCOUNTER WITH NEGATIVE HYDROGEN ION

B. K. GUHA

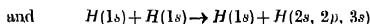
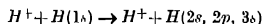
DEPARTMENT OF PHYSICS, B. N. COLLEGE, PATNA-4

(Received for Publication, August 27, 1963)

ABSTRACT Born's approximation is used to calculate the cross-sections of the following processes :



which are compared with the similar excitation processes

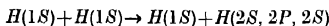
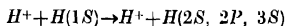


investigated by Bates, *et al*. It is found that the cross section curves for excitation of hydrogen atom by hydrogen negative ion is characterised by two maxima, somewhat similar to those observed by Moisewitch and Stewart in excitation of helium by hydrogen. Results are presented mainly in graphical form

INTRODUCTION

The negative hydrogen ion in the photosphere of the sun has long been recognised as responsible for its continuous opacity in the visible spectrum. Recently Weinman and co-workers (Weinman-1955) have produced negative hydrogen ion by passing positive hydrogen ion from a magnetic ion source through a capillary tube containing hydrogen. Muschlitz-Bailey group at University of Florida (1955) have measured scattering cross section of low energy negative hydrogen ion in hydrogen and helium respectively using method of Simon and co-workers (Simon, 1943). In recent years detailed theoretical study of fast collision processes involving hydrogen and helium atoms and positive ions have been carried out by Bates and his group (1953) using Born's approximation. Considerable interest is attached to the study of the comparable processes involving H^- . The present paper is devoted to the investigation of collision of H^- and hydrogen atom, where the hydrogen atom is excited to various higher states from the initial ground state by the process. Born's approximation is used, no account is taken of exchange, though the range of validity of Born's approximation in present type of problem is still uncertain.

Problems of similar nature as



have been studied by Bates, *et al.*

THEORY

We consider collision of a hydrogen atom and a negative hydrogen ion, both particles being initially in their ground states. Ignoring the effect of the exchange identity of the protons and making use of the Born's approximation the cross-section of the process for which the hydrogen atom is excited to the state characterised by the quantum number $n l$, (the negative ion remaining at the ground state) is given by

$$Q(1S-nl, 1S^2) = \frac{8\pi^3 M^2}{K_i^2 h^4} \int \frac{K_{max}}{K_{min}} |N|^2 K dK \quad \dots (1)$$

where ' h ' is Planck's constant, ' M ' is the reduced mass of the system and

$$\bar{K} = K_i - K_f$$

$$\bar{K}_i = \frac{2M\pi\bar{V}_i}{h}; K_f = \frac{2M\pi\bar{V}_f}{h}$$

\bar{V}_i and \bar{V}_f are the initial and the final velocities of the relative motion, and

$$N = \int e^{-iR.K_f} \chi^*(nl, \rho) \phi^*(1s^2; r_1, r_2)$$

$$\times \left\{ \frac{e^2}{|\bar{R}|} - \frac{e^2}{|\bar{R}+\bar{\rho}|} - \frac{e^2}{|\bar{R}-\bar{r}_1|} - \frac{e^2}{|\bar{R}-\bar{r}_2|} + \frac{e^2}{|\bar{R}+\bar{\rho}-\bar{r}_1|} - \frac{e^2}{|\bar{R}+\bar{\rho}-\bar{r}_2|} \right\} \\ \times e^{i\bar{R} \cdot \bar{K}_f} \chi(1S; \rho) \Phi(1S^2; r_1, r_2) d\bar{r}_1 d\bar{r}_2 d\rho d\bar{R}$$

where \bar{R} is the relative position vector of the nuclei of the two atoms, $\bar{\rho}$ the position vector of the electron of the hydrogen atom relative to the proton, χ 's are the wave function of the hydrogen atom in the state indicated, and \bar{r}_1, \bar{r}_2 are the position vectors of the electrons in the negative hydrogen ion relative to the proton; Φ being the wave function of the hydrogen ion :

$$\phi = \frac{\alpha^3}{\pi a_0^3} \exp \left\{ -\frac{\alpha}{a_0} (r_1 + r_2) \right\}$$

with

$$\alpha = 0.688.$$

It can be seen that in the integral for ' N ' $\frac{1}{|\bar{R}|}$, $\frac{1}{|\bar{R}-\bar{r}_1|}$ and $\frac{1}{|\bar{R}-\bar{r}_2|}$ do not

contribute due to the orthogonality of hydrogen atom wave functions. Therefore we get after integrating

$$N = \frac{-\alpha_0^2 4\pi e^2}{t^2} \left[1 - \frac{2.16.\alpha^4}{[(2\alpha)^2 + t^2]^2} \right] \int \chi_{nl}^*(\rho) e^{-ik.\rho} \chi_{1s}(\rho) d\rho \quad \dots (2)$$

where

$$t = Ka_0.$$

From (1) and (2) we have

$$Q_{nl} = \frac{4c^2}{v_i^2} \left(\frac{2\pi e^2}{\hbar c} \right)^2 \int_{t_{min}}^{t_{max}} \left[1 - \frac{2.16.\alpha^4}{[(2\alpha)^2 + t^2]^2} \right]^2 I_{nl}^2 t^{-3} dt \quad \dots (3)$$

where

$$I_{nl} = \int \chi_{nl}^*(\rho) e^{-ik.\rho} \chi_{1s}(\rho) d\rho.$$

Now

$$t_{max} = a_0 K_{max} = a_0(K_i + K_f)$$

$$t_{min} = a_0 K_{min} = a_0(K_i - K_f)$$

As is usual in the treatment of heavy particle collisions, it is sufficient to take t_{max} as infinite (Bates *et. al.* 1953) and if ΔE is the difference in energy between the two states for a particular excitation processes then

$$t_{min} = a_0 K_{min} = \frac{a_0 \Delta E}{\hbar v_i} \left[1 + \frac{\Delta E}{2Mv_i^2} \right]$$

2.2. For discrete transitions I_{nl} 's can be calculated from (4) by elementary methods. They have been tabulated by Bates and Griffing. We quote their value; :

$$I(1s-2s) = \frac{2^{17/2} t^2}{(4t^2+9)^3}$$

$$I(1s-2p) = \frac{2^{15/2} \cdot 3t}{(4t^2+9)^3}$$

$$I(1s-3s) = \frac{2^4 \cdot 3^{7/2} (27t^2+16)t^2}{(9t^2+16)^4}$$

On substituting them in (3) one can obtain analytical expressions for cross-sections. But they are in general cumbersome and are very tedious to evaluate. It is much easier to evaluate the integrals numerically, which is actually done in this paper.

2.3. It can be seen from the expression (3) that if

$$\frac{2.16.\alpha^4}{[(2\alpha)^2 + t_{min}^2]^2} \ll 1$$

then the expression for the cross-section becomes

$$Q(1s-nl) = \frac{4c^2}{v_i^2} \left(\frac{2\pi e^2}{\hbar c} \right)^2 \int_{t_{min}}^{t_{max}} I(1s-nl)^2 \cdot t^{-3} \cdot dt$$

which is the same as that of the excitation of hydrogen atom by proton. Thus the screening of the negative hydrogen ion has no effect on scattering if the incident energy is below certain value. If we take as first approximation

$$t_{min} = \frac{\alpha_0 \Delta E}{\hbar v_i}$$

it follows that for $(1s-2s)$ and $(1s-2p)$ transitions the hydrogen atom-hydrogen negative ion cross-section will differ from hydrogen atom-hydrogen positive ion (proton) cross-section provided incident energy is greater than 500 ev.

RESULTS

The cross-sections associated with the processes mentioned in the introduction are computed from the formula developed. Figures 1 to 3 show the values obtained. It should be noted that a log-log scale is used, and that the independent variable chosen is not E , the energy of relative motion, but the energy of the incident particle, the atom undergoing transition being taken to be at rest. For comparison the cross-sections of proton-hydrogen atom and hydrogen-hydrogen atom as calculated by Bates and Griffing are also plotted in the same figures.

On comparing the cross-section curve of $(H-H^-)$ with corresponding curves for $(p-H)$ and $(H-H)$ respectively it will be observed that at low energy the cross-sections of $(H-H^-)$ impact lie close to but above the cross-section of the latter processes. When energy is sufficiently low the $(H-H^-)$ cross-section almost coincides with that of $(p-H)$ impact. This is in conformity with the trend observed in $(p-H)$ and $(H-H)$ impact.

The curve for $(H-H^-)$ is characterised by two maxima, somewhat similar to the double peaks observed by Moiseiwtsch and Stewart (1954) in collision between hydrogen and helium atoms. Moiseiwtsch attributed the phenomena to double transition. Essentially the same shape of curve has been obtained by Bates and Griffing who however remark that if a better approximation method is used in the lower part of the energy region, the first maximum may be partially suppressed and the true curve may conceivably show a single broad maxima.

For $(1s-2s)$ and $(1s-3s)$ excitation the maximum cross-section is below that of the corresponding $(H-H)$ cross-section and is shifted to considerable lower energy. But for $(1s-2p)$ transition the maximum cross-section is in between that of $(H-H)$ and $(p-H)$ cross-section and is at higher energy.

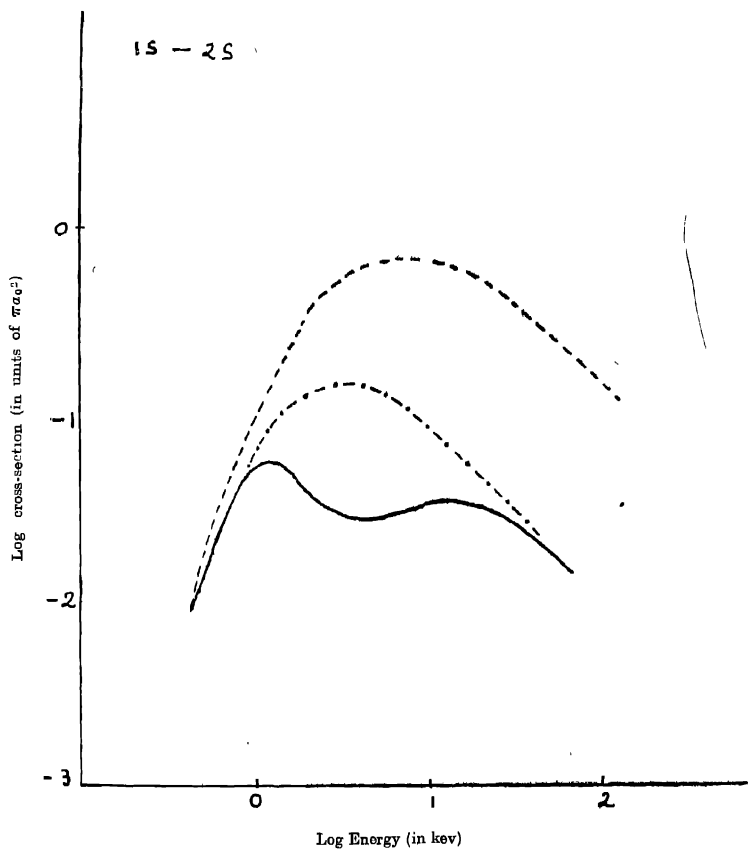
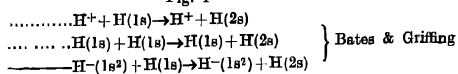


Fig. 1



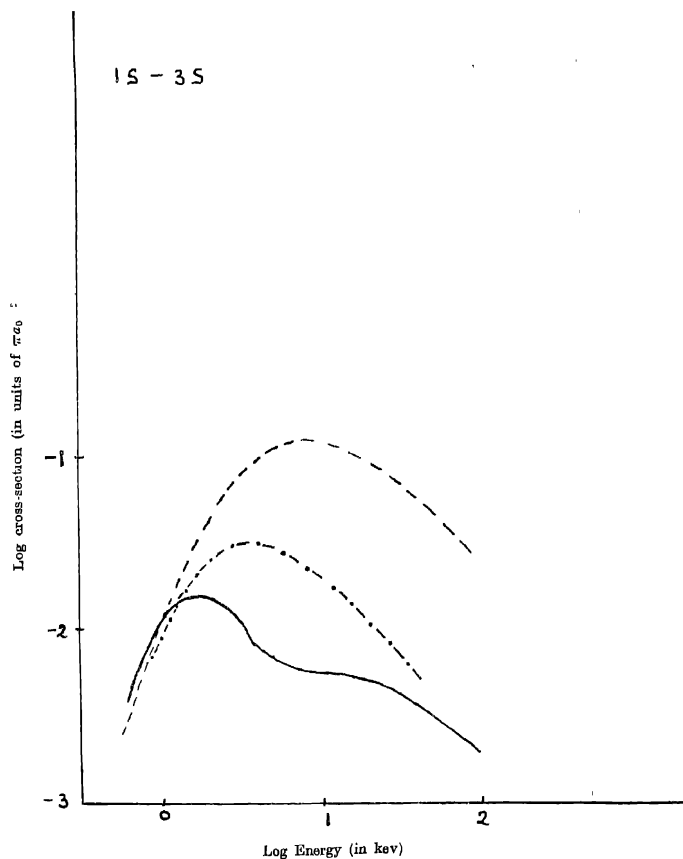


Fig. 2

- | | | |
|-------|---|--------------------|
| | $H^+ + H(1s) \rightarrow H^+ + H(2p)$ | } Bates & Griffing |
| —o—o— | $H(1s) + H(1s) \rightarrow H(1s) + H(2p)$ | |
| ———— | $H^-(1s^2) + H(1s) \rightarrow H^-(1s^2) + H(2p)$ | |

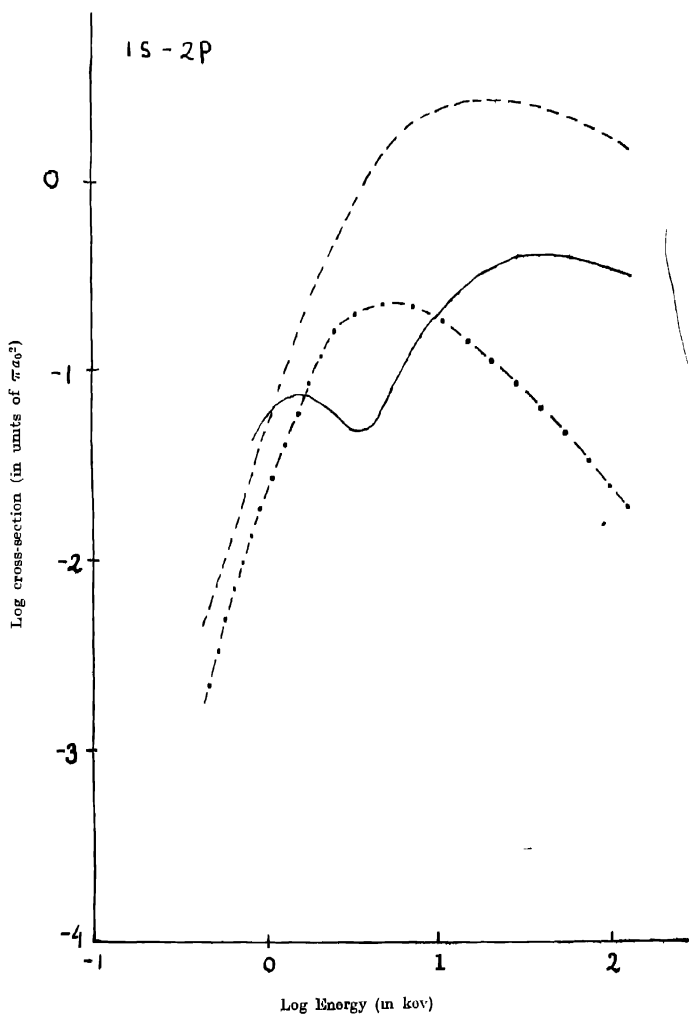
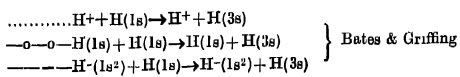


Fig. 3



At higher energy the curve for $(1s-2s)$ and $(1s-3s)$ transitions almost coincides with that of the $(H-H)$ curves for the corresponding transitions, while the curve for $(1s-2p)$ transition lies above $(H-H)$ curve and has a tendency to coincide (with $(p-H)$ curve from below

Unfortunately no experiment is done in the energy region of this calculation. Only available data are due to E. E. Muschlitz who measured the scattering cross-section of H^- in hydrogen and helium in the energy range 4 ev. to 300 ev.

ACKNOWLEDGMENT

I should like to express my gratitude to Dr. H. N. Yadav for continued guidance during the progress of the work. My thanks are also due to Prof. L. M. Chatterjee, Prof. of Physics, P U., for granting every facility to carry out the investigation.

REFERENCES

- Bates, D. R. and Griffing, G. W., 1953, *Proc. Phys. Soc.*, **66**, 961.
Moisewitsch, B. L. and Stewart, A. L., 1954, *Proc. Phys. Soc.*, **67**, 1069.
Muschlitz, E. E. and Bailey, T. L., 1955, *Phys. Rev.*, **100**, 1231.
Sutton, 1943, *J. Chem. Phys.*, **11**, 307.
Weinman and Cameron, 1956, *Rev. Sci. Instr.*, **27**, 288, 1955, *Phys. Rev.*, **100**.

A JEWEL MOUNTED MICRO-BALANCE FOR THE MEASUREMENT OF MAGNETIC SUSCEPTIBILITIES OF CRYSTALS

(Miss) D. DAS

DEPARTMENT OF MAGNETISM,
INDIAN ASSOCIATION FOR THE CULTIVATION OF
SCIENCE, CALCUTTA-32.

(Received September, 1963)

ABSTRACT. A jewel-mounted microbalance has been designed and constructed for the measurement of the magnetic susceptibilities of the dia- and paramagnetic crystals at various temperatures. The detailed description and method of calibration of the balance are given in the paper. The balance is of robust and stable construction and its deflectional sensitivity is magnified very much by a suitable optical lever arrangement. The magnetic force upon a sample suspended by a thin fibre from one arm of the balance is compensated by the force exerted upon a small current bearing coil by a permanent magnet. The sample when in the form of a single crystal is free to set with its maximum susceptibility in the horizontal plane along the direction of the magnetic field. When the balance is calibrated by a standard sample the above method gives directly the maximum susceptibility in the horizontal plane. The sensitivity of the compensation device is 1.65×10^{-6} gms per microampere of compensating current.

INTRODUCTION

Of the methods (Krishnan and Banerji, 1933, Dutta, 1944; Dutta Roy, 1955; Bates, 1961) which are being utilized here as well as elsewhere for the determination of the magnetic susceptibilities of different types of para- as well as dia-magnetic substances particularly of the single crystals of these, the quartz fibre micro-balance method devised by Bose (1947) has been found to be very convenient, though somewhat less sensitive than some of the other methods, namely, those working on the principle of a Curie balance. In Bose's method the single crystal suspended freely, with a very fine fibre from one arm of the balance, in a horizontal magnetic field with a vertical gradient sets with its maximum susceptibility in the horizontal plane along the field and at the same time moves along the gradient, thus eliminating the uncertainty about the direction of measurement of the susceptibility and affording obvious economy of space in the design of cryostats and heaters.

But the quartz suspension system was very sensitive to disturbances and liable to frequent breakage. Attempts to replace quartz fibre with phosphor-bronze strip did not improve matters and replacement became difficult owing to unavail-

ibility of the strips. Moreover, in horizontal fibre suspension systems there was always sagging of the strips and the usual yielding at the points of attachment. Finally, balancing of magnetic force by manual torsion of the fibre introduced unwanted disturbances in the system and the sharp magnetic gradient used led to uncertainties of calibration. With the object of removing all these objections the manufacture of a jewel mounted micro-balance and other concomitant arrangements were undertaken which will be described in details in the present paper.

THEORY

When a small magnetic crystal is placed in an inhomogeneous magnetic field, it experiences a couple due to its magnetic anisotropy, given by (Nye, 1957)

$$G_{ij} = v(-k_{ik}H_kH_j + k_{jk}H_kH_i) \quad (i, j, k = 1, 2, 3) \quad (1)$$

where k 's and H 's are the components of the volume susceptibilities and magnetic field strengths respectively and v the volume of the crystal.

In addition to this the crystal experiences a translational force given by (Nye 1957)

$$F_i = \frac{1}{2}v(k_{jk} - k_0) \cdot \frac{\partial}{\partial x_i} (H_j H_k) \quad (2)$$

where k_0 is the volume susceptibility of the surrounding medium

If now the experimental arrangement is made such that the magnetic field is in the x_1 direction (horizontal direction from pole to pole) and the gradient in the x_3 direction (vertical), the couple due to magnetic anisotropy will be in the $x_1 x_2$ -plane (horizontal) and about x_3 and the translational magnetic force will be along the x_3 direction. If the experimental set up be so arranged that the crystal is incapable of taking up rotation about any direction except x_3 the major couples due to anisotropy of shape about x_1 and x_2 become totally ineffective. A small residual couple of this type about x_3 may be eliminated by grinding the crystal in the form of a disc in $x_1 x_2$ plane.

Then the magnetic anisotropy which is only effective for the purpose of rotating the crystal in the plane $x_1 x_2$ will be given by

$$\frac{1}{2}v(k_{max} - k_{min}) H^2 \sin 2\psi \quad \dots \quad (3)$$

where k_{max} and k_{min} are the maximum and minimum values of the volume susceptibilities in the $x_1 x_2$ plane and ψ is the angle between the magnetic field and k_{max} . If the crystal is perfectly free to rotate about x_3 , the above couple due to magnetic anisotropy will place k_{max} direction practically along the field (x_1 direction) and at the same time crystal will experience a force due to the gradient in the x_3 direction given by

$$F_3 = v(k_{max} - k_0) H_1 \frac{\partial H_1}{\partial x_3} \quad (4)$$

The measurement of this force will then give us the maximum value of the magne-

the susceptibility in $x_1 x_2$ plane. The above principle is utilised in the balance described below.

Description of the balance

(a) The balance consists of a light horizontal beam made from thin aluminum sheet about 5 millimeters wide and 25 centimeters in length bent along the longitudinal axis to an L -shaped cross section serrated along the vertical section, to take movable wire riders.

The beam is capable of rotation in a vertical plane about a thin non-magnetic stainless steel spindle rigidly fixed at right angles (horizontally) through the balance beam. For sensitiveness in detecting the movement of the beam the spindle is fixed at a point about 18 cm from the end of arm at which the sample is suspended. The spindle is accurately mounted on a pair of jewel bearings set in a U -shaped brass holder and fixed with arms upright on a horizontal aluminum base provided with levelling screws. The jewel bearings consist of a pair of perforated jewels with a pair of flat jewels behind them to prevent any lateral motion of the spindle. The jewels are set within two accurately cut screw heads passing co-axially through threaded holes near the top of the two arms of the brass holder and locked in position by locking nuts.

(b) *Method of observation of the movement of the beam*

The movement of the balance beam could be observed as usual by mounting a vertical mirror upon the spindle, but for very small forces the movements of the beam are not perceptible with this arrangement. Consequently, a simple device for magnifying these movements has been adopted. A small light plane mirror has been kept vertical by means of two horizontal stretched unspun silk fibres attached at the two ends of the horizontal diameter of the mirror. The position of the mirror is about 3 cm above the horizontal balance beam near its end from which samples are suspended for magnetic measurements. A small piece of glass rod about 1 cm in length is attached with the mirror at right angles to its plane so that in undisturbed position the rod is always horizontal and just above the balance beam. A small piece of quartz fibre is attached between the balance beam and the small horizontal rod with the mirror in such a way that the fibre is always taut. Thus any very feeble movements of the beam is now many times magnified and can be observed by lamp and scale arrangement.

(c) *Suspension system*

The suspension system consists of three parts attached successively to one another (i) the upper portion consisting of a thin and short glass rod hooked at the upper end to hang from the balance arm, (ii) the central portion consisting of a fine quartz fibre of sufficient length, and (iii) the lowermost portion consisting of a thin long pyrex rod to the lower end of which is fixed the crystal, with the

known direction vertical and lying accurately in the small region over which the magnetic force is appreciably constant. The pyrex rod is of such a length that the thin index rod fixed at its upper end shows above the heater or the cryostat chamber, between the pole pieces, within which the crystal is suspended for taking measurements at high or low temperatures.

(d) *Method of measurement of the magnetic force on the sample*

It is obvious that the specimen suspended with the fine quartz fibre from one arm of the micro-balance in the non-homogeneous magnetic field, between Sucksmith (1939) type of pole shoes over the flat pole pieces of the electromagnet (as adopted here by Dutta Roy 1955), sets with its maximum susceptibility in the horizontal plane, along the horizontal magnetic field and at the same time moves bodily along the vertical gradient. The magnetic translational force is measured by an electrodynamic arrangement placed at the other end of the balance beam. The arrangement consists of a small coil of 70 turns of enamelled copper wire of 42 s.w.g. wound on a light hollow cylindrical perspex former (about 1 cm in length and 8 mm in diameter) suspended from the end of the balance beam and placed inside the magnetic field of a permanent magnet. Pole pieces of the permanent magnet are shaped to concave cylinders and the coil hangs freely concentrically between them. When a current is passed through the coil, the balance beam experiences the usual electrodynamic force proportional to the current. The terminals from the coil are taken in such a way that very little restriction is imposed on the movement of the balance beam.

The entire balance system consisting of the above described parts is placed firmly screwed over a plane base provided with levelling screws. The entire system is covered by a perspex cover to protect it from draught and dust. There is an arrangement fixed to the base by which the beam can be kept arrested from outside the case when not in use. The specimen to be studied is suspended from one end of the balance beam, passes through a hole in the base into the inhomogeneous magnetic field and is counterpoised by placing riders on the beam.

When the magnetic field is switched on, the beam is deflected due to the magnetic force and can be restored to the original position by sending a suitable current through the balancing coil. The description of the different parts can be better followed by referring to the adjoining diagram (Fig. 1.)

Test of sensitiveness :

In order to test the sensitiveness etc. of the balance, the beam was first made free and horizontal and an accurately weighed rider made of thin aluminium wire is placed successively at different points on the balance beam starting from one extreme end. The corresponding deflections of the mirror was observed by a lamp and scale arrangement and were balanced by sending suitable currents through the balancing coil. The current was observed in an accurate, sensitive and cali-

brated microammeter of which readings are correct to ± 0.5 microampere. The balancing current was more accurately measured by recording the drop of potential

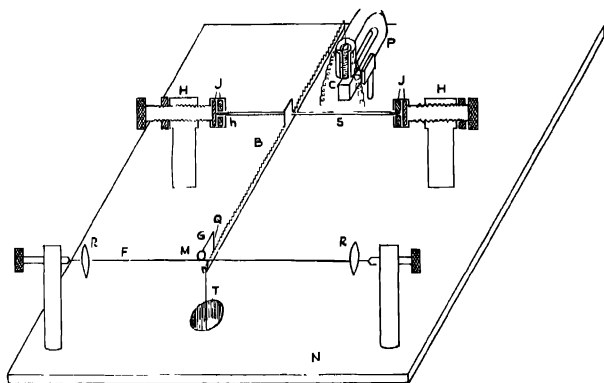


Fig. I Schematic diagram of the balance (not to scale).

B ——— Arm of the balance. S ——— Stainless Steel Spindle.

J, J ——— Jewels. H, H ——— Brass holders. P ——— Permanent Magnet.

C ——— Current bearing coil. M ——— Light plane mirror.

G ——— Pyrex glass rod. Q ——— Quartz fibre. F ——— Unspun Silk fibre.

R, R ——— Copper springs. T ——— Suspension system.

N ——— Aluminum base of the balance.

across a standard resistance placed in the circuit, with the help of a *L*. and *N*. student's type potentiometer while the balancing current was flowing through the circuit. The results of observation are shown in Table I and the variation of current with force shown diagrammatically in Fig. 2.

TABLE I

Weight of the rider in gm	Position of the rider from the spindle in cm.	Effective load at the end of the beam in milligram.	Balancing current in micro-amperes	Sensitiveness in gm/micro-ampere
	0	0	0	
	3.6	333	205.0	
	7.2	667	405.0	
.00165	10.8	1.00	610.0	1.65×10^{-6}
	14.4	1.32	810.0	
	18.0	1.65	1000.0	

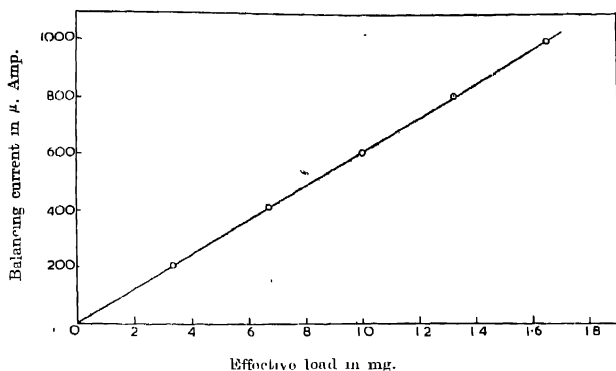


Fig. 2. Sensitivity and accuracy of the balance as shown by the variation of the balancing current with effective load at the end of the beam

It is observed that the relation between force and balancing current is a linear one. It is further observed that with the present arrangement the sensitiveness obtained is about 1.65×10^{-6} gm/micro-ampere.

Calibration and Standardisation

Let a sample of mass m_1 and volume v_1 attached at the end of the suspension system of the balance experience a magnetic force F_1 balanced by a current i_1 and F_2 and i_2 be the corresponding force and current when the above specimen is placed by a standard specimen of mass m_2 and volume v_2 , then

$$\frac{F_1}{F_2} = \frac{i_1}{i_2} = \frac{v_1}{v_2} \frac{k_1}{k_2} \frac{k_0}{k_0}$$

where k_1 and k_2 are the volume susceptibilities of the specimen and the standard substance respectively, k_0 that of the medium in which the samples are placed which is generally air, provided the volumes are comparable and such that

$H \frac{\partial H}{\partial x}$ over them is constant. The mass susceptibility of the specimen will then

be given by $\chi_1 = \frac{i_1}{i_2} \frac{m_2}{m_1} \left(\chi_2 - \frac{k_{air}}{\rho_2} \right) + \frac{k_{air}}{\rho_1}$ where ρ_1 is the density of the specimen χ_2 and ρ_2 are the mass susceptibility and density respectively of standard sample $k_{air} = .028 \times \left(\frac{300}{T} \right)^2 \times 10^{-6}$ at T° absolute. For the measurement of paramagnetic susceptibilities pure crystals of chromium potassium alum have been taken as the standard substance because its susceptibilities at different temperatures have been very accurately measured here and elsewhere (de-Haas and Gorter 1929, Mue. Serres 1932, Dutta Roy 1958).

Mean gm. molecular susceptibility of chromium potassium alum taking the average of these values is given by $\chi_M = 6080.5 \times 10^{-6}$ at 306.8°K .

In the case of diamagnetic samples, conductivity water is taken as the standard substance of which mass susceptibility $\chi = .7225 \times 10^{-6}$ at 30°C .

In order to check the reliability of the balance a number of measurements have been made for paramagnetics with pure crystals of ferric ammonium alum (cubic) and $\text{NiSO}_4 \cdot 6\text{H}_2\text{O}$ (tetragonal) grown from aqueous solutions and for diamagnetics with pure crystals of sodium chloride and potassium chloride (both cubic) obtained from Harshaw Chemicals, (U S A) The detailed results of measurements are given in the adjoining tables (Tables II and III).

TABLE II
Paramagnetic Samples

Substance	Mass, density and balancing current corrected for pull on carrier	Mass susceptibility $\chi \times 10^6$ c g s e m u	P ₂ in Bohr Magnetons at 300°K of unknown substances	
			Present value	Earlier values
Chromium potassium alum (standard)	$m = 1088 \text{ gm}$	$\rho = 1.842 \text{ gm/cc}$ $\epsilon = 77.0 \mu \text{ A}$	34.80	34.81 (Dutta Roy 1958)
				35 (Spin only value)
Ferric ammonium alum (unknown)	$m = 1000 \text{ gm}$	$\rho = 1.724 \text{ gm/cc}$ $\epsilon = 175.2 \mu \text{ A}$	34.80	34.79 (Onnes and Oosterhuis 1926)
				34.78 (Mitra 1963)
Chromium potassium alum (Standard)	$m = 0680 \text{ gm}$	$\rho = 1.842 \text{ gm/cc}$ $\epsilon = 51.0 \mu \text{ A}$	9.677	9.687 (Dutta Roy 1958)
				9.656 (Mookherjee 1946)
$\text{NiSO}_4 \cdot 6\text{H}_2\text{O}$ (along tetragonal axis) (unknown)	$m = 1226 \text{ gm}$ $\rho = 2.080 \text{ gm/cc}$ $\epsilon = 114.5 \mu \text{ A}$	$\rho = 2.080 \text{ gm/cc}$ $\epsilon = 114.5 \mu \text{ A}$	9.677	9.701 (Mitra 1963)

TABLE III
Diamagnetic Samples

Substance	Mass density and balancing current corrected for pull on carrier at 30°C	Mass susceptibility $\chi \times 10^6$ c g s e m u	Earlier values of Mass susceptibility $\chi \times 10^6$ c g s e m u
Water	$m = 1232 \text{ gm}$ $\rho = 99567 \text{ gm/cc at } 30^\circ\text{C}$ $\epsilon = 105.3 \mu \text{ A}$	7225 at 30°C	
Crystals of sodium chloride	$m = 1366 \text{ gm}$ $\rho = 2.165 \text{ gm/cc}$ $\epsilon = 85.0 \mu \text{ A}$	5186	5183*
Crystals of potassium chloride	$m = 1198 \text{ gm}$ $\rho = 1.984 \text{ gm/cc}$ $\epsilon = 75.0 \mu \text{ A}$	5228	5230*

*Tables de constantes et données numériques 1957, Edited by G. Foëx *et al.*, Vol. 7, "Diamagnétisme et Paramagnétisme".

Concluding Remarks :

The lever arrangement for magnification of the deflections could be replaced by some other arrangement such as a balanced photo-cell system Mitra *et al*, 1963 but since this is not easily available here we are to remain content with the present system which is quite simple yet very efficient

It would be interesting to mention in this connection that the present arrangement can easily be utilised with slight modification for the measurement of magnetic anisotropy and maximum absolute susceptibilities in the horizontal plane of a single crystal with the same setting. Only extra arrangement that is necessary is for giving a vertical motion of the magnet by jack-screw so as to bring the crystal in the homogeneous part of the Sucksmith type pole gap and to provide a rotation of the magnet about the vertical suspension axis so that the magnetic couple may be balanced against the torsion of the fibre. From this the anisotropy is calculated. For the susceptibility the crystal is placed in the centre of the inclined parts of the Sucksmith gap as already explained. The arrangement is in course of being set up in our laboratory and the details of it will be published in due course.

ACKNOWLEDGMENT

The author is grateful to Shri A. K. Dutta, Research Officer for his suggestion and guidance and to Professor A. Bose for his constant interest in the work. Sincere thanks are also due to the Workshop staff of the Association for constructing the apparatus efficiently.

REFERENCES

- Bates, L. F., 1961, *Modern Magnetism* (Cambridge University Press), P. 111-131.
Bose, A., 1947, *Ind Jour Phys* **21**, 276.
de-Haas, W. J and Gorter, C. J. 1929-31, *Comm. Londen* No. 208 c.
Dutta, A. K. 1944, *Ind Jour. Phys* **18**, 249.
Dutta Roy, S. K. 1955, *Ind. Jour Phys* **29**, 429.
Dutta Roy, S. K. 1958, Thesis, University of Calcutta, 79.
Krishnan, K. S. and Banerjee, S. 1936, *Phil Trans Roy Soc* **A235**, 343.
Mitra S., Ghosh, P. K., and Dutta Roy, S. K. 1963, (In course of Publication)
Mookherjee, A. 1946, *Ind Jour Phys* **20**, 9.
Nye, J. F. 1957, *Physical Properties of crystals*, (Oxford)
Onnes, H. K. and Oosterhuis, E. 1926, *Comm. Londen*, No. 139 c.
Seares, A. 1932, *Ann. Phys* **17**, 5.
Sucksmith, W. 1939 *Proc Roy. Soc.* **A170**, 551.
Table de constantes et données numériques 1957, Edited by G. Fœx *et al* Vol. 7, "Diamagnétisme et Paramagnétisme."

ELECTRICAL BREAKDOWN IN SPARK COUNTER

N. K. SAHA AND S. L. GUPTA

DEPARTMENT OF PHYSICS AND ASTROPHYSICS, UNIVERSITY OF DELHI, DELHI-6.

(Received, September 11, 1963)

ABSTRACT. Spark counter voltage pulses due to sparks produced by $Po^{210}\alpha$ -particles in atmospheric air were photographed on a Tektronix 531-A Oscilloscope using a fast quenching circuit of RC = 5 ns. Photographs taken at short gaps (~ 1 mm) confirm the occurrence of space-charge type of spark breakdown through streamer formation by the superposed effect of a large number of electron avalanches created by an α -particle. At large gaps (~ 5 to 30 mm), no spark breakdown occurs and only the primary electron pulses are observed. This is understood in the light of the highly non-uniform electric field and the corona zone near the wire in the spark counter geometry. Some finer details of the pulse-forms at large gaps and the possible effect of negative ion formation are also discussed.

INTRODUCTION

Many phenomenological properties of the spark counter have been studied (Connor, 1952, Savel, 1952, Saha and Nath, 1957, Kawata, 1961) and a number of practical applications (Fleury, 1959, Gupta and Saha, 1961, Gupta and Saha, 1962) of these made. Not much work has, however, been done so far to understand the basic mechanism of the spark breakdown in the counter. The spark breakdown processes in gases under overvolted parallel plate gaps have been extensively studied by Raether (1961), Loeb (1956), Meek (1953), Penning (1957) and others (Pfaue and Raether, 1959). The processes in the spark counter are, however, complicated by the strongly non-homogeneous electric field in the wire-to-plate geometry and the existence of the densely charged corona zone near the

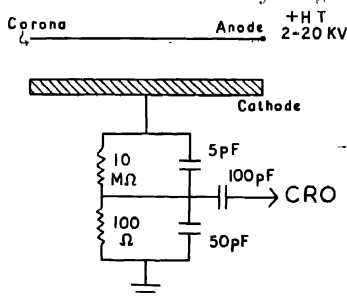


Fig. 1. Schematic diagram of spark counter and the differentiating pulse divider.

wire (Fig 1). It is, therefore, important to study the specific problems in the spark counter in the light of our existing knowledge in the homogeneous field.

An organic vapour or gas between two parallel plates under a steady potential shows two distinct types of electrical breakdown processes (1) the Townsend regenerative gas discharge (γ -process) and (2) the space-charge breakdown by streamer formation (Fig 2). The former is caused by generally strong cathodic

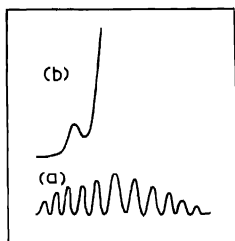


Fig. 2 (a) Typical forms of Townsend regenerative discharge pulses, (b) Space-charge breakdown pulses.

secondary electron emission in gases with large γ_{photon} satisfying $\gamma(e^{ad} - 1) = 1$, even though single primary electron avalanche $e^{ad}(\alpha - \text{the Townsend first coefficient, } d - \text{gap length})$ lies well below 10^8 electrons. In gases with smaller electron emission, a series of secondary electron avalanches may eventually produce large space-charge accumulation and lead to space-charge breakdown. In the second process (2), a single electron avalanche must carry $\geq 10^8$ electrons and positive ions, generating strong space-charge field (near the anode), which in turn sets up conducting electron streamers extending across the entire gap (Loeb *et al.*, 1948, Loeb, 1955, Raether, 1959) and causes spark breakdown. This would take place readily in gases with poor γ_{photon} under sufficiently overvolted gap and much earlier than the process (1) could occur.

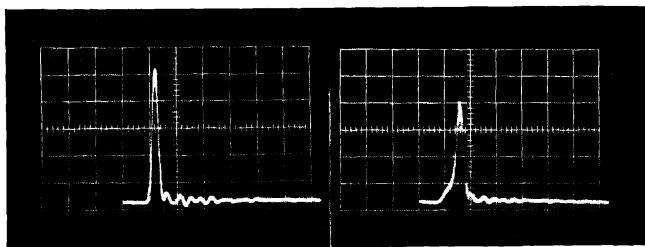
We describe below results of our preliminary study of the structure of the electrical potential pulses produced at the spark counter cathode by α -particles in atmospheric air using a fast quenching circuit ($RC \sim 5$ ns) as shown in Fig. 1, and photographed on a Tektronix 531A oscilloscope. Nine different gap lengths between 0.5 mm and 30 mm were used. The results strongly suggest a space-charge type of breakdown taking place at short distances under the strong non-homogeneous electric field existing. It seems that although the single electron avalanches in the small gaps used do not exceed 10^4 - 10^5 electrons, superposition of the avalanches in time and space due to about 10^4 to 10^5 electrons released by an α -particle within a few nanoseconds enlarges the avalanche due to each α -particle to $\geq 10^8$ electrons. The condition for space charge breakdown by streamer formation is thus set up. This view is supported by a recent work of Schlumbohm (1962) on the α -particle spark breakdown of gases in a homogeneous electric field (published while this manuscript was under preparation). Only

a qualitative interpretation of the mechanism is attempted by us for the present in view of the complications introduced by the non-homogeneous electric field and the corona phenomenon. More measurements with better defined conditions would be required for a quantitative understanding.

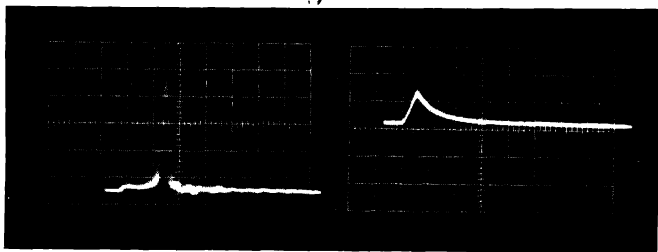
THE OSCILLOGRAMS AND THEIR EXPLANATION

In our previous works on spark counter, only small wire to plate gap (~ 1.5 mm) was used. Here for large spark gap (upto 3 cm) an additional provision had to be made for applying steady D.C. potential up to 20 KV with fine adjustments. Atmospheric air at about 35°C and 40 per cent R. H. was used. The spark gaps ' d ' chosen were, 0.5, 1.0, 1.2, 5.0, 10.0, 15.0, 20.0, 25.0 and 30.0 mm. The potentials across the gaps were adjusted respectively to 2.0, 2.6, 3.0, 4.4, 7.5, 9.6, 12.5, 16.0 and 20 KV. such that they were approximately 200 V above the threshold of the sparking with α -particles in each case. Without the α -particles, the counter showed zero background over long hours.

The photographs of the potential pulses across the series quenching resistor ($R \sim 100\Omega$) were taken at each of the gap lengths. These are reproduced in Figs. 3 and 4.



Traces 3(a) & 3(b)



Traces 3(c) & 3(d)

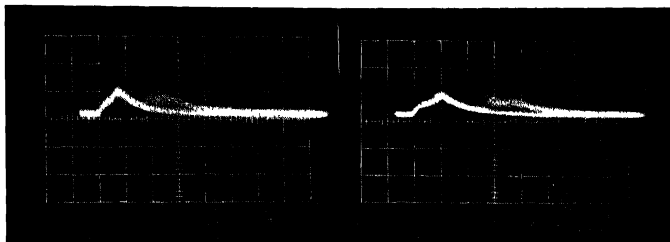
Traces a, b and c are at gap lengths ' d ' = 0.5, 1.0 and 1.2 mm respectively, using oscilloscope sweep speed = $0.1 \mu\text{ sec/cm}$ and vertical sensitivity = 10 V/cm .

Trace d is at 5 mm gap length using sweep speed $0.1 \mu\text{ sec/cm}$ and vertical sensitivity = 0.5 V/cm .

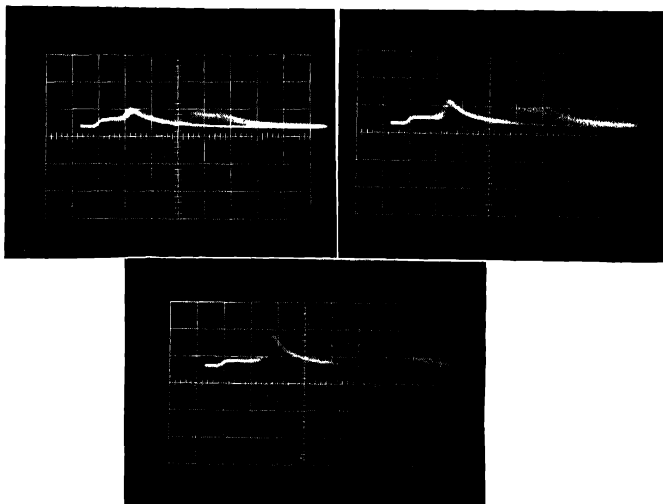
As explained under discussion to follow, we suggest the following interpretation for the observed pulses :

1. In Fig. 3, photographs *a* to *c*, the space-charge type of spark breakdown is occurring with streamer formation precoded by a critically large primary avalanche ($e^{at} \geq 10^6$) electrons) produced by a single α -particle

2. At the smallest gap $d = 0.5$ mm, trace (a), the primary electron pulse is not resolved over the oscilloscope as it is almost instantaneously overtaken by



Traces 4(e) & 4(f)



Traces 4(g), 4(h) & 4(k)

4. Traces e, f, g, h and k are at gap lengths 'd' = 10, 15, 20, 25 and 30 mm. using sweep speed $0.1 \mu \text{ sec/cm}$ and vertical sensitivity = 0.5 V/cm .

the strong streamer breakdown pulse. At the gap $d = 1.2$ mm, trace *c*, the primary electron pulse is clearly resolved first and this is followed by a streamer breakdown pulse after a time delay of about 100 ns. The trace (b) indicates the transition between (a) and (c).

3 At $d = 5$ mm, the trace obtained (d) shows clearly (on a larger vertical sensitivity of the oscilloscope) the primary electron component of the pulse, but there is no trace of any spark breakdown up to about 700 ns. In fact, it never occurs even when observed on a much longer sweep speed

4 In Fig. 4, traces *e* to *k*, a close examination of the traces shows a small electron component of the pulse preceding the main electron component. The latter gradually develops in amplitude and resolves itself more and more from the smaller pulse with increasing gap length. The smaller pulse component seems to arise from the primary electron avalanches within the corona region which has extended considerably at higher gap lengths.

There is again no spark breakdown occurring in these cases.

5. In traces *e* to *k* we find alongside the main electron component pulse a gradually developing hazy and ill-focused broad pulse occurring at an increasing time delay from the main electron peak. Its amplitude has been found to be strongly sensitive to overvoltage of the gap. We suggest that the broad pulse is due to the secondary avalanches produced by electrons released from the negative ions of oxygen (O_2^-) formed by electron capture.

DISCUSSION

(i) *Estimation of electron avalanche size*

The carrier number n_e in the primary electron avalanche should now be estimated in order to justify our proposed explanation of the space-charge breakdown pulses. Values of α/p over a wide range of E/p values in some gases (Schlumbohm, 1959) are known, but they are hardly useful in our calculations because of the strong non-uniformity of the electric field and the presence of the corona region. We know, however, that in a pulse circuit where the potential developed across the external resistance ($\sim 100\Omega$) does not extend beyond a few times T_- (the electron transit time from the cathode to the anode), the time rise \dot{U} of the electron potential pulse $U(t)$ at any instant t is a measure of n_e through the relation

$$n_e = \frac{Cd^* \dot{U}}{ev_-} \quad \dots \quad (1)$$

$$= 0.7 \times 10^{10} \dot{U} d^*,$$

taking $C = 50pF$, $v_- = 5 \times 10^7$ cm/sec and \dot{U} in Volt/ns, where C is the total capacity of the discharge space, v_- the electron drift velocity, e the electronic charge and d^* the remaining gap length outside corona.

The values of n_e estimated by taking \dot{U} from our oscilloscopic traces for $d = 0.5, 1.2$ and 5.0 mm are shown in Table I, taking d for d^* approximately. The accuracy of the n_e values calculated is limited by the rise time of the oscilloscope (~ 20 ns/cm), as well as by the fact that we have used same v , for all the gaps, which may not be strictly correct. Even allowing for ~ 20 per cent uncertainty in the calculated values, their striking regularity with the gap length is remarkable.

TABLE I

$d \rightarrow$	0.5 mm	1.2 mm	5.0 mm
U_{obs}	50 V/10 ns	3 V/20 ns	0.5 V/50 ns
$n_{critical}$	1.7×10^9	1.2×10^8	$\sim 3 \times 10^7$

The avalanche magnitude comes out to be just critical ($\sim 10^8$) for streamer formation* at $d = 1.2$ mm. At $d = 0.5$ mm, n_e very much exceeds the critical value, and that is why the very fast spark breakdown pulse occurring here overlaps the primary electron pulse. Finally, at $d = 5.0$ mm, n_e falls below the critical value, and no streamer breakdown occurs here at all. The reason why the n_e value should fall below the critical value above a certain ' d ' must lie clearly in the electric field strength E_e^* prevailing at a distance r^* , i.e. just outside the corona region, at large gaps and the effective distance within d^* over which the gas amplification takes place (see section iii of discussion).

(ii) *The streamer delay time*

The time duration required for a visible potential rise to occur due to the streamer formation can be measured by the time delay T_d of the point C from the near saturation point B of the primary electron pulse (Fig. 5) on the oscillo-

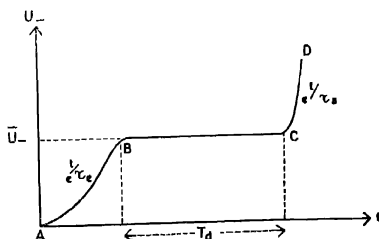


Fig. 5. Typical pulse potential variation with time defining the pulse characteristics. AB=rising primary electron pulse, BC=plateau region, CD=rapidly rising space-charge breakdown pulse.

*Raether (1959) has recently shown that the probability of streamer formation passes through a maximum, when $n_e \geq 10^9$. Hence the increase in the electron number $dn_e/dx > e^{an}$, i.e. there is an over exponential growth.

scope trace. This is an important characteristic in all the streamer phenomena. The time constants τ_c and τ_s are the other two pulse characteristics defining the rise time of the primary electron pulse and the spark breakdown pulse respectively. In general τ_s would be only a few nanoseconds and much shorter than τ_c , on account of the rapidly rising streamer at C . The delay time T_d depends strongly on the saturation (plateau) potential (Schlumbohm, 1962) of the electron pulse \bar{U}_- . As \bar{U}_- reaches the value corresponding to the primary avalanche magnitude $e^{ad} \geq 10^8$, a certain minimum positive ion density n_+ is attained and the space-charge field is strong enough to generate secondary electron avalanches due to gaseous photoelectrons (near the anode). These are at first too small to give any observable potential rise, but as time goes on, more and more space charges accumulate, till the time T_d has elapsed, when the streamer potential starts rising visibly above the plateau. Since T_d is governed by the exact moment of sufficient space-charge accumulation, it may have a large statistical fluctuation (Franke, 1960). Besides this, T_d has been found to depend on the formation of negative ions in certain gases (Schlumbohm, 1962) and the state of the overvoltage (Schlumbohm, 1962) across the gap.

In our photographs, a systematic increase in the delay time from zero to a few nanosecond at 1 mm and then to ~ 100 ns at 1.2 mm gap is noteworthy. This may arise due to a combination of various causes mentioned above. Many more photographs of the pulses at each gap length may have to be taken before assigning a definite reason to the delays, although a strong correlation of T_d with the gap length suggests itself, perhaps due to the gradually weakening field outside the corona region from 0.5 to 1.2 mm gap length.

(iii) *Influence of corona on the electric field distribution*

We have so far disregarded any possible influence of the corona formation on the spark counter action. In reality, the corona seems to play an important role and is something peculiar to the spark counter geometry where a very strong electric field normally exists at the anode wire surface and the field falls off rapidly outside.

In the atmospheric dry air the corona sets in at an electric field strength ≥ 30 KV/cm. A part of it generally contains feebly ionised invisible air molecules, and a visual corona of almost fully ionised gas sets in at a higher field strength ≥ 50 KV/cm nearer to the wire. The corona produces a strongly stabilising effect on the electrostatic stress between electrodes by increasing the wire-radius virtually to r^* , the extension of the visual corona, because the field outside the corona is substantially lower than the original field strength at the wire surface itself, and the chance of any electrical breakdown is therefore reduced.

In the cylindrical wire-to-plate system the field strength at a distance x from the axis of the wire of radius r at a potential V_r is given by

$$E_x = \frac{2d_0 V_r}{x(2d_0 - x) \ln(2d_0 - r)/r} \quad (2)$$

where d_0 = distance of the cathode (at zero potential) from the wire axis. The field strength E_r or E_r^* is maximum at the wire surface and is obtained by substituting $x = r$ or r^* in (2), according as we take the real or the virtual radius.

To calculate roughly the possible gas multiplication by electrons outside the corona, we have evaluated the electric field strength from (2) for two gap lengths $d_0 = 5$ mm and 20 mm at various values of x . A visual corona extension of ~ 2 wire diameters ($r^* \sim 0.2$ mm) is assumed for $d_0 = 5$ mm and ~ 5 wire diameters ($r^* \sim 0.5$ mm) for $d_0 = 20$ mm (from rough eye estimation).

The results of calculation are shown in Fig. 6. It will be seen that for $d_0 = 5$ mm, the electric field strength falls below 20 KV/cm at $x > 0.5$ mm, and

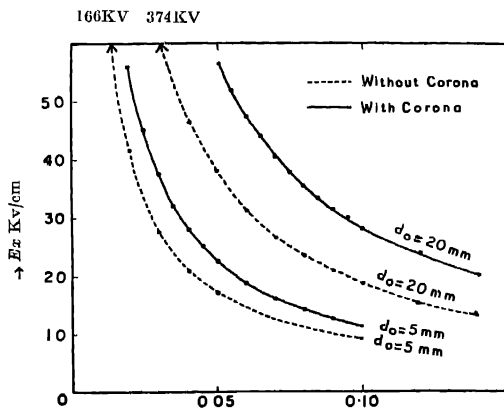


Fig. 6. Electric field strength for two gap lengths $d_0 = 5$ and 20 mm. Full line denotes the calculated field strength corrected for corona and the dotted line denotes the uncorrected field strength.

for $d_0 = 20$ mm, the field falls below 25 KV/cm at $x > 1$ mm, so that beyond these limits of x , the field-strengths are not generally sufficient for gas multiplication and may be left out of account.

The Townsend first coefficient $\alpha(x)$ varies strongly with E_x and can be roughly taken from Schlumbohm's (1959) data. By a graphical plot of $\alpha(x)$ against x

over the effective field region, the average value of αd and the corresponding gas multiplication factor $e^{\alpha d}$ are calculated and shown in Table II. Assuming that an α -particle releases on an average about 1000 electrons in the effective field region the total gas multiplication will be about 10^5 and $10^{3.5}$ in the two cases respectively. These are considerably below the critical value of 10^9 required for streamer formation. The absence of spark breakdown at large gap lengths is thus qualitatively understood.

TABLE II

d_0	corona extension (x^*)	E_r^* KV/cm	Averaged (αd)	$(\alpha d)_{av.}$ e
5 mm	0.2 mm	56.3	3.6	10^2
20 mm	0.5 mm	57.0	8.2	$10^{3.5}$

It is clear from the above two typical cases of field calculation that the increasing extension of corona has a greater stabilising effect on the electrical field outside it, in that the field distribution in the gap tends more towards homogeneity. As a result, the value of αd over the effective field region increases with gap length, giving higher gas multiplication $e^{\alpha d}$.

There is yet another important consequence of the corona phenomenon which is prominent at large gaps. The normal corona region is almost field free on account of strong positive ion density existing over this region. As an α -particle enters the corona region, it releases a large number of electrons very close to the wire which momentarily destroy the normal corona effect and build up a strong field close to the wire. This may exist for a very short time during which the electrons are all collected at the wire and the corona is reestablished. There is, therefore, a weak corona electron pulse of fast rise time having a long plateau, from which eventually will start the main primary electron pulse from outside the corona. The latter may be delayed considerably (upto ~ 100 ns), because during the transition period of the restoration of corona, the field strength at the corresponding points would be much weaker than what would have been with the corona fully established (Fig. 6). The plateau length will depend on the extension of the corona region which increases with the increasing gap length (traces e to k).

This is, therefore, another form of the space-charge effect induced by the α -particle within the corona. It shows itself by a two-step appearance of the primary electron pulse, as is clearly seen in our traces from e to k in Fig. 4.

In small gaps up to $d = 1.2$ mm, the corona extension is very little and the average electric field strength extending up to the cathode outside the corona is stronger than at higher gap lengths. The corona electron collection is therefore much weaker and faster (may not be observable at all), whereas the main electron

component will be much stronger, and may merge into the corona pulse, as appears to be the case in Fig 3 (traces *a* to *d*).

ACKNOWLEDGMENTS

The authors are thankful to Professor R. C. Majumdar, Head of the Department of Physics and Astrophysics, University of Delhi, for giving them facilities to carry out the investigations. Thanks are also due to Mr. Gurbux Singh of the Institute of Nuclear Medicine and Allied Sciences, Delhi-6, for many helpful discussions and suggestions.

REFERENCES

- Connor, R. D., 1952, *J. Sci. Instr.*, **29**, 12.
- Floury, J., 1959, Proc. of the International Symposium on Nuclear Electronics (International Atomic Energy Agency, Wien, Austria), p. 259.
- Franke, W., 1960, *Zeit. f. Physik*, **158**, 96.
- Gupta, S. L. and Saha, N. K., 1961, *Nucl. Instr. and Meth.*, **13**, 258.
- Gupta, S. L. and Saha, N. K., 1962, *Nucl. Instr. and Meth.*, **15**, 95.
- Kawata, S., 1961, *J. Phys. Soc. (Japan)*, **18**, 1.
- Loeb, L. B., 1956, *Encyclopedia of Physics*, ed. S. Flugge (Springer-Verlag), **22**, 445.
- Loeb, L. B., et al., 1948, *J. Appl. Phys.*, **19**, 797.
- Loeb, L. B., 1955, *Basic Processes of Gaseous Electronics*, Univ. of California Press, Berkeley.
- Meek, J. M. and Craggs, J. D., 1963, *Electrical Breakdown of Gases*, Clarendon Press, Oxford.
- Pennung, F. M., 1957, *Electrical Discharges in Gases*, Philips Technical Library, Eindhoven, Holland.
- Pfau, J. and Raether, H., 1959, *Zeit. f. Physik*, **153**, 523.
- Raether, H., 1961, *Ergebnisse der Exakt. Naturwiss.*, **33**, 75.
- Raether, H., 1959, Proc. of the fourth International Conference on Ionisation Phenomena in Gases, Uppsala (North-Holland Publishing Company, Amsterdam, 1960), p. IB 105, 121.
- Saha, N. K. and Nath, N., 1957, *Nucleonics*, **15**, 94.
- Savel, M. P., 1952, *Compt. Rend.*, **234**, 2596.
- Schlumbohm, H., 1959, *Z. Angewandte Physik*, **11**, 156.
- Schlumbohm, H., 1962, *Zeit. f. Physik*, **170**, 233.

Letters to the Editor

The Board of Editors will not hold itself responsible for opinions expressed in the letters published in this section. The notes containing reports of new work communicated for this section should not contain main figures and should not exceed 500 words in length. The contributions must reach the Assistant Editor not later than the 15th of the second month preceding that of the issue in which the letter is to appear. No proof will be sent to the authors.

15

DATING OF SOME NUCLEAR EXPLOSIONS FROM RADIO-ACTIVE FALL-OUT MEASUREMENTS IN CALCUTTA

SUSHIL KUMAR DAS, M. DEB ROY* and S. D. CHATTERJEE

DEPARTMENT OF PHYSICS, JADAVPUR UNIVERSITY, CALCUTTA

(Received for publication, September 11, 1963)

Measurements of the intensity and nature of radio-active fall-out has been systematically carried out in our laboratory since the inception of the last nuclear test series. During the course of our investigation, numerous samples of radio-active fall-out were collected both from rain-borne dusts and from military aeroplanes making routine flights upto altitudes of about 40,000 ft. The samples having high specific activity were normally used for determining the dates of explosion, following the method of Yamasaki and Kaneko¹ as discussed below :

It is well-known that the gross activity of fall-out due to an atomic explosion is given by

$$I_t = I_0 t^{-n}, \quad \dots (1)$$

where I_0 is the activity at the end of unit time (say one day) after the explosion and I_t is that after ' t ' days, and ' n ' usually takes a value between 1.2 and 1.7^{2,3,4,5}. Since the date of explosion T_0 is unknown, the measurements on the samples are made on dates T_1 and T_1' giving activity I_1 and I_1' . Then,

$$\left. \begin{aligned} I_1 &= I_0 t_1^{-n} \\ I_1' &= I_0 t_1'^{-n} \end{aligned} \right\} \quad \dots (2)$$

and

where $t_1 = T_1 - T_0$, $t_1' = T_1' - T_0$ i.e. the time elapsed from the date of explosion.

Squadron Leader, Kalaikunda Air Station, West Bengal.

Putting $T'_1 - T_1 = t'_1 - t_1 = \tau_1$, we obtain from equation (2)

$$\tau_1 = \{(I_1/I'_1)^{1/n} - 1\}t_1, \quad (3)$$

and if we take T'_1 so that the ratio I_1/I'_1 becomes equal to any value K (say 2) and repeat the same procedure at least once more and determine the dates T'_2 for any arbitrary T_2 and so on, satisfying the relation $I_m/I'_m = K$, we obtain a straight line on a $\tau-t$ diagram. Its slope gives the value of ' n ', and by an extrapolation to $\tau = 0$, we can find the date where $t = 0$, i.e. T_0 .

The actual procedure is to measure the β -activity of a sample from time to time, and the counting rates thus obtained are plotted as a function of the date of measurement on a semilogarithmic paper as shown in Figs 1(A) and 2(A). Taking I_1 as the initial count corresponding to any arbitrary time T_1 (date of initial

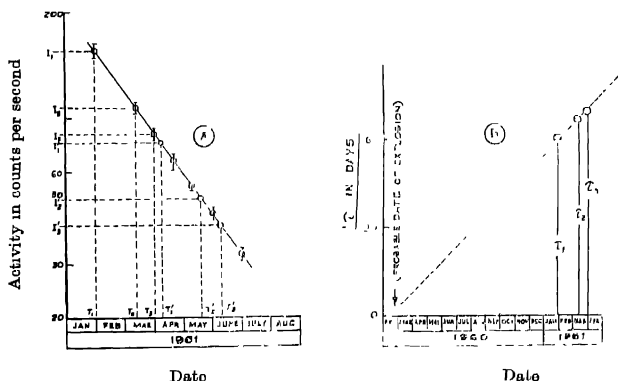


Fig. 1. The determination of I_m and T_m ($I_m/I'_m = 2$) The determination of T_0 .

measurements) one measures I'_1 (equal to, say $\frac{1}{2} I_1$) and determine T'_1 . T_1 and $\tau_1 = T'_1 - T_1$ are thus obtained. Repeating the same procedure, T_2 and τ_2 , T_3 and τ_3 , and so on are obtained. The values of ' τ ' are plotted as a function of the date of measurement ' T ' on a graph paper as shown in Figs. 1(B) and 2(B). These plots should lie on a straight line so long as ' n ' remains constant throughout the measurements. Then the straight line is extrapolated back to τ_0 , and the date of explosion T_0 is found.

The results of two typical cases are given below, one of which (case 1) corresponds to the French test in Sahara on 13th February 1960, while the other (case 2) relates to the Russian '50' megaton Hydrogen Bomb test in the Arctic region on 23rd October 1961.

Case 1

The sample was collected on 30th January, 1961. Fig. 1(A) shows the decay curve plot of β -activity measurements extending over a period of about seven months. The date of explosion has been determined from the plot in Fig. 1(B). The extrapolated date of explosion in this case has been found to be 12th February 1960, while the actual date of French test in Sahara was 13th February 1960. The value of ' n ' in this case has been found to be 1.2.

Case 2.

The sample was collected on 3rd January 1962. Fig. 2(A) shows the decay curve plot of β -activity measurements extending over a period of about

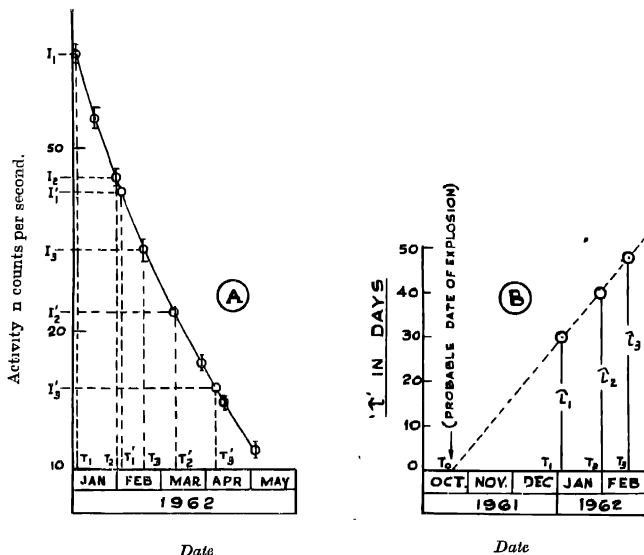


Fig. 2. The determination of I_m and T_m ($I_m/t_m = 2$)

The determination of T_0

six months. The date of explosion has been determined from the plot in Fig. 2(B). The extrapolated date of the explosion in this case has been found to be 21st October 1961, while the actual date of Russian '50' Megaton Hydrogen Bomb explosion was 23rd October 1961. The value of ' n ' in this case has been found to be 1.3.

It is interesting to note that the β -activity of the radio-active debris from the Russian Megaton bomb explosion, as shown in Fig. 2(A), exhibits a rapid rate

of decay while that from the French atomic bomb as shown in Fig. 1(A). exhibits a relatively slower rate of decay.

We are indebted to Air Vice-Marshal K. L. Sondhi, Air Officer Commanding in Chief, the then Eastern Air Command, for giving us every facilities to attach our equipments into Fighter planes in order to collect the radio-active dust samples over Calcutta.

REFERENCES

- Yamasaki, F. and Kanoko, H , 1955, *Jour. Sci. Research Ins.* , **49**, 137
Yamasaki, F., 1952, *J. Sci. Res. Inst.* , **46**, 59.
Abribat, M., Pouradier, J. and Venet, A. M , 1952, *Compt. rend.* , **235**, 157
Clark, H. M , 1954, *Science*, **119**, 619
Chatterjee, S., Patro, A. P., Basu, B., Bhattacharyya, R. L., and Banerjee, M. 1955, *Science & Culture*, **20**

AN X-RAY STUDY OF RUTHENIUM BIGUANIDE SULPHATE

K. N. GOSWAMI and SANKAR K. DATTA

INDIAN ASSOCIATION FOR THE CULTIVATION OF SCIENCE, CALCUTTA-32

(Received for publication, August 9, 1963)

Biguanide combines with many elements of the transition series to give highly coloured chelate complexes of the inner-metallic type. Though the complex compounds of biguanide with copper (II) and nickel (II) were described more than three quarters of century ago, their structure forms a subject of controversy to the present time and a number of possible structures (Ray, 1961) have been proposed. The crystal structure of ruthenium salt of biguanide $[\text{Ru}(\text{C}_2\text{H}_7\text{N}_3)_3]_2(\text{SO}_4)_3 \cdot 7\text{H}_2\text{O}$ (Sen, 1962) has been undertaken in order to determine the nature of metal-biguanide bond

A sample of ruthenium biguanide sulphate was kindly made available to us by Dr. D. Sen, Department of Inorganic Chemistry, Indian Association for the Cultivation of Science, Calcutta. Crystals were prepared by slow evaporation of hot aqueous solution. The crystals were needle shaped, brownish yellow in colour. All these crystals have developed the forms $\{100\}$, $\{104\}$ and $\{001\}$.

The parameters of the unit cell were determined by oscillation and Weissenberg photographs using $\text{CuK}\alpha$ radiation. The crystals were dusted with aluminium powder so as to standardize the radius of the camera.

The parameters are :

$$\begin{aligned} a &= 20.26 \text{ \AA} \pm .02 \\ b &= 11.65 \text{ \AA} \pm .05 \\ c &= 22.19 \text{ \AA} \pm .02 \\ \beta &= 117^\circ 48' \end{aligned}$$

Systematic extinctions were observed for (*h**o**l*) when $l \neq 2n$, and for (*o**k**o*) when $k \neq 2n$. The space group was therefore determined as P_{21}/C . This space group has four fold general positions and consequently one molecule of the chelate forms the asymmetric unit.

The density, obtained by flotation method in a mixture of Carbon tetrachloride and bromoform, was found to be 1.755 gm cm^{-3} . The calculated density for four molecules per unit cell is 1.754 gm.cm^{-3} . Further work is in progress.

ACKNOWLEDGEMENTS

Authors wish to express their sincere thanks to Prof. B. N. Srivastava, D.Sc., F.N.I., for his keen interest in this work, and to Dr. D. Sen who supplied the sample.

REFERENCES

- Ray, P., 1961, *Chem. Rev.*, **61**, 313.
Sen, D., 1962, *Science and Culture*, **28**, 84.

CONTENTS

Indian Journal of Physics

Vol. 37, No. 11

November, 1963

PAGE

61. A 1.2 cm E.P.R. Spectrometer and Paramagnetic Resonance in some Copper Salts—U. S. Ghosh, R. N. Bagchi and A. K. Pal ... 555
 62. A Note on the Electrostatic Model of Hydrogen Bond Applied to Hydrogen Bonding in Aniline and Substituted Anilines in Different Environments—G. S. Kastha and K. C. Medhi ... 568
 63. Excitation of Hydrogen Atom in fast Encounter with Negative Hydrogen Ion—B. K. Guha ... 574
 64. A Jewel Mounted Micro-balance for the Measurement of Magnetic Susceptibilities of Crystals—(Miss) D. Das ... 582
 65. Electrical Breakdown in Spark Counter—N. K. Saha and S. L. Gupta ... 590
- LETTERS TO THE EDITOR—
15. Dating of some Nuclear Explosions from Radio-Active fall-out Measurements in Calcutta—Sushil Kumar Das, M. Deb Roy and S. D. Chatterjee ... 600
 16. An X-ray Study of Ruthenium Biguanide Sulphate—K. N. Goswami and Sankar K. Dutta ... 604

Regd. No. C-3911

VOL. 37. INDIAN JOURNAL OF PHYSICS No. 12

(Published in collaboration with the Indian Physical Society)

AND

VOL. 46 PROCEEDINGS No. 12

OF THE

**INDIAN ASSOCIATION FOR THE
CULTIVATION OF SCIENCE**

DECEMBER 1963

**PUBLISHED BY THE
INDIAN ASSOCIATION FOR THE CULTIVATION OF SCIENCE
JADAVPUR, CALCUTTA 88**

BOARD OF EDITORS

K. BANERJEE	D. S. KOTHARI
D. M. BOSE	B. D. NAG CHAUDHURI
S. N. BOSE	K. R. RAO
S. D. CHATTERJEE	D. B. SINHA
P. S. GILL	S. C. SIKKAR (<i>Secretary</i>)
S. R. KHASTGIR	B. N. SRIVASTAVA

EDITORIAL COLLABORATORS

PROF. R. K. ASUNDI, Ph.D., F.N.I.
PROF. D. BASU, Ph.D.
PROF. J. N. BHAR, D.Sc., F.N.I.
PROF. V. G. BHIDE, Ph.D. (Nag), Ph.D. (Lond).
PROF. A. BOSE, D.Sc., F.N.I.
PROF. S. K. CHAKRABARTY, D.Sc., F.N.I.
DR. J. S. CHATTERJEE
DR. K. DAS GUPTA, Ph.D.
PROF. N. N. DAS GUPTA, Ph.D., F.N.I.
DR. J. DHAR, D.Phil. (So)
PROF. A. K. DUTTA, D.Sc., F.N.I.
PROF. C. S. GHOSH, M.Sc., S.M., F.N.I., M.I.E.E.
PROF. S. GHOSH, D.Sc., F.N.I.
PROF. S. N. GHOSH, D.Sc.
PROF. S. GUPTA, M.Sc., F.N.I.
PROF. D. N. KUNDU, Ph.D., F.N.I.
PROF. R. C. MAJUMDER, Ph.D., F.N.I.
PRINCIPAL Y. G. NAIR, Ph.D.
PROF. S. R. PALIT, D.Sc., F.R.I.C., F.N.I.
PROF. H. RAKSHIT, D.Sc., F.N.I.
PROF. A. SAHA, D.Sc., F.N.I.
DR. VIKRAM A. SARABHAI, M.A., Ph.D., F.N.I.
DR. A. K. SENGUPTA, D.Sc.
PROF. NAND LAL SINGH, D.Sc.
DR. M. S. SINHA, D.Sc., F.N.I.
PROF. N. R. TAWDE, Ph.D., F.N.I.
DR. P. VENKATESWARLU

NOTICE

TO INTENDING AUTHORS

Manuscripts for publication should be sent to the Assistant Editor, Indian Journal of Physics, Jadavpur, Calcutta-32.

The manuscripts submitted must be type-written with double space on thick foolscap paper with sufficient margin on the left and at the top. The original copy, and not the carbon copy, should be submitted. Each paper must contain an abstract at the beginning.

All references should be given in the text by quoting the surname of the author, followed by year of publication, e.g., (Ghosh, 1954). The full reference should be given in a list at the end, arranged alphabetically, as follows; Ghosh, D. K., 1954, *Ind. J. Phys.*, 28, 485.

Line diagrams should be drawn on white Bristol board or tracing paper with black India ink, and letters and numbers inside the diagrams should be written neatly in capital type with India ink. The size of the diagrams submitted and the lettering inside should be large enough so that it is legible after reduction to one-third the original size. A simple style of lettering such as gothic, with its uniform line width and no serifs should be used,

A·B·E·F·G·M·P·T·W·

Photographs submitted for publication should be printed on glossy paper with somewhat more contrast than that desired in the reproduction, and should, if possible, be mounted on thick white paper.

Captions to all figures should be typed in a separate sheet and attached at the end of the paper.

The mathematical expressions should be written carefully by hand. Care should be taken to distinguish between capital and small letters and superscripts and subscripts. Repetition of a complex expression should be avoided by representing it by a symbol. Greek letters and unusual symbols should be identified in the margin. Fractional exponents should be used instead of root

Annual Subscription—

Inland Rs. 25.00

Foreign £ 2-10-0 or \$ 7.00

BENGAL CHEMICAL & PHARMACEUTICAL WORKS LD.

Pioneer Indian Manufacturers of Pharmaceuticals & Chemicals.

Manufacturers of:

Pharmaceutical Chemicals:

Caffeine and its salts, Strychnine Hydrochlor, Strychnine Sulphate, Brucine Sulphate, Nicotinic Acid, B.P., Nicotinamide, B.P., Potassium Citrate B.P., I.P., Sodium Citrate B.P., I.P., Potassium Acetate B.P., I.P., Potassium Iodide B.P., I.P., Sodium Iodide B.P., I.P., Ferri et Ammon Citrate B.P., I.P., and various other Pharmaceutical Chemicals.

Heavy & Reagent Quality Fine Chemicals:

Alum, Alum Sulphate (Iron Free), Ferro Alum, Zinc Chloride Tech. Naphthalene Pure, Sodium Citrate A.R., Potassium Citrate A.R., Magnesium Sulphate A.R., Sodium Sulphate Anhydrous A.R., Potassium Iodide A.R., Sodium Chloride A.R., Zinc Sulphate A.R., and various other reagent quality analytical chemicals.

Please refer your enquiries for the above items and other chemicals in the line to :—

BENGAL CHEMICAL

6, GANESH CHUNDER AVENUE,
CALCUTTA-13, INDIA.

(INDIA MADE)

X'RAY DIFFRACTION APPARATUS

Complete with

MACHLETT SHOCKPROOF BERYLLIUM WINDOW SEALED TUBES OF
DIFFERENT TARGET MATERIALS.

SINGLE VALVE HALF-WAVE RECTIFIED OR TWO VALVE
FULL-WAVE RECTIFIED.

MACHINE already incorporates voltage compensator to compensate plus
or minus 15 volts supply change.

Electro-Magnetic, Electronic, Servo-Mechanical or Chemo-Electric STABILISER
can be added to the filament circuit or
to the entire MACHINE for further STABILISATION.

CAMERAS OF VARIOUS TYPES CAN ALSO BE SUPPLIED
FOR THE MACHINE.

ALSO

X'RAY PLANT FOR BIOLOGICAL RESEARCH & INDUSTRIAL RADIOGRAPHY
AND HIGH TENSION TESTING SETS.

DELIVERY EX-STOCK : : NO LICENCE REQUIRED.

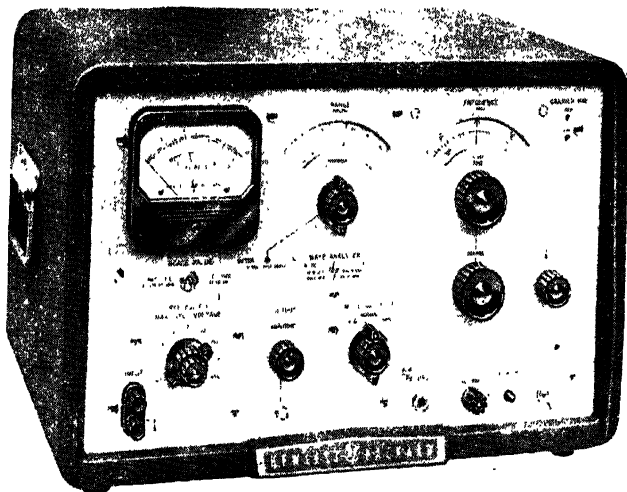
Further details from :-

RADON HOUSE P. LTD.,

7, Sirdar Sankar Road, Calcutta-26.

HEWLETT PACKARD

NEW: HIGHLY SELECTIVE: TRANSISTORIZED: MEASURES WAVE
Components Directly
302A WAVE ANALYZER



The new Model 302A Wave Analyzer represents a significant improvement in wave analyser design—completely transistorized, sophisticated in design, highly selective, free of tedious calibration and stabilization before use, are a few of the important convenience and accuracy features.

Specifications :-

Frequency range	— 20 cps to 50 KC
Frequency calibration	— Linear graduation 1 division per 10 cycles.
Warm up time	— Nil
Input Impedance	— Determined by setting of input attenuator: 100000 ohms on 4 most sensitive ranges, 1 megohm on remaining ranges.

For further particulars, please write to :

Sole Distributors :

**THE SCIENTIFIC INSTRUMENT
COMPANY, LIMITED.**

ALLAHABAD : BOMBAY : CALCUTTA : MADRAS :
NEW DELHI

Head Office : 6, Tej Bahadur Sapru Road, Allahabad



the projector lens were free from spherical aberration, all axial as well as marginal rays from MN which are parallel to the optic axis, would pass through the focal point of the lens F_0 . Hence the object point M would have Q as its image point on the screen. But due to spherical aberration of the lens L , the marginal ray MA would cross the axis at F which is nearer to the lens than F_0 . Thus the point Q' will be really the image of M and QQ' will be the amount of distortion of the point Q . From Fig. 1

$$\begin{aligned}
 QQ' &= PQ' - PQ = PF \tan \alpha - PF_0 \tan \alpha_0 \\
 &= (PF_0 + \Delta Z) \cdot OA/OF - PF_0 \cdot OA/OF_0 \\
 &= (V - f + \Delta Z) \cdot \frac{r_a}{f - \Delta Z} - (V - f) \cdot \frac{r_a}{f} \\
 &= r_a \left[\frac{V - f + \Delta Z}{f} \right] \left(1 + \frac{\Delta Z}{f} \right) - (V - f) \cdot \frac{r_a}{f}, \text{ as } \Delta Z < f \\
 &= r_a \cdot \frac{\Delta Z \cdot V}{f^2} = r_a \cdot \frac{\Delta Z}{f} \cdot \frac{V}{f} = \frac{r_a \Delta Z}{f} (M_p - 1) \\
 &= \frac{r_a \Delta Z}{f} \cdot M_p, \text{ if } M_p \gg 1 \quad \dots (1)
 \end{aligned}$$

where r_a is the radius of the aperture fitted to the projector pole piece, V is the distance of the screen from the pole piece centre, M_p is the magnification of the projector lens. Here ΔZ is the amount of longitudinal spherical aberration, which can be expressed, according to Liebmann (1949), as

$$\Delta Z = C_s \cdot \left(\frac{r_a}{f} \right)^2 \quad \dots (2)$$

where C_s is the spherical aberration constant of the lens. From the equations (1) and (2), the amount of distortion is given by

$$QQ' = d = C_s \cdot M_p \left(\frac{r_a}{f} \right)^3 \quad \dots (3)$$

Now, the focal length of a projector lens is given by

$$f = V/(M_p + 1) = \frac{V}{M_p}, \text{ if } M_p \gg 1 \quad \dots (4)$$

Therefore equation (3) can be written as

$$C_s = \frac{d}{(M_p)^3} \cdot \left(\frac{V}{r_a} \right)^3 \quad \dots (5)$$

The method underlying the measurement of d is as follows. Let the illuminated circle in Fig. 2 represent the image of the aperture fitted with the projector pole

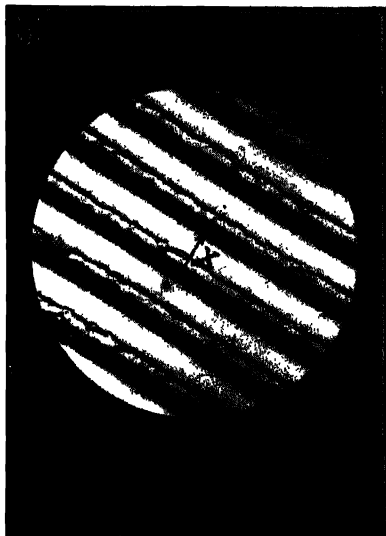


Fig. 2 A typical micrograph of a grating replica

piece. The lines thus projected within the illuminated circle are the rulings of a grating replica whose mean spacing width W is known. If X , the width of the central spacing in the micrograph, be measured, then

$$M_T = X/W \quad \dots (6)$$

and

$$M_p = M_T/M_o \quad \dots (7)$$

where M_T , M_p and M_o are the total, the projector and the objective lens magnifications respectively. Hence the aberration-free radius of the projector aperture in the micrograph should be given by

$$R_0 = r_a \cdot M_p \quad \dots (8)$$

If the radius of the aperture as measured on the micrograph be R_a , then the amount

of distortion d , at the projector lens magnification M_p and for the aperture radius r_a , is obviously expressed as

$$d = R_a - R_0 \quad \dots (9)$$

Hence, working with an aperture of known bore radius r_a , and knowing the distance of the screen from the pole piece centre of the projector lens, the projector lens magnification M_p and the corresponding distortion d , the spherical aberration constant C'_s of the lens can be found out with the help of equation (5).

EXPERIMENTAL METHOD AND RESULTS

A grating replica of known grating constant was chosen as the object and the microscope was operated at 60 kv at a constant objective lens magnification of 75 15X. To test the uniformity of the grating spaces, several micrographs were taken with different grating space at the centre of the field of view at a constant magnification of both the objective and projector lenses. From about 30 micrographs thus taken, the widths of the grating spacings were found to vary within ± 4 per cent of the mean value. Then a particular grating space was brought to the centre of the field of view and micrographs were taken at several settings of the projector lens current, which were noted and are shown in column 1 in Table I. Since the object occupies a very small zone around the optic axis, paraxial imaging condition may be assumed and the images of the grating space in the centre of the field of view may be considered to be free from aberration. The width of the central spacings of the micrographs at the various magnifications were measured. Dividing these widths by the grating constant W , the total magnification M_T of the different micrographs were estimated, and by further dividing these total magnifications by the objective lens magnification M_o , the corresponding magnifications due to the projector lens M_p were calculated as shown in column 2 of Table I.

The radii R_a of the circular contour of the micrographs, taken at different projector lens magnifications, were measured and tabulated in column 3 of Table I. With the help of equation (8), the aberration-free radii R_0 of the micrographs were calculated and entered in the 4th column of Table I, where, in column 5, the respective amount of distortions as obtained from equation (9) are also shown. With these values of M_p and d of the columns 2 and 5 respectively in Table I and with the fixed value of $V = 367$ mm and $r_a = 0.1925$ mm the corresponding C'_s values were calculated and tabulated in column 6 of Table I.

DISCUSSION

In the literature, C'_s is usually expressed in terms of the pole piece bore radius R as a function of the lens excitation NI . For the lens excitation, however, a parameter k^2 is used where k^2 is given by

TABLE I
 $r_a = 0.1925$ mm, $M_0 = 75.15$, $I = 367$ mm

Projector lens current I in mA	Magnification of the projector lens $M_p = M_T / M_0$	Measured radius R_a in mm	Aberration free radius $R_a - r_a < M_p$ in mm	Distortion $d = R_a - R_0$ in mm	Spherical aberration constant $C_s = \frac{d}{(M_p)^2} = \left(\frac{V}{r_a} \right)^{-1}$
1	2	3	4	5	6
75	76.56	16.0	14.74	1.26	244.5
90	104.8	22.1	20.20	1.90	106.4
100	128.3	26.9	24.71	2.19	54.80
105	140.9	29.6	27.14	2.46	41.48
118	170.0	35.6	32.73	2.87	23.81
125	191.8	40.2	36.92	3.28	16.55
130	196.4	41.2	37.81	3.39	15.53
135	207.5	43.5	39.94	3.56	13.09
140	226.0	47.1	43.52	3.88	10.17

$$k^2 = \beta(NI)^2/\phi, \quad \dots (10)$$

where NI is the ampere turns of the lens winding, $\phi = \phi(1 \pm 0.978 \times 10^{-6}\phi)$ is the relativistically corrected accelerating voltage, and β is a factor which depends on pole piece parameter viz. bore radius R or bore diameter D , and spacing S . Magnitudes of β for various values of S/D have been given by Liebmann *et al.* (1951), from which for our case, with $D = 1.0$ mm, $S = 1.0$ mm, the corresponding value of β is 0.006, and since the beam energy is 60 kv, equation (10) can be written as

$$k^2 = 9.448 \times 10^{-8}(NI)^2 \quad (11)$$

The number of coils in our case is 12,650, hence from equation (11) k^2 values were calculated with different values of lens current I (column 1, Table I). For our case, the values of k^2 , thus obtained, were plotted against C_s/R (curve P), as shown in Fig. 3 where the computed values of C_s/R (curve LG) obtained from Liebmann and Grad's (1951) data are also shown for comparison.

CONCLUSION

It is shown that the experimental values of C_s/R , represented here, are consistently higher than the values of Liebmann *et al.* (1951), whose results are obtained analytically. However, at the maximum attainable value of the projector lens

magnification $226\times$, the amount of distortion is 8.9 per cent, which seems to be a very reasonable value. So, it may be concluded that, from the practical point

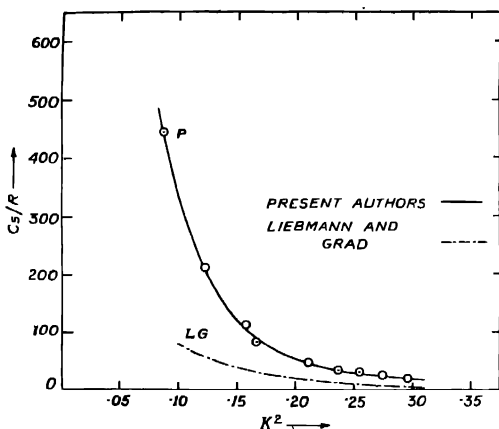


FIG. 1. Variation of C_s/R with the excitation parameter, K^2 .

of view, the values of spherical aberration constants at different magnifications, that are represented here, may be used with more confidence than those obtained analytically.

ACKNOWLEDGMENT

The authors are indebted to Prof. N. N. Das Gupta and Mr. M. L. De for valuable discussions. One of the authors (D. N. M.) is indebted to the Ministry of Scientific Research and Cultural Affairs, Govt. of India, for the award of a Research Training Scholarship.

REFERENCES

- Liebmann, G., 1949, *Proc. Phys. Soc., B*, **62**, 753.
- Liebmann, G. and Grad, E. M., 1951, *Proc. Phys. Soc., B*, **62**, 956.
- Zworykin, V. K. and others, 1948, *Electron Optics and the Electron Microscope*, 1st Ed., p. 639, p. 640.

ELECTRON CAPTURE BY He^+ IONS PASSING THROUGH He ATOMS

D. M. BHATTACHARYA, S. C. MUKHERJEE and N. C. SILL

DEPARTMENT OF THEORETICAL PHYSICS, INDIAN ASSOCIATION FOR THE CULTIVATION
OF SCIENCE, CALCUTTA-32

(Received, October 21, 1963)

ABSTRACT. The expression for the cross section of the electron capture by He^+ ions passing through normal He atoms has been derived by applying a variational method. The effect of exchange of the electrons and the influence of their transitory motion on the cross section have been taken into account.

INTRODUCTION

The first theoretical investigation of charge exchange between He^+ ions and He atoms has been done by Massey and Smith (1933) with the perturbed stationary states method which has been further applied by Dallaportea and Bonfiglioli (1943), Firsov (1951), Jackson (1954) and Moiseiwitsch (1956). The above authors have used a linear combination of the two lowest helium molecular ion states like He_2^+ , viz, the ground state which is symmetric with respect to the exchange of the two nuclei and the antisymmetric state just above the ground state and have approximately solved the time dependent Schrodinger equation. In the above method the cross section depends mainly on the difference of the electronic binding energies of those two states for which Massey and Smith have used, with suitable extension, the electronic energy for He_2^+ calculated by Pauling. The range of energies of the incident ion covered by Massey and Smith was from 500 ev. to 12 kev, whereas the same was further extended by Jackson from 200 ev. to 100 kev. Moiseiwitsch covered a still wider range of energies from 0.1 ev to 10 kev, further he used three sets of wave function to calculate the electronic binding energies. For the high energy region (100 kev. to 700 kev.) Schiff (1954) has given an estimate of the electron capture cross section for He^+ ions passing through He atoms by applying Born approximation method; he has used complete interaction including the nucleus-nucleus interaction in the Hamiltonian and has assumed unit effective charge of the incident ionized helium atom. Snitzer (1953) has experimentally measured the capture cross section for He^+ ions on He atoms for the energy region 100 kev. to 450 kev. further extension has been made recently by Everhart and his collaborators (1963) who covered a wide range of incident ion energy starting from 0.4 kev, to 25 kev. Everhart *et al* have further

observed that at a fixed scattering angle, the electron capture probability when plotted against the incident ion energy gives several resonant peaks and valleys

In the present paper we have derived the expression for electron capture by He^+ ions passing through He atoms by applying a variational method which is valid for both moderately high and low velocities of the incident ions. In our formulation the momentum transfer term is included in the wave function and the effect of exchange of electrons is taken into account.

THEORY

We consider the capture of an electron from the ground state of a helium atom A by the singly ionised helium ion B . We assume the nuclei B and A move with uniform velocities $\frac{1}{2}\mathbf{v}$ and $-\frac{1}{2}\mathbf{v}$ respectively, the effect of the nucleus-nucleus interaction is neglected. Initially at $t = -\infty$ we have the two electrons attached to the nucleus A and one in nucleus B . We symmetrize the initial state wave functions by taking proper account of the effect of electron exchange.

The time rate of change of electron state wave function is given by the time-dependent Schrödinger equation

$$H\psi = i\hbar \frac{\partial \psi}{\partial t} \quad \dots (1)$$

where H is the Hamiltonian corresponding to the motion of the electrons in the coulomb field of the two nuclei

$$H = -\frac{\hbar^2}{2m} \sum_{i=1,2,3} \nabla_i^2 + V, \quad V = -2e^2 \sum_{i=1,2,3} \left(\frac{1}{r_{Ai}} + \frac{1}{r_{Bi}} \right) + e^2 \sum_{i,j} \frac{1}{r_{ij}}$$

and \mathbf{r}_{Ai} , \mathbf{r}_{Bi} are the position vectors of the i -th electron from the nucleus A and B respectively and r_{ij} 's are the inter electronic distances. The Schrödinger equation (1) is obtained by making stationary the following variation integral I ,

$$I = \int \left(\frac{1}{2} \bar{\psi} H \psi - \frac{1}{2} \psi H \bar{\psi} + \frac{1}{2} i\hbar \bar{\psi} \frac{\partial \psi}{\partial t} - \frac{1}{2} i\hbar \psi \frac{\partial \bar{\psi}}{\partial t} \right) d\mathbf{v} dt \quad \dots (2)$$

with respect to small arbitrary variation of ψ and $\bar{\psi}$ for a suitable approximation, we choose a trial wave function ψ_T ,

$$\psi_T = A(t)\psi_i + B(t)\psi_f \quad \dots (3)$$

where ψ_i is the product of the two ground state wave functions, one for the helium atom with the nucleus A and the other for the ionised helium atom with the

Electron Capture by He^+ Ions Passing through He Atoms 613

nucleus B , ψ_f is the product with A and B interchanged. Here we have restricted our calculations to two electron states. The ψ_i and ψ_f can be written as

$$\psi_i = \frac{1}{\sqrt{3}} (\psi_1 + \psi_2 + \psi_3) - (4\alpha), \quad \psi_f = \frac{1}{\sqrt{3}} (\psi_1' + \psi_2' + \psi_3') \quad (4b)$$

$$\text{where} \quad \psi_1 = u_A(2, 3) v_B^+(1) \left\{ \frac{\alpha(2) \beta(3) - \alpha(3) \beta(2)}{\sqrt{2}} \right\} \alpha(1)$$

$$\psi_2 = u_A(3, 1) v_B^+(2) \left\{ \frac{\alpha(3) \beta(1) - \alpha(1) \beta(3)}{\sqrt{2}} \right\} \alpha(2)$$

$$\psi_3 = u_A(1, 2) v_B^+(3) \left\{ \frac{\alpha(1) \beta(2) - \alpha(2) \beta(1)}{\sqrt{2}} \right\} \alpha(3)$$

$$\psi_1' = v_B(2, 3) u_A^+(1) \left\{ \frac{\alpha(2) \beta(3) - \alpha(3) \beta(2)}{\sqrt{2}} \right\} \alpha(1)$$

$$\psi_2' = v_B(3, 1) u_A^+(2) \left\{ \frac{\alpha(3) \beta(1) - \alpha(1) \beta(3)}{\sqrt{2}} \right\} \alpha(2)$$

$$\psi_3' = v_B(1, 2) u_A^+(3) \left\{ \frac{\alpha(1) \beta(2) - \alpha(2) \beta(1)}{\sqrt{2}} \right\} \alpha(3)$$

ψ_1, ψ_2, \dots etc are each normalised, the factor $1/\sqrt{3}$ in equations (4a and 4b) is included so as to normalise ψ_i and ψ_f for infinite separation between A and B . Here $u_A(1, 2)$ denotes the normalised ground state wave function of the helium atom with electrons 1 and 2 around the nucleus A ; this wave function consists of two parts—one due to the orbital motion of the electrons around the nucleus A and the other due to the translatory motion of the electrons. $u_A^+(3)$ is the normalised ground state wave function of helium ion with the electron 3 around the nucleus A and consists of two parts—one orbital and the other translatory. Similarly, v_B and v_B^+ denote ground state normalised wave functions of He atom and He^+ ion respectively with B as the nucleus. α and β are the spin wave functions. In our calculation we shall use Hylleraas type wave function for the

orbital part of u_A with effective charge $\lambda = \frac{27}{16}$.

$$u_A(1, 2) = \frac{\lambda^3}{\pi} \exp \left\{ -\lambda(r_{A1} + r_{A2}) + \frac{v}{\hbar} Et \right\} \exp \left[-\frac{im}{\hbar} \left\{ \frac{1}{2} \mathbf{v} \cdot (\mathbf{r}_1 + \mathbf{r}_2) + \frac{1}{4} v^2 t \right\} \right]$$

$$v_B^+(3) = \sqrt{\frac{8}{\pi}} \exp \left\{ -2r_{B3} + \frac{v}{\hbar} ct \right\} \exp \left[\frac{im}{\hbar} \left(\frac{1}{2} \mathbf{v} \cdot \mathbf{r}_3 - \frac{1}{8} v^2 t \right) \right]$$

$$v_B(1, 2) = \frac{\lambda^3}{\pi} \exp \left\{ -\lambda(r_{B_1} + r_{B_2}) + \frac{i}{\hbar} Et \right\} \exp \left[\frac{im}{\hbar} \left\{ \frac{1}{2} \mathbf{v} \cdot (\mathbf{r}_1 + \mathbf{r}_2) - \frac{1}{4} v^2 t \right\} \right]$$

$$u_A^+(3) = \sqrt{\frac{8}{\pi}} \exp \left\{ \left(-2r_{A_3} + \frac{i}{\hbar} \epsilon t \right) \right\} \exp \left[\frac{-im}{\hbar} \left(\frac{1}{2} \mathbf{v} \cdot \mathbf{r}_3 + \frac{1}{8} v^2 t \right) \right]$$

$\mathbf{r}_1, \mathbf{r}_2, \mathbf{r}_3$ are the respective position vectors of the three electrons with respect to the centre of mass C (at rest) of A , and B . E and ϵ are the binding energies of normal He atom and ground state He^+ atom respectively

Performing the space integration, we may write

$$I = \int L dt \quad \dots (5)$$

where $L = \frac{1}{2} [2(A\dot{A} + B\dot{B})F_1 + 4(\dot{A}A + \dot{B}B)F_4 + 2(\dot{A}B + \dot{B}A)F_2 + 4(\dot{B}A + \dot{A}B)F_3]$

$$+ i\hbar \{ (\dot{A}A - A\dot{A} + \dot{B}B - B\dot{B})f_1 + 2(\dot{A}A - A\dot{A} + \dot{B}B - B\dot{B})f_4 \\ + (\dot{A}B - B\dot{A} + \dot{B}A - A\dot{B})f_2 + 2(\dot{B}A - A\dot{B} + \dot{A}B - B\dot{A})f_3 \}$$

where

$$F_1 = -\int \tilde{\psi}_1 V_1 \psi_1 dV, \quad V_1 = -e^2 \left(\frac{2}{r_{B_1}} + \frac{2}{r_{B_2}} + \frac{2}{r_{A_1}} - \frac{1}{r_{13}} - \frac{1}{r_{23}} \right)$$

$$F_2 = -\int \tilde{\psi}_1 V_2 \psi'_1 dV, \quad V_2 = -e^2 \left(\frac{2}{r_{A_1}} + \frac{2}{r_{A_2}} + \frac{2}{r_{B_3}} - \frac{1}{r_{13}} - \frac{1}{r_{21}} \right)$$

$$F_3 = -\int \tilde{\psi}_2 V_3 \psi'_3 dV, \quad V_3 = -e^2 \left(\frac{2}{r_{B_1}} + \frac{2}{r_{B_3}} + \frac{2}{r_{A_2}} - \frac{1}{r_{13}} - \frac{1}{r_{23}} \right)$$

$$F_4 = -\int \tilde{\psi}_3 V_3 \psi_2 dV$$

$$f_1 = \int \tilde{\psi}_1 \psi_1 dV, \quad f_2 = \int \tilde{\psi}_1 \psi'_1 dV, \quad f_3 = \int \tilde{\psi}_2 \psi'_3 dV, \quad f_4 = \int \tilde{\psi}_3 \psi_2 dV$$

where dots denote differentiation with respect to time.

Finally from the variational principle, by making I stationary with respect to the small arbitrary variations of A and B , we get the following differential equations

$$2(F_1 + 2F_4)A + 2(F_2 + 2F_3)B + i\hbar \{ 2(f_1 + 2f_4)\dot{A} + 2(f_2 + 2f_3)\dot{B} \\ + (\dot{f}_1 + 2\dot{f}_4)A + (\dot{f}_2 + 2\dot{f}_3)B \} = 0 \quad \dots (6)$$

$$2(F_2 + 2F_3)A + 2(F_1 + 2F_4)B + i\hbar \{ 2(f_1 + 2f_3)\dot{A} + 2(f_2 + 2f_4)\dot{B} \\ + (\dot{f}_2 + 2\dot{f}_3)A + (\dot{f}_1 + 2\dot{f}_4)B \} = 0 \quad \dots (7)$$

From the above two equations we obtain

$$(F_1 + F_2 + 2F_3 + 2F_4)(A + B) + i\hbar \{ (f_1 + f_2 + 2f_3 + 2f_4)(\dot{A} + \dot{B}) \\ + \frac{1}{2}(\dot{f}_1 + \dot{f}_2 + 2\dot{f}_3 + 2\dot{f}_4)(A + B) \} = 0 \quad \dots (8)$$

$$(F_1 + 2F_4 - F_2 - 2F_3)(A - B) + i\hbar\{(\dot{f}_1 + 2\dot{f}_4 - \dot{f}_2 - 2\dot{f}_3)(\dot{A} - \dot{B}) \\ + \frac{1}{2}(\dot{f}_1 + 2\dot{f}_4 - \dot{f}_2 - 2\dot{f}_3)(A - B)\} = 0 \quad \dots (9)$$

Applying the initial conditions i.e. at $t = -\infty$, $A = 1$, $B = 0$ we finally get by solving the above two equations the capture probability as

$$|B_{t \rightarrow \infty}|^2 = \sin^2 \phi_2$$

where
$$\phi_2 = \frac{1}{\hbar} \int_{-\infty}^{\infty} \frac{(F_2 + 2F_3)(1 + 2f_4) - (F_1 + 2F_4)(f_2 + 2f_3)}{(1 + 2f_4)^2 (f_2 + 2f_3)^2} dt$$

For the case of very low relative velocity of the incident ion with respect to the helium atom we may evaluate F 's and f 's after neglecting the translatory part of the electron wave functions. We expect, from the expression for the capture probability resonance structure with changes of energy. The details of calculations for the capture cross-section will be published soon.

ACKNOWLEDGMENT

The authors wish to thank Prof. D. Basu for his valuable comments and helpful discussions.

REFERENCES

- Bates, D. R., Mc Carroll, R., 1962, *Advances in Physics*, **11**, 39.
 Massey, H. S. W. and Smith, R. A., 1933, *Proc. Roy. Soc. A*, **142**, 142.
 Dallaportier, N. and Bonfiglioli, P., 1943, *Comment. Pontif. Acad. Sci.*, **7**, 141.
 Firsov, O. B., 1951, *F. Exp. Theor. Phys.*, **21**, 1001.
 Jackson, J. D., 1954, *Canad. J. Phys.*, **32**, 60.
 Moiseiwitsch, B. L., 1956, *Proc. Phys. Soc.*, **69**, 653.
 Schiff, H., 1954, *Canad. J. Phys.*, **32**, 393.
 Snitzer, 1953, *Phys. Rev.*, **89**, 1237.
 Everhart, E., Helbig, H. F. and Lockwood, G. J., 1963, *Proc. Third International Conference on the Physics of Electronic and Atomic Collision* (in press).
 Lockwood, G. J., Helbig, H. F. and Everhart, E., 1963, *Phys. Rev.* (in press).
 Everhart, E., 1963, *Phys. Rev.* (in press).

A METHOD OF MEASURING MAGNETIC PROPERTIES OF FERROMAGNETIC AND OTHER SUBSTANCES

A K MUKERJEE AND N. G. SUTRADHAR

DEPARTMENT OF MAGNETISM, INDIAN ASSOCIATION FOR THE CULTIVATION OF SCIENCE,
CALCUTTA-32

(Received, October 14, 1963)

ABSTRACT In connection with the study of the magnetic properties of Indian minerals, meteorites and various semiconductors which may be Ferro-, Antiferro-, Ferri-, Para- or Dia-magnetic at various temperatures, a horizontal translation type balance has been designed and constructed here. This balance is particularly suitable for measurements at high temperatures as convection disturbances are eliminated by having a horizontal oven. Description and working of the balance are given in the paper.

INTRODUCTION

In connection with the study of the magnetic properties of certain Indian minerals and materials meteorites and various semiconductors which may be ferro-, antiferro-, ferri-, para- or diamagnetic, it has been observed that none of the magnetic balances used in this laboratory are suitable for measurements at high temperatures, —so essential for these studies. —owing to convection disturbances set up in the ovens. Moreover, a method suitable for the said purpose should evidently be versatile, robust and at the same time sensitive. A balance working on the principles of Félix and Forrer (1926) with certain innovations has been found to meet the above requirements to a considerable extent. In such a balance the sample is attached at the end of a horizontal balance beam supported from a pair of bifilar suspensions with the sample arm protruding into a horizontal magnetic field with a gradient perpendicular to it in the same plane, so that the tubular heater enclosing the sample end of the beam is also to be placed in a horizontal position, thereby minimising disturbances due to convection currents. Further, with such a balance not only the temperatures and the field variations, if any, of the above properties but the magneocrystalline anisotropy of the ferromagnetics can also be studied more reliably and conveniently than by other existing methods. The present communication gives a description and working of such a balance.

THEORY

When any small crystalline body of permeability μ_{jk} surrounded by a isotropic medium of permeability μ_0 is placed in a magnetic field H it acquires magnetic potential energy given by (Nye, 1957)

$$V = -\frac{(\mu_{jk}-\mu_0)}{8\pi} H_j H_k$$

per unit volume, $j, k = 1, 2, 3$

Leaving for the present moment the intrinsic magnetic field within the magnetised body, the magnetic force acting on the small body of volume v is then given by

$$F_i = - \frac{\partial}{\partial x_i} \left(\frac{\mu_{jk}-\mu_0}{8\pi} \right) v H_j H_k$$

$$= v(K_{jk} - K_0) H_k \frac{\partial H_j}{\partial x_i}$$

$$i, j, k = 1, 2, 3,$$

where K_{jk} and K_0 are the volume susceptibilities of the specimen and the medium respectively

If the magnetic field is so arranged that, $\frac{\partial H_1}{\partial x_1} = \frac{\partial H_1}{\partial x_3} = 0$, $H_2 = H_3 = 0$ and further the crystal is set with its K_1 direction along H_1 , then we are left with the sole component of the force given by

$$F_2 = v(K_1 - K_0) H_1 \frac{\partial H_1}{\partial x_2} \quad \dots (1)$$

Now for a very small volume of a ferromagnetic substance of suitable shape for estimating the shape effect, placed in a field of very small constant gradient over the sample so that the field dependence of K_1 is negligible, the force (neglecting K_0 compared to large value of K_1 for a ferromagnetic sample) is

$$F_2 = I_1 \frac{\partial H_1}{\partial x_2} v \quad \dots (2)$$

where I_1 is the component of magnetic moment per unit volume of the substance. The above conditions are conveniently obtained in a Fox-Forrer type of balance in which motion is allowed only in one particular direction in the horizontal plane with a specially shaped pole gap

DESCRIPTION

The different parts of the balance are described concisely but with special reference to the modification of the standard Fox-Forrer arrangement, in the

following paragraphs and can be followed easily with reference to the adjoining diagram (fig.1.)

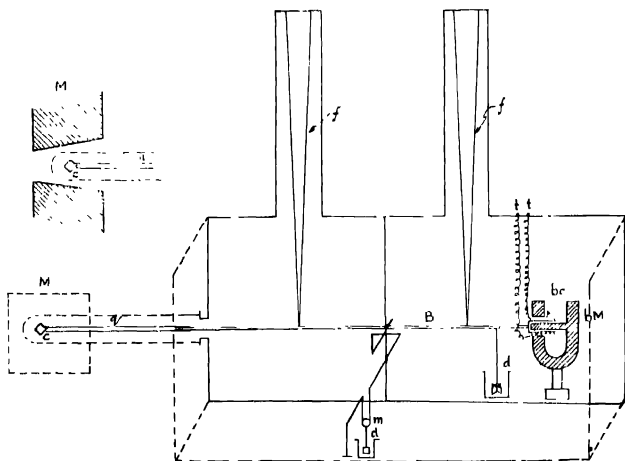


Fig. 1. A sketch of the magnetic balance (not to the scale)

(a) *Balance beam (B)*

This is a thin uniform glass tube about 30 cms long and 0.3 cms in diameter suspended horizontally by a pair of fine glass bifilar suspensions f from a height of about 60 cms the upper ends of the two fibres of each being fixed 21 cms apart. This allows the motion of the beam only in a horizontal direction perpendicular to the planes of the bifilar fibres and the horizontal magnetic field is here so arranged that it lies at right angles to, while its gradient lies along the above direction in which the beam is free to move. At the end of the beam which slightly protrudes out of the balance case is attached a small length of quartz tube q to the other end of which the specimen c is to be attached. The distance between the balance and the magnet M is so adjusted that the specimen is always at a place within the pole gaps of the magnet where (i) $\frac{\partial H_1}{\partial x_2}$ is small and constant during the

measurements with ferromagnetics or (ii) $H_1 \frac{\partial H_1}{\partial x_2}$ is constant during the measure-

ments with non-ferromagnetics. At the other end of the balance beam is attached coaxially a small solenoidal coil bc of about 100 turns of superenamelled copper wire (42 S.W.G) which can freely move within specially designed poles (after Foëx and Forrer 1926) of a small permanent magnet δM . This arrangement is for balancing any force which is exerted at the other end of the balance beam.

(b) *Detection of movement of the balance beam.*

The movement of the balance beam and restoration of its position is observed by a light spot on a scale reflected from a mirror *m* suspended by means of a bifilar arrangement attached at the other end of a thin glass lever rod *l* connected by a short length of quartz fibre to the balance beam

(c) *Damping (d)*

Proper damping arrangements have been made for the balance beam and the bifilar mirror. These are mica vanes, hanging from the balance beam and the mirror immersed in light oil kept in appropriate dash pots

(d) *The magnet (M)*

The theoretical condition for measurements on ferromagnetics, that is a constant gradient transverse to the magnetic field and over a considerable region, is provided for here by having a proper angle ($\sim 6^\circ$) between the two large rectangular pole pieces of the electromagnet (10 cm \times 11 cm) for a particular pole gap (5.7 cm at the central region). The field was measured at intervals of 2 mm. throughout the length of the pole gap at right angles to the field by a sensitive fluxmeter. From the graphs showing the variations of the field with distance the most useful region was selected which showed small and steady variations of the field. Such graphs (Fig. 2.) have also been obtained for different exciting currents of the magnet so that measurements on different samples can easily be taken at different fields.

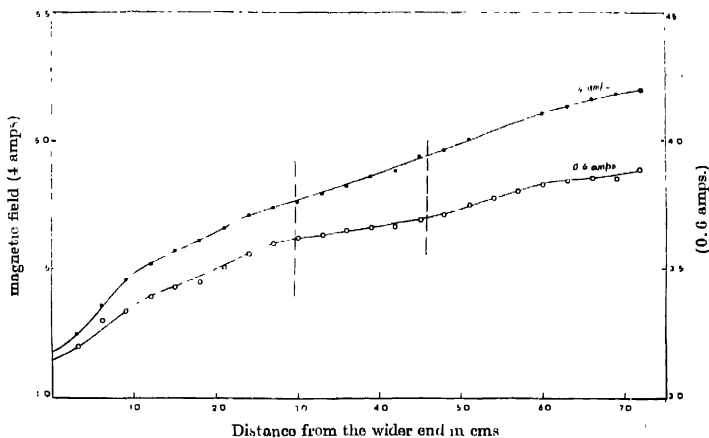


Fig. 2 Variation of the magnetic field with distance from the wider end along the length of the pole gap in arbitrary units.

For non-ferromagnetic substances two Sucksmith types of pole shoes (Sucksmith 1929) are to be attached in the usual way to the pole pieces so that the necessary conditions of uniform H_1 , $\frac{\partial H_1}{\partial x_2}$ is obtained. Switching, reversing, controlling,

and reading arrangements for the magnet current are the same as already adopted here (Dutta Roy 1955).

(c) *Working of the balance*

(i) *Measurement of magnetic force and test of sensitiveness*

As pointed out earlier, the magnetic force exerted on the specimen placed at one end of the beam is balanced by sending a suitable current through the coil at the other end. Now the magnetic forces per unit volume on different samples are proportional to their susceptibilities but it is also necessary to check whether the balancing currents in the coil are exactly proportional to the magnetic forces, since balancing forces upon the coil may depend in a complicated way upon the geometry of the system. In order to ascertain this point and also find the limit of sensitiveness of the balance the following experiment was performed.

An unspun silk fibre connected to the sample end of the balance beam runs horizontally over a jewel pivoted pulley having almost no friction at the bearings, from which weights varying from 1 m.gm. to 100 m.gm are successively suspended. This caused a forward motion of the beam and the light spot from the mirror is widely deflected. It is brought back to its initial position by sending a requisite current through the balancing coil. The current is indicated by a sensitive and accurate milli-or micro-ammeter put in the circuit. The actual value of the current was however obtained by measuring the drop of potential across a standard resistance. The results of the measurement are represented graphically in Fig. 3

It will be seen from the graph that the balancing current is accurately directly proportional to the force acting at the other end. Also it is observed that the sensitiveness of the balance with the present coil is about 1.25×10^{-5} gms./ μA which however can be further increased by changing the number of turns of the coil.

CALIBRATION

(a) *For ferromagnetics*

Since the ferromagnetic susceptibility is field dependent the usual method of using a standard substance for calibrating the balance is not applicable. This has, however, been overcome by using instead a coil of known dimension and number of turns attached at other end of the quartz tube (g), so that the coil is at the same position within the poles of the magnet (M) where there is small and constant gradient, the axis of the coil being parallel to magnetic field direction

A known current is passed through it which is read by a calibrated milliammeter. When the magnet is switched on a force acts on this coil and can be balanced by passing current through the balancing coil (*bc*).

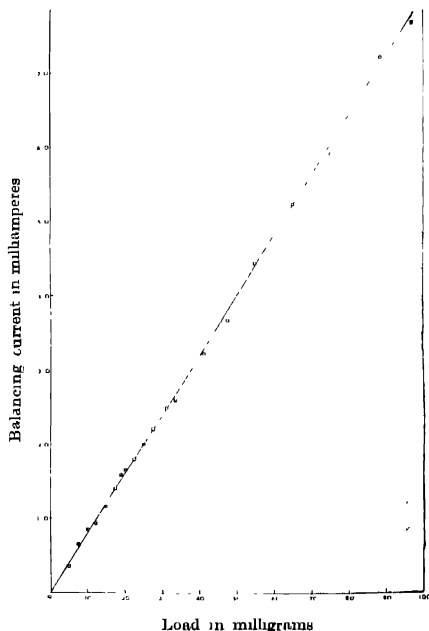


Fig. 3. Load-Balancing current curve for a particular balancing coil

For the purpose of actual measurement the specimen is first attached at the end of the quartz tube (*q*) and the magnetic force is balanced by passing a current say i_1 through the balancing coil. Now the specimen is replaced by the standardising coil mentioned above and the magnetic force is balanced at the same value of the magnetic field as that of the specimen by passing a current i_2 through the coil (*bc*). Then the intensity of magnetisation, I , of the specimen is given by (from eq. 2)

$$I_s = \frac{i_1}{i_2} \frac{NAc\rho}{m}$$

where N is the total number of turns of the standardising coil, A the area of the section of the coil, c the current through it. ρ the density and m the mass of the specimen.

As a test measurement different currents were passed through such a coil and the force exerted on it when the magnetic field is switched on is balanced in the usual way by sending appropriate currents through the balancing coil

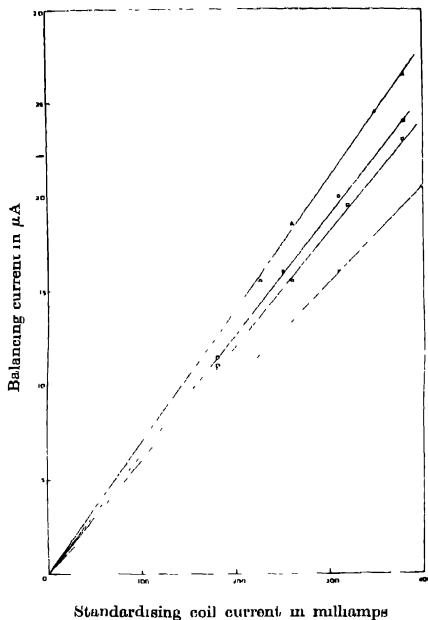


Fig 4 Balancing current for different currents in the standardising coil at different magnetic fields. Coil I 1780 oe ● ; 2050 oe ⊙ ; coil II 1780 oe □ ; 2050 oe ○ .

This procedure is repeated for different magnetic fields and with coils having different number of turns. The results of measurement are shown in Fig 4. The relationship between the current through the standardising coil (i.e. its moment) and the current in the balancing coil (i.e. the force exerted on the standardising coil) is a linear one for a fixed value of the field. Thus in order to find the field variation of the magnetisation of the ferromagnetic specimen, the force acting on it and the standardising coil with known current flowing through it (i.e. the respective balancing currents) are compared at the different desired fields.

(b) *For non-ferromagnetics*

For non-ferromagnetics, as has been pointed out above, two Sucksmith type of pole shoes are attached over the flat pole pieces of the magnet and the

magnetic force exerted on the specimen and on the standard substance, both placed in the same position within the pole gaps with uniform $H_1 \frac{\partial H_1}{\partial x_2}$ over considerable region, are successively balanced by sending currents through the balancing coil, when one is replaced by the other. Then the mass susceptibility of the specimen is given by (from eq. 1)

$$\chi = \frac{i}{i_s} \frac{m_s}{m} \left(\chi_s - \frac{K_a}{\rho_s} \right) + \frac{K_a}{\rho}$$

where χ_s is the mass susceptibility of the standard substance, i and i_s the balancing currents for the specimen and the standard substance respectively, m and m_s the corresponding masses, ρ and ρ_s the densities and K_a the volume susceptibility of the surrounding medium i.e., air at the temperature at which the measurements were taken

For checking the reliability of the balance so far as the non-ferromagnetics are concerned the susceptibilities of a number of freshly prepared crystals of Ferric ammonium Alum ($\text{Fe}_2(\text{SO}_4)_3(\text{NH}_4)_2\text{SO}_4 \cdot 24\text{H}_2\text{O}$) grown from aqueous solution using G.R. quality samples of E. Merck were measured using a crystal of Chrome Potassium Alum ($\text{Cr}_2(\text{SO}_4)_3\text{K}_2\text{SO}_4 \cdot 24\text{H}_2\text{O}$) grown in the same way as

TABLE I
 p_{eff}^2 for Fe^{3+} Alum

	Standard	Unknown	Earlier values for p_{eff}^2 of the unknown sample at 300°K
Substance	Cr^{3+} Alum	Fe^{3+} Alum	
Density	1.842 gms/cc	1.724 gms/cc	
Mass	15720 gms	09020 gms	
Balancing current	127.0 μA	180.0 μA	
$\chi \times 10^6$	11.98 at 300°K	29.56 at 300°K	
p_{eff}^2 (in Bohr magneton units)	14.91	34.75	34.80 (Dutta Roy 1955, 1956) 35.0 (Spin only value)
Substance	NiCl_2 Soln.	Fe^{3+} Alum.	
Density	1.2903 gms/cc	1.724 gms/cc	34.60 (Onnes and Oosterhuis 1927)
Mass	33400 gms, of concentration 2590 gms. of NiCl_2 per gms. of soln	07245 gms	
Balancing current	280.0 μA .	225.0 μA	
$\chi \times 10^6$	8.1067 at 302°K	29.60 at 302°K	
p_{eff}^2 (in Bohr magneton units)	—	34.79	

above, as a standard. The results of measurements are shown in Table I and are found to agree well with other reported values, and are very consistent amongst themselves for a number of different samples. Also the susceptibility of Fe^{3+} Alum was determined using a nickel chloride (NiCl_2) solution of known strength as a standard and the result was found in agreement with standard values.

CONCLUDING REMARKS

It is found that the balance described above is very convenient for measurements of a variety of substances of widely different susceptibilities both ferromagnetic and nonferromagnetic. A horizontal cryostat or an oven eliminating convectional disturbances is very suitable for use with this balance. The stability, reproducibility, and sensitivity are very high and it is now planned to start measurements on some natural ferromagnetic minerals such as ilmenite, magnetite etc., both above and below their Curie temperatures and especially in the region close to this temperature.

ACKNOWLEDGMENT

The authors are grateful to Shri A. K. Dutta, Research Officer, for his guidance and help and Prof. A. Bose, D.Sc., F.N.I., for his keen interest in the work. Also they wish to thank the Workshop for the efficient construction of the balance.

REFERENCES

- Dutta Roy, S. K., 1955, *Ind. Jour. Phys.*, **29**, 429.
 Dutta Roy, S. K., 1956, *Ind. Jour. Phys.*, **30**, 169.
 Fox, G. and Foner, R., 1926, *Journ. de Phys.*, **7**, 180.
 Nye, J. F., 1957, *Physical Properties of Crystals*, Oxford, pp. 57-63.
 Onnes, H. R., and Oosterhuis, E., 1927, *Comms. Leid.*, no. 139C.
 Sucksmith, W., 1929, *Phil. Mag.*, **8**, 158.

DIMENSIONAL AND STRUCTURAL CHANGES DURING DENATURATION OF HELICAL TYPE MACROMOLECULES

A. V. TOBOLSKY* AND V. D. GUPTA**

(Received, November 27, 1963)

ABSTRACT A theory for quantitative description of reversible helix-coil type phase transition in macromolecular systems is given. The transition is characterized by (1) the fraction of helical content, (2) sequence length of the crystalline regions, (3) sequence length of the amorphous regions, and (4) mean square end-to-end distance. The results for per cent helical or crystalline content are compared with experimental values for polybenzyl glutamate and oligoadenylic acid.

INTRODUCTION

Certain macromolecules such as synthetic polypeptides, proteins, synthetic polynucleotides and deoxyribonucleic acid (DNA) and ribo-nucleic acid (RNA) undergo a reversible phase transition as the temperature is raised. For the natural proteins and nucleic acids, this diffuse phase transition has frequently been termed denaturation. For isolated synthetic linear polypeptides in solution this phase change has been identified as a transition from a helical (crystalline) state to a randomly coiled amorphous state, and has been denoted as the helix-coil transition (Doty *et al.*, 1954-57). This transition occurs for single strand helical macromolecules and also for multiple strand helical macromolecules.

The purpose of this paper is to give a quantitative description of this transition. In particular we wish to characterize the macromolecule through the region of transition by the following parameters: (a) per cent helical or crystalline content, (b) sequence length of the crystalline regions, (c) sequence length of the amorphous regions, and (d) mean square end-to-end distance of the macromolecules.

To achieve these purposes we utilize two theoretical developments. The first is a statistical thermodynamic treatment of the phase transition. The second is a theory of chain dimensions of crystalline macromolecules.

* Department of Chemistry, Princeton University, Princeton, New Jersey.

** Department of Physics, University of Allahabad, Allahabad, India.

STATISTICAL THERMODYNAMIC TREATMENT. ZIMM-BRAGG THEORY

The prototype theory for the phase transition for linear polypeptides is the theory of Zimm and Bragg (1958). The authors considered the sequence of amide residues in a linear polypeptide chain. The oxygen atom of any given amide residue is either hydrogen-bonded to the hydrogen atom of the third preceding residue or it is not. The first three amide residues are considered unbonded. The notation zero is assigned to an unbonded amide residue (segment) and the notation unity is assigned to a bonded residue. A particular configuration of the chain therefore, would be

$$000111000011. \dots \quad \dots \quad (1)$$

The following statistical weights were assigned to the various residue pairs

- (1) the quantity s for the residue pair 1 1,
- (2) the quantity σs for the residue pair 0 1,
- (3) the quantity 1 for the residue pair 0 0,
- (4) the quantity 1 for the residue pair 1 0

The above assumptions correspond to the simplest form of the Zimm-Bragg treatment. σ is a quantity much smaller than unity and expresses the difficulty of the transition from a non-bonded segment to a bonded segment in a sequence such as (1). The quantity s which is larger than unity when the helix is favoured expresses the tendency for bonded segments to follow bonded segments.

Zimm and Bragg used the matrix method to derive the partition function for the polypeptide chain and an expression for the fraction of bonded segments as a function of s and σ . Their matrix can be expressed as follows, (we have exchanged rows with columns in their notation for consistency with our further discussion)

$$M = \begin{vmatrix} \overrightarrow{0 \rightarrow 1} & \overrightarrow{0 \rightarrow 1} \\ \overrightarrow{1 \rightarrow 0} & \overrightarrow{1 \rightarrow 1} \end{vmatrix} = \begin{vmatrix} 1 & \sigma s \\ 1 & s \end{vmatrix} \quad \dots \quad (2)$$

The partition function for a chain of n segments is related to the maximum root λ_{max} of matrix M .

$$Q = \lambda_{max}^n \quad \dots \quad (3)$$

where

$$\lambda_{max} = \frac{1}{2} \{1 + s + [(1-s)^2 + 4\sigma s]^{\frac{1}{2}}\}. \quad \dots \quad (4)$$

The fraction of bonded segments θ is equal to

$$\theta = \frac{d \ln \lambda_{max}}{d \ln s} \quad \dots \quad (5)$$

A GENERALIZATION OF THE STATISTICAL THERMODYNAMIC TREATMENT

A modification and generalization of the Zimm-Bragg treatment has been presented by Tobolsky (In Press). One reinterprets the partially helical macromolecule as being a sequence of segments which are either in amorphous regions (randomly coiled) and denoted as r or as segments which are in crystalline (helical) regions and denoted as h . A macromolecule can be written, therefore, as

$$r r r h h h h r r h h h r r \dots \quad (6)$$

The question of hydrogen bonded versus non-hydrogen bonded residues is only a special case for the above way of conceptualizing the chain. For a single strand helical macromolecule the crystallization has to be intramolecular sometimes aided by hydrogen bonding but not necessarily so. For a double or multiple strand helical macromolecule, the crystallization will have to be at least partially intermolecular. We may even imagine that the sequence (6) refers to a macromolecule which is part of a semi-crystalline macromolecular system as in bulk poly-ethylene. Here the crystallization is mainly intermolecular.

We also generalize the notation to develop a 2×2 matrix, analogous to the Zimm and Bragg matrix.

- (1) a segment pair rr is assigned the segment pair partition function f_{rr} ,
- (2) a segment pair rh is assigned the segment pair partition function f_{rh} ,
- (3) a segment pair hr is assigned the partition function f_{hr} ,
- (4) a segment pair hh is assigned the partition function f_{hh} .

The matrix corresponding to (6) can be written as

$$M = \begin{matrix} & \begin{matrix} r \rightarrow r & r \rightarrow h \end{matrix} \\ \begin{matrix} h \rightarrow r & h \rightarrow h \end{matrix} & \begin{bmatrix} f_{rr} & f_{rh} \\ f_{hr} & f_{hh} \end{bmatrix} \end{matrix} \quad \dots \quad (7)$$

The mathematical treatment is identical with the Zimm and Bragg treatment if the following identification is made:

$$\begin{aligned} f_{rr} &= 1 \\ f_{hh} &= s \\ f_{rh}f_{hr} &= \sigma s \end{aligned} \quad (8)$$

One can utilize this matrix to develop expressions for the average sequence size in the crystalline regions, the average sequence size in the amorphous regions, etc.

It is very helpful, however, to solve the problem in an alternate manner through the use of segment partition functions rather than segment pair partition

functions. This requires a rewriting of the sequence (6) and redesignating the first segment of every crystalline sequence as k ,

$$r r r k h h h h r r k h h r \dots \quad \dots \quad (9)$$

The segment partition functions are taken as f_r , f_k and f_h . The solution of the problem now involves the use of a 3×3 matrix as shown by Tobolsky (1962)

$$M = \begin{array}{ccc|ccc} \overline{r \rightarrow r} & \overline{r \rightarrow k} & \overline{r \rightarrow h} & f_r^{\frac{1}{2}} f_r^{\frac{1}{2}} & f_r^{\frac{1}{2}} f_k^{\frac{1}{2}} & 0 \\ k \rightarrow r & k \rightarrow k & k \rightarrow h & f_k^{\frac{1}{2}} f_r^{\frac{1}{2}} & 0 & f_k^{\frac{1}{2}} f_h^{\frac{1}{2}} \\ h \rightarrow r & h \rightarrow k & h \rightarrow h & f_h^{\frac{1}{2}} f_r^{\frac{1}{2}} & 0 & f_h^{\frac{1}{2}} f_h^{\frac{1}{2}} \end{array} \quad \dots \quad (10)$$

The solutions of this matrix are equivalent to the solutions of matrix (2) if :

$$\begin{aligned} f_r &= 1 \\ f_h &= s \\ \frac{f_k}{f_r} &= \sigma s \end{aligned} \quad \dots \quad (11)$$

At this point the advantage of this formulation appears. Inasmuch as we use segment partition functions, we can easily interpret these quantities in the following manner :

$$\begin{aligned} f_r &= g_r \\ f_h &= g_h \exp\left(\frac{\Delta H_f}{RT}\right) \\ f_k &= \epsilon \end{aligned} \quad \dots \quad (12)$$

In equation (12) g_r is the statistical weight of an r segment, g_h is the statistical weight of an h segment, and ΔH_f is the heat of fusion from the crystalline to the amorphous state. The partition function f_k of the k segments which represent the boundary between amorphous and crystalline regions is taken to be temperature independent (an approximation) and very small, to represent the difficulty of entering such a boundary region.

The following results ensue from equations (10) and (12)

$$T_f = -\frac{\Delta H_f}{R \ln \frac{g_r}{g_h}} = \frac{\Delta H_f}{\Delta S_f} \quad \dots \quad (13)$$

$$\Delta S_f = R \ln \frac{g_r}{g_h}$$

In equation (13) T_f is the transition temperature and ΔS_f is the entropy of fusion.

The results for fractional crystallinity θ as a function of temperature, for the average sequence length \bar{h} in the crystalline regions and the average sequence length \bar{r} in the amorphous regions, both as functions of temperature, are written below.

$$1 - \theta = \frac{1 - e^{\frac{\Delta F_f}{RT}} + 2 \frac{f_k}{f_r} + \sqrt{\left(e^{\frac{\Delta F_f}{RT}} - 1 \right)^2 + 4 \frac{f_k}{f_r}}}{\left(\sqrt{\left(e^{\frac{\Delta F_f}{RT}} - 1 \right)^2 + 4 \frac{f_k}{f_r}} \right) \left(1 - e^{\frac{\Delta F_f}{RT}} + \sqrt{\left(e^{\frac{\Delta F_f}{RT}} - 1 \right)^2 + 4 \frac{f_k}{f_r}} \right)}, \quad \dots \quad (14)$$

$$\bar{r} = \frac{\left(1 - e^{\frac{\Delta F_f}{RT}} \right) + \sqrt{\left(e^{\frac{\Delta F_f}{RT}} - 1 \right)^2 + 4 \frac{f_k}{f_r}}}{2 \frac{f_k}{f_r}} + 1, \quad \dots \quad (15)$$

$$\bar{h} = \frac{e^{\frac{\Delta F_f}{RT}} \left[e^{\frac{\Delta F_f}{RT}} - 1 + \sqrt{\left(e^{\frac{\Delta F_f}{RT}} - 1 \right)^2 + 4 \frac{f_k}{f_r}} \right]}{2 \frac{f_k}{f_r}} + 1. \quad \dots \quad (16)$$

$$\frac{n_{seq}}{n} = \frac{\theta}{\bar{h}} \quad \dots \quad (17)$$

Here

$$\Delta F_f = \Delta H_f - T \Delta S_f. \quad \dots \quad (18)$$

The expression for θ is essentially equivalent to that given by Zimm and Bragg. We also present explicit equations for \bar{h} and \bar{r} . The quantity $\frac{n_{seq}}{n}$ given in equation (17) is the ratio of the number of crystalline sequences to the total number of segments.

Equations (14)–(16) are exact equations deduced from the formulae of reference (4). Simple approximate equations were given also in (4) but, for the purposes of the exact calculations carried out in the subsequent portions of this paper, it was desirable to use the exact equations and machine computations.

CHAIN DIMENSIONS DURING THE PHASE TRANSITION

Tobolsky and Gupta (1962) have developed a theory for the end-to-end dimensions R^2 of semi-crystalline macromolecules in terms of two probability parameters.

When statistical thermodynamic equilibrium obtains, these parameters can be related to the partition functions f_r , f_h , and f_k introduced in the previous section. An extremely simple approximate formula results

$$R^2 = \left[\frac{\theta}{3} (2\bar{h} + 1) + (1 - \theta) \right] n l^2_0 \quad \dots \quad (19)$$

where θ and \bar{h} can be identified with equations (14) and (15).

Equation (19), however, applies only to the simplest case where the unit cell of the helix is such that the completely helical form of the molecule is essentially a rigid rod. In other words, we are not considering here the cases where there is complex coiling within the unit cell, as occurs in globular proteins, nor do we consider here the effects which may be produced by long range folding within the crystallites. Although modifications of equation (19) to encompass these phenomena have been given (Tobolsky, 1962; Tobolsky *et al.*, 1962) we feel that it is premature to examine these more complex formulae without more experimental evidence than is now available.

Calculations based on equation (19) are nevertheless valuable because in certain cases the completely helical macromolecules do appear to approximate rigid rods.

APPLICATION TO EXPERIMENTAL DATA

In this paper we apply the theoretical results to three helix-coil transitions

(1) The helix-coil transition of polybenzyl glutamate in a dichloroacetic acid-ethylene dichloride mixture. This is a *reverse* transition, i.e., the helix is stable at high temperatures. This case has been treated by Zimm, Doty and Iso (1959) using the method of Zimm and Bragg. These authors obtain the expression for θ as a function of T by choosing a proper value of σ and ΔH . We repeat these calculations in our notation and in addition present results for \bar{h} , \bar{r} , $\frac{n_{seq}}{n}$, and R^2 .

(2) Schellman postulated that the heat of hydrogen bonding, stabilizing the helix in linear polypeptides is $\Delta H = -1500$ calories/mole. In our notation this means that $\Delta H_f = 1500$ calories/mole. We compute θ , \bar{h} , \bar{r} , $\frac{n_{seq}}{n}$, and R^2 for the normal helix-coil transition for this type of polypeptide assuming the same σ , and the same transition temperature as in case (1). (The Zimm, Doty and Iso case)

(3) Prof. J. R. Fresco has made available to us preliminary data of Fresco, Blake and Doty for the helix-coil transition of the double stranded helix of oligoadenylic acid. We compute $\bar{\theta}$, \bar{r} , \bar{h} , $\frac{n_{seq}}{n}$, and R^2 for $\Delta H_f = -1336$ cal/mole and different values of σ .

(1) Helix-Coil Transition For Polybenzyl Glutamate

Zimm, Doty and Iso have explained the transition in polybenzyl glutamate in a dichloroacetic acid-ethylene dichloride mixture using the following values for the quantities that appear in the Zimm-Bragg treatment:

$$\sigma = 2 \times 10^{-4} = f_k/f_r = c/g_r \quad (\text{in our notation}),$$

$$\frac{d \ln S}{dT} = \frac{\Delta H}{RT^2}, \quad \Delta H = +890 \text{ cal.} - -\Delta H_f \quad (\text{in our notation}),$$

$$T_f = 11.8^\circ\text{C}, \quad \Delta S_f = \Delta H_f/T_f = 3.12 \text{ cal/deg.},$$

$$\Delta F_f = \Delta H_f - T\Delta S_f = -890 + 3.12T_f$$

Using these values in equations (14), (15), (16), (17), and (18) we evaluated

θ , \bar{r} , h , $\frac{n_{\text{seg}}}{n}$, and R^2 as functions to temperature, using a Bendix (4-151D) type computer. The results are shown graphically in Figures 1-4. The computations for R^2 are purely hypothetical based on the assumption that the helical form of the polypeptide is a rigid rod. We know that this isn't true in this case, since intrinsic viscosity measurements in this system show remarkably little change through the temperature region of the helix-coil transition.

We would like to emphasize that the reverse transition treated by Zimm, Doty and Iso as an application of the Zimm-Bragg theory in fact introduces some grave conceptual difficulties for any statistical thermodynamic model of the types discussed here. These authors correctly stated that the positive value of ΔH (a negative ΔH_f in our notation) can be explained only by solvent effects. However, a negative ΔH_f also means a negative ΔS_f and it is certainly difficult to conceive of the ordered helical state as having a higher entropy than the randomly coiled state.

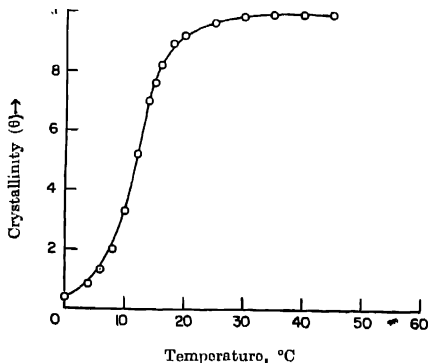


Fig. 1. Crystallinity versus Temperature curve for Polybenzyl Glutamate (Zimm, Doty and Iso case).

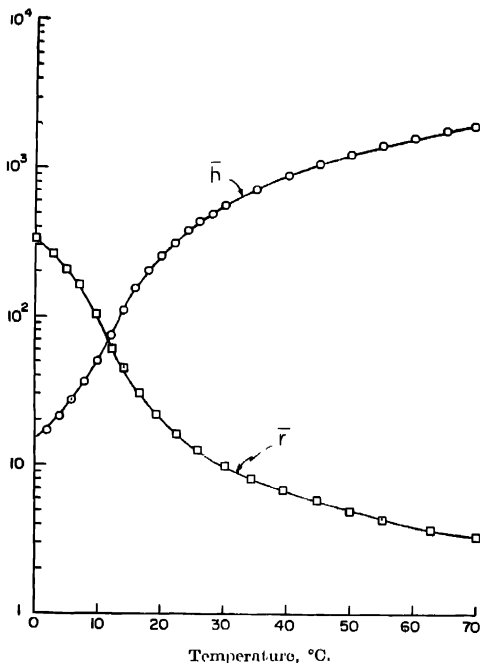


Fig. 2 Curve showing variations of sequence lengths in the crystalline and Amorphous Regions with Temperature for Polybenzyl Glutamate

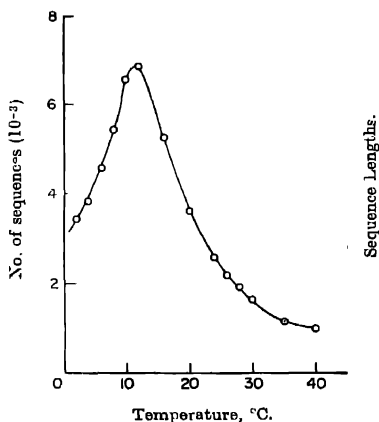


Fig. 3. Number of Sequences Versus Temperature for Polybenzyl Glutamate

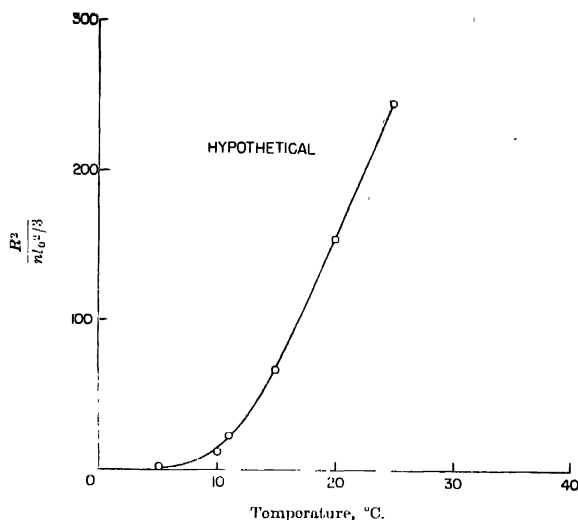


Fig. 4 Variation of the Expected Square of the End-to-End Distance with Temperature for Polybenzyl Glutamate.

(2) Schellman case

Schellman (1955) postulated that the heat of dissociation of the hydrogen bond is $+1500$ cal/mole. In other words, the heat of hydrogen bonding stabilizing the helix in linear polypeptides is -1500 cal/mole. We use the following values of the various parameters which occur in the expressions for θ , \bar{r} , \bar{h} , $\frac{n_{\text{seg}}}{n}$, and R^2 .

$$\Delta H_u \text{ (Schellman's notation)} = -\Delta H_f \text{ (our notation),}$$

$$\Delta H_f = +1500 \text{ cal/mole}$$

For the sake of definiteness in our calculations, we assume that a particular Schellman polypeptide has the same T_f and the same σ as used by Zimm, Doty and Iso.

$$\sigma = 2 \times 10^{-4} = f_h/f_r = \epsilon/g_r \quad (\text{in our notation})$$

$$T_f = 11.8^\circ\text{C}, \Delta S_f = 5.2668$$

$$\Delta F_f = \Delta H_f - T\Delta S_f = 1500 - T\Delta S_f.$$

The calculations are made for the normal helix-coil transition for this type of polypeptide and the results are shown graphically in Figures 5-8.

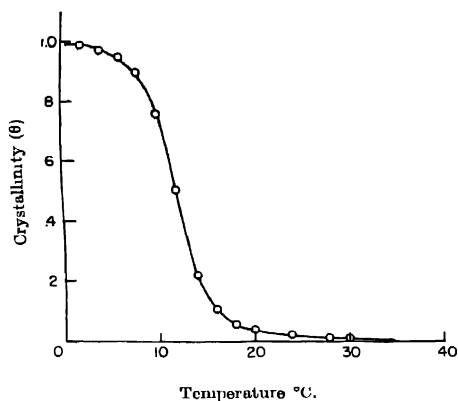


Fig. 5. Crystallinity Versus Temperature Curve for Linear Polypeptides (Schellman Case).

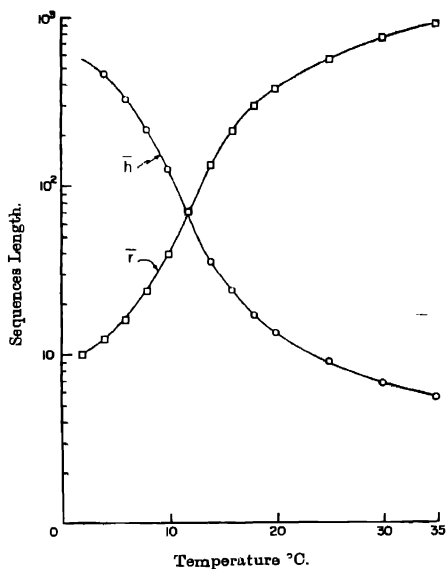


Fig. 6. Curve showing Variation of Sequence Lengths in the Crystalline and Amorphous Regions with Temperature for Linear Polypeptides.

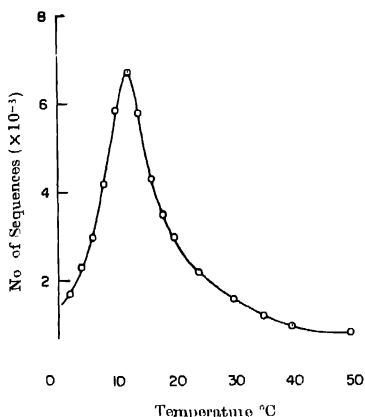


Fig. 7. Number of Sequences Versus Temperature for Linear Polypeptide.

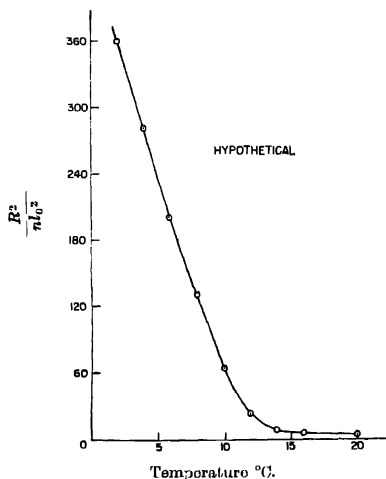


Fig. 8. Variation of the Expected Square of the End-to-End Distance with Temperature for Linear Polypeptides.

(3) *Helix-Coil Transition for Oligoadenylic Acid (Poly A)*

We utilize in this instance some preliminary experimental data on crystallinity versus temperature for a series of oligonucleotides of adenylic acid of vary-

ing degrees of polymerization including data on θ versus T for a very high molecular weight Poly *A*. The data were kindly supplied to us in advance of publication by Prof. J. R. Fresco (private communication).

The Poly *A* polymers exist in aqueous solution at low temperatures as double stranded helices. At higher temperatures they undergo a gradual helix-coil transition. The primary experimental data consisted of values for T_f versus the degree of polymerization P . We compute the values of ΔH_f from the formula (Flory, 1957).

$$\frac{1}{T_f} - \frac{1}{T_f^\infty} = -\frac{R}{\Delta H_f} \ln \left(1 - \frac{2}{P}\right) \quad \dots (20)$$

In equation (20) T_f^∞ is the melting temperature for the polymer of "infinite" molecular weight and T_f is the melting temperature for the polymer of degree of polymerization P . A plot of $1/T_f$ versus $1/(1 - 2/P)$ gave a straight line from whose slope we obtained a value of $\Delta H_f = 1152$ cal/mole. The data in Table I were kindly supplied by Professor J. R. Fresco.

The data for θ versus T for the "infinite" molecular weight poly *A* were also supplied by Professor Fresco using the optical density method.

The value of $\sigma - f_k/f$, which gave the best fit with the experimental θ versus T data is 1.5×10^{-5} . With this value of σ we then computed θ , \bar{r} and \bar{h} . The results are given in Table II.

TABLE I

T_f versus P for Oligo and Polynucleotides of Adenylic Acid in a Sodium Citrate Buffered Solution at $pH = 4.0$.

P	$T_f^\circ C$
2	—
3	—
4	—
5	14
6	26
7	—
8	44.5
9	48.5
10	58.5
11	61
infinite	112

TABLE II
Computation of θ , \bar{r} and \bar{h} for Poly A
($f_k/f_s = 0.00015$)

Temperature (°C)	0 (Experi- mental)	0 (Theore- tical)	i	h
99	1 0	995	18 5	3800
102 3	97	991	26	2500
105	96	98	39	1900
106 3	95	97	50	1500
108 3	92	94	71	860
109 7	86	88	100	650
111 0	75	73	165	450
111 6	69	61	220	340
112 0	50	50	260	260
112 4	23	40	310	240
112 8	0	28	400	205

Experimental discussions of the helix-coil transition in poly A is given in earlier papers by Fresco and co-workers (1957-59)

A "hypothetical value" for R^2 as a function of temperature could, of course be calculated from Table II and equation (19)

A P P E N D I X

A Fundamental Critique of the Zimm Bragg Theory

The Zimm Bragg theory has been presented by its authors as a theory for the phase change occurring in linear polypeptides (i.e., the helix-coil transition). It is our contention that this theory is not a true theory of phase transition but rather a *model* for diffuse melting

In order to make our point clear, we first consider a very simple model for the melting of a simple liquid.

Consider a lattice-cell model for the liquid state in which all atoms have the partition function $f_L = g_L \exp(E_L/RT)$, consider a lattice model for the solid state in which all atoms have the partition function $f_s = g_s \exp(E_s/RT)$ and consider g_L larger than g_s . Only these two configurations (or microstates) are allowed for the system as a whole.

The partition function of the assembly is

$$A. \quad 1. \quad Q = f_s^N + f_L^N$$

When f_s is larger than f_L , only the first term contributes to Q , when f_L is larger than f_s only the second term contributes to Q . The melting condition occurs when f_s equals f_L . At that point

$$\begin{aligned}
 A. \quad 2. \quad \Delta H_{\text{fusion}} &= E_L - E_s \\
 \Delta S &= R \ln (g_L/g_s) \\
 T_m &= \Delta H/\Delta S
 \end{aligned}$$

If, on the other hand in our cell model we allowed cells of partition function f_L to mix indiscriminately with cells of partition function f_s , the partition function of the assembly would be

$$A. 3. \quad Q = (f_s + f_L)^N$$

Equation (3) shows no phase transition

Although equation (1) definitely shows a phase transition, it was put in there by the assumptions of the model, namely, that there are only two configurations and that the partition functions of the cells are f_L in one configuration and f_s in the other. It is what the old text-books would call a "heuristic proof".

The Zimm-Bragg model when σ equals zero is exactly the same as the model represented by equation (1). The Zimm-Bragg model then gives

$$A. 4. \quad Q = 1^N + S^N$$

We do not regard the Zimm-Bragg treatment as a true theory of phase transition, whether σ is zero or finite.

However, when σ is finite, we regard the Zimm-Bragg treatment as an excellent model for diffuse melting. The introduction of finite σ introduces other suitably weighted intermediate configurations in addition to the two displayed in equations (1) and (4). It does not give the same weight to all configurations as was done in equation (3). The mere fact that we assign partition functions 1 and S to segments in random and in helical configurations means that we have preassumed the existence of the two phases. The assignment of finite σ means we preassume a boundary phase. This is not justifiable if we are considering this treatment as a fundamental theory of phase transition. It is perfectly justifiable if we regard the treatment as a mathematical model for diffuse melting.

The very interesting question arises for what problems in diffuse melting can the Zimm-Bragg treatment be applied? Tobolsky's extension of the treatment, including the generalization of the notation, liberates this model from restriction to the helix coil transition in polypeptides. The effect of the hydrogen bonds, the particular structure of the alpha helix, *perhaps* even the one dimensional aspect of the problem, no longer have central or unique roles.

What systems display diffuse melting? Isolated polypeptides in solution, globular proteins which denature reversibly, double and triple strand helices such as poly A, DNA, etc. It is perhaps an open question as to whether crystalline polymers in bulk, such as high molecular weight monodisperse polyethylene would show a sharp or diffuse melting under conditions of complete equilibrium. What about selenium, whose crystal structure displays long chains? Perhaps one requires very thin fibres of polyethylene or thin whiskers of selenium to bring out diffuse one dimensional melting. However, even in low molecular weight systems diffuse meltings are sometimes known to occur. It would be interesting

to know what inherent physical principle underlies diffuse melting (excluding trivial cases such as the effects of impurities). In response to our questionings Professor F. R. Eirich made the interesting suggestion that the basic thing that might underlie diffuse melting is anisotropy of the radial distribution function in the liquid state

The basic question is to what extent would a generalized Zimm-Bragg treatment, such as that presented by Tobolsky, be an apt model for diffuse melting in general? The double strand helix of poly A may be a crucial case. If the treatment presented in this paper is a good approximation for poly A it might encourage further application of the concept to other cases of diffuse melting.

BIBLIOGRAPHY

- Doty, P., Holtzer, A. M., Bradbury, J. H. and Blout, E. R., 1954, *J. Amer. Chem. Soc.*, **76**, 4493.
- Doty, P. and Yang, J. T., 1956, *Ibid.*, **78**, 498.
- Doty, P., Bradbury, J. H. and Holtzer, A. M., 1956, *Ibid.*, **78**, 947.
- Doty, P., Wada, A., Yang, J. T. and Blout, E. R., 1957, *J. Polymer Sci.*, **23**, 851.
- Fresco, J. R. (private communication).
- Flory, P. J., 1957, *Principles of Polymer Chemistry*, Cornell University Press, pp. 565-576.
- Fresco, J. R., Blake, R. D. and Doty, P., (in press).
- Fresco, J. R. and Doty, P., 1957, *Journal of the Am. Chem. Soc.*, **79**, 3928.
- Fresco, J. R. and Klumperman, E., 1959, *Annals of the New York Acad. Sci.*, **81**, 730.
- Schellmann, J. A., 1955, *Compt. rend. Lab. Carlsberg. Ser. Chim.*, **29**, No. 15.
- Tobolsky, A. V., *J. Polymer Sci.* (in press).
- Tobolsky, A. V., 1962, *J. Chem. Phys.*, **37**, 1139.
- Tobolsky, A. V., Gupta, V. D., 1962, *J. Chem. Phys.*, **36**, 430, 1962, **36**, 1999.
- Zimm, B. H., Doty, P., and Iso, K., 1959, *Proc. Nat. Acad. Sciences*, **45**, 1601.
- Zimm, B. H. and Bragg, J. K., 1958, *J. Chem. Phys.*, **28**, 1246; 1959, **31**, 526.

EMISSION SPECTRUM OF MgCl : A NEW DOUBLET SYSTEM

V. SATYANARAYANA RAO AND P. TIRUVENGANNA RAO

SPECTROSCOPIC LABORATORIES, DEPARTMENT OF PHYSICS, ANDHRA UNIVERSITY, WALTAIR

(Received, July 5, 1963, resubmitted, December 23, 1963)

Plate IX

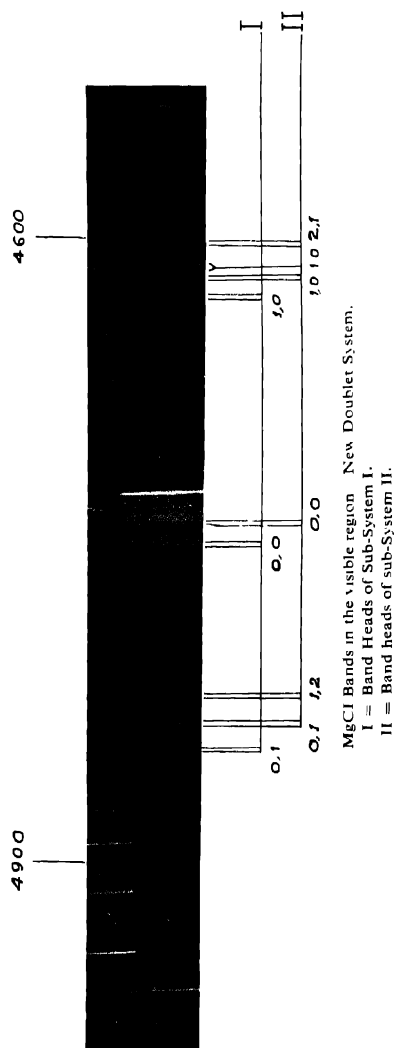
ABSTRACT A new doublet system of bands attributed to MgCl molecule has been observed in the visible region $\lambda 5000\text{--}\lambda 4550$ in the high frequency discharge. From the vibrational analysis of the system it is concluded that the lower state of this system is same as the first excited $A^2\Pi$ state of MgCl with a doublet separation of 55 cm^{-1} . The approximate vibrational constants of the upper state are estimated as $\omega_0' = 563\text{ cm}^{-1}$ and $\omega_0'\omega_e' = 5.5\text{ cm}^{-1}$.

The electronic structures of the ground and excited states of MgCl are discussed in relation to those of BeF and MgF .

INTRODUCTION

The band spectrum of MgCl was investigated by Querbach (1930), Parker (1935), Morgan (1936) and known to consist of only one discrete band system in the region $\lambda 3600\text{--}\lambda 3950\text{ \AA}$. According to Morgan (1936) this system is a doublet system arising from a transition of the type $^2\Pi - ^2\Sigma$ analogous to the well known $^2\Pi_1 - X^2\Sigma$ system of BeF and MgF . The electronic structures of the diatomic halides of Beryllium and Magnesium are expected to be similar in their ground state as they contain the same number of outer valence electrons. By analogy with BeF and MgF one might expect that the ground state of these molecules is a $^2\Sigma$ state. The transition from the first excited $A^2\Pi$ state to the 'X' ground state gives rise to a strong system of bands degraded to violet in the spectra of each of the molecules MgF , MgCl and MgBr . In addition to this main system, transitions from two excited states $B^2\Sigma$ and $C^2\Sigma$ to the common $X^2\Sigma$ ground state have been identified by early workers. In the case of MgCl , fragments of four band systems are given at 12700 cm^{-1} by Querbach (1930), at 25900 cm^{-1} by Parker (1935), at 37060 cm^{-1} and 40850 cm^{-1} by Harrington (1942) in absorption. However no detailed analysis of any of these systems appears to have been reported so far.

During the course of an investigation on the emission spectrum of diatomic MgCl excited in high frequency discharge the authors have obtained a new system of bands in the region $\lambda 5000\text{--}\lambda 4550$, in addition to the well known $A^2\Pi - X^2\Sigma$ system. The results of the vibrational analyses of the systems reported in this paper definitely indicate that the bands are to be attributed to diatomic MgCl .



The electronic structures of MgF and MgCl in their ground and excited states are also discussed in this paper

EXPERIMENTAL

The spectrum of MgCl was excited in high frequency discharge from a 500 Watt oscillator working at a frequency of 30 to 40 Mc/s., using an anhydrous specpure *P* sample of MgCl₂ in a conventional discharge tube. The discharge which was bright green in colour was photographed under low pressure vapour conditions using 3 prism Glass Littrow Spectrograph having a dispersion 7 Å/mm at 4000 Å. Exposures of 5 minutes duration were found sufficient for obtaining good spectrograms using Agfa Isopan superspecial plates. For preliminary survey spectra were also photographed on Fness and Medium Quartz instruments in the visible and ultra violet regions. Measurements of band heads were made on Hilger comparator using iron arc lines as standards and are accurate upto 2 cm⁻¹.

RESULTS AND ANALYSIS

In addition to the well known *A*²Π - *X*²Σ system in the spectrum of MgCl a new system of bands was observed in the region λ5000—λ4550 as can be seen in Fig (I). This system consists of three marked sequences of bands degraded towards the violet. The wave number, intensity and other data of the bands are given in table (I). The measurements of the band heads do not agree with the bands of any of the previously known systems of MgO, MgF, MgBr or with any of the commonly occurring impurity bands.

TABLE I

Wave number in cm ⁻¹	Intensity	Classification v' v''	Band head
20641.4	4	0,1	⁰ P ₁₂
20650.2	2	0,1	P ₂
20696.4	3	0,1	P ₁
20708.0	5	0,1	Q ₁
20761.8	2	1,2	P ₁
20772.1	4	1,2	Q ₁
21128.2	5	0,0	⁰ P ₁₂
21136.8	10	0,0	P ₂
21183.3	5	0,0	P ₁
21191.0	10	0,0	Q ₁
21679.3	2	0,0	⁰ P ₁₂
21687.8	5	1,0	P ₁₂
21720.9	1	1,0	P ₁
21735.9	3	1,0	P ₁
21739.8	3	1,0	Q ₁
21745.4	6	1,0	Q ₁
21798.3	1	2,1	P ₁
21800.4	2	2,1	Q ₁

The analysis of the system was greatly facilitated by identification of the strongest group as $\Delta v = 0$ sequence. The two weaker sequences $\Delta v = -1$ and -2 were easily identified on the longer wave length side and $\Delta v = +1$ sequence on the shorter wave length side of these. Of these the $\Delta v = -2$ sequence is too weak for measurement. The observed double double headed nature of the bands in $\Delta v = 0$ sequence immediately suggested the possibility that the system arises from a ${}^2\Sigma - {}^2\Pi {}^2\Sigma$ or ${}^2\Pi - {}^2\Sigma$ transition. From the structure of ${}^2\Sigma - {}^2\Pi$ transition we expect the following head forming branches ${}^oP_{12}$, $P_2 + pQ_{12}$, P_1 and $Q_1 + qP_{21}$ for bands degraded towards the violet. Thus each band with a particular value of v' and v'' is expected to consist of the above four heads. The intensities of the Q heads is

TABLE II
Vibrational analysis of the sub-system I of MgCl Bands

v'	v''		
	0		1
0	21128.2	486.8	20641.4
	21136.8	480.6	20650.2
	551.1		
	551.0		
1	21679.3		
	21687.8		

TABLE III
Vibrational analysis of the sub-system II of MgCl Bands

v'	v''		
	0	1	2
0	21183.3	486.9	20690.4
	21191.9	483.9	20708.0
	552.6		
	553.5		
1	21735.9		20761.8
	21745.4		20772.1
2		21790.8	
		21800.4	

expected to be twice as strong as the P heads. The detailed classifications of the band heads are given in columns 3 and 4 of Table I. The observed intensities of band heads given in column (2) are in accordance with those expected for ${}^2\Sigma \rightarrow {}^2\Pi$ transition. The vibrational analyses of the two sub-systems are displayed in Tables II and III. The first ΔG_v interval of the lower state of the two sub-systems agrees very well with the first vibrational quantum of $A^2\Pi$ state of MgCl. Further the corresponding bands of the two systems are separated by wave number interval of about 55 cm^{-1} which agrees very closely with the doublet interval of 55 cm^{-1} , of the first excited $A^2\Pi$ state of MgCl. Thus the lower state of the new doublet system was easily identified as the upper state of the main $A^2\Pi \rightarrow X^2\Sigma$ system. All the observed features of the band system are in accordance with the predicted $B^2\Sigma \rightarrow A^2\Pi$. The position of v_0 for the $B^2\Sigma$ state is obtained as $26520.4 \pm 21136.8 = 47657.2\text{ cm}^{-1}$. The approximate vibrational frequency of the upper state is estimated as 563 cm^{-1} . The lower state vibrational constants are the same as those of the main system. Thus the analysis reported above shows conclusively that the emitter of the band system is diatomic MgCl.

Isotope Effect. The calculated isotopic separations of the less abundant molecule MgCl³⁷ according to the formula

$$\begin{aligned}
 \nu_1 - \nu_2 &= (p-1)[\omega'_e(v' + 1/2) - \omega''_e(v'' + 1/2)] \\
 &+ (p^2 - 1)[x'_e\omega'_e(v' + 1/2)^2 - x''_e\omega''_e(v'' + 1/2)^2] + \dots
 \end{aligned}$$

for 0, 1 and 1, 0 bands are 5.03 and 6.5 wave numbers respectively. While this separation is resolvable under dispersion used in the present work, the bands of 0, 1 and 1, 0 sequences are too weak for a detailed study of the chlorine isotopic effect. The weaker MgCl³⁷ heads for 0, 1 bands which are expected to occur on the shorter wave length side are overlapped by the shading of the stronger heads of the more abundant molecule MgCl³⁵. The bands of 1, 0 sequence, though weak, are more favourable for the detection of the weaker MgCl³⁷ heads as they are expected to occur on longer wavelength side. The P_1 and Q_1 heads of the 1, 0 band of the sub-system II were accompanied by the weaker isotopic heads. Although the observed separations of these two solitary heads agree fairly well with the calculated separations as can be seen from table IV, it may be remarked that the agreement tends to support the analysis and may not be taken as too significant or too substantial a support.

TABLE IV
 Isotopic Shifts

Band head	Observed Isotopic shift in cm^{-1}	Calculated Isotopic shifts in cm^{-1}
1,0 P_1	6	6.5
1,0 Q_1	5.6	6.5

ELECTRONIC CONFIGURATIONS AND ELECTRONIC STATES OF MgCl AND MgF

The electronic structures of the ground states of BeF , MgCl are expected to be similar as they contain the same number outer valence electrons. The ground state of the diatomic molecules BeF and MgF is well known to be $^2\Sigma$ state. Following Mullikan's notation the electron configuration of the ground state can be represented as

$$(z\sigma)^2 (y\sigma)^2 (W\pi)^4 (x\sigma) \dots ^2\Sigma \quad \dots (1)$$

The first excited $A^2\Pi_1$ state in BeF and MgF may be represented by the configuration

$$(z\sigma)^2 (y\sigma)^2 (W\pi)^3 (x\sigma) \dots ^2\Pi_1 \quad \dots (2)$$

By analogy with BeF and MgF the $^2\Sigma$ and $^2\Pi_1$ terms arising from configurations from (1) and (2) account for the observed ground $X^2\Sigma$ and first excited $A^2\Pi$ states of MgCl . The observed $B^2\Sigma$ state (upper state of the new doublet system) may be attributed to the configuration

$$(z\sigma)^2 (y\sigma)^2 (W\pi)^3 (x\sigma)(r\pi) \dots ^2\Sigma^+ \quad \dots (3)$$

in which an electron from $(x\sigma)$ orbital goes to the $(r\pi)$ orbital. A transition from the observed $B^2\Sigma$ state to the ground state cannot occur as configuration (3) involves a two electron jump from configuration (1). This might account for the fact that the $B^2\Sigma - X^2\Sigma$ transition was not experimentally observed.

ACKNOWLEDGMENT

The authors wish to express their thanks of Prof. K. R. Rao for his kind interest in this work. One of the authors (V. S. N. Rao) is grateful to the C.S.I.R. (New Delhi) for the financial assistance.

REFERENCES

- Harrington, R. E., 1942, Dissertation (University of California).
 Heugberg, G., 1953, Molecular spectra and Molecular structure. I Spectra of Diatomic Molecules. 2nd Edition (Van Nostrand Co., New York).
 Jevons, W., 1932, Report on Band Spectra of Diatomic Molecules (Physical Society, London).
 Morgan, F., 1936, *Physical Review*, **50**, 603.
 Parker, A. E., 1935, *Physical Review*, **47**, 349.
 Quonbach, J., 1930, *Z. Physik*, **60**, 109.

OBSERVATION OF B_c^8 -DIRECT PRODUCTION

G. C. DEKA AND A. K. GOSWAMI

DEPARTMENT OF PHYSICS, COTTON COLLEGE, GAUHATI (INDIA)

(Received, July 17, 1963; resubmitted, September 7, 1963)

Plate X

ABSTRACT. 105 pairs of alpha particles are observed and analysed as due to the decays of a B_c^8 -nucleus. The kinetic energy of B_c^8 at production and the Q value of the reaction $B_c^8-2\alpha$ are calculated. The energy distribution indicates that the B_c^8 -nuclei were possibly produced during the 'evaporation' of the nucleus. The Q value so obtained has also fair agreement with the expected Q value.

INTRODUCTION

In high energy disintegrations of emulsion nuclei various nuclear fragments of charge $Z > 2$ are often emitted. Ever since the cosmic ray study using nuclear emulsions quite a few workers have been interested in the study of such heavy fragments, i.e., their emission frequency, angular distribution and decay modes. Considerable attention of workers for the study of Li^8 , Li^9 and B^8 has been engaged in the recent times. In addition to these nuclei one can expect that B_c^8 -nucleus should similarly be emitted during the 'evaporation' of the nucleus. The only difficulty for its observation lies in the fact that B_c^8 is very unstable against alpha decay and, in fact, a B_c^8 nucleus disintegrates into two alpha particles in about 10^{-17} second after its production. Because of such a short life it decays before it gets out of the disintegrating nucleus, the two alpha particles then come out of the nucleus as the 'evaporation' particles. The energy released in B_c^8 decay is ~ 90 kev., and B_c^8 when produced gets some kinetic energy. These are then shared between the two alphas. If the kinetic energy of B_c^8 is ~ 40 Mev. a particular value, then the two alpha particles so formed will have nearly equal energy and will diverge in directions inclined at angles $< 6^\circ$. In emulsions they should produce two identical tracks of nearly equal range and it should be possible to observe them. A few such pairs of alpha tracks were observed and analysed first by Perkins (1950) and then by Crussard (1950) in their cosmic ray studies.

EXPERIMENTAL PROCEDURE

Ilford G_5 emulsions were exposed to an intense beam of 4.5 Bev negative π -mesons at the Berkely Bevatron. Two shots of the beam were injected to the

stack and the intensity of pions was 10^6 per cm^2 . As a result of such exposure the production of stars was very large. The stack was processed and developed in the Bristol Physical Laboratory. Emulsion plates were area scanned under X20 objective and X15 eyepieces. Every star was carefully examined looking for two identical black tracks having angle $< 20^\circ$.

The following criteria are adopted in order to select α pairs as due to possible Be^8 -decay:

- (1) Both the tracks must stop in the same plate and they must have an angle $< 20^\circ$ between them.
- (2) Both of them must be identical in appearance so far as their residual ranges, ionisation and coulomb scattering at the end are concerned.

In view of the fact that there are number of experimental biases in selecting the pairs, one should apply the above criteria in order to minimise such biases which includes that the two tracks of the pair may be quite unrelated to each other, they may be just evaporation tracks in the neighbourhood. As both the tracks are, in general, short there is no definite method of identifying them. In addition to the visual inspections profile-measurements are made on some good pairs selected and average track width obtained is compared with those of known tracks of Li and alpha particles. Although it is not so easy to separate alpha tracks from Li ones by this method, still there is some indication that the selected pairs could possibly be due to α particles. We have obtained the average α -track width $= 0.56 \pm 0.03\mu$ and the average Li track width $= 0.60 \pm 0.03\mu$.

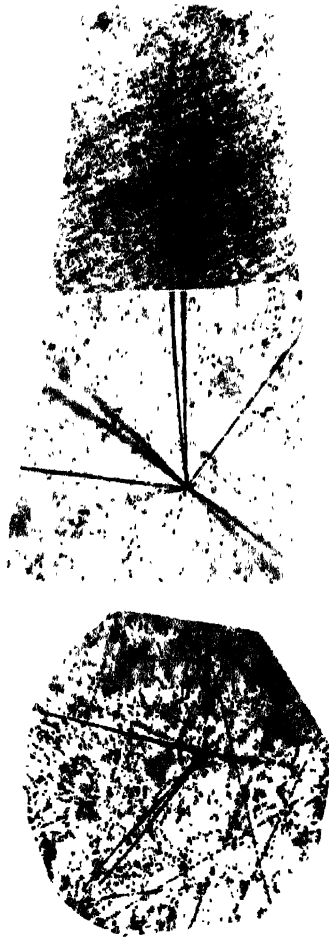
At the same time there is no other method to identify such short tracks. It is not quite justified also to take them as α -particles. It is also very unlikely that two protons or a proton and an alpha particle will be emitted during evaporation in such a manner so as to give the Q value which is very close to the expected Q -value of Be^8 -decay.

Crussard (1950) confined to those events with Q -value < 500 kev whereas Perkins (1950) considered only alpha pairs between which the direction of ejection was $< 10^\circ$. We have accepted events with angles $< 20^\circ$ because the uncertainties in measurement will make the observed spread as big as 20° .

EXPERIMENTAL RESULTS

The experimental results are presented graphically as follows:

Fig. 1 shows the energy distribution of the 105 Be^8 -nuclei which are supposed to be produced during 'evaporation' of the heavy nuclei. To evaluate such energy, the resultant momentum of each alpha-pair is obtained from their observed ranges



Microphotographs of two α pairs.

and the angle between them. This momentum is attributed to the initial momentum of Be^8 —which breaks into two alphas. Assuming that Be^8 nuclei are produced in the evaporation process, one expects the energy distribution to be of Maxwellian type as suggested by Le Counteur (1950). The continuous curve is drawn according to the equation.

$$N(E)dE = \frac{E-V}{T^{1/2}} \exp \left(-\frac{E-V}{T} \right) dE.$$

The two parameters, V —the average potential height and T —the average nuclear temperature are taken from the observed histogram. As is seen in Fig. 1 the agreement between the two graphs is as good as those found by other workers in the study of other fragments, indicating thereby the production of Be^8 -nuclei during 'evaporation process'.

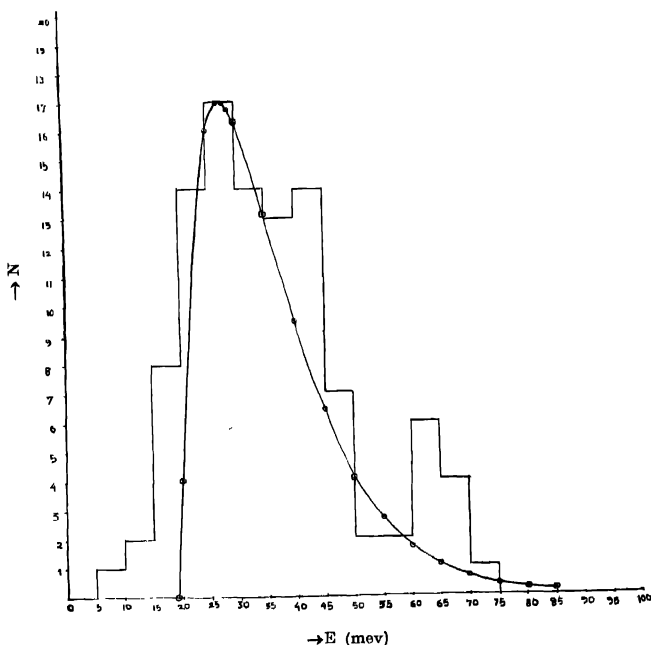


Fig. 1 Energy histogram of Be^8 . the continuous curve is drawn with $V = 19.2$ mev; $T = 8.3$ mev

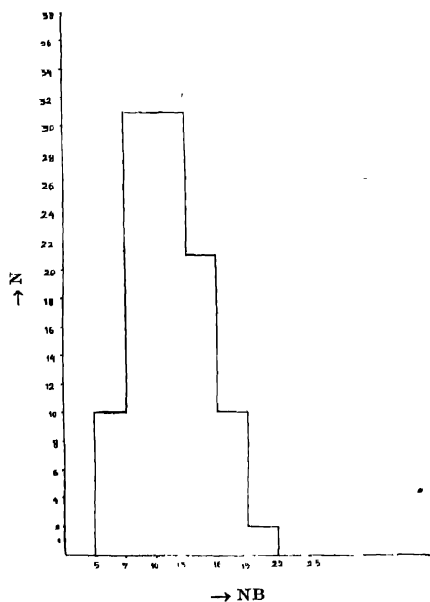


Fig 2 N_1 —distribution of stars with α -pairs

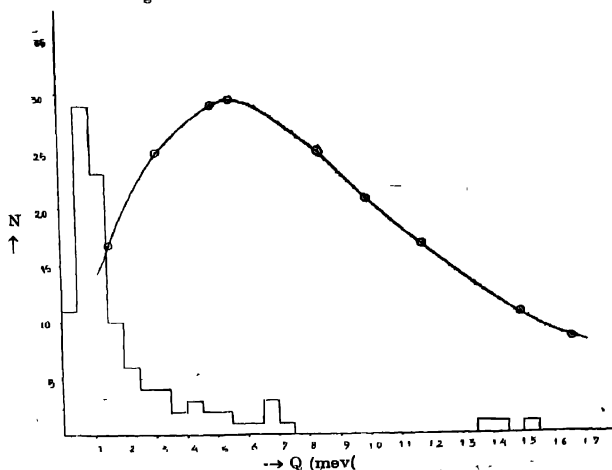


Fig. 3. Q-Value distribution of B_c^0 -decay.
The Continuous curve is the probability curve expected for the Q-distribution of the α -pairs due to chance associations,

Fig. 2 shows the black prong N_b -distribution of the stars with α pairs. The average star size is $N_b = 12$ which indicates that Be^8 was mostly emitted from the disintegration of heavy emulsion nuclei.

Fig. 3 shows the Q -value distribution obtained from the observed α -pairs emitted during 'evaporation' process. The experimental histogram is seen to have a peak at (100 ± 50) Kev. The calculated Q -value for the reaction $\text{Be}^8 \rightarrow 2\alpha$ being 90 Kev, this shows an excellent agreement between these two values. The continuous curve is a probability curve of the Q -distribution for the same, as is expected from α -pairs which may be just the chance association of any two random α -particles emitted during the 'evaporation' of the nuclei.

Micro-photographs of two such α pairs are reproduced

DISCUSSION

The continuous curve in Fig. 3 shows that for random pairs of α particles only 20% of the apparent Q values lie in the interval from 0 to 200 kev. In a sample of 105 stars from most of which one α pair per star is emerged 77 are found to give Q -value less than 250 kev (within 3 standard deviations) and only 28 events with Q lying between 250 to 1500 kev. It is, therefore, reasonable to attributes all but the 28 events with $Q < 250$ kev to be decay of Be^8 fragments. It is expected that the absolute frequency of emission of Be^8 fragments should be appreciably greater than that of the Li^8 -particles and within the present large uncertainties our observed number is consistent with the 'evaporation' theory.

Further, the pairs of α -particles which may be due to the decay of Be^8 from its first excited state of energy 2.9 Mev can not be distinguished from two unrelated α -particles, since their tracks are expected to be widely inclined with a considerable difference in ranges. Also this excited level of Be^8 has a large spread in energy due to its short life time. The result is that a large fraction of α -pairs which are ignored as unrelated ones could also be attributed to Be^8 decay at the first excited state. In a similar way it has sometimes been suggested that groups of tracks from stars may be attributed to the emission of short lived nuclei in highly excited or virtual states. And the procedure we have followed here does not appear fruitful, however, because the observed values of direction and energy for various combinations of tracks which may be chosen from a complex star, can all be made compatible with one or another of the known nuclei and their excited states.

ACKNOWLEDGMENT

Authors like to thank the Department of Atomic Energy, Government of India, for the annual research grant for the project. They are further grateful

to the Government of Assam for giving facilities for such a piece of research in Cotton College. Thanks are also due to Mr K. M. Pathak for his useful suggestions and to Mr M. Das for his scanning works.

REFERENCES

- Crussard, C. R., 1950, *Acad. Sciences, Paris*, **231**, 141.
Lo-Coutour, K. J., 1950, *Proc. Phy. Soc. A.*, **63**, 259.
Perkins, D. H., 1949, *Proc. Roy. Soc. A*, **203**, 399.

Letters to the Editor

The Board of Editors does not hold itself responsible for opinions expressed in the letters published in this section. The notes containing short reports of original investigations communicated to this section should not contain many figures and should not exceed 500 words in length. The contributions reaching that the Secretary by the 15th of any month may be expected to appear in the issue for the next month. No proof will be sent to the author.

17

CRYSTALLOGRAPHIC STUDY OF 3-NITRO-4-HYDROXY PHENYLARSONIC ACID

K. N. GOSWAMI AND SANKAR K. DATTA

INDIAN ASSOCIATION FOR THE CULTIVATION OF SCIENCE, CALCUTTA-32

(Received, August 20, 1963)

As analytical reagents, arsonic acid and substituted arsonic acids combine more or less preferentially with quadrivalent metals. The 3-nitro-4-hydroxy phenylarsonic acid has been used to precipitate cadmium from acetic acid solutions. Very little structural work has been done on this series so far and therefore we have undertaken an x-ray study of this compound to elucidate its molecular structure.

Satisfactory single crystals were grown by slow evaporation of an alcoholic solution of this compound. The crystals were small thin yellow plates. Oblique extinctions were observed when the crystals were examined in polarized light. The crystals were biaxial positive.

The unit-cell dimensions were obtained from oscillation and Weissenberg photographs along [010] and [001] axes using nickel filtered CuK_α radiation. The camera diameter was standardized from the powder lines obtained by sprinkling the crystals with aluminum powder. The axes were so labelled as to confirm to standard crystallographic practice, as shown below.

$$\begin{aligned} a &= 5.54 \text{ \AA}, & \alpha &= 95^\circ 32' \\ b &= 8.39 \text{ \AA}, & \beta &= 99^\circ 15' \\ c &= 11.81 \text{ \AA}, & \gamma &= 125^\circ 9' \end{aligned}$$

No systematic extinctions were observed for (*h*0*l*) and (*h**k*0) reflections. The space group could therefore be either *P*1 or *P* $\bar{1}$.

The density, measured by flotation method in a mixture of Carbontetrachloride and bromoform was found to be 2.05 gm. cm⁻³ which compares favourably with the calculated value 2.03 gm.cm⁻³ on the basis of 2 molecules per unit cell. Further work is in progress.

ACKNOWLEDGMENT

Authors wish to express their sincere thanks to Prof. B. N. Srivastava, D.Sc., F.N.I., for his keen interest in this work.

NOTICE

No claims will be allowed for copies of journal lost in the mail or otherwise unless such claims are received within 4 months of the date of issue.

RATES OF ADVERTISEMENTS

1. Ordinary pages :

Full page Rs. 50/- per insertion

Half page Rs. 28/- per insertion

2. Pages facing 1st inside cover, 2nd inside cover and first and last page of book matter :

Full page Rs. 55/- per insertion

Half page Rs. 30/- per insertion

3. Cover pages by negotiation

25% commissions are allowed to *bona fide* publicity agents securing orders for advertisements.

CONTENTS

Indian Journal of Physics

Vol. 37, No. 12

December, 1963

PAGE

66. On the Measurement of Spherical Aberration Constants of the Projector
Lens of an Electron Microscope—N. H. Sarkar and D. N. Misra ... 605
67. Electron Capture by He^+ Ions passing through He Atoms—D. M.
Bhattacharya, S. C. Mukherjee and N. C. Sil ... 611
68. A Method of Measuring Magnetic Properties of Ferromagnetic and other
Substances—A. K. Mukerjee and N. G. Sutradhar ... 616
69. Dimensional and Structural changes during Denaturation of Helical type
Macromolecules—A. V. Tobolsky and V. D. Gupta ... 625
70. Emission Spectrum of MgCl : A new Doublet System—V. Satyanarayana
Rao and P. Tiruvenganna Rao ... 640
71. Observation of B^8 -Direct Production—G. C. Deka and A. K. Goswami ... 645

LETTERS TO THE EDITOR—

16. Crystallographic Study of 3-Nitro-4-Hydroxy Phenylarsonic Acid—K. N.
Goswami and Sankar K. Dutta ... 651